EMERGING INFECTIOUS DISEASES®

CDC
Centers for Disease Control and Prevention

Viruses

September 2023

Attributed to Ferdinand Georg Waldmüller (1793–1869), *Portrait of Beethoven*, 1823. Oil on canvas, 28.1 in x 30.5 in/71.5 cm x 77.5 cm. Kunsthistorisches Museum, Vienna, Austria. Digital image from Art Resource, New York, New York, USA.

EMERGING INFECTIOUS DISEASES®

Emerging Infectious Diseases is published monthly by the Centers for Disease Control and Prevention, 1600 Clifton Rd NE, Mailstop H16-2, Atlanta, GA 30329-4027, USA. Telephone 404-639-1960; email, eideditor@cdc.gov

EMERGING INFECTIOUS DISEASES®

Viruses **September 2023**

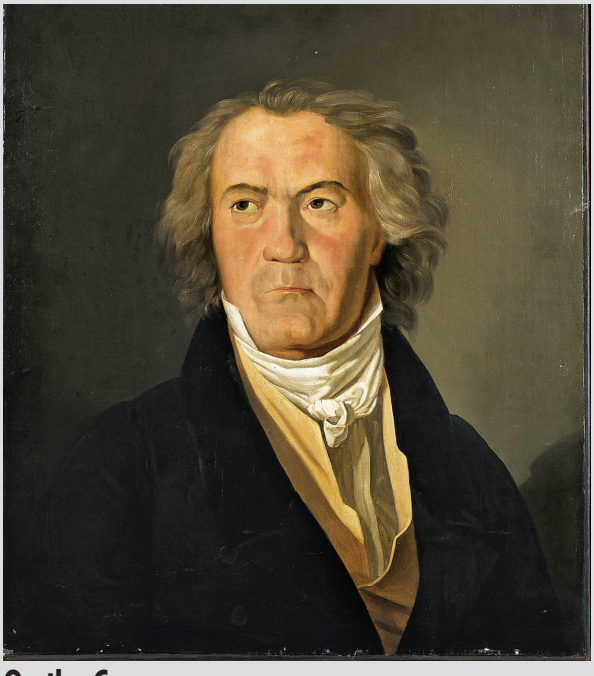

On the Cover

Attributed to Ferdinand Georg Waldmüller (1793–1869), *Portrait of Beethoven*, 1823. Oil on canvas, 28.1 in x 30.5 in/71.5 cm x 77.5 cm. Kunsthistorisches Museum, Vienna, Austria. Digital image from Art Resource, New York, New York, USA.

About the Cover p. 1948

Synopses

Medscape EDUCATION ACTIVITY

Medscape EDUCATION ACTIVITY

Research

Historical Review

Dispatches

EMERGING INFECTIOUS DISEASES®

September 2023

EMERGING INFECTIOUS DISEASES®
September 2023

Photo Quiz

Research Letters

About the Cover

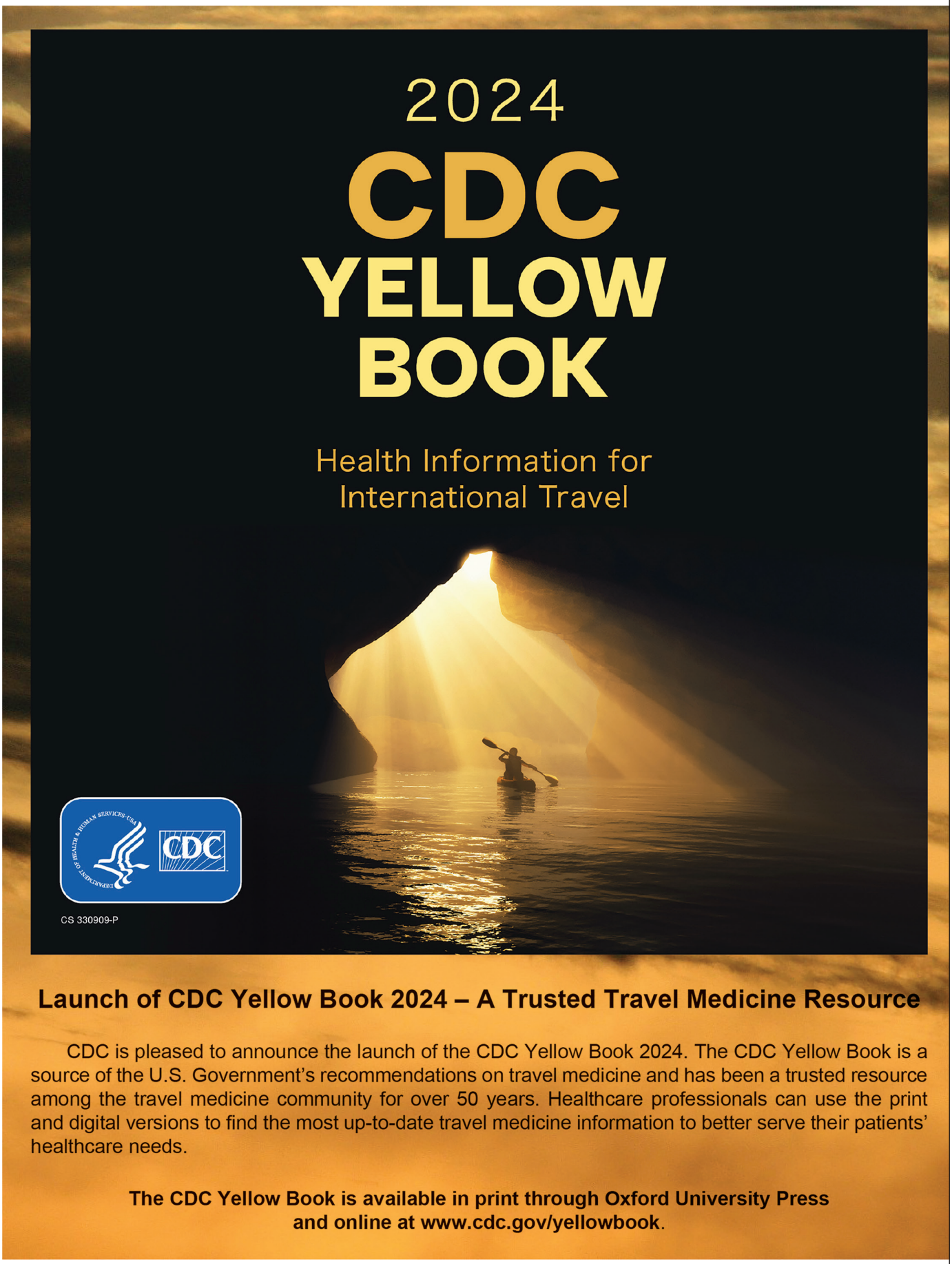

Launch of CDC Yellow Book 2024 – A Trusted Travel Medicine Resource

CDC is pleased to announce the launch of the CDC Yellow Book 2024. The CDC Yellow Book is a source of the U.S. Government's recommendations on travel medicine and has been a trusted resource among the travel medicine community for over 50 years. Healthcare professionals can use the print and digital versions to find the most up-to-date travel medicine information to better serve their patients' healthcare needs.

The CDC Yellow Book is available in print through Oxford University Press and online at www.cdc.gov/yellowbook.

Characteristics of Hard Tick Relapsing Fever Caused by *Borrelia miyamotoi*, United States, 2013–2019

David W. McCormick, Catherine M. Brown, Jenna Bjork, Kim Cervantes, Brenda Esponda-Morrison, Jason Garrett, Natalie Kwit, Abigail Mathewson, Charles McGinnis, Marco Notarangelo, Rebecca Osborn, Elizabeth Schiffman, Haris Sohail, Amy M. Schwartz, Alison F. Hinckley, Kiersten J. Kugeler

In support of improving patient care, this activity has been planned and implemented by Medscape, LLC and Emerging Infectious Diseases. Medscape, LLC is jointly accredited with commendation by the Accreditation Council for Continuing Medical Education (ACCME), the Accreditation Council for Pharmacy Education (ACPE), and the American Nurses Credentialing Center (ANCC), to provide continuing education for the healthcare team.

Medscape, LLC designates this Journal-based CME activity for a maximum of 1.00 ***AMA PRA Category 1 Credit(s)™***. Physicians should claim only the credit commensurate with the extent of their participation in the activity.

Successful completion of this CME activity, which includes participation in the evaluation component, enables the participant to earn up to 1.0 MOC points in the American Board of Internal Medicine's (ABIM) Maintenance of Certification (MOC) program. Participants will earn MOC points equivalent to the amount of CME credits claimed for the activity. It is the CME activity provider's responsibility to submit participant completion information to ACCME for the purpose of granting ABIM MOC credit.

All other clinicians completing this activity will be issued a certificate of participation. To participate in this journal CME activity: (1) review the learning objectives and author disclosures; (2) study the education content; (3) take the post-test with a 75% minimum passing score and complete the evaluation at http://www.medscape.org/journal/eid; and (4) view/print certificate. For CME questions, see page 1951.

NOTE: It is Medscape's policy to avoid the use of Brand names in accredited activities. However, in an effort to be as clear as possible, the use of brand names should not be viewed as a promotion of any brand or as an endorsement by Medscape of specific products.

Release date: August 18, 2023; Expiration date: August 18, 2024

Learning Objectives

Upon completion of this activity, participants will be able to:

- Describe characteristics of *Borrelia miyamotoi*
- Assess trends in the prevalence of infection with *Borrelia miyamotoi* in the US
- Distinguish the peak month for infection with *Borrelia miyamotoi* in the US
- Evaluate the clinical presentation and outcomes of infection with *Borrelia miyamotoi*

CME Editor

Thomas J. Gryczan, MS, Technical Writer/Editor, Emerging Infectious Diseases. *Disclosure: Thomas J. Gryczan, MS, has no relevant financial relationships.*

CME Author

Charles P. Vega, MD, Health Sciences Clinical Professor of Family Medicine, University of California, Irvine School of Medicine, Irvine, California. *Disclosure: Charles P. Vega, MD, has the following relevant financial relationships: consultant or advisor for Boehringer Ingelheim; GlaxoSmithKline; Johnson & Johnson.*

Authors

David W. McCormick, MD; Catherine M. Brown, DVM; Jenna Bjork, DVM; Kim Cervantes, MPH; Brenda Esponda-Morrison; Jason Garrett, MPH; Natalie Kwit, DVM; Abigail Mathewson, DVM; Charles McGinnis, BSN; Marco Notarangelo, MS; Rebecca Osborn, MPH; Elizabeth Schiffman, MPH; Haris Sohail, MPH; Amy M. Schwartz, MPH; Alison F. Hinckley, PhD; Kiersten J. Kugeler, PhD.

Borrelia miyamotoi, transmitted by *Ixodes* spp. ticks, was recognized as an agent of hard tick relapsing fever in the United States in 2013. Nine state health departments in the Northeast and Midwest have conducted public health surveillance for this emerging condition by using a shared, working surveillance case definition. During 2013–2019, a total of 300 cases were identified through surveillance; 166 (55%) were classified as confirmed and 134 (45%) as possible. Median age of case-patients was 52 years (range 1–86 years); 52% were male. Most cases (70%) occurred during June–September, with a peak in August. Fever and headache were common symptoms; 28% of case-patients reported recurring fevers, 55% had arthralgia, and 16% had a rash. Thirteen percent of patients were hospitalized, and no deaths were reported. Ongoing surveillance will improve understanding of the incidence and clinical severity of this emerging disease.

Tickborne diseases are an increasing public health problem, accounting for ≈75% of reported vectorborne illnesses in the United States (*1*–*3*). Continued discovery of new tickborne pathogens in recent years suggests they remain an underrecognized cause of human illness (*4*–*6*). *Borrelia miyamotoi* is a gram-negative spirochete transmitted by *Ixodes* spp. ticks (*7*–*9*) that was initially identified in ticks in Japan during 1995 (*7*). It was recognized as a cause of human illness in Russia during 2011 (*10*) and in the United States during 2013 (*11*). Human infection has since been detected throughout the Holarctic region (*10*,*12*–*17*).

Phylogenetically, *B. miyamotoi* is a relapsing fever group *Borrelia* (*18*). Diseases caused by this diverse group of spirochetes are differentiated by their vector, such as louseborne relapsing fever, transmitted by body lice, and tickborne relapsing fever or soft tick relapsing fever, transmitted by soft-bodied (argasid) ticks in several areas, including the western United States (*19*). *B. miyamotoi* is an agent of hard tick relapsing fever (HTRF), although resulting illness has also been referred to as *B. miyamotoi* disease. In the United States, *B. miyamotoi* is transmitted by *I. scapularis* ticks in the Northeast and Midwest (*20*,*21*) and by *I. pacificus* ticks on the Pacific Coast (*22*). Those tick species also transmit the causative agents of Lyme disease (*23*), anaplasmosis (*24*), babesiosis (*25*), Powassan virus disease (*26*), and a form of ehrlichiosis (*27*). Data from tick testing indicate that the geographic range of *B. miyamotoi* is similar to that of those pathogens (*28*,*29*).

The incidence of HTRF caused by *B. miyamotoi* and its public health role are largely unknown. In the United States, prevalence of *B. miyamotoi* in *Ixodes* spp. ticks is relatively low, but consistent across geographic regions at ≈2% (*3*,*29*). A seroprevalence evaluation conducted in several states in the northeastern United States in 2018 suggested that 2.8% of persons might have evidence of previous infection, compared with 11% of persons who had evidence of previous Lyme disease (*30*). Data from previous case series suggest that HTRF caused by *B. miyamotoi* most often manifests as a nonspecific febrile illness. Among identified cases, fever, myalgia, arthralgia, and headache are common, but recurring fevers similar to those documented in patients who have soft tick relapsing fever are relatively uncommon (4%–11% of total) (*10*,*17*). Immunocompromised persons who have HTRF might have more severe symptoms, including meningoencephalitis (*11*,*16*,*31*).

Specific laboratory diagnosis of *B. miyamotoi* infection is achieved through PCR detection of *B. miyamotoi* DNA (*10*,*17*,*32*). Serologic reactivity to surface proteins, especially glycerophosphodiester phosphodiesterase (GlpQ), is also used, but reactivity is not specific to *B. miyamotoi* infection or HTRF (*33*,*34*). GlpQ is found in all relapsing fever group borreliae but not in the *B. burgdorferi* sensu lato species that cause Lyme disease (*34*). However, GlpQ cannot distinguish between *B. miyamotoi* infection and infections caused by other relapsing fever group *Borrelia* spp., including agents of soft tick relapsing fever. In addition, related GlpQ proteins are found in common bacterial pathogens, such as *Haemophilus influenzae* and *Escherichia coli,* further reducing specificity of those serologic assays (*34*).

After initial cases of HTRF were identified in the United States, several states that had a high incidence of Lyme disease and other *Ixodes*-transmitted illnesses initiated public health surveillance to clarify

Author affiliations: Centers for Disease Control and Prevention, Fort Collins, Colorado, USA (D.W. McCormick, A.M. Schwartz, A.F. Hinckley, K.J. Kugeler); Massachusetts Department of Public Health, Boston, Massachusetts, USA (C.M. Brown); Minnesota Department of Health, Minneapolis, Minnesota, USA (J. Bjork, E. Schiffman); New Jersey Department of Health, Trenton, New Jersey, USA (K. Cervantes); Connecticut Department of Public Health, Hartford, Connecticut, USA (B. Esponda-Morrison); Rhode Island Department of Health, Providence, Rhode Island, USA (J. Garrett, C. McGinnis); Vermont Department of Health, Burlington, Vermont, USA (N. Kwit); New Hampshire Department of Health and Human Services, Concord, New Hampshire, USA (A. Mathewson, M. Notarangelo); Wisconsin Department of Health Services, Madison, Wisconsin, USA (R. Osborn); Maine Center for Disease Control and Prevention, Augusta, Maine, USA (H. Sohail)

DOI: https://doi.org/10.3201/eid2909.221912

the epidemiology of this novel tickborne condition. We summarize available information on HTRF as ascertained through public health surveillance efforts in the United States beginning in 2013.

Methods

Case Definition

The Centers for Disease Control and Prevention (CDC) and state health departments in areas that had a high incidence of Lyme disease jointly created an informal working surveillance case definition to identify and classify potential cases of HTRF caused by *B. miyamotoi* in a standardized manner. Clinical manifestations considered compatible with HTRF were broadly defined as acute onset of fever or chills with ≥1 of the following additional signs or symptoms: headache, sweats/chills, myalgia, arthralgia, malaise/fatigue, rash, abdominal cramps, nausea, vomiting, diarrhea, dizziness, confusion/altered mental status, photophobia, leukopenia, thrombocytopenia, or increased aminotransferase levels.

For purposes of surveillance data as summarized, we defined a confirmed case of HTRF caused by *B. miyamotoi* as compatible clinical manifestations with ≥1 of the following: isolation of *B. miyamotoi* from a clinical specimen; detection of *B. miyamotoi* DNA in a clinical specimen by using nucleic acid amplification techniques (NAAT) such as PCR; or evidence of seroconversion between acute phase and convalescent phase serum samples, including but not limited to a ≥4-fold change in serum antibody titer to *B. miyamotoi* between paired specimens. We defined a possible case as compatible clinical manifestations with ≥1 of the following: direct observation of spirochetes consistent with *B. miyamotoi* on a peripheral blood smear or detectable IgM or IgG to *B. miyamotoi* from a serum specimen.

We characterized cases as possible rather than probable to reflect the uncertainty of the spectrum of clinical manifestations of HTRF and the specificity of a single positive serologic titer. We excluded positive laboratory test results for which no clinical information was obtained or for which there was no associated clinical illness. Data on specific test manufacturers or antigenic targets used in serologic assays were not available to ascertain level of specificity for *B. miyamotoi* versus other relapsing fever *Borrelia* spp.

Public Health Investigation

Commercial or clinical laboratories reported positive laboratory results for *B. miyamotoi* in accordance with local regulations in states in which *B. miyamotoi* infection/HTRF was a reportable condition. Public health personnel conducted case investigations according to local practices to ascertain demographic, clinical, and exposure information to the extent possible through patient or provider interviews or medical chart reviews.

Analytic Methods

We classified symptoms as present or absent. We categorized age as <18 years, 18–64 years, and ≥65 years. We compared categorical and binary variables by using χ^2 or Fisher exact tests and continuous variables by using the Wilcoxon rank-sum test. We performed all statistical analyses by using SAS software (SAS Institute). This study was deemed to be a nonresearch activity by CDC under provision of public health surveillance.

Results

A total of 300 HTRF cases caused by *B. miyamotoi* were identified during 2013–2019 by the 9 state health departments in the Northeast and upper Midwest United States that conducted public health surveillance for this condition (Connecticut, Maine, Massachusetts, Minnesota, New Hampshire, New Jersey, Rhode Island, Vermont, and Wisconsin). The number of states in which HTRF was reportable increased from 1 in 2013 to 9 by 2019 (Figure 1). The number of cases identified annually concomitantly increased; more cases were identified during 2017–2019 (median 82, range 78–83 cases/y) than during 2013–2015 (median 9, range 8–10 cases/y) (Figure 2).

Of the 300 identified cases, 166 (55%) were classified as confirmed and 134 (45%) as possible. Of the 300 cases, 157 (52%) were in male and 143 (48%) among female patients; median age was 52 (range 1–86) years. Almost all cases were among non-Hispanic White persons (107/110, 97%). Median age of persons who had confirmed illness was older than persons who had possible illness (median age 56 [range 4–86] years vs. median 50 [1–86] years; p = 0.03) (Table 1). A higher proportion of confirmed versus possible cases occurred among persons <18 years of age (9% vs. 4%) and among persons ≥65 years of age (34% vs. 21%; p = 0.004) (Figure 3). Among confirmed cases, 56% of patients were male and 44% female; among possible cases, 49% of patients were male and 51% female (p = 0.23). Most case-patients had symptom onset during June–September, with a peak in August (Figure 4). Compared with confirmed HTRF illness, possible illness had a less pronounced seasonal pattern.

The median duration of time from symptom onset to seeking medical attention was 5 (range 0–311)

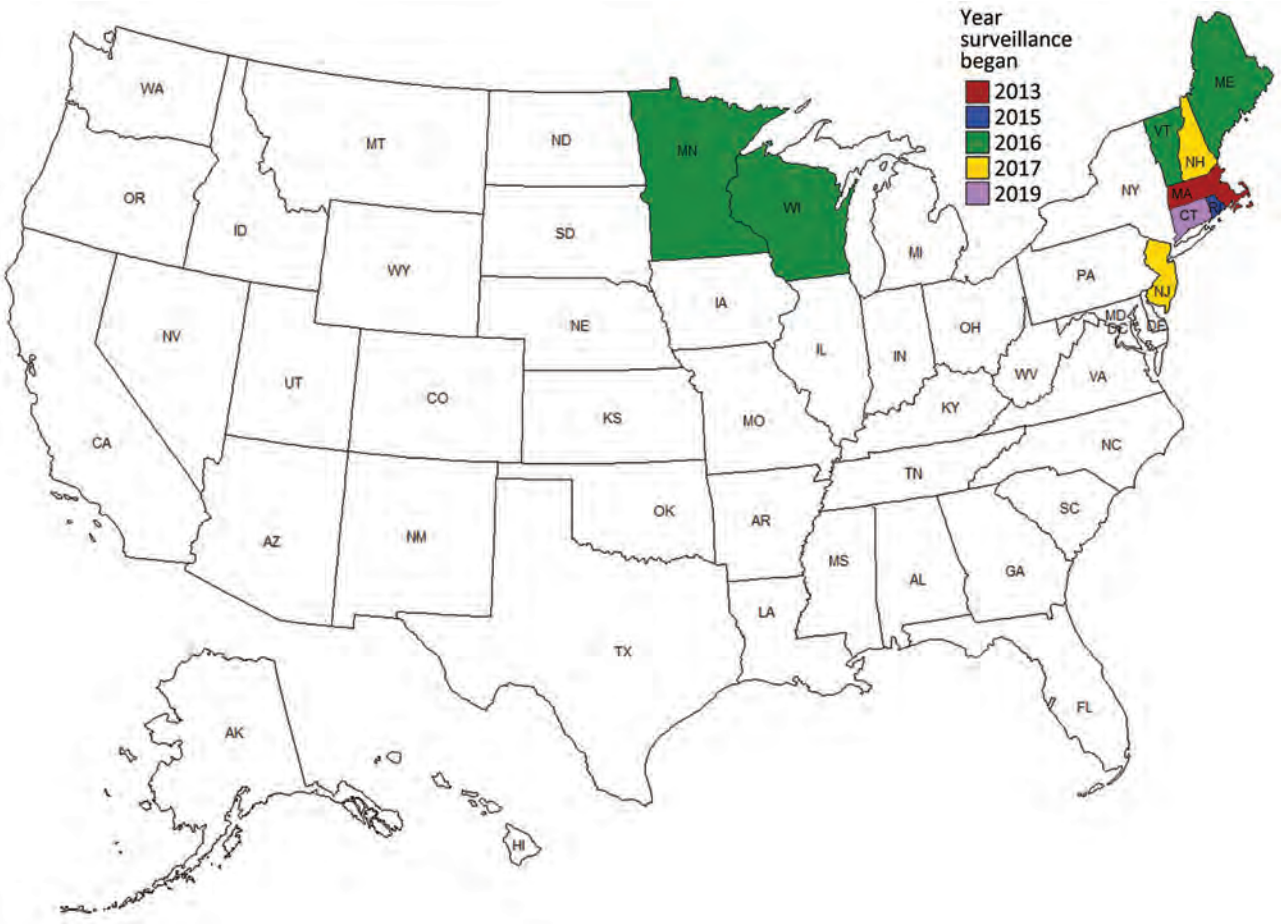

Figure 1. US states that conducted surveillance for hard tick relapsing fever caused by *Borrelia miyamotoi* during 2013–2019 and year in which surveillance began.

days for the 69 persons for whom this information was available (Table 2). Persons who had possible illness had a longer duration from symptom onset to medical attention (median 9, interquartile range [IQR] 3–29 days) than persons who had confirmed cases (median 3, IQR 2–7 days; p = 0.03). Overall, the most common symptoms were fever (89%), fatigue (75%), headache (72%), and chills (68%). Among 64 patients

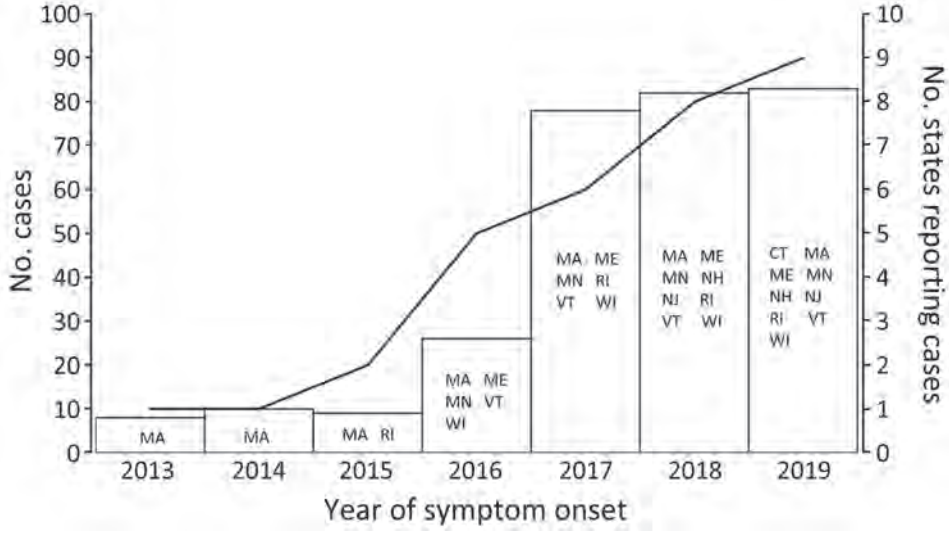

Figure 2. Number of annual cases of hard tick relapsing fever (vertical bars) and number of states reporting cases of hard tick relapsing fever caused by *Borrelia miyamotoi* (line), United States, 2013–2019. The left y-axis corresponds to the vertical bars, and the right y-axis corresponds to the line; scales for the y-axes differ substantially to underscore patterns but do not permit direct comparisons. States reporting cases in that year are shown. CT, Connecticut; MA, Massachusetts; ME, Maine; MN, Minnesota; NH, New Hampshire; NJ, New Jersey; RI, Rhode Island; VT, Vermont; WI, Wisconsin.

Table 1. Demographic characteristics for confirmed and possible cases of hard tick relapsing fever caused by *Borrelia miyamotoi* identified by public health surveillance, United States, 2013–2019*

Characteristic	Confirmed, n = 166	Possible, n = 134	p value
Median age, y (range)†	56 (4–86)	50 (1–86)	0.03‡
Categorical age			
<18	15/166 (9)	5/134 (4)	
18–65	95/166 (57)	101/134 (75)	0.004
>65	56/166 (34)	28/134 (21)	
Sex			
M	92/166 (56)	65/134 (49)	0.23
F	74/166 (44)	69/134 (51)	
Year of illness onset§			
2013	8/165 (5)	0/132 (0)	
2014	9/165 (5)	1/132 (1)	
2015	1/165 (1)	8/132 (6)	
2016	16/165 (10)	10/132 (8)	<0.0001¶
2017	56/165 (34)	22/132 (17)	
2018	38/165 (23)	44/132 (34)	
2019	37/165 (22)	46/132 (35)	

*Values are no. positive/no. tested (%) unless indicated otherwise.
†Missing information for 25 persons.
‡By Wilcoxon rank-sum test.
§Missing information for 4 persons.
¶By Fisher exact test.

who had fever for whom a temperature was available, the median recorded temperature was 102.5°F (range 99.7°F –105.7°F). A total of 28% reported recurring fevers of some kind, 55% had arthralgia, and 16% had a rash. A description of the rash was available for 18 patients; the rash was noted to be generalized for 3 patients (1 confirmed and 2 possible cases) and focal for 15 patients (9 confirmed and 6 possible cases). An erythema migrans–like rash was reported for 1 possible HTRF case. Thrombocytopenia (51/105, 49%), increased levels of aspartate and alanine aminotransferases (40/96, 42%), and leukopenia (39/105, 37%) were common laboratory abnormalities.

When compared with persons who had possible illness, a higher proportion who had confirmed illness also had fever (95% vs. 81%; p<0.0001), leukopenia (46% vs. 22%; p = 0.02), and thrombocytopenia (58% vs. 25%; p = 0.001), and a higher proportion of possible cases had recurring fever (35% vs. 22%; p = 0.01), arthralgia (63% vs. 48%; p = 0.02), and cognitive impairment or mood disturbance (16% vs. 4%; p = 0.0004). Approximately one eighth (39/300, 13%) of persons who had HTRF were hospitalized; the percentage hospitalized was similar among persons who had confirmed (20/166, 12%) and possible (19/134, 12%) illness (p = 0.78). There were no deaths.

All laboratory tests performed were either by using PCR or serologic analysis for *B. miyamotoi* infection. PCR was performed for 167 (56%) patients, and serologic analysis was performed for 137 (46%) patients (Table 3). Serologic analysis for paired serum samples was specifically performed for 19 (14%) persons. Among persons who had confirmed illness, 162/164 (99%) had a positive PCR result. Five (3%) of those persons also had a single positive IgM or IgG serologic test result, of whom 2 had a positive IgM result and none had a positive IgG or IgM/IgG combined test result. Among persons who had possible illness, 5/134 (4%) also had PCR performed; all results were negative. No microscopy or culture results were reported for any case.

Among persons for whom exposure information were available, most (63/69, 91%) reported exposure to ticks or tick habitat; more than half reported a tick bite (46/82, 56%). Travel within (16/70, 23%) or outside (21/79, 27%) the state of residence was infrequently reported. Compared with persons who had possible cases, a higher proportion of persons who had confirmed illness reported exposure to ticks or tick habitat (48/51 [94%] vs. 15/18 [83%]; p = 0.16) or having a known tick bite (37/60, 62% vs. 9/22, 41%, p = 0.09). A total of 15 persons (15/72, 21%) reported receipt of a blood transfusion or organ transplant within the previous 30 days; those occurred among 9 confirmed and 6 possible cases. Among 7 persons who received a blood transfusion and for whom tick exposure information was available, all reported a recent tick bite.

Information on antimicrobial drug treatment was available for 124 (41%) patients. Among those patients, 110 (89%) were given a single antimicrobial drug; 101 (92%) received doxycycline, 5 (5%) amoxicillin, 1 (1%) minocycline, 1 (1%) with cefuroxime, 1 (1%) azithromycin, and 1 (1%) trimethoprim/sulfamethoxazole. Among the 14 patients who received a combination regimen, 13 (93%) were given a regimen of doxycycline and another antimicrobial drug; 1 patient received amoxicillin and cefuroxime.

Discussion

A total of 300 cases of HTRF caused by *B. miyamotoi* in the United States were identified by using public health surveillance. Case-patients were most commonly male and older adults. Case investigations showed that nonspecific symptoms, including fever and headache, were common, and rash was relatively uncommon. Those clinical features are similar to those of previous large case series of HTRF (*10*,*17*), although the overall proportion of cases with recurring fevers in this report was higher, and recurring fevers were more common among possible cases than among confirmed cases. The percentage of cases associated with hospitalization in this report was lower than reported among a large case series in the northeastern United States (*17*), and there were no reported deaths. However, the data in this summary might include cases reflected in previous case series if those previously reported cases were captured through public health surveillance.

We observed a summertime seasonal pattern for confirmed cases, similar to findings for other infections transmitted by *Ixodes* spp. ticks in the United States (*23*,*35*,*36*). The frequency of HTRF peaked later in the summer than that for Lyme disease (*3*,*23*,*37*). This shifted seasonality supports a role for larval blacklegged ticks in *B. miyamotoi* transmission to humans in the United States because those ticks are more likely to be questing for blood meals during mid-to-late summer than during other tick life stages (*38*), and there is documented transovarial transmission of *B. miyamotoi* (*39*).

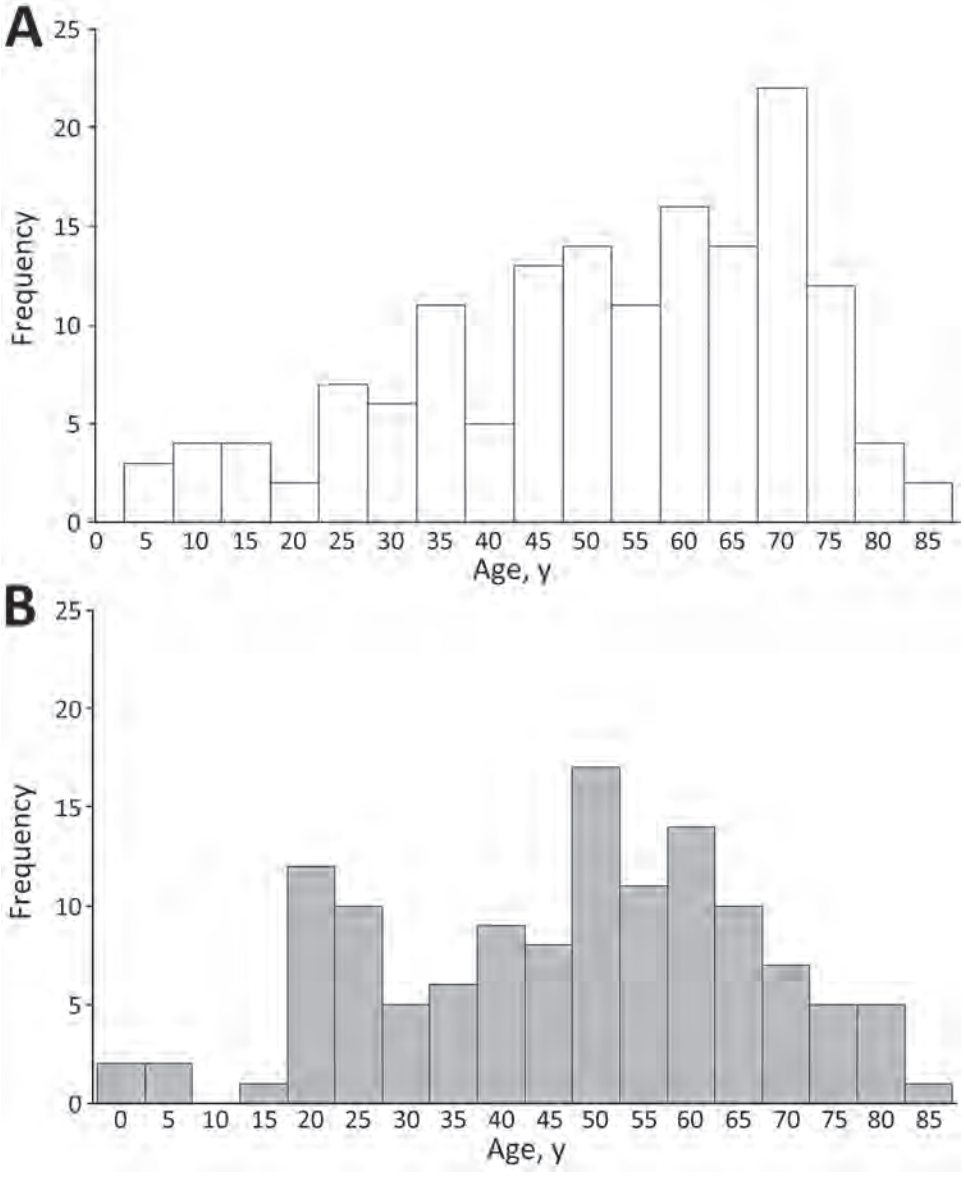

Figure 3. Patient age distribution for confirmed (A) and possible (B) cases of hard tick relapsing fever caused by *Borrelia miyamotoi* identified by using public health surveillance, United States, 2013–2019.

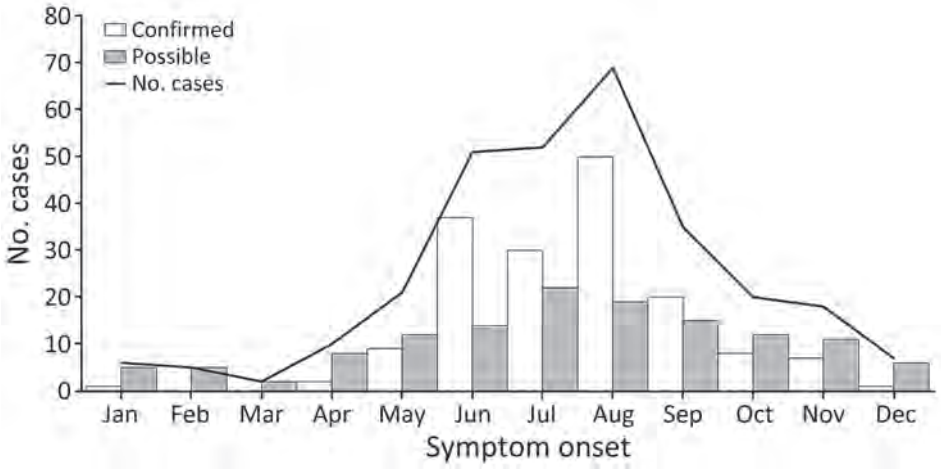

Figure 4. Reported cases of hard tick relapsing fever caused by *Borrelia miyamotoi* by month of symptom onset, United States, 2013–2019. Solid line indicates total number of reported cases each month, and bars indicate number of confirmed (white) and possible (gray) cases each month.

Several features differed between confirmed and possible cases. Confirmed cases occurred more commonly among older persons and among male persons than did possible cases. Confirmed cases were more frequently characterized by fever, thrombocytopenia, and increased levels of aminotransferases. Possible cases were more frequently characterized by confusion, mood disorder, abdominal pain, shortness of breath, and recurring fevers. Although possible case-patients tended to have a longer duration of illness before seeking medical care, this difference might simply reflect the bias of the case definition itself, in which direct detection by

Table 2. Clinical and laboratory findings for persons who have confirmed and possible hard tick relapsing fever caused by *Borrelia miyamotoi* among reported cases with available laboratory findings identified by public health surveillance, United States, 2013–2019*

Characteristic	Confirmed, n = 165	Possible, n = 133	p value
Hospitalized	20 (12)	19 (14)	0.61
Median duration of illness, d† (IQR)	3 (2–7)	9 (3–29)	0.03
Required symptoms			
Fever	157 (95)	108 (81)	<0.0001
Chills	115 (70)	87 (65)	0.27
Supporting signs and symptoms			
Headache	118 (72)	96 (72)	0.85
Myalgia	104 (63)	94 (71)	0.20
Arthralgia	79 (48)	84 (63)	0.02
Malaise/fatigue	125 (76)	99 (74)	0.55
Rash	21 (13)	28 (21)	0.06
Abdominal pain	16 (10)	27 (20)	0.01
Nausea	55 (33)	36 (27)	0.26
Vomiting	23 (14)	15 (11)	0.44
Diarrhea	8 (5)	17 (13)	0.01
Dizziness	26 (16)	33 (25)	0.06
Confusion	7 (4)	24 (18)	<0.0001
Photophobia	8 (5)	11 (8)	0.29
Leukopenia‡	31 (46)	8 (22)	0.02
Thrombocytopenia§	40 (58)	9 (25)	0.001
Increased levels of aminotransferases¶	27 (45)	13 (36)	0.41
Other symptoms			
Recurring fevers	37 (22)	47 (35)	0.01
Shortness of breath	5 (3)	14 (11)	0.01
Cough	15 (9)	10 (8)	0.53
Anorexia	32 (19)	26 (20)	0.99
Jaundice	2 (1)	4 (3)	0.21
Lymphadenopathy	0 (0)	0 (0)	NA
Cognitive impairment/mood disturbance	7 (4)	21 (16)	0.0004
Meningitis/encephalitis	0 (0)	5 (4)	0.01
Neutropenia	6 (4)	2 (2)	0.11
Abnormal chest radiograph	11 (7)	2 (2)	0.04

*Values are no. (%) unless indicated otherwise. IQR, interquartile range; NA, not available.
†Defined as duration from symptom onset to first seeking medical care.
‡Information regarding a patient's leukocyte count was available for 68 confirmed and 37 possible cases.
§Information regarding a patient's platelet count was available for 69 confirmed and 36 possible cases.
¶Information regarding a patient's alanine and aspartate aminotransferase levels was available for 60 confirmed and 36 possible cases.

Table 3. Diagnostic results for confirmed and possible cases of hard tick relapsing fever caused by *Borrelia miyamotoi* reported by public health surveillance, United States, 2013–2019*

Characteristic	Confirmed, n = 166†	Possible, n = 134
PCR results		
Detected	162/164 (99)	0/5 (0)
Not detected	0/164 (0)	5/5 (100)
Serologic analysis results		
Single IgM alone		
Positive	2/2 (100)	36/127 (28)
Negative	0/2 (0)	89/127 (70)
Indeterminate	0/2 (0)	2/127 (2)
Single IgG alone		
Positive	0/2 (0)	111/127 (87)
Negative	2/2 (100)	16/127 (13)
Indeterminate	0/2 (0)	0/127 (0)
Single combined IgM/IgG		
Positive	1/2 (50)	6/7 (86)
Negative	0/2 (0)	1/7 (14)
Indeterminate	1/2 (50)	0/7 (0)
Paired serologic samples		
≥4-fold change in titer	1/1 (100)	0/18 (0)
<4-fold change in titer	0/1 (0)	18/18 (100)

*Values are no. positive/no. tested (%).
†Missing diagnostic information for 2 cases.

using PCR was laboratory evidence for the confirmed case definition and a single positive serologic result was laboratory evidence for the possible case definition. Serologic analysis (particularly for IgG) is unlikely to show increased levels during acute illness (*34*). In addition, increased reactivity against GlpQ alone might not be a specific measure of past HTRF infection (*33*,*34*). In this study, all possible case-patients had detectable IgG, suggesting that they might have had illness onset >20 days before testing, and so results might not represent acute *B. miyamotoi* infection or possibly not *B. miyamotoi* infection at all. However, longer duration of illness before seeking medical care for the possible case-patients might enable increased opportunity for observation of recurrent fevers. We observed less striking seasonality of illness onset for possible case-patients than for confirmed case-patients. Those findings collectively decrease our confidence that the possible cases summarized here reflect acute HTRF illness.

The older age distribution among confirmed HTRF cases is similar to that of anaplasmosis and babesiosis cases and differs from Lyme disease cases, even though all are transmitted in the United States by the same species of *Ixodes* ticks (*24*). Lyme disease most commonly affects children 5–14 years of age, as well as older adults (*40*). In contrast, anaplasmosis rarely affects children, and HTRF in children was uncommon in public health surveillance. The older age distribution of anaplasmosis is believed to reflect host susceptibility differences and immune-related factors linked to aging, rather than age-related differences in tick exposure; those potential age-based susceptibility differences might account for the older age distribution associated with persons who have HTRF. However, diverging clinical or diagnostic approaches might be used for children versus adults, such as lower levels of testing or lower clinical awareness that bias the cases identified through public health surveillance toward adults. Because the clinical manifestations of HTRF and anaplasmosis might be similar (*24*), increased clinical education should highlight the potential for anaplasmosis and HTRF to resemble one another.

Fifteen persons in this study reported receiving a blood transfusion or organ transplant in the 30 days before symptom onset. Although no cases of *B. miyamotoi* infection after blood transfusion have been documented, other tickborne pathogens, including *Babesia microti*, *A. phagocytophilum*, and *Ehrlichia chaffeensis*, have caused infections after blood transfusion (*41*,*42*). Spirochetemia might be higher or more prolonged for *B. miyamotoi* infection than for *B. burgdorferi* infection, suggesting that the risk for transmission from blood transfusion is greater for *B. miyamotoi* (*17*,*46*). Nevertheless, all 7 patients who had a confirmed infection and an available exposure history available reported a recent tick bite, suggesting that receipt of blood products or organs might simply reflect risk factors for more severe illness caused by compromised immune status, rather than a potential route of *B. miyamotoi* transmission.

The frequency of recurring febrile episodes in HTRF caused by *B. miyamotoi* is not well understood. The percentage of patients with confirmed illness who had recurring fever (22%) was higher than those reported in a case series from Russia (11%) (*10*) and in a case series from the United States (4%) (*17*). All relapsing fever group borreliae display antigenic variation, a shift in expressed proteins that creates recurring febrile episodes (*43*,*44*). *B. miyamotoi* infection

generates a lower level of spirochetemia than its soft tick–transmitted relatives, which might affect severity of illness and ability to generate recurrent fevers in untreated infection (*17*,*45*). Direct detection and treatment early in the illness course could result in clinical cure before antigenic variation occurs. It is difficult to compare the frequency of recurrent fevers in persons who have *B. miyamotoi* infection with persons who have soft tick relapsing fever because of variable methods of ascertainment. Also, no objective capture of details regarding fever recurrence frequency, intervals between febrile episodes, and maximum temperature of each febrile episode were captured through this public health surveillance practice; those details are best captured through detailed clinical case series.

Low clinical awareness, limited availability of PCR testing, and limited specificity of available serologic assays make HTRF case identification challenging. Currently, diagnosis of tickborne infections requires clinicians to order tests specific to each suspected pathogen; the expanded use of multiplex direct detection assays, or tickborne panels, in commercial laboratories might improve detection of *B. miyamotoi* and other tickborne infections. Metagenomics approaches are also an increasing opportunity to improve direct detection of tickborne infections, including co-infections (*46*,*47*). Those approaches are particularly appealing for improved detection of *B. miyamotoi* infection because the spirochetes appear to be present in sufficient quantities in blood for detection by using molecular methods (*17*,*46*,*48*). Highlighting the usefulness of PCR-based diagnostic methods for *B. miyamotoi* infection, a study found that among patients with PCR-confirmed *B. miyamotoi* infection, the sensitivity of GlpQ IgG was <55% when assayed <20 days after illness onset, which increased to 74%–86% when assayed 21–150 days after illness onset (*33*). GlpQ is a common serologic target for differentiating infection with relapsing fever group borreliae from those that cause Lyme disease. However, there is limited information on its specificity for relapsing fever group borreliae, constraining its clinical usefulness.

Without sufficiently specific serologic assays, the frequency of exposure in the population and characteristics of more mild illness is difficult to ascertain. In addition, GlpQ-based assays cannot distinguish between infection with hard tick and soft tick relapsing fever borreliae, which can co-occur in some areas (i.e., along the Pacific Coast). In those circumstances, a comprehensive exposure history is necessary to direct public health intervention. However, many patients who have suspected tickborne infections, including HTRF, receive doxycycline empirically, which would effectively treat *B. miyamotoi* even if clinicians had not suspected this specific infection. People with mild symptoms who live in a Lyme disease–endemic area might be more likely to receive empiric therapy.

The first limitation of the surveillance data we describe is that cases identified through passive surveillance probably represent more severe disease because all persons necessarily sought medical care for an illness and obtained laboratory testing. As previously mentioned, persons who have mild symptoms or asymptomatic infections would not be detected by current public health surveillance approaches. Thus, the severity of HTRF caused by *B. miyamotoi* is difficult to reliably measure through this mechanism. Accordingly, the frequency of hospitalization in those data are probably an overestimate caused by inherent ascertainment bias. Second, the nature of public health surveillance activities precludes knowledge of the targets and performance of assays used by commercial laboratories. Third, *B. miyamotoi* might cause human infection in states where the condition is not subject to public health reporting. A recent case of HTRF caused by *B. miyamotoi* was identified in California; that finding, in combination with acarologic and seroprevalence assessments, suggests potential for additional cases of human illness along the Pacific Coast (*28*,*29*,*49*,*50*). Fourth, detailed data on clinical features, such as rash, clinical course and resolution, or immunocompromised status or other medical concurrent conditions, were not collected consistently as part of surveillance-based case investigations, limiting our ability to thoroughly describe the clinical course or examine the effect of immunocompromising conditions or other concurrent conditions on clinical severity or presentation of HTRF caused by *B. miyamotoi* infection. Fifth, data on positive laboratory findings for other tickborne diseases were not regularly compiled as part of public health surveillance; thus, these HTRF cases could reflect patients co-infected with other tickborne diseases.

Public health surveillance in the United States supports that HTRF manifests as a nonspecific febrile illness during the summer months. *B. miyamotoi* is among the group of pathogens transmitted to humans by *Ixodes* spp. ticks, and the clinical manifestations might be similar to that of other tickborne diseases in the same geographic areas. The frequency of asymptomatic or mild illness caused by HTRF that resolves without treatment is not known, nor is the potential for longer-term complications of untreated infection.

At present, *B. miyamotoi* is the only recognized cause of HTRF; if additional pathogens are identified, public health surveillance approaches will necessarily adapt, including through expansion of molecular testing to detect those pathogens. Infections identified through public health surveillance can enable expanded understanding of the clinical spectrum of emerging infectious diseases than what is possible through limited case series or reports, but surveillance depends on clinical suspicion, laboratory diagnostic test access, and state-based public health regulations that enable mandatory reporting of positive laboratory results to the public health system. Ongoing, coordinated public health surveillance for HTRF caused by *B. miyamotoi* will better define its clinical spectrum, severity, incidence, and geographic distribution, and inform associated clinical and public outreach efforts to improve recognition. However, improved access to direct detection of *B. miyamotoi* through unbiased and widely available PCR-based assays, as well as clinically validated serologic markers, are needed to clarify the frequency and severity of the illness.

Acknowledgments

We thank Paul Mead and Jeannine Petersen for helpful discussions on hard tick relapsing fever.

About the Author

Dr. McCormick is a medical officer in the Rickettsial Zoonoses Branch, Division of Vector-Borne Diseases, National Center for Emerging and Zoonotic Infectious Diseases, Centers for Disease Control and Prevention, Atlanta, GA. His primary research interests are the epidemiology and prevention of vector-borne diseases.

References

1. Rosenberg R, Lindsey NP, Fischer M, Gregory CJ, Hinckley AF, Mead PS, et al. Vital signs: trends in reported vectorborne disease cases—United States and territories, 2004–2016. MMWR Morb Mortal Wkly Rep. 2018;67:496–501. https://doi.org/10.15585/mmwr.mm6717e1
2. Kugeler KJ, Schwartz AM, Delorey MJ, Mead PS, Hinckley AF. Estimating the frequency of Lyme disease diagnoses, United States, 2010–2018. Emerg Infect Dis. 2021;27:616–9. https://doi.org/10.3201/eid2702.202731
3. Nelson CA, Saha S, Kugeler KJ, Delorey MJ, Shankar MB, Hinckley AF, et al. Incidence of clinician-diagnosed Lyme disease, United States, 2005–2010. Emerg Infect Dis. 2015;21:1625–31. https://doi.org/10.3201/eid2109.150417
4. Eisen RJ, Kugeler KJ, Eisen L, Beard CB, Paddock CD. Tick-borne zoonoses in the United States: persistent and emerging threats to human health. ILAR J. 2017;58:319–35. https://doi.org/10.1093/ilar/ilx005
5. Eisen RJ, Paddock CD. Tick and tickborne pathogen surveillance as a public health tool in the United States. J Med Entomol. 2021;58:1490–502. https://doi.org/10.1093/jme/tjaa087
6. Madison-Antenucci S, Kramer LD, Gebhardt LL, Kauffman E. Emerging tick-borne diseases. Clin Microbiol Rev. 2020;33:e00083-18.
7. Fukunaga M, Takahashi Y, Tsuruta Y, Matsushita O, Ralph D, McClelland M, et al. Genetic and phenotypic analysis of *Borrelia miyamotoi* sp. nov., isolated from the ixodid tick *Ixodes persulcatus*, the vector for Lyme disease in Japan. Int J Syst Bacteriol. 1995;45:804–10. https://doi.org/10.1099/00207713-45-4-804
8. Wormser GP, Shapiro ED, Fish D. *Borrelia miyamotoi*: an emerging tick-borne pathogen. Am J Med. 2019;132:136–7. https://doi.org/10.1016/j.amjmed.2018.08.012
9. Branda JA, Rosenberg ES. *Borrelia miyamotoi*: a lesson in disease discovery. Ann Intern Med. 2013;159:61–2. https://doi.org/10.7326/0003-4819-159-1-201307020-00009
10. Platonov AE, Karan LS, Kolyasnikova NM, Makhneva NA, Toporkova MG, Maleev VV, et al. Humans infected with relapsing fever spirochete *Borrelia miyamotoi*, Russia. Emerg Infect Dis. 2011;17:1816–23. https://doi.org/10.3201/eid1710.101474
11. Gugliotta JL, Goethert HK, Berardi VP, Telford SR III. Meningoencephalitis from *Borrelia miyamotoi* in an immunocompromised patient. N Engl J Med. 2013;368:240–5. https://doi.org/10.1056/NEJMoa1209039
12. Sato K, Takano A, Konnai S, Nakao M, Ito T, Koyama K, et al. Human infections with *Borrelia miyamotoi*, Japan. Emerg Infect Dis. 2014;20:1391–3. https://doi.org/10.3201/eid2008.131761
13. Kadkhoda K, Dumouchel C, Brancato J, Gretchen A, Krause PJ. Human seroprevalence of *Borrelia miyamotoi* in Manitoba, Canada, in 2011–2014: a cross-sectional study. CMAJ Open. 2017;5:E690–3. https://doi.org/10.9778/cmajo.20170070
14. Gao Y, Lv X-L, Han S-Z, Wang W, Liu Q, Song M. First detection of *Borrelia miyamotoi* infections in ticks and humans from the northeast of Inner Mongolia, China. Acta Trop. 2021;217:105857. https://doi.org/10.1016/j.actatropica.2021.105857
15. Hoornstra D, Koetsveld J, Sprong H, Platonov AE, Hovius JW. *Borrelia miyamotoi* disease in an immunocompetent patient, western Europe. Emerg Infect Dis. 2018;24:1770–2. https://doi.org/10.3201/eid2409.180806
16. Hovius JWR, de Wever B, Sohne M, Brouwer MC, Coumou J, Wagemakers A, et al. A case of meningoencephalitis by the relapsing fever spirochaete *Borrelia miyamotoi* in Europe. Lancet. 2013;382:658. https://doi.org/10.1016/S0140-6736(13)61644-X
17. Molloy PJ, Telford SR III, Chowdri HR, Lepore TJ, Gugliotta JL, Weeks KE, et al. *Borrelia miyamotoi* disease in the northeastern United States a case series. Ann Intern Med. 2015;163:91–8. https://doi.org/10.7326/M15-0333
18. Barbour AG. Phylogeny of a relapsing fever *Borrelia* species transmitted by the hard tick *Ixodes scapularis*. Infect Genet Evol. 2014;27:551–8 https://doi.org/10.1016/j.meegid.2014.04.022
19. Forrester JD, Kjemtrup AM, Fritz CL, Marsden-Haug N, Nichols JB, Tengelsen LA, et al. Tickborne relapsing fever—United States, 1990–2011. MMWR Morb Mortal Wkly Rep. 2015;64:58–60.
20. Scoles GA, Papero M, Beati L, Fish D. A relapsing fever group spirochete transmitted by *Ixodes scapularis* ticks. Vector Borne Zoonotic Dis. 2001;1:21–34. https://doi.org/10.1089/153036601750137624
21. Barbour AG, Bunikis J, Travinsky B, Hoen AG, Diuk-Wasser MA, Fish D, et al. Niche partitioning of *Borrelia burgdorferi* and *Borrelia miyamotoi* in the same tick vector and mammalian reservoir species. Am J Trop

Med Hyg. 2009;81:1120–31. https://doi.org/10.4269/ajtmh.2009.09-0208
22. Mun J, Eisen RJ, Eisen L, Lane RS. Detection of a *Borrelia miyamotoi* sensu lato relapsing-fever group spirochete from *Ixodes pacificus* in California. J Med Entomol. 2006;43:120–3. https://doi.org/10.1093/jmedent/43.1.120
23. Mead PS. Epidemiology of Lyme disease. Infect Dis Clin North Am. 2015;29:187–210. https://doi.org/10.1016/j.idc.2015.02.010
24. Dahlgren FS, Heitman KN, Drexler NA, Massung RF, Behravesh CB. Human granulocytic anaplasmosis in the United States from 2008 to 2012: a summary of national surveillance data. Am J Trop Med Hyg. 2015;93:66–72. https://doi.org/10.4269/ajtmh.15-0122
25. Krause PJ. Human babesiosis. Int J Parasitol. 2019;49:165–74. https://doi.org/10.1016/j.ijpara.2018.11.007
26. Ebel GD. Update on Powassan virus: emergence of a North American tick-borne flavivirus. Annu Rev Entomol. 2010;55:95–110. https://doi.org/10.1146/annurev-ento-112408-085446
27. Xu G, Pearson P, Rich SM. *Ehrlichia muris* in *Ixodes co*okei ticks, northeastern United States, 2016–2017. Emerg Infect Dis. 2018;24:1143–4 https://doi.org/10.3201/eid2406.171755
28. Fleshman AC, Foster E, Maes SE, Eisen RJ. Reported county-level distribution of seven human pathogens detected in host-seeking *Ixodes scapularis* and *Ixodes pacificus* (Acari: Ixodidae) in the contiguous United States. J Med Entomol. 2022;59:1328–35. https://doi.org/10.1093/jme/tjac049
29. Xu G, Luo C-Y, Ribbe F, Pearson P, Ledizet M, Rich SM. *Borrelia miyamotoi* in human-biting ticks, United States, 2013–2019. Emerg Infect Dis. 2021;27:3193–5. https://doi.org/10.3201/eid2712.204646
30. Johnston D, Kelly JR, Ledizet M, Lavoie N, Smith RP, Parsonnet J, et al. Frequency and geographic distribution of *Borrelia miyamotoi*, *Borrelia burgdorferi*, and *Babesia microti* infections in New England residents. Clin Infect Dis. 2022;Mar23:ciac107.
31. Mukerji SS, Ard KL, Schaefer PW, Branda JA. Case 32-2020: a 63-year-old man with confusion, fatigue, and garbled speech. N Engl J Med. 2020;383:1578–86. https://doi.org/10.1056/NEJMcpc2004996
32. Krause PJ, Barbour AG. *Borrelia miyamotoi*: the newest infection brought to us by deer ticks. Ann Intern Med. 2015;163:141–2. https://doi.org/10.7326/M15-1219
33. Koetsveld J, Kolyasnikova NM, Wagemakers A, Stukolova OA, Hoornstra D, Sarksyan DS, et al. Serodiagnosis of *Borrelia miyamotoi* disease by measuring antibodies against GlpQ and variable major proteins. Clin Microbiol Infect. 2018;24:1338.e1–7. https://doi.org/10.1016/j.cmi.2018.03.009
34. Schwan TG, Schrumpf ME, Hinnebusch BJ, Anderson DE Jr, Konkel ME. GlpQ: an antigen for serological discrimination between relapsing fever and Lyme borreliosis. J Clin Microbiol. 1996;34:2483–92. https://doi.org/10.1128/jcm.34.10.2483-2492.1996
35. Finch C, Al-Damluji MS, Krause PJ, Niccolai L, Steeves T, O'Keefe CF, et al. Integrated assessment of behavioral and environmental risk factors for Lyme disease infection on Block Island, Rhode Island. PLoS One. 2014;9:e84758. https://doi.org/10.1371/journal.pone.0084758
36. Bron GM, Fernandez MD, Larson SR, Maus A, Gustafson D, Tsao JI, et al. Context matters: contrasting behavioral and residential risk factors for Lyme disease between high-incidence states in the northeastern and midwestern United States. Ticks Tick Borne Dis. 2020;11:101515. https://doi.org/10.1016/j.ttbdis.2020.101515
37. Schwartz AM, Hinckley AF, Mead PS, Hook SA, Kugeler KJ. Surveillance for Lyme disease— United States, 2008–2015. MMWR Surveill Summ. 2017;66:1–12. https://doi.org/10.15585/mmwr.ss6622a1
38. Wilson ML, Spielman A. Seasonal activity of immature *Ixodes da*mmini (Acari: Ixodidae). J Med Entomol. 1985;22:408–14. https://doi.org/10.1093/jmedent/22.4.408
39. Breuner NE, Hojgaard A, Replogle AJ, Boegler KA, Eisen L. Transmission of the relapsing fever spirochete, *Borrelia miyamotoi*, by single transovarially-infected larval Ixodes scapularis ticks. Ticks Tick Borne Dis. 2018;9:1464–7. https://doi.org/10.1016/j.ttbdis.2018.07.006
40. Kugeler KJ, Mead PS, Schwartz AM, Hinckley AF. Changing trends in age and sex distributions of Lyme disease, United States, 1992–2016. Public Health Rep. 2022; 137:655–9. https://doi.org/10.1177/00333549211026777
41. Mowla SJ, Drexler NA, Cherry CC, Annambholta PD, Kracalik IT, Basavaraju SV. Ehrlichiosis and anaplasmosis among transfusion and transplant recipients in the United States. Emerg Infect Dis. 2021;27:2768–75. https://doi.org/10.3201/eid2711.211127
42. Pantanowitz L, Telford SR, Cannon ME. Tick-borne diseases in transfusion medicine. Transfus Med. 2002;12:85–106. https://doi.org/10.1046/j.1365-3148.2002.00358.x
43. Wilske B, Barbour AG, Bergström S, Burman N, Restrepo BI, Rosa PA, et al. Antigenic variation and strain heterogeneity in *Borrelia* spp. Res Microbiol. 1992;143:583–96. https://doi.org/10.1016/0923-2508(92)90116-6
44. Stone BL, Brissette CA. Host immune evasion by Lyme and relapsing fever Borreliae: findings to lead future studies for *Borrelia miyamotoi*. Front Immunol. 2017;8:12. https://doi.org/10.3389/fimmu.2017.00012
45. Dworkin MS, Schwan TG, Anderson DE Jr, Borchardt SM. Tick-borne relapsing fever. Infect Dis Clin North Am. 2008;22:449–68, viii. https://doi.org/10.1016/j.idc.2008.03.006
46. Branda JA, Lemieux JE, Blair L, Ahmed AA, Hong DK, Bercovici S, et al. Detection of *Borrelia burgdorferi* cell-free DNA in human plasma samples for improved diagnosis of early Lyme borreliosis. Clin Infect Dis. 2021;73:e2355–61. https://doi.org/10.1093/cid/ciaa858
47. Kingry LC, Anacker M, Pritt B, Bjork J, Respicio-Kingry L, Liu G, et al. Surveillance for and discovery of *Borrelia* species in US patients suspected of tickborne illness. Clin Infect Dis. 2018;66:1864–71. https://doi.org/10.1093/cid/cix1107
48. Liveris D, Schwartz I, McKenna D, Nowakowski J, Nadelman R, Demarco J, et al. Comparison of five diagnostic modalities for direct detection of *Borrelia burgdorferi* in patients with early Lyme disease. Diagn Microbiol Infect Dis. 2012;73:243–5. https://doi.org/10.1016/j.diagmicrobio.2012.03.026
49. Brummitt SI, Kjemtrup AM, Harvey DJ, Petersen JM, Sexton C, Replogle A, et al. *Borrelia burgdorferi* and *Borrelia miyamotoi* seroprevalence in California blood donors. PLoS One. 2020;15:e0243950. https://doi.org/10.1371/journal.pone.0243950
50. Rubio LA, Kjemtrup AM, Marx GE, Cronan S, Kilonzo C, Saunders MEM, et al. *Borrelia miyamotoi* infection in immunocompromised man, California, USA, 2021. Emerg Infect Dis. 2023;29:1011–4. https://doi.org/10.3201/eid2905.221638

Address for correspondence: Kiersten J. Kugeler, Centers for Disease Control and Prevention, 3156 Rampart Rd, Mailstop P02, Fort Collins, CO 80521, USA; bio1@cdc.gov

Foodborne Botulism, Canada, 2006–2021[1]

Richard A. Harris, Christine Tchao, Natalie Prystajecky, Kelly Weedmark, Yassen Tcholakov, Manon Lefebvre, John W. Austin

In support of improving patient care, this activity has been planned and implemented by Medscape, LLC and Emerging Infectious Diseases. Medscape, LLC is jointly accredited with commendation by the Accreditation Council for Continuing Medical Education (ACCME), the Accreditation Council for Pharmacy Education (ACPE), and the American Nurses Credentialing Center (ANCC), to provide continuing education for the healthcare team.

Medscape, LLC designates this Journal-based CME activity for a maximum of 1.00 ***AMA PRA Category 1 Credit(s)™***. Physicians should claim only the credit commensurate with the extent of their participation in the activity.

Successful completion of this CME activity, which includes participation in the evaluation component, enables the participant to earn up to 1.0 MOC points in the American Board of Internal Medicine's (ABIM) Maintenance of Certification (MOC) program. Participants will earn MOC points equivalent to the amount of CME credits claimed for the activity. It is the CME activity provider's responsibility to submit participant completion information to ACCME for the purpose of granting ABIM MOC credit.

All other clinicians completing this activity will be issued a certificate of participation. To participate in this journal CME activity: (1) review the learning objectives and author disclosures; (2) study the education content; (3) take the post-test with a 75% minimum passing score and complete the evaluation at http://www.medscape.org/journal/eid; and (4) view/print certificate. For CME questions, see page 1952.

NOTE: It is Medscape's policy to avoid the use of Brand names in accredited activities. However, in an effort to be as clear as possible, the use of brand names should not be viewed as a promotion of any brand or as an endorsement by Medscape of specific products.

Release date: August 15, 2023; Expiration date: August 15, 2024

Learning Objectives

Upon completion of this activity, participants will be able to:

- Distinguish the average annual incidence of foodborne botulism in Canada
- Compare prevalence rates for serotypes of botulinum neurotoxins
- Identify the types of foods associated with foodborne botulism in the current study
- Analyze clinical outcomes associated with foodborne botulism in the current study

CME Editor

Amy J. Guinn, BA, MA, Technical Writer/Editor, Emerging Infectious Diseases. *Disclosure: Amy J. Guinn, BA, MA, has no relevant financial relationships.*

CME Author

Charles P. Vega, MD, Health Sciences Clinical Professor of Family Medicine, University of California, Irvine School of Medicine, Irvine, California. *Disclosure: Charles P. Vega, MD, has the following relevant financial relationships: consultant or advisor for Boehringer Ingelheim; GlaxoSmithKline; Johnson & Johnson.*

Authors

Richard A. Harris, PhD; Christine Tchao, BMLSc, MLT, CSMLS; Natalie Prystajecky, PhD; Kelly Weedmark, PhD; Manon Lefebvre, BSc; Yassen Tcholakov, MD, MSc, MIH; John W. Austin, PhD.

Author affiliations: Health Canada, Ottawa, Ontario, Canada (R.A. Harris, K. Weedmark, J.W. Austin); British Columbia Centre for Disease Control Public Health Laboratory, Vancouver, British Columbia, Canada (C. Tchao, N. Prystajecky); McGill University, Montreal, Quebec, Canada (Y. Tcholakov); Nunavik Regional Board of Health and Social Services, Kuujjuaq, Quebec, Canada (M. Lefebvre)

DOI: https://doi.org/10.3201/eid2909.230409

[1]Results of this study were originally presented at the 58th Annual Interagency Botulism Research Coordinating Committee (IBRCC) Meeting, Richmond, California, USA, October 17–18, 2022.

During 2006–2021, Canada had 55 laboratory-confirmed outbreaks of foodborne botulism, involving 67 cases. The mean annual incidence was 0.01 case/100,000 population. Foodborne botulism in Indigenous communities accounted for 46% of all cases, which is down from 85% of all cases during 1990–2005. Among all cases, 52% were caused by botulinum neurotoxin type E, but types A (24%), B (16%), F (3%), and AB (1%) also occurred; 3% were caused by undetermined serotypes. Four outbreaks resulted from commercial products, including a 2006 international outbreak caused by carrot juice. Hospital data indicated that 78% of patients were transferred to special care units and 70% required mechanical ventilation; 7 deaths were reported. Botulinum neurotoxin type A was associated with much longer hospital stays and more time spent in special care than types B or E. Foodborne botulism often is misdiagnosed. Increased clinician awareness can improve diagnosis, which can aid epidemiologic investigations and patient treatment.

Human foodborne botulism is a neuroparalytic disease that results from ingestion of foods containing botulinum neurotoxin (BoNT) serotypes A, B, E, or F, produced by *Clostridium botulinum* groups I and II or, rarely, neurotoxigenic strains of *C. baratii* type F or *C. butyricum* type E (*1*). BoNTs prevent muscle contraction through cleavage of the proteins responsible for fusion of acetylcholine-containing synaptic vesicles in nerve terminals at neuromuscular junctions (*2*).

Clinical symptoms of botulism include symmetric cranial nerve palsies of the eyes, mouth, and throat. Paralysis can descend to the diaphragm, causing respiratory arrest that can necessitate use of mechanical ventilation (*1*). In some instances, patients can take months or years to recover from prolonged disability caused by skeletal muscle paralysis (*3*). Treatment options are limited to use of botulinum antitoxin (BAT) that binds to and neutralizes circulating BoNTs (*4*). BAT is especially effective when administered early (*5*), and its use should be based on clinical diagnosis, rather than waiting for results from diagnostic tests.

Manifestations of botulism are classified according to the route of exposure to BoNTs. Wound botulism occurs when *C. botulinum* colonizes an infected wound, and intestinal toxemia botulism occurs in the adult intestinal tract when BoNTs are released in situ (*6*,*7*). Infant botulism is a form of intestinal toxemia botulism that occurs in children <1 year of age (*8*). Foodborne botulism is an acute intoxication resulting from ingestion of BoNTs preformed in foods supporting *C. botulinum* growth. *C. botulinum* endospores are widely distributed in soils throughout the world and survive heating processes that inactivate vegetative bacterial cells (*9*). Foods contaminated with viable *C. botulinum* spores can germinate, grow, and produce BoNTs when they are stored under permissive growth conditions, including low oxygen, low acidity (pH >4.6), sufficient temperature (>10°C), and water activity (a_w >0.93) (*10*).

Investigations of foodborne botulism provide valuable information regarding food sources and storage conditions that permit *C. botulinum* growth and BoNT production. Previous reports of foodborne botulism in Canada are available, including the periods of 1919–1973 (*11*), 1971–1984 (*12*), and 1985–2005 (*13*). Here, we present a summary of foodborne botulism in Canada during 2006–2021, including incidence over the course of time, geographic distribution by province and territory, BoNT serotype, and food source when available. In addition, we used hospital records that match cases from laboratory-confirmed outbreaks to determine clinical disease outcomes.

Methods

Microbiology Laboratory and National Surveillance Data

We examined 2 independent laboratory databases for laboratory-confirmed outbreaks of foodborne botulism during 2006–2021, one maintained by the Botulism Reference Service (BRS) for Canada at Health Canada, Ottawa, Ontario, and the other from British Columbia Centre for Disease Control (BCCDC) Public Health Laboratory (PHL), in Vancouver, British Columbia. BRS receives and tests clinical and food specimens associated with suspected botulism cases from all provinces and territories, when requested. The BCCDC PHL provides clinical and foodborne botulism testing services for British Columbia but also tests specimens from the Yukon. Thus, the 2 databases do not overlap and, when combined, represent all the laboratoryconfirmed outbreaks of botulism in Canada. We extracted information regarding patient age and sex, outbreak date and location, implicated food source, and BoNT serotype from those databases. We also extracted case information from the 2006–2019 Canadian Notifiable Disease Surveillance System (CNDSS) and compared those cases to laboratory data for completeness (*14*). CNDSS maintains basic surveillance on nationally notifiable diseases by collecting voluntarily submitted data from provinces and territories. We calculated the rates of disease per 100,000 population by using population data from Statistics Canada (*15*).

National Case Definition for Foodborne Botulism

We used the national case definition for confirmed cases of foodborne botulism in Canada to ensure

consistency in data recording. That definition is as follows: laboratory confirmation of intoxication with clinical evidence, such as detection of botulinum neurotoxin in serum, stool, gastric aspirate, or food; or isolation of *C. botulinum* from stool or gastric aspirate; or clinical evidence and indication that the client ate the same suspect food as a person with laboratory-confirmed botulism (*16*). Because of the urgency of the disease, 1 case of botulism constitutes an outbreak.

Laboratory Confirmation of Clinical Cases

Detection of BoNT and isolation of viable *C. botulinum* from food and clinical specimens were performed according to Health Canada standard methods by using a mouse bioassay to detect BoNT in foods and clinical specimens (*17*). BoNT serotype was determined by neutralization of toxicity with serotype-specific antibodies provided by the US Centers for Disease Control and Prevention. If isolates were not obtained from clinical or food specimens, cases caused by *C. baratii* (type F) or *C. butyricum* (type E) might not have been detected.

Clinical Outcome Data

We retrieved records on patient clinical information by querying the Canadian Institute for Health Information (CIHI) 2005–2021 Discharge Abstract Database (https://www.cihi.ca/en/discharge-abstract-database-metadata-dad) and the 2005–2010 Hospital Morbidity Database (HMDB), which is specific to Quebec (*18*). Data were also collected as part of epidemiologic investigations conducted in Quebec by the Nunavik Regional Board of Health and Social Services (NRBHSS), including records from 2010–2021 that were validated with patient files from the relevant hospitals and were not available in HMDB. We then matched those data to BRS records by age, sex, date of admission, and province of residence. We defined a special care unit in accordance with HMDB as an inpatient unit that is specifically designed, staffed and equipped for the observation and treatment of patients who cannot be cared for in a general acute care unit; these include intensive care units and step-down units (*18*). Formal ethics approval was not required because this study used deidentified healthcare data that were obtained under an agreement with CIHI.

Results

Incidence of Foodborne Botulism in Canada

During 2006–2021, a total of 55 laboratory-confirmed outbreaks of foodborne botulism occurred in Canada, comprising 67 cases (Figure 1). During the reporting period, we determined the average annual

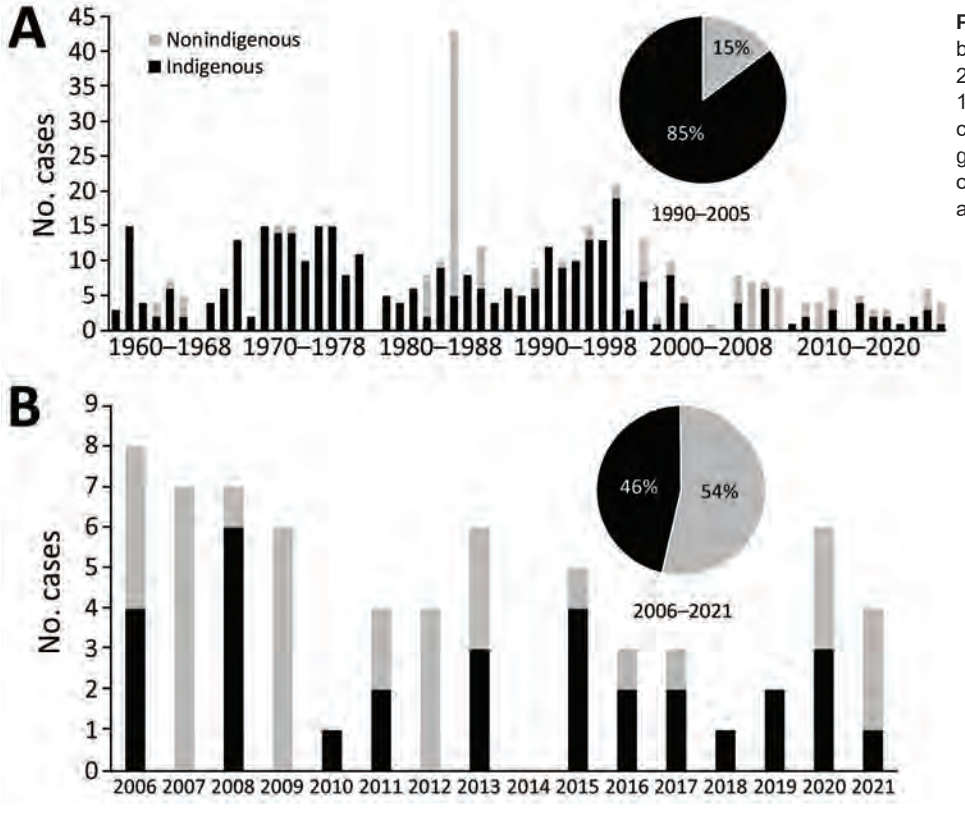

Figure 1. Number of foodborne botulism cases, Canada, 1960–2021. A) Number of cases during 1960–2021; B) detail of number of cases during 2006–2021. Inset pie graphs represent the percentage of cases among non-Indigenous and Indigenous persons.

Table 1. Foodborne botulism cases by province or territory and BoNT serotype, Canada, 2006–2021

Province/territory	Serotype, no. cases						Total
	A	B	E	F	AB	Unknown	
Quebec	5	2	21	1	1	1	31
Ontario	4	6	4	1	0	0	15
Alberta	4	1	0	0	0	1	6
Nunavut	0	0	5	0	0	0	5
British Columbia	1	1	1	0	0	0	3
Northwest Territories	0	0	3	0	0	0	3
Manitoba	1	1	0	0	0	0	2
Saskatchewan	1	0	0	0	0	0	1
Newfoundland and Labrador	0	0	1	0	0	0	1
Total	16	11	35	2	1	2	67

incidence of foodborne botulism in Canada was 0.01 case/100,000 population. The CNDSS reported 60 cases of foodborne botulism during 2006–2019, which compares to 55 laboratory-confirmed cases of foodborne botulism from the same reporting period. That discrepancy was not unexpected because the reference laboratories only record laboratory-confirmed cases, but public health authorities include unconfirmed cases or cases that might have been epidemiologically linked but not laboratory tested.

Geographic Distribution and BoNT Serotype Breakdown

During the reporting period, 31 foodborne botulism cases occurred in Quebec, 15 in Ontario, 6 in Alberta, 5 in Nunavut, 3 in British Columbia, 3 in Northwest Territories, 2 in Manitoba, 1 in Saskatchewan, and 1 in Newfoundland and Labrador (Table 1). Type E was implicated in the most cases (52%, n = 35) across Canada during the reporting period (Table 1). Other serotypes of foodborne botulism across Canada included 16 cases of type A, 11 cases of type B, and 2 cases of type F. Two cases involved clinical samples that were neutralized by multivalent antiserum but were not typed due to insufficient sample. One case was typed as AB because the toxin in the food sample was neutralized by a combination of type A and type B antisera. Indigenous communities represented the most (86%, n = 30) type E cases. Type E was implicated in 21 (68%) cases in Quebec and all (100%) cases in each of Nunavut, the Northwest Territories, and Newfoundland and Labrador.

Foods Associated with Outbreaks

Apart from a single outbreak from salmon eggs in British Columbia in 2013, all the outbreaks in Indigenous communities were caused by products from marine mammals, including seal, whale, and walrus, that were incubated in conditions favorable to *C. botulinum* growth and consumed without cooking. Commercial retail foods were responsible for 4 outbreaks, including an international outbreak of contaminated carrot juice in 2006 that affected 2 persons in Canada (*3*) and an outbreak in Canada caused by salted fish in 2012 that affected 3 persons (*19*). The 2 other outbreaks attributed to retail foods were caused by ground beef that affected 2 persons in 2009 and Alfredo sauce that affected 1 person in 2021 (*20*). In those cases, the cooked ground beef was left at room temperature on the stove top, and the Alfredo sauce was recalled because of storage at room temperature by the retailer, despite a label indicating the product should be kept refrigerated (*20*). Of note, no outbreaks from restaurant dining occurred through the reporting period. Home-prepared foods were responsible for only 2 outbreaks, 1 from spaghetti sauce that affected 2 persons in 2006 and 1 from watermelon jelly that affected 1 person in 2011.

Clinical Outcomes

To examine the health outcomes of foodborne botulism, we cross-referenced cases to 52 (78% matching) hospital records obtained from CIHI and NRBHSS. In 2 instances from the NRBHSS data, the only hospital records available were that the patient died, and in 1 instance the time spent in special care was unknown. The average age of patients was 57.0 years (SD 16.1 years); 27 (52%) were female and 25 (48%) were male. Most case-patients had severe illness: 38 (78%) patients were transferred to special care units, and 35 (70%) required mechanical ventilation. The average length of hospital stay was 48.3 days (SD 84.3 days). The average length of time spent in special care was 36.3 days (SD 72.7 days). Most (52%, n = 27) case-patients were discharged to home without continuing support, but 4 (8%) were discharged to home with support from healthcare workers, 4 (8%) were transferred to continuing care, 9 (17%) were transferred to acute care, and 1 (2%) was transferred to other (palliative) care. In 7 (14%) cases, the patient died.

Clinical Outcomes by BoNT Serotype

To examine the relationship between BoNT serotype and clinical severity of disease, we performed 1-way

analysis of variance tests to compare the serotype of intoxication with the length of hospital stay and time spent in special care (Figure 2). Serotype had a significant effect on the length of hospital stay ($p<0.0001$) and the length of time spent in special care ($p<0.0001$). A Tukey honest significant difference post hoc comparison test indicated that cases of type A were associated with significantly longer hospital stays than were type B ($p<0.01$) or type E ($p<0.0001$), and type A case-patients spent significantly longer times in special care than did patients with type B ($p<0.001$) or type E ($p<0.0001$). We noted no significant difference between types B and E for length of hospital stay ($p = 0.17$) or time in special care ($p = 0.48$). We removed 1 case of type A from analysis because the patient was hospitalized for 497 days and that case was identified as an outlier by a 2-sided Grubb test ($p<0.01$). Type F was not included in this analysis because only a single case that matched hospital records was identified within the reported period. Our results suggest that BoNT type A is associated with more severe clinical outcomes than types B and E. Of note, the 7 deaths during the reporting period were associated with 2 cases of type A, 1 case of each type B and type E, and 1 case of undetermined serotype.

Discussion

The average annual incidence of foodborne botulism cases in Canada (0.01 case/100,000 population) during 2006–2021 is the same as that of the United States during 2001–2017 (*21*). Canada's incidence also was less than the overall incidence (0.02 case/100,000 population) in European Union or European Economic Area countries in 2014 and less than incidences in France (0.02–0.03 case/100,000 population) during 2013–2016, Italy (0.03 case/100,000 population) during 1986–2015, Poland (0.04 case/100,000 population) during 2010–2018, and the Republic of Georgia (0.3–0.9 case/100,000 population) during 1980–2002 (*22*–*26*). The average annual incidence of foodborne botulism in Canada has decreased in recent years. During 1985–2005, the incidence was 0.03 case/100,000 population, and during 1971–1984 the incidence was 0.04 case/100,000 population (*12*,*13*).

The reduction in foodborne botulism was most pronounced in Indigenous communities. During 2006–2021, foodborne botulism in Indigenous communities accounted for 46% of all cases, which is a reduction from 85% of all cases for the previous 16-year period of 1990–2005 (Figure 1). In addition, during 2006–2021 the average annual rate of foodborne botulism in Indigenous communities was 1.9 cases/year, but incidence was 6.7 cases/year during 1985–2005 and 8.7 cases/year during 1971–1984 (*12*,*13*). The incidence of type E botulism in Indigenous communities corresponds to the geographic distribution of *C. botulinum* type E spores in shoreline soils along the Hudson Strait and Ungava Bay in northern Quebec (*27*). Contamination occurs during butchering of marine mammal meat, but *C. botulinum* spore germination and production of BoNTs occurs during storage of the traditional Indigenous foods (*27*). Type E strains

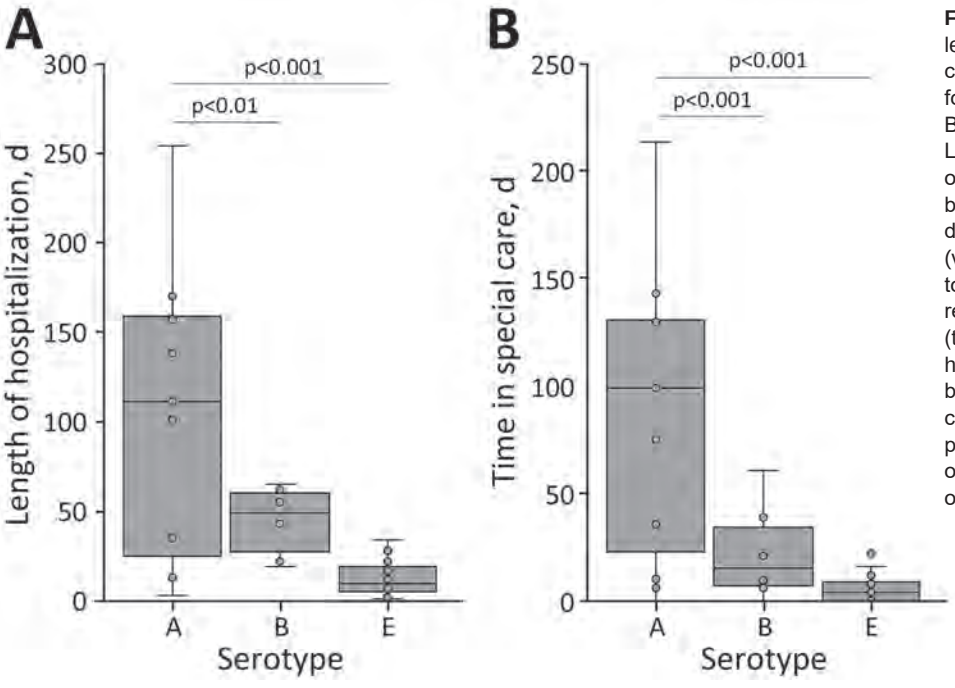

Figure 2. Box and whisker plots of length of hospitalization and special care among persons affected by foodborne botulism serotypes A, B, and E, Canada, 2006–2021. A) Length of hospitalization; B) length of time in a special care unit. The box and whiskers represent the data as quartiles; the whiskers (vertical lines) represent the top and bottom values, the box represents the 1st (bottom) to 3rd (top) quartiles of values, and the horizontal line in the middle of the box represents the median. The circles indicate individual data points including outliers. A single outlier for time in special care occurred for serotype E.

Table 2. Foodborne botulism outbreaks, cases, deaths, and serotype, by year and food source, Canada, 2006–2021

Food source	Years	Outbreaks	Cases	Deaths	Serotype
Commercial retail foods					
Carrot juice	2006	1	2	0	A
Ground beef	2009	1	2	0	B
Salted fish	2012	1	3	0	E
Alfredo sauce	2021	1	1	0	AB
Home-prepared foods					
Spaghetti sauce	2006	1	2	0	A
Watermelon jelly	2011	1	1	0	B
Traditionally prepared Indigenous foods (traditional name)					
Blubber in oil (misiraq)	2006–2021	7	8	1	E
Meat and fat (igunaq)	2006–2021	5	10	1	E
Beluga skin (muktuk)	2006–2021	3	3	0	E
Aged meat	2006–2021	3	3	0	A, E
Salmon eggs	2013	1	1	1	E
Unknown*	2006–2021	30	31	4	A, B, E, F

*Food was either not submitted for analysis or was submitted but not found to be toxic.

belong to group II *C. botulinum*, which possesses a lower minimum growth temperature of 2.5°C–3°C than group I strains (*28*), permitting growth in northern climates.

Outbreaks in the Nunavik region of northern Quebec were most associated with igunaq (meat and blubber) and misiraq (a product consisting of oil from the blubber of marine mammals) and occurred most often in the summer months; 70% of cases occurred from July through September. According to the *Qanuilirpitaa*? (How are we now?) 2017 Health Survey, the consumption of country foods (traditional foods that are largely only available in Canada's far north) did not decline during 2004–2017 and accounted for ≈40% of all meat and fish consumed (*29*). That finding underlines the importance of working closely with Indigenous communities to communicate the risk for disease and the ways of reducing risk, while continuing to practice traditional subsistence activities that are linked with numerous health benefits (*30*,*31*). The NRBHSS collaborates with the Nunavik Hunting, Fishing and Trapping Organization to inform the population about safe traditional food preparation techniques, and symptoms of foodborne botulism intoxications. The NRBHSS recommends chilling butchered meat to below 4°C as soon as possible and storing meat in a freezer (home or community) and to wait to begin the traditional outdoor aging process in the fall when temperatures are cooler. Those interventions might have contributed to the observed decrease of botulism cases in Indigenous communities in Quebec in recent years. In addition, the NRBHSS maintains clinical guidance documents and provides training to clinicians in the region to ensure prompt recognition and management of cases of botulism intoxication.

Foodborne botulism occurs via ingestion of preformed BoNTs in foods contaminated by *C. botulinum*, but identification of a toxic food source remains a significant challenge (*32*). Only 36 (54%) cases were associated with laboratory-confirmed foods in which BoNTs were detected (Table 2). That rate is comparable to the United States, which identified a laboratory-confirmed food vehicle in 47% of all cases during 2001–2017 (*21*), and Italy, which identified a food vehicle in 31% of all laboratory-confirmed cases during 1986–2015 (*24*). The low success rate for food origin tracing might be because most (97%, n = 29) outbreaks without an identified food source involved only a single (sporadic) case. Of those sporadic cases, 24 (83%) had no food submitted for testing. Outbreaks involving several linked individual cases enable epidemiologic identification of foods patients have in common. Of the 8 outbreaks involving >1 case during the reporting period, 7 were traced to a food source. The 1 multicase outbreak that was not traced to a food source was because no food was submitted for testing.

The data obtained from CIHI and NRBHSS hospital records are consistent with previous reviews indicating that foodborne botulism is a rare disease in the population but is associated with severe clinical outcomes. Recent reports from the World Health Organization (2007–2015), Taiwan (2012–2015), and Greece (1996–2006) have estimated that botulism has one of the lowest overall disability-adjusted life years (accounting for prevalence in the population) of all foodborne illnesses, yet severe botulism ranks as one of the highest disability weights based strictly on clinical outcomes (*33*–*35*).

In Canada, ≈4 million episodes of domestically acquired foodborne illness occur each year, attributed to 30 known and unknown pathogens (*36*). *C. botulinum* ranks at 28 out of 30 for prevalence (i.e., estimated cases per 100,000 population) but has the highest proportion of hospitalizations and deaths per case of all known pathogens. We found illness

caused by BoNT type A was associated with significantly longer hospital stays and more time spent in special care than illness caused by types B and E. That finding is consistent with previous reports showing that BoNT type A has higher rates of severe illness than types B, E, or F, based on a higher proportion of patients requiring mechanical ventilation and longer average hospital stays (*37*,*38*). Another study in the United States (1975–2009) found that type F had a higher mortality rate than types A or B (*39*), although the authors noted that heptavalent antitoxin, which is effective for type F, only became available in 2010.

Two limitations of this study highlight potential opportunities for improved prevention and surveillance of foodborne botulism in Canada: identifying toxic foods associated with outbreaks and comprehensively cross-referencing cases with hospital records. First, the difficulty in identifying a food source can be caused in part by misdiagnosis of botulism as stroke, Guillain-Barré syndrome, or myasthenia gravis. Food history and collection can be delayed by misdiagnosis after an outbreak, resulting in discarding of toxic foods. Improved communication between hospital staff, diagnostic laboratories, and public health officials would help ensure that a food history and sampling is performed for each laboratory-confirmed case of foodborne botulism. The second limitation of this study is the proportion of foodborne botulism cases that were cross-referenced to hospital records. Missing hospital records might in part be a result of the narrow range of years that are available from CIHI databases (2005–2010 for HMDB), which is specific to Quebec and required collaboration with local public health units for records after 2010. In addition, 9 laboratory-confirmed cases did not match any records in CIHI databases, even within the years available. The missing CIHI records for laboratory-confirmed cases of foodborne botulism likely were a result of a missing diagnostic code in the databases. Treatment with BAT was not recorded in CIHI databases as a treatment under the Canadian Classification of Health Interventions (code 8.BB.70.HA-BX); therefore, we found no records for this life-saving therapeutic (*4*,*5*).

In conclusion, we found that foodborne botulism rates in Canada decreased during 2006–2021 compared with previous years, especially among Indigenous populations. However, cases might have been underreported because of misdiagnosis or lack of appropriate diagnostic coding. Expanding the years available for the HMDB database in CIHI and ensuring the use of proper coding for suspected diagnoses and treatments would help to capture more instances of foodborne botulism in Canada and aid in evaluation of BAT as a therapeutic for patients of this severe illness.

Acknowledgments

We thank Ryan Boone for helpful manuscript edits.

This work was supported by Health Canada, the British Columbia Centre for Disease Control Public Health Laboratory, and the Nunavik Regional Board of Health and Social Services.

About the Author

Dr. Harris is a laboratory technician with the Botulism Reference Service of Canada at Health Canada in Ottawa, Ontario, Canada. His primary research interests are infectious diseases and food safety.

References

1. Sobel J. Botulism. Clin Infect Dis. 2005;41:1167–73. https://doi.org/10.1086/444507
2. Montecucco C, Schiavo G. Mechanism of action of tetanus and botulinum neurotoxins. Mol Microbiol. 1994;13:1–8. https://doi.org/10.1111/j.1365-2958.1994.tb00396.x
3. Sheth AN, Wiersma P, Atrubin D, Dubey V, Zink D, Skinner G, et al. International outbreak of severe botulism with prolonged toxemia caused by commercial carrot juice. Clin Infect Dis. 2008;47:1245–51. https://doi.org/10.1086/592574
4. Yu PA, Lin NH, Mahon BE, Sobel J, Yu Y, Mody RK, et al. Safety and improved clinical outcomes in patients treated with new equine-derived heptavalent botulinum antitoxin. Clin Infect Dis. 2017;66(suppl_1):S57–64. https://doi.org/10.1093/cid/cix816
5. Richardson JS, Parrera GS, Astacio H, Sahota H, Anderson DM, Hall C, et al. Safety and clinical outcomes of an equine-derived heptavalent botulinum antitoxin treatment for confirmed or suspected botulism in the United States. Clin Infect Dis. 2020;70:1950–7. https://doi.org/10.1093/cid/ciz515
6. Chatham-Stephens K, Fleck-Derderian S, Johnson SD, Sobel J, Rao AK, Meaney-Delman D. Clinical features of foodborne and wound botulism: a systematic review of the literature, 1932–2015. Clin Infect Dis. 2017;66(suppl_1):S11–6. https://doi.org/10.1093/cid/cix811
7. Harris RA, Anniballi F, Austin JW. Adult intestinal toxemia botulism. Toxins (Basel). 2020;12:81. https://doi.org/10.3390/toxins12020081
8. Arnon SS. Infant botulism. Annu Rev Med. 1980;31:541–60. https://doi.org/10.1146/annurev.me.31.020180.002545
9. Dodds KL. *Clostridium botulinum* in foods. In: Hauschild AHW, Dodds KL, editors. *Clostridium botulinum*: ecology and control in foods. New York: Marcel Dekker, Inc.; 1993. p. 53.
10. Hauschild AHW. *Clostridium botulinum*. In: Doyle M, editor. Foodborne bacterial pathogens. New York: Marcel Dekker, Inc.; 1989. p. 111.
11. Dolman CE. Human botulism in Canada (1919–1973). Can Med Assoc J. 1974;110:191–7 passim.

12. Hauschild AH, Gauvreau L. Food-borne botulism in Canada, 1971–84. Can Med Assoc J. 1985;133:1141–6.
13. Leclair D, Fung J, Isaac-Renton JL, Proulx JF, May-Hadford J, Ellis A, et al. Foodborne botulism in Canada, 1985–2005. Emerg Infect Dis. 2013;19:961–8. https://doi.org/10.3201/eid1906.120873
14. Government of Canada. Canadian notifiable disease surveillance system (CNDSS) [cited 2020 Sep 28]. https://diseases.canada.ca/notifiable
15. Statistics Canada. Census profile 2016 [cited 2020 Sep 28]. https://www12.statcan.gc.ca/census-recensement/index-eng.cfm
16. Health Canada. National case definition: botulism 2008 [cited 2020 Sep 28]. https://www.canada.ca/en/public-health/services/diseases/botulism/professionals/national-case-definition.html
17. Government of Canada. HPB methods for the microbiological analysis of foods; MFHPB-16: detection of clostridium botulinum and its toxins in suspect foods and clinical specimens 2009 [cited 2023 Mar 30]. https://www.canada.ca/en/health-canada/services/food-nutrition/research-programs-analytical-methods/analytical-methods/compendium-methods/methods-microbiological-analysis-foods-compendium-analytical-methods.html
18. Canadian Institute for Health Information. DAD abstracting manual (for use with ICD-10-CA/CCI), 2014–2015. Toronto: The Institute; 2014.
19. Walton RN, Clemens A, Chung J, Moore S, Wharton D, Haydu L, et al. Outbreak of type E foodborne botulism linked to traditionally prepared salted fish in Ontario, Canada. Foodborne Pathog Dis. 2014;11:830–4. https://doi.org/10.1089/fpd.2014.1783
20. Government of Quebec. Notice not to consume Vegan Touch brand Alfredo sauce sold at room temperature at some retailers [in French] [cited 2023 Mar 30]. https://www.quebec.ca/nouvelles/actualites/details/avis-de-ne-pas-consommer-de-la-sauce-de-type-alfredo-de-marque-vegan-touch-vendue-a-temperature-ambiante-chez-certains-detaillants-33851
21. Lúquez C, Edwards L, Griffin C, Sobel J. Foodborne botulism outbreaks in the United States, 2001–2017. Front Microbiol. 2021;12:713101. https://doi.org/10.3389/fmicb.2021.713101
22. European Centre for Disease Prevention and Control. Botulism: annual epidemiological report 2016. Stockholm: The Centre; 2016.
23. Rasetti-Escargueil C, Lemichez E, Popoff MR. Human botulism in France, 1875–2016. Toxins (Basel). 2020;12:338. https://doi.org/10.3390/toxins12050338
24. Anniballi F, Auricchio B, Fiore A, Lonati D, Locatelli CA, Lista F, et al. Botulism in Italy, 1986 to 2015. Euro Surveill. 2017;22:30550. https://doi.org/10.2807/1560-7917.ES.2017.22.24.30550
25. Krzowska-Firych J, Mikłaszewska A, Tomasiewicz K. Foodborne botulism in eastern Poland: a hospital-based retrospective study and epidemiological data review. Int J Food Prop. 2020;23:609–15. https://doi.org/10.1080/10942912.2020.1749065
26. Varma JK, Katsitadze G, Moiscrafishvili M, Zardiashvili T, Chokheli M, Tarkhashvili N, et al. Foodborne botulism in the Republic of Georgia. Emerg Infect Dis. 2004;10:1601–5. https://doi.org/10.3201/eid1009.030806
27. Leclair D, Farber JM, Doidge B, Blanchfield B, Suppa S, Pagotto F, et al. Distribution of *Clostridium botulinum* type E strains in Nunavik, northern Quebec, Canada. Appl Environ Microbiol. 2013;79:646–54. https://doi.org/10.1128/AEM.05999-11
28. Peck MW, Stringer SC, Carter AT. *Clostridium botulinum* in the post-genomic era. Food Microbiol. 2011;28:183–91. https://doi.org/10.1016/j.fm.2010.03.005
29. Nunavik Regional Board of Health and Social Services. Where are we now? [in Inuktitut, English, and French] [cited 2023 Mar 30]. http://nrbhss.ca/en/nrbhss/public-health/nunavik-health-surveys/qanuilirpitaa-2017#topics
30. Batal M, Johnson-Down L, Moubarac J, Ing A, Fediuk K, Sadik T, et al. Quantifying associations of the dietary share of ultra-processed foods with overall diet quality in First Nations peoples in the Canadian provinces of British Columbia, Alberta, Manitoba and Ontario. Public Health Nutr. 2018;21(1):103–13. https://doi.org/10.1017/S1368980017001677
31. Batal M, Chan HM, Fediuk K, Ing A, Berti P, Sadik T, et al. Importance of the traditional food systems for First Nations adults living on reserves in Canada. Can J Public Health. 2021;112(Suppl 1):20–9. https://doi.org/10.17269/s41997-020-00353-y
32. Maslanka S. Botulism as a disease of humans. In: Foster K, editor. Molecular aspects of botulinum neurotoxin: current topics in neurotoxicity, vol 4. New York: Springer; 2014.
33. World Health Organization. WHO estimates of the global burden of foodborne diseases; foodborne diseases burden epidemiology reference group 2007–2015. Geneva: The Organization; 2015.
34. Lai YH, Chung YA, Wu YC, Fang CT, Chen PJ. Disease burden from foodborne illnesses in Taiwan, 2012–2015. J Formos Med Assoc. 2020;119:1372–81. https://doi.org/10.1016/j.jfma.2020.03.013
35. Gkogka E, Reij MW, Havelaar AH, Zwietering MH, Gorris LG. Risk-based estimate of effect of foodborne diseases on public health, Greece. Emerg Infect Dis. 2011;17:1581–90. https://doi.org/10.3201/eid1709.101766
36. Thomas MK, Murray R, Flockhart L, Pintar K, Pollari F, Fazil A, et al. Estimates of the burden of foodborne illness in Canada for 30 specified pathogens and unspecified agents, circa 2006. Foodborne Pathog Dis. 2013;10:639–48. https://doi.org/10.1089/fpd.2012.1389
37. Hughes JM, Blumenthal JR, Merson MH, Lombard GL, Dowell VR Jr, Gangarosa EJ. Clinical features of types A and B food-borne botulism. Ann Intern Med. 1981;95:442–5. https://doi.org/10.7326/0003-4819-95-4-442
38. Woodruff BA, Griffin PM, McCroskey LM, Smart JF, Wainwright RB, Bryant RG, et al. Clinical and laboratory comparison of botulism from toxin types A, B, and E in the United States, 1975–1988. J Infect Dis. 1992;166:1281–6. https://doi.org/10.1093/infdis/166.6.1281
39. Jackson KA, Mahon BE, Copeland J, Fagan RP. Botulism mortality in the USA, 1975–2009. Botulinum J. 2015;3:6–17. https://doi.org/10.1504/TBJ.2015.078132

Address for correspondence: John Austin, 251 Sir Frederick Banting Driveway, Ottawa, Ontario K1A 0K9, Canada; email: john.austin@hc-sc.gc.ca

Participatory Mathematical Modeling Approach for Policymaking during the First Year of the COVID-19 Crisis, Jordan

Saverio Bellizzi,[1] Nicholas Letchford,[1] Keyrellous Adib,[1] William J.M. Probert, Penelope Hancock, Lora Alsawalha, Alessio Santoro, Maria C. Profili, Ricardo Aguas, Christian Popescu, Lubna Al Ariqi, Lisa White, Wail Hayajneh, Nathir Obeidat, Pierre Nabeth

We engaged in a participatory modeling approach with health sector stakeholders in Jordan to support government decision-making regarding implementing public health measures to mitigate COVID-19 disease burden. We considered the effect of 4 physical distancing strategies on reducing COVID-19 transmission and mortality in Jordan during March 2020–January 2021: no physical distancing; intermittent physical distancing where all but essential services are closed once a week; intermittent physical distancing where all but essential services are closed twice a week; and a permanent physical distancing intervention. Modeling showed that the fourth strategy would be most effective in reducing cases and deaths; however, this approach was only marginally beneficial to reducing COVID-19 disease compared with an intermittently enforced physical distancing intervention. Scenario-based model influenced policy-making and the evolution of the pandemic in Jordan confirmed the forecasting provided by the modeling exercise and helped confirm the effectiveness of the policy adopted by the government of Jordan.

Jordan reported ≈1.1 million confirmed COVID-19 cases and ≈12,500 deaths by the end of December 2021 (*1*), accounting for ≈6.0% of the total confirmed cases and ≈4.0% of the total number of deaths in the World Health Organization (WHO) Eastern Mediterranean Region (*1*). The COVID-19 epidemiologic curve in Jordan during the first 2 years of the pandemic followed distinct phases that reflected the complex interrelation between the natural evolution of the outbreak and the implementation of public health and social measures (PHSMs), which were also modulated in relation to the COVID-19 vaccination campaign (*2*) and the introduction of different variants of concern.

Jordan was particularly successful in flattening the epidemiologic curve during the first months of the pandemic until April 2020 because of implementation of strict PHSMs (*3*). However, the progressive easing of restrictions resulted in an exponential increase in cases, and the first 2 epidemic peaks in November 2020 and March 2021 led to ≈10,000 confirmed cases per day (*4*). Throughout that and subsequent phases of the pandemic, public health policies focused on reducing COVID-19 transmission and mortality in Jordan were supported by a participatory, epidemiologic scenario-based modeling approach.

We provide an overview of lessons learned and challenges in conducting modeling efforts to simulate the transmission of SARS-CoV-2 in Jordan during the first year of the pandemic. Specifically, we assess the likely effectiveness of different combinations of physical distancing measures, and we describe the approach taken to ensure national level buy-in to the modeling results.

Efficacy of Physical Distancing Interventions

During the earliest stages of the COVID-19 pandemic, in the absence of proven antiviral medication and

Author affiliations: World Health Organization Jordan Country Office, Amman, Jordan (S. Bellizzi, L. Alsawalha, A. Santoro, M.C. Profili, C. Popescu); World Health Organization Regional Office for Eastern Mediterranean, Cairo, Egypt (N. Letchford, K. Adib, W.J.M. Probert, Penelope Hancock, L. Al Ariqi, P. Nabeth); Nuffield Department of Medicine, University of Oxford, Oxford, UK (R. Aguas, L. White); SSM Health Cardinal Glennon Children's Hospital, St. Louis University, St. Louis, Missouri, USA (W. Hayajneh); Jordan University Hospital, Amman (N. Obeidat)

DOI: https://doi.org/10.3201/eid2909.221493

[1]These first authors contributed equally to this article.

vaccines, PHSMs represented the only option available for reducing COVID-19 community transmission and mortality (*5*). Among the wide variety of PHSMs applied in different settings, physical distancing interventions (PDIs) and curfews were considered among the most effective (*6*). For the purpose of our analysis, we considered PDIs to be interventions that require persons to maintain a physical distance of ≥1 m from other persons in all essential services (e.g., services conducted by grocery stores and healthcare facilities) and the closure of public places. The purpose of such interventions was ultimately to reduce the probability of COVID-19 transmission among persons (*7*). Evidence on the importance of this variety of PHSMs in limiting the transmission of COVID-19 emerged in Europe and Asia (*8*,*9*) and in the United States, where school closures have been found to reduce COVID-19 incidence and mortality rates by as much as 60% (*10*). Of note, several PHSMs, including PDIs, were substantially more effective when implemented while incidence rates remained low (*11*).

However, PDIs are unsustainable and may have wider-reaching detrimental effects. For example, home confinement considerably increased the rate of domestic violence in many countries, affecting women and children the most (*12*), and limited access to essential services for vulnerable populations (*13*–*17*). Therefore, tailored interventions that maintain persons' livelihoods and keep economies functional while protecting persons at high risk need to be considered (*11*).

Curfews and Physical Distancing Interventions in Jordan

The PHSM strategy adopted in Jordan included imposing a nightly curfew (6 hours) from 12 AM to 6 AM, closing schools and universities, increasing community awareness of hygiene and enforcing a mask mandate in public places (*18*), and prohibiting mass gatherings (*19*). Community transmission in September 2020 triggered the imposition of an intermittent PDI, enforced on Fridays and Saturdays, lasting for 4 weeks. Shortly afterwards, physical distancing was only enforced on Fridays during October 2020–January 2021 (Figure 1). On those Fridays, all city activities, shops, and public places had to be closed (*19*). Furthermore, leaving the house was prohibited, except for persons who held a permit, such as healthcare personnel. Restrictions on other days of the week

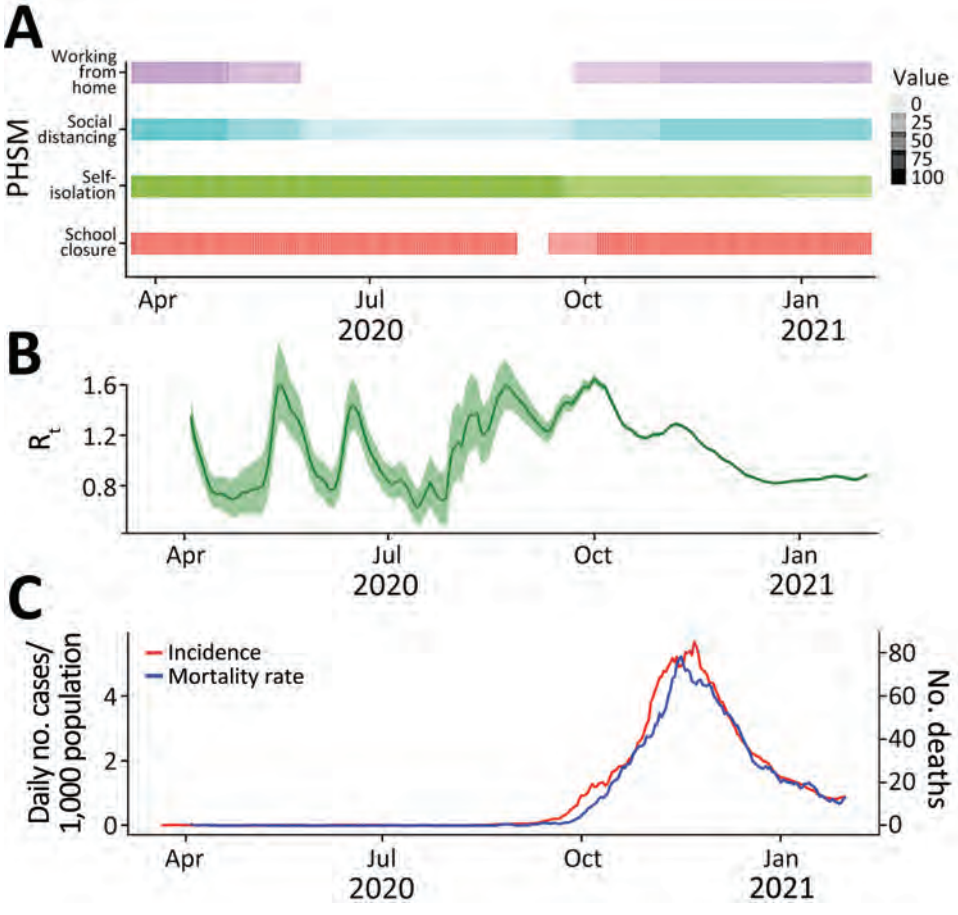

Figure 1. Epidemiologic indicators and PHSMs in a COVID-19 modeling study, Jordan, March 2020–January 2021. A) Timeline of implemented PHSMs. Colors indicate individual PHSMs; level of shading represents the coverage of each intervention in the timeline, ranging from 0% to 100%. B) Estimated R_t, calculated using the EpiEstem package in R (https://CRAN.R-project.org/package=EpiEstim), which presents the number of new case-patients infected by an average case-patient at time t. Green shading indicates 95% CI. C) Daily incidence and mortality rates for COVID-19 in Jordan. PHSM, public health and social measure; Rt, effective reproduction number.

consisted of a 6-hour curfew period after midnight (from 12 AM to 6 AM), with no restriction on persons' movement during the rest of the day (*19*). Such a unique approach was debated, and physical distancing for 1 day a week was questioned in terms of its healthcare benefit based on evidence (*20*).

The Jordan Ministry of Health, with the support of WHO, launched 3 rounds of a nationwide seroprevalence survey from the onset of the pandemic through the beginning of 2021. Findings revealed that seroprevalence steadily increased over time; only a tiny fraction of persons were seropositive in August 2020 (0.3%), a more than 20-fold increase was observed by October 2020 (7.0%), and up to one third of the overall population had been exposed by January 2021 (34.2%) (*4*).

Using Mathematical Modeling in Decision-Making

In the context of infectious diseases, epidemiologic models play a critical role in anticipating the transmission of the disease and driving public health policies designed to limit illness and death (*21*). Specifically, epidemiologic models represent a tool for policy makers to design and evaluate targeted interventions. To do so, a range of factors specific to a setting are taken into consideration, such as demographic features, healthcare capacity, and the concurrent interaction among multiple PHSMs. When limited data are available, mathematical models can provide key elements to decision-makers on the effect of various future policy scenarios (*22*,*23*).

In Jordan, including relevant country stakeholders at each stage of the modeling process ensured that data were reliable and accurate and that the analysis was focused on addressing specific policy questions (*24*,*25*). The senior management of the Ministry of Health requested a series of scenarios on a regular basis (on average, once every 5–6 weeks) and worked directly with WHO to run the model and present the model's findings to inform high-level and evidence-based decision-making. Starting after the second modeling round in October 2020, the Strategic Planning Department of the Jordanian Royal Hashemite Court supported those modeling techniques and bolstered them by expanding data availability, which was critical to initiate the process.

Model Selection

At the onset of the pandemic, the WHO Jordan Country Office approached the Minister of Health to propose the use of mathematical modeling to estimate the epidemiologic outcomes under different scenarios. We selected and adapted the COVID-19 International Modeling Consortium (CoMo) model for implementing mathematical modeling analysis because of its suitability for conducting modeling analysis in low- to middle-income countries (*26*) and because it provided other desirable features, including the ongoing support from CoMo (*26*), an active team of software developers, and epidemiologic modelers. Additional resource requirements for implementing our participatory modeling approach were minimal (e.g., a stable internet connection, the R open-source statistical software [The R Foundation for Statistical Computing, https://www.r-project.org], and standard desktop applications).

The CoMo model is an age-dependent, deterministic, susceptible–exposed–infectious–recovered compartmental design that models transmission of SARS-CoV-2 in the population and can be used to estimate the relative effect of various PHSMs (Appendix, https://wwwnc.cdc.gov/EID/article/29/9/22-1493-App1.pdf). The model considers 5 levels of infection severity: asymptomatic, symptomatic, infections requiring hospitalization, infections requiring intensive care treatment, and infections requiring ventilated intensive care treatment. Infection severity and associated mortality rates are age-dependent, in that the proportion of infected persons requiring hospitalization and the proportion who die varies with age. In addition to predicting case and death rates at various timepoints, the CoMo model also incorporates 2 submodels: hospital and critical care requirements and implementation of public health and safety measures. The CoMo model incorporates a hospital submodel that suggests when hospital and critical care requirements will exceed the capacity of the country's healthcare system (e.g., in terms of hospital beds, intensive care units, and ventilators available for use).

Participatory Modeling of the COVID-19 Pandemic in Jordan

Participatory modeling approaches engage a range of stakeholders from academia, public health sectors, and government throughout the entire modeling process and promote the translation of model results into public health decision-making (*27*). We applied the participatory modeling process developed by WHO's Eastern Mediterranean Region Office (EMRO) modeling support team to analyze the COVID-19 pandemic in Jordan. Specifically, WHO EMRO established a modeling support team in mid-March 2020 as part of the information management component within its COVID-19 Incident Management Support Team with the objective of addressing imminent decision-making needs and promoting awareness of how models work (*24*). When approaching the Minister of Health at the onset of the pandemic, the WHO Jordan Country Office proposed the use of the CoMo model.

The participatory modeling began, therefore, with an initial meeting to communicate the modeling methodology and develop common expectations regarding the outcomes of the modeling exercise. The participants of this process included the WHO Jordan Country Office, the Minister of Health of Jordan, the Ministry of Health Secretary General for the COVID-19 portfolio (appointed to oversee COVID-19 response in Jordan), epidemiologic modeling researchers from the University of Oxford, and mathematical modelers, surveillance officers, and policy analysts from WHO EMRO. Although no specific declaration of interest was signed, there was no remuneration for any stakeholder.

We collected input parameters for the CoMo model by using a standardized template (developed in Excel [Microsoft, https://www.microsoft.com]) accompanied by a guidance document describing the model parameters and their definitions. We conducted 3 rounds of modeling analysis over a period of ≈3 months (November 2020–February 2021).

The participatory modeling process was instrumental in meeting recommended standards of practice associated with mathematical modeling for public health decision-making. Throughout the continued engagement of participants, communication of model uncertainty was reinforced, and key aspects of uncertainty, such as parameters related to viral transmission, were identified. Model outputs were routinely discussed among partners; satisfaction around model outputs paved the way for codevelopment of modeling results in the policy and decision-making process. In addition, patterns of reported and modeled COVID-19 disease and mortality were used for discussions regarding public health surveillance to identify possible challenges and misreporting of COVID-19 with specialists at the Ministry of Health, concerns that were evident from the experience of COVID-19 collaborative modeling in the Philippines by the WHO Western Pacific Region Office (*28*).

The participatory process helped to define the context for the modeling exercise, including questions of importance to policymakers, and make it easier to collect country-specific model inputs (Appendix). Those communications also were productive in developing interpretations of the analysis that were relevant and useful to all participants.

Scenario-Based Modeling of the COVID-19 Pandemic in Jordan

We considered 4 scenarios in the analysis: the baseline scenario and 3 other scenarios (A, B, and C). All scenarios considered interventions that were designed to reduce the rate at which persons come into contact with each other, stemming COVID-19 transmission in Jordan. Common to each scenario are 2 parameters that can be used to define the extent of the PDI: coverage and adherence. Coverage refers to the percentage of the population that is following physical distancing regulations; adherence refers to the extent individual persons follow those guidelines. An intervention with low adherence but high coverage would mean that most of the population loosely follow the physical distancing regulations. Conversely, an intervention with high adherence but low coverage would mean a small percentage of the population follow the physical distancing regulations to a high standard. All other parameters in the model were held constant throughout the duration of the simulation. We developed the scenarios considered through an iterative process of engaging with relevant policy makers, updating the scenarios as more information became available (since the last analysis), and adapting the scenarios to reflect the effect of potential future changes to PHSMs.

The baseline scenario considers the situation of no government intervention but assumed 50% of the population would continue to physically distance themselves. This percentage was suggested by public health experts in Jordan and is in line with available literature (*29*). Scenario A assumed the Jordan population would physically distance themselves for a period of 24 hours every Friday (considering Friday prayer observance), applying to all but basic services, such as hospitals and grocery stores. No government restrictions were assumed to be imposed on the other days of the week, yet, as in the baseline scenario, we assumed a portion of the population (50%) would continue to practice a degree of physical distancing regardless of government guidelines. Similarly, scenario B is an extension of scenario A in that all but essential services were required to close over the entire weekend, reducing contacts as much as possible. Last, scenario C, being the most extreme scenario considered in our analysis, assumed all but essential services were closed for the entire week until the end of the simulation period. Consistent across each scenario we assumed the interventions came into effect on October 31, 2020, and lasted until the end of the simulation period on January 31, 2021.

Estimated Effect of Continuation of Planned Measures on Health Outcomes

The timing of the predicted peak incidence, which was estimated to occur in mid-November 2020, varied only marginally across the different scenarios

(Figure 2, panel A). However, soon after the interventions in scenarios A, B, and C were implemented, their effect was observed in reduced incidence (Figure 2, panel A) and cumulative mortality (Figure 2, panel B). Unsurprisingly, the most impactful scenario was scenario C, where a sharp and rapid reduction in cases and deaths was predicted to occur shortly after implementation. However, the economic cost of such an intervention would likely have been substantial for the population.

Exploring Variation in Efficacy of Different Scenarios

We estimated the effect of scenarios A, B, and C in terms of the percentage reduction of COVID-19 cases and deaths during November 2020–January 2021 relative to the baseline scenario (Figure 3). The coverage of the PDI in each scenario was assumed to only be relevant during the days of the week the intervention was enforced. During the nonintervention days of the week, we assumed 50% of the population continued to practice physical distancing regardless of government guidelines. Consistently across each scenario, the model estimated that the greatest reduction in COVID-19 incidence and death was associated with increasing adherence to the respective physical distancing guidelines implemented by the government. When the adherence of the population was low, increasing the coverage of the PDI had relatively little effect on reducing disease. Conversely, however, if the adherence of persons who follow government regulations was high (>80%), the model estimated that increasing the coverage of the population had compounded effects on reducing COVID-19 disease incidence and death.

The greatest effect was observed under scenario C, with high coverage and high adherence (97% reduction in cases and deaths relative to the baseline scenario, assuming 100% coverage and adherence). However, assuming adherence and coverage >90% for either scenario A or B, the model predicted that reported cases and deaths would have reduced by ≈90% relative to the baseline scenario. In contrast, any scenario (either A, B, or C) with low coverage (<25%) had almost no effect, decreasing disease incidence and death by as little as 10% relative to the baseline scenario. The difference in disease incidence and death between scenarios A and C equates to roughly 7% fewer cases and deaths (assuming the coverage and adherence are both high [>90%]). As coverage and particularly adherence decreases, diseases incidence and death increase rapidly. Those results suggest that implementing scenario C during October 31, 2020–January 31, 2021, would be only marginally beneficial at reducing COVID-19 disease and death compared with scenario A or B with high coverage and adherence. The findings of our analysis and the subsequent decision-making was supported by epidemiologic and economic modeling for COVID-19 policy in Australia; although tighter

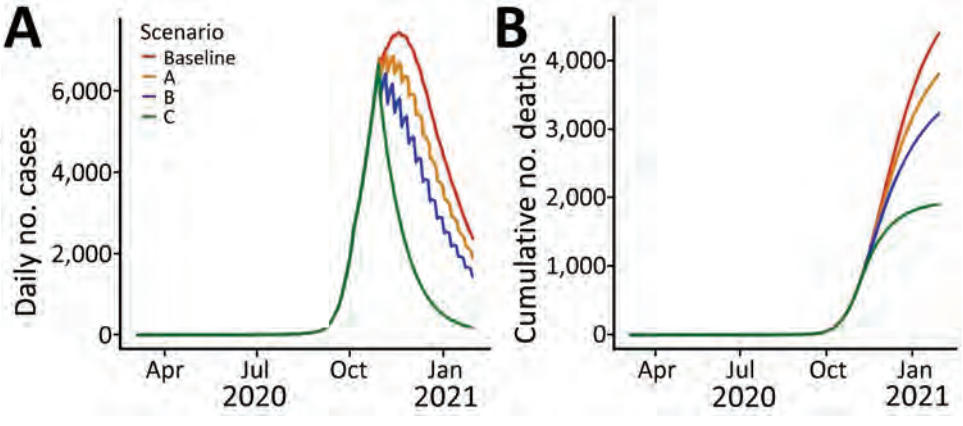

Figure 2. Model-predicted reported number of COVID-19 cases and cumulative number of associated deaths under scenarios A, B, C, and the baseline scenario in a COVID-19 modeling study, Jordan, March 2020–January 2021. Scenario A assumes the entire population, excepting essential services, will physically distance themselves for 24 hours every Friday while reverting to their usual behavior on the other days of the week. Scenario B assumes the population will physically distance themselves for the entire weekend (Friday and Saturday) while reverting to their usual behavior throughout the week. Scenario C assumes the entire population, except for essential services, will physically distance themselves for the entire week while never reverting to their usual behavior. Baseline scenario assumes no government intervention and half the population instinctively physically distancing themselves to avoid infection. Common to each scenario are 2 parameters used to define the extent of the physical distancing intervention: coverage, which refers to the percentage of the population following physical distancing regulations, and adherence, which refers to the extent to which individual persons follow those guidelines. On days when the interventions are not enforced, simulations assume 80% adherence and 50% coverage of the population practice physical distancing, while on days when the interventions are enforced it is assumed that 80% adherence and 90% coverage of the population physically distance themselves.

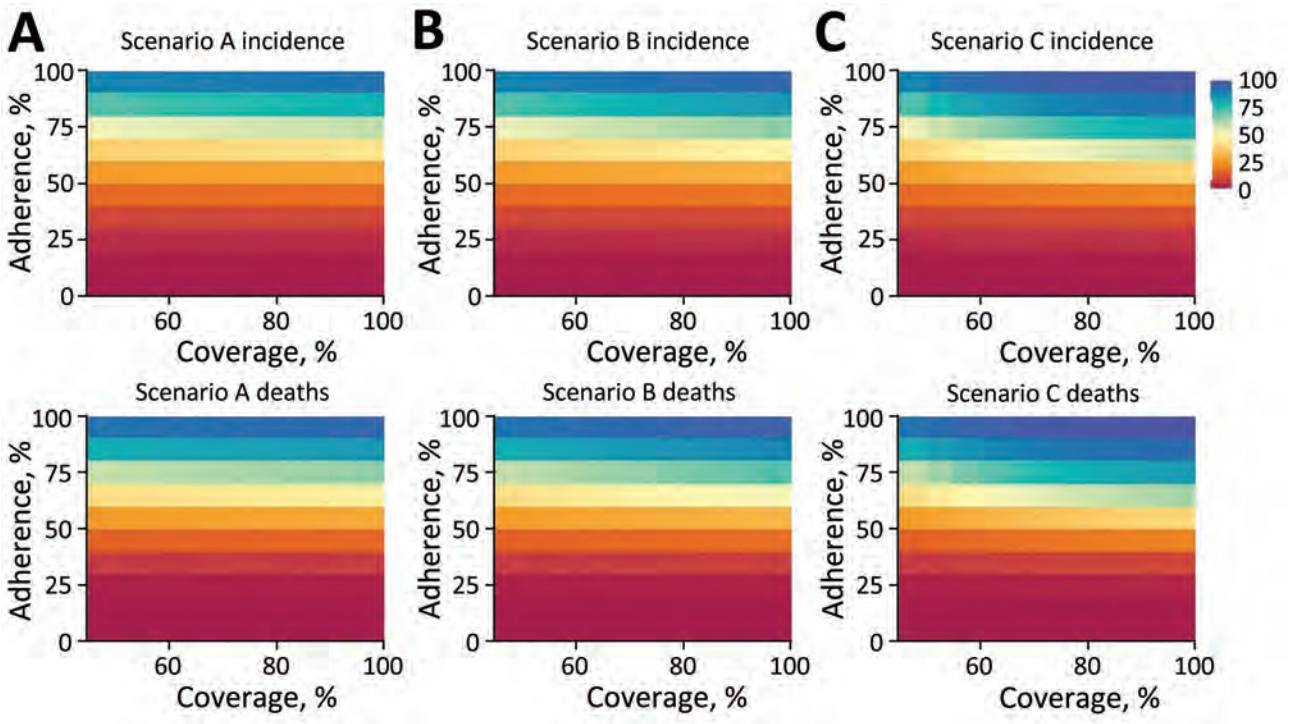

Figure 3. Model-predicted heat map showing percentage reduction in COVID-19 incidence (top row) and deaths (bottom row) in a COVID-19 modeling study in Jordan under 3 different scenarios (A, B, and C), relative to the baseline scenario, aggregated for the period November 2020–January 31, 2021. Dark blue corresponds to nearly 100% reduction in incidence and cases relative to the baseline scenario; dark red corresponds to 0% reduction. Scenario A assumes the entire population, excepting essential services, will physically distance themselves for 24 hours every Friday while reverting to their usual behavior on the other days of the week. Scenario B assumes the population will physically distance themselves for the entire weekend (Friday and Saturday) while reverting to their usual behavior throughout the week. Scenario C assumes the entire population, except for essential services, will physically distance themselves for the entire week while never reverting to their usual behavior. Baseline scenario assumes no government intervention and half the population instinctively physically distances themselves to avoid infection. Common to each scenario are 2 parameters used to define the extent of the physical distancing intervention: coverage, which refers to the percentage of the population following physical distancing regulations, and adherence, which refers to the extent to which individual persons follow those guidelines. The coverage parameter was varied between values of 50% and 100% (presented on the horizontal axis of each heat map) on the days when the physical distancing intervention was enforced. On respective days when the interventions were not enforced, simulations assume the coverage was constant at 50%. The adherence parameter varied between 0% and 100% (presented on the vertical axis of each heat map), remaining constant throughout each simulation.

stringency PHSMs remarkably reduced cumulative infections in that country, that effect had the trade-off of higher expected societal economic losses (*29*). Therefore, ranking of policy options should be based on optimality and cost-effectiveness, possibly leading to a mix of higher-stringency PHSMs (*30*).

We retrospectively compared the results of scenario A to historical reported data (Figure 4). We found the incidence under scenario A closely resembled the reported data for an assumed coverage of 60% and adherence of 80% and even more so for cumulative mortality (Figure 4). The coverage and adherence parameters for another scenario (Figure 5) closely resemble the reported Google mobility data for Jordan (*31*). We considered the average of the Google mobility data reported from retail and recreational facilities, grocery and pharmacy stores, and parks and transit locations. Changes in the average Google mobility data occurred on weekly intervals, representing the reduced mobility of persons during the weekend (Figure 5).

Challenges and Limitations

As in all modeling studies, we made various assumptions in this analysis. We cannot accurately estimate COVID-19 transmission rates and the effective reproduction number (R_t) when the burden of COVID-19 in the country is underestimated because of underreporting of cases and associated deaths. This limitation prevented us from performing model fitting, for example, using Bayesian particle filtering methods, to estimate the actual dynamics of COVID-19 and perform inference on key parameters such as the basic reproduction number (R_0). Moreover, although

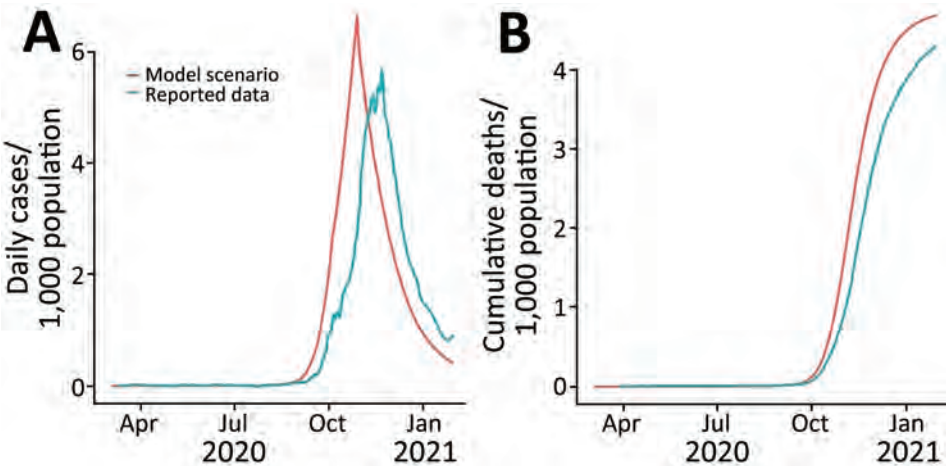

Figure 4. Comparison of COVID-19 daily incidence (A) and cumulative deaths (B) under model scenario A compared with reported data in a COVID-19 modeling study, Jordan, March 2020–January 2021. Scenario A assumes the entire population, excepting essential services, will physically distance themselves for 24 hours every Friday while reverting to their usual behavior on the other days of the week. The scenario is defined by 2 key parameters: coverage and adherence. On days when the physical distancing intervention was enforced, the simulation assumes 60% of the population is following physical distancing regulations (coverage) and that those persons spend 80% of their time adhering to the intervention (adherence).

our models included age-specific mixing patterns, geographic location–specific mixing patterns were ignored. This analysis modeled Jordan as a whole, whereas differences between governorates may have warranted a spatially explicit approach to modeling. The analysis did not account for the introduction of variants of concern and assumed that natural infection provided lifelong protection against reinfection. Ensuring policy makers understand the limitations of these assumptions through clear communication is vital to ensure the model's relevance.

Conclusions

COVID-19 modeling has been a substantial achievement (*32*). Strong and consistent national support and inputs from a wide range of critical stakeholders, such as the Ministry of Health and the Royal Hashemite Court, ensured that estimations of relative effect have been constantly refined over time.

The participatory scenario-based approach we describe considered the effect of intermittent PDIs on reducing COVID-19 transmission in Jordan. We show that enforcing a PDI with no intermittent periods is only marginally beneficial to reducing COVID-19 disease burden compared with an intermittently enforced PDI. The evolution of the pandemic in Jordan confirmed the forecasting provided by the modeling exercise and helped confirm the effectiveness of the policy adopted by the government of Jordan. The insights from scenario-based modeling influenced the implementation of PHSMs and PDIs; specifically, scenario-based models were used to updating PHSM and PDI guidelines in addition to other evidence-based actions, such as infection prevention and control (*33*).

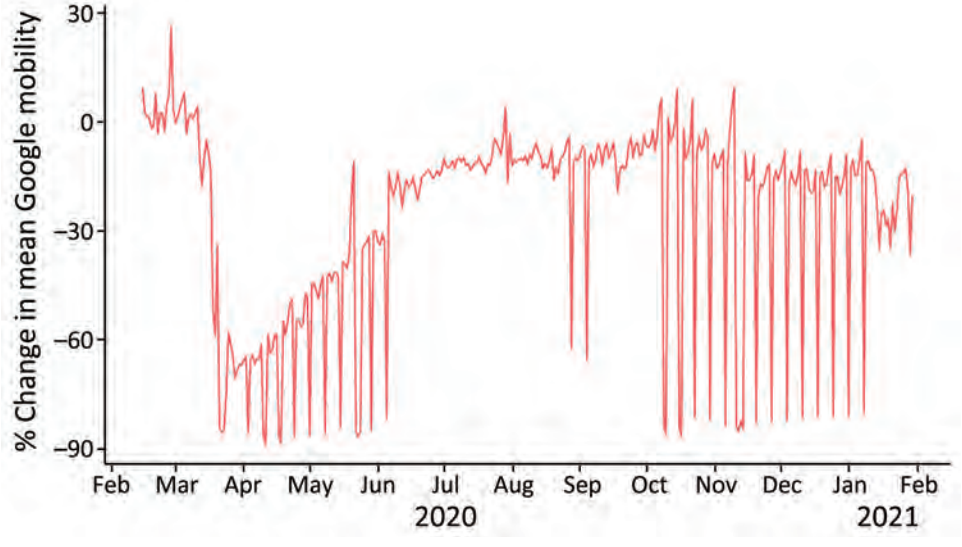

Figure 5. Percentage changes in mean mobility among the population, Jordan, February 2020–January 2021, including around retail and recreational facilities, grocery and pharmacy stores, parks, and transit locations. Google mobility data are used as a proxy for the population's coverage and adherence to COVID-19–related physical distancing interventions.

By interacting directly with the policy decision-makers, we were able to define the context of the modeling exercise and address specific policy questions they posed. Furthermore, communicating what mathematical modeling is capable of and its limitations at every stage of the analysis was vital to the success of the project. This level of engagement strengthened communication between stakeholders and encouraged insights learned through the modeling process to be incorporated into policy decisions.

This modeling initiative for the pandemic confirmed the comparative advantage in providing hands-on support to national health authorities for developing evidence-based policies. The participatory approach in running COVID-19 modeling research provided the chance to convey the model's caveats and limitations and disseminate modeling results among governing bodies and partners as appropriate. By leveraging and investing in WHO resources and providing essential assistance for the pandemic (e.g., procurement, research, and capacity building), WHO created crucial evidence to help with decision-making within and beyond Jordan's health sector.

About the Author

Dr. Bellizzi is the Emergency Team Leader for the Jordan WHO Country Office. His research interests include policy support in the area of public health emergency, with a focus on low- and middle-income countries.

References

1. World Health Organization. Weekly epidemiological update on COVID-19—28 December 2021 [cited 2023 Apr 1]. https://www.who.int/publications/m/item/weekly-epidemiological-update-on-covid-19—28-december-2021
2. Bellizzi S, Aidyralieva C, Alsawhala L, Al-Shaikh A, Santoro A, Profili MC. Vaccination for SARS-CoV-2 of migrants and refugees, Jordan. Bull World Health Organ. 2021;99:611. https://doi.org/10.2471/BLT.21.285591
3. Brookings Institution. Policy and institutional responses to COVID-19 in the Middle East and North Africa: Jordan [cited 2023 Apr 1]. https://www.brookings.edu/research/policy-and-institutional-responses-to-covid-19-in-the-middle-east-and-north-africa-jordan
4. Bellizzi S, Alsawalha L, Sheikh Ali S, Sharkas G, Muthu N, Ghazo M, et al. A three-phase population based sero-epidemiological study: assessing the trend in prevalence of SARS-CoV-2 during COVID-19 pandemic in Jordan. One Health. 2021;13:100292. https://doi.org/10.1016/j.onehlt.2021.100292
5. Qualls N, Levitt A, Kanade N, Wright-Jegede N, Dopson S, Biggerstaff M, et al.; CDC Community Mitigation Guidelines Work Group. Community mitigation guidelines to prevent pandemic influenza—United States, 2017. MMWR Recomm Rep. 2017;66:1–34. https://doi.org/10.15585/mmwr.rr6601a1
6. Haug N, Geyrhofer L, Londei A, Dervic E, Desvars-Larrive A, Loreto V, et al. Ranking the effectiveness of worldwide COVID-19 government interventions. Nat Hum Behav. 2020;4:1303–12. https://doi.org/10.1038/s41562-020-01009-0
7. World Health Organization. COVID-19: physical distancing [cited 2023 Apr 1]. https://www.who.int/westernpacific/emergencies/covid-19/information/physical-distancing
8. Flaxman S, Mishra S, Gandy A, Unwin HJT, Mellan TA, Coupland H, et al.; Imperial College COVID-19 Response Team. Estimating the effects of non-pharmaceutical interventions on COVID-19 in Europe. Nature. 2020;584:257–61. https://doi.org/10.1038/s41586-020-2405-7
9. Park YJ, Choe YJ, Park O, Park SY, Kim YM, Kim J, et al.; COVID-19 National Emergency Response Center, Epidemiology and Case Management Team. Contact tracing during coronavirus disease outbreak, South Korea, 2020. Emerg Infect Dis. 2020;26:2465–8. https://doi.org/10.3201/eid2610.201315
10. Auger KA, Shah SS, Richardson T, Hartley D, Hall M, Warniment A, et al. Association between statewide school closure and COVID-19 incidence and mortality in the US. JAMA. 2020;324:859–70. https://doi.org/10.1001/jama.2020.14348
11. Talic S, Shah S, Wild H, Gasevic D, Maharaj A, Ademi Z, et al. Effectiveness of public health measures in reducing the incidence of covid-19, SARS-CoV-2 transmission, and covid-19 mortality: systematic review and meta-analysis. BMJ. 2021;375:e068302. https://doi.org/10.1136/bmj-2021-068302
12. Bellizzi S, Nivoli A, Lorettu L, Farina G, Ramses M, Ronzoni AR. Violence against women in Italy during the COVID-19 pandemic. Int J Gynaecol Obstet. 2020;150:258–9. https://doi.org/10.1002/ijgo.13270
13. Bellizzi S, Nivoli A, Lorettu L, Ronzoni AR. Human rights during the COVID-19 pandemic: the issue of female genital mutilations. Public Health. 2020;185:53–4. https://doi.org/10.1016/j.puhe.2020.05.037
14. Bellizzi S, Pichierri G, Napodano CMP, Picchi S, Fiorletta S, Panunzi MG, et al. Access to modern methods of contraception in Italy: will the COVID-19 pandemic be aggravating the issue? J Glob Health. 2020;10:020320. https://doi.org/10.7189/jogh.10.020320
15. Bellizzi S, Alsawalha L, Samawi L, Al-Shaikh A, Alfar H, Muthu N, et al. The impact of the SARS-CoV-2 pandemic on mental health in vulnerable population settings: the case of Jordan. Front Psychiatry. 2021;12:692541. https://doi.org/10.3389/fpsyt.2021.692541
16. Bellizzi S, Ronzoni AR, Pichierri G, Cegolon L, Salaris P, Panu Napodano CM, et al. Safe abortion amid the COVID-19 pandemic: the case of Italy. Int J Gynaecol Obstet. 2020;150:254–5. https://doi.org/10.1002/ijgo.13233
17. Bellizzi S, Muthu N, Khader Y, Boukerdenna H, Darwish D, Al-Sheikh A, et al. COVID-19 and non-communicable diseases in complex vulnerable populations: evidence from Jordan. Prim Health Care Res Dev. 2023;24:e8. https://doi.org/10.1017/S1463423622000731
18. Bubbico L, Mastrangelo G, Larese-Filon F, Basso P, Rigoli R, Maurelli M, et al. Community use of face masks against the spread of COVID-19. Int J Environ Res Public Health. 2021;18:3214. https://doi.org/10.3390/ijerph18063214
19. AlRyalat SA, Elubous KA, Al-Ebous AD, Mahafzah A. Impact of a single-day lockdown on COVID-19: an interrupted time series analysis. Cureus. 2021;13:e17299. https://doi.org/10.7759/cureus.17299
20. Al Mostafa M, et al. Friday lockdown in Jordan: Good lessons to be learned from Jordan? Ethics Med Public Health. 2021 Jun 16 [letter]. https://doi.org/10.1016/j.jemep.2021.100663

21. Aylett-Bullock J, Gilman RT, Hall I, Kennedy D, Evers ES, Katta A, et al. Epidemiological modelling in refugee and internally displaced people settlements: challenges and ways forward. BMJ Glob Health. 2022;7:e007822. https://doi.org/10.1136/bmjgh-2021-007822
22. Teslya A, Pham TM, Godijk NG, Kretzschmar ME, Bootsma MCJ, Rozhnova G. Impact of self-imposed prevention measures and short-term government-imposed social distancing on mitigating and delaying a COVID-19 epidemic: a modelling study. PLoS Med. 2020;17:e1003166. https://doi.org/10.1371/journal.pmed.1003166
23. McBryde ES, Meehan MT, Adegboye OA, Adekunle AI, Caldwell JM, Pak A, et al. Role of modelling in COVID-19 policy development. Paediatr Respir Rev. 2020; 35:57–60.
24. Adib K, Hancock PA, Rahimli A, Mugisa B, Abdulrazeq F, Aguas R, et al. A participatory modelling approach for investigating the spread of COVID-19 in countries of the Eastern Mediterranean Region to support public health decision-making. BMJ Glob Health. 2021;6:e005207. https://doi.org/10.1136/bmjgh-2021-005207
25. Aguas R, White L, Hupert N, Shretta R, Pan-Ngum W, Celhay O, et al.; CoMo Consortium. Modelling the COVID-19 pandemic in context: an international participatory approach. BMJ Glob Health. 2020;5:e003126. https://doi.org/10.1136/bmjgh-2020-003126
26. CoMo Consortium. The COVID-19 International Modelling Consortium [cited 2023 Apr 1]. https://como.bmj.com
27. Adams S, Rhodes T, Lancaster K. New directions for participatory modelling in health: redistributing expertise in relation to localised matters of concern. Glob Public Health. 2022;17:1827–41. https://doi.org/10.1080/17441692.2021.1998575
28. Hughes A, Ragonnet R, Jayasundara P, Ngo HA, de Lara-Tuprio E, Estuar MRJ, et al. COVID-19 collaborative modelling for policy response in the Philippines, Malaysia and Vietnam. Lancet Reg Health West Pac. 2022;29:100563. https://doi.org/10.1016/j.lanwpc.2022.100563
29. Kim HY, Bershteyn A, McGillen JB, Shaff J, Sisti J, Ko C, et al. Social distancing and mask-wearing could avoid recurrent stay-at-home restrictions during COVID-19 respiratory pandemic in New York City. Sci Rep. 2022;12:10312. https://doi.org/10.1038/s41598-022-13310-1
30. Szanyi J, Wilson T, Howe S, Zeng J, Andrabi H, Rossiter S, et al. Epidemiologic and economic modelling of optimal COVID-19 policy: public health and social measures, masks and vaccines in Victoria, Australia. Lancet Reg Health West Pac. 2023;32:100675. https://doi.org/10.1016/j.lanwpc.2022.100675
31. Google. COVID-19 community mobility reports [cited 2023 Apr 1]. https://www.google.com/covid19/mobility
32. World Health Organization. WHO supports generating evidence for decision-making in Jordan during COVID-19 [cited 2023 Apr 1]. https://www.who.int/about/accountability/results/who-results-report-2020-mtr/country-story/2020/jordan
33. Tarif AB, Ramadan M, Yin M, Sharkas G, Ali SS, Gazo M, et al. Infection prevention and control risk factors in health workers infected with SARS-CoV-2 in Jordan: a case control study. PLoS One. 2022;17:e0271133. https://doi.org/10.1371/journal.pone.0271133

Address for correspondence: Saverio Bellizzi, Mohammad Jamjoum St, Ministry of Interior Circle, Bldg 5, Amman, Jordan; email: bellizzis@who.int

Compliance Trajectory and Patterns of COVID-19 Preventive Measures, Japan, 2020–2022

Taro Kusama, Kenji Takeuchi, Yudai Tamada, Sakura Kiuchi, Ken Osaka, Takahiro Tabuchi

COVID-19 remains a global health threat. Compliance with nonpharmaceutical interventions is essential because of limited effectiveness of COVID-19 vaccines, emergence of highly contagious variants, and declining COVID-19 antibody titers over time. We evaluated compliance with 14 nonpharmaceutical intervention–related COVID-19 preventive behaviors, including mask wearing, ventilation, and surface sanitation, in a longitudinal study in Japan using 4 waves of Internet survey data obtained during 2020–2022. Compliance with most preventive behaviors increased or remained stable during the 2-year period, except for surface sanitation and going out behaviors; compliance with ventilation behavior substantially decreased in winter. Compliance patterns identified from latent class analysis showed that the number of persons in the low compliance class decreased, whereas those in the personal hygiene class increased. Our findings reflect the relaxation of mobility restriction policy in Japan, where the COVID-19 pandemic continues. Policymakers should consider behavioral changes caused by new policies to improve COVID-19 prevention strategies.

COVID-19, caused by SARS-CoV-2, remains a global health threat (*1*). Although COVID-19 vaccinations have covered most of the population in many countries (*2*), vaccine effectiveness is limited because of the emergence of highly contagious variants and a decrease in SARS-CoV-2 antibody titer over time (*3*,*4*). Therefore, individual compliance with nonpharmaceutical interventions (NPIs), such as physical distancing, mask wearing, and increased building ventilation, remains essential for COVID-19 prevention (*5*–*7*).

Temporal changes in compliance with several NPI-related preventive behaviors have been reported (*8*–*11*). However, those studies were followed up for a short period (e.g., within 0.5–1 year) and included limited types of preventive behaviors. Since the first case of COVID-19 was confirmed, some preventive measures, such as surface sanitation, have been considered less effective, whereas others, such as increased building ventilation, have been confirmed as more effective in general settings (*12*,*13*). Previous studies have not examined changes in preventive measure compliance over time. A cross-sectional study reported patterns of compliance with multiple preventive measures (*14*); however, whether those compliance patterns changed over time remained unclear. We performed a 2-year longitudinal study in Japan to determine changes in compliance with 14 NPI-related COVID-19 preventive behaviors; identify compliance patterns for those behaviors over time; and define sociodemographic characteristics associated with compliance for each preventive behavior and characteristics associated with compliance patterns for multiple preventive behaviors.

Methods

Study Design and Participants

We conducted a 2-year follow-up longitudinal study by using unbalanced panel data obtained from 2 Japan COVID-19 and Society Internet Surveys (JACSIS) and 2 Japan Society and New Tobacco Internet Surveys (JASTIS). JACSIS aimed to evaluate health conditions and social determinants during the COVID-19 pandemic in Japan, whereas JASTIS aimed to evaluate the status of new tobacco products and

Author affiliations: Tohoku University Graduate School of Dentistry, Sendai, Japan (T. Kusama, K. Takeuchi, Y. Tamada, S. Kiuchi, K. Osaka); Nagoya University Graduate School of Medicine, Nagoya, Japan (K. Takeuchi, Y. Tamada); Tohoku University Frontier Research Institute for Interdisciplinary Sciences, Sendai (S. Kiuchi); Osaka International Cancer Institute, Osaka, Japan (T. Tabuchi); The Tokyo Foundation for Policy Research, Tokyo, Japan (T. Tabuchi)

DOI: https://doi.org/10.3201/eid2909.221754

their related factors in Japan (*11*,*15*). Surveys were administered via Internet questionnaires. The surveys were conducted during the following periods: August 25–September 30, 2020 (JACSIS2020); February 8–26, 2021 (JASTIS2021); September 27–October 29, 2021 (JACSIS2021); and February 1–28, 2022 (JASTIS2022). Daily numbers of newly confirmed COVID-19 cases in Japan were determined during the survey periods (https://www.mhlw.go.jp/stf/covid-19/open-data.html) (Appendix Figure 1, https://wwwnc.cdc.gov/EID/article/29/9/22-1754-App1.pdf). The original population of all 4 surveys came from the same panel data. Candidates registered as panelists at an Internet research company (Rakuten Insight, https://insight.rakuten.com) in Japan and responded to multiple surveys; therefore, the number of survey waves encountered by participants ranged from 1 to 4. We excluded participants who provided inconsistent or unreliable responses in the questionnaires (e.g., selected applicable for all questions regarding various types of current drug use or chronic diseases, including major noncommunicable diseases) from the analysis. In addition, we excluded participants who were <20 or >79 years of age.

Outcome Variables

The evaluated outcomes in each survey were compliance with COVID-19 preventive behaviors. We selected 14 preventive behaviors related to COVID-19 NPIs: mask wearing, ventilation, social distancing, avoiding crowds, hand sanitation, hand washing, gargling, respiratory hygiene, avoiding touching one's face, surface sanitation, avoiding travel, avoiding going out, avoiding talking closely, and avoiding meeting high-risk persons. We asked the participants about their compliance with each of those preventive behaviors; participants who answered that they always complied were considered compliant with each preventive behavior (Appendix Table 1). Mask wearing, ventilation, social distancing, and avoiding crowds were behaviors mandated by the government of Japan campaign called the 3 Cs, which requests that the public should avoid closed spaces, crowded places, and close-contact settings to prevent COVID-19 (*1*,*16*).

Predictors

For predictors, we used a continuous scale for survey waves (recorded as 0 for JACSIS2020, 1 for JASTIS2021, 2 for JACSIS2021, and 3 for JASTIS2022), survey type (JACSIS or JASTIS), sex, age categories, education, and equivalent income. For age, education, and equivalent income, we used the values from each survey. Surveys were conducted in the summer/autumn (JACSIS) and winter (JASTIS). In addition, we included population density at the prefecture level as a geographic predictor as a binary variable categorized as the top 20% of densely populated prefectures in Japan, which are Tokyo, Osaka, Kanagawa, Saitama, Aichi, Chiba, Fukuoka, Okinawa, and Hyogo.

Statistical Analysis

We estimated the absolute differences in percentages and 95% CIs for each preventive behavior according to generalized estimating equations, fitting the Gaussian distribution and identity link function by using a Huber–White sandwich estimator for SEs (*17*). We identified compliance patterns for multiple preventive behaviors to simplify interpretation and gain a holistic understanding of preventive behavior compliance during the COVID-19 pandemic and used latent class analysis to identify those patterns (*18*). We estimated the probability of being in each class on the basis of the generalized structural equation model fitting the logistic regression model and included the binary variables of preventive behavior compliance as dependent variables. We determined the final number of latent classes according to a scree plot of the Bayesian information criterion and proportion of participants belonging to the smallest class. For the scree plot, we estimated the Bayesian information criterion for each model by using a different number of latent classes from 1 to 6; the elbow of the scree plot was considered to have an appropriate number of classes (*18*). Furthermore, a class representing a small portion of the population would violate the generalizability and interpretability of the result; therefore, we excluded the model that estimated ≥1 class that included <15% of participants (*18*). To avoid violating the local independence assumption within the class, we excluded the preventive behavior that had a ϕ coefficient of >0.7 with the other behaviors (*18*). We found a strong correlation between social distancing and avoiding talking closely behaviors (Appendix Table 2); therefore, we excluded the avoiding talking closely behavior from latent class analysis.

We also used the estimated class as the outcome and evaluated its association with predictors. We fitted the multinomial logistic regression model with generalized estimating equations and estimated the absolute difference in probability (percentage and 95% CIs) of belonging to each class according to each predictor by using the parametric g-formula (*19*). To evaluate the mobility of latent classes through the 4 surveys, we created a Sankey plot of the proportion of each class at each survey point for participants who

responded to all 4 survey waves. To reduce selection bias, in all statistical analyses, including descriptive statistics and regression analysis, we used the inverse probability weighting method and propensity score estimated from the Comprehensive Survey of Living Conditions, which is representative of a sociodemographic random sample in Japan (*20*). We used generalized estimating equations for data with multiple responses among persons and addressed interindividual correlations; therefore, the results obtained from regression analysis can be interpreted as a population-average difference in preventive behavior compliance (*21*). Only the candidates who completed the whole questionnaire could register their responses within the online system created by the Internet research company; no missing values existed for any participant in this study. We used Stata version 17.0 (StataCorp LLC, https://www.stata.com) for all analyses and set statistical significance at $\alpha = 0.05$.

Ethical Issues

Both the JACSIS and JASTIS conducted during 2020–2022 followed procedures approved by the Ethics Committee on Research of Human Subjects at the Osaka International Cancer Institute (no. 20084-8). In addition, we followed Strengthening the Reporting of Observational studies in Epidemiology guidelines, known as STROBE, to report our observational study.

Results

Initially, the numbers of responses to the questionnaires were 28,000 for JACSIS2020, 26,000 for JASTIS2021, 31,000 for JACSIS2021, and 33,000 for JASTIS2022. After excluding respondents who did not meet eligibility criteria, we included 103,312 responses from a total of 41,510 participants (Table 1; Appendix Figure 2) and determined response patterns and distribution (Appendix Table 3). Characteristics of the respondents were recorded; the average age (±SD) of participants was 47.2 ±17.3 SD years; 49.9% were men and 50.1% women (Table 2).

We evaluated compliance with each preventive behavior according to the survey period (Figure 1). Compliance with most behaviors slightly increased or remained stable among the surveys; however, compliance with ventilation and avoiding going out behaviors decreased among the surveys. Compliance with ventilation showed apparent seasonal

Table 1. Preventive behaviors of participants in each survey in study of compliance trajectory and patterns of COVID-19 preventive measures, Japan, 2020–2022*

Characteristics	Compliance	Surveys				
		All responses	JACSIS2020	JASTIS2021	JACSIS2021	JASTIS2022
No. responses	NA	103,312 (100.0)	24,651 (100.0)	22,350 (100.0)	27,348 (100.0)	28,963 (100.0)
Preventive behaviors						
Mask-wearing	Yes	91,377 (88.5)	20,624 (83.7)	19,415 (86.9)	24,930 (91.2)	26,407 (91.2)
	No	11,935 (11.5)	4,027 (16.3)	2,935 (13.1)	2,418 (8.8)	2,556 (8.8)
Ventilation	Yes	42,240 (40.9)	11,221 (45.5)	8,066 (36.1)	13,464 (49.2)	9,489 (32.8)
	No	61,072 (59.1)	13,430 (54.5)	14,284 (63.9)	13,884 (50.8)	19,474 (67.2)
Social distancing	Yes	45,759 (44.3)	10,317 (41.8)	9,884 (44.2)	12,855 (47.0)	12,703 (43.9)
	No	57,553 (55.7)	14,334 (58.2)	12,466 (55.8)	14,493 (53.0)	16,260 (56.1)
Avoiding crowds	Yes	61,679 (59.7)	14,771 (59.9)	13,216 (59.1)	17,092 (62.5)	16,600 (57.3)
	No	41,633 (40.3)	9,880 (40.1)	9,134 (40.9)	10,256 (37.5)	12,363 (42.7)
Hand sanitation	Yes	68,435 (66.2)	14,550 (59.0)	14,696 (65.8)	19,034 (69.6)	20,155 (69.6)
	No	34,877 (33.8)	10,101 (41.0)	7,654 (34.2)	8,314 (30.4)	8,808 (30.4)
Handwashing	Yes	57,316 (55.5)	13,551 (55.0)	11,962 (53.5)	15,986 (58.5)	15,817 (54.6)
	No	45,996 (44.5)	11,100 (45.0)	10,388 (46.5)	11,362 (41.5)	13,146 (45.4)
Gargling	Yes	47,298 (45.8)	10,859 (44.0)	10,736 (48.0)	12,373 (45.2)	13,330 (46.0)
	No	56,014 (54.2)	13,792 (56.0)	11,614 (52.0)	14,975 (54.8)	15,633 (54.0)
Respiratory hygiene	Yes	75,845 (73.4)	16,817 (68.2)	15,810 (70.7)	20,967 (76.7)	22,250 (76.8)
	No	27,467 (26.6)	7,834 (31.8)	6,540 (29.3)	6,381 (23.3)	6,713 (23.2)
Avoiding touching face	Yes	45,945 (44.5)	10,633 (43.1)	9,707 (43.4)	12,451 (45.5)	13,154 (45.4)
	No	57,367 (55.5)	14,018 (56.9)	12,643 (56.6)	14,897 (54.5)	15,809 (54.6)
Surface sanitation	Yes	21,378 (20.7)	5,101 (20.7)	4,880 (21.8)	5,648 (20.6)	5,748 (19.8)
	No	81,935 (79.)3	19,550 (79.3)	17,470 (78.2)	21,700 (79.4)	23,215 (80.2)
Avoiding travel	Yes	74,478 (72.1)	17,323 (70.3)	16,542 (74.0)	20,571 (75.2)	20,042 ()69.2
	No	28,834 (27.9)	7,328 (29.7)	5,808 (26.0)	6,777 (24.8)	8,921 (30.8)
Avoiding going out	Yes	58,274 (56.4)	14,648 (59.4)	12,839 (57.4)	15,726 (57.5)	15,061 (52.0)
	No	45,038 (43.6)	10,003 (40.6)	9,511 (42.6)	11,622 (42.5)	13,902 (48.0)
Avoiding talking closely	Yes	43,499 (42.1)	9,796 (39.7)	9,160 (41.0)	12,266 (44.8)	12,277 (42.4)
	No	59,813 (57.9)	14,855 (60.3)	13,190 (59.0)	15,082 (55.2)	16,686 (57.6)
Avoiding meeting persons at high risk	Yes	61,173 (59.2)	14,402 (58.4)	12,339 (55.2)	17,405 (63.6)	17,028 (58.8)
	No	42,139 (40.8)	10,249 (41.6)	10,011 (44.8)	9,943 ()36.4	11,935 (41.2)

*Values are no. (%) of responses to questionnaires. JACSIS, Japan COVID-19 and Society Internet Survey (2020, 2021); JASTIS, Japan Society and New Tobacco Internet Survey (2021, 2022).

Table 2. Sociodemographic characteristics of participants in each survey in study of compliance trajectory and patterns of COVID-19 preventive measures, Japan, 2020–2022*

Characteristics	All responses	Surveys			
		JACSIS2020	JASTIS2021	JACSIS2021	JASTIS2022
No. responses	103,312	24,651	22,350	27,348	28,963
Sex					
M	51,540 (49.9)	12,422 (50.4)	11,467 (51.3)	13,473 (49.3)	14,179 (49.0)
F	51,772 (50.1)	12,229 (49.6)	10,882 (48.7)	13,875 (50.7)	14,784 (51.0)
Age, y					
20–29	15,650 (15.1)	3,323 (13.5)	2,816 (12.6)	3,544 (13.0)	5,967 (20.6)
30–39	15,158 (14.7)	3,794 (15.4)	3,208 (14.4)	4,165 (15.2)	3,990 (13.8)
40–49	20,151 (19.5)	4,954 (20.1)	4,467 (20.0)	5,446 (19.9)	5,284 (18.2)
50–59	17,928 (17.3)	4,283 (17.4)	4,245 (19.0)	4,794 ()17.5	4,606 (15.9)
60–69	18,033 (17.5)	4,290 (17.4)	4,185 (18.7)	4,844 (17.7)	4,715 (16.3)
70–79	16,392 (15.9)	4,007 (16.2)	3,429 (15.3)	4,555 (16.7)	4,401 (15.2)
Education					
Junior high school, high school	50,397 (48.8)	11,639 (47.2)	11,026 (49.4)	13,602 (49.7)	14,130 (48.8)
Vocational school, junior college	20,820 (20.2)	4,962 (20.1)	4,365 (19.5)	5,576 (20.4)	5,917 (20.4)
University, graduate school	31,341 (30.3)	7,908 (32.1)	6,887 (30.8)	7,930 (29.0)	8,617 (29.8)
Other	754 (0.7)	142 (0.6)	72 (0.3)	240 (0.9)	299 (1.0)
Equivalent income, million JPY					
<2.00	18,261 (17.7)	4,388 (17.8)	3,994 (17.9)	4,743 (17.3)	5,136 (17.7)
2.00–3.99	37,976 (36.8)	9,235 (37.5)	8,422 (37.7)	9,953 (36.4)	10,366 (35.8)
4.00–5.99	14,305 (13.8)	3,183 (12.9)	3,103 (13.9)	3,894 (14.2)	4,125 (14.2)
≥6.00	9,741 (9.4)	2,673 (10.8)	2,036 (9.1)	2,428 (8.9)	2,604 (9.0)
Not answered	23,029 (22.3)	5,172 (21.0)	4,795 (21.5)	6,330 (23.2)	6,732 (23.3)
Population density of residential prefecture					
High, top 20%	30,580 (29.6)	7,413 (30.1)	6,422 (28.7)	8,296 (30.3)	8,448 (29.2)
Low, <80%	72,732 (70.4)	17,238 (69.9)	15,928 (71.3)	19,052 (69.7)	20,515 (70.8)

*Values are no. (%) of responses to questionnaires. JACSIS, Japan COVID-19 and Society Internet Survey (2020, 2021); JASTIS, Japan Society and New Tobacco Internet Survey (2021, 2022); JPY, Japanese yen.

fluctuations. We reported the characteristics of participants who complied with each preventive behavior (Appendix Table 4) and estimated the associations among participant characteristics and each preventive behavior by using a multivariable regression model (Table 3; Appendix Tables 5–7). Compliance with most preventive behaviors did not significantly decrease among the survey waves, except for the surface sanitation and avoiding going out behaviors. Ventilation compliance decreased by 13.4% (95% CI −14.4% to −12.3%) for JASTIS (winter season). For all preventive behaviors, compliance was significantly higher among women than men. Older age, higher education, and higher income (i.e., incremental increases of each variable) were associated with greater compliance with most preventive behaviors. Compliance with COVID-19 preventive behaviors differed according to population density of residential prefectures; however, the direction of associations differed depending on the preventive behavior.

We determined that the number of latent classes was 4 according to the scree plot, distribution of class allocation, and interpretability (Appendix Figure 3). We evaluated the distribution of compliance with each preventive behavior for the 4 identified classes (Figure 2; Appendix Table 8). Class 1 was low compliance, which was characterized by lower than average compliance with all preventive behaviors. Class 2 was personal hygiene, which was characterized by higher than average compliance with personal hygiene measures, such as hand sanitation or respiratory hygiene, and lower than average compliance with the other measures. Class 3 was avoiding social contact, which was characterized by higher than average compliance with measures related to social contacts, such as avoiding travel or avoiding crowds, whereas compliance with other measures was similar to the overall average. Class 4 was comprehensive, which was characterized by higher than average compliance with all measures within the other classes. The percentage of persons in the low compliance class decreased over time, whereas the percentage in the personal hygiene class increased (Figure 3). We categorized the characteristics of the participants belonging to each latent class (Appendix Table 9). Using the multinomial logistic regression model, we estimated associations between participant characteristics and latent classes by determining percentage differences and odds ratios (Table 4, https://wwwnc.cdc.gov/EID/article/29/9/22-1754-T4.htm; Appendix Table 10). The percentage of persons in the low compliance class significantly decreased (−2.8% [95% CI −3.3% to −2.3%] per wave; p<0.001) with each survey wave, whereas those in the personal hygiene class significantly increased (2.6% [95% CI 2.1%–3.0%] per wave; p<0.001). Women were less likely to belong to the low

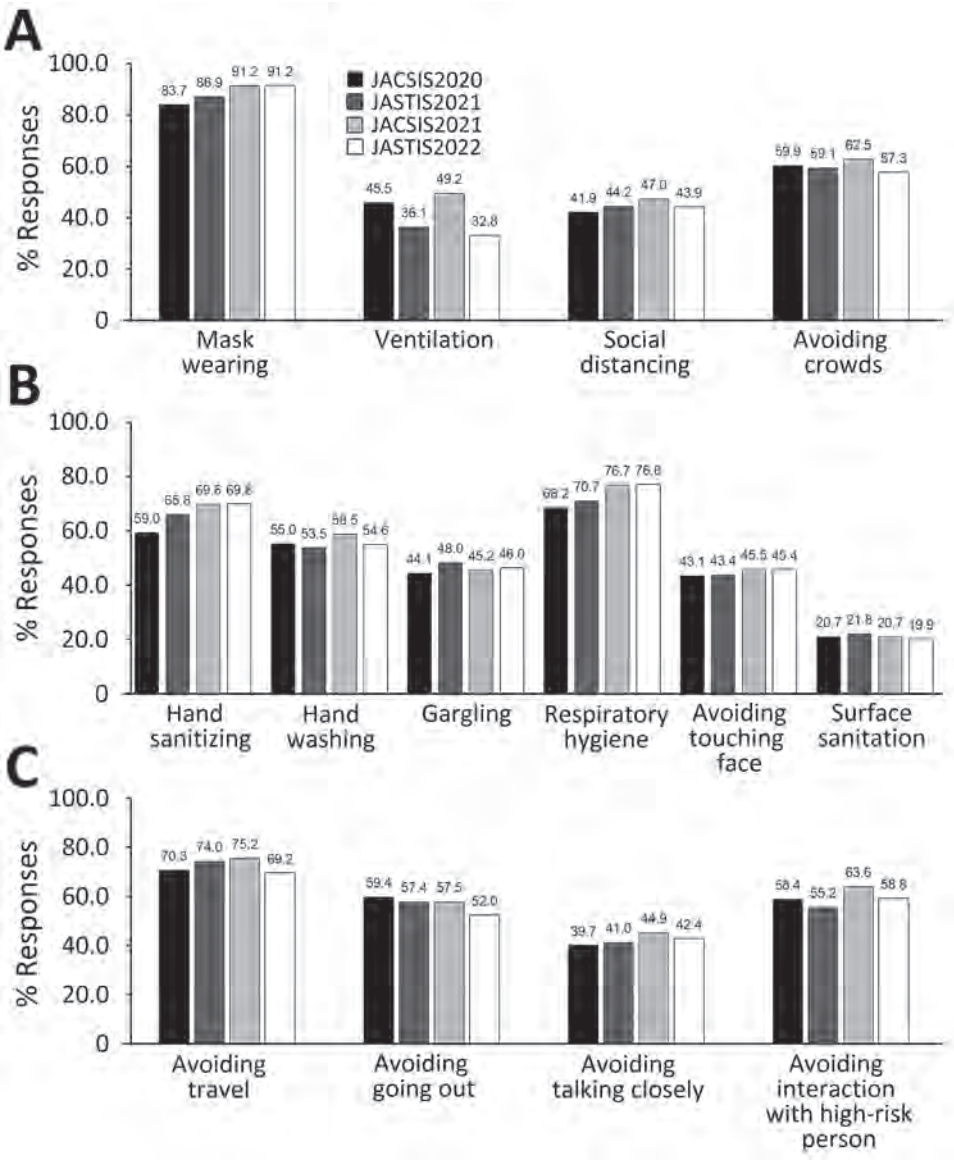

Figure 1. Transition of compliance with COVID-19 preventive behaviors over time in study of compliance trajectory and patterns of COVID-19 preventive measures, Japan, 2020–2022. Four surveys were conducted during August 25–September 30, 2020 (JACSIS2020); February 8–26, 2021 (JASTIS2021); September 27–October 29, 2021 (JACSIS2021); and February 1–28, 2022 (JASTIS2022). Percentages of responses from study participants indicate compliance with behaviors related to 3 behavioral areas: A) 3 Cs, a government of Japan campaign mandating the public to avoid closed spaces, crowded places, and close-contact settings to prevent COVID-19; B) personal hygiene; and C) avoiding social contact. Number of questionnaire responses was 103,312 from a total of 41,510 study participants. Values above bars indicate specific percentages. JACSIS, Japan COVID-19 and Society Internet Survey; JASTIS, Japan Society and New Tobacco Internet Survey.

compliance class than men (−15.8% [95% CI −17.0% to −14.7%]). Furthermore, younger participants tended to belong to the low compliance or personal hygiene class, whereas those who were older tended to be categorized into the avoiding social contact class. In addition, those with lower education tended to be allocated to the low compliance class; those with higher education tended to belong to the comprehensive class. Participants with lower income tended to be allocated to the low compliance or avoiding social contact class, whereas those with higher income tended to be categorized into the personal hygiene or comprehensive class. Participants who lived in highly populated prefectures were less likely to belong to the avoiding social contact class and more likely to be in the comprehensive class.

For participants who completed the 4 survey waves (n = 11,804), we used a Sankey diagram to compare patterns of the 4 latent classes among the 4 survey waves (Figure 4). Although most preventive behavior patterns were consistent, some changed among the 4 survey periods. We observed a large influx of participants into the personal hygiene class from the low compliance and avoiding social contact classes over time.

Discussion

Our results show that compliance with most COVID-19 preventive behaviors included in this study either increased or remained stable over the 4 survey waves; however, compliance with surface sanitation and avoiding going out behaviors decreased.

Compliance with ventilation substantially decreased during the winter seasons. Female sex, older age, higher education, and higher equivalent income were positively associated with compliance with most preventive behaviors. The percentage of persons in the low compliance class decreased over time and increased in the personal hygiene class, which could be partially attributed to the change in the overall pattern toward personal hygiene compliance.

Previous studies reported changes in compliance with COVID-19 preventive behaviors. A 1-year follow-up study conducted in the United States reported that compliance with mask wearing continuously increased from April 2020 to April 2021; however, compliance with physical distancing and reduced movement was stable or decreased slightly over time (*9*). Another study also reported that compliance with mask wearing increased over time, and compliance with physical distancing decreased (*10*). Similarly, our study showed increased compliance with mask wearing; however, although compliance with the avoiding going out behavior decreased, compliance with social distancing increased over time. This result could be because of changes in Japan's policy that relaxed social distancing rules and promoted travel and going out (*22*). Previous studies have mainly investigated changes in preventive behaviors related to COVID-19 prevention guidelines (e.g., mask wearing and physical distancing) within a relatively short period (<1 year). We studied changes in other preventive behaviors over a 2-year follow-up period, especially noting the seasonal fluctuation of compliance with ventilation and decreased compliance with surface sanitation, avoiding travel, and avoiding going out behaviors.

We showed that women, older and more educated participants, and those with higher income were highly compliant with most preventive behaviors. A previous study also reported that compliance with COVID-19 preventive behaviors was higher among women than men (*23*). Our study showed a large gap in compliance behaviors between men and women. Social desirability bias might have been responsible for those results because compliance was self-reported. However, a previous study suggested that higher self-reported compliance with preventive behaviors reflects actual compliance and is less affected by social desirability bias because of a participant's sex (*23*). The tendency of older adults to comply with preventive behaviors has also been reported (*24*). Furthermore, socioeconomic disparities have been reported to affect compliance with COVID-19 preventive behaviors, and persons with higher education or income were more compliant with those behaviors (*24*,*25*). Our results also showed that persons with higher education or income were more compliant

Table 3. Trends in associations between preventive behaviors and participant characteristics (n = 82,201 responses) in study of compliance trajectory and patterns of COVID-19 preventive measures, Japan, 2020–2022*

Preventive behavior	Per wave†	JASTIS‡	Women§	Older age¶	Higher education#	Higher equivalent income**	High population density††
Mask wearing	+	–	+ + +	+	NS	+	NS
Ventilation	NS	– – –	+ + +	+	+	NS	+
Social distancing	+	–	+ +	+	+	NS	+
Avoiding crowds	NS	–	+ + +	+	+	NS	+
Hand sanitation	+	NS	+ + +	NS	NS	+	NS
Hand washing	+	–	+ + +	NS	NS	+	NS
Gargling	NS	+	+ +	NS	+	NS	+ +
Respiratory hygiene	+	–	+ + +	NS	+	+	–
Avoiding touching face	+	NS	+ + +	+	+	+	+
Surface sanitation	–	+	+ +	–	NS	+	NS
Avoiding travel	NS	NS	+ + +	+	–	–	–
Avoiding going out	–	–	+ + +	+	+	–	–
Avoiding talking closely	+	–	+ +	+	+	NS	+
Avoiding high-risk person	+	–	+ + +	+	NS	NS	NS

*p value for trend was <0.05. +, 0%–5% difference; + +, >5%–10% difference; + + +, >10% difference; –, indicates >–5% to 0% difference; – –, indicates –10% to –5% difference; – – –, indicates <–10% difference. Differences were estimated by increments within each category. JACSIS, Japan COVID-19 and Society Internet Survey; JASTIS, Japan Society and New Tobacco Internet Survey; NS, not significant.
†Surveys were conducted in 4 waves: August 25–September 30, 2020 (JACSIS2020); February 8–26, 2021 (JASTIS2021); September 27–October 29, 2021 (JACSIS2021); and February 1–28, 2022 (JASTIS2022).
‡Referent was JACSIS.
§Referent was men.
¶Age was treated as a continuous variable (i.e., 20–29 y = 1, 30–39 y = 2, 40–49 y = 3, 50–59 y = 4, 60–69 = 5, 70–79 = 6); associations were estimated according to an incremental increase in age.
#Participants who answered as other for education were excluded. Education was treated as a continuous variable (i.e., junior high school, high school = 1, vocational school, junior college = 2, university, graduate school = 3); associations were estimated according to an incremental increase in education level.
**Participants who did not answer income question were excluded. Equivalent income (million yen) was treated as a continuous variable (i.e., <2.00 = 1, 2.00–3.99 = 2, 4.00–5.99 = 3, ≥6.00 = 4); associations were estimated according to an incremental increase in income.
††Top 20% of residential prefecture population density. Referent was low (<80%) density.

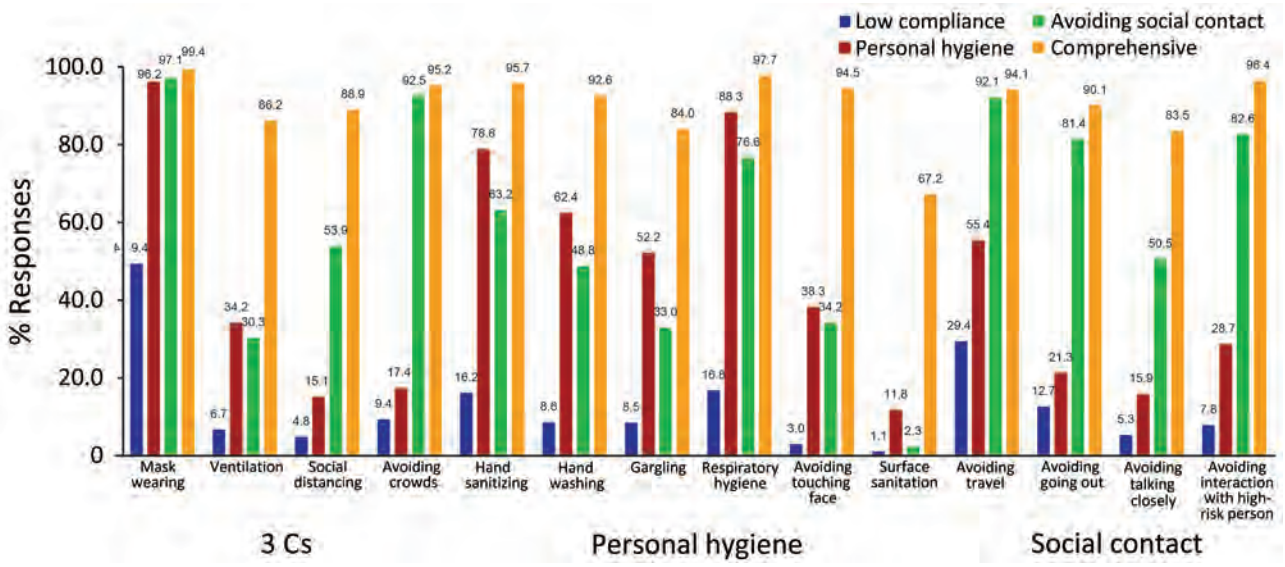

Figure 2. Compliance with each preventive behavior according to 4 latent classes in study of compliance trajectory and patterns of COVID-19 preventive measures, Japan, 2020–2022. Percentage of responses to questions regarding each behavior is shown; 3 Cs is a government of Japan campaign mandating the public to avoid closed spaces, crowded places, and close-contact settings to prevent COVID-19. Values above bars indicate specific percentages.

with all preventive behaviors except for avoiding travel and avoiding going out behaviors.

Our results revealed differences in compliance with COVID-19 preventive behaviors according to sociodemographic status, including sex, age, education, and income level. Although the government of Japan emphasized the importance of NPIs in preventing COVID-19 through various media sources, such important information might not have reached specific groups, including those with low socioeconomic status. The source of information related to COVID-19 affects preventive behavior compliance in Japan (*11*). For risk communications during a health crisis, the sociodemographic features of groups for which the government attempts to provide essential information should be considered (*26*). In addition, during the initial waves of the COVID-19 pandemic, a severe shortage of surgical and N95 masks existed even in clinical settings (*27*,*28*); therefore, low-income persons would have had difficulty preparing sufficient masks because of the mask shortage and increased cost from reselling. Although the government of Japan provided all citizens with 1 supply of cloth masks (*29*), the distribution and cost of surgical and N95 masks should have been controlled to increase affordability and availability for citizens.

To determine patterns of compliance with multiple preventive behaviors, we identified 4 latent classes on the basis of compliance with each of the 14 preventive behaviors. A previous cross-sectional study identified similar compliance patterns for COVID-19 prevention (*14*). Although that study only considered 6 preventive behaviors, the authors identified a group with low compliance and 1 with high compliance with all preventive behaviors. Moreover, similar to the findings in our study, participants in that study who were included in the low compliance group were predominantly younger, male, and less educated (*14*).

Our study results suggested that the percentage of persons in the low compliance class decreased over time, but the percentage of persons in the personal hygiene class increased. A study in the United Kingdom reported that compliance with COVID-19 prevention guidelines decreased slightly during 1 year (*30*). Although relaxation of mask-wearing rules for vaccinated persons occurred in other countries, including the United States (*31*), the government of Japan did not relax compliance with any preventive behaviors, except for traveling and going out (*22*). Therefore, compliance with the preventive behaviors showed a continuous increase over time in Japan. Moreover, we observed an increased percentage of persons in the personal hygiene class and an influx from the avoiding social contact class to the personal hygiene class. This influx also reflects relaxation of the avoiding social contact policy for COVID-19 prevention (*22*).

The first limitation of our study is possible information bias. Compliance with COVID-19 preventive behaviors was self-reported, and misclassification of responses might have affected our results to some extent. However, as previously described, self-reported

compliance is less affected by social desirability bias in both sexes (*23*). In addition, a study using an Internet survey reported that ≈50% of persons did not tell others about their actual compliance with COVID-19 preventive behaviors (*32*). The high level of anonymity of that survey method helped identify actual compliance with preventive behaviors. Therefore, our Internet survey also likely obtained more correct answers from participants than an interview-based survey. A future study using objective measurements for preventive behavior compliance, such as tracking mobile phones, might decrease potential information bias (*33*). The second limitation is selection bias. We recruited participants from the registry of an Internet survey company, and the distribution of characteristics was different from that of the general population in Japan. We calculated a sampling weight by using a representative sample of the population in Japan for analysis in this study; therefore, the representativeness of our results was improved. Furthermore, although some participants did not participate in all 4 survey waves, we could partially eliminate the bias caused by dropout by applying a sampling weight for all 4 waves.

COVID-19 prevention policies varied among nations (*34*), and the magnitude of associations among sociodemographic characteristics and preventive behavior compliance also differed among them (*24*). Therefore, caution should be exercised when generalizing the results of this study to countries outside of Japan.

In conclusion, we conducted a longitudinal follow-up study by using 4 multiple-panel surveys over a 2-year period and showed that compliance with most of the 14 NPI-related COVID-19 preventive behaviors increased or remained stable over time, except for surface sanitation and avoiding going out behaviors; compliance with ventilation decreased during the winter season. Moreover, latent class analysis suggested that compliance patterns changed; the number

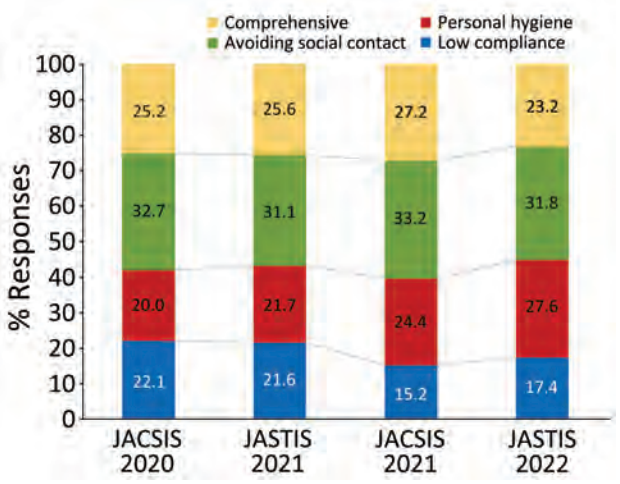

Figure 3. Percentage of persons belonging to each of 4 latent classes according to survey waves (n = 103,312 responses) in study of compliance trajectory and patterns of COVID-19 preventive measures, Japan, 2020–2022. Four surveys were conducted during August 25–September 30, 2020 (JACSIS2020); February 8–26, 2021 (JASTIS2021); September 27–October 29, 2021 (JACSIS2021); and February 1–28, 2022 (JASTIS2022). Values within bar sections indicate specific percentages. JACSIS, Japan COVID-19 and Society Internet Survey; JASTIS, Japan Society and New Tobacco Internet Survey.

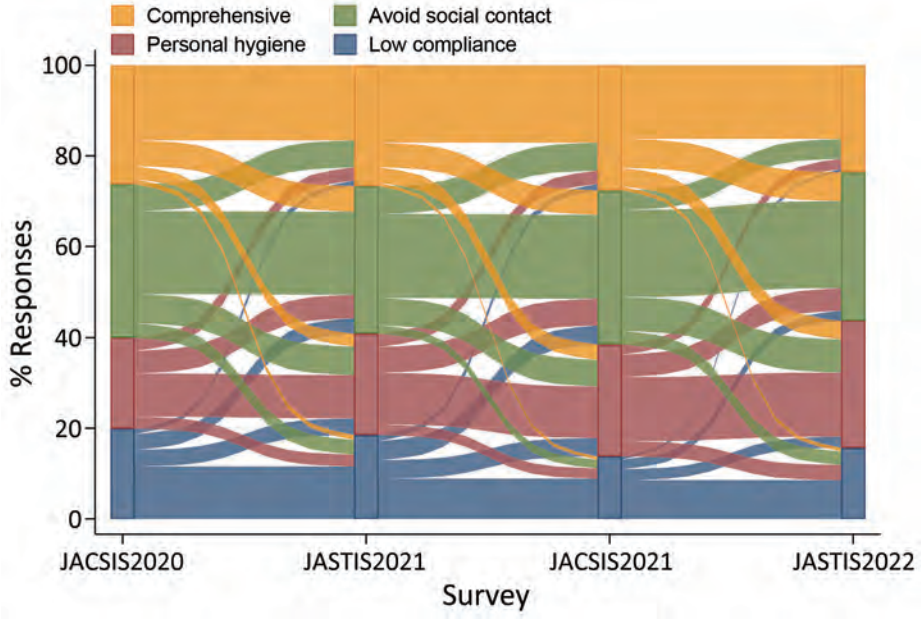

Figure 4. Compliance patterns for survey participants who responded to all 4 surveys waves (11,804 participants) in study of compliance trajectory and patterns of COVID-19 preventive measures, Japan, 2020–2022. Four surveys were conducted during August 25–September 30, 2020 (JACSIS2020); February 8–26, 2021 (JASTIS2021); September 27–October 29, 2021 (JACSIS2021); and February 1–28, 2022 (JASTIS2022). The Sankey plot shows compliance patterns of persons in 4 latent classes for each survey wave. JACSIS, Japan COVID-19 and Society Internet Survey; JASTIS, Japan Society and New Tobacco Internet Survey.

of persons in the low compliance class decreased over time, whereas the number of persons in the personal hygiene class increased. Overall, compliance with NPI-related COVID-19 preventive behaviors in Japan has increased, which can be partially attributed to changes in compliance patterns among persons. Changes in compliance with NPI-related preventive behaviors in Japan might be because persons prefer to comply with personal hygiene measures under the relaxed mobility restriction policy during the ongoing COVID-19 pandemic. From a public health perspective, policymakers should anticipate potential changes in preventive behavior patterns caused by new policy introduction to improve strategies for future prevention of COVID-19 and other public health threats.

This study was supported by the Japan Society for the Promotion of Science KAKENHI Grants (grant nos. 17H03589, 19K10671, 19K10446, 18H03107, 18H03062, 19H03860, and 21H04856) and Grant-in-Aid for Young Scientists (grant no. 19K19439); Research Support Program to Apply the Wisdom of the University to tackle COVID-19 Related Emergency Problems, University of Tsukuba, and Health Labor Sciences Research Grant (grant nos 19FA1005, 19FG2001, 19FA1012, and 21HA2016); and Japan Agency for Medical Research and Development (grant no. 2033648).

About the Author

Dr. Kusama is an epidemiologist at the Division of Statistics and Data Science, Liaison Center for Innovative Dentistry, Tohoku University Graduate School of Dentistry. His primary research interests focus on oral health and health-related behaviors.

References

1. Koelle K, Martin MA, Antia R, Lopman B, Dean NE. The changing epidemiology of SARS-CoV-2. Science. 2022;375:1116–21. https://doi.org/10.1126/science.abm4915
2. Huang C, Yang L, Pan J, Xu X, Peng R. Correlation between vaccine coverage and the COVID-19 pandemic throughout the world: based on real-world data. J Med Virol. 2022;94:2181–7. https://doi.org/10.1002/jmv.27609
3. Araf Y, Akter F, Tang Y-D, Fatemi R, Parvez MSA, Zheng C, et al. Omicron variant of SARS-CoV-2: genomics, transmissibility, and responses to current COVID-19 vaccines. J Med Virol. 2022;94:1825–32. https://doi.org/10.1002/jmv.27588
4. Feikin DR, Higdon MM, Abu-Raddad LJ, Andrews N, Araos R, Goldberg Y, et al. Duration of effectiveness of vaccines against SARS-CoV-2 infection and COVID-19 disease: results of a systematic review and meta-regression. Lancet. 2022;399:924–44. https://doi.org/10.1016/S0140-6736(22)00152-0
5. Chu DK, Akl EA, Duda S, Solo K, Yaacoub S, Schünemann HJ, et al.; COVID-19 Systematic Urgent Review Group Effort (SURGE) study authors. Physical distancing, face masks, and eye protection to prevent person-to-person transmission of SARS-CoV-2 and COVID-19: a systematic review and meta-analysis. Lancet. 2020;395:1973–87. https://doi.org/10.1016/S0140-6736(20)31142-9
6. Nair AN, Anand P, George A, Mondal N. A review of strategies and their effectiveness in reducing indoor airborne transmission and improving indoor air quality. Environ Res. 2022;213:113579. https://doi.org/10.1016/j.envres.2022.113579
7. Wang X, Pasco RF, Du Z, Petty M, Fox SJ, Galvani AP, et al. Impact of social distancing measures on coronavirus disease healthcare demand, central Texas, USA. Emerg Infect Dis. 2020;26:2361–9. https://doi.org/10.3201/eid2610.201702
8. Wright L, Fancourt D. Do predictors of adherence to pandemic guidelines change over time? A panel study of 22,000 UK adults during the COVID-19 pandemic. Prev Med. 2021;153:106713. https://doi.org/10.1016/j.ypmed.2021.106713
9. Levitt EE, Gohari MR, Syan SK, Belisario K, Gillard J, DeJesus J, et al. Public health guideline compliance and perceived government effectiveness during the COVID-19 pandemic in Canada: findings from a longitudinal cohort study. Lancet Reg Health Am. 2022;9:100185. https://doi.org/10.1016/j.lana.2022.100185
10. Petherick A, Goldszmidt R, Andrade EB, Furst R, Hale T, Pott A, et al. A worldwide assessment of changes in adherence to COVID-19 protective behaviours and hypothesized pandemic fatigue. Nat Hum Behav. 2021;5:1145–60. https://doi.org/10.1038/s41562-021-01181-x
11. Kusama T, Kiuchi S, Takeuchi K, Ikeda T, Nakazawa N, Kinugawa A, et al. Information usage and compliance with preventive behaviors for COVID-19: a longitudinal study with data from the JACSIS 2020/JASTIS 2021. Healthcare (Basel). 2022;10:521. https://doi.org/10.3390/healthcare10030521
12. Gonçalves J, da Silva PG, Reis L, Nascimento MSJ, Koritnik T, Paragi M, et al. Surface contamination with SARS-CoV-2: a systematic review. Sci Total Environ. 2021;798:149231. https://doi.org/10.1016/j.scitotenv.2021.149231
13. Tang JW, Bahnfleth WP, Bluyssen PM, Buonanno G, Jimenez JL, Kurnitski J, et al. Dismantling myths on the airborne transmission of severe acute respiratory syndrome coronavirus-2 (SARS-CoV-2). J Hosp Infect. 2021;110:89–96. https://doi.org/10.1016/j.jhin.2020.12.022
14. Wright L, Steptoe A, Fancourt D. Patterns of compliance with COVID-19 preventive behaviours: a latent class analysis of 20,000 UK adults. J Epidemiol Community Health. 2022;76:247–53. https://doi.org/10.1136/ jech-2021-216876
15. Tabuchi T, Shinozaki T, Kunugita N, Nakamura M, Tsuji I. Study profile: the Japan "Society and New Tobacco" Internet Survey (JASTIS): a longitudinal Internet cohort study of heat-not-burn tobacco products, electronic cigarettes, and conventional tobacco products in Japan. J Epidemiol. 2019;29:444–50. https://doi.org/10.2188/jea.JE20180116
16. The Government of Japan. Avoiding the three Cs: a key to preventing the spread of COVID-19 [cited 2021 Sep 8]. https://www.japan.go.jp/kizuna/2020/avoiding_the_three_cs.html
17. Naimi AI, Whitcomb BW. Estimating risk ratios and risk differences using regression. Am J Epidemiol. 2020;189:508–10. https://doi.org/10.1093/aje/kwaa044
18. Sinha P, Calfee CS, Delucchi KL. Practitioner's guide to latent class analysis: methodological considerations and common pitfalls. Crit Care Med. 2021;49:e63–79. https://doi.org/10.1097/CCM.0000000000004710

19. Smith MJ, Mansournia MA, Maringe C, Zivich PN, Cole SR, Leyrat C, et al. Introduction to computational causal inference using reproducible Stata, R, and Python code: a tutorial. Stat Med. 2022;41:407–32. https://doi.org/10.1002/sim.9234
20. Tabuchi T, Gallus S, Shinozaki T, Nakaya T, Kunugita N, Colwell B. Heat-not-burn tobacco product use in Japan: its prevalence, predictors and perceived symptoms from exposure to secondhand heat-not-burn tobacco aerosol. Tob Control. 2018;27:e25–33. https://doi.org/10.1136/tobaccocontrol-2017-053947
21. Hubbard AE, Ahern J, Fleischer NL, Van der Laan M, Lippman SA, Jewell N, et al. To GEE or not to GEE: comparing population average and mixed models for estimating the associations between neighborhood risk factors and health. Epidemiology. 2010;21:467–74. https://doi.org/10.1097/EDE.0b013e3181caeb90
22. Karako K, Song P, Chen Y, Tang W, Kokudo N. Overview of the characteristics of and responses to the three waves of COVID-19 in Japan during 2020–2021. Biosci Trends. 2021;15:1–8. https://doi.org/10.5582/bst.2021.01019
23. Galasso V, Pons V, Profeta P, Becher M, Brouard S, Foucault M. Gender differences in COVID-19 attitudes and behavior: panel evidence from eight countries. Proc Natl Acad Sci USA. 2020;117:27285–91. https://doi.org/10.1073/pnas.2012520117
24. Fujii R, Suzuki K, Niimi J. Public perceptions, individual characteristics, and preventive behaviors for COVID-19 in six countries: a cross-sectional study. Environ Health Prev Med. 2021;26:29. https://doi.org/10.1186/s12199-021-00952-2
25. Lee GB, Jung SJ, Yiyi Y, Yang JW, Thang HM, Kim HC. Socioeconomic inequality in compliance with precautions and health behavior changes during the COVID-19 outbreak: an analysis of the Korean Community Health Survey 2020. Epidemiol Health. 2022;44:e2022013. https://doi.org/10.4178/epih.e2022013
26. Kusama T, Aida J, Tsuboya T, Sugiyama K, Yamamoto T, Igarashi A, et al. The association between socioeconomic status and reactions to radiation exposure: a cross-sectional study after the Fukushima Daiichi nuclear power station accident. PLoS One. 2018;13:e0205531. https://doi.org/10.1371/journal.pone.0205531
27. Oda J, Muguruma T, Matsuyama S, Tanabe S, Nishimura T, Sugawara Y, et al. JAAM nationwide survey on the response to the first wave of COVID-19 in Japan. Part II: how did medical institutions overcome the first wave and how should they prepare for the future? Acute Med Surg. 2020;7:e592. https://doi.org/10.1002/ams2.592
28. Umazume T, Miyagi E, Haruyama Y, Kobashi G, Saito S, Hayakawa S, et al. Survey on the use of personal protective equipment and COVID-19 testing of pregnant women in Japan. J Obstet Gynaecol Res. 2020;46:1933–9. https://doi.org/10.1111/jog.14382
29. Wright J. Overcoming political distrust: the role of 'self-restraint' in Japan's public health response to COVID-19. Japan Forum. 2021;33:453–75. https://doi.org/10.1080/09555803.2021.1986565
30. Wright L, Steptoe A, Fancourt D. Trajectories of compliance with COVID-19 related guidelines: longitudinal analyses of 50,000 UK adults. Ann Behav Med. 2022;56:781–90. https://doi.org/10.1093/abm/kaac023
31. Tanne JH. Covid-19: CDC relaxes rules on mask wearing. BMJ. 2022;376:o524. https://doi.org/10.1136/bmj.o524
32. Levy AG, Thorpe A, Scherer LD, Scherer AM, Drews FA, Butler JM, et al. Misrepresentation and nonadherence regarding COVID-19 public health measures. JAMA Netw Open. 2022;5:e2235837. https://doi.org/10.1001/jamanetworkopen.2022.35837
33. Mendolia S, Stavrunova O, Yerokhin O. Determinants of the community mobility during the COVID-19 epidemic: the role of government regulations and information. J Econ Behav Organ. 2021;184:199–231. https://doi.org/10.1016/j.jebo.2021.01.023
34. Li Y, Campbell H, Kulkarni D, Harpur A, Nundy M, Wang X, et al.; Usher Network for COVID-19 Evidence Reviews (UNCOVER) group. The temporal association of introducing and lifting non-pharmaceutical interventions with the time-varying reproduction number (R) of SARS-CoV-2: a modelling study across 131 countries. Lancet Infect Dis. 2021;21:193–202. https://doi.org/10.1016/S1473-3099(20)30785-4

Address for correspondence: Kenji Takeuchi, Department of International and Community Oral Health, Tohoku University Graduate School of Dentistry, 4-1 Seiryo-machi, Aoba-ku, Sendai, Miyagi 980-8575, Japan; email: kenji.takeuchi.c4@tohoku.ac.jp

COVID-19 Epidemiology during Delta Variant Dominance Period in 45 High-Income Countries, 2020–2021

Christine J. Atherstone, Sarah Anne J. Guagliardo, Anthony Hawksworth, Kevin O'Laughlin, Kimberly Wong, Michelle L. Sloan, Olga Henao, Carol Y. Rao, Peter D. McElroy, Sarah D. Bennett

The SARS-CoV-2 Delta variant, first identified in October 2020, quickly became the dominant variant worldwide. We used publicly available data to explore the relationship between illness and death (peak case rates, death rates, case-fatality rates) and selected predictors (percentage vaccinated, percentage of the population >65 years, population density, testing volume, index of mitigation policies) in 45 high-income countries during the Delta wave using rank-order correlation and ordinal regression. During the Delta-dominant period, most countries reported higher peak case rates (57%) and lower peak case-fatality rates (98%). Higher vaccination coverage was protective against peak case rates (odds ratio 0.95, 95% CI 0.91–0.99) and against peak death rates (odds ratio 0.96, 95% CI 0.91–0.99). Vaccination coverage was vital to preventing infection and death from COVID-19 during the Delta wave. As new variants emerge, public health authorities should encourage the uptake of COVID-19 vaccination and boosters.

The Delta variant of SARS-CoV-2, first identified in India in October 2020 (*1*), became the dominant variant in ≥130 countries worldwide during June–November 2021 (*2*). Global vaccination coverage during that time remained low; <50% of the world's population had received ≥1 dose and <25% had completed a primary vaccination series (*3*). Despite the increased transmissibility of Delta compared with previous variants, countries experienced varying levels of illness and death (*4*).

With each new wave of COVID-19, governments' responses varied depending on the understanding of SARS-CoV-2, variant characteristics, and societal factors such as healthcare system capacity, vaccination coverage, and the public's willingness to follow public health mitigation measures. Policies ranged from flattening the curve (i.e., slowing down infection rates to alleviate pressure on healthcare systems) to zero-COVID policies that aimed to completely prevent infections in the community (*5*–*7*).

As the COVID-19 pandemic continues and new variants emerge (*8*), governments are working to identify and implement a combination of effective yet socially and economically acceptable measures. For example, previous works showed the effectiveness of nonpharmaceutical interventions (e.g., remote work, mask-wearing in indoor public spaces) in reducing case rates and death rates (*9*–*11*). In addition, 1 study showed that fewer deaths were reported in countries with earlier and more stringent mitigation policies, such as business closures, restrictions on public gatherings, and stay-at-home orders (*12*). Some countries employing zero-COVID policies experienced rising cases and deaths during the initial Omicron period and beyond (*13*). The benefits and social acceptability of prolonged lockdowns and mass testing policies to prevent new cases and deaths remain unclear (*14*).

We aimed to describe the epidemiology during the pre-Delta and Delta wave periods of the COVID-19 pandemic among high-income countries (HICs) and characterize the relationship between public health policies and epidemiologic burden. Specifically, we assessed the degree to which key measures of illness and death (case rate, death rate, and case-fatality rate) were correlated with vaccination coverage, testing volume, mitigation stringency, population density, and demographics.

Author affiliation: Centers for Disease Control and Prevention, Atlanta, Georgia, USA

DOI: https://doi.org/10.3201/eid2909.230142

Methods

Inclusion Criteria

We restricted our analysis to HICs because more accessible testing in those countries likely provides a more accurate assessment of the case and death burdens (*15*,*16*). We included HICs that reported ≥200 SARS-CoV-2 sequences during the full period of interest (April 1, 2020–November 30, 2021) and ≥20 Delta sequences in the first month of Delta dominance. The cutoff of 200 sequences was chosen to ensure adequate reflection of variant burden. In August 2021, the World Health Organization (WHO) recommended a minimum of 15 specimens per week (*1*); 200 sequences would provide >3 months' worth of data. We chose 20 Delta sequences as a minimum to prevent the overrepresentation of a few sequences during weeks that had slower reporting. We defined Delta dominance as the time during which ≥50% of sequenced samples were Delta.

Data Sources

We obtained data for this study from 4 publicly available sources. First, we used World Bank country income classifications for 2020 (*17*) to select HICs. This classification is updated annually on July 1 on the basis of the gross national income per capita data from the previous calendar year. Second, information about when the Delta variant became dominant in each country was gleaned from SARS-CoV-2 genomic sequences published in the GISAID (*18*) and GenBank (*19*) databases. Last, we used Our World in Data (OWID) (*15*,*20*) to obtain data on confirmed cases, deaths, percentage of the population fully vaccinated, percentage of the population >65 years of age, population density, SARS-CoV-2 testing volume, and stringency (a composite index of 9 mitigation policies and strategies). OWID compiles data from Johns Hopkins University, World Bank, national government reports, and Oxford University. Data were reported daily (confirmed cases and deaths, stringency index), every weekday (vaccinations), weekly (testing), or annually (population >65 years of age, population density) during the period of interest.

Data Management

We downloaded sequence data from GISAID and GenBank, aggregated at the country-level, and removed duplicate sequences that were in both databases. Then, for each country, we calculated the weekly proportions of Delta variant sequences during the period of interest, April 1, 2020–November 30, 2021.

To enable easy comparisons between the periods before and after the emergence of the Delta variant, we defined the Delta dominance date as the Monday of the first week in which ≥50% of sequenced samples were Delta. We defined the pre-Delta period as April 1, 2020, to the Delta dominance date and the Delta dominance period as the Delta dominance date through November 30, 2021.

Outcome and Predictor Variables

We used measures of illness and death as outcomes. For the pre-Delta and Delta dominance periods, we calculated the peak 7-day rolling averages for case

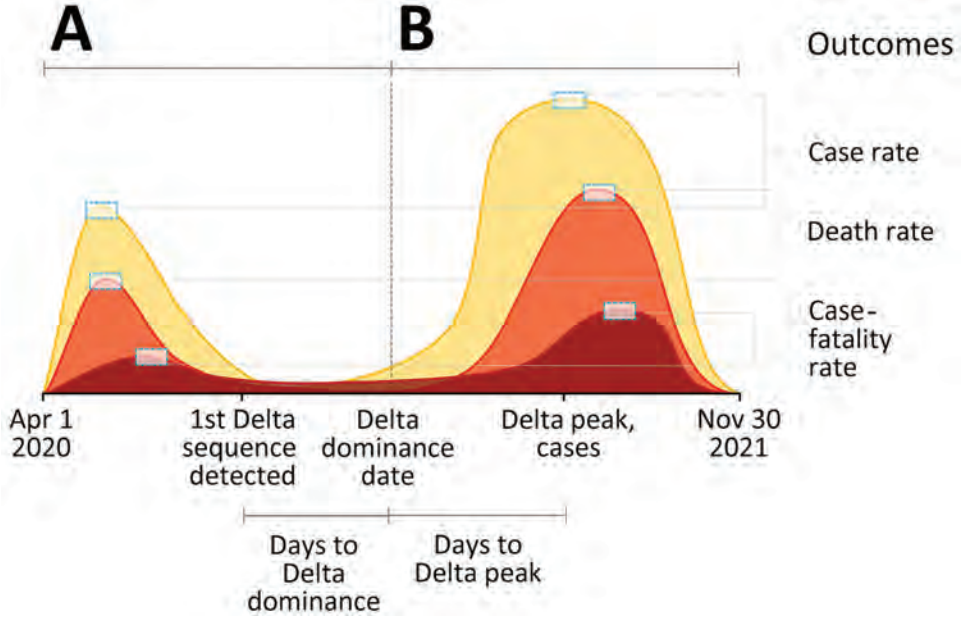

Figure 1. Example of COVID-19 outcomes during pre-Delta variant (A) and Delta dominance (B) periods. Ratio of Delta-dominant period to pre-Delta period is shown for peak case rate, peak death rate, and peak case-fatality rate.

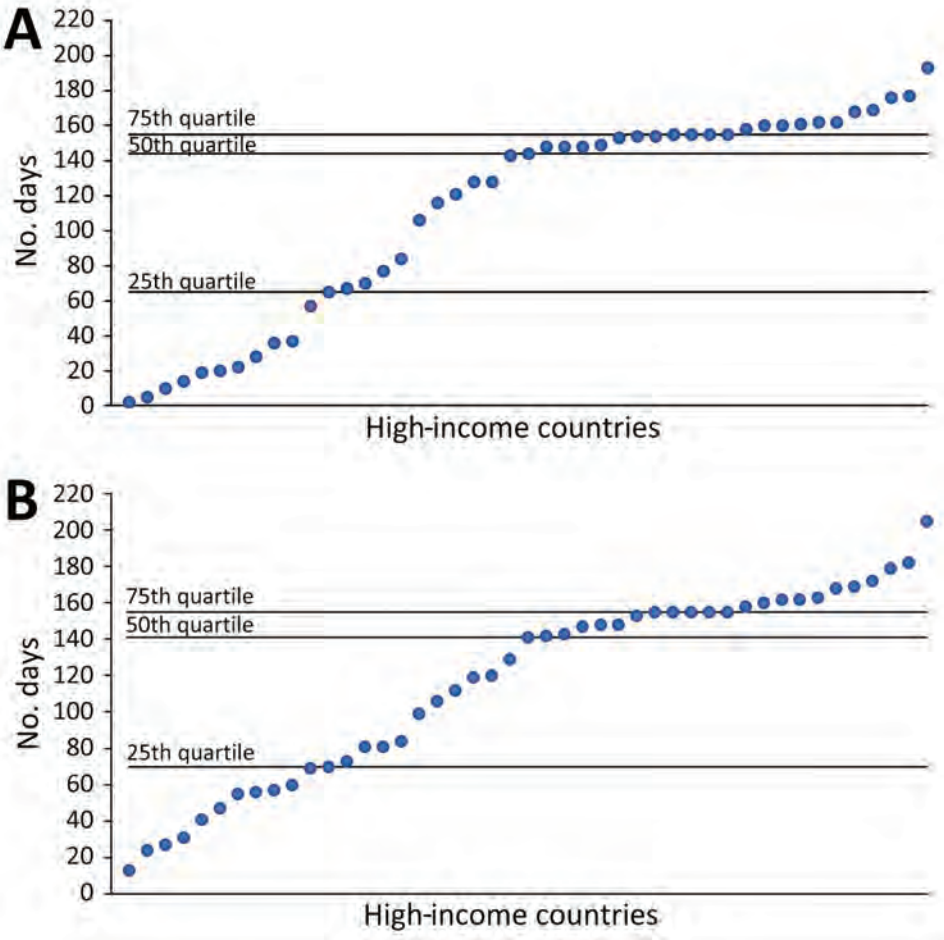

Figure 2. Number of days from SARS-CoV-2 Delta variant dominance to peak case rates (A) and peak death rates (B) in 45 high-income countries, December 2020–November 2021. Each dot represents an individual high-income country. The Delta dominance date for each country was defined as the Monday of the first week in which ≥50% of sequenced samples in GISAID (https://www.gisaid.org) were Delta.

rates, death rates, and case-fatality rates (CFRs) per million persons. We chose the 7-day peak rolling average to indicate the intensity of the outbreak while also minimizing the effect of bulk data uploads. CFRs used a 14-day lag between daily new cases and daily new deaths (*21*) and was calculated as a ratio of reported deaths to reported cases. Death rates and CFRs offer different types of information about deaths: death rates account for the probability of death in an entire population, whereas CFRs only measure the probability of death among those with the disease. Adherence to case and death reporting might vary by country. To standardize outcomes across countries, we calculated a Delta dominance to pre-Delta ratio (DD:PD) for each outcome. We calculated 3 outcomes of interest as a 7-day rolling average: peak case rate DD:PD, peak death rate DD:PD, and peak CFR DD:PD.

We classified outcome variables into quartiles to enable easier interpretation and statistical evaluation of small datasets. For example, the outcome variable peak case rate DD:PD predictor variables included the percent of the total population fully vaccinated with a primary series at the date of Delta dominance, the percentage of the population >65 years of age, and population density (persons/km^2). We also included the median 7-day rolling average daily testing volume DD:PD (comparing the period of Delta predominance to the pre-Delta period, as described). Last, we calculated the median stringency index DD:PD. The stringency index, as defined by other scholars (*22*), ranges from 0–100 (100 = strictest) and increases over time if more stringent mitigation policies are implemented or decreases if policies are rescinded (*23*).

Statistical Analysis

We managed and analyzed data using SPSS Statistics 1.0.0.1406 (IBM Corp., https://www.ibm.com) and RStudio 1.4.1717 (PBC, https://posit.co/blog/rstudio-pbc). To characterize the speed at which Delta supplanted previous variants, we calculated the number of days from the date of the first Delta sequence collection to the date of Delta dominance and from the start of Delta dominance to peak case and death rates (Figure 1). We calculated descriptive statistics (range, mean, median, peak, quartiles) for all

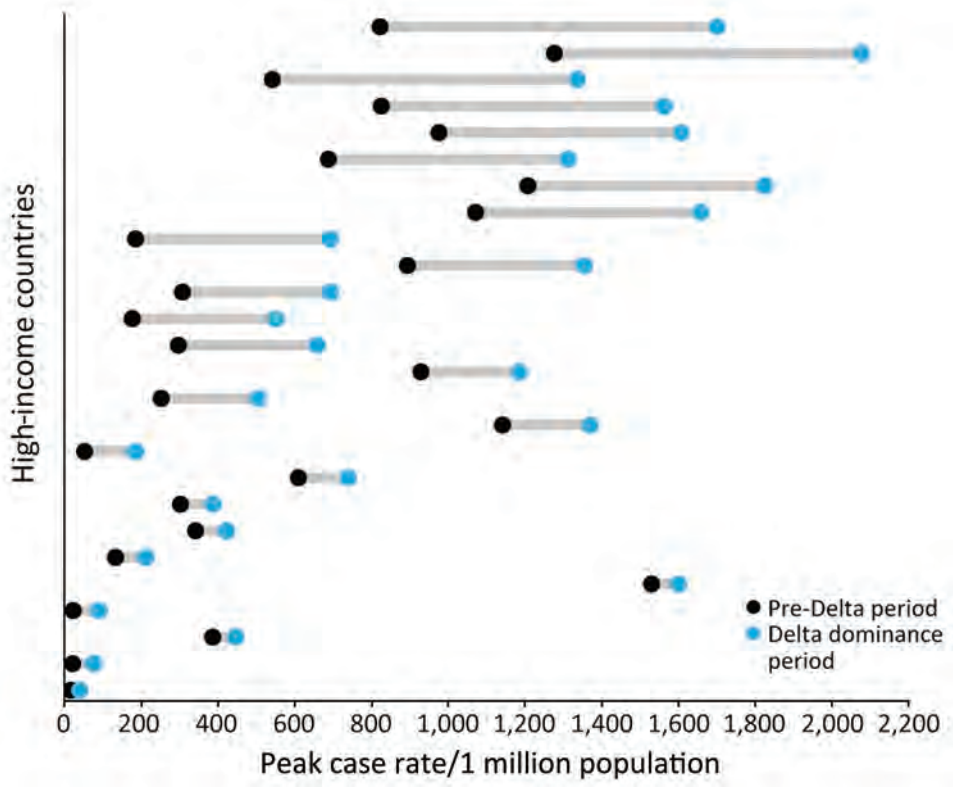

Figure 3. Countries with increased peak COVID-19 case rates during Delta dominance period compared with pre-Delta period in study of COVID-19 epidemiology in 45 high-income countries, December 2020–November 2021. Each data line represents 1 country (n = 26 countries).

measures of illness and death and predictor variables during the pre-Delta and Delta dominance periods.

We used Spearman rank-order correlation to assess the strength and direction of the association between quartile outcomes with predictor variables. For bivariate correlations with p values <0.25, we further assessed relationships between outcomes and predictors in multivariable ordinal regression models. Each of the outcomes were modeled separately. We explored all possible combinations of predictor variables meeting the above criteria and selected the model with the lowest Akaike Information Criterion score as the best model. We evaluated multicollinearity among the predictor variables using a Condition Index cutoff of <15. This activity was reviewed by Centers for Disease Control and Prevention and conducted consistent

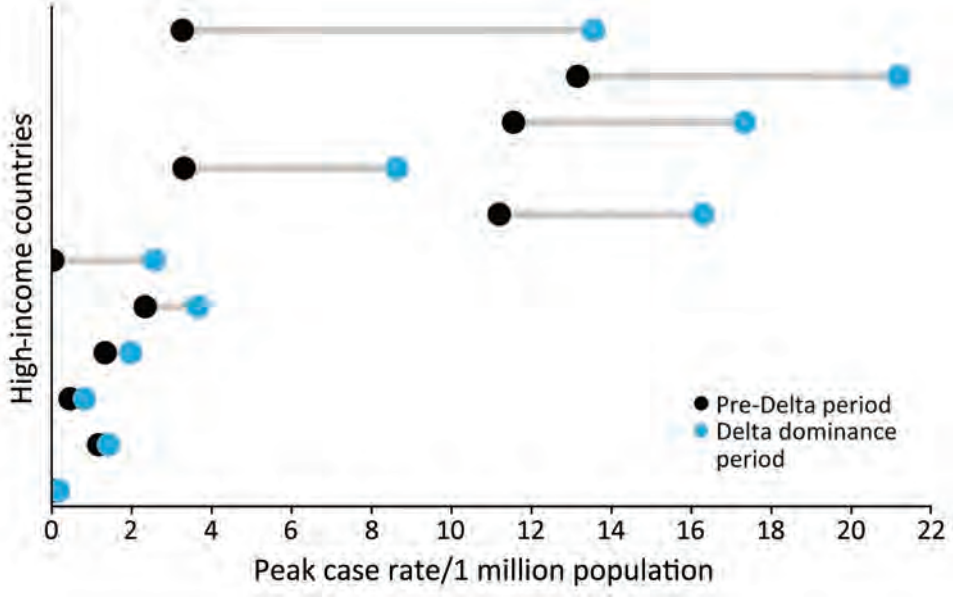

Figure 4. Countries with increased peak COVID-19 death rates during Delta dominance period compared with pre-Delta period in study of COVID-19 epidemiology in 45 high-income countries, December 2020–November 2021. Each data line represents 1 country (n = 11 countries).

Table 1. Descriptive statistics for COVID-19 outcomes and predictor variables in Delta dominance period and pre-Delta period for 45 high-income countries, December 2020–November 2021*

Outcome variables: peak rate ratios†	Min	Mean	Median	Peak	IQR
Cases	0.06	1.4	1.2	4.2	0.65–1.91
Deaths	0.05	2.9	0.49	99	0.25–0.93
CFR	0.00	0.21	0.08	2.3	0.02–0.27
Predictor variables					
% Vaccination coverage‡	1.0	32	31	72	24–37
% Population >65 y of age	1.1	16	18	27	14–20
Population density, persons/km^2	3.2	544	123	7,916	36–237
Median stringency index†	0.5	0.86	0.78	3.5	0.67–0.90
Median daily testing volume†	0.6	2.3	1.7	19.2	1.2–2.4

*CFR, case-fatality rate; IQR, interquartile range.
†Delta dominance (DD) period to pre-Delta period ratio.
‡Indicates persons with primary vaccine series at date of Delta predominance.

with applicable federal law and CDC policy (see, e.g., 45 C.F.R. part 46.102(l) (2), 21 C.F.R. part 56; 42 U.S.C. §241(d); 5 U.S.C. §552a; 44 U.S.C. §3501 et seq.).

Results

Descriptive Analysis

Among 79 HICs, 45 met the inclusion criteria. The first Delta sequence collection dates ranged from December 28, 2020, to July 26, 2021; more than half (n = 25, 55%) of the countries reported a Delta sequence by the end of March 2021. The median time between the first Delta sequence collected to the start of the Delta dominance period was 77 days (interquartile range [IQR] 49–140). The median time from the start of the Delta dominance period to the peak case rates was 144 (IQR 65–155) days and to the peak death rate was 141 (IQR 70–155) days (Figure 2). Weekly case incidence during the Delta dominance period varied by country and WHO region (Appendix Figure, https://wwwnc.cdc.gov/EID/article/29/9/23-0142-App1.pdf). Average peak case rates ranged from 180 in the WHO Western Pacific region to 1,699 in the African region.

Most countries (57%, n = 26) reported higher peak case rates (Figure 3) but lower peak CFRs (98%, n = 44) and peak death rates (75%, n = 34) (Figure 4) during the Delta dominance period than during the pre-Delta period. Ten (22%) countries reported both higher peak case rates and death rates during the Delta dominance period than during the pre-Delta period.

Vaccination coverage with a primary series at the start date of Delta dominance ranged from 1% to 72% in 44 of 45 countries for which data were available (Table 1). The percentage of the population >65 years of age averaged 15.7% (IQR 13.9%–19.5%) in 44 countries for which data were available. Most countries (84%, n = 38) had a lower stringency index during the Delta dominance period than during the pre-Delta period.

Peak Case Rate DD:PD Ratio

Higher vaccination coverage was protective against higher case rates; that is, vaccination resulted in lower peak case rate DD:PD ratios (Spearman rank correlation coefficient [ρ] = −0.36; p = 0.018) (Table 2). The same association was held in the ordinal regression model (odds ratio [OR] 0.95, 95% CI 0.91–0.99; p = 0.01) (Tables 3, 4). There was a positive correlation between median daily testing volume and peak case rate DD:PD ratios (Spearman ρ = 0.30; p = 0.048) (Table 2), although that relationship did not hold in the ordinal regression models (Table 4).

Peak Death Rate DD:PD Ratio

A higher percentage of the population being persons >65 years of age was protective against death rates (peak death rate DD:PD ratios), both in bivariate

Table 2. Spearman rank-order correlations in study of COVID-19 epidemiology in Delta variant dominance period in 45 high-income countries, December 2020–November 2021*

	Peak Rate Ratio†					
	Cases		Deaths		CFR	
Predictor variables	ρ	p value	ρ	p value	ρ	p value
% Vaccination coverage‡	−0.36	**0.018**	−0.21	0.17	−0.09	0.58
% Population >65 y of age	0.04	0.82	−0.31	**0.039**	−0.48	**0.001**
Population density, persons/km^2	−0.05	0.75	−0.12	0.45	0.05	0.76
Median stringency index†	0.04	0.78	0.07	0.63	−0.14	0.35
Median daily testing volume†	0.30	**0.048**	0.24	0.12	0.18	0.24

*Bold indicates statistical significance (p<0.05). CFR, case-fatality rate; ρ, Spearman rank correlation coefficient.
†Delta dominance period to pre-Delta period ratio.
‡Indicates persons with primary series at date of Delta predominance.

Table 3. Ordinal regression results in study of COVID-19 epidemiology in Delta variant dominance period in 45 high-income countries, December 2020–November 2021*

Model	Peak rate ratio outcome†	Predictor variable	OR (95% CI)	p value
1	Cases	% Vaccination coverage‡	0.95 (0.91–0.99)	**0.014**
2	Deaths	% Vaccination coverage‡	0.96 (0.92–0.99)§	**0.025**
		% Population >65 y of age	0.88 (0.78–0.98)§	**0.021**
3	CFR	% Population >65 y of age	0.89 (0.80–0.98)	**0.013**

*Bold indicates statistical significance (p<0.05). CFR, case-fatality rate; OR, odds ratio.
†Delta dominance (DD) period: pre-Delta (PD) period ratio.
‡Indicates persons with primary series at date of Delta predominance.
§Values shown are adjusted OR (95% CI).

comparisons (Spearman ρ = −0.31; p = 0.039) (Table 2) and in the regression models (OR 0.88, 95% CI 0.78–0.98; p = 0.02). In addition, higher vaccination coverage was associated with lower peak death rate DD:PD ratios (OR 0.96, 95% CI 0.92–0.99; p = 0.03) in the regression models.

Peak CFR DD:PD Ratio

A higher percentage of the population being persons >65 years of age was associated with lower CFRs (lower peak CFR DD:PD ratios, Spearman ρ = −0.48; p = 0.001) (Table 2). This association held in the ordinal regression model (OR 0.89, 95% CI 0.80–0.98; p = 0.01).

Discussion

Most HICs had higher case rates but lower death rates and CFRs during the Delta dominance period than in their pre-Delta periods. Achieving higher vaccination coverage appeared to be the main public health measure associated with a decrease in the intensity (peak) of COVID-19 cases and deaths. Each quartile increase in vaccination coverage resulted in a 5% reduction in peak case rates and a 4% reduction in peak death rates. Countries with a larger percentage of persons >65 years of age had lower death rates and CFRs during the Delta dominance period, likely because of focused early vaccination activities in this age group and case management protocols prioritizing older populations for close observation and hospital admission (*24*,*25*).

Many HICs recorded increased case rates during the Delta dominance period, but those increases did not often result in higher death rates than for the pre-Delta period. Previous studies reported mixed results on death rates during the period of Delta variant prevalence; 2 studies reported no differences in mortality rates (*26*) or in-hospital deaths (*27*), and 3 studies indicated an increase in mortality rates (*28*; A. Kumar et. Al, unpub. Data, https://www.medrxiv.org/content/10.1101/2021.09.23.21263948v1) and in-hospital deaths (R.S. Khedar et al., unpub. Data, https://www.medrxiv.org/content/10.1101/2021.09.03.21263091v1). The lower death rates and CFRs among HICs in this study may be the result of advances in therapeutics, improvements in case management protocols, increased natural immunity from previous infection, and the availability of vaccines, rather than decreased virulence of the Delta variant virus (*29*–*31*). Among global studies from HICs, the early prioritization of vaccination in the elderly and achievement of high coverage appeared to protect older adults against death during the Delta dominance period. Studies have shown that, during the Delta wave, vaccines were less effective against infection (*32*,*33*; R.S. Barlow et al., unpub. data, https://www.medrxiv.org/content/10.1101/2021.08.30.21262446v1) but highly protective against symptomatic disease (*29*,*33*), hospitalization (*34*), and death (*33*). This lack of protection against infection among vaccinated persons, combined with the increased transmissibility of the Delta variant, likely contributed to an overall higher case burden during the Delta predominance period in HICs. Nevertheless, despite Delta's high transmissibility, peak case and death rates occurred in many countries >4 months after the date of

Table 4. Heat map of bivariate analyses and ordinal regression model results in study of COVID-19 epidemiology in Delta variant dominance period in 45 high-income countries, December 2020–November 2021*

	Peak rate ratio†					
	Bivariate analysis			Ordinal regression results		
Predictor variables	Cases	Deaths	CFR	Cases	Deaths	CFR
% Vaccination coverage‡†						
% population >65 y of age						
Population density, persons/km^2						
Median stringency index†						
Median daily testing volume†						

*Blue shading indicates negative (protective) association, yellow shading indicates positive association, and no shading indicates no significant association. CFR, case-fatality rate.
†Delta dominance (DD) period: pre-Delta (PD) period ratio.
‡Indicates persons with primary series at date of Delta predominance.

Delta's dominance, which would have allowed time for strategies such as vaccination to be implemented and have an effect (*35*).

The first limitation of this study is that we used publicly available datasets, which might be affected by fluctuations in reporting, including reporting of at-home testing. Death rates might not be a robust indicator of severity in HICs. Hospitalization data might have provided another measure of illness severity, but OWID hospitalization data were available for <50% of countries included in the study and had many reporting gaps. The goal of this study was to identify population-level associations between COVID-19 illness and death and disease control metrics; a priori testing of more specific hypotheses might be addressed in other assessments using different study designs (e.g., a community-wide, cluster-randomized trial that evaluated masking in Bangladesh [*36*]). This analysis was ecologic in nature, and therefore population-level associations might not apply at the individual level. We also focused on the outcomes of peak cases, deaths, and CFRs and therefore did not capture the total burden of cases and deaths. Finally, the variety of COVID-19 vaccines available and changing recommendations on the number of doses for maximal effectiveness make it difficult to generalize the findings associated with vaccination coverage to all COVID-19 variants and coverage effectiveness over time.

In conclusion, this characterization of epidemiologic outcomes in high-income countries during the Delta dominance period shows that many countries reported higher case rates but lower death and case fatality rates compared to the pre-Delta period; higher vaccination coverage and completion of a primary vaccination series were associated with lower case and death rates; and >4 months elapsed between Delta introduction and peaks in case rates and death rates, which might have allowed time for mitigation strategies such as vaccination to be implemented and have an impact. These findings might be useful in informing public health authorities of the importance of achieving high vaccination coverage as the pandemic continues to evolve. The ability to continue implementing measures to combat COVID-19 might be limited by authorities' willingness to implement stronger measures and the willingness of the public to comply. However, across multiple HICs, our findings consistently indicate that higher vaccination coverage can result in fewer cases and deaths.

Acknowledgments

We thank Barbara Marston, Zachary Myles, David Shih, and Xinjian Zhang for their contributions to this research.

About the Author

Dr. Atherstone is an epidemiologist with broad experience in zoonotic infectious disease surveillance, outbreak response, and research in the United States and sub-Saharan Africa. She has expertise working in multiple countries, alongside dozens of partners, in remote, difficult conditions implementing complex investigations.

References

1. World Health Organization. Tracking SARS-CoV-2 variants [cited 2022 Jan 26]. https://www.who.int/en/activities/tracking-SARS-CoV-2-variants
2. GISAID. Tracking of hCoV-19 variants. 2020 [cited 2022 Jan 26]. https://www.gisaid.org/hcov19-variants
3. World Health Organization. COVID-19 vaccination data. 2022 [cited 2022 Jan 26]. https://covid19.who.int/who-data/vaccination-data.csv
4. Our World in Data. COVID-19 data explorer [cited 2022 Jan 26]. https://ourworldindata.org/explorers/coronavirus-data-explorer
5. New Zealand Ministry of Health. COVID-19 community response framework. 2022 [cited 2022 Apr 14]. https://www.health.govt.nz/covid-19-novel-coronavirus/covid-19-response-planning/covid-19-community-response-framework
6. Soo Z, Fung A. Hong Kong orders mandatory COVID-19 tests for all residents. Associated Press. 2022 Feb 22 [cited 2022 Apr 14]. https://apnews.com/article/coronavirus-pandemic-health-hong-kong-4bb8dd1225887f-06f5a0d981a4b52505
7. Chen J-M, Chen Y-Q. China can prepare to end its zero-COVID policy. Nat Med. 2022;28:1104–5. https://doi.org/10.1038/s41591-022-01794-3
8. World Health Organization. Statement on Omicron sublineage BA.2. 2022 Feb 22 [cited 2022 Apr 13]. https://www.who.int/news/item/22-02-2022-statement-on-omicron-sublineage-ba.2
9. Pan A, Liu L, Wang C, Guo H, Hao X, Wang Q, et al. Association of public health interventions with the epidemiology of the COVID-19 outbreak in Wuhan, China. JAMA. 2020;323:1915–23. https://doi.org/10.1001/jama.2020.6130
10. Dehning J, Zierenberg J, Spitzner FP, Wibral M, Neto JP, Wilczek M, et al. Inferring change points in the spread of COVID-19 reveals the effectiveness of interventions. Science. 2020;369:eabb9789. https://doi.org/10.1126/science.abb9789
11. Medline A, Hayes L, Valdez K, Hayashi A, Vahedi F, Capell W, et al. Evaluating the impact of stay-at-home orders on the time to reach the peak burden of Covid-19 cases and deaths: does timing matter? BMC Public Health. 2020;20:1750. https://doi.org/10.1186/s12889-020-09817-9
12. Fuller JA, Hakim A, Victory KR, Date K, Lynch M, Dahl B, et al.; CDC COVID-19 Response Team. Mitigation policies and COVID-19–associated mortality—37 European countries, January 23–June 30, 2020. MMWR Morb Mortal Wkly Rep. 2021;70:58–62. https://doi.org/10.15585/mmwr.mm7002e4
13. Smith DJ, Hakim AJ, Leung GM, Xu W, Schluter WW, Novak RT, et al. COVID-19 mortality and vaccine coverage—Hong Kong Special Administrative Region, China, January 6, 2022–March 21, 2022. China CDC Wkly. 2022;4:288–92. https://doi.org/10.46234/ccdcw2022.071
14. Talic S, Shah S, Wild H, Gasevic D, Maharaj A, Ademi Z, et al. Effectiveness of public health measures in reducing the

incidence of covid-19, SARS-CoV-2 transmission, and covid-19 mortality: systematic review and meta-analysis. BMJ. 2021;375:e068302. https://doi.org/10.1136/bmj-2021-068302
15. Hasell J, Mathieu E, Beltekian D, Macdonald B, Giattino C, Ortiz-Ospina E, et al. A cross-country database of COVID-19 testing. Sci Data. 2020;7:345.
16. Ohlsen EC, Hawksworth AW, Wong K, Guagliardo SAJ, Fuller JA, Sloan ML, et al. Determining gaps in publicly shared SARS-CoV-2 genomic surveillance data by analysis of global submissions. Emerg Infect Dis. 2022;28:S85–92. https://doi.org/10.3201/eid2813.220780
17. The World Bank. World Bank country and lending groups [cited 2021 Nov 30]. https://datahelpdesk.worldbank.org/knowledgebase/articles/906519-world-bank-country-and-lending-groups
18. Elbe S, Buckland-Merrett G. Data, disease and diplomacy: GISAID's innovative contribution to global health. Glob Chall. 2017;1:33–46.
19. Clark K, Karsch-Mizrachi I, Lipman DJ, Ostell J, Sayers EW. GenBank. Nucleic Acids Res. 2016;44(D1):D67–72. https://doi.org/10.1093/nar/gkv1276
20. Mathieu E, Ritchie H, Ortiz-Ospina E, Roser M, Hasell J, Appel C, et al. A global database of COVID-19 vaccinations. Nat Hum Behav. 2021;5:947–53.
21. Baud D, Qi X, Nielsen-Saines K, Musso D, Pomar L, Favre G. Real estimates of mortality following COVID-19 infection. Lancet Infect Dis. 2020;20:773.
22. Hale T, Angrist N, Goldszmidt R, Kira B, Petherick A, Phillips T, et al. A global panel database of pandemic policies (Oxford COVID-19 Government Response Tracker). Nat Hum Behav. 2021;5:529–38. https://doi.org/10.1038/s41562-021-01079-8
23. Blavatnik School of Government. Coronavirus government response tracker [cited 2021 Dec 7]. https://www.bsg.ox.ac.uk/research/research-projects/coronavirus-government-response-tracker
24. Ministry of Health and Family Welfare, Government of India. Clinical guidance for management of adult COVID-19 patients [cited 2022 May 30]. https://www.mohfw.gov.in/pdf/ClinicalGuidanceforManagementofAdultCOVID19Patientsupdatedason05thjan2023.pdf
25. World Health Organization. COVID-19 clinical management: living guidance. 2021 Jan 25 [cited 2022 May 30]. https://apps.who.int/iris/handle/10665/338882
26. Christensen PA, Olsen RJ, Long SW, Subedi S, Davis JJ, Hodjat P, et al. Delta variants of SARS-CoV-2 cause significantly increased vaccine breakthrough COVID-19 cases in Houston, Texas. Am J Pathol. 2022;192:320–331.
27. Taylor CA, Patel K, Pham H, Whitaker M, Anglin O, Kambhampati AK, et al.; COVID-NET Surveillance Team. Severity of disease among adults hospitalized with laboratory-confirmed COVID-19 before and during the period of SARS-CoV-2 B. 1.617. 2 (Delta) predominance—COVID-NET, 14 states, January–August 2021. MMWR Morb Mortal Wkly Rep. 2021;70:1513–9. https://doi.org/10.15585/mmwr.mm7043e1
28. Fisman DN, Tuite AR. Evaluation of the relative virulence of novel SARS-CoV-2 variants: a retrospective cohort study in Ontario, Canada. CMAJ. 2021;193:E1619–25. https://doi.org/10.1503/cmaj.211248
29. Bernal JL, Andrews N, Gower C, Gallagher E, Simmons R, Thelwall S, et al. Effectiveness of COVID-19 vaccines against the B. 1.617. 2 (Delta) variant. N Engl J Med. 2021;385:585–94.
30. Johnson AG. COVID-19 incidence and death rates among unvaccinated and fully vaccinated adults with and without booster doses during periods of Delta and Omicron variant emergence—25 US jurisdictions, April 4–December 25, 2021. MMWR Morb Mortal Wkly Rep. 2022;71:132–8.
31. Saban M, Myers V, Wilf-Miron R. Changes in infectivity, severity and vaccine effectiveness against Delta COVID-19 variant ten months into the vaccination program: the Israeli case. Prev Med. 2022;154:106890. https://doi.org/10.1016/j.ypmed.2021.106890
32. Sheikh A, McMenamin J, Taylor B, Robertson C; Public Health Scotland and the EAVE II Collaborators. SARS-CoV-2 Delta VOC in Scotland: demographics, risk of hospital admission, and vaccine effectiveness. Lancet. 2021;397:2461–2. https://doi.org/10.1016/S0140-6736(21)01358-1
33. Ng OT, Koh V, Chiew CJ, Marimuthu K, Thevasagayam NM, Mak TM, et al. Impact of Delta variant and vaccination on SARS-CoV-2 secondary attack rate among household close contacts. Lancet Reg Health West Pac. 2021;17:100299. https://doi.org/10.1016/j.lanwpc.2021.100299
34. Grannis SJ, Rowley EA, Ong TC, Stenehjem E, Klein NP, DeSilva MB, et al.; VISION Network. Interim estimates of COVID-19 vaccine effectiveness against COVID-19–associated emergency department or urgent care clinic encounters and hospitalizations among adults during SARS-CoV-2 B. 1.617. 2 (Delta) variant predominance—nine states, June–August 2021. MMWR Morb Mortal Wkly Rep. 2021;70:1291–3. https://doi.org/10.15585/mmwr.mm7037e2
35. Li H, Wang L, Zhang M, Lu Y, Wang W. Effects of vaccination and non-pharmaceutical interventions and their lag times on the COVID-19 pandemic: comparison of eight countries. PLoS Negl Trop Dis. 2022;16:e0010101. https://doi.org/10.1371/journal.pntd.0010101
36. Abaluck J, Kwong LH, Styczynski A, Haque A, Kabir MA, Bates-Jefferys E, et al. Impact of community masking on COVID-19: a cluster-randomized trial in Bangladesh. Science. 2022;375:eabi9069. https://doi.org/10.1126/science.abi9069

Address for correspondence: Christine Atherstone, Centers for Disease Control and Prevention, 1600 Clifton Rd NE, Mailstop H24-12, Atlanta, GA 30329-4027, USA; email: qdw2@cdc.gov

Temporally Associated Invasive Pneumococcal Disease and SARS-CoV-2 Infection, Alaska, USA, 2020–2021

Katherine Newell, Marc Fischer, Stephanie Massey, Laurie Orell, Jonathan Steinberg, Megan Tompkins, Louisa Castrodale, Joseph McLaughlin

Streptococcus pneumoniae can co-infect persons who have viral respiratory tract infections. However, research on *S. pneumoniae* infections that are temporally associated with SARS-CoV-2 infections is limited. We described the epidemiology and clinical course of patients who had invasive pneumococcal disease (IPD) and temporally associated SARS-CoV-2 infections in Alaska, USA, during January 1, 2020–December 23, 2021. Of 271 patients who had laboratory-confirmed IPD, 55 (20%) had a positive SARS-CoV-2 test result. We observed no major differences in age, race, sex, or underlying medical conditions among IPD patients with and without SARS-CoV-2. However, a larger proportion of IPD patients with SARS-CoV-2 died (16%, n = 9) than for those with IPD alone (4%, n = 9) (p<0.01). IPD patients with SARS-CoV-2 were also more likely to be experiencing homelessness (adjusted OR 3.5; 95% CI 1.7–7.5). Our study highlights the risk for dual infection and ongoing benefits of pneumococcal and COVID-19 vaccination, especially among vulnerable populations.

Invasive pneumococcal disease (IPD) occurs when *Streptococcus pneumoniae* infects a normally sterile site, such as blood or cerebrospinal fluid. Viral respiratory tract infections caused by rhinovirus, respiratory syncytial virus, and influenza virus are known to predispose patients to secondary bacterial infections, including IPD (*1*,*2*). Bacterial infections in patients who have viral respiratory tract infections also have been associated with greater disease severity and increased mortality rates (*3*–*7*).

Despite the widespread global circulation of SARS-CoV-2, a limited number of studies have examined IPD and SARS-CoV-2 co-infections. A meta-analysis of case series reported that only 4% of patients who had COVID-19 had a bacterial co-infection and 14% had a bacterial secondary infection (*8*); no predominant bacterial pathogen was reported. Those bacterial infections occurred mainly among patients in intensive care units. Based on previous studies, only a small proportion of SARS-CoV-2 infections are accompanied by IPD (*9*,*10*); however, outcomes of such cases might be more severe (*11*). A recent national cohort study in England reported that, although substantial nationwide decreases were observed in IPD incidence during the COVID-19 pandemic, persons who had IPD and SARS-CoV-2 co-infections had higher case-fatality rates than did patients who had IPD alone, particularly among older adults (*12*).

In the United States, Alaska has consistently had among the highest IPD rates in recent years, and a disproportionate burden occurs among Alaska Native persons (*13*–*16*). However, the possible interactions between IPD and SARS-CoV-2 infections are unclear. We evaluated and compared the epidemiology and clinical course of patients with IPD with and without temporally associated SARS-CoV-2 infection in Alaska during 2020–2021.

Methods

Data Sources

The Alaska Division of Public Health and the US Centers for Disease Control and Prevention Arctic Investigations Program maintain statewide laboratory-based

Author affiliations: Centers for Disease Control and Prevention, Atlanta, Georgia, USA (K. Newell, M. Fisher, L. Orell, J. Steinberg); Alaska Division of Public Health, Anchorage, Alaska, USA (K. Newell, S. Massey, M. Tompkins, L. Castrodale, J. McLaughlin)

DOI: https://doi.org/10.3201/eid2909.230080

surveillance for invasive disease caused by *S. pneumoniae*. Data are collected regarding patient demographic characteristics, clinical syndrome, pneumococcal vaccination, and illness outcomes through medical records. We included patients with IPD in Alaska during January 1, 2020–December 23, 2021. SARS-CoV-2 infection status was determined from nucleic acid amplification test and antigen test results reported to the Alaska Division of Public Health. COVID-19 testing procedures were based on State of Alaska COVID-19 guidance, including testing all symptomatic persons, as well as any asymptomatic person at admission to a healthcare facility. We linked cases by unique patient identifiers. We excluded patients with IPD who had no SARS-CoV-2 testing performed within 30 days before or after their positive *S. pneumoniae* culture. COVID-19 vaccination status was assigned through linkage with the immunization information system of Alaska.

Definitions

We defined a case of IPD as *S. pneumoniae* isolated from or bacterial DNA detected in a normally sterile site, including blood, cerebrospinal fluid, pleural fluid, peritoneal fluid, pericardial fluid, joint fluid, bone, or deep tissue, in an Alaska resident. We defined temporally associated SARS-CoV-2 infection as a positive SARS-CoV-2 test result detected on a respiratory specimen collected within 30 days before or after the specimen collection date of the *S. pneumoniae* culture or positive DNA test result. We defined underlying medical conditions as those conditions specified at the time of IPD reporting that are established risk factors for IPD, including chronic lung disease, cardiovascular disease, immunosuppression, alcoholism, chronic renal disease, current smoking, or diabetes (*17*). We defined patients as being fully vaccinated against COVID-19 if they had received the second dose of the Pfizer-BioNTech (https://www.pfizer.com) or Moderna (https://www.modernatx.com) mRNA vaccines or 1 dose of the J&J/Janssen (https://www.jnj.com) vaccine ≥14 days before *S. pneumoniae* detection. We assigned COVID-19 vaccination status only to IPD patients who were eligible for COVID-19 vaccination at the time of IPD detection, based on the initial COVID-19 vaccine introduction schedule of Alaska. Pneumococcal vaccination was having received ≥1 dose of 13-valent pneumococcal conjugate vaccine (PCV13) or 23-valent pneumococcal polysaccharide vaccine (PPSV23) ≥14 days before *S. pneumoniae* detection. We defined IPD serotype groups as *S. pneumoniae* serotypes contained in PCV13 plus serotype 6C, those contained in PPSV23 but not in PCV13, and nonvaccine and unknown serotypes.

Statistical Analysis

We compared demographic, epidemiologic, and clinical characteristics of IPD patients with and without a temporally associated SARS-CoV-2 infection. We used χ^2 or Fisher exact tests for categorical variables. We performed multivariable logistic regression to identify risk factors for IPD and temporally associated SARS-CoV-2 infection among all patients with IPD. We included known risk factors associated with SARS-CoV-2 infection and retained those that resulted in the best fit models selected by the Akaike Information Criteria through backward stepwise selection. We used R version 4.1.1 (https://www.R-project.org) for all statistical analyses. This activity was reviewed by CDC and was conducted consistent with applicable federal law and CDC policy (see, e.g., 45 C.F.R. part 46.102(l)(2), 21 C.F.R. part 56; 42 U.S.C. §241(d); 5 U.S.C. §552a; 44 U.S.C. §3501 et seq.).

Results

During January 2020–December 2021, we identified 330 IPD case-patients. Of those persons, 59 (18%) had no SARS-CoV-2 testing performed within 30 days before or after IPD specimen collection date and were thus excluded from the analysis. Of the excluded persons, 38 (64%) did not undergo SARS-CoV-2 testing because of having a positive culture for *S. pneumoniae* before COVID-19 testing was initiated in Alaska in March 2020. Other persons might have obtained a positive test result for COVID-19 within the previous 90 days; per testing guidance, these persons were exempted from further testing.

Of the remaining 271 IPD case-patients, 55 (20%) had a temporally associated SARS-CoV-2 infection (Figure). Of those 55 patients, 49 (89%) had a positive SARS-CoV-2 test result on a specimen collected within 30 days before or on the same day as specimen collection for *S. pneumoniae* detection (Table 1). Only 6 patients had a positive SARS-CoV-2 test result on a specimen collected after their positive test for *S. pneumoniae.* All IPD patients who died and had a temporally associated SARS-CoV-2 infection (n = 9) had SARS-CoV-2 detected before or concurrent with their IPD; no deaths occurred among patients who had SARS-CoV-2 detected >24 hours after a positive test result for *S. pneumoniae*.

Seven (3%) IPD cases were reported among patients <20 years of age (Table 2), including 1 patient who had a temporally associated SARS-CoV-2 infection (detected 9 days before IPD). The remaining 264 (97%) patients who had IPD were adults ≥20 years of age (median age 52 years, range 20–88 years); 54 had a temporally associated SARS-CoV-2 infection.

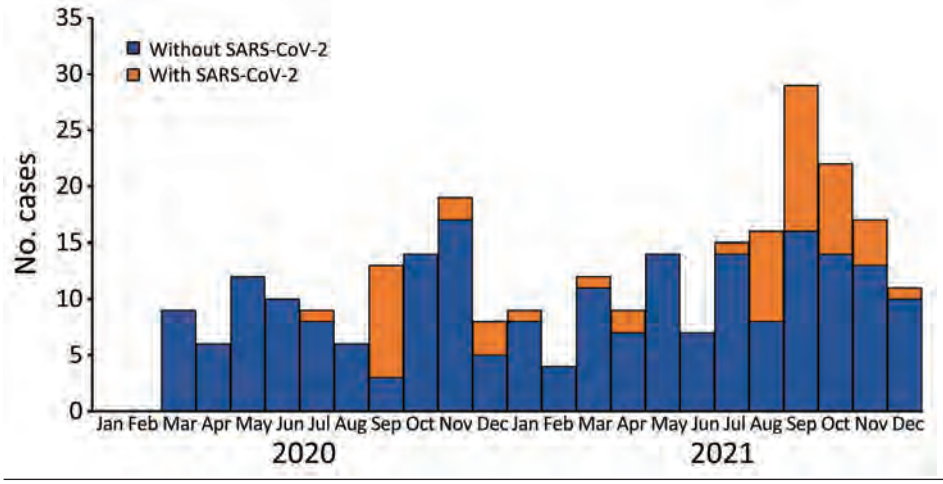

Figure. Epidemic curve for invasive pneumococcal disease case-patients with and without temporally associated SARS-CoV-2 infections, by month invasive pneumococcal disease specimen was collected, Alaska, USA, 2020–2021.

No major differences in sex, age, race, region, or underlying medical conditions were reported among IPD patients with and without temporally associated SARS-CoV-2 infection (Table 2). A total of 19 (35%) of 55 patients who had IPD and temporally associated SARS-CoV-2 infections were persons experiencing homelessness, compared with 39 (18%) of 216 patients with IPD alone (p = 0.01). IPD cases with temporally associated SARS-CoV-2 infection were more likely to occur during July–September 2021, the period when COVID-19 hospitalizations peaked in Alaska (Table 2) (*18*).

Patients who had IPD and temporally associated SARS-CoV-2 infection were more likely to show a clinical syndrome of pneumonia defined in the patient's medical records, but we found no differences in rates of hospitalization between patients with or without temporally associated SARS-CoV-2 infection. Among 55 IPD patients who had temporally associated SARS-CoV-2 infection, 9 (16%) died, compared with 9 (4%) of 216 patients who had IPD alone (p<0.01).

Of 271 patients who had IPD, 133 (49%) had received ≥1 dose of pneumococcal vaccine; no difference was reported in pneumococcal vaccination coverage rates between patients with or without temporally associated SARS-CoV-2 infection. Of 139 patients who had IPD and were eligible for COVID-19 vaccination, only 52 (37%) had completed a COVID-19 vaccine primary series. No difference in COVID-19 vaccination rates was reported between patients with or without temporally associated SARS-CoV-2 infection.

Overall, 30 (55%) of the IPD cases among patients who had SARS-CoV-2 infections were caused by *S. pneumoniae* serotypes contained in the PCV13 vaccine, compared with 167 (63%) of the IPD cases in patients without SARS-CoV-2 infection (Table 3). Serotype 4 was the most common cause of IPD among both groups, including 44% (24/55) of IPD cases with SARS-CoV-2 infection and 56% (120/216) of IPD cases without SARS-CoV-2. In contrast, a higher proportion of patients who had temporally associated SARS-CoV-2 infection had IPD attributable to a serotype contained in PPSV23 but not PCV13 or a serotype that is not in either vaccine. Multivariable analysis showed that, among patients who had IPD, persons experiencing homelessness were more likely to have a temporally associated SARS-CoV-2 infection than persons not experiencing homelessness (adjusted odds ratio 3.5, 95% CI 1.7–7.5) (Table 4).

Discussion

We found that, among 271 patients who had laboratory confirmed IPD, 55 (20%) also had a temporally associated SARS-CoV-2 infection. For most of those patients, SARS-CoV-2 infection was detected before or concurrent with IPD. This finding is similar to what has been observed for other viral infections, such as influenza viruses, rhinoviruses, and adenoviruses (*19*–*22*). The mechanism through which SARS-CoV-2

Table 1. Timing of SARS-CoV-2 detection in patients who had IPD and temporally associated SARS-CoV-2 infection, Alaska, USA, 2020–2021*

Timing of SARS-CoV-2 detection†	Nonfatal cases, no. (%), n = 46	Fatal cases, no. (%), n = 9
1–30 d before IPD	21 (46)	6 (66)
Same day as IPD	19 (41)	3 (33)
1–30 d after IPD	6 (13)	0

*IPD, invasive pneumococcal disease.
†Difference between dates of specimen collection.

infection might predispose a person to IPD is unclear. However, as for other viral infections, the cause is likely multifactorial, including epithelial damage, changes in airway function, upregulation and exposure of receptors, inhibited immune response, or enhancement of inflammation (*23*–*26*).

We found that IPD patients who died were more likely to have a temporally associated SARS-CoV-2 infection. All patients who died and had IPD and a temporally associated SARS-CoV-2 infection also had their infection detected either before or concurrently with the IPD. This finding suggests secondary

Table 2. Characteristics of patients who had IPD temporally associated with a SARS-CoV-2 infection, compared with patients who had IPD alone, Alaska, USA, 2020–2021*

Characteristic	IPD patients with SARS-CoV-2 infection, no. (%), n = 55	IPD patients without SARS-CoV-2 infection, no. (%), n = 216	p value†
Sex			0.29
M	31 (56)	141 (65)	
F	24 (44)	75 (35)	
Age, y			0.90
<20	1 (2)	6 (3)	
20–39	12 (22)	57 (26)	
40–59	25 (46)	93 (43)	
≥60	17 (31)	60 (28)	
Race			0.98
Alaska Native/American Indian	29 (53)	117 (54)	
White	16 (30)	62 (29)	
Other/unknown	10 (18)	37 (17)	
Region			0.70
Anchorage	28 (51)	111 (51)	
Interior	7 (13)	31 (14)	
Gulf	4 (7)	16 (7)	
Matanuska-Susitna	5 (9)	15 (7)	
Northern	2 (4)	20 (9)	
Southeast	2 (4)	7(3)	
Southwest	7 (13)	16 (7)	
Underlying medical condition			1.0
≥1	44 (80)	175 (81)	
None	11 (20)	41 (19)	
Seasonality			<0.01
Summer, June–August	10 (18)	54 (25)	
Fall, September–December	37 (67)	76 (35)	
Winter, December–February	5 (9)	27 (13)	
Spring, March–May	3 (6)	59 (27)	
Person experiencing homelessness			0.01
Yes	19 (34)	39 (18)	
No	36 (66)	177 (82)	
Pneumococcal vaccine received			0.80
PCV13	5 (9)	26 (12)	
PPSV23	17 (31)	70 (32)	
Both	2 (4)	13 (6)	
Neither	31 (56)	107 (50)	
COVID-19 vaccine received			0.09
Fully vaccinated	9 (16)	43 (20)	
Not fully vaccinated	28 (51)	59 (27)	
Not eligible‡	18 (33)	114 (53)	
Clinical syndrome§			<0.01
Pneumonia	46 (84)	155 (72)	
Bacteremia without source	9 (16)	43 (20)	
Other	2 (4)	49 (23)	
Hospitalized			0.26
Yes	49 (89)	179 (83)	
No/unknown	6 (11)	37 (17)	
Died			<0.01
Yes	9 (16)	9 (4)	
No	46 (84)	196 (91)	
Unknown	0	11 (5)	

*IPD, invasive pneumococcal disease; PCV13, 13-valent pneumococcal conjugate vaccine; PPSV23, 23-valent pneumococcal polysaccharide vaccine.
†By χ^2 test.
‡Not eligible for COVID-19 vaccination at the time of IPD detection based on Alaska's initial COVID-19 vaccine introduction schedule. Not included in $\chi 2$ calculation.
§Clinical syndromes are not mutually exclusive.

Table 3. *Streptococcus pneumoniae* serotype by vaccine type among patients who had IPD temporally associated with SARS-CoV-2 infection or IPD alone, Alaska, USA, 2020–2021*

S. pneumoniae serotype by vaccine type	IPD patients with SARS-CoV-2 infection, no. (%), n = 55	IPD patients without SARS-CoV-2 infection, no. (%), n = 216
PCV13 + 6C†	30 (55)	137 (63)
PPSV23, non-PCV13‡	18 (33)	50 (23)
Nonvaccine type	6 (11)	9 (4)
Unknown	1 (2)	20 (9)

*IPD, invasive pneumococcal disease; PCV13, 13-valent pneumococcal conjugate vaccine; PPSV23, 23-valent pneumococcal polysaccharide vaccine.
†Serotypes contained in PCV13 (i.e., 1, 3, 4, 5, 6A, 6B, 7F, 9V, 14, 18C, 19A, 19F, 23F) plus serotype 6C.
‡Serotypes contained in PPSV23 but not in PCV13 (i.e., 2, 8, 9N, 10A, 11A, 12F, 15B, 17F, 20, 22F, 33F).

bacterial infection as a possible complicating factor for death. All deceased patients with a SARS-CoV-2 infection had COVID-19 listed as a cause of death. However, because of a lack of detailed clinical data and similar clinical manifestations of both diseases, we were unable to determine how IPD, SARS-CoV-2 infection, or a combination of both contributed to the patients' deaths.

Among all reported patients who had IPD, persons experiencing homelessness were more likely to have a temporally associated SARS-CoV-2 infection. People experiencing homelessness are known to be at increased risk for IPD, probably attributable to staying in congregate settings, limited uptake of routine vaccinations, and higher prevalence of predisposing medical conditions (*27*–*31*). However, the possibility also exists that our findings were caused by increased detection of SARS-CoV-2 infection from routine screening in homeless shelters.

The first limitation of our study was that we were not able to obtain symptom onset dates for IPD or SARS-CoV-2 infection, indicating that timing of infection might differ from timing of detection in our results. Second, we were unable to determine how many SARS-CoV-2 tests persons experiencing homelessness received during the study period relative to the general population. Therefore, we could not calculate whether increased SARS-CoV-2 testing contributed to the observed increased odds of SARS-CoV-2 infection in persons experiencing homelessness. Third, our study was limited in assessing the interaction between homelessness and death because of the small number of deaths among persons experiencing homelessness. However, it is useful to recognize that homelessness itself has consistently been associated as an independent risk factor for increased deaths. Fourth, we were unable to obtain detailed clinical information regarding those patients who died and had IPD and a temporally associated SARS-CoV-2 infection, which indicates that we could not determine the etiologic role that SARS-CoV-2 had in their death. We also assigned COVID-19 vaccination eligibility based on the phased rollout in the Alaska general population. Certain IPD patients might have been eligible before this date on the basis of immunocompromising conditions and occupational risk factors (e.g., healthcare workers) and underestimated the number of eligible persons not vaccinated. We also did not examine risk factors for IPD and deaths because the total number of patients who died was small (n = 18) probably resulting in small sample bias from maximum-likelihood estimation in multivariable models. Fifth, because we only included patients who had IPD, we cannot infer the association concerning other noninvasive pneumococcal infections with SARS-CoV-2. Nevertheless, the study has multiple strengths, including linkage of statewide data sources to effectively capture all reported cases of IPD and COVID-19 in the state during the study period and a robust epidemiologic comparison of persons co-infected with IPD and SARS-CoV-2 to those infected with IPD alone.

In conclusion, we found that ≈1 of 5 patients who had IPD in Alaska during 2020–2021 had a

Table 4. Multivariable analysis of risk factors for invasive pneumococcal disease temporally associated with a SARS-CoV-2 infection compared with patients who had with IPD alone, Alaska, USA, 2020–2021

Characteristic	Adjusted odds ratio* (95% CI)
Person experiencing homelessness	
No	Referent
Yes	3.0 (1.4–6.7)
Sex	
M	Referent
F	1.8 (0.9–3.6)
Age, y	
<50	Referent
≥50	2.0 (1.0–3.9)
Race	
White	Referent
American Indian/Alaska Native	0.9 (0.4–1.9)
Other/unknown	0.9 (0.3–2.5)
Underlying medical condition	
None	Referent
One or more	0.8 (0.3–1.8)
Season	
Summer, June–August	Referent
Fall, September–December	2.7 (1.2–6.4)
Winter, December–February	0.9 (0.3–3.1)
Spring, March–May	0.3 (0.1–1.2)
Fully vaccinated for COVID-19	
Yes	Referent
No	2.0 (0.9–4.1)

*Multivariable logistic regression model mutually adjusted for other variables.

temporally associated SARS-CoV-2 infection, and a greater proportion of patients who had IPD and temporally associated SARS-CoV-2 infection died compared with persons who had IPD alone. Persons experiencing homelessness who had IPD were at increased risk for temporally associated SARS-CoV-2 infection. Healthcare providers should be aware of the added risks associated with dual infection and the ongoing benefits of pneumococcal and COVID-19 vaccination, especially among vulnerable populations (*17*,*32*,*33*).

About the Author

Dr. Newell is an Epidemic Intelligence Service officer in the Center for Surveillance, Epidemiology, and Laboratory Services, Centers for Disease Control and Prevention, Atlanta, GA, assigned to the Alaska Division of Public Health. Her primary research interests focus on the epidemiology of infectious diseases.

References

1. Klein EY, Monteforte B, Gupta A, Jiang W, May L, Hsieh YH, et al. The frequency of influenza and bacterial coinfection: a systematic review and meta-analysis. Influenza Other Respir Viruses. 2016;10:394–403. https://doi.org/10.1111/irv.12398
2. Metersky ML, Masterton RG, Lode H, File TM Jr, Babinchak T. Epidemiology, microbiology, and treatment considerations for bacterial pneumonia complicating influenza. Int J Infect Dis. 2012;16:e321–31. https://doi.org/10.1016/j.ijid.2012.01.003
3. Paddock CD, Liu L, Denison AM, Bartlett JH, Holman RC, Deleon-Carnes M, et al. Myocardial injury and bacterial pneumonia contribute to the pathogenesis of fatal influenza B virus infection. J Infect Dis. 2012;205:895–905. https://doi.org/10.1093/infdis/jir861
4. Martín-Loeches I, Sanchez-Corral A, Diaz E, Granada RM, Zaragoza R, Villavicencio C, et al.; H1N1 SEMICYUC Working Group. Community-acquired respiratory coinfection in critically ill patients with pandemic 2009 influenza A(H1N1) virus. Chest. 2011;139:555–62. https://doi.org/10.1378/chest.10-1396
5. Kneyber MC, Blussé van Oud-Alblas H, van Vliet M, Uiterwaal CS, Kimpen JL, van Vught AJ. Concurrent bacterial infection and prolonged mechanical ventilation in infants with respiratory syncytial virus lower respiratory tract disease. Intensive Care Med. 2005;31:680–5. https://doi.org/10.1007/s00134-005-2614-4
6. Jennings LC, Anderson TP, Beynon KA, Chua A, Laing RT, Werno AM, et al. Incidence and characteristics of viral community-acquired pneumonia in adults. Thorax. 2008;63:42–8. https://doi.org/10.1136/thx.2006.075077
7. Templeton KE, Scheltinga SA, van den Eeden WC, Graffelman AW, van den Broek PJ, Claas EC. Improved diagnosis of the etiology of community-acquired pneumonia with real-time polymerase chain reaction. Clin Infect Dis. 2005;41:345–51. https://doi.org/10.1086/431588
8. Langford BJ, So M, Raybardhan S, Leung V, Westwood D, MacFadden DR, et al. Bacterial co-infection and secondary infection in patients with COVID-19: a living rapid review and meta-analysis. Clin Microbiol Infect. 2020;26:1622–9. https://doi.org/10.1016/j.cmi.2020.07.016
9. Lansbury L, Lim B, Baskaran V, Lim WS. Co-infections in people with COVID-19: a systematic review and meta-analysis. J Infect. 2020;81:266–75. https://doi.org/10.1016/j.jinf.2020.05.046
10. Suzuki M, Hayakawa K, Asai Y, Terada M, Kitajima K, Tsuzuki S, et al. Characteristics of hospitalized COVID-19 patients with other respiratory pathogens identified by rapid diagnostic test. J Infect Chemother. 2023;29:539–45. https://doi.org/10.1016/j.jiac.2023.02.006
11. Musuuza JS, Watson L, Parmasad V, Putman-Buehler N, Christensen L, Safdar N. Prevalence and outcomes of co-infection and superinfection with SARS-CoV-2 and other pathogens: A systematic review and meta-analysis. PLoS One. 2021;16:e0251170. https://doi.org/10.1371/journal.pone.0251170
12. Amin-Chowdhury Z, Aiano F, Mensah A, Sheppard CL, Litt D, Fry NK, et al. Impact of the COVID-19 pandemic on invasive pneumococcal disease and risk of pneumococcal coinfection with SARS-CoV-2: prospective national cohort study, England. Clin Infect Dis. 2021;72:e65–75. https://doi.org/10.1093/cid/ciaa1728
13. Massay S, Bobo M, Stewart P, Fischer M, Bressler S, Bruden D, et al. Updated adult pneumococcal vaccination recommendations. Epi Bulletin 2022;8 [cited 2023 Jul 20]. http://www.epi.alaska.gov/bulletins/docs/b2022_08.pdf
14. Bruce MG, Singleton R, Bulkow L, Rudolph K, Zulz T, Gounder P, et al. Impact of the 13-valent pneumococcal conjugate vaccine (pcv13) on invasive pneumococcal disease and carriage in Alaska. Vaccine. 2015;33:4813–9. https://doi.org/10.1016/j.vaccine.2015.07.080
15. Singleton R, Wenger J, Klejka JA, Bulkow LR, Thompson A, Sarkozy D, et al. The 13-valent pneumococcal conjugate vaccine for invasive pneumococcal disease in Alaska native children: results of a clinical trial. Pediatr Infect Dis J. 2013;32:257–63. https://doi.org/10.1097/INF.0b013e3182748ada
16. Wenger JD, Zulz T, Bruden D, Singleton R, Bruce MG, Bulkow L, et al. Invasive pneumococcal disease in Alaskan children: impact of the seven-valent pneumococcal conjugate vaccine and the role of water supply. Pediatr Infect Dis J. 2010;29:251–6. https://doi.org/10.1097/INF.0b013e3181bdbed5
17. Kobayashi M, Farrar JL, Gierke R, Britton A, Childs L, Leidner AJ, et al. Use of 15-valent pneumococcal conjugate vaccine and 20-valent pneumococcal conjugate vaccine among U.S. adults: updated recommendations of the Advisory Committee on Immunization Practices — United States, 2022. MMWR Morb Mortal Wkly Rep. 2022;71:109–17. https://doi.org/10.15585/mmwr.mm7104a1
18. Alaska Division of Public Health. Alaska State COVID-19 cases dashboard [cited 2023 Jul 27]. https://experience.arcgis.com/experience/af2efc8bffbf4cdc83c2d1a134354074.
19. O'Brien KL, Walters MI, Sellman J, Quinlisk P, Regnery H, Schwartz B, et al. Severe pneumococcal pneumonia in previously healthy children: the role of preceding influenza infection. Clin Infect Dis. 2000;30:784–9. https://doi.org/10.1086/313772
20. Brundage JF. Interactions between influenza and bacterial respiratory pathogens: implications for pandemic preparedness. Lancet Infect Dis. 2006;6:303–12. https://doi.org/10.1016/S1473-3099(06)70466-2
21. Peltola V, Heikkinen T, Ruuskanen O, Jartti T, Hovi T, Kilpi T, et al. Temporal association between rhinovirus circulation in the community and invasive pneumococcal disease in children. Pediatr Infect Dis J. 2011;30:456–61. https://doi.org/10.1097/INF.0b013e318208ee82

22. Håkansson A, Kidd A, Wadell G, Sabharwal H, Svanborg C. Adenovirus infection enhances in vitro adherence of *Streptococcus pneumoniae*. Infect Immun. 1994;62:2707–14. https://doi.org/10.1128/iai.62.7.2707-2714.1994
23. Deinhardt-Emmer S, Böttcher S, Häring C, Giebeler L, Henke A, Zell R, et al. SARS-CoV-2 causes severe epithelial inflammation and barrier dysfunction. J Virol. 2021;95:e00110–21. https://doi.org/10.1128/JVI.00110-21
24. Lee JS, Park S, Jeong HW, Ahn JY, Choi SJ, Lee H, et al. Immunophenotyping of COVID-19 and influenza highlights the role of type I interferons in development of severe COVID-19. Sci Immunol. 20201;5:eabd1554.
25. Pallikkuth S, Williams E, Pahwa R, Hoffer M, Pahwa S. Association of flu specific and SARS-CoV-2 specific CD4 T cell responses in SARS-CoV-2 infected asymptomatic heath care workers. Vaccine. 2021;39:6019–24. https://doi.org/10.1016/j.vaccine.2021.08.092
26. Hoepel W, Chen HJ, Geyer CE, Allahverdiyeva S, Manz XD, de Taeye SW, et al. High titers and low fucosylation of early human anti-SARS-CoV-2 IgG promote inflammation by alveolar macrophages. Sci Transl Med. 2021;13:eabf8654. https://doi.org/10.1126/scitranslmed.abf8654
27. Mosites E, Zulz T, Bruden D, Nolen L, Frick A, Castrodale L, et al. Risk for invasive streptococcal infections among adults experiencing homelessness, Anchorage, Alaska, USA, 2002–2015. Emerg Infect Dis. 2019;25:1911–8. https://doi.org/10.3201/eid2510.181408
28. Steinberg J, Bressler SS, Thompson GC. Invasive pneumococcal disease among adults experiencing homelessness in Anchorage, Alaska 2005–2020. Presented at: 12th International Symposium on Pneumococci and Pneumococcal Diseases; Toronto, Ontario Canada; June 19–23, 2022.
29. Lemay J-A, Ricketson LJ, Zwicker L, Kellner JD. Homelessness in adults with invasive pneumococcal disease in Calgary, Canada. Open Forum Infect Dis. 2019;6:ofz362. https://doi.org/10.1093/ofid/ofz362
30. McKee G, Choi A, Madill C, Marriott J, Kibsey P, Hoyano D II. Outbreak of invasive Streptococcus pneumoniae among an inner-city population in Victoria, British Columbia, 2016–2017. Can Commun Dis Rep. 2018;44:317–22. https://doi.org/10.14745/ccdr.v44i12a02
31. Beall B, Walker H, Tran T, Li Z, Varghese J, McGee L, et al. Upsurge of conjugate vaccine serotype 4 invasive pneumococcal disease clusters among adults experiencing homelessness in California, Colorado, and New Mexico. J Infect Dis. 2021;223:1241–9. https://doi.org/10.1093/infdis/jiaa501
32. Kobayashi M, Farrar JL, Gierke R, Leidner AJ, Campos-Outcalt D, Morgan RL, et al.; ACIP Pneumococcal Vaccines Work Group; CDC Contributors. Use of 15-valent pneumococcal conjugate vaccine among U.S. children: updated recommendations of the Advisory Committee on Immunization Practices—United States, 2022. MMWR Morb Mortal Wkly Rep. 2022;71:1174–81. https://doi.org/10.15585/mmwr.mm7137a3
33. Centers for Disease Control and Prevention. Overview of COVID-19 vaccines [cited 2023 Jul 20]. https://www.cdc.gov/coronavirus/2019-ncov/vaccines/different-vaccines/overview-COVID-19-vaccines.html.

Address for correspondence: Katherine Newell, Centers for Disease Control and Prevention, 3601 C St, Ste 540, Anchorage AK, USA; email: katherine.newell@alaska.gov

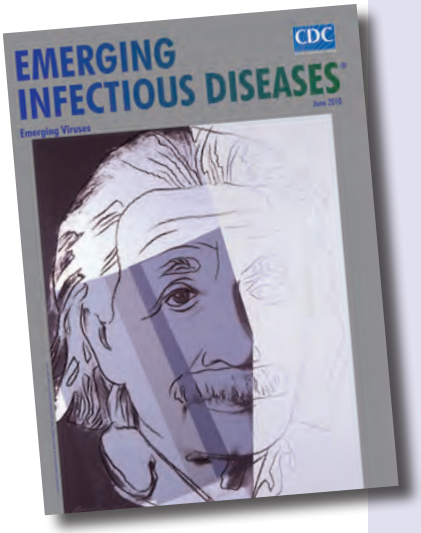

Originally published in June 2010

https://wwwnc.cdc.gov/ei

etymologia revisited

Lassa Virus

[lah sə] virus

This virus was named after the town of Lassa at the southern end of Lake Chad in northeastern Nigeria, where the first known patient, a nurse in a mission hospital, had lived and worked when she contracted this infection in 1969. The virus was discovered as part of a plan to identify unknown viruses from Africa by collecting serum specimens from patients with fevers of unknown origin. Lassa virus, transmitted by field rats, is endemic in West Africa, where it causes up to 300,000 infections and 5,000 deaths each year.

References:

1 Frame JD, Baldwin JM Jr, Gocke DJ, Troup JM. Lassa fever, a new virus disease of man from West Africa. I. Clinical description and pathological findings. Am J Trop Med Hyg. 1970;19:670–6
2. Mahy BW. The dictionary of virology, 4th ed. Burlington (MA): Elsevier; 2009.

Validation of Claims-Based Algorithm for Lyme Disease, Massachusetts, USA

Noelle M. Cocoros, Sheryl A. Kluberg, Sarah J. Willis, Susan Forrow, Bradford D. Gessner, Cameron T. Nutt, Alejandro Cane, Nathan Petrou, Meera Sury, Chanu Rhee, Luis Jodar, Aaron Mendelsohn, Emma R. Hoffman, Robert Jin, John Aucott, Sarah J. Pugh, James H. Stark

Compared with notifiable disease surveillance, claims-based algorithms estimate higher Lyme disease incidence, but their accuracy is unknown. We applied a previously developed Lyme disease algorithm (diagnosis code plus antimicrobial drug prescription dispensing within 30 days) to an administrative claims database in Massachusetts, USA, to identify a Lyme disease cohort during July 2000–June 2019. Clinicians reviewed and adjudicated medical charts from a cohort subset by using national surveillance case definitions. We calculated positive predictive values (PPVs). We identified 12,229 Lyme disease episodes in the claims database and reviewed and adjudicated 128 medical charts. The algorithm's PPV for confirmed, probable, or suspected cases was 93.8% (95% CI 88.1%–97.3%); the PPV was 66.4% (95% CI 57.5%–74.5%) for confirmed and probable cases only. In a high incidence setting, a claims-based algorithm identified cases with a high PPV, suggesting it can be used to assess Lyme disease burden and supplement traditional surveillance data.

Lyme disease is the most commonly reported vectorborne disease in the United States (*1*) and is an economic burden for patients and society (*2*–*4*). As a notifiable disease, standard Lyme disease case definitions and reporting criteria have identified ≈30,000 cases annually via traditional surveillance (*5*). Several jurisdictions have used alternative methods to approximate Lyme disease incidence, including sampling (*6*), estimation techniques (*7*), and supplementing laboratory-based surveillance data with information from electronic health records (*8*).

To complement traditional surveillance, the Centers for Disease Control and Prevention (CDC) used a commercial health care administrative claims database to estimate Lyme disease incidence in the United States. In 2015, claims-based algorithms were developed for inpatient and outpatient settings; the outpatient algorithm combined diagnosis codes from the International Classification of Diseases, 9th Revision, Clinical Modification (ICD-9-CM), for Lyme disease with dispensing of an antimicrobial drug within 30 days (*9*). That study estimated that ≈329,000 annual cases of Lyme disease occurred during 2005–2010 after applying several correction factors to account for database limitations. The analysis was repeated for cases during 2010–2018 after the addition of diagnosis codes from the International Classification of Diseases, 10th Revision, Clinical Modification (ICD-10-CM), for Lyme disease, estimating that ≈476,000 Lyme disease cases occurred annually during this period (*10*). However, the accuracy of the algorithms is unknown (*11*). We validated this outpatient algorithm by assessing algorithm performance across age groups, healthcare facility type, and periods in a single Lyme disease–endemic state.

Methods

Study Population

We used Harvard Pilgrim Health Care (HPHC) administrative claims data to identify the initial Lyme disease cohort in Massachusetts, USA. HPHC is a not-for-profit health insurance company serving >3 million members primarily in the New England region of the United States. HPHC members are approximately

Author affiliations: Harvard Medical School and Harvard Pilgrim Health Care Institute, Boston, Massachusetts, USA (N.M. Cocoros, S.A. Kluberg, S.J. Willis, S. Forrow, C. Rhee, A. Mendelsohn, E.R. Hoffman, R. Jin); Pfizer Inc., New York, New York, USA (S.J. Willis); Pfizer Inc., Collegeville, Pennsylvania, USA (B.D. Gessner, A. Cane, L. Jodar, S.J. Pugh, J.H. Stark); Brigham and Women's Hospital, Boston (C.T. Nutt, N. Petrou, M. Sury, C. Rhee); Johns Hopkins School of Medicine, Baltimore, Maryland, USA (J. Aucott)

DOI: https://doi.org/10.3201/eid2909.221931

half female and half male, and ≈20% of members are >65 years of age. We included HPHC members who were enrolled in medical and pharmacy benefits for ≥6 months from July 1, 2000, through June 30, 2019, and who were residents of Massachusetts at the time of enrollment.

To validate cases identified in the administrative claims database, we reviewed medical charts for a subset of patients with Lyme disease episodes who received care from any facility that was part of the Mass General Brigham (MGB) healthcare system. We limited chart review to a single healthcare system to simplify accessing medical charts. MGB, the largest provider system in Massachusetts, comprises 16 institutions across the care continuum and has 6,500 physicians. The system includes academic medical centers, specialty and community hospitals, and urgent and community-based care via community health centers that are geographically dispersed across eastern Massachusetts. In 2020, the MGB healthcare system was responsible for ≈20% of inpatient discharges and ≈27% of outpatient revenue in Massachusetts (*12*). We expected the MGB healthcare system to be representative of care delivered across the state.

Algorithm Criteria and Descriptive Analyses

Lyme disease was defined by ≥1 diagnosis code (ICD-9-CM code 088.81; ICD-10-CM codes A69.20, A69.21, A69.22, A69.23, and A69.29) and ≥1 outpatient dispensing of an antimicrobial drug used to treat Lyme disease according to Infectious Diseases Society of America guidelines (*13*). We defined antimicrobial drugs by using the US Food and Drug Administration National Drug Codes for doxycycline, amoxicillin, cefuroxime axetil, azithromycin, penicillin G, ceftriaxone, and cefotaxime; we included oral and nonoral formulations. We required a minimum 7-day supply of antimicrobial drug dispensed within 30 days of the Lyme disease diagnosis and included oral and nonoral formulations. We evaluated the use of doxycycline, amoxicillin, cefuroxime axetil, azithromycin, penicillin G, ceftriaxone, and cefotaxime to treat Lyme disease.

To identify Lyme disease episodes, we required that HPHC members did not have a Lyme disease diagnosis code documented within 180 days before meeting the Lyme disease definition (i.e., if someone had a Lyme disease diagnosis code but no antimicrobial drug dispensed and then had another Lyme disease diagnosis code <180 days later with a qualifying antimicrobial drug dispensed, we did not include the second episode). For members who had multiple Lyme disease episodes, we used recurrence intervals to exclude episodes in which the diagnosis code and antimicrobial drug were likely used for treating Lyme disease–related sequelae from the first infection; we used intervals according to those used by others for ICD-9-CM (*9*) and ICD-10-CM (*10*) codes. During the ICD-9-CM era (before October 1, 2015), the recurrence interval was 365 days. During the ICD-10 era (beginning October 1, 2015), if a member met the algorithm definition with code A69.2 (Lyme disease) or A69.20 (Lyme disease, unspecified) on or after October 1, 2015, the recurrence interval was 180 days, as long as the second Lyme disease case date was in the next calendar year. If the second Lyme disease case date was in the same calendar year, then the second episode was not included. If a member met the algorithm definition with code A69.21 (meningitis), A69.22 (other neurologic disorders), A69.23 (arthritis), or A69.29 (other conditions) on or after October 1, 2015, the recurrence interval was 365 days.

We summarized characteristics of HPHC members with algorithm-defined Lyme disease during the full study period by using descriptive statistics. We examined the frequencies and percentages of patient demographic and clinical characteristics associated with Lyme disease episodes that were available in the administrative claims data. Acute signs and symptoms were rash, fever, chills, fatigue, headache, joint and muscle pain, radiculopathy, and paresthesia, and those were identified by ICD-9-CM and ICD-10-CM diagnosis codes reported within 14 days before or after meeting the Lyme disease algorithm definition (Appendix Table, https://wwwnc.cdc.gov/EID/article/29/9/22-1931-App1.pdf). Musculoskeletal, nervous system, cardiovascular, and ocular manifestations of Lyme disease were examined up to 1 year after Lyme disease diagnosis and were also identified by diagnosis codes (Appendix Table). Among those patients with obtainable MGB medical records that were reviewed and adjudicated, we evaluated demographic and clinical characteristics and summarized acute symptoms and disseminated manifestations by using the same criteria described previously. We also assessed laboratory data captured in the medical records to determine how many cases were laboratory-confirmed.

Algorithm Validation via Medical Chart Reviews

We had an a priori goal of reviewing 125 medical charts for algorithm validation; we prioritized cases from the ICD-10-CM era and then included ICD-9-CM era episodes to obtain ≥125 charts. We identified 193 medical charts for persons with HPHC insurance who had evidence of Lyme disease–related care at a facility

within the MGB system and who met the algorithm criteria during January 2015–June 2019; we sought medical records for a convenience sample of 171 cases.

Under the supervision of an infectious disease clinical faculty member (C.R.), 3 MGB medical residents (C.T.N., N.P., M.S.) conducted all chart abstraction and adjudication activities. Prior to conducting those activities, they received training from a Lyme disease clinical expert (J.A.). To assess interrater reliability, all 3 clinicians initially abstracted and adjudicated the same 20 medical charts. We calculated a single κ-like statistic that summarized interrater reliability across all clinicians by computing the mean of the weighted κ for each clinician pair (*14*). We divided the remaining charts among the 3 clinicians for single adjudications.

We conducted medical chart reviews assuming that the clinician-determined adjudication was the standard for definitively assigning Lyme disease status according to surveillance case definitions. We developed standardized abstraction and adjudication forms for chart reviews that had definitions consistent with the 2017 Council of State and Territorial Epidemiologists' Lyme disease case definitions for confirmed, probable, and suspected cases (*15*) (Appendix). Abstracted data from each medical record were evidence of erythema migrans or rash; tick bite or exposure to ticks; signs and symptoms of Lyme disease; cardiovascular, musculoskeletal, or nervous system manifestations of Lyme disease; antimicrobial drugs or other medications used to treat Lyme disease; laboratory tests and results; physician diagnosis of Lyme disease; evidence of persistent signs and symptoms of Lyme disease; and healthcare facility type. Claims-based Lyme disease cases were adjudicated, and we classified each case as confirmed, probable, suspected, or not a Lyme disease case (Table 1).

Table 1. Case classification, definitions, and instructions used by clinician adjudicators for chart review in study of validation of claims-based algorithm for Lyme disease, Massachusetts, USA*

Classification	Definitions†
Confirmed	Erythema migrans with known exposure in a high-incidence state (e.g., Massachusetts), erythema migrans with known exposure in a low-incidence state and laboratory-confirmed Lyme disease, or ≥1 late manifestation of Lyme disease and laboratory-confirmed Lyme disease
Probable	Diagnosis of Lyme disease in clinical notes and laboratory-confirmed Lyme disease but no evidence of erythema migrans and no eligible late manifestations of disease
Suspected	Diagnosis of Lyme disease in clinical notes and antimicrobial drugs ordered by healthcare provider to treat Lyme disease but no laboratory confirmation, no evidence of erythema migrans, and no eligible late manifestations of Lyme disease; or erythema migrans with no known exposure, no laboratory confirmation, and no eligible late manifestations of Lyme disease

*Definitions were based on the 2017 Council of State and Territorial Epidemiologists case definitions (*15*).
†Laboratory-confirmed Lyme disease was indicated by positive Lyme cultures, PCR, or 2-tiered tests. For a positive 2-tiered test, if the patient experienced signs or symptoms for <30 d before a positive or equivocal enzyme immunoassay or immunofluorescence assay, they must have a positive IgG or IgM Western blot result; if the patient has experienced signs or symptoms for >30 d before a positive or equivocal enzyme immunoassay or immunofluorescence assay, they must have a positive IgG Western blot result (a positive IgM Western blot result does not confirm Lyme disease in this scenario). Late manifestations of Lyme disease include musculoskeletal involvement defined as inflammatory arthritis or recurrent and brief attacks of swelling in >1 joint that lasts for several weeks or months; nervous system involvement defined as lymphocytic meningitis, cranial neuritis, radiculoneuropathy, or encephalomyelitis (headache, fatigue, paresthesia, or mildly stiff neck alone did not meet criteria for neurologic involvement); or cardiovascular involvement defined as acute onset of high-grade atrioventricular conduction defects that resolve in days to weeks, such as complete heart block, third degree heart block, or high-grade atrioventricular block (palpitations, bradycardia, bundle branch block, or myocarditis alone did not meet criteria for cardiovascular involvement).

We calculated positive predictive values (PPV) for claims-based Lyme disease cases adjudicated as confirmed, probable, or suspected and PPV values for confirmed or probable cases only. We calculated PPVs according to age group, healthcare facility type, period, and patients with Lyme disease–related laboratory tests to determine how performance varied across those subgroups. We used the Clopper-Pearson method to calculate 95% CIs for all PPVs (*16*). The study was approved by the Harvard Pilgrim Health Care Institutional Review Board.

Results

Claims Data

From July 1, 2000, through June 30, 2019, by using the Lyme disease claims-based algorithm, we identified 12,229 Lyme disease episodes among 11,823 HPHC members who lived in Massachusetts; a total of 11,452 members had 1 Lyme disease episode, 339 had 2 episodes, and 32 had 3 or 4 qualifying episodes. Most (77.7%) episodes were identified during the ICD-9-CM era; the only applicable code was 088.81, Lyme disease. During the ICD-10-CM era, the most common cohort-defining diagnosis code was A69.20, Lyme disease unspecified (93.0%); 4.9% were identified as A69.23, arthritis due to Lyme disease; 1.4% as A69.29, other conditions associated with Lyme disease; and <1% as A69.22, other neurologic disorders in Lyme disease, or A69.21, meningitis due to Lyme disease.

We analyzed demographic and clinical characteristics of patients with Lyme disease episodes according to claims data for the overall cohort (n = 12,229) and the subset included in the chart review (n = 128) (Table 2). Most Lyme disease episodes occurred among adults ≥18 years of age, including 71.4% in

Table 2. Demographic and clinical characteristics of Harvard Pilgrim Health Care members who met criteria for a validation study of a claims-based algorithm for Lyme disease during July 2000–June 2019 in Massachusetts, USA*

Characteristics	Total Lyme disease episodes	Lyme disease episodes included in chart review
Total no. cases	12,229	128
Age groups, y		
Pediatric, <18	3,494 (28.6)	25 (19.5)
Adult, ≥18	8,735 (71.4)	103 (80.5)
<1	8 (0.1)	0
1–4	775 (6.3)	8 (6.3)
5–14	2,271 (18.6)	16 (12.5)
15–24	1,208 (9.9)	7 (5.5)
25–39	1,500 (12.3)	16 (12.5)
40–64	5,609 (45.9)	62 (48.4)
≥65	858 (7.0)	19 (14.8)
Median age, y (IQR)	42 (15–55)	48 (29–60)
Sex		
M	6,675 (54.6)	63 (49.2)
F	5,554 (45.4)	65 (50.8)
Antimicrobial drug		
Doxycycline	8,110 (66.3)	107 (83.6)
Amoxicillin	3,594 (29.4)	18 (14.1)
Cefuroxime axetil	341 (2.8)	2 (1.6)
Azithromycin	177 (1.5)	1 (0.8)
Penicillin G	7 (0.1)	0
Acute signs and symptoms†		
No signs or symptoms	6,931 (56.7)	80 (62.5)
Joint pain	1,681 (13.7)	12 (9.4)
Rash‡	1,644 (13.4)	20 (15.6)
Fatigue	1,518 (12.4)	10 (7.8)
Fever	1,091 (8.9)	6 (4.7)
Headache	999 (8.2)	7 (5.5)
Myalgia	654 (5.3)	10 (7.8)
Disseminated manifestations§		
Nervous system	904 (7.4)	9 (7.0)
Musculoskeletal	326 (2.7)	10 (7.8)
Ocular	257 (2.1)	3 (2.3)
Cardiovascular	37 (0.3)	0

*Values are no. (%) except as indicated. All data are from the Harvard Pilgrim Health Care administrative claims database. The 128 Lyme disease episodes included in the chart reviews were also included in the total Lyme disease episode data. IQR, interquartile range.
†Rash, fever, chills, fatigue, headache, joint pain, neck pain or stiff neck, radiculopathy, myalgia, and paresthesia were derived from diagnosis codes from the International Classification of Diseases, 9th Revision, Clinical Modification, and International Classification of Diseases, 10th Revision, Clinical Modification, documented up to 14 d before or after the member met the claims-based definition of Lyme disease.
‡Upon medical record review, 62 of 128 (48.4%) cases had evidence of erythema migrans.
§Nervous system, musculoskeletal, ocular, and cardiovascular manifestations were derived from diagnosis codes from the International Classification of Diseases, 9th Revision, Clinical Modification, and International Classification of Diseases, 10th Revision, Clinical Modification, documented up to 365 d after the member met the claims-based definition of Lyme disease. A patient can have both disseminated manifestations and acute signs and symptoms.

the overall cohort (median age 42 years, interquartile range 15–55 years; 45.9% were 40–64 years of age) and 80.5% in the chart review (median age 48 years, interquartile range 29–60 years; 48.4% were 40–64 years of age). Male patients comprised 49.2% of reviewed charts and 54.6% of all Lyme disease episodes.

Of the total Lyme disease episodes, 66.3% were associated with dispensation of a ≥7-day supply of doxycycline, 29.4% with amoxicillin, and 4.3% with cefuroxime acetyl, azithromycin, or penicillin G. Some cases (2%) were treated with >1 antimicrobial drugs. No cases were treated with ceftriaxone or cefotaxime. Within the subset included in the chart review, the pattern was similar, although more patients (83.6%) were treated with doxycycline.

For the overall Lyme disease cohort, during the 14 days before and after the Lyme disease case date, 56.7% of cases did not have any diagnosis codes recorded in claims data that were indicative of acute signs or symptoms; 13.7% of cases had diagnosis codes for joint pain, 13.4% for rash, and 12.4% for fatigue. During the 365 days after the Lyme disease case date, 7.4% of cases had a diagnosis code indicative of a nervous system manifestation, such as Bell's palsy, meningitis, or radiculopathy. Musculoskeletal (2.7%), ocular (2.1%), or cardiovascular (0.3%) manifestations occurred within 365 days of the Lyme disease case date, according to diagnosis codes. Those findings were generally similar among patients included in chart reviews.

Algorithm Validation via Chart Review

Of the 128 (75%) obtainable medical records that we reviewed and adjudicated, 80.5% were for cases

that occurred during the ICD-10 era. The overall interrater reliability for the 20 charts reviewed by all 3 clinician adjudicators yielded a mean weighted κ of 0.94.

Overall, we adjudicated 120 of 128 reviewed charts as confirmed, probable, or suspected cases. The distribution of those 120 cases followed the expected seasonality of Lyme disease in Massachusetts; the peak was observed in July. Of the 18.8% of cases that were laboratory-confirmed (defined by positive Lyme disease culture, PCR, or standard 2-tiered tests), all were adjudicated as confirmed or probable cases. A clinical diagnosis of Lyme disease was indicated in 55.5% of charts, defined as erythema migrans or Lyme disease–associated carditis, neuroborreliosis, meningitis, or arthritis in the healthcare provider's clinical notes. Upon chart review, erythema migrans was reported for 48% of patients (98.4% of whom were adjudicated as confirmed cases), which was substantially higher than the >15.6% of patients with evidence of rash via claims data alone. Similar to observations for claims data alone, reports of disseminated Lyme disease manifestations were uncommon upon chart review. Musculoskeletal involvement was found in 6.3%, nervous system involvement in 2.3%, cardiovascular involvement in <1%, and ocular involvement in 0% of cases; 75% (n = 9) of patients with a disseminated manifestation were adjudicated as confirmed cases.

For reviewed charts, we calculated PPVs for the algorithm overall and according to select characteristics (Table 3). Most (74.2%) charts were from patients seen in a primary care setting. The overall PPV of the algorithm for cases identified as confirmed, probable, or suspected was 93.8% (95% CI 88.1%–97.3%). When limited to confirmed or probable cases only, the PPV was 66.4% (95% CI 57.5%–74.5%). The PPV for confirmed, probable, or suspected cases was 100% (n = 25) for pediatric patients, compared with 92.2% (n = 103) for adult patients. PPVs for confirmed, probable, and suspected cases were 92.0% for those identified during the ICD-9 era and 92.4% for those identified during the ICD-10 era. When including only confirmed and probable cases, the PPV was 76.0% for the ICD-9 era and 64.1% for the ICD-10 era.

Among the 8 patients who did not have Lyme disease upon adjudication, none had erythema migrans, and 1 patient had a nonspecific rash. Only 1 patient had a documented tick bite. One patient's chart indicated *Borrelia miyamotoi* infection and another noted a suspected *B. miyamotoi* infection. Among 5 patients who had a Lyme disease test, 4 had negative results documented.

Discussion

We report high PPVs for a claims-based algorithm previously used by the CDC to estimate the incidence of Lyme disease in the United States, using claims data and medical record information from sources in Massachusetts. The PPV for cases adjudicated as confirmed, probable, or suspected (according to surveillance case definitions) was 93.8%; PPV was 66.4% when limited to only confirmed or probable. Our results provide support for previous studies (*4*,*9*,*10*,*17*,*18*) and future research aimed at using claims-based algorithms to estimate the total burden of Lyme disease.

Algorithm performance varied depending on the inclusion of suspected cases in PPV calculations. The surveillance definition for a suspected case captures

Table 3. Numbers of reviewed charts and positive predictive values according to case definitions and other factors during January 2015–June 2019 in study of validation of claims-based algorithm for Lyme disease, Massachusetts, USA*

Factors	Reviewed charts	Confirmed	Probable	Suspected	Not LD	% PPV (95% CI)†	% PPV (95% CI)‡
Overall	128	70	15	35	8	93.8 (88.1–97.3)	66.4 (57.5–74.5)
Age group, y							
Pediatric, <18	25 (19.5%)	19	3	3	0	100 (86.3–100)	88 (68.8–97.5)
Adults, ≥18	103 (80.5%)	51	12	32	8	92.2 (85.3–96.6)	61.2 (51.1–70.6)
ICD era§							
ICD-9-CM	25 (19.5%)	16	3	4	2	92.0 (74.0–99.0)	76.0 (54.9–90.6)
ICD-10-CM	103 (80.5%)	54	12	31	6	94.2 (87.8–97.8)	64.1 (54.0–73.3)
Healthcare facility type							
Primary care	95 (74.2%)	51	14	26	4	95.8 (89.6–98.8)	68.4 (58.1–77.6)
Urgent care	17 (13.3%)	12	1	4	0	100 (80.5–100)	76.5 (50.1–93.2)
Other¶	16 (12.5%)	7	0	5	4	75.0 (47.6–92.7)	31.3 (11.0–58.7)
Laboratory tests#	68 (53.1%)	27	15	21	5	92.7 (83.7–97.6)	61.8 (49.2–73.3)

*Values are no. (%) except as indicated. Lyme disease case definitions are confirmed, probable, suspected, and not Lyme disease. ICD, International Classification of Diseases; ICD-9, ICD, 9th Revision, Clinical Modification; ICD-10, ICD, 10th Revision, Clinical Modification; LD, Lyme disease; PPV, positive predictive value.
†Confirmed, probable, or suspected cases.
‡Confirmed or probable cases only.
§Case dates were January 2015–September 2015 for ICD-9 and October 2015–June 2019 for ICD-10.
¶Includes specialist practice (n = 5), emergency department (n = 3), telephone encounter (n = 3), and unknown facility type (n = 5).
#Laboratory testing performed (regardless of result).

persons treated presumptively and those who do not have true Lyme disease as well as those who, for example, have poor recall of a tick bite (and, therefore, no known exposure) or whose erythema migrans resolves before a scheduled medical encounter. Because all suspected cases were treated, they represent a burden on the healthcare system.

The PPV also varied according to the ICD coding era. The ICD-9 era had a higher PPV (76.0% [95% CI 54.9%–90.6%]) than did the ICD-10 era (64.1% [95% CI 54.0%–73.3%]) when restricted to only confirmed and probable cases; 16% of charts reviewed from the ICD-9 era were adjudicated as suspected cases, compared with 30% from the ICD-10 era. The difference in adjudication percentages could be explained by increased awareness of Lyme disease in recent years leading to more presumptive treatment and diagnosis. Of note, most (81%) of the charts reviewed were diagnosed in the ICD-10 era and yielded a narrower CI.

We showed that a low percentage of Lyme disease episodes in both the claims data and chart review subset had evidence of disseminated disease (neurologic, musculoskeletal, and cardiac systems). Some variation existed according to data source; musculoskeletal involvement was the most prevalent (6% of cases) disseminated manifestation identified in the chart review subset, whereas nervous system involvement within 1 year was most common (7% of cases) in the claims-based cohort. Another study also reported low prevalence of disseminated Lyme disease in claims data using the same algorithm (*19*). Overall, that study found that 6% of Lyme disease episodes had disseminated disease within 30 days of diagnosis; arthritis was the most common manifestation at 3%, followed by facial palsy at 2%. Those findings contrast with surveillance reports indicating 27.5% of patients with confirmed Lyme disease had arthritis, 1.5% had carditis, and 12.5% had a neurologic manifestation (*1*) and another report indicating 43.9% of cases reported via laboratory-based surveillance had evidence of disseminated Lyme disease (*20*). This discrepancy might be because of lack of capture of those conditions in claims data or a lack of ascertainment of disseminated disease with this algorithm, which requires a Lyme disease diagnosis code. Alternatively, estimates of disseminated manifestations in surveillance data might be overestimates because of reporting bias. Previous claims data–based studies have found that >50% of Lyme disease patients did not have a Lyme disease–specific diagnosis code (*9*,*21*). Future studies should aim to elucidate this discrepancy by validating other case-identifying algorithms. Another explanation might be that the algorithm required data on outpatient dispensing of a 7-day antimicrobial drug supply; we did not include procedure codes for treatment with intravenous antimicrobial drugs. Therefore, the algorithm might have underperformed for identifying nervous system disease because treatment of those manifestations includes intravenous antimicrobial drugs.

We validated the claims-based algorithm to support its use in retrospectively estimating Lyme disease incidence, but claims data can be used for routine ongoing surveillance if data lags are anticipated and understood. The timeliness of settled (closed) claims data varies according to care settings and specific data elements. For example, outpatient drug dispensing data are generally available and complete within several weeks of service, whereas hospital-based claims data can take months to be near-complete.

The first limitation of our study is that we obtained 128 (75%) of 171 charts that were sought for our analysis. Although the number is slightly higher than for other studies that identified charts from claims data for review (*22*–*24*), whether the charts that were unobtainable were more or less likely to contain a Lyme disease diagnosis is unknown. Charts were often unobtainable because the electronic medical records lacked information on the encounter of interest. Second, we validated the algorithm in a Lyme disease–endemic state, and the algorithm might not perform similarly in nonendemic states because of differences in physician awareness and Lyme disease testing, treatment, and coding practices. One study validated a claims-based algorithm for outpatient Lyme disease in Tennessee, a non–Lyme disease–endemic state, and reported a PPV of 5%. However, that study used a different algorithm, which was defined by ≥3 occurrences of the ICD-9 diagnosis code for Lyme disease (*25*). Future studies should consider validating the algorithm developed by CDC in a non–Lyme disease–endemic state. Third, we were unable to assess the sensitivity or specificity of the algorithm given our study design. Fourth, the chart reviews were conducted within 1 Massachusetts healthcare system, albeit a large system with many different clinical practices and sites. Any claims-based algorithm will perform differently according to testing, treatment, and coding practices, which might vary by clinical practice and system. However, the algorithm we used was not highly specialized, and we hypothesize that its performance would be similar in other Lyme disease–endemic regions. Finally, diagnosis codes for symptoms are generally undercaptured in administrative claims data. Therefore, we might have underestimated the frequency of acute signs

and symptoms of a Lyme disease in our claims-based analysis and, perhaps, the frequency of late manifestations of Lyme disease as well.

In conclusion, we found that a claims-based algorithm defined by documentation of a Lyme disease diagnosis code and dispensation of an outpatient antimicrobial drug had a high PPV upon chart validation. Our analysis bolsters previous claims-based estimates of Lyme disease, indicating a substantial burden of medically attended Lyme disease in high-incidence states. Our findings suggest that claims data can be used to estimate Lyme disease incidence by state or nationally. More accurate estimates of Lyme disease incidence can inform decisions related to prevention, both clinically and from a policy perspective.

This study was supported and jointly funded by Valneva and Pfizer as part of their co-development of a Lyme disease vaccine. Funders provided salary support via contract with Harvard Pilgrim Health Care Institute for N.M.C. S.F., E.R.H., R.J., S.A.K., A.M., and S.J.W. (S.J.W. was a Harvard Pilgrim Health Care Institute employee at the time of the study); consulting fees via contract with Harvard Pilgrim Health Care Institute (C.T.N., C.R., N.P., M.S.); clinical consultant fees for work related to manuscript (J.A.); and support in the form of stock and salaries (A.C., B.D.G., J.H.S., L.J., S.P.).

About the Author

Dr. Cocoros is a principal research scientist at the Harvard Pilgrim Health Care Institute and a principal associate in the Department of Population Medicine at Harvard Medical School in Boston. Her primary research interests focus on infectious disease epidemiology, pharmacoepidemiology, and the use of electronic health data for research, surveillance, and pandemic responses.

References

1. Schwartz AM, Hinckley AF, Mead PS, Hook SA, Kugeler KJ. Surveillance for Lyme disease—United States, 2008–2015. MMWR Surveill Summ. 2017;66:1–12. https://doi.org/10.15585/mmwr.ss6622a1
2. Hook SA, Jeon S, Niesobecki SA, Hansen AP, Meek JI, Bjork JKH, et al. Economic burden of reported Lyme disease in high-incidence areas, United States, 2014–2016. Emerg Infect Dis. 2022;28:1170–9. https://doi.org/10.3201/eid2806.211335
3. Schwartz AM, Shankar MB, Kugeler KJ, Max RJ, Hinckley AF, Meltzer MI, et al. Epidemiology and cost of Lyme disease-related hospitalizations among patients with employer-sponsored health insurance—United States, 2005–2014. Zoonoses Public Health. 2020;67:407–15. https://doi.org/10.1111/zph.12699
4. Adrion ER, Aucott J, Lemke KW, Weiner JP. Health care costs, utilization and patterns of care following Lyme disease. PLoS One. 2015;10:e0116767. https://doi.org/10.1371/journal.pone.0116767
5. Centers for Disease Control and Prevention. Lyme disease. Data and surveillance [cited 2022 Sep 13]. https://www.cdc.gov/lyme/datasurveillance/index.html
6. Bjork J, Brown C, Friedlander H, Schiffman E, Neitzel D. Validation of random sampling as an estimation procedure for Lyme disease surveillance in Massachusetts and Minnesota. Zoonoses Public Health. 2018;65:266–74. https://doi.org/10.1111/zph.12297
7. Lukacik G, White J, Noonan-Toly C, DiDonato C, Backenson PB. Lyme disease surveillance using sampling estimation: evaluation of an alternative methodology in New York state. Zoonoses Public Health. 2018;65:260–5. https://doi.org/10.1111/zph.12261
8. Moon KA, Pollak J, Hirsch AG, Aucott JN, Nordberg C, Heaney CD, et al. Epidemiology of Lyme disease in Pennsylvania 2006–2014 using electronic health records. Ticks Tick Borne Dis. 2019;10:241–50. https://doi.org/10.1016/j.ttbdis.2018.10.010
9. Nelson CA, Saha S, Kugeler KJ, Delorey MJ, Shankar MB, Hinckley AF, et al. Incidence of clinician-diagnosed Lyme disease, United States, 2005–2010. Emerg Infect Dis. 2015;21:1625–31. https://doi.org/10.3201/eid2109.150417
10. Schwartz AM, Kugeler KJ, Nelson CA, Marx GE, Hinckley AF. Use of commercial claims data for evaluating trends in Lyme disease diagnoses, United States, 2010–2018. Emerg Infect Dis. 2021;27:499–507. https://doi.org/10.3201/eid2702.202728
11. Nam YH, Willis SJ, Mendelsohn AB, Forrow S, Gessner BD, Stark JH, et al. Healthcare claims-based Lyme disease case-finding algorithms in the United States: a systematic literature review. PLoS One. 2022;17:e0276299. https://doi.org/10.1371/journal.pone.0276299
12. Center for Health Information and Analysis. Hospital health systems [cited 2023 Apr 6]. https://www.chiamass.gov/hospital-health-systems
13. Lantos PM, Rumbaugh J, Bockenstedt LK, Falck-Ytter YT, Aguero-Rosenfeld ME, Auwaerter PG, et al. Clinical practice guidelines by the Infectious Diseases Society of America (IDSA), American Academy of Neurology (AAN), and American College of Rheumatology (ACR): 2020 guidelines for the prevention, diagnosis and treatment of Lyme disease. Clin Infect Dis. 2021;72:e1–48. https://doi.org/10.1093/cid/ciaa1215
14. Hallgren KA. Computing inter-rater reliability for observational data: an overview and tutorial. Tutor Quant Methods Psychol. 2012;8:23–34. https://doi.org/10.20982/tqmp.08.1.p023
15. Centers for Disease Control and Prevention. Lyme disease (*Borrelia burgdorferi*) 2017 case definition [cited 2022 Oct 5]. https://ndc.services.cdc.gov/case-definitions/lyme-disease-2017
16. Clopper CJ, Pearson ES. The use of confidence or fiducial limits illustrated in the case of the binomial. Biometrika. 1934;26:404–13. https://doi.org/10.1093/biomet/26.4.404
17. Kugeler KJ, Schwartz AM, Delorey MJ, Mead PS, Hinckley AF. Estimating the frequency of Lyme disease diagnoses, United States, 2010–2018. Emerg Infect Dis. 2021;27:616–9. https://doi.org/10.3201/eid2702.202731
18. Tseng YJ, Cami A, Goldmann DA, DeMaria A Jr, Mandl KD. Incidence and patterns of extended-course antibiotic therapy in patients evaluated for Lyme disease. Clin Infect Dis. 2015;61:1536–42. https://doi.org/10.1093/cid/civ636

19. Kwit NA, Nelson CA, Max R, Mead PS. Risk factors for clinician-diagnosed Lyme arthritis, facial palsy, carditis, and meningitis in patients from high-incidence states. Open Forum Infect Dis. 2017;5:ofx254. https://doi.org/10.1093/ofid/ofx254
20. Ertel SH, Nelson RS, Cartter ML. Effect of surveillance method on reported characteristics of Lyme disease, Connecticut, 1996–2007. Emerg Infect Dis. 2012;18:242–7. https://doi.org/10.3201/eid1802.101219
21. Rutz H, Hogan B, Hook S, Hinckley A, Feldman K. Exploring an alternative approach to Lyme disease surveillance in Maryland. Zoonoses Public Health. 2018;65:254–9. https://doi.org/10.1111/zph.12446
22. Epstein MM, Dutcher SK, Maro JC, Saphirak C, DeLuccia S, Ramanathan M, et al. Validation of an electronic algorithm for Hodgkin and non-Hodgkin lymphoma in ICD-10-CM. Pharmacoepidemiol Drug Saf. 2021;30:910–7. https://doi.org/10.1002/pds.5256
23. Ammann EM, Leira EC, Winiecki SK, Nagaraja N, Dandapat S, Carnahan RM, et al. Chart validation of inpatient ICD-9-CM administrative diagnosis codes for ischemic stroke among IGIV users in the Sentinel Distributed Database. Medicine (Baltimore). 2017;96:e9440. https://doi.org/10.1097/MD.0000000000009440
24. Lo Re V 3rd, Carbonari DM, Jacob J, Short WR, Leonard CE, Lyons JG, et al. Validity of ICD-10-CM diagnoses to identify hospitalizations for serious infections among patients treated with biologic therapies. Pharmacoepidemiol Drug Saf. 2021;30:899–909. https://doi.org/10.1002/pds.5253
25. Clayton JL, Jones SG, Dunn JR, Schaffner W, Jones TF. Enhancing Lyme disease surveillance by using administrative claims data, Tennessee, USA. Emerg Infect Dis. 2015;21:1632–4. https://doi.org/10.3201/eid2109.150344

Address for correspondence: Noelle M. Cocoros, Harvard Pilgrim Health Care Institute, 401 Park Dr, Ste 401 East, Boston, MA 02215, USA; email: Noelle_Cocoros@harvardpilgrim.org

Genomic Characteristics of Emerging Intraerythrocytic *Anaplasma capra* and High Prevalence in Goats, China

Zhe-Tao Lin, Li-Feng Du, Ming-Zhu Zhang, Xiao-Yu Han, Bai-Hui Wang, Jiao Meng, Fu-Xun Yu, Xiao-Quan Zhou, Ning Wang, Cheng Li, Xiao-Yang Wang, Jing Liu, Wan-Ying Gao, Run-Ze Ye, Luo-Yuan Xia, Yi Sun, Na Jia, Jia-Fu Jiang, Lin Zhao,[1] Xiao-Ming Cui,[1] Lin Zhan,[1] Wu-Chun Cao[1]

Anaplasma capra is an emerging tickborne human pathogen initially recognized in China in 2015; it has been reported in ticks and in a wide range of domestic and wild animals worldwide. We describe whole-genome sequences of 2 *A. capra* strains from metagenomic sequencing of purified erythrocytes from infected goats in China. The genome of *A. capra* was the smallest among members of the genus *Anaplasma*. The genomes of the 2 *A. capra* strains contained comparable G+C content and numbers of pseudogenes with intraerythrocytic *Anaplasma* species. The 2 *A. capra* strains had 54 unique genes. The prevalence of *A. capra* was high among goats in the 2 endemic areas. Phylogenetic analyses revealed that the *A. capra* strains detected in this study were basically classified into 2 subclusters with those previously detected in Asia. Our findings clarify details of the genomic characteristics of *A. capra* and shed light on its genetic diversity.

Anaplasma capra is an emerging tickborne zoonotic pathogen in the genus *Anaplasma*, family Anaplasmataceae, and was initially identified in blood samples from asymptomatic goats (*Capra aegagrus hircus*) and a febrile human patient with tick-bite history in China in 2015 (*1*). The patient infected with *A. capra* had fever, headache, malaise, dizziness, myalgia, gastrointestinal symptoms, rash, lymphadenopathy, and abnormalities in cerebrospinal fluid pleocytosis and hepatic aminotransferase. Since then, *A. capra* has been detected in various domestic animals (e.g., goats, sheeps, cattle, yaks, and dogs) (*2*–*5*) and wild animals (e.g., takins, muntjacs, water deer, musk deer, onagers, serows, and brown hares) (*6*–*10*), and in a wide range of ticks (e.g., *Ixodes persulcatus*, *Haemaphysalis longicornis*, *H. qinghaiensis*, *Dermacentor abaensis*, *D. nuttalli*, *and Rhipicephalus microplus* [*1*,*11*–*14*]) across China and around the world (*2*,*7*–*10*,*15*,*16*), posing a potential threat to the health of humans and animals.

Members of the family Anaplasmataceae have complex life cycles involving vertebrate hosts and hematophagous ticks, many of which have emerged as human pathogens. The genus *Anaplasma* was proposed according to the phylogenetic analyses based on 16S rRNA and *groEL* sequences (*17*) and initially encompassed 6 species: *A. phagocytophilum*, *A. marginale*, *A. centrale*, *A. ovis*, *A. platys*, and *A. bovis*. Subsequently, 2 candidate novel species (*A. capra* and *A. odocoilei*) and other unclassified genovariants (*1*,*18*–*20*) were included in the List of Prokaryotic Names with Standing in Nomenclature (https://www.bacterio.net) pending validation. To date, 5 *Anaplasma* species have been known to infect humans: *A. phagocytophilum*, *A. capra*, *A. ovis*, *A. platys*, and *A. bovis* (*21*). Since the *A. marginale* genome sequence was reported in 2005 (*22*), a total of 24 *A. marginale* genomes (*23*), 32 *A. phagocytophilum* genomes (*24*,*25*), 1 *A. centrale* genome

Author affiliations: State Key Laboratory of Pathogen and Biosecurity, Beijing Institute of Microbiology and Epidemiology, Beijing, China (Z.-T. Lin, L.-F. Du, M.-Z. Zhang, X.-Y. Han, Y. Sun, N. Jia, J.-F. Jiang, X.-M. Cui, W.-C. Cao); Institute of EcoHealth, School of Public Health, Shandong University, Jinan, China (L.-F. Du, M.-Z. Zhang, B.-H. Wang, N. Wang, C. Li, X.-Y. Wang, J. Liu, W.-Y. Gao, R.-Z. Ye, L.-Y. Xia, L. Zhao); National Health Commission Key Laboratory of Pulmonary Immunological Diseases, Guizhou Provincial People's Hospital, Guiyang, China (J. Meng, F.-X. Yu, L. Zhan); Guizhou Provincial Blood Center, Guiyang (X.-Q. Zhou)

DOI: https://doi.org/10.3201/eid2909.230131

[1]These senior authors contributed equally to this article.

(*26*), 2 *A. ovis* genomes (*27*), and 1 *A. platys* genome (*28*) have been sequenced and deposited in GenBank. Although *A. capra* has been extensively detected in ticks and animal hosts worldwide, no genome of the emerging pathogen has been determined so far, which has hindered us from better understanding its genetic features and pathogenesis. Considering *A. capra* is an intraerythrocytic pathogen and abundant in blood samples of host goats (*1*,*29*), we separated erythrocytes from the blood of infected goats to enrich the bacteria and generated the entire genome of *A. capra* using metagenome assembly to promote better understanding of this emerging pathogen, to compare the characteristics of *A. capra* genomes with previously published genomes of other *Anaplasma* and related species, and to evaluate intraspecies genetic diversity of *A. capra* in different geographic locations and tick species across China.

Materials and Methods

Sample Collection and Preparation

We collected EDTA blood samples from 3 flocks of goats in Shandong Province and a flock of goats in Guizhou Province, China (Appendix Figure 1, https://wwwnc.cdc.gov/EID/article/29/9/23-0131-App1.pdf), during September 2021–July 2022. Meanwhile, we prepared blood smears for some goats. We collected host-seeking ticks in the same areas where the infected goats lived by dragging white flags over vegetation. An entomologist (Y.S.) identified all ticks to the species level and developmental stage. We extracted DNA from each goat blood sample or tick by using a High Pure PCR Template Preparation Kit (Roche, https://www.roche.com) according to the manufacturer's instructions.

PCRs and Sequencing

We conducted a nested PCR specific for the citrate synthase (*gltA*) gene of *A. capra* (Appendix Table 1) to screen all goat blood and tick samples, as previously described (*1*). We amplified all the positive samples for *gltA* by specific PCRs targeting the 16S rRNA, *msp4*, and *groEL* genes of *A. capra* (Appendix Table 1). We sequenced all amplicons to confirm the correctness of PCR results and conducted a SYBR Green–based quantitative PCR (qPCR) targeting different regions of the *gltA* gene by using a specific primer (Appendix Table 1).

Fluorescence In Situ Hybridization

We used fluorescence in situ hybridization (FISH) to observe the *A. capra* on blood smears. We designed the probe on the basis of the 16S rRNA full-length sequence of *A. capra* (Appendix Table 2) and labeled it with Quasar 570. We resuspended the pooled FISH probes in a final concentration of 25 μmol/L in RNase-free storage buffer, which we protected from light and stored at –20°C. We performed FISH on the prepared blood smear with a commercial kit (Biosearch Technologies, https://www.biosearchtech.com), according to the manufacturer's instructions.

Enrichment of *A. capra* for Genomic Sequencing

We separated erythrocytes from infected goats by conducting gradient centrifugation using cell separation solution (Eppendorf, https://www.eppendorf.com) for 20 min at 200 × *g* at 4°C. Then, we added 4 times volume of precooled (4°C) erythrocyte lysis buffer (Solarbio, http://www.solarbio.net) to the isolated erythrocytes by gentle pipetting to ensure adequate mixing. After placing the lysis solution at 4°C for 10 min, we centrifuged the solution at 350 × *g* for 10 min to remove residual blood cells. After that treatment, we maximally removed the host DNA in samples. Finally, we centrifuged the supernatant at 20,000 × *g* at 4°C for 30 min. We resuspended the pooled *A. capra* for DNA extraction by using the High Pure PCR Template Preparation Kit (Roche). We then constructed a sequencing library by using the AxyPrep MAG PCR Clean Up Kit (Fisher Scientific, https://www.fishersci.com) for an MGI sequencing set (https://en.mgi-tech.com). We prepared the sequencing library according to the Whole Genome Sequencing Library Preparation Protocol (MGI). We sequenced the paired-end libraries with a read length of 2 × 150 bp on a DNBseq-T7 platform at Grandomics Gene Technology Beijing Co. Ltd (Beijing, China).

Genome Assembly and Comparative Analyses

We mapped the clean reads to the goat (*Capra hircus*) reference genome (GenBank accession no. GCF_001704415) by using SAMtools 1.14 (*30*) to discard host-derived reads. We de novo assembled contigs from the unmapped reads by using metaSPAdes 3.15.3 (*31*). We performed contig binning by using MetaBAT 2.15 (*32*) and evaluated assembly quality by using CheckM version 1.1.3 in linage_wf mode, which searches for universal single-copy marker genes and deduces completeness and contamination on the basis of presence and absence of these genes (*33*). We generated G+C content, genome completeness, and annotation information and depicted them by using an approach described previously (*34*,*35*). We estimated average nucleotide identity (ANI) and DNA–DNA

hybridization (DDH) by using fastANI 1.32 (*36*) and GGDC (https://ggdc.dsmz.de/ggdc.php).

Phylogenetic Analyses

We deposited in GenBank the results of the phylogenetic analysis of the whole genomes of the 2 *A. capra* strains and all the genomes of *Anaplasma* species by using Orthofinder 2.5.4 (*37*), after eliminating the poorly aligned positions and divergent regions by using Gblocks 0.91b. We aligned trimmed sequence by using Muscle 5.1 (R.C. Edgar, unpub. data, https://doi.org/10.1101/2021.06.20.449169) and constructed the phylogenetic tree by using iqtree 2.2.0.3 (*38*). Furthermore, we conducted phylogenetic analyses on *A. capra gltA*, *groEL*, 16S rRNA, and *msp4* genes obtained from infected goats and ticks by using the maximum-likelihood method in MEGA11 (*39*).

Functional Analysis of Predicted Genes

To find difference in the Kyoto Encyclopedia of Genes and Genomes (KEGG) between the 2 strains of *A. capra* and other species in the genus *Anaplasma*, were annotated orthogroup sequences by using KOfam 1.4.0 (*40*) and illustrated them using a Venn diagram. We used the software eggNOG-Mapper 2.1.7 to determine the Clusters of Orthologous Group (COG) categories for protein encoding regions (*41*).

Results

Forty-three (59.7%) of 72 goat blood samples were positive for *gltA* gene of *A. capra*. We chose 2 blood samples (1 from a 2-year-old female goat in Shandong Province and another from a 10-month-old female goat in Guizhou Province) (Appendix Figure 1) for next-generation sequencing because they had high bacterial loads (8.4×10^6 *gltA* gene copies/mL blood for the goat in Shandong Province and 2.0×10^6 *gltA* gene copies/mL blood for the goat in Guizhou Province) as estimated by qPCR (Appendix Table 1). In addition, we visualized *A. capra* by specific FISH in erythrocytes on the blood smear prepared from the goat in Shandong Province for next-generation sequencing (Figure 1).

The metagenome sequencing resulted in >38 million 150-bp clean reads from each sample. Despite primary removing of host DNA, 95.9% and 93.3% of reads in the 2 samples were mapped to the goat genome and discarded. The remaining reads were subsequently de novo assembled into contigs by using the SPAdes 3.15.3 with meta parameters (*31*). The 2 assembled *A. capra* genomes were named *A. capra* str. BIME1 (GenBank accession no. GCA_025628785.1) and *A. capra* str. BIME2 (GenBank accession no. GCA_025628805.1), and had a higher level of completeness (99.79% for BIME1 and 99.36% for BIME2). The genome of *A. capra* was the smallest (≈1.07 Mb) among those in the genus *Anaplasma* and the second smallest genome of the family Anaplasmataceae, just after *Neorickettsia sennetsu* (0.859 Mb) (*24*). The genome sequences of the 2 strains shared 99.89% nucleotide similarity with each other.

We compared the 2 *A. capra* genomes with other representative species strains in the genus *Anaplasma* (Appendix Table 3). The G+C content (48.3% for both) of the 2 *A. capra* genomes was similar to those of *A. ovis*, *A. marginale*, *and A. centrale*, which are all intraerythrocytic pathogens. The *A. capra* genomes yielded a total of 929 and 932 genes, of which 862 and 863, respectively, represented coding sequences. They possessed 37 tRNAs and a complete ribosomal RNA operon, in which the 16S rRNA gene was separated from the 23S-5S rRNA gene pair (Figure 2) as displayed by other members of the order Rickettsiales (*42*). The 2 strains of *A. capra* and other intraerythrocytic *Anaplasma* species, including *A. ovis*, *A. centrale*, and *A. marginale*, contained comparable numbers of pseudogenes that have lost functions owing to mutation accumulation and are observed more frequently in obligate intracellular bacteria where the lost gene functions are compensated by the host cells (*43*). Of note, *A. phagocytophilum* has ≈4-fold more pseudogenes than the other *Anaplasma* species (Appendix Table 3).

The estimated values of ANI and DDH between *A. capra* and other *Anaplasma* species suggested that *A. capra* were distinct from the other species. On the basis of ANI values, *A. capra* str. BIME1 was most similar to *A. marginale*, whereas *A. capra* str. BIME2 was most similar to *A. ovis*. The DDH results revealed that both *A. capra* strains were most close to *A. marginale* (Appendix Table 4). The phylogenetic analysis based on the single copy genes revealed that the 2 *A. capra* strains together occupied a distinct branch and were more closely related to *A. ovis*, *A. marginale*, and *A. centrale* than to *A. phagocytophilum* and *A. platys* in the genus *Anaplasma* (Figure 3, panel A). To explore the gene differences in species in the genus *Anaplasma*, we used Orthofinder (*37*) to identify the homologous genes. All species in the genus *Anaplasma* shared 643 genes in common, and the 2 *A. capra* strains together with other intraerythrocytic *Anaplasma* species (*A. ovis*, *A. centrale*, and *A. marginale*) shared 75 genes that are not present in the other 2 species, *A. phagocytophilum* and *A. platys*. Compared with other members of the genus *Anaplasma*, 14 genes were not possessed by *A. capra*. Of note, a total of 54 genes were only shared by the 2 *A. capra* strains, which had other 14 distinct genes in BIME1 and 10 in

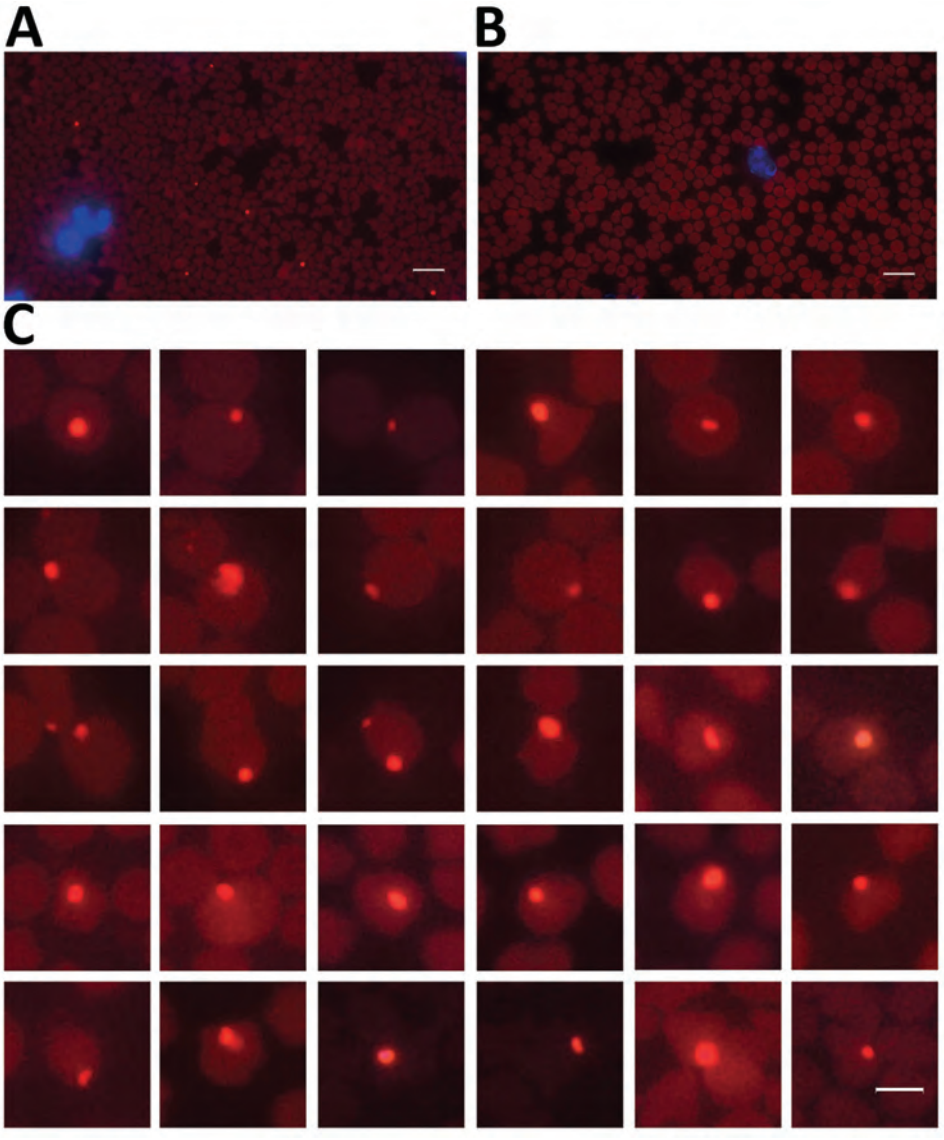

Figure 1. *Anaplasma capra* in the erythrocytes of an infected goat detected by fluorescence in situ hybridization (FISH) in study of emerging intraerythrocytic *A. capra* and high prevalence in goats, China. Glowing red indicates *A. capra*; blue indicates leukocyte nucleus stained with fluorescent antibody blocker containing DAPI. A) FISH results under fluorescence microscope of *A. capra*. B) FISH results of *A. capra*–negative blood smear. C) FISH results showing different shapes and sizes of *A. capra* in erythrocytes.

BIME2 (Figure 3, panel B). In addition, we identified 25 virulent genes in the 2 *A. capra* strains that were shared by all the species in the genus of *Anaplasma*, including *virB2* gene family, *virB6* gene family, *virB4* gene family, *virB8* gene family, *virB9* gene family, and *virB3*, *virB7*, *virB10*, *virB11*, *virD4*, *and Ats-1* genes that encode the type 4 secretion system and membrane protein-encoding genes (Appendix Table 5).

Among the 54 unique genes of *A. capra*, a total of 37 were unclassified, none of which was assigned to any KEGG category. Six of the remaining 17 genes were associated with metabolic processing, 5 genes were related to genetic information processing, and 6 were involved in signaling and cellular processing (Appendix Table 6). Among them, the most noteworthy of genes were *RSF1*, a gene related to the repair of DNA double-strand breaks (*44*), and *desk*, which encodes a protein acting as a kinase at cold temperatures in *Bacillus subtilis* (*45*).

We classified the coding proteins of the 2 *A. capra* strains (BIME1 and BIME2) into functional clusters of orthologous group (COG) categories and compared them with those of representative species strains in the genus *Anaplasma* (Appendix Table 7). Most proteins were involved in translation, ribosomal structure and biogenesis, energy production and conversion, and nutrient (including amino acid, nucleotide, carbohydrate, coenzyme, and lipid) transport and metabolism, all of which were essential for bacterial survival. Of note, the number of genes encoding cell wall and membrane in *A. platys* was substantially lower than those of other *Anaplasma* species. In addition, ≈10% of the proteins did not assign to any COG category and were classified as function unknown in each species.

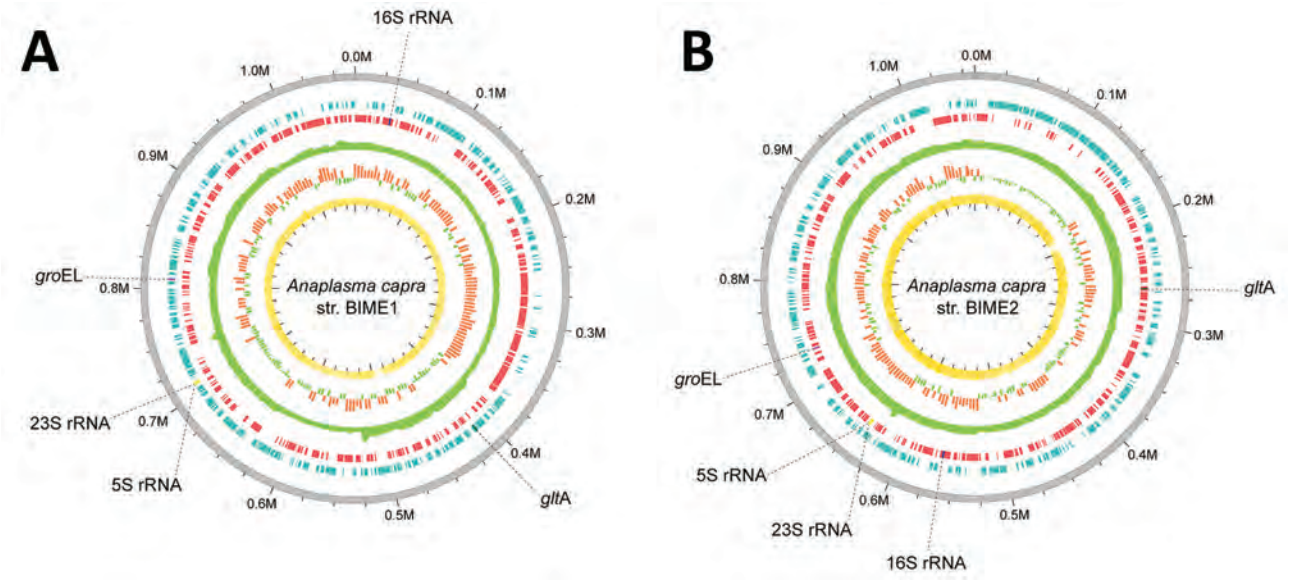

Figure 2. Circular map of *Anaplasma capra* strains BIME1 and BIME2 genomes in study of emerging intraerythrocytic *A. capra* and high prevalence in goats, China. The outermost ring shows the genome size in 100-kb increments. Moving inward, the blue-green and red marks indicate the coding sequences on the reverse and forward strands. The fourth ring represents the sequencing depth. The fifth ring shows the G+C skew, and the sixth rings show and G+C content. The location of *groEL and gltA* genes and the complete ribosomal RNA genes (5S rRNA, 16S rRNA, and 23S rRNA) within the genome are indicated.

We screened blood samples from 3 flocks of 54 goats in Shandong Province and a flock of 18 goats in Guizhou Province (Appendix Figure 1) by using nested PCR and qPCR targeting different regions of the *gltA* gene (Appendix Table 1). The overall positive rate was 59.7% (95% CI 48.4%–71.0%), and the positive rate was significantly higher among goats in Guizhou Province than in Shandong Province (77.8% vs. 53.7%; p<0.001). Accordingly, among the *H. longicornis* ticks collected from the same sites of the positive goats, the overall positive rate was 8.0% (95% CI 4.2%–11.8%), and the *A. capra* infection rate was significantly higher among ticks in Guizhou Province than that in Shandong Province (15.8% vs. 4.9%; p<0.001) (Appendix Table 8). To understand the genetic diversity, we amplified *A. capra* 16S rRNA (1,500 bp), *groEL* (1264 bp), and *msp4* (799 bp) genes from those positive samples. We compared the nucleotide identities for each gene sequence and (Appendix Figures 2–5; GenBank accession numbers are provided).

The *gltA* genes amplified from either goats or ticks in this study had 99.7%–100% identity with each other and with the strain that infected humans (Appendix Figure 2). The phylogenetic analysis based on *gltA* gene revealed that the *A. capra* sequences in this study were in an independent cluster from those previously reported in various animals from China and South Korea but distinct from those detected in wild and domestic animals from Europe and Kyrgystan. The South Korea water deer seemed to be capable of carrying both variants of *A. capra* (Figure 4, panel A). No *A. capra groEL* gene was acquired from tick samples, and the sequences from goats shared 99.4%–100% identity with each other and 99.8%–100% with sequences from humans (Appendix Figure 3). Similarly, the phylogenetic analyses based on the *groEL* gene revealed that *A. capra* strains of this study clustered with those from humans, dogs, and domestic ruminants in Asia but were distinguished from those in Europe (Figure 4, panel B). The entire 16S rRNA gene sequences (1,500 bp) of *A. capra* detected in goats and *H. longicornis* ticks from either Shandong or Guizhou Province shared average similarity of >99.7% from each other and from the sequence detected in humans (Appendix Figure 4). The phylogenetic tree based on 16S rRNA gene sequences indicated that all the *A. capra* strains detected in this study were in the same clade with previously reported strains in Asia (Figure 4, panel C). The *A. capra msp4* gene sequences were also relatively conserved (Appendix Figure 5) among the goats and ticks, and the topology of phylogenetic tree based on *msp4* gene were similar to that based on the 16S rRNA gene, in which all *A. capra* sequences clustered in the clade different from other members of *Anaplasma* species (Figure 4, panel D).

Discussion

Whole-genome assembly of obligate intracellular bacteria has usually been hindered by the DNA presence

of host cells. In this study, we first assembled 2 complete genomes of *A. capra* from the red blood cells of infected goats by using the metagenomic sequencing strategy. Because *A. capra* is an intraerythrocytic pathogen (*1*,*29*), we separated erythrocytes from the periphery blood of the infected goats and then lysed them for maximum removal of goat DNA. After metagenomic next-generation sequencing, we discarded the remaining goat genomic sequences and successfully assembled the *A. capra* genomes from 2 infected goats. The high percentage of reads from goat could be attributable to the low abundance of *A. capra* in erythrocytes or the fact that all other host cells rather than erythrocytes were not totally removed during the isolation of erythrocytes. In any case, the completeness of the 2 *A. capra* genomes are up to 99.79% for BIME1 and 99.36% for BIME2. The genome sizes obtained in this study reach 1,066,874 bp for BIME1 and 1,059,758 bp for BIME2. Therefore, their predicted sizes are ≈1.07 Mbp, which remain the smallest genome in the genus of *Anaplasma*. The phylogenetic analysis based on genome sequences and the comparative analyses of genomic characteristics provide the evidence that *A. capra* is closely related to other intraerythrocytic *Anaplasma* species, including *A. ovis*, *A. centrale*, and *A. marginale*.

The genome of *A. capra* consists of a single circular chromosome with a total size of 1.07 Mbp and has 862 protein-coding genes, which is smaller than other *Anaplasma* species. In fact, all the *Anaplasma* genomes sequenced so far are relatively small compared with free-living bacteria. The small genome size might be because a part of the intracellular bacterial functions has been compensated by the host cells, a process of reductive evolution that has occurred in the order Rickettsiales because of long-term intracellular association with eukaryotic hosts (*46*). This reductive evolution is associated with the frequent formation of pseudogenes, affecting distinct loci in different species (*47*). Moreover, we found that the G+C content of *A. capra* is close to that of *A. ovis*, *A. marginale*, and *A. centrale*. Of note, their relatedness also seems to be closest according to the phylogenetic analysis. The common invasiveness of erythrocytes also accounts for their high similarity.

A limitation of this study is that both the *A. capra* genomes were directly derived from the blood samples of infected goats through metagenomic next-generation sequencing. Unfortunately, we did not obtain the genomes at chromosome level, which usually relies on 3rd-generation sequencing of an isolate. In any case, this study reveals the genomic characteristics of *A. capra* and sheds light on its genetic diversity.

The high prevalence of *A. capra* in goats from Shandong and Guizhou Provinces in this study

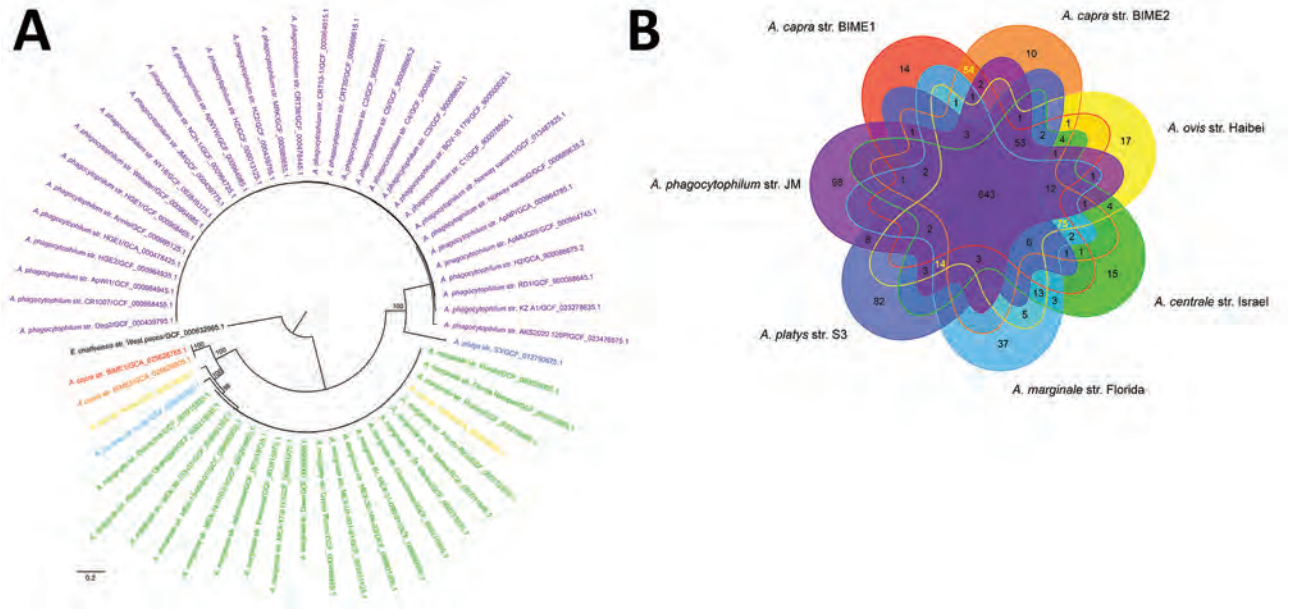

Figure 3. Phylogenetic tree and genomic comparison among *Anaplasma* species in study of emerging intraerythrocytic *A. capra* and high prevalence in goats, China. A) Phylogenetic tree of *Anaplasma* species based on all the genomic sequences deposited in GenBank, constructed by using maximum-likelihood method with *Ehrlichia chaffeensis* as an outgroup. The percentages of replicate trees in which the associated taxa clustered together in the bootstrap test (1,000 replicates) are shown next to the branches. B) Differences in gene contents among *Anaplasma* species strains. Venn diagrams show the distribution of shared and unique gene clusters among representative *Anaplasma* species.

further indicate that domestic ruminants might be the main animal hosts, as suggested by previous studies (*2*–*5*). *H. longicornis* ticks collected from the same sites of the positive goats either in Shandong Province or Guizhou Province are naturally infected with *A. capra*, implying the role of the tick species in transmission of the pathogen. Phylogenetic analyses based on the *gltA* and *groEL* genes demonstrate that *A. capra* strains detected from goats and *H. longicornis* ticks in this study are clustered in the same clade with those

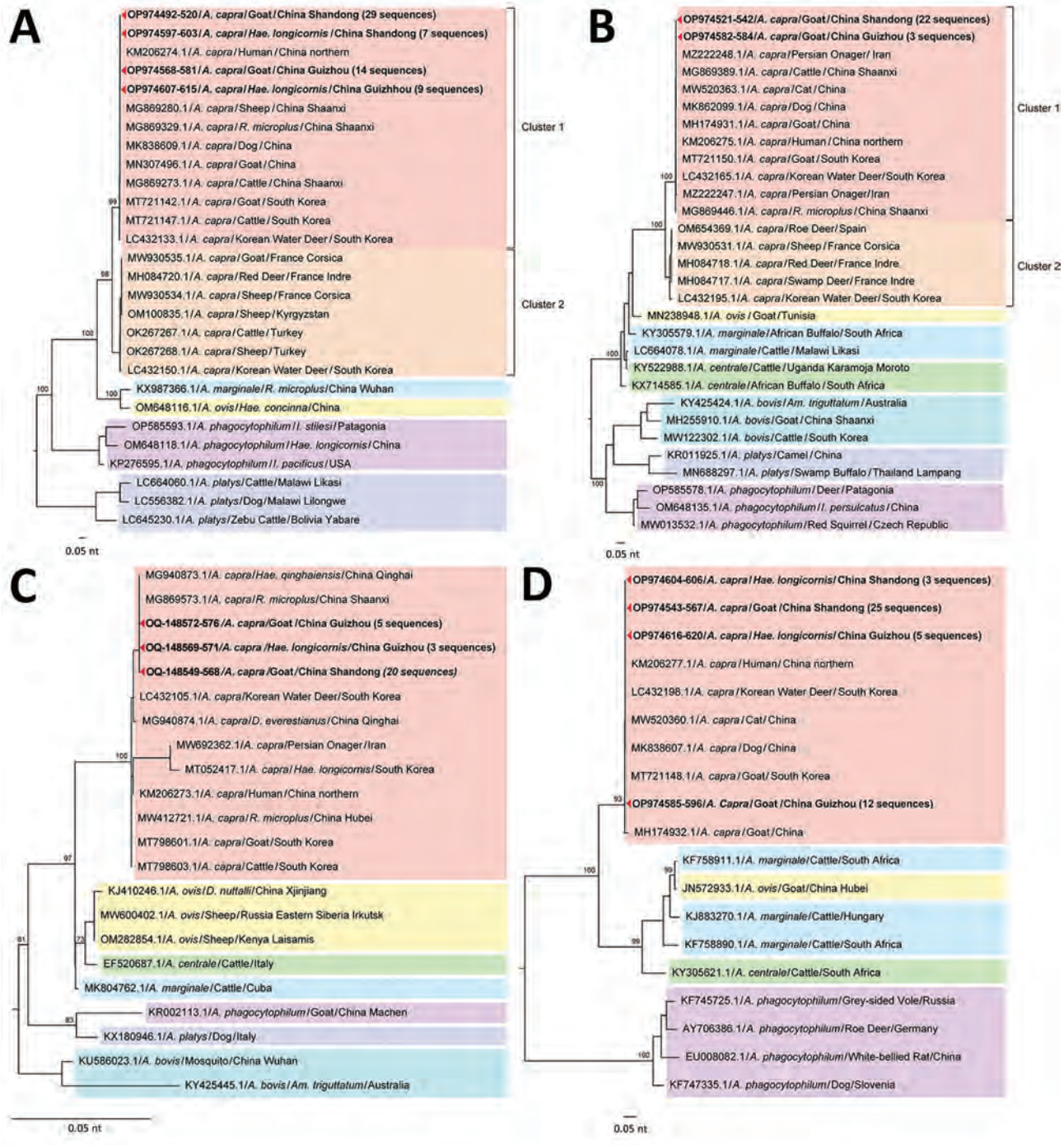

Figure 4. Phylogenetic analysis of *Anaplasma capra* based on nucleotide sequences of 4 genes in study of emerging intraerythrocytic *A. capra* and high prevalence in goats, China. A) Phylogenetic tree based on 536 bp nucleotide sequence of *gltA*. B) Phylogenetic tree based on 620 bp nucleotide sequence of *groEL*. C) Phylogenetic tree based on 860 bp nucleotide sequence of 16S rRNA. D) Phylogenetic tree based on 642 bp nucleotide sequence of *msp4*. We performed bootstrap analysis of 1,000 replicates to assess the reliability of the reconstructed phylogenies. GenBank accession numbers are provided. Scale bars show estimated evolutionary distance.

from humans, domestic ruminants, dogs, and Korean water deer (*2*,*3*,*5*,*10*). Of note, another clade of *A. capra* strains is mainly found in the wild and domestic animals from Europe and Kyrgyzstan (*6*,*10*,*48*). Those findings suggest that the enzootic cycles in various regions of the world might be different. Public health professionals should pay enough attention and formulate prevention and control strategies to reduce the health threat of the emerging tickborne pathogen to humans in other countries besides China.

This study was supported by the Natural Science Foundation of China (grant no. 81621005 to W.-C.C.; grant nos. 81760605, 82160633, and 82103897 to L.Z.), the Natural Science Foundation of Shandong Province, China (grant no. ZR2020QH299 to L.Z.), and the Cheeloo Young Scholar Program of Shandong University.

About the Author

Mr. Lin is an MPH candidate in the State Key Laboratory of Pathogen and Biosecurity at the Beijing Institute of Microbiology and Epidemiology. His primary research interests are the prevention and control of tickborne pathogens.

References

1. Li H, Zheng YC, Ma L, Jia N, Jiang BG, Jiang RR, et al. Human infection with a novel tick-borne *Anaplasma* species in China: a surveillance study. Lancet Infect Dis. 2015;15:663–70. https://doi.org/10.1016/S1473-3099(15)70051-4
2. Yang J, Liu Z, Niu Q, Liu J, Han R, Guan G, et al. A novel zoonotic *Anaplasma* species is prevalent in small ruminants: potential public health implications. Parasit Vectors. 2017;10:264. https://doi.org/10.1186/s13071-017-2182-9
3. Seo MG, Ouh IO, Lee H, Geraldino PJL, Rhee MH, Kwon OD, et al. Differential identification of *Anaplasma* in cattle and potential of cattle to serve as reservoirs of *Anaplasma capra*, an emerging tick-borne zoonotic pathogen. Vet Microbiol. 2018;226:15–22. https://doi.org/10.1016/j.vetmic.2018.10.008
4. Wang Y, Zhang Q, Han S, Li Y, Wang B, Yuan G, et al. *Ehrlichia chaffeensis* and four *Anaplasma* species with veterinary and public health significance identified in Tibetan sheep (*Ovis aries*) and yaks (*Bos grunniens*) in Qinghai, China. Front Vet Sci. 2021;8:727166. https://doi.org/10.3389/fvets.2021.727166
5. Shi K, Li J, Yan Y, Chen Q, Wang K, Zhou Y, et al. Dogs as new hosts for the emerging zoonotic pathogen *Anaplasma capra* in China. Front Cell Infect Microbiol. 2019;9:394. https://doi.org/10.3389/fcimb.2019.00394
6. Yang J, Liu Z, Niu Q, Mukhtar MU, Guan G, Liu G, et al. A novel genotype of "*Anaplasma capra*" in wildlife and its phylogenetic relationship with the human genotypes. Emerg Microbes Infect. 2018;7:210. https://doi.org/10.1038/s41426-018-0212-0
7. Staji H, Yousefi M, Hamedani MA, Tamai IA, Khaligh SG. Genetic characterization and phylogenetic of *Anaplasma capra* in Persian onagers (*Equus hemionus onager*). Vet Microbiol. 2021;261:109199. https://doi.org/10.1016/j.vetmic.2021.109199
8. Rocchigiani G, Ebani VV, Nardoni S, Bertelloni F, Bascherini A, Leoni A, et al. Molecular survey on the occurrence of arthropod-borne pathogens in wild brown hares (*Lepus europaeus*) from central Italy. Infect Genet Evol. 2018;59:142–7. https://doi.org/10.1016/j.meegid.2018.02.005
9. Sato M, Nishizawa I, Fujihara M, Nishimura T, Matsubara K, Harasawa R. Phylogenetic analysis of the 16S rRNA gene of *Anaplasma* species detected from Japanese serows (*Capricornis crispus*). J Vet Med Sci. 2009;71:1677–9. https://doi.org/10.1292/jvms.001677
10. Amer S, Kim S, Yun Y, Na KJ. Novel variants of the newly emerged *Anaplasma capra* from Korean water deer (*Hydropotes inermis argyropus*) in South Korea. Parasit Vectors. 2019;12:365. https://doi.org/10.1186/s13071-019-3622-5
11. Yang J, Liu Z, Niu Q, Liu J, Han R, Liu G, et al. Molecular survey and characterization of a novel *Anaplasma* species closely related to *Anaplasma capra* in ticks, northwestern China. Parasit Vectors. 2016;9:603. https://doi.org/10.1186/s13071-016-1886-6
12. Zhang H, Sun Y, Jiang H, Huo X. Prevalence of severe febrile and thrombocytopenic syndrome virus, *Anaplasma* spp. and *Babesia microti* in hard ticks (Acari: Ixodidae) from Jiaodong Peninsula, Shandong Province. Vector Borne Zoonotic Dis. 2017;17:134–40. https://doi.org/10.1089/vbz.2016.1978
13. Han R, Yang JF, Mukhtar MU, Chen Z, Niu QL, Lin YQ, et al. Molecular detection of *Anaplasma* infections in ixodid ticks from the Qinghai-Tibet Plateau. Infect Dis Poverty. 2019;8:12. https://doi.org/10.1186/s40249-019-0522-z
14. Guo WP, Zhang B, Wang YH, Xu G, Wang X, Ni X, et al. Molecular identification and characterization of *Anaplasma capra* and *Anaplasma platys*–like in *Rhipicephalus microplus* in Ankang, Northwest China. BMC Infect Dis. 2019;19:434. https://doi.org/10.1186/s12879-019-4075-3
15. Remesar S, Prieto A, García-Dios D, López-Lorenzo G, Martínez-Calabuig N, Díaz-Cao JM, et al. Diversity of *Anaplasma* species and importance of mixed infections in roe deer from Spain. Transbound Emerg Dis. 2022;69:e374–85. https://doi.org/10.1111/tbed.14319
16. Elhachimi L, Rogiers C, Casaert S, Fellahi S, Van Leeuwen T, Dermauw W, et al. Ticks and tick-borne pathogens abound in the cattle population of the Rabat-Sale Kenitra Region, Morocco. Pathogens. 2021;10:1594. https://doi.org/10.3390/pathogens10121594
17. Dumler JS, Barbet AF, Bekker CP, Dasch GA, Palmer GH, Ray SC, et al. Reorganization of genera in the families *Rickettsiaceae* and *Anaplasmataceae* in the order *Rickettsiales*: unification of some species of *Ehrlichia* with *Anaplasma, Cowdria* with *Ehrlichia* and *Ehrlichia* with *Neorickettsia*, descriptions of six new species combinations and designation of *Ehrlichia equi* and 'HGE agent' as subjective synonyms of *Ehrlichia phagocytophila.* Int J Syst Evol Microbiol. 2001;51:2145–65. https://doi.org/10.1099/00207713-51-6-2145
18. Tate CM, Howerth EW, Mead DG, Dugan VG, Luttrell MP, Sahora AI, et al. *Anaplasma odocoilei* sp. nov. (family Anaplasmataceae) from white-tailed deer (*Odocoileus virginianus*). Ticks Tick Borne Dis. 2013;4:110–9. https://doi.org/10.1016/j.ttbdis.2012.09.005
19. Calchi AC, Vultão JG, Alves MH, Yogui DR, Desbiez ALJ, De Santi M, et al. *Ehrlichia* spp. and *Anaplasma* spp. in Xenarthra mammals from Brazil, with evidence of novel '*Candidatus Anaplasma* spp.'. Sci Rep. 2020;10:12615. https://doi.org/10.1038/s41598-020-69263-w
20. Vanstreels RET, Yabsley MJ, Parsons NJ, Swanepoel L, Pistorius PA. A novel candidate species of *Anaplasma* that infects avian erythrocytes. Parasit Vectors. 2018;11:525. https://doi.org/10.1186/s13071-018-3089-9

21. Rar V, Tkachev S, Tikunova N. Genetic diversity of *Anaplasma* bacteria: twenty years later. Infect Genet Evol. 2021;91:104833. https://doi.org/10.1016/j.meegid. 2021.104833
22. Brayton KA, Kappmeyer LS, Herndon DR, Dark MJ, Tibbals DL, Palmer GH, et al. Complete genome sequencing of *Anaplasma marginale* reveals that the surface is skewed to two superfamilies of outer membrane proteins. Proc Natl Acad Sci U S A. 2005;102:844–9. https://doi.org/10.1073/pnas.0406656102
23. Dall'Agnol B, Webster A, Souza UA, Barbieri A, Mayer FQ, Cardoso GA, et al. Genomic analysis on Brazilian strains of *Anaplasma marginale*. Rev Bras Parasitol Vet. 2021;30:e000421. https://doi.org/10.1590/s1984-29612021043
24. Dunning Hotopp JC, Lin M, Madupu R, Crabtree J, Angiuoli SV, Eisen JA, et al. Comparative genomics of emerging human ehrlichiosis agents. PLoS Genet. 2006;2:e21. https://doi.org/10.1371/journal.pgen.0020021
25. Barbet AF, Al-Khedery B, Stuen S, Granquist EG, Felsheim RF, Munderloh UG. An emerging tick-borne disease of humans is caused by a subset of strains with conserved genome structure. Pathogens. 2013;2:544–55. https://doi.org/10.3390/pathogens2030544
26. Herndon DR, Palmer GH, Shkap V, Knowles DP Jr, Brayton KA. Complete genome sequence of *Anaplasma marginale* subsp. *centrale*. J Bacteriol. 2010;192:379–80. https://doi.org/10.1128/JB.01330-09
27. Liu Z, Peasley AM, Yang J, Li Y, Guan G, Luo J, et al. The *Anaplasma ovis* genome reveals a high proportion of pseudogenes. BMC Genomics. 2019;20:69. https://doi.org/10.1186/s12864-018-5374-6
28. Llanes A, Rajeev S. First whole genome sequence of *Anaplasma platys*, an obligate intracellular rickettsial pathogen of dogs. Pathogens. 2020;9:277. https://doi.org/10.3390/pathogens9040277
29. Peng Y, Lu C, Yan Y, Song J, Pei Z, Gong P, et al. The novel zoonotic pathogen, *Anaplasma capra*, infects human erythrocytes, HL-60, and TF-1 cells in vitro. Pathogens. 2021;10:600. https://doi.org/10.3390/pathogens10050600
30. Danecek P, Bonfield JK, Liddle J, Marshall J, Ohan V, Pollard MO, et al. Twelve years of SAMtools and BCFtools. Gigascience. 2021;10:giab008.
31. Nurk S, Meleshko D, Korobeynikov A, Pevzner PA. metaSPAdes: a new versatile metagenomic assembler. Genome Res. 2017;27:824–34. https://doi.org/10.1101/gr.213959.116
32. Prjibelski A, Antipov D, Meleshko D, Lapidus A, Korobeynikov A. Using SPAdes de novo assembler. Curr Protoc Bioinformatics. 2020;70:e102. https://doi.org/10.1002/cpbi.102
33. Parks DH, Imelfort M, Skennerton CT, Hugenholtz P, Tyson GW. CheckM: assessing the quality of microbial genomes recovered from isolates, single cells, and metagenomes. Genome Res. 2015;25:1043–55. https://doi.org/10.1101/gr.186072.114
34. Seemann T. Prokka: rapid prokaryotic genome annotation. Bioinformatics. 2014;30:2068–9. https://doi.org/10.1093/bioinformatics/btu153
35. Syberg-Olsen MJ, Garber AI, Keeling PJ, McCutcheon JP, Husnik F. Pseudofinder: detection of pseudogenes in prokaryotic genomes. Mol Biol Evol. 2022;39:msac153.
36. Jain C, Rodriguez-R LM, Phillippy AM, Konstantinidis KT, Aluru S. High throughput ANI analysis of 90K prokaryotic genomes reveals clear species boundaries. Nat Commun. 2018;9:5114. https://doi.org/10.1038/s41467-018-07641-9
37. Emms DM, Kelly S. OrthoFinder: phylogenetic orthology inference for comparative genomics. Genome Biol. 2019;20:238. https://doi.org/10.1186/s13059-019-1832-y
38. Minh BQ, Schmidt HA, Chernomor O, Schrempf D, Woodhams MD, von Haeseler A, et al. IQ-TREE 2: new models and efficient methods for phylogenetic inference in the genomic era. Mol Biol Evol. 2020;37:1530–4. https://doi.org/10.1093/molbev/msaa015
39. Tamura K, Stecher G, Kumar S. MEGA11: Molecular Evolutionary Genetics Analysis version 11. Mol Biol Evol. 2021;38:3022–7. https://doi.org/10.1093/molbev/msab120
40. Aramaki T, Blanc-Mathieu R, Endo H, Ohkubo K, Kanehisa M, Goto S, et al. KofamKOALA: KEGG ortholog assignment based on profile HMM and adaptive score threshold. Bioinformatics. 2020;36:2251–2. https://doi.org/10.1093/bioinformatics/btz859
41. Cantalapiedra CP, Hernández-Plaza A, Letunic I, Bork P, Huerta-Cepas J. eggNOG-mapper v2: functional annotation, orthology assignments, and domain prediction at the metagenomic scale. Mol Biol Evol. 2021;38:5825–9. https://doi.org/10.1093/molbev/msab293
42. Andersson SG, Zomorodipour A, Andersson JO, Sicheritz-Pontén T, Alsmark UC, Podowski RM, et al. The genome sequence of *Rickettsia prowazekii* and the origin of mitochondria. Nature. 1998;396:133–40. https://doi.org/10.1038/24094
43. Beare PA, Sandoz KM, Omsland A, Rockey DD, Heinzen RA. Advances in genetic manipulation of obligate intracellular bacterial pathogens. Front Microbiol. 2011;2:97. https://doi.org/10.3389/fmicb.2011.00097
44. Helfricht A, Wiegant WW, Thijssen PE, Vertegaal AC, Luijsterburg MS, van Attikum H. Remodeling and spacing factor 1 (RSF1) deposits centromere proteins at DNA double-strand breaks to promote non-homologous end-joining. Cell Cycle. 2013;12:3070–82. https://doi.org/10.4161/cc.26033
45. Albanesi D, Martín M, Trajtenberg F, Mansilla MC, Haouz A, Alzari PM, et al. Structural plasticity and catalysis regulation of a thermosensor histidine kinase. Proc Natl Acad Sci U S A. 2009;106:16185–90. https://doi.org/10.1073/pnas.0906699106
46. Darby AC, Cho NH, Fuxelius HH, Westberg J, Andersson SG. Intracellular pathogens go extreme: genome evolution in the Rickettsiales. Trends Genet. 2007;23:511–20. https://doi.org/10.1016/j.tig.2007.08.002
47. Ogata H, Audic S, Renesto-Audiffren P, Fournier PE, Barbe V, Samson D, et al. Mechanisms of evolution in *Rickettsia conorii* and *R. prowazekii*. Science. 2001;293:2093–8. https://doi.org/10.1126/science.1061471
48. Jouglin M, Rispe C, Grech-Angelini S, Gallois M, Malandrin L. *Anaplasma capra* in sheep and goats on Corsica Island, France: a European lineage within *A. capra* clade II? Ticks Tick Borne Dis. 2022;13:101934. https://doi.org/10.1016/j.ttbdis.2022.101934

Address for correspondence: Wu-Chun Cao, State Key Laboratory of Pathogen and Biosecurity, Beijing Institute of Microbiology and Epidemiology, 20 Dong-Da St, Fengtai District, Beijing 100071, China; email: caowuchun@126.com; Lin Zhao, Institute of EcoHealth, School of Public Health, Shandong University, 44 Wenhuaxi St, Jinan 250012, Shandong, China; email: zhaolin1989@sdu.edu.cn; Lin Zhan, NHC Key Laboratory of Pulmonary Immunological Diseases, Guizhou Provincial People's Hospital, 83 Zhongshan East Rd, Nanming District 550002, Guiyang, Guizhou, China; email: zhanlin300@hotmail.com

Global Estimate of Human Brucellosis Incidence

Christopher G. Laine, Valen E. Johnson, H. Morgan Scott, Angela M. Arenas-Gamboa

Brucellosis is a major public health concern worldwide, especially for persons living in resource-limited settings. Historically, an evidence-based estimate of the global annual incidence of human cases has been elusive. We used international public health data to fill this information gap through application of risk metrics to worldwide and regional at-risk populations. We performed estimations using 3 statistical models (weighted average interpolation, bootstrap resampling, and Bayesian inference) and considered missing information. An evidence-based conservative estimate of the annual global incidence is 2.1 million, significantly higher than was previously assumed. Our models indicate Africa and Asia sustain most of the global risk and cases, although areas within the Americas and Europe remain of concern. This study reveals that disease risk and incidence are higher than previously suggested and lie mainly within resource-limited settings. Clarification of both misdiagnosis and underdiagnosis is required because those factors will amplify case estimates.

Brucellosis is a bacterial disease that affects populations of livestock and humans, as well as their respective economies, throughout the world (*1*–*4*). Three of the *Brucella* species are highly virulent to their natural hosts, as well as to humans, and are considered endemic in most countries, predominantly in resource-limited settings (*1*,*2*,*4*,*5*). Those species are *B. abortus*, which primarily infects cattle; *B. melitensis*, which infects sheep and goats; and *B. suis*, which infects mainly swine (*4*). Of interest, although *Brucella* infections are a considerable concern for livestock and are known to be zoonotic, human brucellosis is less recognized and understood (*1*,*4*). In humans, the disease is typically characterized by nonspecific influenza-like illness manifesting as undulating fever, sweats, fatigue, and malaise, which are similar signs and symptoms to those of malaria, one of the most commonly acquired infectious diseases in resource-limited regions (*1*,*2*,*4*). Furthermore, undulant fever, arthritis, myocarditis, and neuropathies can occur among chronic cases of human brucellosis (*1*,*4*). Humans are normally exposed to *Brucella* spp. by consuming unpasteurized milk products or handling contaminated tissues such as aborted livestock placentas (*4*). Those exposure pathways put raw milk–product consumers, livestock owners, abattoir workers, and veterinarians at high risk of acquiring the disease within endemic areas (*4*).

Despite the established recognition of the zoonotic risk worldwide (*2*,*6*,*7*), the number of new human brucellosis cases annually remains unclear (*8*). For decades, researchers have attempted to identify the global and regional impact of this disease. However, all previous efforts to quantify the annual number of new cases either have not been based on sufficient, documented evidence (*9*) or have concluded that it was not possible to accurately determine the global incidence of this disease using results available from the scientific literature (*10*,*11*). In addition, annual incidence cannot be estimated solely from human brucellosis cases reported to intergovernmental public health institutions because of incomplete data and lack of representation among geographic regions (*8*).

To enhance understanding of the disease's effects worldwide, we aimed to identify at-risk human populations worldwide, estimate the risk for populations for which there are currently no available data, estimate the risk of acquiring human brucellosis both globally and regionally, and estimate annual incidence. We produced these estimates using animal and human brucellosis data reported to the World Organization of Animal Health (WOAH, formerly OIE) and human population data reported to the World Bank. To the best of our knowledge, the use of this approach has not previously been attempted. To accomplish these goals, we used 3 data sources: reported animal data that indicates the presence of *B. abortus*, *B. melitensis*, and *B. suis* among the 182 WOAH member states; reported human data compiled by WOAH demonstrating the presence of human brucellosis by country, without regard for *Brucella* species; and rural human population counts within these countries

Author affiliation: Texas A&M University, College Station, Texas, USA

DOI: http://doi.org/10.3201/eid2909.230052

(those with the highest likelihood of contact with livestock) from the World Bank. We used 3 distinct statistical approaches, weighted average interpolation, bootstrap resampling, and Bayesian hierarchical modeling, to estimate incidence and assess the confidence of our results. Our findings suggest that the severity and magnitude of global human brucellosis incidence have been significantly underestimated.

Materials and Methods

Although precise estimates of the annual incidence of human brucellosis cannot be obtained using existing data repositories or scientific reports alone (*8*,*10*,*11*), this study combines existing data sources and analyses from 3 statistical models to provide estimates of the annual incidence rates and characterize the uncertainty of these estimates. The data used in our analyses represent a combination of open-source data provided by WOAH, showing the presence of disease in animals and human case counts, and by the World Bank, showing national human populations and percentage of rural human populations. The statistical models we propose range from simple weighted average interpolation, to bootstrap resampling, and finally to Bayesian hierarchical models. We also estimate the risk by geographic region (Appendix Figure, https://wwwnc.cdc.gov/EID/article/29/9/23-0052-App1.pdf). We define population risk (i.e., incidence proportion) as the ratio of new cases within a population relative to the total population at risk. Consequently, the number of new cases could be calculated by multiplying the total population at risk by the population risk. This relationship between incidence, the population at risk, and population risk served as the basic framework for all statistical models. Because of the sharp decline in available information during the COVID-19 pandemic (*8*), we used data from the most recent uninterrupted 5-year timeframe (i.e., 2014–2018) (Appendix). To ensure best reporting practices, we conducted the study under the Guidelines for Accurate and Transparent Health Estimates Reporting (GATHER) (*12*).

General Modeling Procedures

To estimate the baseline human brucellosis incidence data at country and regional levels, we followed the methods described in Laine et al. (*8*). We first stratified the global human population into mutually exclusive country and region groups. To provide a population scale for individual countries, we added the World Bank estimates for each year (2014–2018) (*13*,*14*) into the dataset. Second, to provide a means of geographic comparison, we grouped the individual WOAH member countries into 4 continental regions (Africa, Americas, Asia, or Europe), as specified by WOAH (*5*). We excluded Oceania because its 7 countries and 132 total reported case counts (RCCs) during 2014–2018 provided insufficient data to statistically estimate case counts; those countries have small populations relative to the rest of the world, so they do not substantially affect the overall results. Subsequently, we categorized differences in reporting methods by each country into a mutually exclusive group (e.g., informative versus uninformative) on the basis of the information presented. Informative reports specified a quantified RCC within the report (RCC $\geq$0). Uninformative reports provided no quantified information on the human brucellosis status of the country. Because we assessed a 5-year timeframe and not every country reported annually, we took the average RCC as the input parameter from each of the countries that reported $\geq$3 of 5 years.

We used our observed RCC input parameters to estimate case counts for the uninformative reports, providing values for the overall regional and global incidence estimates. Specifically, to calculate the overall incidence, we divided the RCC input parameters by their respective populations at risk for the country-level risk (Appendix Figure); this parameter is essential for estimating among each of the models. Country-level risk is equivalent to incidence proportion, which can simply be referred to as risk. We applied this risk, through 3 models (Appendix), to estimate risk for those countries that did not provide RCCs for the study timeframe. After we used each model to estimate the risk for nonreporting countries, we multiplied the risk against each of the respective populations at risk to estimate incidence.

One of the most important risk factors for acquiring brucellosis is close contact with infected livestock, especially by engagement in activities known to increase the risk for infection, such as consuming raw milk and handling infected tissues (*4*,*15*,*16*). Of interest, we found no evidence in previous studies to suggest a certain livestock-to-human ratio as a risk factor. Furthermore, brucellosis is known to be routinely maintained and transmitted in transhumant herds, and wild animals and can propagate in areas with sparse livestock populations (*17*–*20*). What matters for transmission is the probability of contact, driven by the infected to susceptible ratio (routine sustained contact between infectious livestock or products and susceptible humans is more likely on smallholder farms in rural settings) (*17*). The degree of infection in the human population is, therefore, representative of the amount of interaction between infected animals or products and susceptible humans. Worldwide, most livestock reside in rural areas where it is

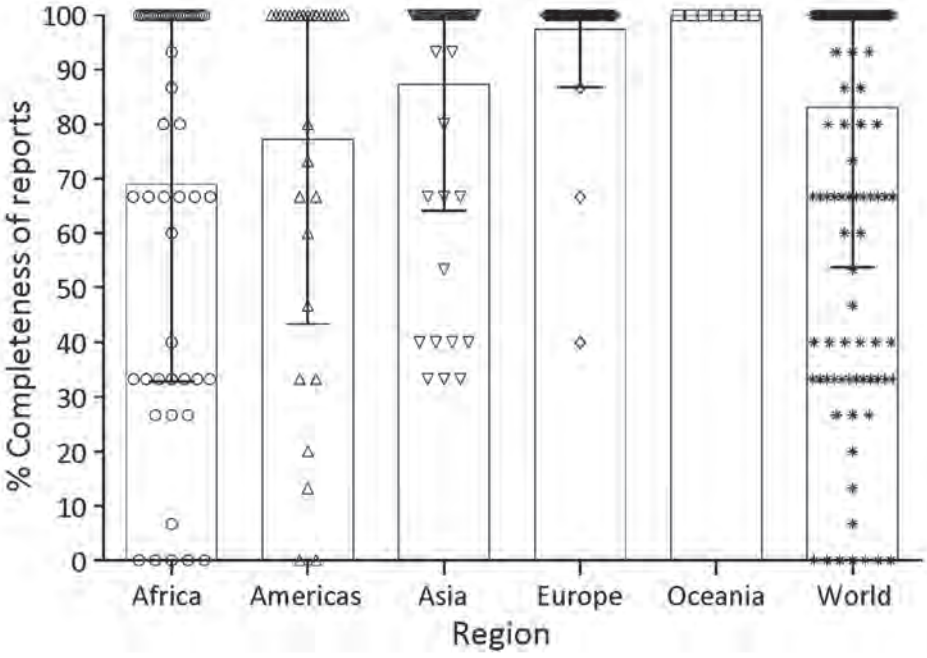

Figure 1. Percentage completeness of World Organization of Animal Health annual reports that provide information on each of the zoonotic *Brucella* species, by worldwide region, 2014–2018. Each point on the plot denotes the 5-year average percentage completeness of reports from an individual country. Reporting the presence or absence of all *Brucella* species (*B. abortus*, *B. melitensis*, and *B. suis*) equates to 100%. Bar tops indicate mean % completeness for each region and error bars indicate SDs from each mean.

common practice to consume raw milk; therefore, we used the World Bank dataset identifying the percentage of each country's population that resides in rural areas and multiplied it by the total population of each country to calculate the population at risk for each country (Appendix Figure). We segregated at-risk populations at the country level into different categories: rural populations in every country where brucellosis was reported in humans, rural populations in every country that reported the disease in livestock but that had not submitted RCCs, and rural populations in every country that did not report RCCs or the absence of *Brucella* spp. in livestock (Appendix).

Results

Previous studies have indicated that an accurate global disease incidence estimation is not possible using reported human data (*8*). Therefore, we used a novel approach to estimate disease incidence along with the uncertainties of those estimates. Our estimates used both human and animal information to identify human at-risk populations worldwide, estimate risk for populations for which there is currently no available data, estimate the risk of acquiring human brucellosis globally and regionally, and estimate annual global and regional incidence.

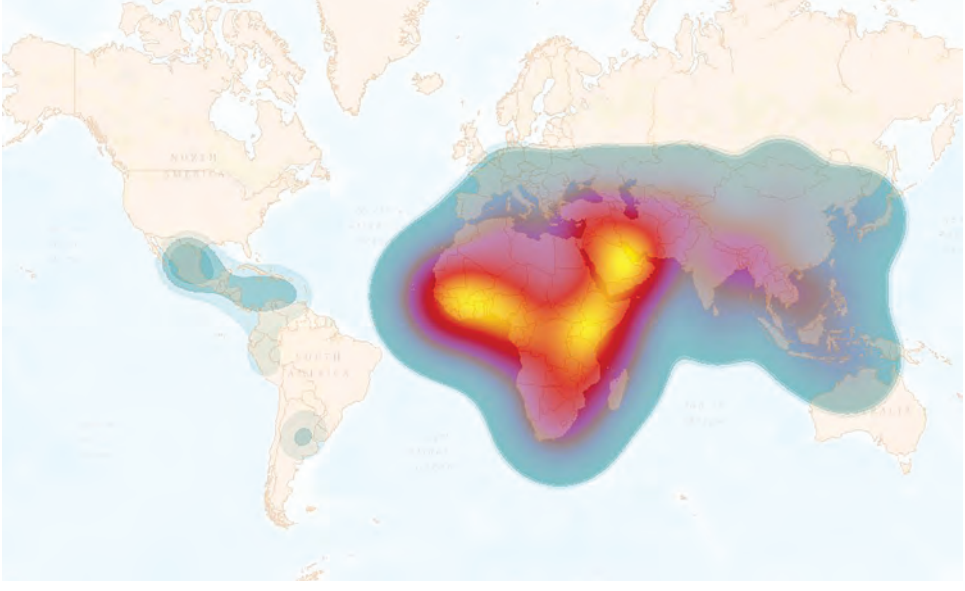

Figure 2. Heat map of global annual incidence of human brucellosis estimated per 1 million population at risk. Overall global risk is defined by the weighted average interpolation data (total number of new cases/total population at risk × 1 million). The global average is ≈500 new cases per 1 million persons at risk. The heat scale shows high risk to low risk; yellow (≥4,000 cases) to blue (≤1 case). This heatmap is intended to represent transnational zones that require priority control or surveillance initiative, not to represent the risk for individual countries.

Table. Estimated annual incidence of human brucellosis worldwide determined by using 3 statistical models*

Region	Estimated human cases						
	Total	Mean (SD)	2.5% Quantile	25% Quantile	Median	75% Quantile	97.5% Quantile
Weighted average interpolation							
World	1,621,468						
Asia	1,103,122						
Africa	514,001						
Americas	3,335						
Europe	1,010						
Bootstrap resampling							
World		1,691,666 (975,292)	679,393	1,080,049	1,416,482	1,906,564	4,651,474
Asia		1,172,573 (959,859)	261,493	566,081	887,126	1,355,607	4,107,355
Africa		513,928 (171,607)	257,863	380,681	487,549	624,155	902,139
Americas		3,343 (214)	3,133	3,181	3,272	3,448	3,912
Europe		1,821 (424)	1,595	1,632	1,688	1,818	3,717
Hierarchical Bayes†							
World		2,096,080 (1,754,315)	568,038	1,063,620	1,592,291	2,511,881	6,616,334
Asia		1,622,446 (1,680,985)	246,536	639,906	1,117,309	1,993,573	5,972,342
Africa		468,321 (291,337)	168,919	283,125	393,384	562,957	1,210,226
Americas		3,425 (362)	3,133	3,215	3,319	3,503	4,347
Europe		1,889 (446)	1,593	1,654	1,746	1,944	3,050

*Calculation of uncertainty intervals in the weighted average interpolation method was not performed due to the nature of the model. During bootstrap resampling, uncertainty intervals were calculated using one million resampled risk estimates based on observed reported case count values.
†The hierarchical Bayes model intervals were calculated using 1 million posterior samples. Posterior distributions were estimated using a Markov chain Monte Carlo (MCMC) algorithm based on observed reported case count values. For the MCMC algorithm, 50,000 burn-in iterations were performed before the samples were retained.

Determination of At-Risk Human Populations

Analysis of the livestock datasets indicates that during 2014–2018 a total of 83.1% (2,269/2,730) (population SD 29.4%) of the livestock brucellosis data were provided for the 3 *Brucella* species (Figure 1), compared to 48.4% of human brucellosis data (*8*). Specifically, from the lowest to the highest percentage of reports, Africa provided 69.1% of the expected information on *Brucella* spp. (549/795, SD 36.2%), the Americas 77.2% (359/465, SD 33.9%), Asia 87.3% (642/735, SD 23.2%), and Europe 97.5% (614/630, SD 10.6%) (Figure 1). Because we had more complete data for livestock than human disease at both the global and regional levels, we used livestock data as the basis to estimate disease incidence. Even so, a limiting factor in using the livestock data was the incompleteness of *B. suis*, 76.5% (696/910, SD 40.0%) data compared with *B. melitensis*, 81.4% (741/910, SD 35.5%) and *B. abortus*, 91.4% (832/910, SD 24.4%) data. That information is unavailable for human disease, which further supports our decision to base our analyses on livestock data to identify which *Brucella* species is afflicting each population.

Worldwide, 82.3% (144/175) of countries and 43.2% (3.2 billion/7.4 billion) of persons were considered at risk. By region, 92.5% (49/53) of the countries and 57.5% (0.69 billion/1.2 billion) of persons in Africa, 85.7% (42/49) of countries and 47.7% (2.1 billion/4.4 billion) of persons in Asia, 80.6% (25/31) of countries and 19.4% (0.19 billion/0.98 billion) of persons in the Americas, and 66.7% (28/42) of countries and 24.3% (0.18/0.74 billion) of persons in Europe were at risk. As noted, the model included only 175/182 countries; all of the countries from Oceania were excluded because of incomplete reporting, the small number of countries (7 total) and at-risk population numbers (7.6 million) involved, and the small number of RCCs (132 RCCs over 5 years).

Determining the Risk of Acquiring Human Brucellosis

Identifying the human populations that are most at risk of acquiring brucellosis is pivotal for the design and implementation of interventions to mitigate disease spread. Therefore, we used the information from countries that reported human disease to calculate the level of risk for their populations at risk. We entered generated data into ArcMap (Esri, https://www.arcgis.com) to produce heat maps. The global average risk was ≈500 new cases/1 million persons (Figure 2). As expected, the maps demonstrate distinct epidemiologic differences between the regions; Africa reflects most of the risk, followed by Asia, then the rest of the world.

Estimating Annual Incidence

After population risk assessment, we used 3 models to determine annual incidence. By weighted average interpolation model, the estimated incidence was 1,621,468; by bootstrap resampling model, the mean estimated incidence was 1,691,666; and by Bayesian hierarchical model, the mean estimated incidence was 2,096,080 (Table). Of interest, the models computed similar results between the means and medians both regionally and globally (Table), suggesting some robustness in each approach despite the individual strengths and weaknesses of each. The conservative

global annual incidence was 1.6–2.1 million new cases across models. When we analyzed the data by region, Asia (1.2–1.6 million cases) and Africa (0.5 million cases) accounted for most of the cases. Nonetheless, there were also a substantial number of cases in the Americas and Europe. Differences in the results between models were mainly between the smoothness of the resampling histograms (Figures 3, 4) and the distribution of CIs (Table) produced by the bootstrap resampling and hierarchical Bayes frameworks. All models indicated that the global annual incidence of human brucellosis is many times larger than previously thought (*9*).

Using the observed information provided from Europe, the region with the strongest surveillance systems and most complete reports for both humans and livestock, we determined each model's accuracy in representing the behavior of the system. We estimated 1,010 new cases by weighted average interpolation model, 1,821 cases by bootstrap resampling, and 1,889 cases by hierarchical Bayes model annually in Europe. The average value of empirical annual RCCs from Europe provided by WOAH was 1,771 cases/year; range was 727–5,329. Together with similar results between the means and medians of the models, our findings support both internal and external model validity.

Overall Regional Risk Assessment

We assessed the overall risk at the regional level of acquiring human brucellosis using the incidence and population at risk data and subsequently applying this information to generate heat maps for a visual interpretation of regional risk. As we expected, all regions analyzed in this study have some degree of disease risk, which is primarily focused within the tropics. However, the magnitude of the risk differed substantially among and within regions (Figure 5). Africa is at most significant risk (Figure 5, panel A), followed by Asia (Figure 5, panel B), the Americas (Figure 5, panel C), and Europe (Figure 5, panel D). Within Africa (Figure 5, panel A), all but 4 countries are considered high risk, and 3 of those countries are island nations. Major hotspots

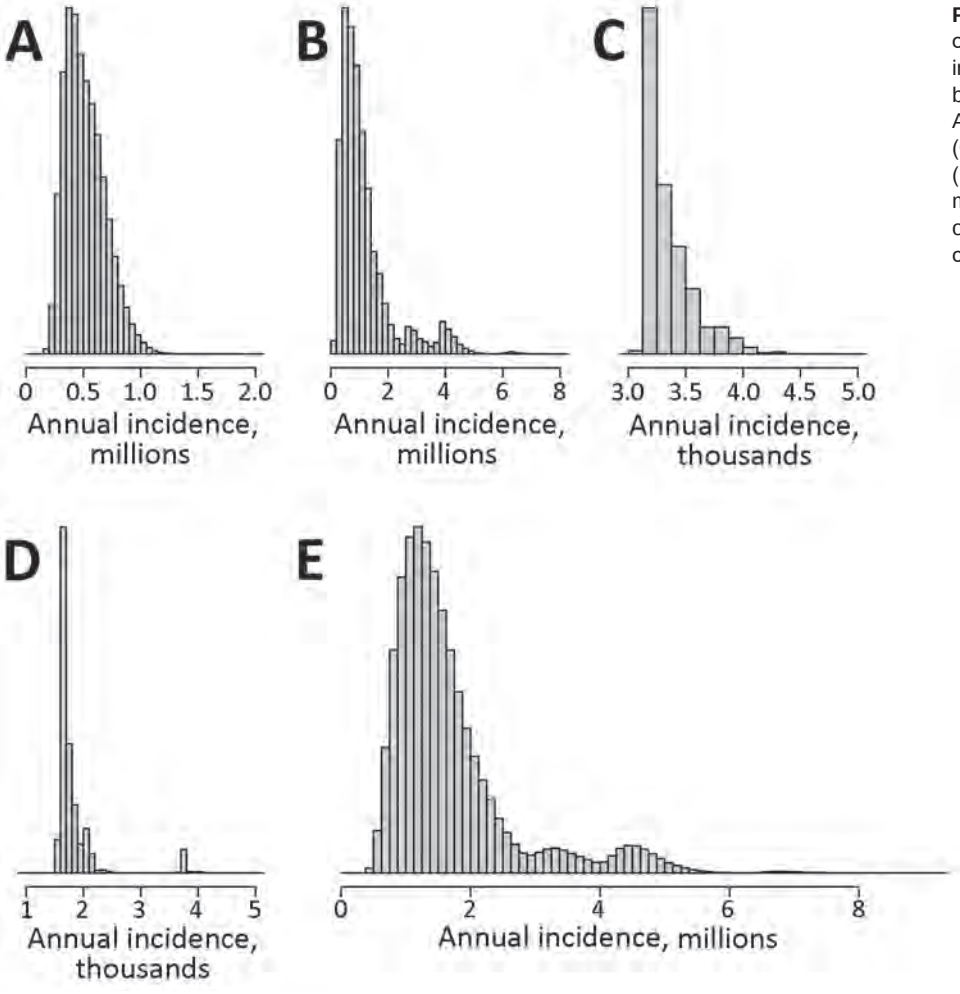

Figure 3. Estimated distribution of annual human brucellosis incidence as determined by bootstrap resampling model for Africa (A), Asia (B), Americas (C), and Europe (D) and globally (E). Histograms generated via 1 million sample iterations based on observed reported case count values.

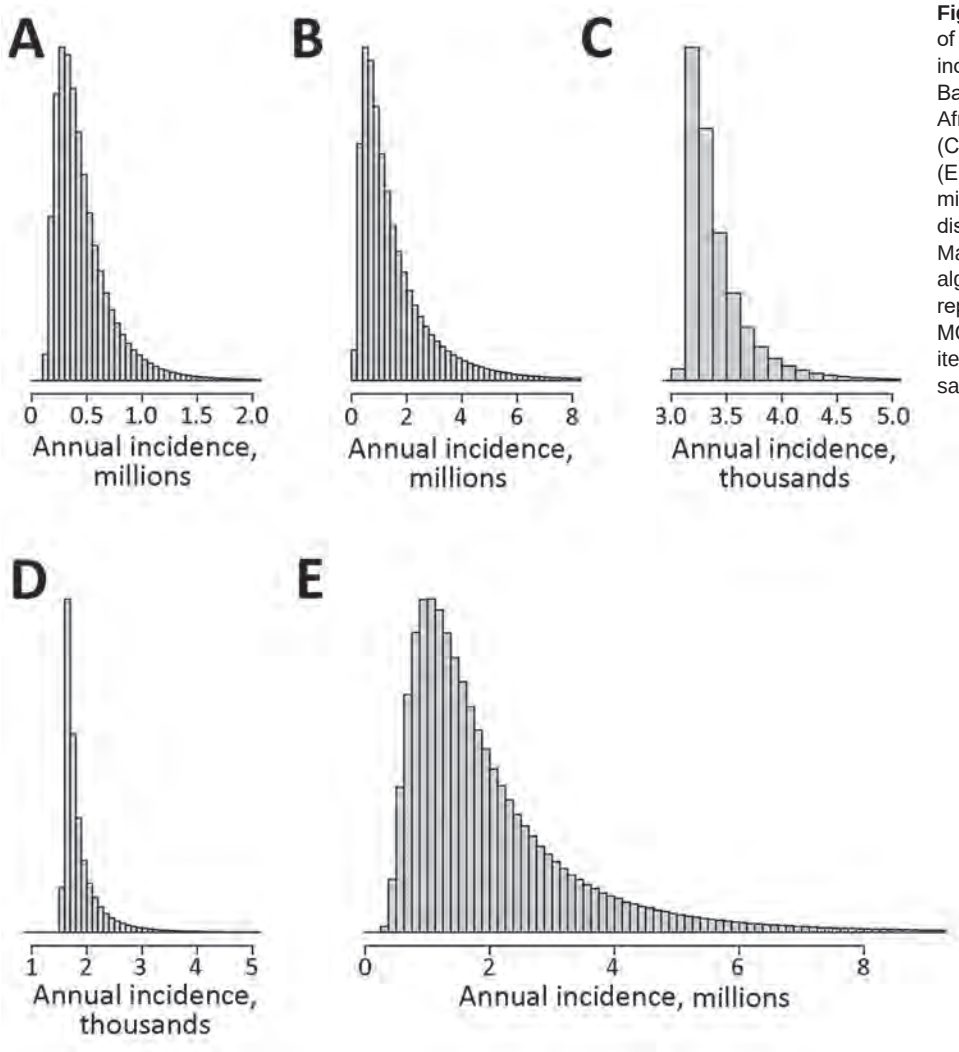

Figure 4. Estimated distribution of annual human brucellosis incidence as determined by Bayesian hierarchical model for Africa (A), Asia (B), Americas (C), and Europe (D) and globally (E). Histograms generated via 1 million sample iterations. Posterior distributions were estimated using a Markov chain Monte Carlo (MCMC) algorithm based on observed reported case count values. For the MCMC algorithm, 50,000 burn-in iterations were performed before the samples were retained.

occur in the equatorial regions of the east and west, followed by the southern region, and the northern Saharan subregion. In Asia, the major risk hotspot is localized in the Middle East subregion (Figure 5, panel B). With the exception of 6 countries, 5 of which are island nations, all countries in Asia are considered to be at risk, and risk levels are increased in the central, south, and southeast subregions. Although the Americas (Figure 5, panel C) experience less risk, there is more significant subregional variation than in Asia and Africa. Central America experiences most human brucellosis risk. South America follows, having major hotspots in the northern and southern portions of the continent. North America experiences the least risk in this region. Finally, Europe (Figure 5, panel D) is considered to have the least risk of all the analyzed regions, having a major hotspot in the Eastern Mediterranean area and increased risk in the central subregion.

Discussion

This study provides an empirically based estimate of human brucellosis incidence and associated risk for persons worldwide, suggesting a reality that at least 1.6–2.1 million new cases of human brucellosis likely occur every year. This estimate differs significantly from one of the most cited references in the brucellosis field (*9*), which predicts an incidence of 500,000 new cases yearly. Although that previous estimate was not rigorously justified using empirical data, the estimate of 500,000 new cases has been assumed and used worldwide as a key factor for determining the disease's global significance and effect on humans. The continued use of that estimate can be attributed mainly to the paucity of data presented by the international reporting system and a lack of empirical evidence that caused the scientific community to ignore the burden of this disease (*8*). As a solution, in this study, we used

human and animal data and a range of statistical methods to provide a better understanding of global brucellosis incidence.

It is essential to highlight that we did not incorporate disease misdiagnosis and underdiagnosis into our statistical models as parameters because of limited data. If we had, brucellosis estimates would have been even higher. In areas to which malaria and brucellosis are endemic, recent scientific data indicate that 21%–50% of human brucellosis cases were initially misdiagnosed as malaria, and 4%–11% of the total cases initially diagnosed as malaria were later identified as brucellosis (*14*,*15*). In 1 study, 51% of brucellosis cases were initially misdiagnosed as typhoid fever or pneumonia, and 13% of the total cases initially diagnosed as those 2 diseases were later identified as brucellosis (*14*). Underdiagnosis can arise from several deficiencies in medical and public health systems. Examples include a lack of diagnostic capacity, a lack of knowledge by diagnosticians, and a lack of awareness of public health practitioners to prioritize the disease. Current data are inadequate to estimate the extent of those problems worldwide. Given the magnitude of the reported malaria and typhoid incidence within brucellosis-endemic zones, incorporating those effects would likely increase the estimated disease incidence by millions of cases per year. Future research into human brucellosis misdiagnosis and underdiagnosis is necessary for further insight into disease burden (Appendix).

The data and analyses we present demonstrate that only a small proportion of the world's population is not subject to brucellosis disease risk. Most human brucellosis cases come from regions with highly dense at-risk populations (Figures 2, 5). These results should be considered in the context of previous studies, which suggest that far less data were being collected in 2022 than 15 years earlier (*8*). Combined with the continuing increase in the world population, particularly in Africa (*8*), there is substantial evidence that world populations are more at risk now than in the past. When the regions are viewed separately, Asia and Africa account for most of the risk and incidence of human brucellosis (Figures 2, 5). Moreover, among countries in Africa, inadequate or nonexistent public and animal health programs perpetuate the status quo (*7*,*8*,*16*,*21*). This uncontrolled disease situation, accompanied by rapid population growth and increased demand

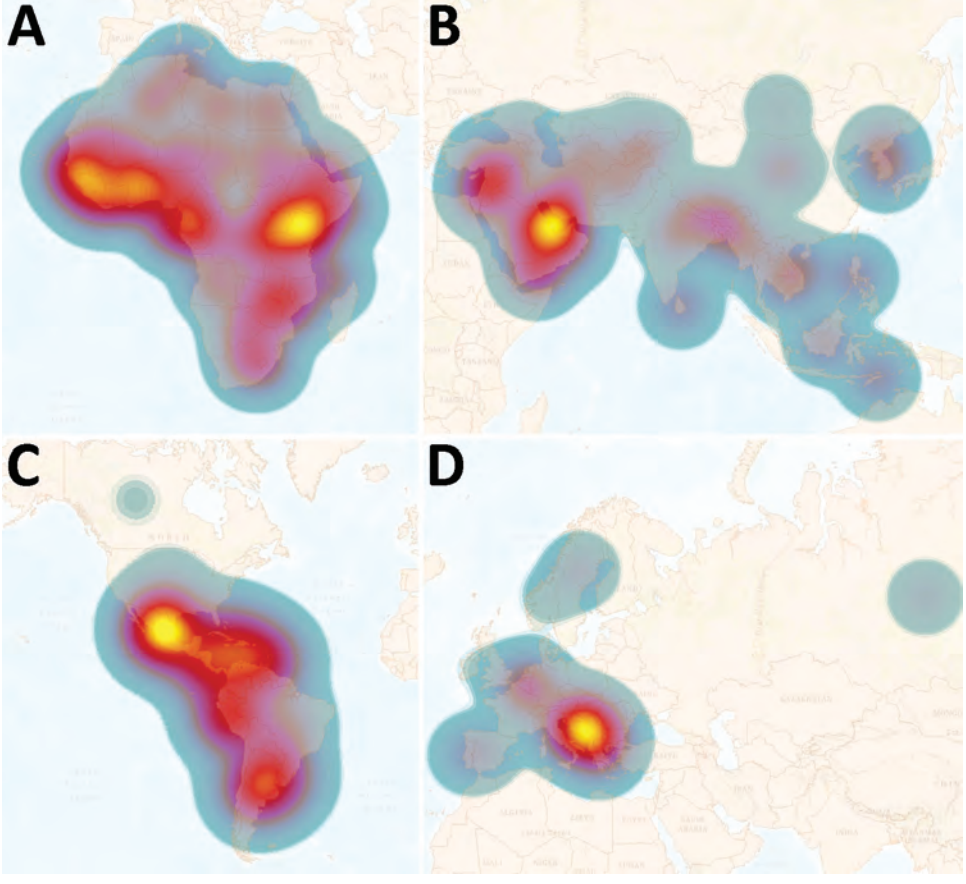

Figure 5. Heatmaps of regional annual incidence of human brucellosis estimated per 1 million population at risk. Each region has a different scale for incidence per 1 million population at risk. Heatmaps are intended to represent transnational zones that require priority control or surveillance initiative, not to represent the risk of individual countries. The heat scale shows high risk to low risk; yellow to blue. A) Africa: average risk is ≈750 new cases per million; high is >3,000. B) Asia: average risk is ≈500 new cases per million; high is ≥4,000. C) Americas: average risk is ≈20 new cases per million; high is ≥75. D) Europe: average risk is ≈10 new cases per million; high ≥100.

for animal products, provides an unfortunate outlook for the future of brucellosis control across this entire region. Although risk is spread across the entire Asia region, the primary hotspot occurs in the Middle East. This increased risk is likely the result of having close contact with small ruminants and consuming their raw milk products (*22*).

The Americas also have a uniform spread of risk across the region with distinct hotspots. Central America has the highest risk, followed by northern and southern South America. Farming in this region includes cattle, small ruminants, and pigs and routinely includes interaction with their infected tissues and fluids. In addition, countries not endemic for the disease incur cases resulting from travel and from trade of raw milk products across national borders (*23*).

Europe has the most advanced brucellosis surveillance and control programs. Countries in this region account for the most complete and representative data, along with the lowest RCCs (*8*), translating to the lowest estimated case counts and risk (Table; Figures 2, 5). Although Europe generally is less of a concern than the other regions, hotspots are present in the Mediterranean area; a subset of the population is at risk for traveler's brucellosis, which probably accounts for the increased risk within the central subregion. The differences in incidence and risk can be seen in the Eastern Mediterranean area. Similar to the case for the Americas, countries in Europe that are not endemic for the disease also incur cases related to factors such as travel, laboratory-acquired infections, and trade of raw milk products across national borders (*23*). Fortunately, in Europe, the medical infrastructure is adept in identifying and reporting cases to integrated surveillance networks. Because of the high level of completeness within that data, each of the 3 model estimates are close to the reported account, further supporting the model validity.

In conclusion, although the true annual incidence of human brucellosis remains elusive, we have compiled an evidence-based, scientifically computed estimate. This study reveals that the contemporary disease risk conditions most likely translate to an approximate global annual incidence that is many times higher than what has been previously suggested (i.e., conservatively 1.6–2.1 million). Furthermore, the risk of acquiring the disease was highest within resource-limited regions. It is critical that research be conducted to understand the role of misdiagnosis and underdiagnosis of human brucellosis, because those factors will undoubtably amplify case estimates and risk profiles within those regions.

The US Department of the Defense, Defense Threat Reduction Agency sponsored this project (contract no. HDTRA11910032). The content of the information does not necessarily reflect the position or the policy of the United States federal government, and no official endorsement should be inferred.

About the Author

Dr. Laine is a research scientist of epidemiology in the Department of Veterinary Pathobiology, School of Veterinary Medicine & Biomedical Sciences, Texas A&M University, College Station. His research interests include epidemiological modeling, brucellosis transmission dynamics, and data analytics. His current research focuses on the efficient implementation of vaccine programs and diagnostic tests for zoonotic and transboundary infectious diseases, used under resource-limited settings to reduce biothreats.

References

1. Franco MP, Mulder M, Gilman RH, Smits HL. Human brucellosis. Lancet Infect Dis. 2007;7:775–86. https://doi.org/10.1016/S1473-3099(07)70286-4
2. Franc KA, Krecek RC, Häsler BN, Arenas-Gamboa AM. Brucellosis remains a neglected disease in the developing world: a call for interdisciplinary action. BMC Public Health. 2018;18:125. https://doi.org/10.1186/s12889-017-5016-y
3. McDermott J, Grace D, Zinsstag J. Economics of brucellosis impact and control in low-income countries. Rev Sci Tech. 2013;32:249–61. https://doi.org/10.20506/rst.32.1.2197
4. Corbel MJ. Brucellosis in humans and animals. Geneva: World Health Organization; 2006.
5. World Organisation for Animal Health. WAHIS: World Animal Health Information System [cited 2023 Jul 20]. https://wahis.oie.int
6. Akakpo AJ, Têko-Agbo A, Koné P. The impact of brucellosis on the economy and public health in Africa. Presented at: Conference of the OIE Regional Commission for Africa; February 23–27, 2009; N'Djamena, Chad.
7. Cárdenas L, Awada L, Tizzani P, Cáceres P, Casal J. Characterization and evolution of countries affected by bovine brucellosis (1996–2014). Transbound Emerg Dis. 2019;66:1280–90. https://doi.org/10.1111/tbed.13144
8. Laine CG, Scott HM, Arenas-Gamboa AM. Human brucellosis: widespread information deficiency hinders an understanding of global disease frequency. PLoS Negl Trop Dis. 2022;16:e0010404. https://doi.org/10.1371/journal.pntd.0010404
9. Pappas G, Papadimitriou P, Akritidis N, Christou L, Tsianos EV. The new global map of human brucellosis. Lancet Infect Dis. 2006;6:91–9. https://doi.org/10.1016/S1473-3099(06)70382-6
10. Dean AS, Crump L, Greter H, Hattendorf J, Schelling E, Zinsstag J. Clinical manifestations of human brucellosis: a systematic review and meta-analysis. PLoS Negl Trop Dis. 2012;6:e1929. https://doi.org/10.1371/journal.pntd.0001929
11. Dean AS, Crump L, Greter H, Schelling E, Zinsstag J. Global burden of human brucellosis: a systematic review

of disease frequency. PLoS Negl Trop Dis. 2012;6:e1865. https://doi.org/10.1371/journal.pntd.0001865
12. Stevens GA, Alkema L, Black RE, Boerma JT, Collins GS, Ezzati M, et al.; The GATHER Working Group. Guidelines for accurate and transparent health estimates reporting: the GATHER statement. Lancet. 2016;388:e19–23. https://doi.org/10.1016/S0140-6736(16)30388-9
13. World Bank Group. Population estimates and projections. In: Data catalog. 2021 [cited 2023 Jul 20]. https://databank.worldbank.org/home.aspx
14. United Nations Department of Economic and Social Affairs. 2019 Revision of world population prospects. New York: United Nations; 2019 [cited 2023 Jul 250]. https://population.un.org/wpp
15. Njeru J, Wareth G, Melzer F, Henning K, Pletz MW, Heller R, et al. Systematic review of brucellosis in Kenya: disease frequency in humans and animals and risk factors for human infection. BMC Public Health. 2016;16:853. https://doi.org/10.1186/s12889-016-3532-9
16. McDermott JJ, Arimi SM. Brucellosis in sub-Saharan Africa: epidemiology, control, and impact. Vet Microbiol. 2002; 90:111–34. https://doi.org/10.1016/S0378-1135(02)00249-3
17. Roy S, McElwain TF, Wan Y. A network control theory approach to modeling and optimal control of zoonoses: case study of brucellosis transmission in sub-Saharan Africa. PLoS Negl Trop Dis. 2011;5:e1259. https://doi.org/10.1371/journal.pntd.0001259
18. Jackson DS, Nydam DV, Altier C. Prevalence and risk factors for brucellosis in domestic yak *Bos grunniens* and their herders in a transhumant pastoralist system of Dolpo, Nepal. Prev Vet Med. 2014;113:47–58. https://doi.org/10.1016/j.prevetmed.2013.09.016
19. Ndengu M, Matope G, de Garine-Wichatitsky M, Tivapasi M, Scacchia M, Bonfini B, et al. Seroprevalence of brucellosis in cattle and selected wildlife species at selected livestock/wildlife interface areas of the Gonarezhou National Park, Zimbabwe. Prev Vet Med. 2017;146:158–65. https://doi.org/10.1016/j.prevetmed.2017.08.004
20. Assenga JA, Matemba LE, Muller SK, Malakalinga JJ, Kazwala RR. Epidemiology of *Brucella* infection in the human, livestock and wildlife interface in the Katavi-Rukwa ecosystem, Tanzania. BMC Vet Res. 2015;11:189. https://doi.org/10.1186/s12917-015-0504-8
21. Ibironke AA, McCrindle CM, Fasina FO, Godfroid J. Evaluation of problems and possible solutions linked to the surveillance and control of bovine brucellosis in sub-Saharan Africa, with special emphasis on Nigeria. Vet Ital. 2008;44:549–56.
22. Bagheri Nejad R, Krecek RC, Khalaf OH, Hailat N, Arenas-Gamboa AM. Brucellosis in the Middle East: current situation and a pathway forward. PLoS Negl Trop Dis. 2020;14:e0008071. https://doi.org/10.1371/journal.pntd.0008071
23. Negrón ME, Kharod GA, Bower WA, Walke H. Notes from the field: human *Brucella abortus* RB51 infections caused by consumption of unpasteurized domestic dairy products—United States, 2017–2019. MMWR Morb Mortal Wkly Rep. 2019;68:185. https://doi.org/10.15585/mmwr.mm6807a6

Corresponding author: Angela M. Arenas-Gamboa, Department of Veterinary Pathobiology, School of Veterinary Medicine and Biomedical Sciences, Texas A&M University, 4467 TAMU, College Station, TX 77843-4467, USA; email: aarenas@cvm.tamu.edu

Interspecies Transmission of Swine Influenza A Viruses and Human Seasonal Vaccine-Mediated Protection Investigated in Ferret Model

Pauline M. van Diemen, Alexander M.P. Byrne, Andrew M. Ramsay, Samantha Watson, Alejandro Nunez, Ana v Moreno, Chiara Chiapponi, Emanuela Foni, Ian H. Brown, Sharon M. Brookes, Helen E. Everett

We investigated the infection dynamics of 2 influenza A(H1N1) virus isolates from the swine 1A.3.3.2 (pandemic 2009) and 1C (Eurasian, avian-like) lineages. The 1C-lineage virus, A/Pavia/65/2016, although phylogenetically related to swine-origin viruses, was isolated from a human clinical case. This strain infected ferrets, a human influenza model species, and could be transmitted by direct contact and, less efficiently, by airborne exposure. Infecting ferrets and pigs (the natural host) resulted in mild or inapparent clinical signs comparable to those observed with 1A.3.3.2-lineage swine-origin viruses. Both H1N1 viruses could infect pigs and were transmitted to cohoused ferrets. Ferrets vaccinated with a human 2016–17 seasonal influenza vaccine were protected against infection with the antigenically matched 1A pandemic 2009 virus but not against the swine-lineage 1C virus. Our results reaffirm the need for continuous influenza A virus surveillance in pigs and identification of candidate human vaccine viruses.

Influenza A viruses (IAVs) have pandemic potential and remain a threat to human and animal health, mainly owing to their intrinsic ability to continually diversify and infect a broad range of host species. Genetic heterogeneity in the 8-segmented IAV genome arises from the gradual accumulation of mutations (drift) owing to the low fidelity of the viral RNA polymerase. In addition, sporadic IAV gene segment exchange (shift) events can lead to the emergence of reassortant viruses with novel gene constellations and functional attributes. IAVs are characterized antigenically based on the hemagglutinin (HA) and neuraminidase (NA) envelope glycoproteins; HA incorporates the major epitopes conferring protective immunity (*1*–*3*).

Pigs are a key intermediate host species for IAV diversification; their susceptibility to IAVs originating from numerous mammalian (including human) and avian hosts enables virus reassortment and contributes to the expanding genetic heterogeneity of circulating swine IAV (swIAV) lineages (*2*,*4*,*5*). Because of this genetic heterogeneity, swIAVs are categorized according to HA phylogeny (*6*). Predominant viruses detected globally in swine populations belong to 3 main H1 genetic lineages (1A, 1B, and 1C) and multiple H3 clades, although antigenic and genetic differences might occur within these groupings according to geographic location (*6*,*7*). In Europe, the Eurasian avian-like H1 1C lineage (formerly termed the H1avN1 clade) has been enzootic in swine since the 1970s; phylogenetic evidence suggests direct incursion of an avian (duck)–origin virus into pigs (*8*). Subsequent reassortment with human-origin viruses produced the human-like H1 1B lineage (formerly known as the H1huN2 clade) and human-like H3N2 clades that cocirculated in pig populations in Europe as antigenically distinct IAV lineages until the introduction of the H1 1A.3.3.2 pandemic H1N1 (H1pdmN1) lineage in 2009 (*9*–*12*). The 1A.3.3.2 lineage continues to circulate and adapt in both pig and human populations globally and, in the swine reservoir, genetic mutation together with reassortment with

Author affiliations: Animal and Plant Health Agency, Addlestone, UK (P.M. van Diemen, A.M.P. Byrne, A.M. Ramsay, S. Watson, A. Nunez, I.H. Brown, S.M. Brookes, H.E. Everett); Istituto Zooprofilattico Sperimentale della Lombardia e dell'Emilia Romagna, Brescia, Italy (C. Chiapponi, E. Foni, A. Moreno)

DOI: https://doi.org/10.3201/eid2909.230066

established lineages is driving the expansion of viral diversity (*1*,*7*,*13*). This diversification of swIAVs circulating in pigs, combined with occasional transmission across the species barrier followed by host adaptation and escape from previous immunity, further elevates potential pandemic risk (*1*,*3*) and presents a challenge for disease control.

Sporadic human infection with so-called variant (v) influenza viruses that normally circulate in swine continue to be reported (*3*,*13*). In recent years, H1N1v infections with H1 1C swIAVs have been characterized in Europe (*14*–*18*) and Asia (*19*,*20*), and zoonotic infections caused by reassortant viruses incorporating gene segments from those 1C lineages have also been described (*21*–*27*). Experimental data indicate that some isolates have increased virulence profiles (*20*,*26*–*29*). Variant cases are frequently linked to persons or their contacts who have occupational exposure to pigs or exposure at animal exhibits. Onward transmission, assessed serologically, is reportedly limited or does not occur.

Vaccination remains the primary approach used to mitigate the disease burden of seasonal influenza in the human population and is the main defense against emergent IAVs with pandemic and epidemic potential, which occurred most recently in 2009. The most widely used human season influenza vaccines are trivalent or quadrivalent and contain inactivated antigens from 2 IAV subtypes (H1 and H3) and 1 or 2 influenza B virus lineages. However, because of constant antigenic change, contemporary IAVs are assessed biannually for antigenic match with vaccine antigens at the World Health Organization Vaccine Candidate Meeting, and candidate vaccine virus (CVV) recommendations are provided. The increased diversification of swIAVs and reports of zoonotic transmission have necessitated additional assessment of the antigenic match between CVVs and variant viruses and recommendation of swine-origin CVVs by OFFLU, the global network of expertise on animal influenza, should rapid vaccine antigen update be required (*1*,*30*).

We used the well-established ferret model of human influenza infection (*31*–*33*) to investigate 2 H1N1 viruses. The first virus was a 1A.3.3.2 lineage, swine-origin virus, A/swine/England/1353/2009 (*34*), incorporating all gene segments highly homologous to 2009 pandemic strains isolated from humans and swine (*9*). The second virus was a 1C.2.1 lineage virus, A/Pavia/65/2016 (*15*), which was associated with a human clinical case of influenza, but phylogenetic analysis confirmed that all gene segments were derived from contemporary 1C.2.1 viruses circulating in swine herds in Italy. We first assessed the ability of this virus to infect ferrets and undergo onward ferret-to-ferret transmission by direct or airborne exposure. We then evaluated the zoonotic potential of this 1C.2.1 virus by assessing transmission from infected pigs to cohoused ferrets and compared this virus in parallel with the swine-origin 1A.3.2.2 strain. Because swIAVs exhibit a higher degree of genetic and antigenic diversity than IAVs circulating in the human population at any one time, we also used the ferret model to investigate whether the human 2016–17 seasonal influenza vaccine could provide immune protection against the 2 swIAV strains.

Materials and Methods

Ethics Statement

We conducted in vivo studies at the Animal and Plant Health Agency (APHA), Addlestone, UK, in accordance with the Animal (Scientific Procedures) Act (ASPA) 1986 under license 70–8329 and approved by the APHA Ethical Review Panel. Results are reported according to the ARRIVE guidelines (*35*).

Vaccines and Viruses

We immunized ferrets with a 2016–17 Northern Hemisphere seasonal influenza vaccine (Agrippal; CSL Seqirus, https://www.csl.com) that incorporated 3 inactivated virus antigens, A/California/7/2009 from the 1A.3.3.2 pandemic 2009 lineage (H1pdmN1), A/Hong Kong/4801/2014 (H3N2), and B/Brisbane/60/2008 (B/Victoria lineage). The H1N1 challenge strains were the 1A.3.3.2 (H1pdmN1) swine-origin virus A/swine/England/1353/2009 (*34*) and the 1C.2.1 (H1avN1) virus, A/Pavia/65/2016 (*15*). We propagated virus stocks in cell culture or specific-pathogen-free embryonated chicken eggs (Appendix, https://wwwnc.cdc.gov/EID/article/29/9/23-0066-App1.pdf). For consistency, we used the standard MDCK cell line for propagation and 50% tissue culture infectious dose ($TCID_{50}$) titration of the inoculum for both virus strains (*36*).

Animals

We conducted the studies using 34 three-month-old male ferrets from a registered breeder and 10 six-week-old Landrace cross male pigs from a commercial, high–health status herd. All animals were negative for influenza A virus infection, as determined by absence of viral RNA in nasal samples using real-time quantitative reverse transcription PCR (*37*) and swIAV-specific antibodies by hemagglutination

inhibition (HI) assays against 4 antigens (*38*) and ID Screen competitive ELISA (Innovative Diagnostics, https://www.innovative-diagnostics.com) recognizing the viral nucleoprotein (NP) (Appendix). All ferrets and pigs were implanted with a subcutaneous biothermal IDentiChip (Destron Fearing, http://destronfearing.com) to monitor temperature. We monitored clinical signs, such as demeanor, appetite, temperature, and respiratory signs (e.g., coughing and sneezing), daily using a clinical scoring system designed for each species (Appendix Tables 1–4). We used a single subcutaneous injection of medetomidine (0.04 mg/kg; Vetoquinol, https://www.vetoquinolusa.com) and butorphanol (0.1 mg/kg; MSD Animal Health, https://www.msd-animal-health.com) to place ferrets under general anesthesia for virus inoculation and blood sample collection. We reversed the medetomidine anesthesia with a subcutaneous injection of atipamezole hydrochloride (0.4 mg/kg; Vetoquinol). We humanely killed animals by intravenous injection with pentobarbital sodium at study end.

Study Design

The first study assessed the ability of the H1avN1 isolate, A/Pavia/65/2016, to infect ferrets and transmit to other ferrets by direct or airborne exposure (Figure 1, panel A). We randomly divided 12 male ferrets into 2 groups (n = 6). In each group, 2 animals were inoculated by intranasal instillation of 2×10^5 $TCID_{50}$ of strain A/Pavia/65/2016 in 0.5 mL (0.25 mL per nostril) and cohoused them with 2 ferrets in direct contact; we housed 2 additional ferrets in an adjacent cage separated by a perforated double divider to enable airborne exposure to respiratory droplets without nose-to-nose contact. We collected nasal wash samples daily from alert ferrets and took blood samples (clotted) from the jugular vein of anesthetized ferrets before inoculation and at study completion (14 days postinoculation [dpi]).

The second study (Figure 1, panel B) evaluated the infection dynamics of the H1avN1 and H1pdmN1 viruses in pigs and assessed the interspecies transmission of these viruses from pigs to vaccinated or naive ferrets. We randomly distributed 20 male ferrets into 4 groups (n = 5), then prime-boost vaccinated 2 groups with 1 dose (0.5 mL) of human seasonal vaccine administered by intramuscular injection into the thigh muscle at a 21-day interval. Two unvaccinated ferrets were not virus exposed and were housed separately to serve as negative control animals. Blood samples (clotted and heparin

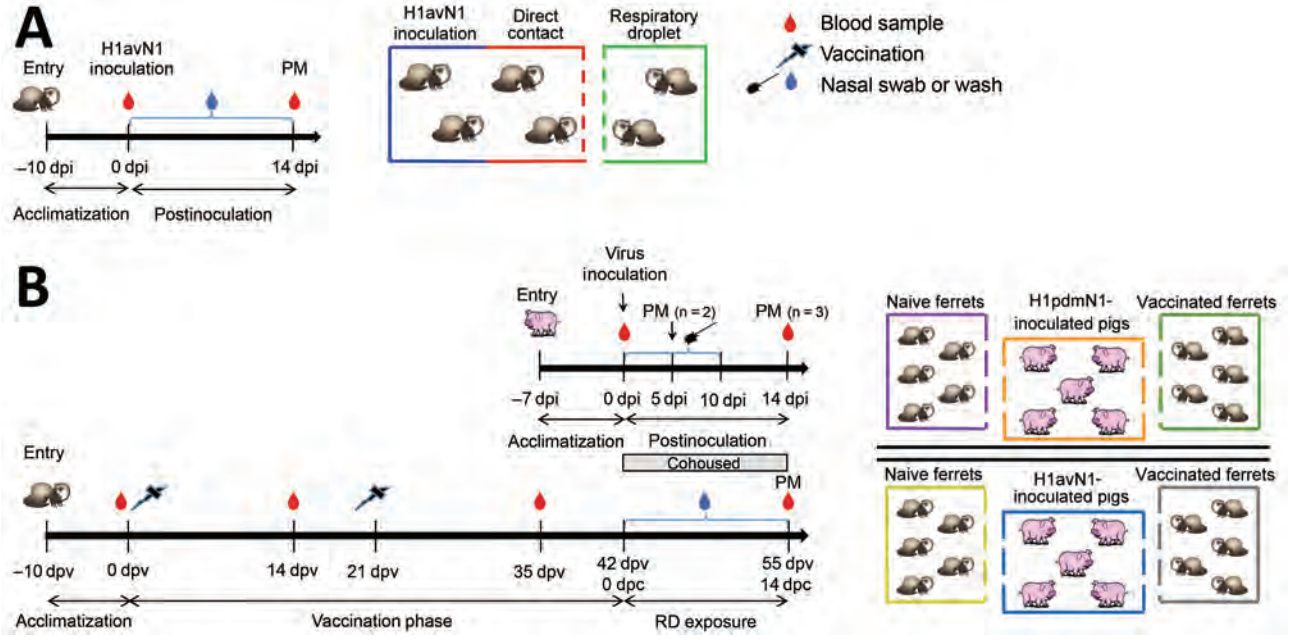

Figure 1. Outlines of 2 studies using ferret model to investigate interspecies transmission of swine influenza A viruses and human seasonal vaccine-mediated protection. A) Study 1 investigated the transmission ability of the A/Pavia/65/2016 (H1avN1) isolate in the ferret model of human infection. In 2 replicates, ferrets (n = 2) were intranasally inoculated and then cohoused with ferrets in direct contact (n = 2) and another group of ferrets (n = 2) separated by a perforated double divider to enable airborne exposure to respiratory droplets. B) Study 2 assessed airborne respiratory droplet transmission of 2 viruses from pigs to ferrets. In separate rooms, 2 groups of pigs (n = 5) were inoculated with either A/Pavia/65/2016 H1avN1 or A/swine/England/1353/2009 (H1pdmN1) virus and cohoused with naive (n = 5) and human seasonal 2016–17 influenza vaccine prime-boost–vaccinated ferrets (n = 5). Symbols on the timeline represent samples taken. dpc, days postcontact; dpi, days postinoculation; dpv, days postvaccination; PM, postmortem examination; RD, respiratory droplet.

anticoagulated) were taken under anesthesia from the jugular vein of all ferrets before first vaccination, before boost, at 35 days after vaccination, and at study completion.

We randomly assigned pigs to 2 groups (n = 5) and housed them in separate rooms for inoculation with either 4×10^6 $TCID_{50}$ A/swine/England/1353/2009 or 2×10^6 $TCID_{50}$ A/Pavia/65/2016 virus stocks in 4 mL (2 mL/nostril) using a MAD Nasal Intranasal Mucosal Atomization Device (Teleflex, https://www.teleflex.com). After 24 hours (corresponding to 42 days after vaccination), we cohoused a vaccinated and a nonvaccinated ferret group (each n = 5) in each pig room to enable airborne respiratory droplet exposure in the shared airspace. We obtained nasal swab (pig) and wash (ferret) samples daily from alert animals after inoculation or contact to monitor viral shedding. We obtained blood samples (clotted and heparin anticoagulated) from the left jugular vein of pigs before inoculation and before euthanasia. At 5 dpi, we humanely killed 2 pigs from each group to perform postmortem examination. We humanely killed the remaining pigs at 14 dpi when virus shedding had ceased; we humanely killed ferrets at 14 dpc.

Sample Analysis

We performed sample processing as described (Appendix). To monitor nasal shedding of viral RNA, we extracted nasal samples using a QIAamp Viral RNA Biorobot Kit (QIAGEN, https://www.qiagen.com) and quantified the RNA present using real-time quantitative reverse transcription PCR directed against the matrix (M) gene (*37*). Viral RNA quantity is expressed as relative equivalent units (REUs) per milliliter and was evaluated according to a standard 10-fold dilution series of RNA prepared from each challenge virus stock, with known $TCID_{50}$ titer. REUs provide a relative quantification of infectious virus present, inferred from the linear, proportional relationship between viral infectivity and viral RNA quantity standardized by volume of nasal sample (*38*), and enables rapid, sensitive, and direct analysis of clinical samples. We evaluated the humoral response as described (Appendix). We used a commercial, competitive ELISA (IDVet, Innovative Diagnostics) to detect NP-specific antibodies. The competition percent is calculated as $(OD_{sample}/OD_{negative}) \times 100\%$ and is expressed as the inverse, such that results <50% are considered negative. We used HI and virus neutralization assays (*39*,*40*) to evaluate antibody titers elicited by the challenge virus for each group. To monitor the cellular response, we assessed interferon-γ–producing peripheral blood mononuclear cells using the ELISpot assay (Appendix). During the postmortem at 5 dpi, we collected pig respiratory tissues (nasal turbinate, trachea, and lung) in 10% (vol/vol) phosphate-buffered formalin for immunohistochemical analysis of NP to assess viral distribution (Appendix) (*41*).

Statistical Analysis

We performed statistical analyses using GraphPad Prism7 (GraphPad, https://www.graphpad.com) to calculate arithmetic and geometric means, associated standard deviation or error of the mean, analysis of variance, and associated post-hoc Tukey tests. Titer and REU values were logarithmically transformed. We used a 2-way repeated measures analysis of variance to analyze repeated measurements such as viral RNA quantity and immune response values. We identified statistically significant differences using the Tukey multiple comparisons test and considered results significant when $p<0.05$.

Results

Intranasal inoculation of ferrets with the A/Pavia/65/2016 isolate in study 1 (Figure 1, panel A) resulted in productive infection (Figure 2, panels A–C), as revealed by nasal shedding of viral RNA detected at 2–8 dpi and seroconversion by 14 dpi, evaluated by NP ELISA and HI assays. Clinical signs, such as demeanor, appetite, temperature, and respiratory signs (e.g., coughing and sneezing), were normal/not apparent or mild and did not exceed a total score of 4 for any individual ferret (Appendix Tables 1–2). One of 4 ferrets did not shed viral RNA after direct inoculation, although seroconversion was detected by NP ELISA and HI assays, indicating immune exposure to virus. This observation could reflect differences in the susceptibility of a genetically outbred ferret population or experimental variation. Cohoused ferrets also demonstrated evidence of productive infection, indicating virus transmission by direct contact. Viral transmission by the airborne route was not detected. However, respiratory droplet exposure did elicit an antibody response in some ferrets that was at or below the lower limit of detection of the assays, possibly indicating immune exposure. Those results indicated that ferrets were a suitable challenge model for the A/Pavia/65/2016 H1avN1 isolate.

In study 2 (Figure 1, panel B), 10 ferrets were prime-boost vaccinated with a trivalent human influenza vaccine from the 2016–17 season; 10 ferrets were not vaccinated to serve as naive control animals. The interval between prime and boost vaccinations was 3 weeks, and the vaccination phase continued for a

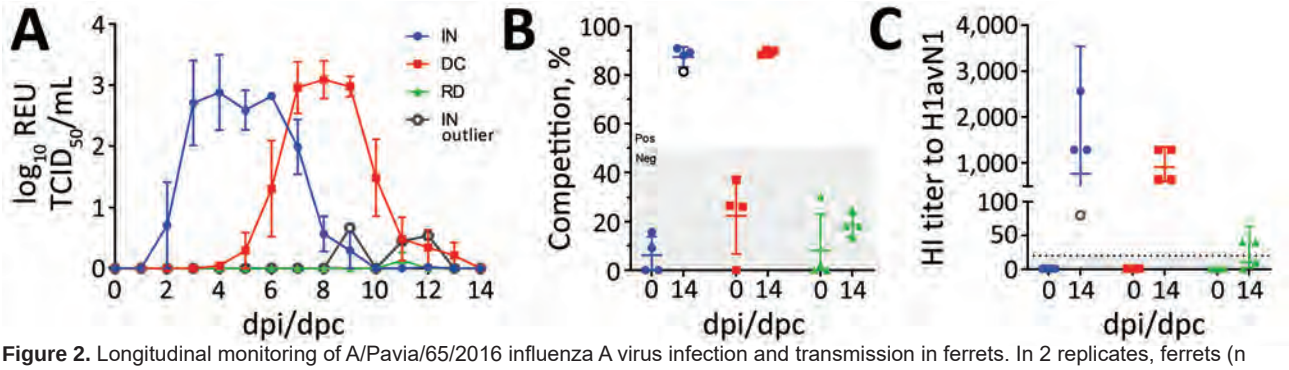

Figure 2. Longitudinal monitoring of A/Pavia/65/2016 influenza A virus infection and transmission in ferrets. In 2 replicates, ferrets (n = 2) were intranasally inoculated with the A/Pavia/65/2016 strain and cohoused with ferrets in direct contact (n = 2) or in the same airspace (n = 2) enabling airborne exposure to respiratory droplets. Infection was evaluated by (A) monitoring daily nasal shedding of viral RNA between 0–14 dpi expressed as REUs. The specific humoral immune response was evaluated at 0 and 14 dpi using (B) a competitive ELISA to determine nucleoprotein-specific antibody titer, expressed as the inverse of the competition percentage (%) or (C) HI titer with the homologous virus. Competition percentage was calculated as (1 – sample/negative) × 100. Nucleoprotein competition percentage <50% or HI titer of <20 are considered negative (gray shaded areas). Outlier results for a single ferret in the intranasally inoculated group (IN-outlier) were excluded from the analysis and are shown by hollow black symbols. DC, direct contact; dpc, days postcontact; dpi, days postinoculation; HI, hemagglutination inhibition; IN, intranasally inoculated; Neg, negative; Pos, positive; RD, respiratory droplet; REU, relative equivalent unit; TCID50, 50% tissue culture infectious dose.

further 3 weeks. We then housed 2 groups of pigs (n = 5) in separate rooms and inoculated with either the 1A.3.2.2 swine-origin (H1pdmN1) virus A/swine/England/1353/2009 (room 1) or the 1C.2.1 human isolate (H1avN1) virus, A/Pavia/65/2016 (room 2). We then cohoused a group of naive ferrets (n = 5) and a group of vaccinated ferrets (n = 5), held in separate cages, with the infected pigs in each room. We monitored all animals daily; clinical signs were mild or absent according to the clinical scoring systems for ferrets and pigs (Appendix Tables 1–4), indicating that both virus strains had similar, mild pathogenesis profiles and infection was effectively resolved in both host species.

We quantified viral RNA in daily nasal samples to assess virus shedding (Figure 3, panels A, B). In pigs, nasal shedding of viral RNA peaked at 2–6 dpi and ceased by 8 dpi, indicating that both virus strains caused a productive infection that resolved quickly. We detected viral RNA in nasal wash samples collected from all naive, unvaccinated ferrets as well as in samples collected from vaccinated ferrets that had been exposed to the 1C.2.1 virus. Conversely, the ferret group that had received the human seasonal vaccine and was then exposed to the swine-origin 1A.3.2.2 virus (Figure 3, panel A) showed a significant reduction in viral shedding in nasal samples. A single ferret in this vaccinated group showed an outlier response of transient, low level of viral RNA shedding on nonconsecutive days. Taken together, those shedding profiles indicated that both viruses could be transmitted from infected pigs to naive ferrets by the airborne route and cause productive infection. In addition, the human seasonal vaccine

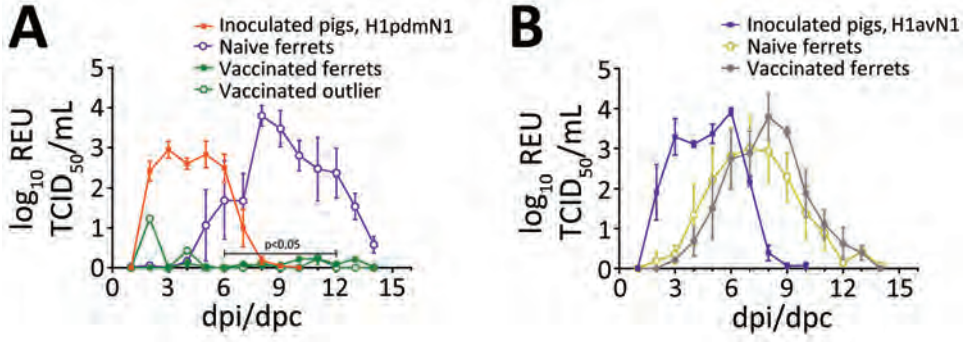

Figure 3. Nasal shedding of viral RNA monitored in pigs intranasally inoculated with influenza A virus strains A/swine/England/1353/2009 (H1pdmN1) (A) or A/Pavia/65/2016 (H1avN1) (B) and in naive or vaccinated ferrets cohoused in the same airspace as inoculated pigs. Viral RNA was quantified by real-time quantitative reverse transcription PCR in longitudinal nasal samples collected daily until 14 dpi (pigs) or 14 dpc (ferrets) and is expressed as REU based on an RNA quantification standard prepared from the corresponding virus stock. In vaccinated ferrets (n = 4) exposed to the H1pdmN1 strain, nasal shedding of viral RNA between 6 dpc and 12 dpc was significantly different from the naive ferret group ($p<0.05$). Results for the remaining ferret in this group are shown as outlier data (hollow green circles). dpc, days postcontact; dpi, days postinoculation; REU, relative equivalent unit; $TCID_{50}$, 50% tissue culture infectious dose.

could only elicit protective immunity against an antigenically similar challenge virus, namely the swine-origin 1A.3.3.2 virus but not the antigenically distinct 1C.2.1 virus.

Immunohistochemical analysis of pig tissues collected at 5 dpi (Figure 4) demonstrated immunolabelling of viral NP antigen in the nucleus and cytoplasm of epithelial cells of the respiratory mucosae, including nasal turbinate, trachea, and bronchi and bronchioles in the lungs of pigs inoculated with either virus, indicating comparable replication of both virus strains. Specific humoral responses were detected in both groups of pigs at 14 dpi, indicated by the increase in NP (Figure 5, panels A, B) and HI (Figure 5, panels C, D) antibody titers. Furthermore, we detected a specific neutralizing antibody response (Figure 5, panels E, F) for each inoculated virus at 14 dpi, although titers were considerably lower in H1pdmN1 virus–infected pigs. Taken together, those results indicate that all pigs seroconverted after virus inoculation and that infections were productive.

Humoral immune responses in virus-exposed ferrets were evaluated by NP ELISA (Figure 6, panels A, B) as well as HI (Figure 6, panels C, D) and virus neutralization (Figure 6 panels, E, F), using the homologous viruses. Antibody responses to vaccination were low or undetectable. Unvaccinated ferrets in both groups seroconverted after virus exposure, as did vaccinated ferrets cohoused with pigs inoculated with the 1C.2.1 virus. In contrast, vaccinated ferrets cohoused with pigs infected with the swine-origin 1A.3.3.2 virus mounted no detectable influenza-specific humoral response, apart from the single ferret that showed transient, low-level nasal shedding (Figure 3, panel A). The humoral responses shown separately for this ferret as an outlier from the group data (Figure 6, panels A, C, E) could reflect differences in the immune response elicited by vaccination in this individual ferret, as observed in outbred populations. Two nonvaccinated, nonexposed negative control animals did not produce specific humoral immune responses, as was expected. ELISpot analysis (Figure 6, panels G, H) showed that infection elicited a detectable cellular response after stimulation with NP peptides, but it was considerably reduced ($p<0.0002$) in vaccinated ferrets exposed to the H1pdmN1 virus, although the single outlier ferret showed an intermediate response.

Collectively, those results indicate that naive ferrets became productively infected after airborne exposure to virus shed by infected pigs but nevertheless mounted an effective humoral and cellular response, resulting in resolution of infection. Conversely, productive infection did not occur in the 1A.3.3.2 H1N1–exposed ferrets with previous vaccine-mediated immunity when the vaccine antigen was well matched to the challenge strain, although we did not identify corresponding immune determinants. Vaccination did not prevent infection of ferrets with the 1C.2.1 virus.

Discussion

H1 1C Eurasian avian-like viruses have been circulating in swine herds in Europe for >40 years, most likely following direct introduction from an avian host into pigs (*8*). This virus clade remains a potential zoonotic

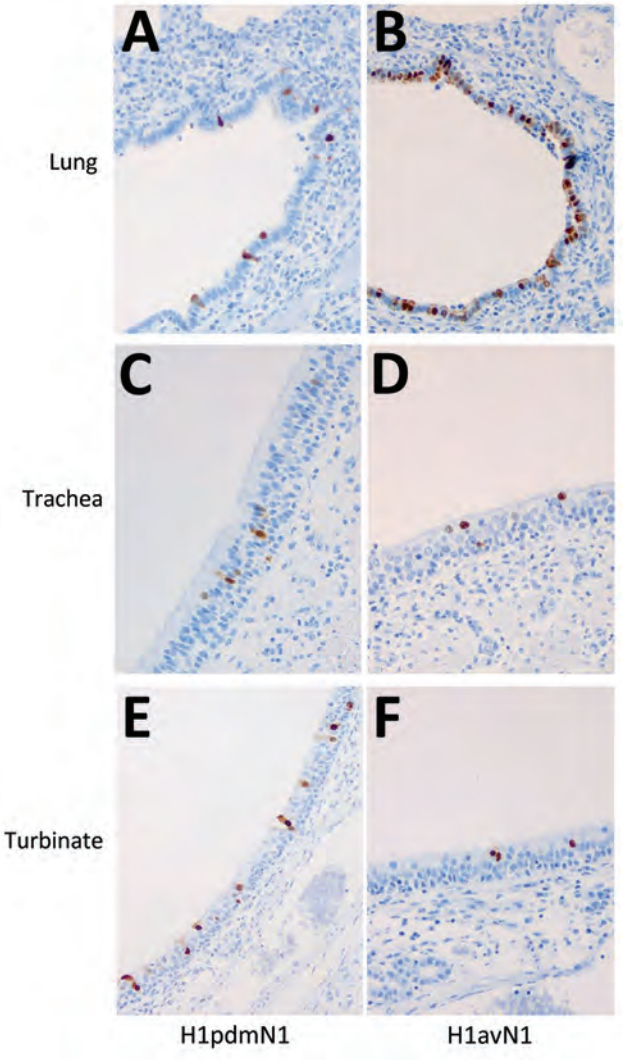

Figure 4. Immunohistochemical detection of viral nucleoprotein in pig tissues. Immunolabelling of influenza A viral nucleoprotein in respiratory tissues collected from pigs at 5 dpi after inoculation with A/swine/England/1353/2009 (H1pdmN1; panels A, C, and E) or A/Pavia/65/2016 (H1avN1; panels B, D, and F) viruses reveals presence of viral nucleoprotein antigen (brown staining) in respiratory epithelial cells of the lung, trachea, and nasal turbinate for both viruses. Original magnification × 400.

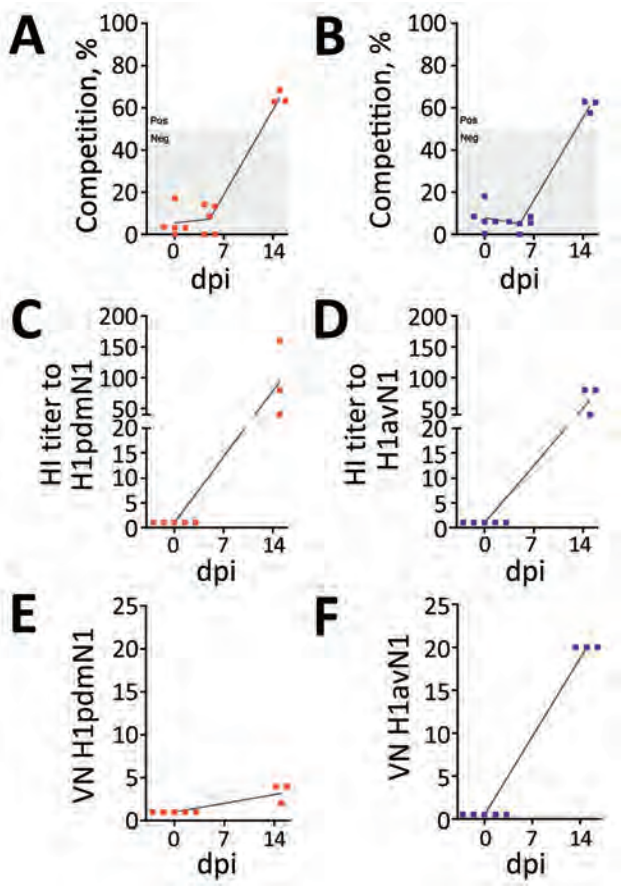

Figure 5. Characterization of virus-specific humoral responses following intranasal inoculation of pigs with A/swine/England/1353/2009 (H1pdmN1, panels A, C, E) or A/Pavia/65/2016 (H1avN1, panels B, D, F). Antibody titers were monitored at 0, 5, and 14 dpi by nucleoprotein competitive ELISA (A, B) and are expressed as competition percentage and considered negative if <50% (gray area). Competition percentage was calculated as (1 – sample/negative) × 100. Hemagglutination inhibition (C, D) and virus neutralization (E, F) titers were assessed at 0 and 14 dpi using the homologous virus for each group. Both titers were normalized to the individual prevaccination titers (0 days postvaccination). dpi, days postinoculatinon.

risk, as highlighted by sporadic human H1N1v cases caused by this swIAV lineage and reassortant viruses, as well as by experimental data obtained using the ferret model (*20*,*24*,*26*,*28*,*29*).

The ferret is a robust animal model species for studying influenza arising from both human- and swine-origin IAV infections (*32*,*42*) and for studying influenza vaccines (*31*); we used that model to characterize the 1C.2.1 lineage virus, A/Pavia/65/2016. Virus infection transmitted effectively between ferrets by the direct contact route but not by airborne respiratory droplet exposure, suggesting that sustained transmission in human populations would be limited, as supported by epidemiologic findings (*15*). Of note, nasal shedding of virus by pigs resulted in respiratory droplet infection of susceptible, cohoused ferrets. We speculate that result occurred because of the larger volume of respiratory droplets exhaled by pigs, which have a larger lung volume than ferrets, thereby increasing the viral load. The virologic profile of the A/Pavia/65/2016 isolate, when compared in the same interspecies transmission model to A/swine/England/1353/2009, a swine-origin H1N1 virus from the 1A.3.3.2 lineage, demonstrated that all experimentally infected animals exhibited mild or no clinical signs of influenza, mounted an effective humoral and cellular immune response, and resolved the infection. Our findings therefore indicate that the A/Pavia/65/2016 strain does not have an increased pathogenicity profile compared to the 1A.3.3.2 strain when assessed in 2 animal models, as predicted from phylogenetic data, despite having originated from a human clinical case. In addition, our study reaffirms the value of the interspecies transmission model for assessing zoonotic potential (*20*,*38*,*42*–*45*).

We assessed immunity provided by the 2016–17 human seasonal influenza vaccine against the 2 swIAV isolates by cohousing naive and vaccinated ferret groups with pigs shedding the respective virus strains. All ferret groups, except the vaccinated ferrets exposed to the H1pdmN1 virus–infected pigs, had a viral nasal shedding profile consistent with productive infection and mounted a detectable humoral and cellular immune response. Conversely, nasal shedding in the vaccinated, 1A.3.3.2 H1N1–exposed ferret group was significantly reduced, suggesting that the human seasonal vaccine provided immune protection from infection by the antigenically matched swine-origin challenge strain. However, the immune response after infection was low in that ferret group, so the correlates of protection remain unknown. In both studies, individual ferrets in single groups displayed outlier responses to infection or vaccination, possibly reflecting the differences observed in outbred populations.

Despite such limitations and the constraints of low group numbers, this study enabled effective modeling of interspecies transmission of influenza. The experimental design benefited from using pigs as a biological host for the virus strains studied. In addition, the study design provided a controlled and biologically relevant system to study interspecies airborne transmission to ferrets, a well-established animal model for human influenza; including naive and vaccinated ferret groups enabled modeling of human populations with varied prior immunity to influenza (*31*).

As part of the World Health Organization influenza pandemic preparedness initiative, CVVs for

human seasonal vaccines are identified twice a year. Considering the increase in reports of zoonotic infections, OFFLU has contributed data for selecting swIAV-origin CVVs should a zoonotic spillover event necessitate a rapid update of human seasonal vaccine antigens. Within-clade diversity of 1C-lineage swIAVs hampers the selection of candidate antigens, as has also been observed for 1B viruses (*24*,*43*,*46*) and, despite the A/Pavia/65/2016 strain being in the same 1C2.1 genetic lineage as the CVV A/Netherlands/3315/2016, antigenic cross-reactivity is low (*1*). Those findings reinforce the need for continued CVV assessment for swIAVs to ensure pandemic preparedness. Furthermore, recent studies in the ferret model have demonstrated the potential for IAV and SARS-CoV-2 co-infection. Clinical severity was ameliorated by influenza vaccination, thereby demonstrating the potential importance of ensuring vaccine immunity to circulating influenza strains in the human population (*47*).

Our study confirms that vaccine and challenge strains must be antigenically matched to elicit vaccine-mediated protective immunity and that the immune status of the human population might not provide complete immunity to all currently circulating swine influenza A virus H1N1 strains. Continual

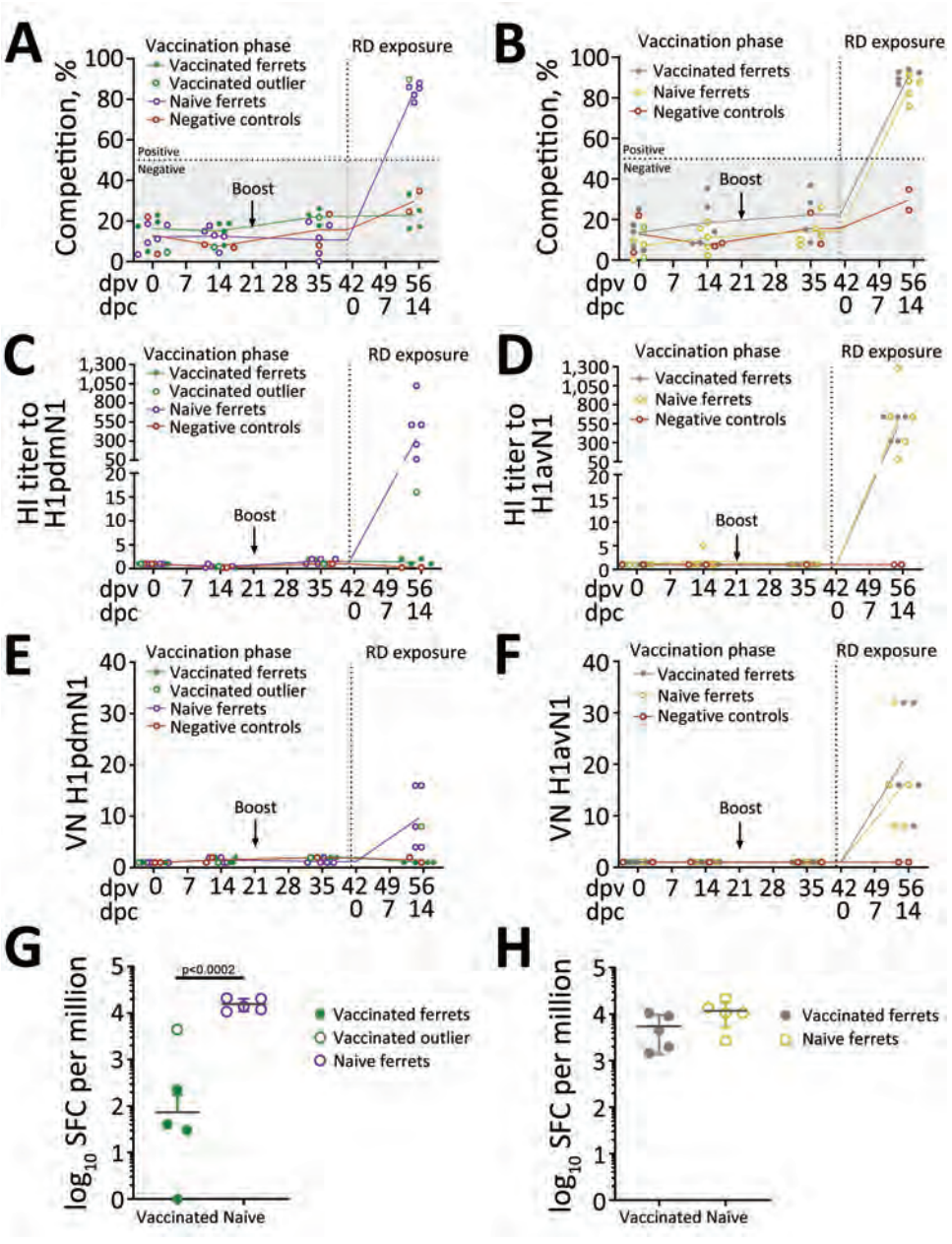

Figure 6. Immune parameters assessed in naive and vaccinated ferrets before and after exposure to pigs infected with influenza A viruses A/swine/England/1353/2009 (H1pdmN1, panels A, C, E, and G) or A/Pavia/65/2016 (H1avN1, panels B, D, F, and H). Data from a single outlier, a vaccinated ferret exposed to the H1pdmN1 virus, were excluded from analysis but are shown. Negative control ferrets (n = 2) were not vaccinated or exposed to infectious virus. Specific humoral responses were assessed longitudinally in serum. Antibody titers detected by NP competition ELISA (A, B) are expressed as competition percentage and considered negative if <50% (gray area). Competition percentage was calculated as (1 – sample/negative) × 100. HI (C, D) and VN (E, F) were determined using the homologous virus for each group. Both HI and VN titers are normalized to the individual prevaccination titers (0 dpv). ELISpot analysis (G, H) evaluated the number of interferon-γ–producing peripheral blood mononuclear cells induced by 18-mer nucleoprotein peptides, represented as SPC per 1 million, at 14 dpc (RD exposure). dpv, days postvaccination; dpc, days postcontact; HI, hemagglutination inhibition; NP, nucleoprotein; RD, respiratory droplets; SFC, spot-forming cells;VN, virus neutralization.

evaluation and monitoring of IAVs circulating in human and swine populations is required to identify potential pandemic threats; broadly effective vaccines for both human and veterinary use are needed to mitigate these threats.

Acknowledgments

We thank the staff of the APHA Animal Sciences Unit for excellent animal care.

This work was conducted under the FluFutures research program (SE2211), and mammalian influenza research is supported by FluFutures2 (SE2213), both funded by the UK Department for the Environment, Food and Rural Affairs (Defra) and the devolved Scottish and Welsh Administrations.

About the Author

Dr. van Diemen is senior scientist in the Mammalian Influenza Research team at the Animal and Plant Health Agency, an agency of the UK Department for Environment, Food and Rural Affaires (Defra). Her research focuses on mammalian influenza, particularly viral pathogenesis, interactions between host and virus, and generation of vaccine-mediated protection.

References

1. Anderson TK, Chang J, Arendsee ZW, Venkatesh D, Souza CK, Kimble JB, et al. Swine influenza A viruses and the tangled relationship with humans. Cold Spring Harb Perspect Med. 2021;11:a038737. https://doi.org/10.1101/cshperspect.a038737
2. Short KR, Richard M, Verhagen JH, van Riel D, Schrauwen EJ, van den Brand JM, et al. One health, multiple challenges: the inter-species transmission of influenza A virus. One Health. 2015;1:1–13.
3. Pulit-Penaloza JA, Belser JA, Tumpey TM, Maines TR. Sowing the seeds of a pandemic? Mammalian pathogenicity and transmissibility of H1 variant influenza viruses from the swine reservoir. Trop Med Infect Dis. 2019;4:41. https://doi.org/10.3390/tropicalmed4010041
4. Rajao DS, Vincent AL, Perez DR. Adaptation of human influenza viruses to swine. Front Vet Sci. 2019;5:347. https://doi.org/10.3389/fvets.2018.00347
5. Vincent AL, Anderson TK, Lager KM. A brief introduction to influenza A virus in swine. Methods Mol Biol. 2020;2123:249–71. https://doi.org/10.1007/978-1-0716-0346-8_18
6. Anderson TK, Macken CA, Lewis NS, Scheuermann RH, Van Reeth K, Brown IH, et al. A phylogeny-based global nomenclature system and automated annotation tool for H1 hemagglutinin genes from swine influenza A viruses. MSphere. 2016;1:e00275-16. https://doi.org/10.1128/mSphere.00275-16
7. Lewis NS, Russell CA, Langat P, Anderson TK, Berger K, Bielejec F, et al.; ESNIP3 consortium. The global antigenic diversity of swine influenza A viruses. eLife. 2016;5:e12217. https://doi.org/10.7554/eLife.12217
8. Krumbholz A, Lange J, Sauerbrei A, Groth M, Platzer M, Kanrai P, et al. Origin of the European avian-like swine influenza viruses. J Gen Virol. 2014;95:2372–6. https://doi.org/10.1099/vir.0.068569-0
9. Watson SJ, Langat P, Reid SM, Lam TT, Cotten M, Kelly M, et al.; ESNIP3 Consortium. Molecular epidemiology and evolution of influenza viruses circulating within European swine between 2009 and 2013. J Virol. 2015;89:9920–31. https://doi.org/10.1128/JVI.00840-15
10. Simon G, Larsen LE, Dürrwald R, Foni E, Harder T, Van Reeth K, et al.; ESNIP3 consortium. European surveillance network for influenza in pigs: surveillance programs, diagnostic tools and Swine influenza virus subtypes identified in 14 European countries from 2010 to 2013. PLoS One. 2014;9:e115815. https://doi.org/10.1371/journal.pone.0115815
11. Brown IH. History and epidemiology of swine influenza in Europe. Curr Top Microbiol Immunol. 2013;370:133–46. https://doi.org/10.1007/82_2011_194
12. Henritzi D, Petric PP, Lewis NS, Graaf A, Pessia A, Starick E, et al. Surveillance of European domestic pig populations identifies an emerging reservoir of potentially zoonotic swine influenza A viruses. Cell Host Microbe. 2020;28:614–627.e6. https://doi.org/10.1016/j.chom.2020.07.006
13. Hennig C, Graaf A, Petric PP, Graf L, Schwemmle M, Beer M, et al. Are pigs overestimated as a source of zoonotic influenza viruses? Porcine Health Manag. 2022;8:30. https://doi.org/10.1186/s40813-022-00274-x
14. Parys A, Vandoorn E, King J, Graaf A, Pohlmann A, Beer M, et al. Human infection with Eurasian avian-like swine influenza A(H1N1) Virus, the Netherlands, September 2019. Emerg Infect Dis. 2021;27:939–43. https://doi.org/10.3201/eid2703.201863
15. Rovida F, Piralla A, Marzani FC, Moreno A, Campanini G, Mojoli F, et al. Swine influenza A (H1N1) virus (SIV) infection requiring extracorporeal life support in an immunocompetent adult patient with indirect exposure to pigs, Italy, October 2016. Euro Surveill. 2017;22:30456.
16. Fraaij PL, Wildschut ED, Houmes RJ, Swaan CM, Hoebe CJ, de Jonge HC, et al. Severe acute respiratory infection caused by swine influenza virus in a child necessitating extracorporeal membrane oxygenation (ECMO), the Netherlands, October 2016. Euro Surveill. 2016;21:30416.
17. European Centre for Disease Prevention and Control. Threats and outbreaks of swine influenza [cited 2023 Jan 16]. https://www.ecdc.europa.eu/en/swine-influenza/threats-and-outbreaks
18. Dürrwald R, Wedde M, Biere B, Oh DY, Heßler-Klee M, Geidel C, et al. Zoonotic infection with swine A/H1(av)N1 influenza virus in a child, Germany, June 2020. Euro Surveill. 2020;25:2001638.
19. Wang DY, Qi SX, Li XY, Guo JF, Tan MJ, Han GY, et al. Human infection with Eurasian avian-like influenza A(H1N1) virus, China. Emerg Infect Dis. 2013;19:1709–11. https://doi.org/10.3201/eid1910.130420
20. Yang H, Chen Y, Qiao C, He X, Zhou H, Sun Y, et al. Prevalence, genetics, and transmissibility in ferrets of Eurasian avian-like H1N1 swine influenza viruses. Proc Natl Acad Sci USA. 2016;113:392–7. https://doi.org/10.1073/pnas.1522643113
21. Xie JF, Zhang YH, Zhao L, Xiu WQ, Chen HB, Lin Q, et al. Emergence of Eurasian avian-like swine influenza A (H1N1) virus from an adult case in Fujian Province, China. Virol Sin. 2018;33:282–6. https://doi.org/10.1007/s12250-018-0034-1
22. Li X, Guo L, Liu C, Cheng Y, Kong M, Yang L, et al. Human infection with a novel reassortant Eurasian-avian lineage

swine H1N1 virus in northern China. Emerg Microbes Infect. 2019;8:1535–45. https://doi.org/10.1080/22221751.2019.1679611
23. Rambo-Martin BL, Keller MW, Wilson MM, Nolting JM, Anderson TK, Vincent AL, et al. Influenza A virus field surveillance at a swine-human interface. MSphere. 2020; 5:e00822-19. https://doi.org/10.1128/mSphere.00822-19
24. Sun H, Xiao Y, Liu J, Wang D, Li F, Wang C, et al. Prevalent Eurasian avian-like H1N1 swine influenza virus with 2009 pandemic viral genes facilitating human infection. Proc Natl Acad Sci U S A. 2020;117:17204–10. https://doi.org/10.1073/pnas.1921186117
25. Andersen KM, Vestergaard LS, Nissen JN, George SJ, Ryt-Hansen P, Hjulsager CK, et al. Severe human case of zoonotic infection with swine-origin influenza A virus, Denmark, 2021. Emerg Infect Dis. 2022;28:2561–4. https://doi.org/10.3201/eid2812.220935
26. Pulit-Penaloza JA, Belser JA, Tumpey TM, Maines TR. Mammalian pathogenicity and transmissibility of a reassortant Eurasian avian-like A(H1N1v) influenza virus associated with human infection in China (2015). Virology. 2019;537:31–5. https://doi.org/10.1016/j.virol.2019.08.008
27. Zhu W, Zhang H, Xiang X, Zhong L, Yang L, Guo J, et al. Reassortant Eurasian avian-like influenza A(H1N1) virus from a severely ill child, Hunan Province, China, 2015. Emerg Infect Dis. 2016;22:1930–6. https://doi.org/10.3201/eid2211.160181
28. Meng F, Yang H, Qu Z, Chen Y, Zhang Y, Zhang Y, et al. A Eurasian avian-like H1N1 swine influenza reassortant virus became pathogenic and highly transmissible due to mutations in its PA gene. Proc Natl Acad Sci U S A. 2022;119:e2203919119. https://doi.org/10.1073/pnas.2203919119
29. Lakdawala SS, Lamirande EW, Suguitan AL Jr, Wang W, Santos CP, Vogel L, et al. Eurasian-origin gene segments contribute to the transmissibility, aerosol release, and morphology of the 2009 pandemic H1N1 influenza virus. PLoS Pathog. 2011;7:e1002443. https://doi.org/10.1371/journal.ppat.1002443
30. OFFLU. OFFLU VCM summary reports [cited 2023 Jan 16]. https://www.offlu.org/index.php/offlu-vcm-summary-reports
31. Roubidoux EK, Schultz-Cherry S. Animal models utilized for the development of influenza virus vaccines. Vaccines (Basel). 2021;9:787. https://doi.org/10.3390/vaccines9070787
32. Belser JA, Lau EHY, Barclay W, Barr IG, Chen H, Fouchier RAM, et al.; Working Group on the Standardization of the Ferret Model for Influenza Risk Assessment. Robustness of the ferret model for influenza risk assessment studies: a cross-laboratory exercise. MBio. 2022;13:e0117422. https://doi.org/10.1128/mbio.01174-22
33. Belser JA, Barclay W, Barr I, Fouchier RAM, Matsuyama R, Nishiura H, et al. Ferrets as models for influenza virus transmission studies and pandemic risk assessments. Emerg Infect Dis. 2018;24:965–71. https://doi.org/10.3201/eid2406.172114
34. Brookes SM, Núñez A, Choudhury B, Matrosovich M, Essen SC, Clifford D, et al. Replication, pathogenesis and transmission of pandemic (H1N1) 2009 virus in non-immune pigs. PLoS One. 2010;5:e9068. https://doi.org/10.1371/journal.pone.0009068
35. Percie du Sert N, Hurst V, Ahluwalia A, Alam S, Avey MT, Baker M, et al. The ARRIVE guidelines 2.0: updated guidelines for reporting animal research. BMC Vet Res. 2020;16:242. https://doi.org/10.1186/s12917-020-02451-y
36. Karakus U, Crameri M, Lanz C, Yángüez E. Propagation and titration of influenza viruses. In: Yamauchi Y, editor. Influenza virus: methods and protocols. New York: Springer New York; 2018. p. 59–88.
37. Nagy A, Vostinakova V, Pirchanova Z, Cernikova L, Dirbakova Z, Mojzis M, et al. Development and evaluation of a one-step real-time RT-PCR assay for universal detection of influenza A viruses from avian and mammal species. Arch Virol. 2010;155:665–73.
38. Everett HE, Nash B, Londt BZ, Kelly MD, Coward V, Nunez A, et al. Interspecies transmission of reassortant swine influenza A virus containing genes from swine influenza A(H1N1)pdm09 and A(H1N2) viruses. Emerg Infect Dis. 2020;26:273–81. https://doi.org/10.3201/eid2602.190486
39. Gauger PC, Vincent AL. Serum virus neutralization assay for detection and quantitation of serum neutralizing antibodies to influenza A virus in swine. Methods Mol Biol. 2020;2123:321–33. https://doi.org/10.1007/978-1-0716-0346-8_23
40. Kitikoon P, Gauger PC, Vincent AL. Hemagglutinin inhibition assay with swine sera. Methods Mol Biol. 2014;1161:295–301. https://doi.org/10.1007/978-1-4939-0758-8_24
41. Löndt BZ, Brookes SM, Nash BJ, Núñez A, Stagg DA, Brown IH. The infectivity of pandemic 2009 H1N1 and avian influenza viruses for pigs: an assessment by ex vivo respiratory tract organ culture. Influenza Other Respir Viruses. 2013;7:393–402. https://doi.org/10.1111/j.1750-2659.2012.00397.x
42. Pulit-Penaloza JA, Brock N, Jones J, Belser JA, Jang Y, Sun X, et al. Pathogenesis and transmission of human seasonal and swine-origin A(H1) influenza viruses in the ferret model. Emerg Microbes Infect. 2022;11:1452–9. https://doi.org/10.1080/22221751.2022.2076615
43. Kimble JB, Souza CK, Anderson TK, Arendsee ZW, Hufnagel DE, Young KM, et al. Interspecies transmission from pigs to ferrets of antigenically distinct swine H1 influenza A viruses with reduced reactivity to candidate vaccine virus antisera as measures of relative zoonotic risk. Viruses. 2022;14:2398. https://doi.org/10.3390/v14112398
44. Russier M, Yang G, Marinova-Petkova A, Vogel P, Kaplan BS, Webby RJ, et al. H1N1 influenza viruses varying widely in hemagglutinin stability transmit efficiently from swine to swine and to ferrets. PLoS Pathog. 2017;13:e1006276. https://doi.org/10.1371/journal.ppat.1006276
45. Kaplan BS, Kimble JB, Chang J, Anderson TK, Gauger PC, Janas-Martindale A, et al. Aerosol transmission from infected swine to ferrets of an H3N2 virus collected from an agricultural fair and associated with human variant infections. J Virol. 2020;94:e01009-20. https://doi.org/10.1128/JVI.01009-20
46. Meng F, Chen Y, Song Z, Zhong Q, Zhang Y, Qiao C, et al. Continued evolution of the Eurasian avian-like H1N1 swine influenza viruses in China. Sci China Life Sci. 2022.
47. Huang Y, Skarlupka AL, Jang H, Blas-Machado U, Holladay N, Hogan RJ, et al. SARS-CoV-2 and influenza A virus coinfections in ferrets. J Virol. 2022;96:e0179121.

Address for correspondence: Pauline van Diemen or Helen Everett, Virology Department, APHA, New Haw, Addlestone, Surrey, KT15 3NB, UK; email: PaulineM.vanDiemen@APHA.gov.uk or Helen.Everett@APHA.gov.uk

Shifting Patterns of Influenza Circulation during the COVID-19 Pandemic, Senegal

Alexandre Lampros, Cheikh Talla, Maryam Diarra, Billo Tall, Samba Sagne, Mamadou Korka Diallo, Boly Diop, Ibrahim Oumar, Ndongo Dia, Amadou Alpha Sall, Mamadou Aliou Barry,[1] Cheikh Loucoubar[1]

Historically low levels of seasonal influenza circulation were reported during the first years of the COVID-19 pandemic and were mainly attributed to implementation of nonpharmaceutical interventions. In tropical regions, influenza's seasonality differs largely, and data on this topic are scarce. We analyzed data from Senegal's sentinel syndromic surveillance network before and after the start of the COVID-19 pandemic to assess changes in influenza circulation. We found that influenza shows year-round circulation in Senegal and has 2 distinct epidemic peaks: during January–March and during the rainy season in August–October. During 2021–2022, the expected January–March influenza peak completely disappeared, corresponding to periods of active SARS-CoV-2 circulation. We noted an unexpected influenza epidemic peak during May–July 2022. The observed reciprocal circulation of SARS-CoV-2 and influenza suggests that factors such as viral interference might be at play and should be further investigated in tropical settings.

In temperate regions, seasonal influenza commonly follows a regular circulation pattern and has an annual epidemic peak during the colder winter months (*1*–*3*). In contrast, tropical areas have great diversity in influenza seasonality (*1*–*3*). Some countries, including Brazil, Mexico, and the Philippines, report 1 distinct annual peak, but other countries, including Colombia, Burkina Faso, and Thailand, have 2 distinct peaks (*3*). Countries near the equator, such as Venezuela, Cameroon, Indonesia, and Malaysia, show year-round circulation and have no distinct peak (*3*). However, Senegal and other countries in West Africa have year-round influenza activity with 1 or 2 distinct annual peaks; the second most often occurs during the rainy season (*3*).

The diversity of circulation patterns challenges old theories on influenza's seasonality that suggest the increased activity seen in winter mainly is explained by the permissive dry and cold weather (*4*). The determinants of influenza's seasonality remain poorly understood, and studying viral circulation in tropical areas represents a crucial step toward a global understanding of influenza seasonality (*2*,*5*–*7*).

The emergence of SARS-CoV-2 in late 2019 deeply impacted influenza's global circulation (*8*). During 2020–2021, the first years of the pandemic, historically low levels of influenza circulation were noted, but those findings were largely described and discussed from high-income countries in temperate regions that have abundant influenza surveillance data (*9*–*12*). The low-level phenomenon is commonly believed to be a beneficial side effect of nonpharmaceutical interventions (NPIs) implemented to control of the spread of SARS-CoV-2 (*13*,*14*). However, little is known about the impact that SARS-CoV-2 had on influenza's circulation in tropical settings. To clarify SARS-CoV-2–influenza interactions in tropical regions, we investigated usual influenza circulation patterns in Senegal, a subtropical country in West Africa, and whether circulation patterns shifted during the COVID-19 pandemic.

Methods

Syndromic Surveillance in Senegal

Since 2011, Senegal has been managing a sentinel syndromic surveillance system (réseaux de surveillance

Author affiliations: Hôpital Européen Georges Pompidou, Paris, France (A. Lampros); Institut Pasteur de Dakar, Dakar, Senegal (A. Lampros, C. Talla, M. Diarra, B. Tall, S. Sagne, M. Korka Diallo, N. Dia, A.A. Sall, M.A. Barry, C. Loucoubar); Government of Senegal Ministry of Health and Social Action, Dakar (A. Lampros, B. Diop); World Health Organization, Dakar (A. Lampros, I. Oumar)

DOI: https://doi.org/10.3201/eid2909.230307

[1]These authors contributed equally to this article.

sentinelle syndromique du Sénégal), known as the 4S Network (*15*). The 4S Network is concurrently run by the National Ministry of Health and Institut Pasteur de Dakar, which supervises the sites' activities, provides equipment, and manages sample transport, virological testing, and data management and analysis.

The 4S Network functions as any syndromic surveillance system by monitoring and testing persons who have certain syndromes of public health interest, in this case, signs and symptoms suggestive of viral respiratory diseases, as previously described (*16*). The 4S Network comprises 25 sentinel sites: 22 community sites in primary or secondary healthcare facilities that are in charge of influenza-like illness (ILI) surveillance and 3 hospitals located in the region of Dakar that are in charge of severe acute respiratory illness (SARI) surveillance (Figure 1). Sentinel sites are located throughout the country in each of its 14 regions, enabling geographic coverage and providing a fairly accurate representation of Senegal's population. Sites were selected according to their location, number of patients served, willingness to participate, and availability of minimal equipment, such as running water and a refrigerator (*16*).

The 4S Network offers a unique source of epidemiologic data on ILI and SARI in Senegal. During the COVID-19 pandemic, the network also rapidly integrated SARS-CoV-2 testing in its routine surveillance activities. We extracted data from the 4S Network to analyze local dynamics of influenza, SARS-CoV-2, and interactions between the 2 viruses in a remote setting.

Study Population and Case Definition

We focused on ILI and SARI surveillance by using definitions from 2014 World Health Organization criteria (*17*). Those criteria define ILI cases as acute respiratory infection accompanied by a measured temperature of ≥38°C and cough that had an onset within the previous 10 days and define SARI cases as an acute respiratory infection and history of fever or a measured temperature of ≥38°C and cough that had an onset within the previous 10 days and resulted in hospital admission. We included all age groups in the study and had no specific exclusion criteria apart from a patient's refusal to participate. All patients undergoing virological testing and included in the surveillance program gave informed oral consent. All data were fully anonymized in advance.

Study Period and Data Collection

To assess baseline influenza seasonality patterns, we extracted influenza test results from January 1, 2013–March 1, 2020. To describe interactions between SARS-CoV-2 and influenza, we extracted those test results from March 1, 2020–July 31, 2022.

For SARI cases, any patient that fit the case description and was admitted at a sentinel site was subjected to nasal and oropharyngeal swab sampling. For ILI surveillance, ≥5 samples per site were randomly

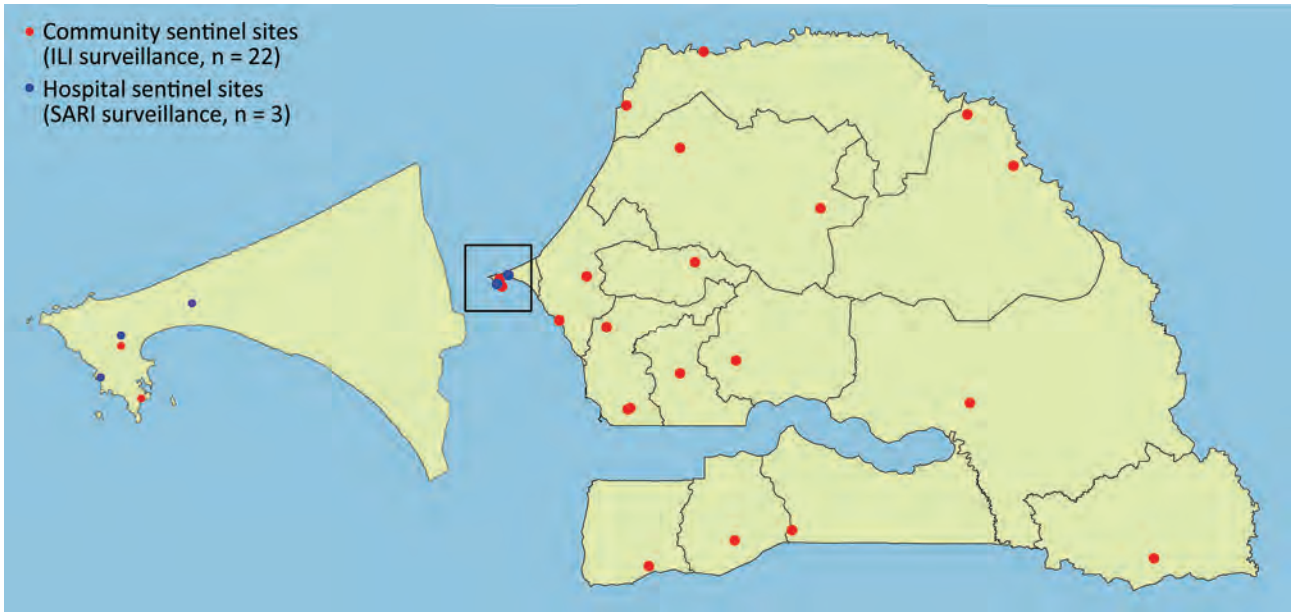

Figure 1. Geographic distribution of community and hospital sentinel sites participating in surveillance for shifting patterns of influenza circulation during the COVID-19 pandemic, Senegal. Sites represent the network of sentinelle syndromique du Sénégal (sentinel syndromic surveillance of Senegal), also known as the 4S Network. Enlarged map at left shows detailed view of the Dakar capital region and 4S Network hospitals located in the region. ILI, influenza-like illness; SARI, severe acute respiratory illness.

collected for surveillance every week. SARI samples are transferred every day and ILI samples are transferred weekly to the national reference center for influenza and other respiratory viruses at the Pasteur Institute in Dakar.

The reference center performs 2-step real-time reverse transcription PCR (rRT-PCR) by using the CFX96 Real-Time PCR Detection System (Bio-Rad, https://www.bio-rad.com) and Anyplex II RV16 Detection Kit (Seegene, https://www.seegene.com). That testing system enables simultaneous testing for influenza A and B viruses; human respiratory syncytial virus A and B; adenovirus; metapneumovirus; coronavirus 229E, NL63, and OC43; parainfluenza virus 1–4; rhinovirus A/B/C; enterovirus; and bocavirus (*18*). Influenza viruses underwent RT-PCR to detect N1, H1, and H3 subtypes and matrix, neuraminidase 2, and hemagglutinin 2 genes, as previously described (*19*).

SARS-CoV-2 surveillance was rapidly integrated into the 4S Network. At the beginning of June 2020, every sample from SARI or ILI cases was subjected to monoplex SARS-CoV-2 RT-PCR testing by using the LightMix CoV E-gene and LightMix Modular Wuhan CoV RdRP-gene kits (TIB MOLBIOL, https://www.tib-molbiol.de). Although a new case definition including other symptoms, such as anosmia or digestive symptoms, for suspected COVID-19 cases was initially added to the surveillance system, ILI and SARI case definitions remained unchanged during that period. Senegal abandoned the new suspected COVID-19 case definition at the end of 2021, following the World Health Organization's international recommendations for COVID-19 surveillance (*20*). Thus, we only included patients that fit the case description for ILI or SARI in this study.

Statistical Analysis

We used R version 4.0.3 (The R Foundation for Statistical Computing, https://www.r-project.org) and the supplementary R package, Moving Epidemic Method version 2.17 (https://github.com/lozalojo/mem), to process data and create epidemiologic curves. We generated average epidemic curves on the basis of percentages of SARI or ILI cases testing positive for influenza during each season. Then, we aligned the seasonal curves to generate an average curve, and set thresholds to define preepidemic, epidemic, and postepidemic periods. We defined the thresholds by calculating the upper limit of the 95% CI around the 30 highest weekly values. Our model also estimated sensitivity by correctly defining the epidemic period and specificity by correctly defining the nonepidemic period, and we calculated 95% CIs for the average season's start date and duration (*21*,*22*).

Results

During the prepandemic period, January 1, 2013–December 31, 2019, the 4S Network detected 74,726 ILI cases in community sites. Of those, 12,530 (17%) were randomly tested for influenza by rRT-PCR, and 3,157 (25%) were influenza-positive. During the same period, 776 SARI cases were hospitalized in sentinel sites and tested for influenza; 145 (19%) were positive (Table).

During the pandemic period, January 1, 2020–July 31, 2022, the 4S Network detected 19,030 ILI cases in community sites. Of those, 2,593 (14%) were randomly tested for influenza, of which 1,409 (54.3%) were also tested for SARS-CoV-2. Among tested samples, 622 (24%) were influenza-positive and 195 (14%) were SARS-CoV-2–positive. During the same period, 1,352 SARI cases were hospitalized in sentinel sites and tested for influenza, and 68 (5%) tested influenza-positive; 1,129 had combined SARS-CoV-2 and influenza testing, and 211 (19%) were SARS-CoV-2–positive (Table). Every specimen tested for SARS-CoV-2 was systematically tested for influenza, but the 2 pathogens were co-detected in only 1 patient.

Table. RT-PCR test results demonstrating shifting patterns of influenza circulation during the COVID-19 pandemic, Senegal*

Testing per timeframe	No. (%) cases		
	ILI	SARI	Total
Prepandemic, 2013–2020			
No. cases enrolled	74,726	776	75,502
No. influenza RT-PCR performed	12,530 (1)	776 (100)	13,306 (17)
No. influenza-positive tests	3,157 (25)	145 (19)	3,302 (25)
Pandemic period, 2020–2022			
No. cases enrolled	19,030	1,352	20,382
No. influenza RT-PCR performed	2,593 (14)	1,352 (100)	3,945 (19)
No. influenza-positive tests	622 (24)	68 (5)	690 (17)
No. SARS-CoV-2 RT-PCR performed	1,409 (7)	1,129 (84)	2,538 (12)
No. SARS-CoV-2 positive tests	195 (14)	211 (19)	416 (16)

*Cases are from ILI and SARI surveillance during January 2013–July 2022. ILI, influenza-like illness; RT-PCR, reverse transcription PCR; SARI, severe acute respiratory illness

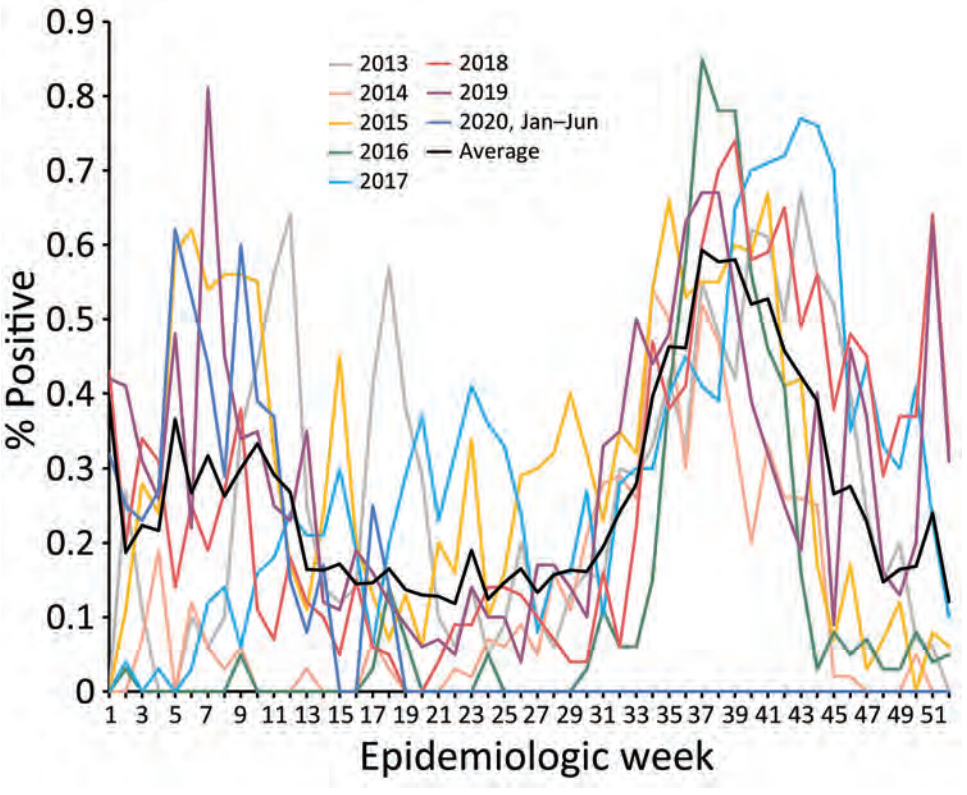

Figure 2. Prepandemic average epidemic curves used to demonstrate shifting patterns of influenza circulation during the COVID-19 pandemic, Senegal. Graphs show annual and overall average percentage of influenza-positive reverse transcription PCR tests per epidemiology week reported by the sentinelle syndromique du Sénégal (sentinel syndromic surveillance of Senegal), also known as the 4S Network, during January 2013–January 2020.

Local Influenza Epidemiology before COVID-19 Pandemic

We found that, before the pandemic, Senegal had continuous circulation of influenza throughout the year and had 2 distinct seasonal peaks. The first peak typically occurred at the beginning of the year during epidemiologic week 5 (range week 1–13). The first peak typically ended around mid-April and had an average duration of 14 (95% CI 12–17) weeks and an average test-positive intensity peak of 34% (95% CI 10%–57%) of samples (Figure 2).

The second peak typically occurred during the second half of the rainy season, around August during epidemiologic week 31 (range week 27–36). That peak usually lasted until the end of November and had an average duration of 18 (95% CI 13–25) weeks and an average test-positive intensity peak of 61% (95% CI 47%–78%) of samples (Figure 2).

Changes Observed in Seasonal Influenza during the COVID-19 Pandemic

We observed that SARS-CoV-2 essentially transformed the biannual profile of influenza's seasonal epidemic peaks in Senegal to a monophasic epidemic. During 2020, influenza circulation in Senegal seemed practically unperturbed. At the start of the year, influenza B (Victoria) virus peaked during January–March, after which a rainy season peak of influenza A(H3N2) and influenza B (Victoria) began during epidemiologic week 37, peaked at 73% of positive tests, and lasted for 11.5 weeks. SARS-CoV-2 started circulating in Senegal at the beginning of March 2020; the first case in Senegal was detected on March 2. However, systematic testing for SARS-CoV-2 was not added to the 4S Network until the beginning of June, which explains the low levels of SARS-CoV-2 detection during March–May 2020 (Figure 3). However, influenza surveillance continued during that period and revealed unusually low levels of influenza (Figures 4, 5).

During 2021, the expected beginning of the year influenza peak was completely absent. That period was marked by high levels of SARS-CoV-2 Alpha variant, after which an unmodified rainy season peak of 2009 pandemic influenza A(H1N1) started during epidemiologic week 37, peaked at 80% test-positivity, and lasted 10 weeks (Figures 4, 5).

The beginning of 2022 also was marked by the absence of the expected January–March influenza peak. That period also showed high levels of circulating SARS-CoV-2, but the Omicron variant dominated. Finally, an unexpected epidemic peak of influenza A(H3N2) was observed completely out of the usual period, starting in May during epidemiologic week 17 when influenza activity is usually the lowest in

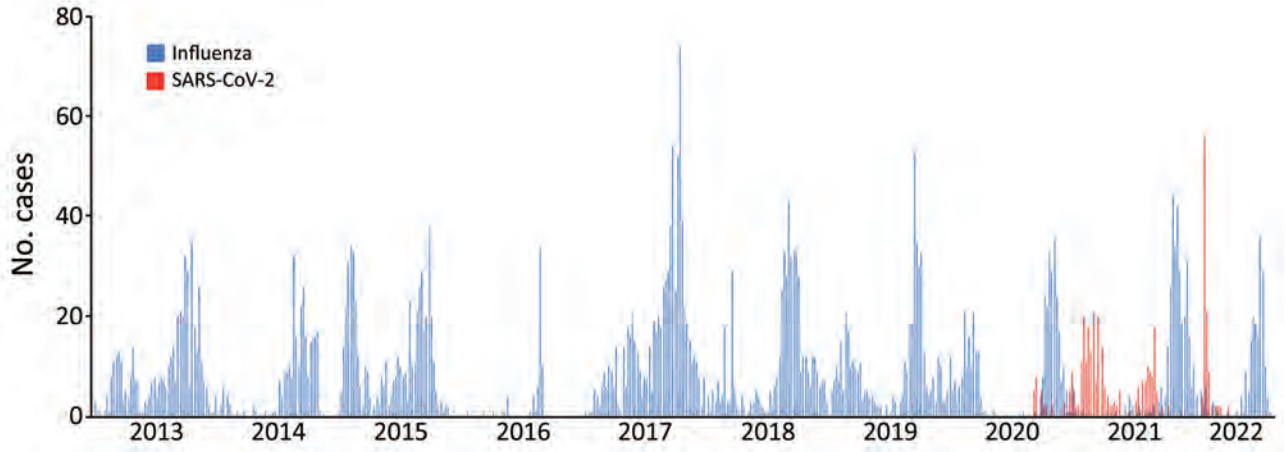

Figure 3. Average number of cases detected in a study of shifting patterns of influenza circulation during the COVID-19 pandemic, Senegal. Bars indicate number of reverse transcription PCR–positive tests for influenza and SARS-CoV-2 per epidemiology week reported by the sentinelle syndromique du Sénégal (sentinel syndromic surveillance of Senegal), also known as the 4S Network, during January 2013–July.

Senegal, and ending in July, during epidemiologic week 29, with a maximum peak of 71% test positivity (Figures 4, 5). Of note, influenza B (Yamagata) has practically disappeared in Senegal since June 2020; the last 2 cases were detected in January 2021.

Discussion

Before the COVID-19 pandemic, the dynamics of influenza in Senegal mostly followed the various patterns seen in tropical regions, showing year-round low-level circulation and increased activity during the rainy seasons (*1*,*2*). Senegal also had a typical smaller influenza peak at the start of the year (Figure 5, panel A).

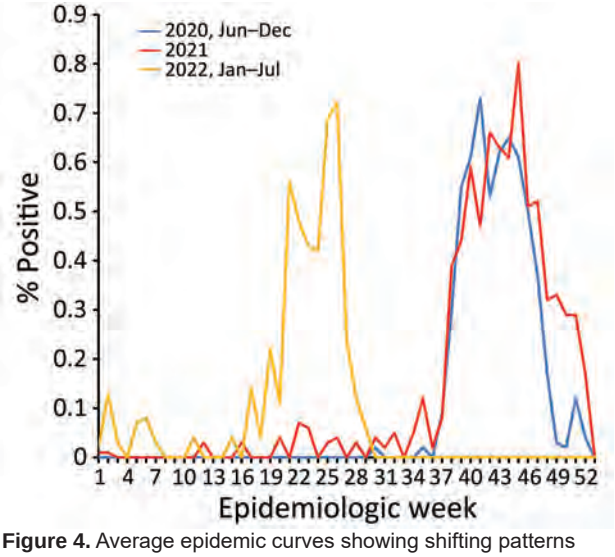

Figure 4. Average epidemic curves showing shifting patterns of influenza circulation during the COVID-19 pandemic, Senegal. Graphs show percentage of influenza-positive reverse transcription PCR tests per epidemiologic week reported by the sentinelle syndromique du Sénégal (sentinel syndromic surveillance of Senegal), also known as the 4S Network, during January 2020–December 2022.

Influenza's seasonal patterns and variability across different climate zones is still only partially understood (*23*). Among other factors, dry and cold weather conditions appear to promote influenza circulation in temperate regions (*23*–*25*), which is supported by in vitro and in vivo models (*24*). However, weather conditions do not account for observations made in tropical areas where circulation often peaks around months with the highest temperature and humidity levels (*25*–*27*).

Many other seasonally dependent factors influence influenza's circulation: fluctuations in host competence and immune response; changes in population behavior, such as school attendance; and the amount of time spent indoors (*23*). In Senegal, the rainy season is a period when most of the population is frequently forced to stay at home because of violent rainfall that disrupts normal traffic and human mobility patterns. The increase in indoor human contact and the return to school of a predominantly young population during the same season certainly contribute to the observed rainy season peak in Senegal and possibly in other countries (*26*).

Increased indoor contact does not account for the peak seen at the start of the year, which is the middle of Senegal's dry season. However, school schedules and international travel might be implicated in the peak. Children returning to school increase influenza circulation. In addition, many persons travel to Europe, which usually experiences its annual influenza season at that time. Travel between Senegal and northern Europe peaks during the end of the year,

when persons from Senegal return from visiting their families in Europe during the winter holidays and tourists from Europe who favor the dry season travel to Senegal to visit. The role of international travel on the January–March influenza peak is also suggested by the absence of influenza at the beginning of 2016, which corresponded to the period of the Ebola epidemic in West Africa that resulted in travel restrictions (Figure 3). Among the NPIs used during the COVID-19 pandemic, travel restrictions might have had a role in reshaping the biannual seasonality of influenza in Senegal into a more monophasic epidemic.

However, Senegal did not have a biannual influenza epidemic profile until after the implantation of the pandemic H1N1 2009 strain in the territory in 2010 (*27*). That observation suggests that climate, host immunity, and behavior might not be the only contributing factors to the seasonality of influenza circulation and that emergence of new competitive viral strains can also have a prolonged effect on periodic influenza circulation patterns.

Changes Observed during COVID-19 Pandemic

During 2020–2021, countries in the Southern Hemisphere that have temperate climates, such as Australia and South Africa, reported close to zero influenza circulation, and influenza remained mostly absent until 2021 (*28*). In the Northern Hemisphere, the

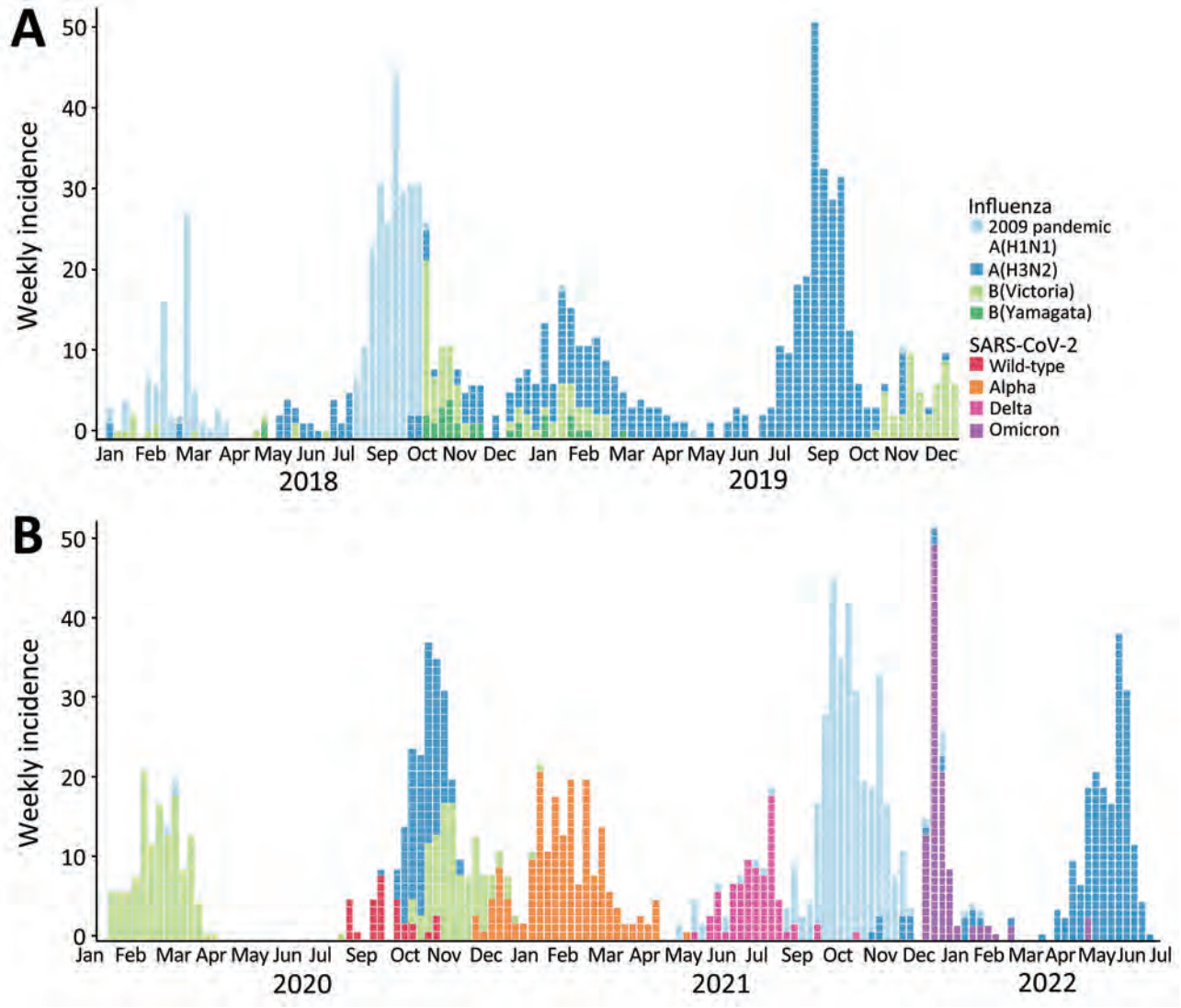

Figure 5. Number of reverse transcription PCR (RT-PCR)–positive samples per week in a study of shifting patterns of influenza circulation during the COVID-19 pandemic, Senegal. Data represent RT-PCR–positive tests per epidemiologic week reported by the sentinelle syndromique du Sénégal (sentinel syndromic surveillance of Senegal), also known as the 4S Network, including influenza subtypes and SARS-CoV-2 variants. A) Weekly influenza incidence during the prepandemic period, January 2018–2019. B) Weekly influenza and SARS-CoV-2 incidence during the pandemic period, January 2020–July 2022.

influenza seasonal peak of the 2020–21 winter was also absent (*29*,*30*). Those periods showed high levels of SARS-CoV-2 circulation during the second pandemic wave of the Alpha variant and subsequent reinforcement of NPIs (*31*).

In Senegal, at the end of March 2020, face masks became mandatory in public places, public gatherings were forbidden, international flights were closed, and a curfew was put in place (*32*). Those measures were gradually alleviated at the end of July 2020, when curfew hours were lightened and international flights were reopened, but Senegal maintained a high level of border control. A noticeable reduction of population mobility was recorded during March 2020–March 2021 (*33*).

The arrival of SARS-CoV-2 in Senegal had noticeable effects on local influenza circulation. Unlike reports from temperate regions, only the expected January–March influenza peak was affected in Senegal, but the main rainy season peaks stayed unperturbed in their timing and intensity (Figure 5, panel B). That finding could be partially explained by concurrent reinforcement or alleviation of NPIs. However, influenza activity in Senegal did not seem well correlated with local NPI reinforcement. Senegal noticeably alleviated its contact restriction measures around March 2021 (*34*), as illustrated by the noticeable drop in its estimated COVID-19 Stringency Index (*35*) and the concomitant rise in the population's mobility, as estimated by Google's COVID-19 Community Mobility Reports (*33*). That timeline does not account for influenza's recorded activity during the study period.

The abnormally low levels of influenza in the early months of 2021 and 2022 might be explained by the link between the expected start of the year peak and the winter peak usually seen in the Northern Hemisphere. That start of the year peak would be more dependent on international travel, as described, which might explain the unbalanced effect of the COVID-19 pandemic on influenza circulation in Senegal.

Deciphering the underlying causes of those shifts is challenging because the pandemic affected every level of the human ecosystem. The role of social distancing and other NPIs is undeniable because it necessarily affects the number of potentially contaminating social encounters. However, as those measures were gradually alleviated, influenza and SARS-CoV-2 continued to circulate alternately. The observed reciprocal nature of influenza and SARS-CoV-2 circulation, which is easier to visualize in Senegal's tropical setting, calls into question the prevailing role of NPIs and travel restrictions and invites us to search for other contributors.

Negative viral interference or viral competition—that is, the transient inhibitory effects that a virus can have on secondary infection by other viruses at the host level, essentially through sustained interferon pathway activation—s an old concept that has been studied and confirmed by in vitro and animal models (*36*,*37*) and has been supported by epidemiologic observations and statistical modeling (*36*,*38*,*39*). Although the concept is still controversial, some argue that rhinoviruses might have participated in the dissipation of first the wave of the 2009 pandemic influenza A(H1N1), for instance (*40*). Viral interference between SARS-CoV-2 and influenza has also been studied experimentally (*41*,*42*) and is supported by epidemiologic data (*43*,*44*). The implication of negative viral interference on influenza circulation is further supported by the very low levels of co-detection noticed at the patient level, only 1 case of co-detection out of 2,538 tests performed during our study period. Cases of SARS-CoV-2 and influenza co-infections have been reported in the literature but seem to be rare (<1%) (*43*).

The surveillance network used in this study has certain advantages, such as wide geographic coverage and use of community and hospital settings. However, the 4S Network exclusively provides information on symptomatic patients because of its focus on syndromic surveillance; thus, the network omits some local influenza and SARS-CoV-2 epidemiologic features. Also, locations of sentinel sites might have underrepresented populations from remote areas, especially in the northeastern and southeastern parts of Senegal, the most underpopulated areas of the country.

Because the network provides close to real time information, we were able to integrate recent data and cover more post–COVID-19 influenza seasons. Thus, we could offer a broader view of the effects of SARS-CoV-2 on influenza circulation in Senegal, which has public health implications that seem to be ongoing (*5*).

During March–June 2020, which corresponds to the first SARS-CoV-2 pandemic wave in Senegal, the activity of the surveillance system was drastically decreased. At that time, COVID-19 tests were not available, and local healthcare providers from sentinel sites were asked by the ministry of health to train colleagues in neighboring districts to perform nasopharyngeal sampling and conduct local case investigations. Nevertheless, routine influenza surveillance was not completely abandoned during that period, and approximately one third of the usual number of samples were sent for influenza

testing. Therefore, the absence of influenza notifications during the first SARS-CoV-2 wave was not only because of a lack of testing but also because of low levels of concurrent influenza circulation, consistent with what was seen later.

Data regarding influenza and SARS-CoV-2 circulation in tropical regions are scarce. In addition, our data are limited to a small geographic area and timeframe, just 2 years of co-circulation. Distinguishing crucial and durable changes in influenza's circulation patterns requires a broader scope. Therefore, data from other tropical countries and over longer periods of time are needed to clarify the effects of the COVID-19 pandemic on influenza circulation patterns in tropical regions.

Many questions on how influenza's seasonality will be affected in the long term remain. Influenza seasonality is probably intimately linked to SARS-CoV-2 and its potential for becoming a seasonal virus. In addition, SARS-CoV-2 could interfere with influenza circulation through broad population behavioral responses and host level immunologic and virologic determinants.

In conclusion, although NPIs and travel restrictions most certainly were predominant factors in the disruption of influenza circulation in 2020 and early 2021, those now seem insufficient to account for the more recent observations made in Senegal and other countries. Thus, the role of viral interference in reshaping influenza seasonality should be considered and included in future virologic and epidemiologic studies.

Acknowledgments

We thank Arnaud Fontanet for his careful revision of the present paper and his constructive remarks. We thank the rest of the staff of the Epidemiology, Clinical Research and Data Science Department and the Department of Virology of the Institut Pasteur de Dakar who contributed to sample and lab logistics. We also thank every healthcare provider from the sentinel sites that participated in the sampling and care of the patients included in this study.

The surveillance system from which the data was extracted has received financial support from the US Department of Human Health services. The funding body had no role in the design of the study, analysis, interpretation of data and in writing the manuscript. However, part of its funding was used to transport samples from study sites to the Institut Pasteur de Dakar.

A.L. designed the study, extracted and analyzed the data, and wrote the original draft. M.A.B. participated in the study design, data extraction and analysis, and revised the original draft. S.S. contributed to data curation and management and participated in data extraction. C.L. participated in the study design and supervised and contributed to the review and editing of the paper. M.A.B., C.T., M.D., B.T., M.K.D., C.L., B.D., N.D., Y.S., I.O.B., and A.A.S. all contributed to the management of the surveillance system and edited the paper.

About the Author

Dr. Lampros is an infectious disease specialist at the Hôpital Europeen Georges Pompidou in Paris, France. He is concurrently pursuing an epidemiology and public health master's degree through the Institut Pasteur Network where he worked at the Institut Pasteur de Dakar. His research interests include COVID-19 co-infections, notably fungal superinfections, and more broad pathogen interactions.

References

1. Moura FE. Influenza in the tropics. Curr Opin Infect Dis. 2010;23:415–20. https://doi.org/10.1097/QCO.0b013e32833cc955
2. Leo YS, Lye DC, Chow A. Influenza in the tropics. Lancet Infect Dis. 2009;9:457–8. https://doi.org/10.1016/S1473-3099(09)70182-3
3. Hirve S, Newman LP, Paget J, Azziz-Baumgartner E, Fitzner J, Bhat N, et al. Influenza seasonality in the tropics and subtropics—when to vaccinate? PLoS One. 2016;11:e0153003. https://doi.org/10.1371/journal.pone.0153003
4. Lowen AC, Mubareka S, Steel J, Palese P. Influenza virus transmission is dependent on relative humidity and temperature. PLoS Pathog. 2007;3:1470–6. https://doi.org/10.1371/journal.ppat.0030151
5. Lee SS, Viboud C, Petersen E. Understanding the rebound of influenza in the post COVID-19 pandemic period holds important clues for epidemiology and control. Int J Infect Dis. 2022;122:1002–4. https://doi.org/10.1016/j.ijid.2022.08.002
6. Yazdanbakhsh M, Kremsner PG. Influenza in Africa. PLoS Med. 2009;6:e1000182. https://doi.org/10.1371/journal.pmed.1000182
7. Steffen C, Debellut F, Gessner BD, Kasolo FC, Yahaya AA, Ayebazibwe N, et al. Improving influenza surveillance in sub-Saharan Africa. Bull World Health Organ. 2012;90:301–5. https://doi.org/10.2471/BLT.11.098244
8. Jones N. How COVID-19 is changing the cold and flu season. Nature. 2020;588:388–90. https://doi.org/10.1038/d41586-020-03519-3
9. Kim J, Gómez Gómez RE, Hong K, Yum S, Jang J, Chun BC. Changing influenza activity in the Southern hemisphere countries during the COVID-19 pandemic. Int J Infect Dis. 2021;108:109–11. https://doi.org/10.1016/j.ijid.2021.05.039
10. Huang QS, Wood T, Jelley L, Jennings T, Jefferies S, Daniells K, et al.; NPIsImpactOnFlu Consortium. Impact of the COVID-19 nonpharmaceutical interventions on influenza and other respiratory viral infections in New Zealand. Nat Commun. 2021;12:1001. https://doi.org/10.1038/s41467-021-21157-9
11. Feng L, Zhang T, Wang Q, Xie Y, Peng Z, Zheng J, et al. Impact of COVID-19 outbreaks and interventions on

influenza in China and the United States. Nat Commun. 2021;12:3249. https://doi.org/10.1038/s41467-021-23440-1
12. Sakamoto H, Ishikane M, Ueda P. Seasonal influenza activity during the SARS-CoV-2 outbreak in Japan. JAMA. 2020;323:1969–71. https://doi.org/10.1001/jama.2020.6173
13. Fricke LM, Glöckner S, Dreier M, Lange B. Impact of non-pharmaceutical interventions targeted at COVID-19 pandemic on influenza burden—a systematic review. J Infect. 2021;82:1–35. https://doi.org/10.1016/j.jinf.2020.11.039
14. Qi Y, Shaman J, Pei S. Quantifying the impact of COVID-19 nonpharmaceutical interventions on influenza transmission in the United States. J Infect Dis. 2021;224:1500–8. https://doi.org/10.1093/infdis/jiab485
15. Niang MN, Dosseh A, Ndiaye K, Sagna M, Gregory V, Goudiaby D, et al. Sentinel surveillance for influenza in Senegal, 1996-2009. J Infect Dis. 2012;206:S129–35. https://doi.org/10.1093/infdis/jis576
16. Barry MA, Arinal F, Talla C, Hedible BG, Sarr FD, Ba IO, et al. Performance of case definitions and clinical predictors for influenza surveillance among patients followed in a rural cohort in Senegal. BMC Infect Dis. 2021;21:31. https://doi.org/10.1186/s12879-020-05724-x
17. Fitzner J, Qasmieh S, Mounts AW, Alexander B, Besselaar T, Briand S, et al. Revision of clinical case definitions: influenza-like illness and severe acute respiratory infection. Bull World Health Organ. 2018;96:122–8. https://doi.org/10.2471/BLT.17.194514
18. Kim H-K, Oh S-H, Yun KA, Sung H, Kim M-N. Comparison of Anyplex II RV16 with the xTAG respiratory viral panel and Seeplex RV15 for detection of respiratory viruses. J Clin Microbiol. 2013;51:1137–41. https://doi.org/10.1128/JCM.02958-12
19. Wright KE, Wilson GA, Novosad D, Dimock C, Tan D, Weber JM. Typing and subtyping of influenza viruses in clinical samples by PCR. J Clin Microbiol. 1995;33:1180–4. https://doi.org/10.1128/jcm.33.5.1180-1184.1995
20. World Health Organization. End-to-end integration of SARS-CoV-2 and influenza sentinel surveillance, revised interim guidance [cited 2023 Apr 14]. https://apps.who.int/iris/bitstream/handle/10665/351409/WHO-2019-nCoV-Integrated-sentinel-surveillance-2022.1-eng.pdf
21. Vega T, Lozano JE, Meerhoff T, Snacken R, Mott J, Ortiz de Lejarazu R, et al. Influenza surveillance in Europe: establishing epidemic thresholds by the moving epidemic method. Influenza Other Respir Viruses. 2013;7:546–58. https://doi.org/10.1111/j.1750-2659.2012.00422.x
22. Vega T, Lozano JE, Meerhoff T, Snacken R, Beauté J, Jorgensen P, et al. Influenza surveillance in Europe: comparing intensity levels calculated using the moving epidemic method. Influenza Other Respir Viruses. 2015;9:234–46. https://doi.org/10.1111/irv.12330
23. Tamerius J, Nelson MI, Zhou SZ, Viboud C, Miller MA, Alonso WJ. Global influenza seasonality: reconciling patterns across temperate and tropical regions. Environ Health Perspect. 2011;119:439–45. https://doi.org/10.1289/ehp.1002383
24. Lowen AC, Steel J. Roles of humidity and temperature in shaping influenza seasonality. J Virol. 2014;88:7692–5. https://doi.org/10.1128/JVI.03544-13
25. Paynter S. Humidity and respiratory virus transmission in tropical and temperate settings. Epidemiol Infect. 2015;143:1110–8. https://doi.org/10.1017/S0950268814002702
26. Tamerius JD, Shaman J, Alonso WJ, Bloom-Feshbach K, Uejio CK, Comrie A, et al. Environmental predictors of seasonal influenza epidemics across temperate and tropical climates. PLoS Pathog. 2013;9:e1003194. https://doi.org/10.1371/journal.ppat.1003194
27. Ndongo D, Ousmane MD, Mbayame NN. Influenza seasonality affected by the 2009 pandemic episode in Senegal. Afr J Microbiol Res. 2014;8:217–21. https://doi.org/10.5897/AJMR2013.6228
28. Olsen SJ, Azziz-Baumgartner E, Budd AP, Brammer L, Sullivan S, Pineda RF, et al. Decreased influenza activity during the COVID-19 pandemic—United States, Australia, Chile, and South Africa, 2020. MMWR Morb Mortal Wkly Rep. 2020;69:1305–9. https://doi.org/10.15585/mmwr.mm6937a6
29. Solomon DA, Sherman AC, Kanjilal S. Influenza in the COVID-19 Era. JAMA. 2020;324:1342–3. https://doi.org/10.1001/jama.2020.14661
30. Olsen SJ, Winn AK, Budd AP, Prill MM, Steel J, Midgley CM, et al. Changes in influenza and other respiratory virus activity during the COVID-19 pandemic—United States, 2020–2021. MMWR Morb Mortal Wkly Rep. 2021;70:1013–9. https://doi.org/10.15585/mmwr.mm7029a1
31. World Health Organization. WHO coronavirus (COVID-19) dashboard [cited 2023 Aug 3]. https://covid19.who.int
32. Republic of Senegal. Declaration of a state of emergency in the context of the fight against coronavirus disease COVID-19 [cited 2023 Aug 3]. https://sante.gouv.sn/sites/default/files/Discours%20Pr%C3%A9sident%20de%20la%20R%C3%A9publique%20%20%C3%A9tat%20d%27urgence%20COVID-19.pdf
33. Google. COVID-19 community mobility reports, Senegal [cited 2023 Apr 13]. https://www.gstatic.com/covid19/mobility/2022-10-15_SN_Mobility_Report_en.pdf
34. Republic of Senegal. Press release from the Council of Ministers of March 10, 2021 [cited 2023 Aug 3]. https://www.presidence.sn/actualites/communique-du-conseil-des-ministres-du-10-mars-2021_2204
35. Our World in Data. COVID-19: Stringency index, Senegal [cited 2023 Apr 13]. https://ourworldindata.org/covid-stringency-index
36. Piret J, Boivin G. Viral interference between respiratory viruses. Emerg Infect Dis. 2022;28:273–81. https://doi.org/10.3201/eid2802.211727
37. Chan KF, Carolan LA, Korenkov D, Druce J, McCaw J, Reading PC, et al. Investigating viral interference between influenza A virus and human respiratory syncytial virus in a ferret model of infection. J Infect Dis. 2018;218:406–17. https://doi.org/10.1093/infdis/jiy184
38. Opatowski L, Baguelin M, Eggo RM. Influenza interaction with cocirculating pathogens and its impact on surveillance, pathogenesis, and epidemic profile: A key role for mathematical modelling. PLoS Pathog. 2018;14:e1006770. https://doi.org/10.1371/journal.ppat.1006770
39. Nickbakhsh S, Mair C, Matthews L, Reeve R, Johnson PCD, Thorburn F, et al. Virus-virus interactions impact the population dynamics of influenza and the common cold. Proc Natl Acad Sci U S A. 2019;116:27142–50. https://doi.org/10.1073/pnas.1911083116
40. Wu A, Mihaylova VT, Landry ML, Foxman EF. Interference between rhinovirus and influenza A virus: a clinical data analysis and experimental infection study. Lancet Microbe. 2020;1:e254–62. https://doi.org/10.1016/S2666-5247(20)30114-2
41. Sa Ribero M, Jouvenet N, Dreux M, Nisole S. Interplay between SARS-CoV-2 and the type I interferon response. PLoS Pathog. 2020;16:e1008737. https://doi.org/10.1371/journal.ppat.1008737

42. Essaidi-Laziosi M, Alvarez C, Puhach O, Sattonnet-Roche P, Torriani G, Tapparel C, et al. Sequential infections with rhinovirus and influenza modulate the replicative capacity of SARS-CoV-2 in the upper respiratory tract. Emerg Microbes Infect. 2022;11:412–23. https://doi.org/10.1080/22221751.2021.2021806
43. Nowak MD, Sordillo EM, Gitman MR, Paniz Mondolfi AE. Coinfection in SARS-CoV-2 infected patients: Where are influenza virus and rhinovirus/enterovirus? J Med Virol. 2020;92:1699–700. https://doi.org/10.1002/jmv.25953
44. Stowe J, Tessier E, Zhao H, Guy R, Muller-Pebody B, Zambon M, et al. Interactions between SARS-CoV-2 and influenza, and the impact of coinfection on disease severity: a test-negative design. Int J Epidemiol. 2021;50:1124–33. https://doi.org/10.1093/ije/dyab081

Address for Correspondence: Alexandre Lampros and Mamadou Aliou Barry, Institut Pasteur de Dakar, Pôle d'Épidémiologie, de Recherche Clinique et de Science des Données, 36 Avenue Pasteur, Dakar 12900, Sénégal; email: alexandre.lampros@aphp.fr

Molecular Characterization of Circulating Yellow Fever Viruses from Outbreak in Ghana, 2021–2022

Joseph Humphrey Kofi Bonney, Terrel Sanders, Deborah Pratt, Bright Agbodzi, Dennis Laryea, Nana Kwame Fredua Agyeman, Selassie Kumordjie, Keren Attiku, Patience Lartekai Adams, Gideon Aning Boateng, Sally-Ann Ohene, Christopher Tamal, Gifty Mawuli, Clara Yeboah, Samuel Dadzie, Chrysantus Kubio, Franklin Asiedu-Bekoe, John Kofi Odoom

Yellow fever virus, transmitted by infected *Aedes* spp. mosquitoes, causes an acute viral hemorrhagic disease. During October 2021–February 2022, a yellow fever outbreak in some communities in Ghana resulted in 70 confirmed cases with 35 deaths (case-fatality rate 50%). The outbreak started in a predominantly unvaccinated nomadic community in the Savannah region, from which 65% of the cases came. The molecular amplification methods we used for diagnosis produced full-length DNA sequences from 3 confirmed cases. Phylogenetic analysis characterized the 3 sequences within West Africa genotype II; strains shared a close homology with sequences from Cote d'Ivoire and Senegal. We deployed more sensitive advanced molecular diagnostic techniques, which enabled earlier detection, helped control spread, and improved case management. We urge increased efforts from health authorities to vaccinate vulnerable groups in difficult-to-access areas and to educate the population about potential risks for yellow fever infections.

Yellow fever virus (YFV), transmitted by infected *Aedes* spp. mosquitoes, causes a viral hemorrhagic disease, typically acute, with case-fatality rates up to 50%. The disease remains a major public health problem, especially in West Africa, where outbreaks occur every year. In Ghana, yellow fever outbreaks have been observed in 5-year cycles over the past 20 years. However, increased recorded incidence and death during these outbreaks can be partially attributed to improved diagnostic efforts from laboratory investigations.

Initial influenza-like signs and symptoms from yellow fever typically improve within 5 days; however, 15%–25% of infected persons progress to complications, including liver damage, which increases risk for bleeding and kidney problems (*1*). YFV (strain Asibi), a mosquito-borne flavivirus, was first isolated in 1927 from a patient in Ghana (*2*). Despite having an effective vaccine, 17D strain, with >500 million doses administered to humans (*3*), YFV infection remains a public health threat in certain regions of the world (*1*); ≈1 billion persons are estimated to live in regions endemic for yellow fever. In 2013 alone, YFV caused ≈127,000 severe infections and 45,000 deaths globally (*1*); ≈90% of deaths occur in Africa (*4*).

Yellow fever has been endemic in Ghana since it was first documented (*5*). Major outbreaks have occurred, notably in the 1970s and 1980s (*6*). One recent outbreak, which occurred in the West Gonja district in the Savannah region of Ghana in 2015, resulted in 3 deaths from 12 confirmed cases (*7*). Additional sporadic cases have been rumored or confirmed since the 2015 outbreak.

Little is known about the genetic diversity and evolutionary dynamics of YFV, mainly because few genomic sequences from wild virus isolates have been identified. For this outbreak investigation, we aimed to use molecular assays to rapidly detect and confirm or disprove presence of YFV among case-patients. We also sought to characterize virus strains

Author affiliations: Noguchi Memorial Institute for Medical Research Virology Department, Legon Accra, Ghana (J.H.K. Bonney, D. Pratt, K. Attiku, P.L. Adams, G.A. Boateng, G. Mawuli, J.K. Odoom); US Naval Medical Research Unit, No. 3, Ghana Detachment, Accra, Ghana (T. Sanders, B. Agbodzi, S. Kumordjie, C. Yeboah); Ghana Health Service Public Health Unit, Accra (D. Laryea, N.K.F. Agyeman, F. Asiedu-Bekoe); World Health Organization Ghana Country Office, Accra (S.-A. Ohene, C. Tamal); Noguchi Memorial Institute for Medical Research Department of Parasitology, Legon Accra (S. Dadzie); Ghana Health Service–Savannah Regional Health Directorate, Damongo, Ghana (C. Kubio)

DOI: https://doi.org/10.3201/eid2909.221671

in clinical specimens from YFV-positive case-patients from the most affected communities to discover the molecular epidemiology of the outbreak within the identified regions. The institutional review board of the Noguchi Memorial Institute for Medical Research (NMIMR) approved experimental protocols for molecular detection of viral hemorrhagic fevers (VHFs), including YFV (NMIMR-IRB-003/07-08).

The Ghana Health Service determined this epidemiologic surveillance and outbreak response as a research activity not involving human subjects and thus exempt from further ethics consideration. The Naval Medical Research Center Institutional Review Board Office of Research Administration (NAMRU3-PJT-22-01) also determined this activity as non-human subjects research.

Materials and Methods

Setting and Study Design

Elevated yellow fever incidence during October 2021–February 2022 led to an outbreak being declared in Ghana. We collected clinical specimens of serum from patients in health facilities in the outbreak areas, predominantly Damongo, Busunu, and Kawankura communities in West Gonja district and Daboya and Kagbal communities in North Gonja district, which constitute 2/6 districts of the Savannah region in Ghana (Figure 1). We collected additional specimens from health facilities in adjoining districts and regions, including Sawla-Tuna-Kalba district and Bono East region. We submitted 188 clinical specimens from patients with suspected YFV to NMIMR for molecular diagnosis. Nucleic acid amplification testing of the specimens confirmed 70 yellow fever cases from communities in 4 regions (Savannah, Upper West, Bono, and Oti) in northern Ghana. Because of 35 recorded deaths and a case-fatality ratio of 50%, public health interventions were swiftly initiated among the nomadic populations most affected. Those populations live in forested areas, including in the immediate vicinity of a forest reserve in the Savannah region. We placed all patients with suspected yellow fever based on case definitions in isolation or holding rooms and used requisite infection prevention and control precautions to manage cases. Public health and laboratory staff using appropriate personal protective equipment collected clinical specimens and recorded demographic and health history information, including age, sex, travel history, vaccination status, date of hospital admission, and residential location. We sent the 188 clinical specimens taken during the outbreak period to laboratories for further investigation, including characterizing virus strains. Age range of case-patients was 4 months to 70 years; most exhibited signs/symptoms such as body pain, fever, abdominal pain, vomiting, jaundice, and bleeding from the gums. Slightly more case-patients were male (54%) than female (46%).

Background Observations

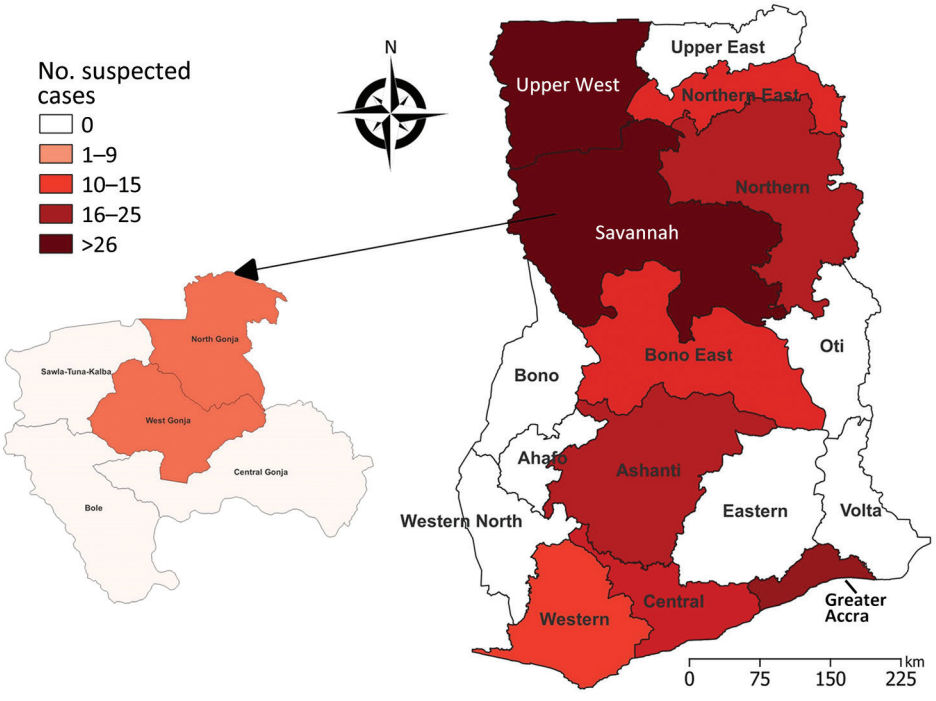

Figure 1. Distribution of suspected yellow fever cases among the 16 regions of Ghana, January 2021–February 2022. Callout map at left shows the high-incidence Savannah region containing 2 districts, North and West Gonja, that had the highest numbers of cases among the 6 districts in the region. Map created using QGIS version 3.26.1-Buenos Aires (https://qgis.org); Ghana boundary coordinates obtained from the Ghana Statistical Service.

An activity for passive surveillance of VHFs, established in 2016 in response to the 2014–2016 Ebola virus disease outbreak in some West Africa countries, provided routine reports on suspected yellow fever cases submitted from health facilities (*8*). From that surveillance activity, 12 suspected cases were reported, and the patients were screened. All 12 reports were submitted during February–September 2021, before the YFV outbreak began, and patients tested negative for all VHFs on the panel of viruses (Table 1): Ebola, Marburg, Lassa, dengue, chikungunya, and yellow fever (Figure 2).

Real-Time Reverse Transcription PCR Assays

We extracted viral nucleic acid from 140 μL of serum using the QIAamp viral RNA kit (QIAGEN, https://www.qiagen.com). We performed all PCR assays in 25 μL of Master Mix with 2.5 μL or 5 μL nucleic acid extract as a template (Table 1). We used real-time reverse transcription PCR (rRT-PCR) for Lassa virus (*9*), YFV (*10*), and filoviruses including Ebola and Marburg viruses (*10*,*11*) and a Trioplex rRT-PCR (*12*) for qualitative detection and differentiation of dengue, chikungunya, and Zika virus RNA in the clinical specimens taken from the suspected case-patients. We performed amplifications using the Applied Biosystems 7500 Fast/Standard Dx Real-Time PCR instrument (ThermoFisher Scientific, https://www.thermofisher.com).

Trioplex rRT-PCR

The Trioplex assay, designed for research purposes only (*12*), was created to test simultaneously for the presence of dengue, chikungunya, and Zika viruses using primers and dual-labeled probes and a reverse transcription step to produce copy DNA (cDNA) from RNA in the sample. The probe binds to the target DNA between the 2 unlabeled PCR primers. During the PCR extension process, the polymerase extends the unlabeled primers using the template strand as a guide. The rRT-PCR instrumentation detects fluorescence; with each successive PCR cycle, fluorescence increases in proportion to the amount of target nucleic acid present. This assay identifies Zika, chikungunya, and dengue virus RNA during the acute phase of infection and up to 14 days after onset of signs/symptoms (*12*).

Whole Genome Sequencing

We prepared sequencing libraries using Illumina DNA prep with enrichment (Illumina, https://www.illumina.com), according to the manufacturer's instructions. We performed viral enrichment using custom target capture probes (Twist Bioscience, https://www.twistbioscience.com). We fragmented the extracted RNA, spiked it with mosquito RNA, and reverse-transcribed it to cDNA. We achieved dual indexing of cDNA libraries using IDT unique dual indexes (Integrated DNA Technologies, https://www.idtdna.com). We enriched libraries by using the 1-plex pooling strategy following a protocol described elsewhere (*13*). We sequenced barcoded pooled libraries on an Illumina MiSeq with version 3 reagent kits.

Sequence Analysis

We quality filtered demultiplexed raw fastq files to Phred scores ≥20, filtered them for minimum read length of 20 bp, and adaptor trimmed them

Table 1. Details of PCR testing and sequence analysis from study of yellow fever in Ghana, 2021–2022*

Virus	Reagent kit	Cycles	Primer sequences, 5′ → 3′	Target gene	Amplicon length, bp
Lassa virus	QIAGEN OneStep RT-PCR	45	36E2:ACCGGGGATCCTAGGCATTT LVS-339-rev:GTTCTTTGTGCAGGAMAGGGGCATKGTCAT	5′ UTR/GPC	320
YFV	QIAGEN/Ambion OneStep rRT-PCR	45	RF:AAATCCTGKGTGCTAATTGAGGTGYATTGG RR:ACATDWTCTGGTCARTTCTCTGCTAATCGC RProbe: gCAAATCgAgTTgCTAggCAATAAACACATT[BHQdT]g[THF]A[FAMdT] TAATTTTRATCgTTC -Ph		
Filovirus	QIAGEN Filo OneStep RT-PCR	45	FiloA2.2:AAGCCTTTCCTAGCAACATGATGGT FiloA2.3:AAGCATTCCCTAGCAACATGATGGT FiloA2.4:AAGCATTTCCTAGCAATATGATGGT FiloA2.4:AAGCATTTCCTAGCAATATGATGGT Filo B-Ra:GTGAGGAGGGCTATAAAAGTCACTGACATG	L	290
Trioplex (*12*)					
Dengue	Invitrogen Superscript III Platinum OneStep qRT-PCR	45	NA	C	171
CHIKV				E1	208
Zika				NS5	209

*QIAGEN, http://www.qiagen.com; Invitrogen, Thermo Fisher, https://www.thermofisher.com. CHIKV, chikungunya virus; RT-PCR, reverse transcription PCR; qRT-PCR, quantitative RT-PCR; YFV, yellow fever virus.

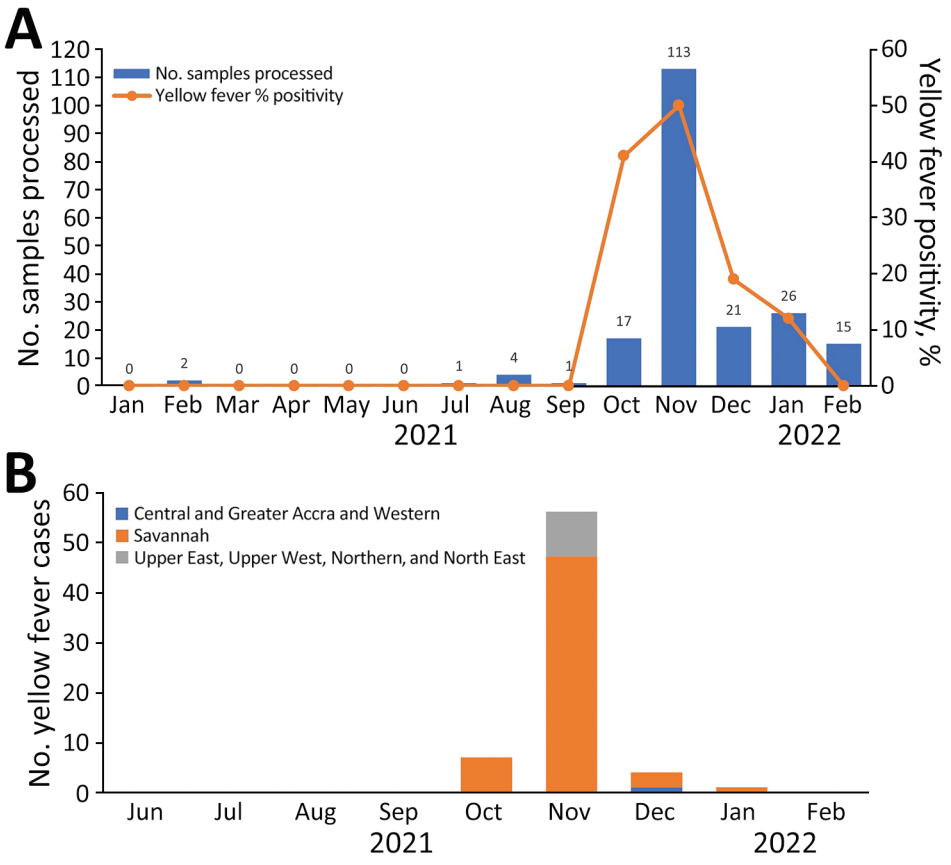

Figure 2. Distribution of yellow fever cases over time, Ghana, January 2021–February 2022. A) Percentage positivity over the outbreak period and total number of samples processed. B) Numbers of yellow fever–positive participants over the outbreak period within the 3 regional categories.

using BBDuk (decontamination using kmers; https://sourceforge.net/projects/bbmap). We confirmed read quality using FastQC tool (https://sourceforge.net/projects/fastqc.mirror). We used the resultant high-quality reads for de novo assembly using the SPAdes assembler version 3.15.2 (https://github.com/ablab/spades) (*14*). We used the largest contig from the de novo assembly to query the nonredundant nucleotide database (GenBank) to obtain the best matching reference sequence. We employed the retrieved reference for reference-based assembly using Bowtie2 (https://bowtie-bio.sourceforge.net/bowtie2/index.shtml) (*15*). To make a consensus call, we required ≥3 times read-depth coverage; we treated positions lacking this depth of coverage as missing (labeled N).

Phylogenetic Analysis

We submitted consensus sequences from the final assemblies to the Genome Detective virus tool (https://www.genomedetective.com) for genotyping. For phylogenetic analysis, we selected complete genomes covering the 4 major YFV genotypes in addition to our strains. We conducted genome alignment using MUSCLE (https://www.ebi.ac.uk/Tools/msa/muscle) and phylogenetic construction using MEGAX software (*16*,*17*). To correct for the effects of ambiguous alignments because of polymorphisms in the 5′ and 3′ untranslated regions, we trimmed the sequences to the open reading frames (ORFs) and conducted all subsequent phylogenetic analyses on the ORFs. We conducted maximum likelihood phylogenetic analysis on the sequences using the generalized time reversible plus gamma distribution substitution model, which was inferred as the best fit model for the data in MEGAX. We ascertained the robustness of each node of the phylogenetic tree using the bootstrap method with 1,000 replicates. We used FigTree version 1.4.4 (http://tree.bio.ed.ac.uk/software/figtree) for tree visualization and annotation.

Accession Numbers

We attempted to sequence all PCR-confirmed positive samples from the outbreak. However, only 3 positive samples yielded DNA sequencing data of sufficiently good quality to be sequenced on the Illumina next-generation sequencing platform. We deposited those sequences into GenBank (accession nos. OM066735–37).

Results

The outbreak lasted from mid-October 2021 through the first week of February 2022; a total of 188 clinical specimens of whole blood serum or plasma were submitted for testing within that period. We submitted one half-portion of each sample from suspected case-patients within the identified outbreak regions (Figure 1) to the virology department of NMIMR, a World Health Organization–recognized laboratory, for molecular confirmation of yellow fever (*18*). We sent the other half-portion to the National Public Health Reference Laboratory (NPHRL) in Accra, Ghana, for serologic testing for YFV IgM. After ruling out dengue, West Nile, and Zika viral infections by differential diagnosis (*18*), YFV-positive samples were forwarded to the WHO-designated regional reference laboratory in Dakar, Senegal.

We determined suspected yellow fever cases on the basis of location in high-incidence regions and signs/symptoms associated with YFV infection: muscle and joint pain, abdominal pain, difficulty swallowing, difficulty breathing, hiccups, loss of appetite, skin rash, anorexia, myalgia, dizziness, malaise, agitation, swollen buttocks, convulsion, chills, runny nose, chest pain, cough, and lethargy. Yellow fever was less common in the Central, Greater Accra, and Western regions than the Savannah region (odds ratio [OR] 0.08, 95% CI 0.01–0.63) (Table 2) and more common among persons who exhibited signs/symptoms (OR 2.03, 95% CI 1.11–3.71; p = 0.022) (Table 2) than those who did not. During the outbreak, we observed the highest number of confirmed cases in November 2021 (Figure 2).

Demographic and Virologic Findings

We performed Trioplex screening for qualitative detection and differentiation of dengue, chikungunya, and Zika viruses and RT-PCR testing for other VHFs existing in the regions, including Lassa, Ebola, and Marburg; all samples tested negative for those viruses. However, rRT-PCR testing confirmed yellow fever (Table 1) in 70/188 (37%) patients, 64% of whom were male (Table 3). Age range of all patients was 4–24 years; mean age was 7 years for YFV-negative and 11 years for YFV-positive patients (Table 3). Health facilities in 10/16 regions in Ghana, in the coastal (Central, Greater Accra, and Western), midlands (Ashanti and Bono East), and northern (Upper East, Upper West, Northern, and Northeast) areas of the country and in the Savannah region, submitted suspected cases for testing (Figure 1). The highest percentage of total (65%), positive (84%), and negative (57%) samples submitted came from the Savannah region (Table 3). Results from the Savannah region, in northwest Ghana, showed a statistically significant higher association with yellow fever relative to other regions, including >2 times as many cases as from other northern regions combined. Calculating percentages of the signs/symptoms of patients screened (Table 3) indicated fever, jaundice, and hemorrhage were the predominate clinical signs among both YFV-negative and -positive patients, although the absolute numbers were not statistically significant.

Table 2. Distributions of patient sex, region, and signs/symptoms in study of yellow fever in Ghana, 2021–2022

Characteristics	Odds ratio (95% CI)	p value
Sex		
M	Referent	0.079
F	0.58 (0.31–1.07)	
Region		
Savannah	Referent	0.024
Central, Greater Accra, Western	0.08 (0.01–0.63)	
Upper East, Upper West, Northern, North East	0.53 (0.23–1.23)	
Ashanti, Bono East		
Signs/symptoms		
Fever	1.68 (0.75–3.75)	0.207
Jaundice	0.6 (0.1–3.75)	0.584
Hemorrhage	3.17 (0.89–11.24)	0.074
Other*	2.03 (1.11–3.71)	0.022

*Muscle and joint pain, abdominal pain, difficulty swallowing, difficulty breathing, hiccups, loss of appetite, skin rash, anorexia, myalgia, dizziness, malaise, agitation, swollen buttocks, convulsions, chills, runny nose, chest pain, cough, and lethargy

Sequence Analysis and Phylogeny

The Genome Detective virus tool grouped all 3 Ghana yellow fever strains within West Africa genotype II. Complete ORF maximum-likelihood phylogeny showed the 3 yellow fever strains from the outbreak area in Ghana to be closely related to each other and to sequences from Senegal and Cote d'Ivoire (Figure 3). Those sequences all clustered within West Africa genotype II, which is less heterogeneous than the other 8 known West Africa genotypes (*19*).

Discussion

The October 2021–February 2022 yellow fever outbreak in parts of Ghana renewed calls and highlighted the need for timely laboratory confirmation of suspected yellow fever cases as an essential part of effective responses. The greater sensitivity of advanced molecular diagnostic techniques deployed for laboratory testing during outbreak investigations distinguished those methods from previous serologic assays. The improved performance of those diagnostic techniques enabled us to characterize the circulating outbreak strains and deposit yellow fever strains from Ghana with GenBank.

Initial outbreak cases were identified at the West Gonja District Hospital in the West Gonja municipality of the Savannah region. Three index case-patients from

Table 3. Demographics and signs/symptoms of patients in study of yellow fever in Ghana, 2021–2022

Variable	Yellow fever test results		p value
	Negative, n = 118	Positive, n = 70	
Sex			0.078
M	58 (50.4)	44 (63.8)	
F	57 (49.6)	25 (36.2)	
Median age, y (interquartile range)	7 (4–19)	11 (4–23.5)	0.172
Region			
Central, Greater Accra, Western	14 (12.2)	1 (1.4)	<0.001
Ashanti, Bono East	15 (13.0)	0	
Savannah	65 (56.5)	58 (84.1)	
Upper East, Upper West, Northern, North East	21 (18.3)	10 (14.5)	
Unknown	3	1	
Signs/symptoms			
Fever	62/88 (70.5)	44/55 (70.0)	0.205
Jaundice	3/47 (6.4)	2/51 (3.9)	0.58
Hemorrhage	4/118 (3.4)	7/70 (10.0)	0.062
Other†	39/118 (33.1)	35/70 (50.0)	0.021

*Values are no. (%) except as indicated.
†Muscle and joint pain, abdominal pain, difficulty swallowing, difficulty breathing, hiccups, loss of appetite, skin rash, anorexia, myalgia, dizziness, malaise, agitation, swollen buttocks, convulsions, chills, runny nose, chest pain, cough, and lethargy

adjoining localities spent an average of 3 days in the hospital and died before their clinical specimens could be tested and results released. In addition to necessary laboratory confirmation, final determination of yellow fever diagnosis must be made on a case-by-case basis, in the context of clinical manifestations, epidemiology, and vaccination history (*18*,*19*). Early identification and diagnosis, leading to prompt response, are essential for successfully controlling communicable disease outbreaks and ensuring global health security.

Implementing the Global Health Security agenda (*20*) developed by health and allied ministries in Ghana has enhanced capacity for outbreak response. Improving advanced laboratory testing capacity and establishing an advanced-level field epidemiology training program were among other core components contributing to quicker response time, reduced illness and death, and controlled risk of spread. Diagnostic specificity was ensured because the molecular methods deployed in our laboratory investigations minimized false-positive test results by targeting the specific molecule of interest. In addition, turnaround times are shorter for molecular diagnostic methods than for serologic testing, decreasing time from specimen receipt to test result reporting.

In disease-endemic areas, outbreaks provide historic patterns or trends to help guide health workers make preliminary diagnoses and begin case management before final diagnoses are laboratory confirmed. The yellow fever outbreak documented in our study began in the Savannah region of Ghana, which also recorded the highest numbers of confirmed cases (70) and 35 deaths (case-fatality rate 50%). In retrospect, analysis of 2011 and 2015–2016 surveillance data on confirmed yellow fever in the region indicated a 5-year cycle of occurrence (*21*). A 2011 outbreak of yellow fever began in November in the Northern region (since delineated into Savannah and Northern regions) and by February 2012 had spread to 10 additional regions and led to 7 deaths (*21*). In comparison, the 2021–2022 outbreak recorded the worst death counts and rates over the intervening period. That greater severity might be because initial cases occurred among Fulani, pastoral nomads who move about in remote settlements and have substantial populations of unvaccinated youth (*22*).

In accordance with the standard algorithm for viral detection and means of differential diagnosis, we used RT-PCRs developed for VHF-associated viruses (*10*,*11*) and multiplex assays (*12*). All 188 clinical specimens of serum or plasma received from the health facilities during the outbreak, in addition to the 12 received before the onset of the outbreak, were screened and tested negative for Lassa fever, Ebola, Marburg, dengue, chikungunya, and Zika viral infections. Those findings are consistent with a previous study in which we established that overall VHF incidence is low in Ghana and contributes little to hospital-identified morbidity (*23*). However, although yellow fever is classified as a VHF, low incidence does not extend to that disease, which is known to be endemic in Ghana.

Using an RT-PCR assay developed to detect YFV RNA, we confirmed that 70/188 suspected case-samples submitted to NMIMR during the 2021–2022 outbreak were positive for yellow fever (*10*). More than half (102/188, 64%) of the samples received during the outbreak were from male patients. Combined with the median age of 11 years (Table 2), that finding suggests that the outbreak affected younger and working-aged men and boys engaged in nomadic pastoral lifestyles more than other demographic groups. This observation corroborates findings made in farming communities in other parts of Africa under similar outbreak conditions

(*24*). Because persons seeking healthcare, especially during outbreak conditions, tend to be more severely affected, the actual number of persons with yellow fever was likely higher than the number for whom we submitted samples to NMIMR for testing; persons with cases of subclinical or mildly symptomatic yellow fever might not have been sampled, so cases might have gone undetected. Reflecting the iceberg concept, which indicates that for each detected case there is considerable potential for many more undetected infections, it has been estimated that 1 severe case of yellow fever might represent an additional 3–20 asymptomatic or mild infections (*25*).

The highest percentages of clinical specimens—total (65%), positive (84%), and negative (57%)—came from the Savannah region (Table 3), which had case numbers >2 times those recorded from the other northern regions combined. That finding supports the assertion that the yellow fever outbreak started and peaked in the region. Past outbreaks in the region have occurred during the dry season months, October–February, as did the 2021–2022 outbreak. Water stored in containers around households provides habitat for mosquitoes and might increase their populations. In addition, an upsurge in farming activities during those periods in preparation for the rainy season might have led to more frequent exposure to mosquito vectors in remote areas. However, mosquito species trapped during outbreak investigations, including *Aedes aegypti aegypti* (2%), *Ae. aegypti formosus* (39%), and *Culex* spp. (58%), tested negative for YFV. This finding suggests either low virus density in the mosquito population sampled or the contribution of forest-dwelling mosquito species that mediate vector infection rates in sylvatic outbreaks.

Yellow fever was commonly detected among symptomatic persons, including those exhibiting

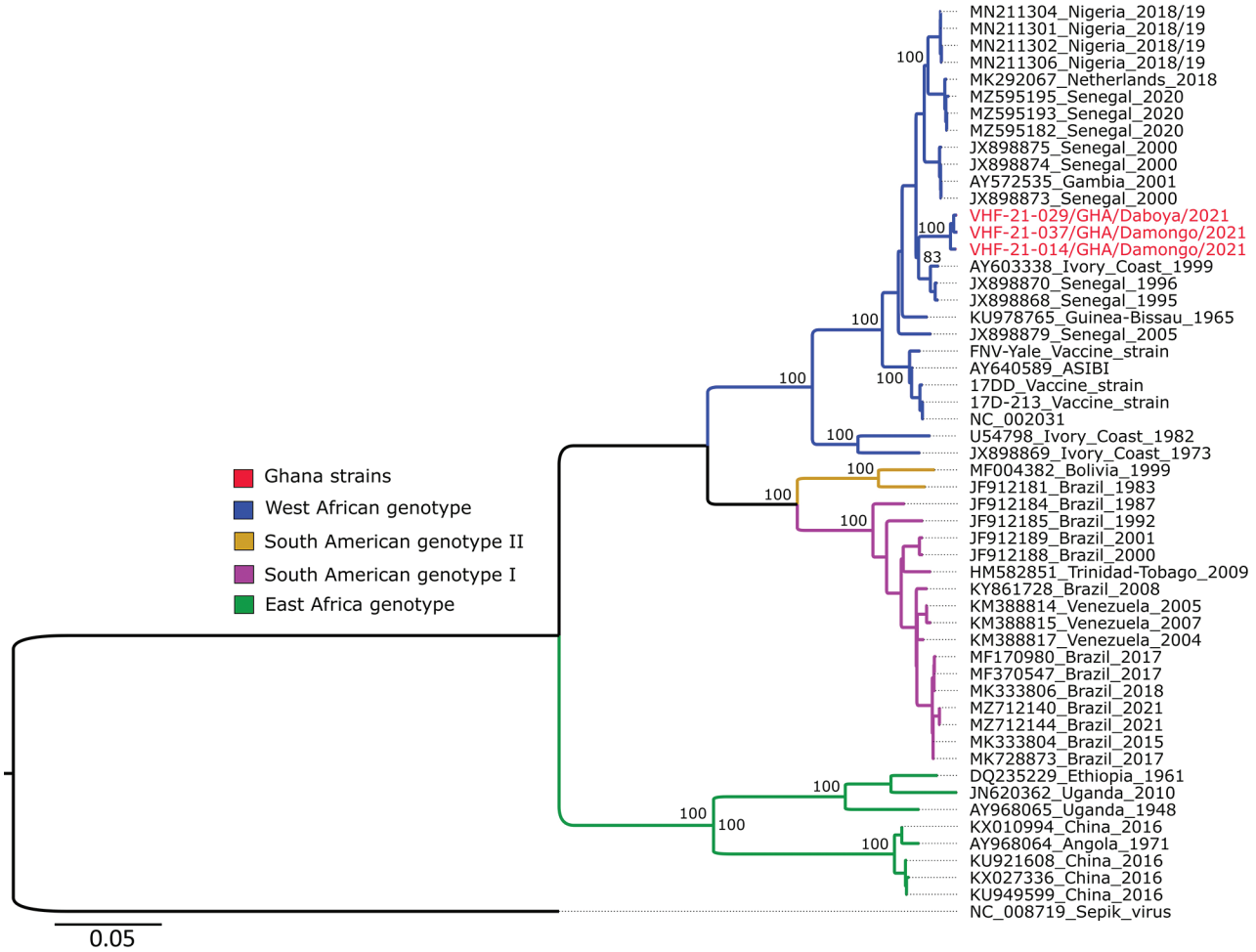

Figure 3. Phylogenetic analysis of yellow fever virus sequences from 3 confirmed cases in Ghana during January 2021–February 2022 (red text) compared with reference sequences obtained from GenBank in January 2022 (identified by GenBank accession number and country of origin).). Virus genotypes are indicated with different color nodes on the tree. Some branches with low support values were collapsed for clarity of presentation. Scale bar indicates substitution per site.

hemorrhage. Calculated percentages of patients screened indicated that fever, hemorrhage, and other signs/symptoms were predominantly observed for both negative and positive patients, although we found no statistically significant association between signs/symptoms and yellow fever detection (Table 3). Yellow fever is classified a VHF because of shared signs/symptoms with other VHFs, aside from fever among some. Patients with yellow fever often initially exhibit fever and general malaise, signs/symptoms common in other tropical diseases, including malaria and typhoid. Those similar manifestations make differentiating VHFs, including yellow fever, from other tropical diseases more difficult but vital for proper management and to curtail spread.

The sequences generated from this outbreak investigation clustered among sequences known in literature and documented to be circulating in Ghana. Phylogenetic analysis revealed some close homology among the sequences from yellow fever–positive patient samples. Although the strains circulated in different outbreak communities, they were closely related to each other and to strains circulating in Senegal and Cote d'Ivoire; the strains all clustered within West Africa genotype II. Seven YFV genotypes have been described (*26*–*30*), 2 in South America and 5 in Africa, namely West Africa genotype I (Nigeria, Cameroon, and Gabon), West Africa genotype II (Senegal, Guinea, Ivory Coast, and Ghana), East and Central Africa genotype (Sudan, Ethiopia, Central African Republic, and Democratic Republic of Congo), East Africa genotype (Kenya), and Angola genotype (Angola). Less homogeneous outbreaks of yellow fever have been documented within areas of endemicity (*21*). Sequences of the 2 West Africa genotypes dominate in outbreaks for reasons possibly attributable to genetic variability that might affect the virulence of the virus. Sequences belonging to West Africa genotype I show more heterogeneity than West Africa II and East/Central Africa genotypes (*26*), which could indicate stronger evolutionary activity.

In conclusion, in this yellow fever outbreak in Ghana, a more sensitive pathogen detection approach during our laboratory outbreak investigations enabled us to reduce time between the outbreak and when first cases were detected, which proved useful for reducing time between when the first cases were detected after the actual beginning of the outbreak and subsequent initiation of disease control interventions leading to more effective disease management. Rapid response is an essential component in successfully controlling infectious disease outbreaks and ensuring global health security interests. Moreover, identifying full-length sequences of 3 confirmed YFV strains provided vital genomic surveillance information about circulating strains and potential risks. On the basis of our findings, we urge increased efforts from health authorities to educate and vaccinate vulnerable groups in difficult-to-access areas to reduce potential risks for yellow fever infections.

Acknowledgments

This work was supported by the Armed Forces Health Surveillance Division, Global Emerging Infections Surveillance Branch (PROMIS ID: P0179_23_N3).

The authors thank all health staff, especially laboratory scientists and disease control officers who supported sample handling and transporting at various health facilities and the US NAMRU-3 Ghana Detachment laboratory for their help in genomic sequencing.

Some authors are military service members or employees of the US government. This work was prepared as part of their official duties. Title 17, U.S.C. §105 provides that copyright protection under this title is not available for any work of the U.S. Government. Title 17, U.S.C. §101 defines a US government work as work prepared by a military service member or employee of the US government as part of that person's official duties. The views expressed in this article are those of the authors and do not necessarily reflect the official policy or position of the Department of the Navy, Department of Defense, nor the US government.

J.H.K.B., T.S., S.D., and J.K.O. designed the study. D.P., S.K., K.A., P.L.A., G.A.B., G.M., and C.Y. conducted experiments and data analyses. D.L., N.K.F.A., C.K., and F.A.B. examined patients, made diagnoses, and collected samples and clinical information. B.A. and C.T. performed statistical analyses and contributed to generating tables and figures. S.A.O., J.H.K.B. and F.A.B. helped interpret data and write the manuscript. All authors reviewed and approved the manuscript.

About the Author

Dr. Bonney is an associate professor of virology at the Noguchi Memorial Institute for Medical Research, University of Ghana. His primary research interest is emerging and reemerging infections, particularly viral zoonoses, including arboviruses and viral hemorrhagic fevers, such as Ebola, Lassa, Crimean-Congo, and Rift valley.

References

1. World Health Organization. Yellow fever [cited 2021 Nov 12]. https://www.who.int/news-room/fact-sheets/detail/yellow-fever
2. Barrett ADT, Weaver SC. Arboviruses: alphaviruses, flaviviruses and bunyaviruses: encephalitis; yellow fever; dengue; haemorrhagic fever; miscellaneous tropical fevers; undifferentiated fever. In: Greenwood D, Barer M, Slack R, Irving W, editors. Medical microbiology: eighteenth edition. London: Churchill Livingstone; 2012.
3. Gardner CL, Ryman KD. Yellow fever: a reemerging threat. Clin Lab Med. 2010;30:237–60. https://doi.org/10.1016/j.cll.2010.01.001
4. Tolle MA. Mosquito-borne diseases. Curr Probl Pediatr Adolesc Health Care. 2009;39:97–140. https://doi.org/10.1016/j.cppeds.2009.01.001
5. Scott DE. Epidemic disease in Ghana, 1901–1960. London: Oxford University Press; 1965.
6. Agadzi VK, Boakye AB, Appawu MA, Mingle JAA, Addy PA. Yellow fever in Ghana, 1977–1980. Bull World Health Organ. 1984;62:577–83
7. Fresh yellow fever claims 3 lives in West Gonja [cited 2022 Mar 23]. https://www.modernghana.com/news/666626/fresh-yellow-fever-outbreak-claims-3-lives-in-west-gonja.html
8. Bonney JH, Asigbee TW, Kotey E, Attiku K, Asiedu-Bekoe F, Mawuli G, et al. Molecular detection of viral pathogens from suspected viral hemorrhagic fever patients in Ghana. Health Sciences Investigations Journal. 2020;1:31–5. https://doi.org/10.46829/hsijournal.2020.6.1.1.31-35
9. Escadafal C, Faye O, Sall AA, Faye O, Weidmann M, Strohmeier O, et al. Rapid molecular assays for the detection of yellow fever virus in low-resource settings. PLoS Negl Trop Dis. 2014;8:e2730. https://doi.org/10.1371/journal.pntd.0002730
10. Towner JS, Rollin PE, Bausch DG, Sanchez A, Crary SM, Vincent M, et al. Rapid diagnosis of Ebola hemorrhagic fever by reverse transcription-PCR in an outbreak setting and assessment of patient viral load as a predictor of outcome. J Virol. 2004;78:4330–41. https://doi.org/10.1128/JVI.78.8.4330-4341.2004
11. Drosten C, Gottig S, Schilling S, Asper M, Panning M, Schmitz H, et al. Rapid detection and quantification of RNA of Ebola and Marburg viruses, Lassa virus, Crimean-Congo hemorrhagic fever virus, Rift Valley fever virus, dengue virus, and yellow fever virus by real-time reverse transcription-PCR. J Clin Microbiol. 2002; 40:2323–30.
12. Santiago GA, Vázquez J, Courtney S, Matías KY, Andersen LE, Colón C, et al. Performance of the Trioplex real-time RT-PCR assay for detection of Zika, dengue, and chikungunya viruses. Nat Commun. 2018;9:1391. https://doi.org/10.1038/s41467-018-03772-1
13. Blackley DJ, Wiley MR, Ladner JT, Fallah M, Lo T, Gilbert ML, et al. Palacios G. Reduced evolutionary rate in reemerged Ebola virus transmission chains. Sci Adv. 2016;2:e1600378. https://doi.org/10.1126/sciadv.1600378
14. Prjibelski A, Antipov D, Meleshko D, Lapidus A, Korobeynikov A. Using SPAdes de novo assembler. Curr Protoc Bioinformatics. 2020;70:e102. https://doi.org/10.1002/cpbi.102
15. Langmead B, Salzberg SL. Fast gapped-read alignment with Bowtie 2. Nat Methods. 2012;9:357–9. https://doi.org/10.1038/nmeth.1923
16. Kumar S, Stecher G, Li M, Knyaz C, Tamura K. MEGA X: molecular evolutionary genetics analysis across computing platforms. Mol Biol Evol. 2018;35:1547–9. https://doi.org/10.1093/molbev/msy096
17. Kalyaanamoorthy S, Minh BQ, Wong TKF, von Haeseler A, Jermiin LS. ModelFinder: fast model selection for accurate phylogenetic estimates. Nat Methods. 2017;14:587–9. https://doi.org/10.1038/nmeth.4285
18. World Health Organization. Yellow fever laboratory diagnostic testing in Africa [cited 2022 Mar 23]. https://apps.who.int/iris/bitstream/handle/10665/246226/who-ohe-yf-lab-16.1-eng.pdf
19. Stock NK, Laraway H, Faye O, Diallo M, Niedrig M, Sall AA. Biological and phylogenetic characteristics of yellow fever virus lineages from West Africa. J Virol. 2013;87:2895–907. https://doi.org/10.1128/JVI.01116-12
20. Global health security agenda [cited 2022 Mar 26]. https://globalhealthsecurityagenda.org
21. International Federation of Red Cross and Red Crescent Societies. Yellow fever outbreak—Disaster Relief Emergency Fund operation no. MDRGH005 [cited 2022 Mar 26]. https://reliefweb.int/report/ghana/yellow-fever-outbreak-dref-operation-n°-mdrgh005
22. Nwaiwu AU, Musekiwa A, Tamuzi JL, Sambala EZ, Nyasulu PS. The incidence and mortality of yellow fever in Africa: a systematic review and meta-analysis. BMC Infect Dis. 2021;21:1089. PubMed https://doi.org/10.1186/s12879-021-06728-x
23. Bonney JHK, Osei-Kwasi M, Adiku TK, Barnor JS, Amesiya R, Kubio C, et al. Hospital-based surveillance for viral hemorrhagic fevers and hepatitides in Ghana. PLoS Negl Trop Dis. 2013;7:e2435. PubMed https://doi.org/10.1371/journal.pntd.0002435
24. Kwagonza L, Masiira B, Kyobe-Bosa H, Kadobera D, Atuheire EB, Lubwama B, et al. Outbreak of yellow fever in central and southwestern Uganda, February–May 2016. BMC Infect Dis. 2018;18:548. PubMed https://doi.org/10.1186/s12879-018-3440-y
25. Johansson MA, Vasconcelos PFC, Staples JE. The whole iceberg: estimating the incidence of yellow fever virus infection from the number of severe cases. Trans R Soc Trop Med Hyg. 2014;108:482–7. https://doi.org/10.1093/trstmh/tru092
26. Mutebi JP, Barrett AD. The epidemiology of yellow fever in Africa. Microbes Infect. 2002;4:1459–68. https://doi.org/10.1016/S1286-4579(02)00028-X
27. Barrett AD, Monath TP. Epidemiology and ecology of yellow fever virus. Adv Virus Res. 2003;61:291–315. https://doi.org/10.1016/S0065-3527(03)61007-9
28. de Souza RP, Foster PG, Sallum MA, Coimbra TL, Maeda AY, Silveira VR, et al. Detection of a new yellowfever virus lineage within the South American genotype I in Brazil. J Med Virol. 2010;82:175–85. https://doi.org/10.1002/jmv.21606
29. Mutebi JP, Wang H, Li L, Bryant JE, Barrett AD. Phylogenetic and evolutionary relationships among yellow fever virus isolates in Africa. J Virol. 2001;75:6999–7008. https://doi.org/10.1128/JVI.75.15.6999-7008.2001
30. von Lindern JJ, Aroner S, Barrett ND, Wicker JA, Davis CT, Barrett ADT. Genome analysis and phylogenetic relationships between east, central and west African isolates of yellow fever virus. J Gen Virol. 2006;87(Pt 4):895–907. https://doi.org/10.1099/vir.0.81236-0

Address for correspondence: Joseph Humphrey Kofi Bonney or John Kofi Odoom, Department of Virology, Noguchi Memorial Institute for Medical Research, PO Box, LG 581, University of Ghana, Legon Accra, Ghana; email: kbonney@noguchi.ug.edu.gh or jodoom@noguchi.ug.edu.gh

Improvements and Persisting Challenges in COVID-19 Response Compared with 1918–19 Influenza Pandemic Response, New Zealand (Aotearoa)

Jennifer Summers, Amanda Kvalsvig, Lucy Telfar Barnard, Julie Bennett, Matire Harwood, Nick Wilson,[1] Michael G. Baker[1]

Exploring the results of the COVID-19 response in New Zealand (Aotearoa) is warranted so that insights can inform future pandemic planning. We compared the COVID-19 response in New Zealand to that for the more severe 1918–19 influenza pandemic. Both pandemics were caused by respiratory viruses, but the 1918–19 pandemic was short, intense, and yielded a higher mortality rate. The government and societal responses to COVID-19 were vastly superior; responses had a clear strategic direction and included a highly effective elimination strategy, border restrictions, minimal community spread for 20 months, successful vaccination rollout, and strong central government support. Both pandemics involved a whole-of-government response, community mobilization, and use of public health and social measures. Nevertheless, lessons from 1918–19 on the necessity of action to prevent inequities among different social groups were not fully learned, as demonstrated by the COVID-19 response and its ongoing unequal health outcomes in New Zealand.

The world is continuing to experience the COVID-19 pandemic, which has resulted in >767 million reported cases and ≈6.9 million deaths (≈870 deaths/1 million persons) through June 2023 (*1*). Those numbers are likely a huge undercount; mortality has been estimated to be ≥3 times higher (*2*). New Zealand (Aotearoa, the commonly used Indigenous Māori language name for the country) experienced ≈2.4 million confirmed COVID-19 cases and ≈3,077 COVID-19 attributed deaths (≈597 per million population) reported up to mid-June 2023 (*3*). The country has also experienced severe effects of the COVID-19 pandemic through disruptions to the healthcare system and economy and wider societal harms (*4*–*7*). However, in terms of deaths, the influenza pandemic of 1918–19 still remains "New Zealand's worst recorded natural disaster" (*8*).

The 1918–19 influenza pandemic occurred in the final stages of World War I (WWI) and is estimated to have killed 50–100 million persons worldwide, equaling >1% of the world's population (*9*). This particularly lethal strain of influenza A(H1N1) virus spread to almost all parts of the globe, leaving just a few isolated locations untouched. In New Zealand, the 1918–19 influenza pandemic spread the length of the country through railway and shipping routes and is estimated to have killed >9,000 persons (*8*). The effects of this pandemic were severe, stressing the existing healthcare system (already stretched by the war effort) and, as in other nations, affecting all aspects of daily life and compounding existing societal and economic inequities.

Past pandemics provide insight into how societies, governments, and communities are affected and how they might respond to an emerging disease threat. Indeed, failure to examine past pandemic experiences limits our understanding and reduces the clarity of evidence and justification for future pandemic management and control. Given this background, we completed a historical review (Appendix, https://wwwnc.cdc.gov/EID/article/29/9/22-1265-App1.pdf) to consider how this island nation responded to these 2 severe pandemics and to explore

Author affiliations: University of Otago, Wellington, New Zealand (J. Summers, A. Kvalsvig, L. Telfar Barnard, J. Bennett, N. Wilson, M.G. Baker); University of Auckland, Auckland, New Zealand (M. Harwood)

DOI: https://doi.org/10.3201/eid2909.221265

[1]These senior authors contributed equally to this article.

whether ongoing lessons exist that are relevant both for today and for future pandemic planning.

1918–19 Influenza Pandemic in New Zealand

The first, relatively mild, wave of the 1918–19 influenza pandemic spread in New Zealand during July–October 1918. The more virulent second wave largely occurred during November–December 1918 (Appendix Table 1, Figure 1, panel A). Most pandemic deaths in New Zealand occurred during this second wave, which spread nationwide in a matter of weeks; some localized examples of prevention measures, such as quarantine and travel restrictions, have been documented (*8*). Vaccine use for bacterial pathogens during this pandemic is documented in New Zealand and in overseas-based New Zealand military personnel, who were part of vaccine studies (*11*). Some limited international evidence of vaccine efficacy for influenza-associated bacterial pneumonia (a common secondary infection) during this pandemic exists, but there was no coordinated distribution of vaccines to the public in New Zealand. This pandemic had a profound effect on children in New Zealand, not only as a result of influenza infection itself but also through detrimental effects on family and caregiving structure and by deaths of caregivers that left children orphaned (*8*). Evidence also exists for a sudden decrease in the annual birth rate in the country in 1918 and particularly 1919, a possible result of the association between influenza infections, social effects, and stillbirths or fetal loss (*12,13*).

In late 2018, we published a systematic review of all known literature on the experience of the 1918–19 influenza pandemic in New Zealand (*12*). We found epidemiologic patterns among residents during this pandemic that were consistent with international literature, such as a w-shaped age distribution for deaths (Figure 1) (*8,14,15*). Mortality rates were high among Indigenous Māori civilian and military populations compared with the European-origin population (*8,16*), and risk for death was higher among New

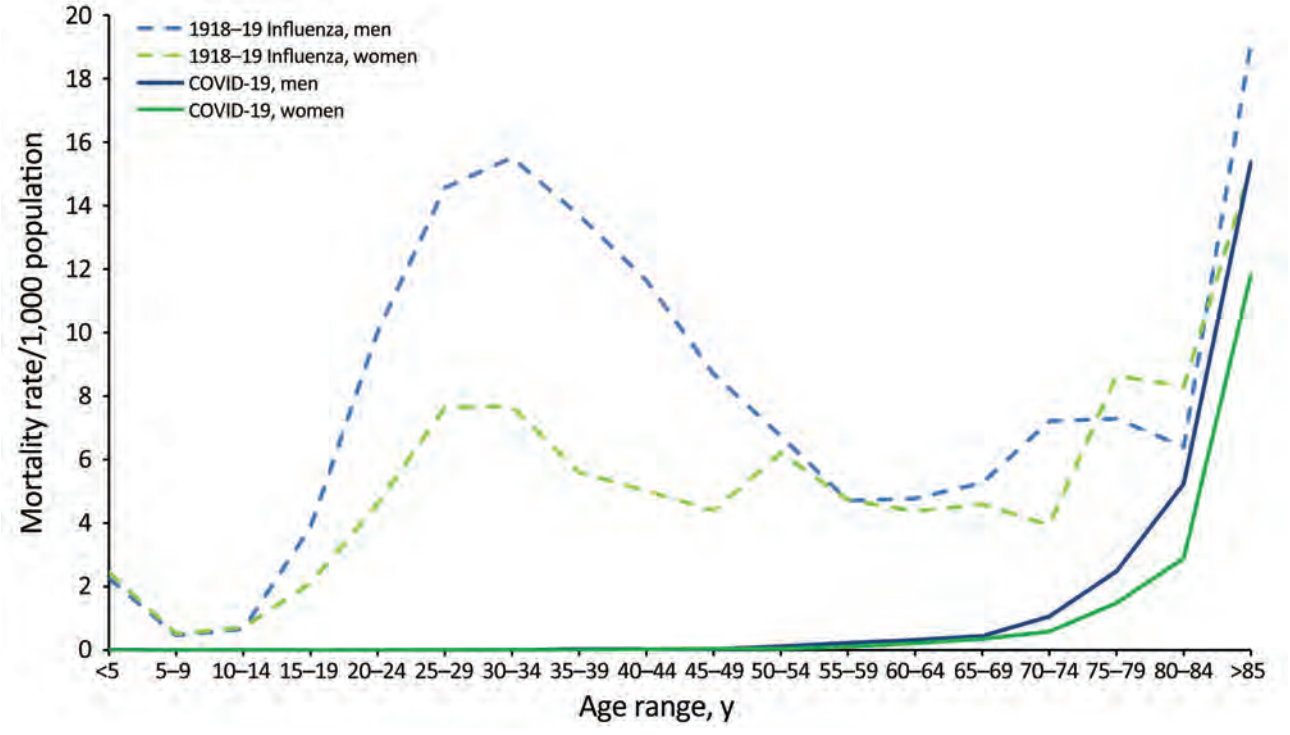

Figure 1. Cumulative mortality rate (deaths/1,000 population) in New Zealand (Aotearoa) during the 1918–19 influenza pandemic (for European-origin persons) and during the COVID-19 pandemic (all origins), by age and sex. The 1918–19 pandemic mortality data cover the entire period of the pandemic in NZ and are reproduced from Summers (*10*) and derived/approximated from publicly available sources (*8*; https://www3.stats.govt.nz/New_Zealand_Official_Yearbooks/1924/NZOYB_1924.html). Mortality data from 1918–19 for the Māori population are not available; therefore, mortality rates are likely underestimates. COVID-19 mortality data cover the period of January 2020–December 31, 2022. Mortality data were provided by the New Zealand Ministry of Health/Manatū Hauora, and population totals were sourced from Stats NZ/Tatauranga Aotearoa (https://www.stats.govt.nz/topics/population). Death was classified as a COVID-19 death when COVID-19 was the underlying cause of death or a contributory cause of death. The figure does not include 3 deaths with missing demographic information or the 589 deaths that were unclassified as of December 31, 2022 (and might subsequently be classified as COVID-19 deaths).

Zealand military personnel who had a preexisting chronic disease or were recent military recruits (*8*,*15*–*17*). Unique findings focused on the novel risk factors for death, such as larger chest size in men (possibly an indicator of a different immune system response in men with larger bodies) (*17*) and lack of difference between mortality rates in men and women in the Māori population. The lack of difference in mortality rates by sex contrasted with the relatively higher death rates of men than women in the European-origin population in New Zealand (as was found in many other countries) (*12*,*15*,*18*). Although this H1N1 influenza virus was considered endemic by 1920, it continued to cause more severe influenza seasons for several more years, and long-term sequelae from the pandemic strain have been documented internationally (*19*,*20*) (Appendix).

COVID-19 in New Zealand

The first identified case of COVID-19 in New Zealand was reported on February 28, 2020; the first outbreak peaked in March 2020 alongside the first national stay-at-home order (lockdown), border closures for noncitizens, and introduction of wide-ranging public health protections (Appendix Figure 1, panel B). The government initially adopted an elimination response strategy to manage the pandemic, which required tight border management to prevent the importation of COVID-19 cases and systems to extinguish outbreaks if they occurred (*21*).

Relatively small COVID-19 outbreaks occurred in 2020 and 2021 because of incursions coupled with new COVID-19 variants (*3*,*22*). In response, local (including iwi [tribal]–led), regional, and national public health and social measures (including lockdowns) were put in place to contain community spread. During those periods, businesses were closed, work was restricted unless deemed essential, and the government provided some financial assistance to businesses and employees.

A switch from an elimination strategy to a suppression strategy occurred in late 2021 during the Delta variant wave with the introduction of the COVID-19 Protection Framework (*21*,*23*). This framework focused on vaccination requirements for various indoor and public venues and included some limited travel restrictions. However, the framework was retired mid-September 2022, and only limited public health protections, such as mask-wearing in healthcare facilities, remained in place. The pandemic plan in New Zealand at the emergence of COVID-19 was (and remains as of mid-June 2023) based on a hypothetical influenza pandemic and predominantly uses a mitigation strategy (*24*). Therefore, the applicability of this plan to the characteristics of COVID-19 has been questioned (*4*).

Compared with other high-income countries, New Zealand experienced decreased excess winter deaths, a net decline in overall deaths, and an increase in life expectancy during the first 2 years of the COVID-19 pandemic (*25*). The largest waves to date in terms of cases, hospitalizations, and deaths have been from the Omicron variant (and its sublineages), which began in early 2022 and spread nationwide (*26*). By mid-June 2023, a total of 3,077 estimated deaths attributed to COVID-19 had occurred in the country (*3*).

The effects of COVID-19 in New Zealand have varied; the burden of hospitalizations and deaths have disproportionately affected Māori and Pacific persons (another ethnic grouping), and those groups have had lower rates of COVID-19 vaccination (although the difference varies by age group) (*3*,*6*). As of June 9, 2023, ≈89.3% of the total eligible New Zealand population had received 2 vaccine doses, and ≈73.2% had received ≥1 booster (third) vaccine dose (*3*). The pandemic has also had a major effect on children and adolescents because of widespread disruption to education at all ages (*27*).

Just over a year into the COVID-19 pandemic, the New Zealand government confirmed that the health system would be restructured to create 1 national service delivery organization to function alongside the continuing Ministry of Health (focused on policy), a dedicated Public Health Agency, and a Māori Health Authority (https://www.futureofhealth.govt.nz). The transformed health system aims to create a "more equitable, accessible, cohesive and people-centered system that will improve the health and wellbeing of all New Zealanders" (https://www.futureofhealth.govt.nz). This health system restructure was planned before the COVID-19 pandemic, however; unlike the health system restructuring and legislative changes that occurred in New Zealand after the 1918–19 influenza pandemic, this restructuring began during the COVID-19 pandemic.

Comparison of 2 Pandemics

We identified key similarities and differences between hazards and responses across the 2 pandemics (Table). Both pandemics occurred among largely immunologically naive populations (with some exceptions in 1918–19) (*43*), and large proportions of the population were infected with marked ethnic health disparities, manifesting as higher rates of illness, hospitalization, and death, among Māori and Pacific peoples.

Table. Comparative summary of distinct features of 1918–19 influenza pandemic and the COVID-19 pandemic hazard and responses, New Zealand*

1918–19 influenza pandemic	COVID-19 pandemic	Similarities
Hazard and effects (both globally and in NZ, where data available)		
Caused by influenza virus H1N1	Caused by SARS-CoV-2	Likely zoonotic origins for the pandemic viruses
RNA virus that showed relatively slow genetic drift through mutation	Global infection fatality risk of 0.1%–2.0% up to June 2021 (*28*); NZ infection fatality risk 0.79% (estimated, January 2021 before vaccination) (*29*)	Transmitted between humans as a respiratory viral pathogen
Probably originated in domestic and wild birds (*30,31*)	RNA virus showing rapid genetic shifts through mutation and recombination, including within-host evolution during chronic infection of immunocompromised patients (*32*)	Immunologically naive population
Moderately transmissible, with R_0 estimated at 2.4–4.3 (*33*)	Probably originated in bats (*31*)	High proportion of population infected
Incubation period of ≈a few hours to 2 d reported in a large US civilian hospital in 1918 (*34*) and general influenza estimates of 1–4 d (*35*)	Highly transmissible with estimated R_0 of 9.5 for Omicron variant (*36*)	Marked ethnic health disparities experienced globally. For example, in NZ, notably higher death rates in the Māori population
Global case-fatality risk ≈1–2.5% (*20,37*)	Incubation period estimates differ by variant, with one meta-analysis reporting a pooled mean incubation time of 6.6 d (*38*)	Higher death rates in men internationally
Global infection fatality risk >2% (*28*)	Global estimate for case fatality risk of 1.12% as of July 26, 2022 (*1*). NZ case-fatality risk of 1.15 in 2020 (before vaccines), reduced to 0.09% as of July 2022 (with high vaccine coverage) (*3*)	Post-acute infection syndrome common
Infection gives long-term immunity (*39*)	Infection gives protection that fades over ≈3 y (*40*)	
Net effect is symptomatic infection in ≈8% of population each year (*41*)	Net effect is reinfections are common (*3*)	
Short, intense pandemic wave, with some smaller waves in subsequent years	Repeated, prolonged pandemic waves	
Relatively more severe illness in young adults and elderly	Relatively more severe illness in elderly and immunosuppressed	
Devastating spread of infection from NZ to surrounding Pacific nations	Regional border quarantine measures probably limited spread from NZ to South Pacific jurisdictions	
Response in NZ		
Lack of strategic response	Highly strategic national control response (elimination for first 20 mo of pandemic) with vigorous public communication	Large community/voluntary sector mobilization
No use of external border controls	Use of tight external border controls (in the first 2 years)	Use of physical distancing through closure of public facilities, businesses, schools, and cancellation of large public events, although less systematically in 1918–19
No specific test for pathogen available	Accurate diagnostic test and organized testing program	Some use of internal border controls
Limited use of case isolation and contact quarantine	Active contact tracing and quarantining of contacts	No specific curative treatment initially (although supportive management and treatment options for COVID-19 sufferers were developed, including antivirals)
Limited infection control in institutions	Infection prevention and control in health care and aged care	Iwi, hapū and marae-led care and support† (*7,8,42*)
No specific vaccine available	Highly effective vaccines in late 2020 (within 1 year)	Royal Commissions of Inquiries to investigate pandemic responses
Lack of economic and social support from government	Extensive economic and social support from government	
No widespread mask-wearing	Requirements (mandates) to use masks in some settings to limit transmission	

*For greater detail of the hazards, response, and various impacts of the two pandemics in NZ, see Appendix Table 1 (https://wwwnc.cdc.gov/EID/article/29/9/22-1265-App1.pdf). NZ, New Zealand; R_0, basic reproductive number.
†Indigenous Māori language terms: iwi refers to tribe and hapū refers to subtribe. Marae (meeting grounds) are the focal point of Māori communities and are a complex of carved buildings and grounds that belongs to a particular iwi, hapū, or whānau (family).

Both viruses are moderately to highly infectious; basic reproductive numbers (R_0) were estimated to be >2.4 (Table) (*37*,*42*). A key difference is that the incubation period (and serial interval) is much shorter for influenza. An estimate of the incubation period for 1918–19 influenza is a few hours to 2 days (*34*); for influenza A, 1.4 days (*35*). For SARS-CoV-2, by contrast, one mean estimate of incubation is 6.57 days (*38*). The longer incubation period for COVID-19 has made contact tracing and quarantine of contacts much more feasible.

The 1918–19 influenza pandemic caused a short, intense pandemic wave with high death rates that swept through New Zealand in <2 months (November–December 1918) and likely infected ≈50% of the population (*8*). The first Omicron variant wave of the COVID-19 pandemic moved through New Zealand in a similarly short period (February–April 2022). Unlike the 1918-19 influenza pandemic, it was followed by a succession of waves; a second occurred in June–August 2022, a third began in November 2022, and a fourth began in April 2023. These waves were each dominated by different Omicron subvariants (BA.1 and BA.2 for the first wave, BA.4 and BA.5 for the second, and a mix of multiple Omicron subvariants in the third and fourth waves) (*3*). Influenza H1N1 (such as the 1918–19 influenza virus) and SARS-CoV-2 are RNA viruses that mutate more readily than DNA viruses (*44*). However, SARS-CoV-2 has demonstrated a capacity for sudden and frequent antigenic shifts that result in new variants and subvariants with multiple mutations, which enables it to escape existing immunity and cause high levels of reinfection and a succession of pandemic waves (*32*). One change in human populations between 1918–19 and 2020 onward is the likely increase in the proportion of persons now living with known immune suppression. SARS-CoV-2 appears able to cause chronic infections in such patients, during which it can have rapid within-host evolution (*32*).

Of note, the lethality of H1N1 in 1918–19 (global infection fatality risk >2%) overlapped with the range reported for SARS-CoV-2 (global infection fatality risk 0.1%– 2%) before vaccines were introduced (*28*,*29*). After widespread COVID-19 vaccination, the case-fatality risk in New Zealand dropped by an order of magnitude, from 1.15% in 2020 to ≈0.13% by the end of May 2023 (*3*). This decline might also reflect the reduced severity of the Omicron variant relative to the Delta variant, although Omicron appears to have similar virulence to the original variant that dominated during the first year of the COVID-19 pandemic (*45*). Furthermore, immunity after infection with H1N1 virus in 1918–19 appeared to be long-lasting (*39*). By contrast, immunity against infection generated by SARS-CoV-2 appears to fade over ≈3 years (*40*). In addition, this immunity is much less effective at preventing infection with subsequent COVID-19 subvariants, although protection against severe infection appears to be well sustained after both natural infection and vaccination (*40*).

We observed a w-shaped distribution of deaths in New Zealand during the 1918–19 pandemic that was more pronounced for men than women in almost all age groups (Figure 1). However, we observed no evidence of a w-shaped distribution of deaths by age for COVID-19 in New Zealand; the mortality rate increased exponentially with older age. The rate of overall attributable deaths was higher among men than women, which is consistent with international findings (*3*,*46*). For both pandemics, higher mortality rates were observed in specific populations, such as Māori and Pacific peoples (*3*,*6*,*8*). Reported rates of COVID-19 illness have been generally higher among children and younger adults in New Zealand (*3*). However, this difference might reflect increased exposure to infection because they have higher levels of social contact than older adults; rates of self-reporting among the younger population could also be higher.

A wide-ranging government response with robust community mobilization was observed during both pandemics, as was a substantial reliance on charitable contributions to support persons and communities (Appendix Table 1) (*4*,*8*,*47*). Physical distancing measures and travel/border restrictions were used in both pandemics, but public health protections were far tighter during the COVID-19 pandemic (particularly during 2020 and 2021). Additional external border controls used the advantage of New Zealand being a remote island nation and having a brief window of time to implement controls before widespread domestic COVID-19 transmission occurred. However, during 1918–19, use of internal border restrictions was limited and inconsistent, and no substantial external travel restrictions or border control was in place. For example, a discriminatory travel ban on public transport for Māori (unless issued a health permit) was implemented, and other unofficial bans were extended to other premises, such as business places (*8*).

Institutional infection control and prevention was limited during 1918–19, although some temporary hospitals were established for influenza patients, in addition to separate hospitals for Māori patients (*8*). The response in 1918–19 was unlike the response during COVID-19, in which extensive prevention and

control measures were used in a range of healthcare and aged-care settings and integrated into the initial Alert Level System and the subsequent COVID-19 Protection Framework (*21*,*47*).

Discussion

More than a century has now passed since the 1918–19 influenza pandemic, but it remains the worst public health disaster in recorded New Zealand history. More than 9,000 influenza deaths occurred in just a couple of months, and during the final stages of WWI, New Zealand residents faced a uniquely difficult period in the nation's history. In particular, the Māori population was disproportionally affected by the pandemic, and many Māori pandemic deaths probably remain undocumented (*8*). The response during and after this period provides insight into how New Zealand society might respond to future disease threats, as well as to the continuing COVID-19 pandemic.

Probably the most fundamental difference in responses to COVID-19 and influenza was the use of a national control strategy, namely an elimination strategy for SARS-CoV-2 (*48*). The early use of the elimination strategy in New Zealand in 2020 helped maintain a relatively low death rate in the first 2 years and reduced the economic impact of the COVID-19 pandemic compared with other nations (*1*). New Zealand also observed an increase in life expectancy during this period (*25*) and low estimates of excess deaths compared with a pre–COVID-19 period (≈0.02% as of May 2023), unlike other high-income nations, such as the United States (12.8%), United Kingdom (10.0%), and Sweden (5.1%) (*1*). This proactive response to COVID-19 is markedly different from 1918–19, when no clear strategy was implemented for preventing or managing the influenza pandemic, resulting in substantial deaths and reduced birth rates in the following years (*12*,*13*).

The death patterns observed in 1918–19 highlighted health inequities and the factors driving them, such as household crowding, comorbidities, and unequal access to healthcare. Reasons for poorer health outcomes among Māori are complex; Māori persons in 1918–19 experienced higher rates of chronic disease (compared to the European-origin population in New Zealand), barriers in access to healthcare, and discriminatory outbreak management approaches. For example, in 1918–19, the Māori population had a substantially higher pandemic influenza mortality rate of 42.3 per 1,000 compared with 5.8 per 1,000 among the European-origin population; as a result, in the final 2 months of 1918, an estimated 4% of the Māori population died from pandemic influenza (*8*).

Those health inequities persist today (*16*). Although the New Zealand government has acknowledged failings in the COVID-19 pandemic response and provided some targeted support to Māori providers (and other services such as those for Pacific and disabled persons), cases, hospitalizations, and death rates for COVID-19 have been disproportionally higher among those groups (*3*). Rates of COVID-19 vaccination are also lower among Māori adults and children than among other ethnic groups. Therefore, the principles of equity, partnership, and active protection, as guaranteed in the Te Tiriti o Waitangi–Treaty of Waitangi between the Government (Crown) and Māori, continue to be inadequately addressed 100 years after the first pandemic. Fortunately, some of this deficit was addressed through Māori-led initiatives during the COVID-19 pandemic, such as basic living support (for example, food parcels to families [*7*]) and health service provision (for example, testing and vaccination drives by community groups, with or without government support). Several iwi (tribes) also initiated border controls for their tribal areas, emulating the approaches used in 1918–19 to limit the spread and severity of disease and thus protect their whānau (families) and communities.

When comparing the 2 pandemics, considering how scientific understanding has progressed and given us better ways of identifying, measuring, and describing the effect of infectious diseases is key. For example, the first human influenza virus was not isolated until 1933, more than a decade after the 1918–19 influenza pandemic (*8*). One distinct research area is the growing awareness of post–acute illness effects. The long-term effects of COVID-19 infection, which include both post–acute infection syndrome (long COVID) and organ system–specific effects (manifesting as excess deaths for at least 1 year after acute infection), appear to be relatively common. Long-term effects after the 1918–19 influenza pandemic were recognized, but fewer scientific tools to investigate them existed (*19*). Recent comparisons of COVID-19 with influenza suggest that sequelae from influenza appear less common (*49*).

During 1918, WWI was continuing to have a substantial impact on daily life; ≈40% of the New Zealand adult male population served in the military during the war, and many doctors and nurses were stationed overseas. This huge disturbance to normal life meant that when the pandemic hit, fewer able-bodied adults were available in traditional roles to provide assistance, and this gap was compounded by the higher rates of illness and death in younger adults. Therefore, many other residents stepped up

Figure 2. Medicine department at the Wellington Town Hall during the 1918 influenza epidemic. Shows where the standard mixture and tonic were prepared and bottled. Mrs. Waters (right) was in charge. Taken by an unidentified photographer. Reproduced from New Zealand Free Lance: 1/2-C-016207-F, 1918, Alexander Turnbull Library: National Library of New Zealand, Wellington, New Zealand.

to help by volunteering in temporary hospitals, providing food and medical supplies, transporting those who were ill, and serving on block committees that managed and supported local communities by coordinating relief (Figure 2) (*8*). Numerous examples of children playing essential roles during the 1918–19 pandemic by delivering supplies and working in hospitals have also been detailed (*8*). Similar examples were observed during the COVID-19 pandemic; local communities provided food and other supplies throughout New Zealand (Figure 3) (*7*), and children in secondary schools took employment in essential roles in supermarkets while schools were closed to support their families and fill labor shortages. The government also provided economic assistance during COVID-19, although this assistance was intermittent and was particularly focused on localities experiencing the tightest controls.

Unlike the 1918–19 influenza pandemic, which was largely over in 2 months, the COVID-19 pandemic has sustained itself globally for >3 years. Consequently, the effect of the COVID-19 pandemic on societal cohesion in New Zealand might be different from that observed during 1918–19; the ongoing COVID-19 response, vaccine provision and mandates, and overall management by the government has led to increased displays of social division. This division suggests the ongoing need for a more equitable and effective pandemic response, at both national and international levels.

Surprisingly, after 3 years of the COVID-19 pandemic, New Zealand still lacks a generic pandemic plan, and little evidence of planning for future disease threats (other than COVID-19 or influenza) exists (*47*). Therefore, it appears that New Zealand has not yet fully learned the lessons of 1918–19; the COVID-19 response has largely taken a reactive approach to new challenges, rather than a proactive stance (*47*). A more proactive approach could have implications

Figure 3. Workers at Kōkiri Marae preparing food and sanitation packages for the Lower Hutt and Wainuiomata communities during COVID-19 pandemic, New Zealand. Photograph by Luke Pilkinton-Ching, University of Otago, Wellington, New Zealand.

for controlling other infectious diseases (for example, improving infrastructure to support improved public health and social measures) and managing COVID-19 aftereffects such as long COVID and long-term effects on children.

Restructuring the health system during the COVID-19 pandemic might not have been optimal timing and is unlikely to incorporate all potentially relevant lessons from the entire period of the pandemic, unlike the restructuring after 1918–19. A Royal Commission of Inquiry investigating the response in New Zealand to the COVID-19 pandemic was announced in December 2022, but the scope of the inquiry is constrained. It excludes, for example, any assessment of the effect of the health system reforms, the epidemiology of the COVID-19 virus, private sector involvement, or various judgments and decisions related to the pandemic in various courts and independent agencies. A major positive feature is its focus on improving future pandemic preparedness (*50*).

New Zealand's "team of 5 million," as former Prime Minister Jacinda Ardern voiced in 2020 in reference to the population, is arguably now somewhat fractured by the prolonged COVID-19 pandemic and spread of the Omicron variant. Every aspect of the pandemic response has also been scaled back, with less use of public health and social measures and slowing uptake of vaccination and boosters. Therefore, it is difficult to identify, from a public health perspective, the government's ongoing strategy for managing COVID-19, how persisting inequities associated with infection are to be addressed, or how those most at-risk are to be protected. However, it is worth remembering that New Zealand emerged from the devastating 1918–19 influenza pandemic by strengthening its health system with the goal of learning lessons from its pandemic response. At this point, there remains an opportunity for New Zealand and the rest of the world, to build capacity to prevent future pandemics and to better respond to them when they are unavoidable.

Acknowledgments

We thank the Centre for Advanced Study (CAS) in Oslo, Norway, for hosting Michael Baker as part of the research project "Social science meets biology: indigenous people and severe influenza outcomes" during the 2022–2023 academic year. Svenn-Erik Mamelund and Lisa Sattenspiel provided helpful comments on the manuscript. We thank the New Zealand Ministry of Health/Manatū Hauora for providing additional COVID-19 data directly for the purposes of this article.

This research was supported by a donation from the late Professor Richard Seddon of Otago University, New Zealand.

About the Author

Dr. Summers is an epidemiologist, medical statistician, and medical historian who is a senior research fellow at Otago University, New Zealand. Her primary research interests are pandemics and infectious disease epidemiology.

References

1. Mathieu E, Ritchie H, Rodés-Guirao L, Appel C, Gavrilov D, Giattino C, et al. Coronavirus pandemic (COVID-19) [cited 2023 Jan 3]. https://ourworldindata.org/coronavirus
2. Jha P, Brown PE, Ansumana R. Counting the global COVID-19 dead. Lancet. 2022;399:1937–8. https://doi.org/10.1016/S0140-6736(22)00845-5
3. Ministry of Health–Manatū Hauora. COVID-19: data and statistics. 2023 [cited 2023 Jan 25]. https://www.health.govt.nz/covid-19-novel-coronavirus/covid-19-data-and-statistics
4. Summers J, Cheng H-Y, Lin H-H, Barnard LT, Kvalsvig A, Wilson N, et al. Potential lessons from the Taiwan and New Zealand health responses to the COVID-19 pandemic. Lancet Reg Health West Pac. 2020;4:100044.
5. Wilson N, Grout L, Summers J, Nghiem N, Baker M. Health and economic impacts of the COVID-19 response: NZ compared to OECD countries. 2020 Dec 3 [cited 2022 Aug 22]. https://www.phcc.org.nz/briefing/health-and-economic-impacts-covid-19-response-nz-compared-oecd-countries
6. Steyn N, Binny RN, Hannah K, Hendy SC, James A, Lustig A, et al. Māori and Pacific people in New Zealand have a higher risk of hospitalisation for COVID-19. N Z Med J. 2021;134:28–43.
7. Davies C, Timu-Parata C, Stairmand J, Robson B, Kvalsvig A, Lum D, et al. A kia ora, a wave and a smile: an urban marae-led response to COVID-19, a case study in manaakitanga. Int J Equity Health. 2022;21:70. https://doi.org/10.1186/s12939-022-01667-8
8. Rice G. Black November: the 1918 influenza pandemic in New Zealand. 2nd ed. Christchurch: Canterbury University Press; 2005.
9. Johnson NP, Mueller J. Updating the accounts: global mortality of the 1918–1920 "Spanish" influenza pandemic. Bull Hist Med. 2002;76:105–15. https://doi.org/10.1353/bhm.2002.0022
10. Summers JA. The burden and risk factors for death from the 1918–19 influenza pandemic amongst the New Zealand military forces of World War One [thesis]. 2013, University of Otago.
11. Chien YW, Klugman KP, Morens DM. Efficacy of whole-cell killed bacterial vaccines in preventing pneumonia and death during the 1918 influenza pandemic. J Infect Dis. 2010;202:1639–48. https://doi.org/10.1086/657144
12. Summers JA, Baker M, Wilson N. New Zealand's experience of the 1918–19 influenza pandemic: a systematic review after 100 years. N Z Med J. 2018;131:54–69.
13. Wilson N, Turner N, Baker MG. One hundred years ago in 1919: New Zealand's birth reduction shock associated with an influenza pandemic. N Z Med J. 2019;132:57–62.

14. Morens DM, Taubenberger JK, Fauci AS. The persistent legacy of the 1918 influenza virus. N Engl J Med. 2009;361:225–9. https://doi.org/10.1056/NEJMp0904819
15. Wilson N, Oliver J, Rice G, Summers JA, Baker MG, Waller M, et al. Age-specific mortality during the 1918–19 influenza pandemic and possible relationship to the 1889–92 influenza pandemic. J Infect Dis. 2014;210:993–5. https://doi.org/10.1093/infdis/jiu191
16. Wilson N, Barnard LT, Summers JA, Shanks GD, Baker MG. Differential mortality rates by ethnicity in 3 influenza pandemics over a century, New Zealand. Emerg Infect Dis. 2012;18:71–7. https://doi.org/10.3201/eid1801.110035
17. Summers JA, Stanley J, Baker MG, Wilson N. Risk factors for death from pandemic influenza in 1918–1919: a case-control study. Influenza Other Respir Viruses. 2014;8:329–38. https://doi.org/10.1111/irv.12228
18. Wilson N, Mansoor OD, Baker MG. The first analytic evidence for socio-economic gradients in 1918 pandemic influenza mortality rates for New Zealand. N Z Med J. 2018;131:50–3.
19. Honigsbaum M, Krishnan L. Taking pandemic sequelae seriously: from the Russian influenza to COVID-19 long-haulers. Lancet. 2020;396:1389–91. https://doi.org/10.1016/S0140-6736(20)32134-6
20. Taubenberger JK, Morens DM. 1918 influenza: the mother of all pandemics. Emerg Infect Dis. 2006;12:15–22. https://doi.org/10.3201/eid1209.05-0979
21. Unite against COVID-19, Ministry of Health, Manatū Hauora. History of the COVID-19 Protection Framework (traffic lights). 2022 [cited 2023 Jan 2]. https://covid19.govt.nz/about-our-covid-19-response/history-of-the-covid-19-protection-framework-traffic-lights
22. Grout L, Katar A, Ait Ouakrim D, Summers JA, Kvalsvig A, Baker MG, et al. Failures of quarantine systems for preventing COVID-19 outbreaks in Australia and New Zealand. Med J Aust. 2021;215:320–4. https://doi.org/10.5694/mja2.51240
23. Baker MG, Kvalsvig A, Crengle S, Harwood M, Tukuitonga C, Betty B, et al. The next phase in Aotearoa New Zealand's COVID-19 response: a tight suppression strategy may be the best option. N Z Med J. 2021;134:8–16.
24. Ministry of Health, Manatū Hauora. New Zealand Influenza Pandemic Plan—a framework for action. 2nd ed. Wellington (New Zealand): Ministry of Health; 2017.
25. Summers J, Baker M, Wilson N. Mortality declines in Aotearoa NZ during the first two years of the Covid-19 pandemic. 2022 Feb 22 [cited 2023 Jan 3]. https://www.phcc.org.nz/briefing/mortality-declines-aotearoa-nz-during-first-two-years-covid-19-pandemic
26. Public Health Agency. COVID-19 mortality in Aotearoa New Zealand: inequities in risk. Wellington (New Zealand): Ministry of Health; 2022.
27. Kvalsvig A, Brooks A, Wilson N, Bennett J, Summers J, Timu-Parata C, et al. Longer-term harm from Covid-19 in children: the evidence suggests greater efforts are needed to protect children in Aotearoa NZ from infection. 2022 Mar 8 [cited 2023 Jan 3]. https://www.phcc.org.nz/briefing/longer-term-harm-covid-19-children-evidence-suggests-greater-efforts-are-needed-protect
28. Mamelund, S-E, Dimka J. Not the great equalizers: Covid-19, 1918–20 influenza, and the need for a paradigm shift in pandemic preparedness. Popul Stud (Camb). 2021;75:179–99.
29. COVID-19 Forecasting Team. Variation in the COVID-19 infection-fatality ratio by age, time, and geography during the pre-vaccine era: a systematic analysis. Lancet. 2022; 399:1469–88. https://doi.org/10.1016/S0140-6736(21)02867-1
30. Worobey M, Han G-Z, Rambaut A. A synchronized global sweep of the internal genes of modern avian influenza virus. Nature. 2014;508:254–7. https://doi.org/10.1038/nature13016
31. Morens DM, Taubenberger JK, Fauci AS. A centenary tale of two pandemics: the 1918 influenza pandemic and COVID-19, part I. Am J Public Health. 2021;111:1086–94. https://doi.org/10.2105/AJPH.2021.306310
32. Harari S, Tahor M, Rutsinsky N, Meijer S, Miller D, Henig O, et al. Drivers of adaptive evolution during chronic SARS-CoV-2 infections. Nat Med. 2022;28:1501–8. https://doi.org/10.1038/s41591-022-01882-4
33. Vynnycky E, Trindall A, Mangtani P. Estimates of the reproduction numbers of Spanish influenza using morbidity data. Int J Epidemiol. 2007;36:881–9. https://doi.org/10.1093/ije/dym071
34. Nuzum JW, Pilot I, Stangl FH, Bonar BE. Pandemic influenza and pneumonia in a large civil hospital. JAMA. 1918;71:1562–5. https://doi.org/10.1001/jama.1918.26020450009011a
35. Lessler J, Reich NG, Brookmeyer R, Perl TM, Nelson KE, Cummings DAT. Incubation periods of acute respiratory viral infections: a systematic review. Lancet Infect Dis. 2009;9:291–300. https://doi.org/10.1016/S1473-3099(09)70069-6
36. Liu Y, Rocklöv J. The effective reproductive number of the Omicron variant of SARS-CoV-2 is several times relative to Delta. J Travel Med. 2022;29:taac037.
37. He D, Zhao S, Li Y, Cao P, Gao D, Lou Y, et al. Comparing COVID-19 and the 1918–19 influenza pandemics in the United Kingdom. Int J Infect Dis. 2020;98:67–70. https://doi.org/10.1016/j.ijid.2020.06.075
38. Wu Y, Kang L, Guo Z, Liu J, Liu M, Liang W. Incubation period of COVID-19 caused by unique SARS-CoV-2 strains: a systematic review and meta-analysis. JAMA Netw Open. 2022;5:e2228008–2228008. https://doi.org/10.1001/jamanetworkopen.2022.28008
39. Yu X, Tsibane T, McGraw PA, House FS, Keefer CJ, Hicar MD, et al. Neutralizing antibodies derived from the B cells of 1918 influenza pandemic survivors. Nature. 2008;455:532–6. https://doi.org/10.1038/nature07231
40. Prillaman M. One coronavirus infection wards off another—but only if it's a similar variant. Nature. 2022 Jul 14 [Epub ahead of print]. http://doi.org/10.1038/d41586-022-01914-6
41. Tokars JI, Olsen SJ, Reed C. Seasonal incidence of symptomatic influenza in the United States. Clin Infect Dis. 2018;66:1511–8. https://doi.org/10.1093/cid/cix1060
42. King M. The 1918 pandemic: 'People were just dying everywhere.' E-Tangata. 2021 Nov 7 [cited 2023 Jan 3]. https://e-tangata.co.nz/history/the-1918-pandemic-people-were-just-dying-everywhere
43. Mamelund S-E. Geography may explain adult mortality from the 1918–20 influenza pandemic. Epidemics. 2011;3:46–60. https://doi.org/10.1016/j.epidem.2011.02.001
44. Telenti A, Arvin A, Corey L, Corti D, Diamond MS, García-Sastre A, et al. After the pandemic: perspectives on the future trajectory of COVID-19. Nature. 2021;596:495–504. https://doi.org/10.1038/s41586-021-03792-w
45. Mefsin YM, Chen D, Bond HS, Lin Y, Cheung JK, Wong JY, et al. Epidemiology of infections with SARS-CoV-2 Omicron BA.2 variant, Hong Kong, January–March 2022. Emerg Infect Dis. 2022;28:1856–8.
46. World Health Organization. 14.9 million excess deaths associated with the COVID-19 pandemic in 2020 and 2021. 2022 [cited 2023 Jan 2]. https://www.who.int/news/

item/05-05-2022-14.9-million-excess-deaths-were-associated-with-the-covid-19-pandemic-in-2020-and-2021
47. Kvalsvig A, Baker MG. How Aotearoa New Zealand rapidly revised its Covid-19 response strategy: lessons for the next pandemic plan. J R Soc N Z. 2021;51:S143–66.
48. Baker MG, Wilson N, Blakely T. Elimination could be the optimal response strategy for COVID-19 and other emerging pandemic diseases. BMJ. 2020;371:m4907. https://doi.org/10.1136/bmj.m4907
49. Taquet M, Dercon Q, Luciano S, Geddes JR, Husain M, Harrison PJ. Incidence, co-occurrence, and evolution of long-COVID features: a 6-month retrospective cohort study of 273,618 survivors of COVID-19. PLoS Med. 2021;18:e1003773. https://doi.org/10.1371/journal.pmed.1003773
50. New Zealand Government–Te Kāwanatanga o Aotearoa. Summary of the terms of reference for the Royal Commission of Inquiry into lessons learned from Aotearoa New Zealand's response to COVID-19 that should be applied in preparation for a future pandemic [cited 2023 Jan 3]. https://www.beehive.govt.nz/sites/default/files/2022-12/Summary%20of%20ToR%20for%20Royal%20Commission%20into%20COVID%20and%20any%20future%20pandemic.pdf

Address for correspondence: Jennifer Summers, University of Otago Wellington Public Health, 23A Mein St, Newtown, Wellington 6242 New Zealand; email: jennifer.summers@otago.ac.nz

Emergence of GII.4 Sydney [P16]-like Norovirus-Associated Gastroenteritis, China, 2020–2022

Yuanyun Ao,[1] Lijuan Lu,[1] Jin Xu

Newly evolved GII.4 Sydney[P16] norovirus with multiple residue mutations, already circulating in parts of China, became predominant and caused an abrupt increase in diagnosed norovirus cases among children with gastroenteritis in Shanghai during 2021–2022. Findings highlight the need for continuous long-term monitoring for SHGII.4-2020 and emergent GII.4 norovirus variants.

Norovirus, the main cause of nonbacterial acute gastroenteritis (AGE) outbreaks worldwide (*1*), is a positive-sense, single-stranded RNA virus within the family Caliciviridae. Its genome contains 3 open reading frames (ORFs): ORF1 encodes a polyprotein cleaved into 6 nonstructural proteins, including RNA-dependent RNA polymerase (RdRp); ORF2 encodes major (VP1) and ORF3 minor (VP2) capsid proteins (*2*). On the basis of VP1 amino acid sequences, noroviruses can be grouped into 10 genogroups (GI–GX) and 49 genotypes (*3*); GI and GII genogroups are the most common in human infections.

Since 2002, GII.4 has been the predominant norovirus genotype worldwide (*4*,*5*). GII.4 Sydney norovirus recombinant with a GII.P31 polymerase, GII.4 Sydney[P31], emerged in 2012 and caused pandemic illness during 2012–2013 (*6*). However, in 2015, a recombinant GII.4 Sydney[P16] norovirus emerged and recently became predominant in some Western countries (*7*–*10*). GII.4 Sydney[P16] norovirus has advantageous epidemic potential because of viral fitness from its recombinant components: emerging GII.P16 polymerase and persistently mutating GII.4 VP1 (*11*,*12*). Although GII.4 Sydney[P16] norovirus prevalence has rarely been reported in China (*13*), its advantageous qualities raise concerns about the virus possibly causing an epidemic. To monitor epidemiologic and genetic data from GII.4 Sydney[P16] norovirus in China, we performed laboratory-based surveillance of noroviruses among children with AGE in Shanghai.

The Study

Beginning in 2016, fecal specimens were collected from children ≤5 years of age with AGE seen as outpatients at Children's Hospital of Fudan University in Shanghai; case-patients from local outbreaks were excluded. AGE is defined as 3 episodes of loose feces or 2 episodes of vomiting within 24 hours. We tested fecal samples for GI and GII norovirus by dual-genotyped reverse transcription PCR (RT-PCR), as described elsewhere (*14*). We genotyped sequences using the norovirus typing tool of the Dutch National Institute for Public Health and the Environment (https://www.rivm.nl/mpf/norovirus/typingtool). We measured concentrations of viral RNA in norovirus-positive samples using real-time RT-PCR with primers/probe targeting the conserved ORF1–ORF2 junction, as described elsewhere (*15*).

We determined that, during January 2016–March 2022, a total of 301/2,419 (12.4%) fecal samples from cases in children were norovirus-positive (Figure 1, panel A). Annually, the peak number of norovirus cases has been detected in samples taken during winter, exhibiting a seasonal characteristic. Each year during 2016–2019, there were <60 norovirus cases; during 2020, the first year of the COVID-19 pandemic, norovirus activity abruptly decreased to 13 cases, but rates then unexpectedly increased to 110 cases in 2021, a trend similar to the proportion of norovirus cases among all gastroenteritis cases (data not shown). Of note, 40 (36.4%) cases were identified in samples taken during November–December 2021; a

Author affiliations: Children's Hospital of Fudan University Department of Clinical Laboratory, Shanghai, China (Y. Ao, L. Lu, J. Xu). Shanghai Institute of Infectious Disease and Biosecurity of Fudan University, Shanghai, China (J. Xu).

DOI: https://doi.org/10.3201/eid2909.230383

[1]These authors contributed equally to this article.

total of 11 cases were detected in samples taken during January–March 2022.

We observed a dynamic profile of norovirus genotypes in cases among children during 2016–2022 (Figure 1, panel B). Before the COVID-19 pandemic, the predominant genotypes were GII.4 Sydney[P31] during 2016–2017 and GII.4 Sydney[P31] and GII.3[P12] during 2018–2019; however, GII.4 Sydney[P16] suddenly emerged in November 2020 and predominated in 2021. Of 110 norovirus samples in 2021, we successfully genotyped 100. GII.4 Sydney[P16], the predominant genotype, was identified in 60 (60%) samples, followed by GII.4 Sydney[P31] in 14 (14%), GII.2[P16] in 9 (9%), GII.3[P12] in 7 (7%), GII.17[P17] in 3 (3%), GII.6[P7] in 3 (3%), and other genotypes in 2 (2%). Of note, the proportion of GII.4 Sydney[P16] cases rose sharply to 42/55 (76.4%) during October–December 2021 and 7/11 (70%) cases during January–March 2022.

Using high-throughput sequencing, we identified 23 complete genomes of GII.4 Sydney[P16] (GenBank accession nos. OP037976–83 and OQ940068–82) from fecal samples. Maximum-likelihood phylogenetic trees of GII.4 Sydney[P16] full-length RdRp and VP1 genes all showed that 22 strains from November 2020–December 2021 clustered together with strains recently identified in Beijing (GenBank accession nos. OL336332.1, OL336335.1–41.1, and OL336352.1–89.1), Taiwan (ON329737.1), and Thailand (MW521126.1–7.1 and MW521129.1–30.1)

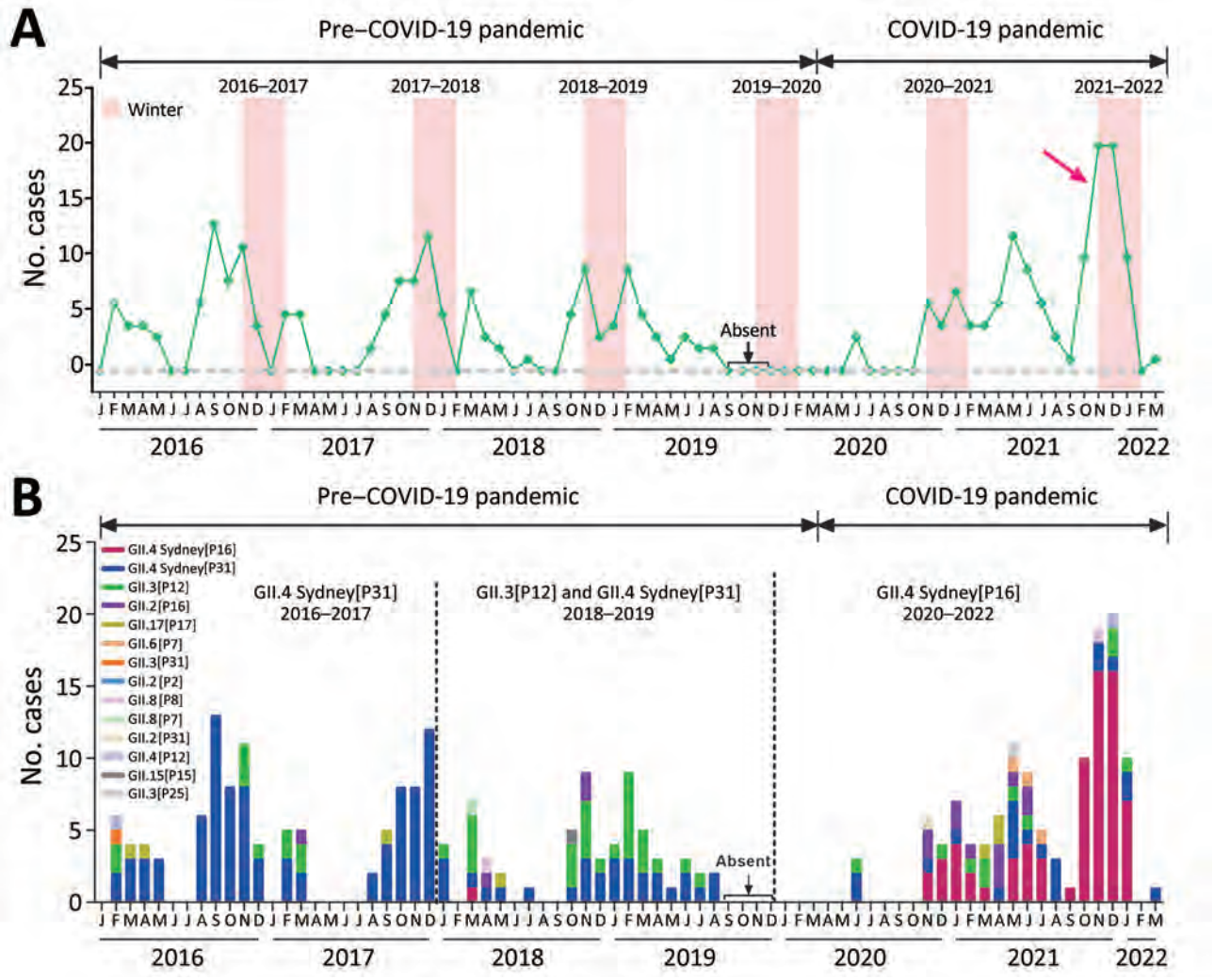

Figure 1. Emergence of recombinant GII.4 Sydney[P16] norovirus associated with acute gastroenteritis among children treated as outpatients in Shanghai, before and during COVID-19 pandemic, Shanghai, China, during January 2016–March 2022. A) Numbers of cases of norovirus-associated acute gastroenteritis. Red arrow indicates an abrupt increase in norovirus activity. B) Genotype (polymerase-capsid) distribution of norovirus. Different norovirus genotypes are indicated by color (key). Start date of COVID-19 pandemic declared by World Health Organization was March 11, 2020; absent labels indicate period (September–December 2019) during which fecal sample collection was paused.

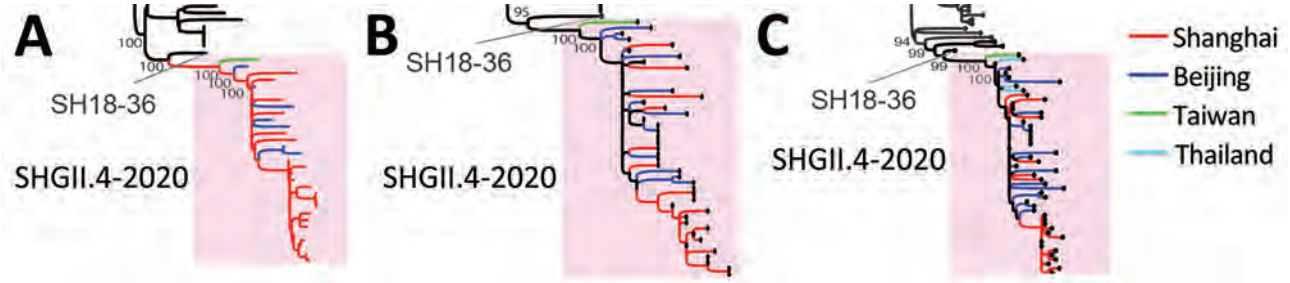

Figure 2. Phylogenetic analysis of newly identified GII.4 Sydney[P16] noroviruses in Shanghai, China, 2020–2022. Maximum-likelihood phylogenetic trees show complete genome (A), RNA-dependent RNA polymerase (RdRp) (B), and VP1 (C) gene sequences for newly identified GII.4 Sydney[P16] strains (n = 23) in Shanghai. A total of 123 genomic sequences, 162 RdRp, and 220 VP1 nucleotide sequences were collected for analyses from GenBank by BLASTN (https://blast.ncbi.nlm.nih.gov/Blast.cgi) relative to sequence of SH18-36. All trees were generated with datasets of 1,000 replicates by PhyML 3.1 (http://www.atgc-montpellier.fr/phyml/versions.php). Pink shading indicates new sublineage (tentatively named SHGII.4-2020) in GII.4 Sydney[P16] cluster. Branches of each strain in SHGII.4-2020 are indicated by color according to identified positions; red indicates GII.4 Sydney[P16] strains identified in this study, except SH18-36. Numbers on ancestral nodes represent node support values.

(Appendix Table, https://wwwnc.cdc.gov/EID/article/29/9/23-0383-App1.pdf), which evolved into a genetically distinct sublineage (tentatively named SHGII.4-2020) in the GII.4 Sydney[P16] cluster (Figure 2). All trees showed SHGII.4-2020 most closely related to SH18-36, the first identified GII.4 Sydney[P16] strain in our study, implying that SH18-36 might constitute an evolutionary ancestor of SHGII.4-2020.

Compared with sequences of GII.4 Sydney[P16] strains from GenBank, SHGII.4-2020 had 19 aa mutations: 10 in nonstructural proteins (T169S and L305F in p48; K84R, V88I and I168V in p22; K103R in VPg; K54R, V125A, A311T and N427T in RdRp), 2 in VP1 (R297H and D372N), and 7 in VP2 (K80R, A108V, A128S, N157T, T164A, I174T and N207S) (Appendix Figure 1). In VP1, R297H and D372N substitutions were mapped to the main antigenic epitope A, and D372N was also present around the HBGA binding site II (Appendix Figure 2). Those 2 residues, 297H and 372N, were only identified in certain previous GII.4 Sydney[P16] strains (MG002631.1, MH922876, and MK754444). Three substitutions, K54R, V125A, and N427T, were located on the surface of RdRp (Appendix Figure 2); A312T resided adjacent to motif B. In addition, we found 7 unique mutations in Shanghai strains. Further studies of these SHGII.4-2020 mutations are needed to better understand their role in its emergence.

We performed comparative clinical analysis of SHGII.4-2020, GII.4 Sydney[P31] and GII.3[P12] cases. The median age of SHGII.4-2020 case-patients (21.5 months, interquartile range [IQR] 15–50.3 months) was older than those for GII.4 Sydney[P12] (12 months, IQR

Table. Comparisons of sociodemographic and clinical characteristics between GII.4 Sydney[P16] norovirus and GII.4 Sydney[P31]/GII.3[P12] norovirus infection in norovirus–positive children, Shanghai, China, January 2016–March 2022*

Characteristic	GII.4 Sydney[P16]	GII.4 Sydney[P31]	p value†	GII.3[P12]	p value‡
Total no. patients	63	120		47	
Median patient age, mo (IQR)	21.5 (15–50.3)	12 (9–19.3)	<0.0001§	12 (8–26.75)	0.004§
Age range, mo					
<12	9 (14.3)	47 (39.2)	**0.001¶**	18 (38.3)	**0.004¶**
12–36	31 (49.2)	63 (52.5)	0.672¶	19 (40.4)	0.360¶
>36	23 (36.5)	10 (8.3)	**<0.001**	10 (21.3)	**0.085¶**
F:M ratio	0.58:1	0.5:1	0.744#	0.48:1	0.688#
Signs/symptoms					
Total no. patients with signs/symptoms	60	112	NA	44	NA
Diarrhea	45 (75.0)	93 (83.0)	0.586¶	33 (75.0)	0.579¶
Duration ≤5 d	33 (73.3)	64 (68.8)	0.821¶	26 (78.8)	0.837¶
Duration >5 d	12 (26.7)	29 (31.2)	0.687¶	7 (21.2)	0.664¶
Vomiting	35 (58.3)	40 (35.7)	**<0.001¶**	17 (38.6)	**0.047¶**
Fever	18 (30.0)	20 (17.9)	0.067¶	17 (38.6)	0.357¶
Abdominal cramps	9 (15)	2 (1.8)	0.02¶	6 (13.6)	0.845¶

*Values are no. (%) patients except as indicated. Bold indicates statistical significance. NA, not applicable
†Denotes comparison between GII.4 Sydney[P16] and GII.4 Sydney[P31].
‡Indicates comparison between GII.4 Sydney[P16] and GII.3[P12].
§By χ^2 test.
¶For the comparison of the median age between groups; calculated by Mann-Whitney U-test.
#By Fisher exact test.

9–19.3 months) and GII.3[P12] (12 months, IQR 8–26.75 months; p<0.005) case-patients (Table). We observed SHGII.4-2020 more commonly than GII.4 Sydney[P31] among children >36 months of age, whereas the converse was true among children <12 months of age (p<0.005) (Table). Vomiting was a more common clinical sign among SHGII.4-2020 case-patients than among GII.4 Sydney[P31] and GII.3[P12] case-patients (p<0.05) (Table). The median viral RNA load (cycle threshold value) for SHGII.4-2020 (15.86, IQR 13.95–18.74) was higher than those for GII.4 Sydney[P31] (17.00, IQR 15.11–20.32; p = 0.0372) and GII.3[P12] (17.98, IQR 15.76–21.75; p = 0.0093) (Appendix Figure 3). Five samples with high cycle threshold values (>25.0) for each genotype were randomly selected for primer/probe sequence mismatch analysis; no mismatch was found.

Conclusions

We provide evidence that GII.4 Sydney[P16] norovirus has evolved into a new sublineage, SHGII.4-2020, that carries multiple mutations and is circulating in different regions of China. We found that SHGII.4-2020 became the predominant norovirus genotype and resulted in an abrupt increase in diagnosed cases among children treated as outpatients at a hospital in Shanghai during 2021–2022. Based on data from CaliciNet China, GII.2[P16] was identified as the dominant genotype in 2016–2020 norovirus outbreaks in China (*13*), but more recent data have not been reported. The viral load for SHGII.4-2020 was higher than for GII.4 Sydney[P31] and GII.3[P12] noroviruses, suggesting the higher viral replication efficiency and transmissibility of SHGII.4-2020. However, further multivariate analyses are needed to exclude potential confounding factors, such as time interval from sign and symptom onset to sample collection, which may have biased those results. The higher proportion of case-patients experiencing vomiting during infection with SHGII.4-2020 is of particular clinical and epidemiologic interest because this symptom profile may affect how that norovirus strain spreads and cause a changes in epidemiology. Although our study was limited by a small number of cases and its single-center setting, our findings highlight the need for continuous long-term monitoring for global spread of SHGII.4-2020 and emergence of newly evolving GII.4 norovirus variants.

This work was supported by grants from the National Natural Science Foundation of China (no. 82202495), General Project of Natural Science Foundation of Shanghai (no. 22ZR1408200), and the Key Development Program of the Children's Hospital of Fudan University (no. EK2022ZX05).

About the Author

Dr. Ao is a virologist in the Department of Clinical Laboratory, Children's Hospital of Fudan University, National Children's Medical Center. His research interests include evolutionary analysis and epidemic mechanisms of emerging enteric viruses.

References

1. Ahmed SM, Hall AJ, Robinson AE, Verhoef L, Premkumar P, Parashar UD, et al. Global prevalence of norovirus in cases of gastroenteritis: a systematic review and meta-analysis. Lancet Infect Dis. 2014;14:725–30. https://doi.org/10.1016/S1473-3099(14)70767-4
2. Robilotti E, Deresinski S, Pinsky BA. Norovirus. Clin Microbiol Rev. 2015;28:134–64. https://doi.org/10.1128/CMR.00075-14
3. Chhabra P, de Graaf M, Parra GI, Chan MC, Green K, Martella V, et al. Updated classification of norovirus genogroups and genotypes. J Gen Virol. 2019;100:1393–406. https://doi.org/10.1099/jgv.0.001318
4. Siebenga JJ, Vennema H, Zheng DP, Vinjé J, Lee BE, Pang XL, et al. Norovirus illness is a global problem: emergence and spread of norovirus GII.4 variants, 2001–2007. J Infect Dis. 2009;200:802–12. https://doi.org/10.1086/605127
5. Vinjé J, Altena SA, Koopmans MP. The incidence and genetic variability of small round-structured viruses in outbreaks of gastroenteritis in the Netherlands. J Infect Dis. 1997;176:1374–8. https://doi.org/10.1086/517325
6. van Beek J, Ambert-Balay K, Botteldoorn N, Eden JS, Fonager J, Hewitt J, et al.; NoroNet. Indications for worldwide increased norovirus activity associated with emergence of a new variant of genotype II.4, late 2012. Euro Surveill. 2013;18:8–9. https://doi.org/10.2807/ese.18.01.20345-en
7. Barclay L, Cannon JL, Wikswo ME, Phillips AR, Browne H, Montmayeur AM, et al. Emerging novel GII.P16 noroviruses associated with multiple capsid genotypes. Viruses. 2019;11:11. https://doi.org/10.3390/v11060535
8. Cannon JL, Barclay L, Collins NR, Wikswo ME, Castro CJ, Magaña LC, et al. Genetic and epidemiologic trends of norovirus outbreaks in the United States from 2013 to 2016 demonstrated emergence of novel GII.4 recombinant viruses. J Clin Microbiol. 2017;55:2208–21. https://doi.org/10.1128/JCM.00455-17
9. Bidalot M, Théry L, Kaplon J, De Rougemont A, Ambert-Balay K. Emergence of new recombinant noroviruses GII.p16-GII.4 and GII.p16-GII.2, France, winter 2016 to 2017. Euro Surveill. 2017;22:30508. https://doi.org/10.2807/1560-7917.ES.2017.22.15.30508
10. Lun JH, Hewitt J, Yan GJH, Enosi Tuipulotu D, Rawlinson WD, White PA. Recombinant GII.P16/GII.4 Sydney 2012 was the dominant norovirus identified in Australia and New Zealand in 2017. Viruses. 2018;10:548. https://doi.org/10.3390/v10100548
11. Tohma K, Lepore CJ, Ford-Siltz LA, Parra GI. Phylogenetic analyses suggest that factors other than the capsid protein play a role in the epidemic potential of GII.2 norovirus. mSphere. 2017;2:e00187-17. https://doi.org/10.1128/mSphereDirect.00187-17
12. Parra GI, Tohma K, Ford-Siltz LA, Eguino P, Kendra JA, Pilewski KA, et al. Minimal antigenic evolution after a decade of norovirus GII.4 Sydney_2012 circulation in

humans. J Virol. 2023;97:e0171622. https://doi.org/10.1128/jvi.01716-22
13. Zhu X, He Y, Wei X, Kong X, Zhang Q, Li J, et al. Molecular epidemiological characteristics of gastroenteritis outbreaks caused by norovirus GII.4 Sydney [P31] strains—China, October 2016–December 2020. China CDC Wkly. 2021;3:1127–32. https://doi.org/10.46234/ccdcw2021.276
14. Ao Y, Wang J, Ling H, He Y, Dong X, Wang X, et al. Norovirus GII.P16/GII.2-associated gastroenteritis, China, 2016. Emerg Infect Dis. 2017;23:1172–5. https://doi.org/10.3201/eid2307.170034
15. Kageyama T, Kojima S, Shinohara M, Uchida K, Fukushi S, Hoshino FB, et al. Broadly reactive and highly sensitive assay for Norwalk-like viruses based on real-time quantitative reverse transcription-PCR. J Clin Microbiol. 2003;41:1548–57. https://doi.org/10.1128/JCM.41.4.1548-1557.2003

Addresses for correspondence: Jin Xu or Yuanyun Ao, Children's Hospital of Fudan University, National Children's Medical Center, 399 Wanyuan Rd, Min-hang District, Shanghai 201102, China; email: jinxu125@163.com or 727643776@qq.com

Highly Pathogenic Avian Influenza A(H5N1) Clade 2.3.4.4b Virus in Wild Birds, Chile

Naomi Ariyama,[1] Catalina Pardo-Roa,[1] Gabriela Muñoz, Carolina Aguayo, Claudia Ávila, Christian Mathieu, Leonardo I. Almonacid, Rafael A. Medina, Barbara Brito, Magdalena Johow, Victor Neira

In December 2022, highly pathogenic avian influenza A(H5N1) clade 2.3.4.4b virus emerged in Chile. We detected H5N1 virus in 93 samples and obtained 9 whole-genome sequences of strains from wild birds. Phylogenetic analysis suggests multiple viral introductions into South America. Continued surveillance is needed to assess risks to humans and domestic poultry.

Highly pathogenic avian influenza (HPAI) A(H5N1) viruses grouped within hemagglutinin (HA) gene clade 2.3.4.4b are spreading globally and causing high mortality among domestic and wild birds (*1*). In addition, the viruses have spilled over to several nonavian species, including humans (*2*). To contain HPAI outbreaks, poultry exposed to or infected with HPAI viruses have been culled, resulting in disposal of ≈131 million domestic birds globally in 2022 (*3*). Therefore, HPAI viruses pose a threat not only to public health because of zoonotic potential but also to food security.

In late 2021, HPAI H5N1 virus clade 2.3.4.4b, which had spread predominantly in Europe, Asia, and Africa, was detected in wild birds in North America and, shortly after, in domestic poultry (*3*–*5*). In October 2022, this virus reached South America and was officially reported in Colombia; it later was also reported in Peru, Ecuador, and Venezuela (*2*). We describe detection of this virus clade in wild birds in Chile.

Author affiliations: Universidad de Chile, Santiago, Chile (N. Ariyama, G. Muñoz, V. Neira); Pontificia Universidad Católica de Chile, Santiago (C. Pardo-Roa, L.I. Almonacid, R.A. Medina); Servicio Agrícola y Ganadero (SAG), Santiago (C. Aguayo, C. Ávila, C. Mathieu, M. Johow); Emory University, Atlanta, Georgia, USA (R.A. Medina); Icahn School of Medicine at Mount Sinai, New York, New York, USA (R.A. Medina); Department of Primary Industries, Menangle, New South Wales, Australia (B. Brito)

DOI: https://doi.org/10.3201/eid2909.230067

The Study

In early December 2022, increased wild bird deaths were detected across the north coast of Chile (Figure 1). Wild birds, mainly pelicans, were found dead or dying (Figure 2). By December 22, 2022, the official Veterinary Services of the Agricultural and Livestock Service of Chile had collected 1,368 samples for HPAI virus detection and epidemiologic investigation: 1,080 from domestic birds and 288 from wild birds (Appendix Table 1, https://wwwnc.cdc.gov/EID/article/29/9/23-0067-App1.pdf). We performed a total of 578 real-time qualitative reverse transcription PCR (qRT-PCR) reactions to detect active avian influenza virus (AIV) infection and 754 agar gel immunodiffusion (AGID) tests to detect previous AIV exposure (Appendix Table 2).

We initially performed qRT-PCR by using VetMAX-Gold AIV Detection Kit (Applied Biosystems/Thermo Fisher Scientific, https://www.thermofisher.com), targeting the AIV matrix gene. Then, we tested positive samples with specific H5 qRT-PCR according to US Department of Agriculture (USDA) National Veterinary Services Laboratories standard protocols (nos. 1732.02, 1767.01, and 1768.01). We tested 13 tissue samples, 2 (15%) of which were positive; 248 tracheal swab samples, 43 (17%) of which were positive; 314 cloacal swab samples, 47 (15%) of which were positive; and 3 oral swab samples, 1 (33%) of which was positive. Among all samples tested by qRT-PCR, 93 (16%) were H5 AIV–positive with cycle threshold (Ct) values <40. Among positive samples, 18 were from the Arica y Parinacota region, 18 were from Tarapaca, 53 were from Antofagasta, and 4 were from Atacama (Figure 1). No domestic poultry samples were AIV-positive, but among wild bird species, H5 AIV was detected most frequently among Peruvian pelicans (*Pelecanus thagus*) (n = 50, 54%), turkey vultures

[1]These first authors contributed equally to this article.

(*Cathartes aura*) (n = 12, 13%), and Peruvian boobies (*Sula variegata*) (n = 10, 11%) (Appendix Table 1).

We evaluated 754 serum samples by using the official AGID against AIV antigens ribonucleoprotein and matrix protein, according to USDA protocols (https://www.aphis.usda.gov/animal_health/lab_info_services/downloads/Avian_AGID_SOP.pdf) (*6*). We found no positive serum samples (Appendix Table 2).

We selected 11 H5 AIV–positive samples from the initial outbreak according to Ct values (Ct <27) and location; 9 samples were from pelicans and 2 from gulls, representing 3 administrative regions of Chile. We obtained whole-genome AIV sequences by initial amplification using a multisegment 1-step RT-PCR (*7*), then performed next-generation nanopore sequencing by using the Native Barcoding Kit 96 and MinION platform (Oxford Nanopore Technologies, https://nanoporetech.com), according to the manufacturer's instructions. We filtered nanopore reads in FASTQ (https://github.com/mcollina/fastq) according to the average quality (Phred score ≥7) and length ≤2,600 bp by using NanoFit (*8*). We assembled genomes according to reference by using the nanopore ARTIC pipeline version 1.2.3 (https://artic.network), which we modified by using a relevant reference and to account for the primer sets (Appendix). We used influenza strain A/*Falco_rusticolus*/EdoMex/CPA-19638–22/2022(H5N1) (GenBank accession nos. OP691321–28) as the reference. We used the National Center for Biotechnology Information Influenza Virus Sequence Annotation Tool (*9*) to check and annotate

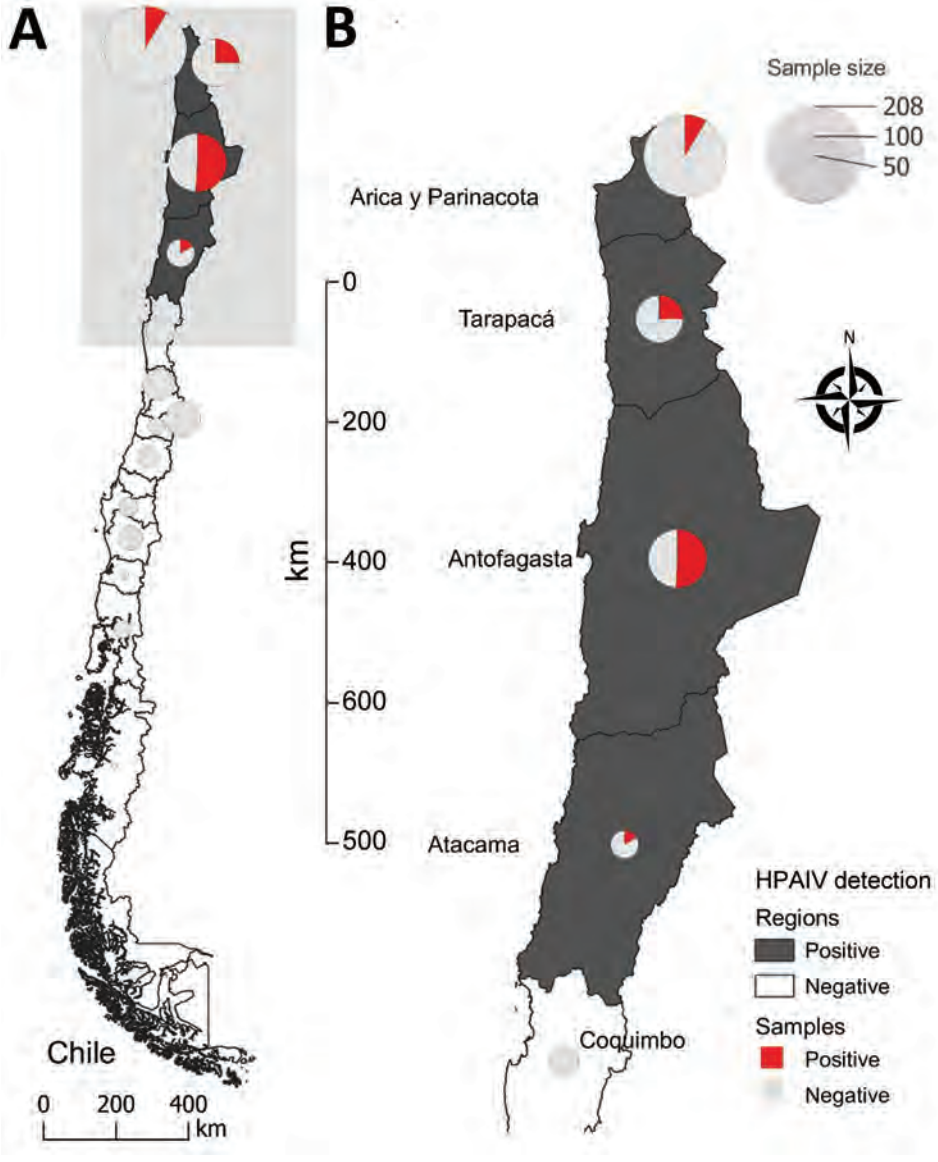

Figure 1. Distribution of samples collected and tested for HPAIV H5N1 clade 2.3.4.4b virus in wild birds, Chile. A) Map of Chile shows regions positive and negative for HPAIV. B) Detail of area in which affected birds were sampled. Size and color of circles indicate sample size and percent positivity. HPAIV, highly pathogenic avian influenza virus.

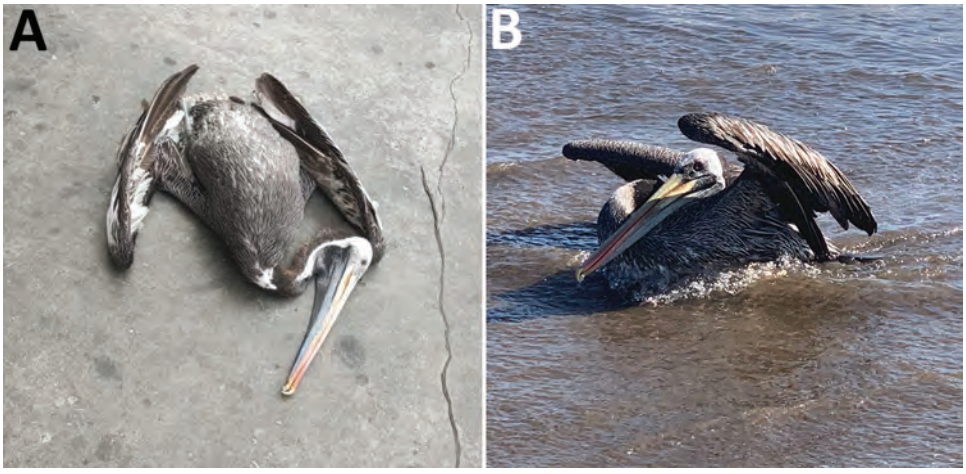

Figure 2. Images of Peruvian pelicans (*Pelecanus thagus*) collected and sampled for highly pathogenic avian influenza virus H5N1 clade 2.3.4.4b, Chile. A) Dead pelican found on land near shoreline; B) ill pelican in water near shoreline.

assembled genomes and conducted H5 clade classification by using an online subspecies classification tool (*10*). We conducted a BLAST search (https://blast.ncbi.nlm.nih.gov/Blast.cgi) to choose the reference from preliminary assembled contigs constructed with filtered reads that we de novo assembled by using Canu (*11*). We obtained sequences with a mean coverage depth of 33,381× for 10 samples; 9 of 10 genomes were complete (Appendix Table 3).

All positive samples were classified as H5 subtype clade 2.3.4.4b. We inferred Bayesian evolutionary analysis sampling trees for HA and neuraminidase (NA), and maximum-likelihood trees for internal segments (Appendix). A/Peru/LIM-003/2022 and A/Peru/LAM-002/2022 (GISAID accession nos. EPI_ISL_16249730 and EPI_ISL_16249681) were the most closely related HA sequences found in the GISAID database (*12*) (Appendix Figure 1). We observed similar results from phylogenies for NA and internal genes (Appendix Figures 2–8). Sequences from Peru corresponded to isolates collected in November 2022 from domestic chickens from Lima (12′S latitude) and Lambayeque (6′S latitude). On internal gene analyses, HPAI virus sequences available from Ecuador and Mexico grouped closely to the Chile–Peru subcluster (Appendix Figures 3–8). For HA, the Chile–Peru subcluster showed a nonsynonymous mutation, T392A (L131Q), previously associated with antigenic variability in H5N1 virus strains (*13*). We found other synonymous and nonsynonymous mutations in NA (L269M and S339P) and internal genes (Appendix Table 4), but those mutations have not been associated with phenotypic changes.

The phylogenetic tree for the HA segment showed that the sequences from Chile and Peru were closely related to a recent ancestor from North America that was detected during October–November 2022, and the Chile–Peru sequences had closely related ancestors among strains from North America (Appendix Figure 1). A sequence from Ecuador grouped in a paraphyletic branch with different sequences from North America and had a time to most recent common ancestor estimated at August 27, 2022 (95% highest posterior density July 10–September 21). The sequences from Venezuela had a longer branch in the phylogeny reconstruction. Those sequences were more closely related to strains collected earlier in the year from North America and had a time to most recent common ancestor estimated at February 2, 2022 (95% highest posterior density January 15–February 23). The NA, matrix, and polymerase acidic sequences from Venezuela also grouped outside the Chile–Peru subcluster in the maximum-likelihood phylogenies (Appendix Figures 2, 5, 7). The phylogenetic clustering with different sequences from North America suggests that viruses from Venezuela might have resulted from separate introductions into South America. However, because of the low availability of HPAI H5N1 virus sequences from Central and South America, conclusions on the origin of the cluster in Chile are limited.

Previous studies suggest that the HPAI H5N1 virus clade 2.3.4.4b was introduced into North America multiple times across the East Asia–Australasia/Pacific and Atlantic Flyways and was subsequently disseminated to other flyways (*4*,*14*,*15*). The flyways reach the southernmost tip of South America, representing a high-risk route for HPAIV dissemination across the continent.

Conclusions

According to official data, as of January 18, 2023, HPAI H5N1 viruses have disseminated as far as the

Maule region (35 south latitude) of Chile; no poultry cases have been confirmed. The Agricultural and Livestock Service of Chile implemented a contingency plan to perform extensive surveillance and reinforce biosecurity measurements to avoid introduction of HPAI virus into domestic poultry. The impact of HPAI H5N1 virus in the country, and the potential for introduction of the virus from Chile to Antarctica, remain to be fully elucidated.

This article was preprinted at https://doi.org/10.1101/2023.04.07.535949.

Acknowledgments

We thank the Agricultural and Livestock Service (SAG) personnel for their support and contributions, especially in sample collection. We are grateful to Belen Aguero and Felipe Berrios for their help in sample processing. We are grateful to the GISAID EpiFlu Database, laboratories, and source of original data of influenza A virus sequences, especially to the Servicio Nacional de Sanidad Agraria del Perú–SENASA, Peru, source of the closest strains.

This study was funded by Fondecyt 1211517 (to V.N.) and the Center for Research on Influenza Pathogenesis and Transmission (contract no. 75N93021C00014, awarded to R.A.M. and V.N.) and Emory CEIRR (contract no. 75N93021C00017 awarded to C.P.R, V.N., and R.A.M.), both part of the National Institute of Allergy and Infectious Diseases Centers of Excellence for Influenza Research and Surveillance.

About the Author

Dr. Ariyama is a veterinarian and PhD candidate at the University of Chile, Santiago, Chile. Her primary focus is the study of emerging viral zoonotic pathogens. Dr. Pardo-Roa is an assistant professor at the Molecular Virology Laboratory at Pontificia Universidad Católica de Chile, Santiago, Chile. Her focus is the study of influenza A viruses and next generation sequencing technologies.

References

1. Cui P, Shi J, Wang C, Zhang Y, Xing X, Kong H, et al. Global dissemination of H5N1 influenza viruses bearing the clade 2.3.4.4b HA gene and biologic analysis of the ones detected in China. Emerg Microbes Infect. 2022;11:1693–704. https://doi.org/10.1080/22221751.2022.2088407
2. World Health Organization. Assessment of risk associated with recent influenza A(H5N1) clade 2.3.4.4b viruses [cited 2023 Jan 18]. https://www.who.int/publications/m/item/assessment-of-risk-associated-with-recent-influenza-a(h5n1)-clade-2.3.4.4b-viruses
3. World Health Organization. Ongoing avian influenza outbreaks in animals pose risk to humans [cited 2023 July 12]. https://www.who.int/news/item/12-07-2023-ongoing-avian-influenza-outbreaks-in-animals-pose-risk-to-humans
4. Bevins SN, Shriner SA, Cumbee JC Jr, Dilione KE, Douglass KE, Ellis JW, et al. Intercontinental movement of highly pathogenic avian influenza A(H5N1) clade 2.3.4.4 virus to the United States, 2021. Emerg Infect Dis. 2022;28:1006–11. https://doi.org/10.3201/eid2805.220318
5. US Department of Agriculture. USDA confirms highly pathogenic avian influenza in a wild bird in South Carolina [cited 2022 Dec 27]. https://www.aphis.usda.gov/aphis/newsroom/stakeholder-info/sa_by_date/sa-2022/hpai-sc
6. Beard CW. Demonstration of type-specific influenza antibody in mammalian and avian sera by immunodiffusion. Bull World Health Organ. 1970;42:779–85.
7. Mena I, Nelson MI, Quezada-Monroy F, Dutta J, Cortes-Fernández R, Lara-Puente JH, et al. Origins of the 2009 H1N1 influenza pandemic in swine in Mexico. eLife. 2016;5:e16777. PubMed https://doi.org/10.7554/eLife.16777
8. De Coster W, D'Hert S, Schultz DT, Cruts M, Van Broeckhoven C. NanoPack: visualizing and processing long-read sequencing data. Bioinformatics. 2018;34:2666–9. https://doi.org/10.1093/bioinformatics/bty149
9. Bao Y, Bolotov P, Dernovoy D, Kiryutin B, Tatusova T. FLAN: a web server for influenza virus genome annotation. Nucleic Acids Res. 2007;35(Web Server issue):W280–4. https://doi.org/10.1093/nar/gkm354
10. Olson RD, Assaf R, Brettin T, Conrad N, Cucinell C, Davis JJ, et al. Introducing the Bacterial and Viral Bioinformatics Resource Center (BV-BRC): a resource combining PATRIC, IRD and ViPR. Nucleic Acids Res. 2023;51(D1):D678–89. https://doi.org/10.1093/nar/gkac1003
11. Koren S, Walenz BP, Berlin K, Miller JR, Bergman NH, Phillippy AM. Canu: scalable and accurate long-read assembly via adaptive *k*-mer weighting and repeat separation. Genome Res. 2017;27:722–36. https://doi.org/10.1101/gr.215087.116
12. Khare S, Gurry C, Freitas L, Schultz MB, Bach G, Diallo A, et al. GISAID's role in pandemic response. China CDC Wkly. 2021;3:1049–51. https://doi.org/10.46234/ccdcw2021.255
13. Li J, Gu M, Liu K, Gao R, Sun W, Liu D, et al. Amino acid substitutions in antigenic region B of hemagglutinin play a critical role in the antigenic drift of subclade 2.3.4.4 highly pathogenic H5NX influenza viruses. Transbound Emerg Dis. 2020;67:263–75. https://doi.org/10.1111/tbed.13347
14. Prosser DJ, Chen J, Ahlstrom CA, Reeves AB, Poulson RL, Sullivan JD, et al. Maintenance and dissemination of avian-origin influenza A virus within the northern Atlantic Flyway of North America. PLoS Pathog. 2022;18:e1010605. https://doi.org/10.1371/journal.ppat.1010605
15. Alkie TN, Lopes S, Hisanaga T, Xu W, Suderman M, Koziuk J, et al. A threat from both sides: Multiple introductions of genetically distinct H5 HPAI viruses into Canada via both East Asia-Australasia/Pacific and Atlantic flyways. Virus Evol. 2022;8(2):veac077. https://doi.org/10.1093/ve/veac077

Address for correspondence: Victor Neira, Departamento de Medicina Preventiva Animal, Facultad de Ciencias Veterinarias y Pecuarias, Universidad de Chile, 11735 Santa Rosa, La Pintana, Santiago, Chile; email: vneiraram@gmail.com; Magdalena Johow, Servicio Agrícola y Ganadero, Santiago, Chile; email: magdalena.johow@sag.gob.cl

Laboratory Diagnosis of Mpox, Central African Republic, 2016–2022

Sandra Garba-Ouangole,[1] Josephine Bourner,[1] Festus Mbrenga, Ella Gonofio, Benjamin Selekon, Alexandre Manirakiza, Ernest Kalthan, Christian Malaka, Yap Boum II, Piero Olliaro,[2] Emmanuel Nakouné[2]

During 2016–2022, PCR testing confirmed 100 mpox cases among 302 suspected cases in the Central African Republic. The highest detection rates were from active lesions (40%) and scabs (36%); cycle thresholds were lower (≈18) than those for blood samples (≈33). Results were consistent for generic primer– and clade I primer–specific PCR tests.

Mpox is caused by the monkeypox virus (MPXV), a double-stranded DNA orthopoxvirus with 2 known clades: clade I (formerly Congo Basin or Central African clade); and clade II (formerly West African clade), which encompasses 2 subclades (IIa and IIb) (*1*–*3*). Cases of mpox have been identified in the Central African Republic (CAR) since 2001 and have increased over time (*4*). The growing number of cases can be explained by the widening geographic spread of the disease and intensified case-finding activities (*5*). However, official figures probably underestimate the incidence of mpox, which principally occurs in remote areas, where many cases may go undetected because of a lack of diagnostic capacity.

The Ministry of Health and Population set up a passive surveillance program for mpox in 2010. Under this program, specimens are collected from all suspected case-patients with illness meeting the standardized case definition (Appendix, https://wwwnc.cdc.gov/EID/article/29/9/23-0514-App1.pdf), which is disseminated to all health professionals in CAR through regular training sessions and posters displayed in health facilities. Specimens are sent for biologic confirmation by PCR to the national reference laboratory at Institut Pasteur de Bangui (IPB). Whenever possible, contact tracing is conducted after identification of confirmed cases.

Since 2016, each specimen received at IPB is tested for MPXV by real-time PCR. After specimen processing, 200 μL of each sample are extracted by using the QIAamp Viral DNA Mini Kit (QIAGEN, https://www.qiagen.com) according to the manufacturer's instructions. The reactions are performed in 25 μL volume containing 12.5 μL of TaqMan Universal PCR Master Mix (Thermo Fisher Scientific, https://www.thermofisher.com), 4.5 μL of nuclease-free water (Thermo Fisher), 1 μL of each 10 μmol/L primer developed by TaqMan technology (Thermo Fisher), using the generic primer (G2RG) and clade I–specific (C3L) primers and 5 μL of extracted DNA (*6*). On the basis of these same concentrations, varicella zoster virus (VZV) primers (VZV open reading frame 63) are also used (*7*).

The Study

We conducted a retrospective descriptive study. By using results from all specimens collected from patients with suspected mpox under the national mpox surveillance program during 2016–2022, we aimed to describe the mpox landscape in CAR and evaluate the agreement of mpox test results (including cycle threshold [Ct] values) generated using the G2RG and C3L primers and different specimen types (blood, active lesion, or scab).

During 2016–2022, a total of 494 specimens (278 blood, 99 active lesion, 95 scab, and 22 oropharyngeal) from 302 patients were received and tested for suspected mpox at IPB. Of the total 302 suspected

Author affiliations: Institut Pasteur de Bangui, Bangui, Central African Republic (S. Garba-Ouangole, F. Mbrenga, E. Gonofio, C. Malaka, Y. Boum II, E. Nakouné); International Severe Acute Respiratory and Emerging Infection Consortium, Pandemic Sciences Institute, University of Oxford, Oxford, UK (J. Bourner); Ministry of Health and Population, Bangui (B. Selekon, A. Manirakiza, E. Kalthan)

DOI: https://doi.org/10.3201/eid2909.230514

[1]These first authors contributed equally to this article.

[2]These senior authors contributed equally to this article.

case-patients, 105 (35%) were positive for MPXV on >1 specimen (varying 19%–64% annually) (Figure 1). Of the 105 MPXV-positive patients, 3 (3%) were also positive for VZV. Of the 197 MPVX-negative patients, 82 (42%) were positive for VZV and 108 (55%) were negative for both MPXV and VZV. The remaining 7 patients were not tested for VZV.

The highest percentage of MPXV-positive specimens derived from the Lobaye and Mbomou prefectures, which together contributed 58% of mpox cases overall. MPXV detection rates varied by prefecture: Sangha Mbaere, 24/40 specimens (60%); Lobaye, 35/106 specimens (33%); Mbomou, 25/74 specimens (34%); and Bangui 2/41 specimens (5%) (Appendix Table 1).

Significantly more female patients were among MPXV-positive than VZV-positive case-patients (p = 0.03) but not among case-patients who were negative for both viruses. The median age across all suspected case-patients was 14 years; we observed no statistically significant difference between the median ages of confirmed case-patients with mpox (17 years) and VZV (20 years) infections. The median age of case-patients who tested negative on both tests was significantly lower (9 years) (Appendix Table 1).

Blood specimens were positive for MPXV on G2RG in 77/278 (28%) of cases, active lesions in 45/102 (44%), scabs in 36/98 (37%), and oropharyngeal specimens in 3/22 (14%) (Table 1). Of specimens returning a positive result on G2RG, the median Ct was 32.11 (interquartile range [IQR] 29.12–35.45) for blood specimens, 18.92 (IQR 17.42–23.43) for active lesions, 18.07 (16.19–19.82) for scabs, and 30.15 (28.04–32.56) for oropharyngeal specimens (Table 2). Similar values were returned by C3L. For paired specimens (Appendix Table 2), we observed either substantial (κ 0.61–0.80) or almost perfect (κ 0.81–1.00) agreement of a positive or negative result on pairwise comparisons of tests conducted on different specimens types on either G2RG or C3L.

The Ct values of G2RG and C3L on blood were significantly higher than in active lesion and scabs, whereas we observed no difference between active lesion and scab specimens. We observed no statistically significant difference between the Ct values generated on G2RG and C3L on the same specimens. (Figure 2)

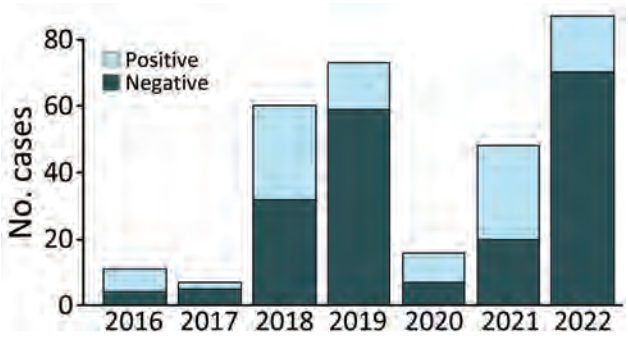

Figure 1. Laboratory test results for persons with suspected mpox cases, by year, Central African Republic, 2016–2022. Of 302 suspected cases during the study period, 105 (35%) had positive results for monkeypox virus on >1 specimen.

Conclusions

Approximately one third of suspected mpox cases in CAR are confirmed MPXV infections; an additional 2/5 are VZV infections, leaving ≈3/5 cases of papulovesicular cutaneous eruptions undiagnosed. Most mpox and VZV infections were diagnosed in teenagers and young adults, with an even younger population remaining undiagnosed.

Although cases of mpox are generally detected across the heavily forested, southern parts of CAR, mpox detection rates vary across prefectures. Some prefectures, such as Sangha Mbaere, have a high detection rate of MPXV (60%) over VZV (5%), whereas in others, such as Bangui, detection is much lower (MPXV 5%, VZV 46%). The varying detection rates between prefectures could be linked to local lifestyles and practices, as well as social instability. In the southwest region, local communities primarily subsist through hunting and gathering, spending long periods in mpox-endemic forest, which may increase the risk for exposure to the virus; however, in the southeast, mpox-endemic bushlands are used for farming and as a place of passage or temporary habitation for communities that have been displaced by social instability.

Our study also detected significantly more female patients among mpox-positive than VZV-positive

Table 1. Test results by specimen type and test type for MPXV and VZV in a study assessing laboratory diagnosis of mpox, Central African Republic, 2016–2022*

	MPXV (G2RG)		MPXV (C3L)		VZV	
Specimen type	Positive	Negative	Positive	Negative	Positive	Negative
Blood	77/278 (28)	201/278 (72)	73/278 (26)	205/278 (74)	62/260 (24)	198/260 (76)
Active lesion	45/102 (44)	57/102 (56)	45/102 (44)	57/102 (56)	42/108 (39)	66/108 (61)
Scab	36/98 (37)	62/98 (63)	37/98 (38)	61/98 (62)	38/100 (38)	62/100 (62)
Oropharyngeal	3/22 (14)	19/22 (86)	2/22 (9)	20/22 (91)	6/22 (27)	16/22 (73)

*Data are no. positive/no. tested (%). C3L, clade I–specific primer; G2RG, generic primer; MPXV, monkeypox virus; VZV, varicella–zoster virus.

Table 2. Cycle threshold values obtained using G2RG and C3L PCR primers on different specimens in a study assessing laboratory diagnosis of mpox, Central African Republic, 2016–2022*

Specimen type	MPXV (G2RG)	MPXV (C3L)	VZV
Blood	32.11 (29.12–35.45)	32.93 (30.25–35.94)	34.41 (31.38–36.01)
Active lesion	18.92 (17.42–23.43)	19.61 (18.05–23.57)	19.23 (17.69–20.82)
Scab	18.07 (16.19–19.82)	18.13 (16.46–21.46)	15.78 (13.63–18.42)
Oropharyngeal	30.15 (28.04–32.56)	28.19 (26.79–29.59)	34.31 (32.95–35.67)

*Data are median cycle threshold value (interquartile range). C3L, clade I–specific primer; G2RG, generic primer; MPXV, monkeypox virus; VZV, varicella–zoster virus.

cases, which may be explained by increased risk for infection through multiple routes of exposure to potentially infected sources. For example, women are primarily responsible for skinning and cooking wild game hunted in the forest and are the primary caretakers for family members who fall ill.

Our results demonstrate very high agreement in PCR results between primers. The results also highlight the need to prioritize active lesion and scab specimens over blood specimens, given that their relatively higher viral loads for MPXV and VZV enable better detection.

CAR faces special geographic, social, and healthcare challenges, leading to substantial delays between symptoms onset, diagnosis, and care. The reported case-fatality ratio for clade I mpox cases varies widely and is often cited as 11% (*8*) but has also been as low as 1.4% in Democratic Republic of Congo (P.R. Pittman et al., unpub. data, https://doi.org/10.1101/2022.05.26.22273379) and 6.7% in CAR (*9*). To improve patient outcomes in CAR, diagnostic capacity needs to be strengthened through greater availability of point-of-care testing and through support by more active epidemiologic and genomic surveillance that can be implemented with a wider range of partners.

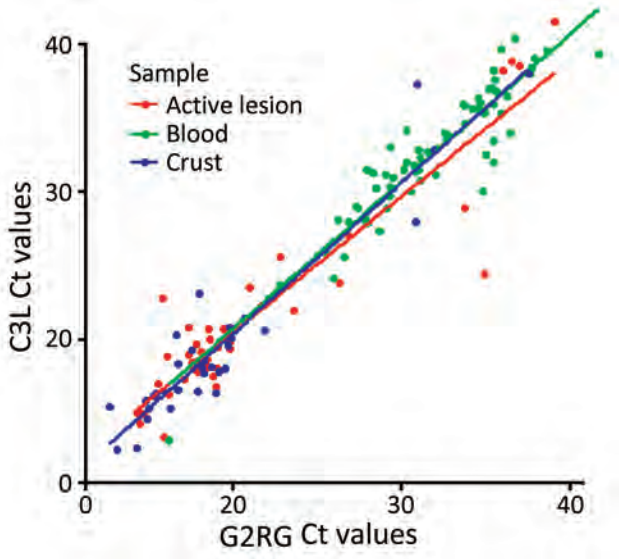

Figure 2. Distribution of Ct values obtained using G2RG and C3L primers of monkeypox virus–positive active lesion, blood, and scab specimens in study assessing laboratory diagnosis of mpox, Central African Republic, 2016–2022. C3L, clade I–specific primer; Ct, cycle threshold; G2RG, generic primer.

This work was supported by the UK Foreign, Commonwealth and Development Office and Wellcome (grant no. 215091/Z/18/Z), the Bill and Melinda Gates Foundation (grant no. OPP1209135), and the African Coalition for Epidemic Research, Response and Training (ALERRT). ALERRT is part of the European and Developing Countries Clinical Trials Partnership 2 program supported by the European Union (grant no. RIA2016E-1612). ALERRT is also supported by the United Kingdom's National Institute for Health Research.

About the Author

Ms. Garba-Ouangole is an assistant technical supervisor at Institut Pasteur de Bangui in the Central African Republic. Her primary research interests include genomic surveillance and surveillance of emerging and reemerging infectious diseases and zoonoses.

References

1. Mitjà O, Ogoina D, Titanji BK, Galvan C, Muyembe JJ, Marks M, et al. Monkeypox. Lancet. 2023;401:60–74. https://doi.org/10.1016/S0140-6736(22)02075-X
2. Gessain A, Nakoune E, Yazdanpanah Y. Monkeypox. N Engl J Med. 2022;387:1783–93. https://doi.org/10.1056/NEJMra2208860
3. Mansour R, Houston A, Majeed A, Boum Y II, Nakouné E, Razai MS. Human monkeypox: diagnosis and management. BMJ. 2023;380:e073352. https://doi.org/10.1136/bmj-2022-073352
4. Berthet N, Descorps-Declère S, Besombes C, Curaudeau M, Nkili Meyong AA, Selekon B, et al. Genomic history of human monkey pox infections in the Central African Republic between 2001 and 2018. Sci Rep. 2021;11:13085. https://doi.org/10.1038/s41598-021-92315-8
5. Petersen E, Kantele A, Koopmans M, Asogun D, Yinka-Ogunleye A, Ihekweazu C, et al. Human monkeypox: epidemiologic and clinical characteristics, diagnosis, and prevention. Infect Dis Clin North Am. 2019;33:1027–43. https://doi.org/10.1016/j.idc.2019.03.001
6. Li Y, Zhao H, Wilkins K, Hughes C, Damon IK. Real-time PCR assays for the specific detection of monkeypox virus West African and Congo Basin strain DNA. J Virol Methods. 2010;169:223–7. https://doi.org/10.1016/j.jviromet.2010.07.012

7. Cohrs RJ, Randall J, Smith J, Gilden DH, Dabrowski C, van Der Keyl H, et al. Analysis of individual human trigeminal ganglia for latent herpes simplex virus type 1 and varicella-zoster virus nucleic acids using real-time PCR. J Virol. 2000;74:11464–71. https://doi.org/10.1128/JVI.74.24.11464-11471.2000
8. Bunge EM, Hoet B, Chen L, Lienert F, Weidenthaler H, Baer LR, et al. The changing epidemiology of human monkeypox—a potential threat? A systematic review. PLoS Negl Trop Dis. 2022;16:e0010141. https://doi.org/10.1371/journal.pntd.0010141
9. Besombes C, Mbrenga F, Schaeffer L, Malaka C, Gonofio E, Landier J, et al. National monkeypox surveillance, Central African Republic, 2001–2021. Emerg Infect Dis. 2022;28:2435–45. https://doi.org/10.3201/eid2812.220897

Address for correspondence: Josephine Bourner, ISARIC Global Support Centre, International Severe Acute Respiratory and Emerging Infection Consortium, New Richards Building, University of Oxford Old Road Campus, Old Road, Oxford OX3 7LG, UK; email: josephine.bourner@ndm.ox.ac.uk

Effects of School-Based Preventive Measures on COVID-19 Incidence, Hong Kong, 2022

Tim K. Tsang, Xiaotong Huang, Min Whui Fong, Can Wang, Eric H.Y. Lau, Peng Wu, Benjamin J. Cowling

We show that school closures reduced COVID-19 incidence rates in children by 31%–46% in Hong Kong in 2022. After school reopening accompanied by mask mandates, daily rapid testing, and vaccination requirements, school-reported cases correlated with community incidence rates. Safe school reopening is possible when appropriate preventive measures are used.

After 2 years of minimal incidence of SARS-CoV-2 infections in Hong Kong, the Omicron BA.2 variant began to spread in January 2022. The resulting 5th COVID-19 wave in Hong Kong's population of 7.3 million persons resulted in >1 million cases and >9,000 deaths during February–April 2022, despite high overall vaccine coverage (*1*). After a low point of <200 cases/day in mid-May, the number of cases resurged, resulting in a 6th wave beginning in June 2022.

Schools in Hong Kong were intermittently closed throughout the 5th wave, and online learning began in February 2022. The summer holiday (conventionally 6 weeks during mid-July–August) was rescheduled to March and April, with a shorter 2-week summer holiday at the end of August. Schools resumed in-person learning in May 2022, and a range of public health and social measures were imposed to reduce COVID-19 transmission risk among staff and students (Table 1; Appendix Tables 1, 2, https://wwwnc.cdc.gov/EID/article/29/9/22-1897-App1.pdf), including mask wearing, requiring negative results of daily self-administered rapid antigen tests (RAT) (Appendix Table 3) for staff and students before entering school, reducing class sizes and lesson durations, and fulfilling certain vaccination requirements.

School closures or class dismissals can cause substantial harm, such as negatively affecting education, social and emotional development, and physical and mental health of children and young persons (*2*,*3*). Hence, rigorous evaluation of public health effects of school-based measures are needed to guide disease control and prevention policies. We analyzed epidemiologic and school-reported data to determine the effects of school-based measures on COVID-19 transmission in Hong Kong during 2022.

The Study

The study was approved by the Institutional Review Board of the University of Hong Kong. We analyzed COVID-19 data reported to the Hong Kong Centre for Health Protection that included PCR-confirmed cases during January 1–November 22, 2022, and RAT-confirmed cases during February 26–November 22, 2022. Confirmative PCR was administered for RAT-confirmed cases reported during June 7–August 28, 2022. We found that age-specific incidence rate ratios for infections in children compared with adults (>18 years of age) in the 6th wave were slightly higher than in the 5th wave (Figure 1).

We divided the study period into 3 segments: school closure, summer holiday, and normal school days (days other than closures and holidays). We stratified cases into 4 age groups: 2–5 years (preschool/kindergarten students), 6–11 years (primary school students), 12–17 years (secondary school students), and ≥18 years (adults). We used a Poisson generalized additive regression model, adjusting for time trend of COVID-19 cases and including the age groups and study periods (Appendix), to determine the effects of school closure and

Author affiliations: The University of Hong Kong, Hong Kong, China (T.K. Tsang, X. Huang, M.W. Fong, C. Wang, E.H.Y. Lau, P. Wu, B.J. Cowling); Laboratory of Data Discovery for Health Limited, Hong Kong Science and Technology Park, Hong Kong (T.K. Tsang, E.H.Y. Lau, P. Wu, B.J. Cowling)

DOI: https://doi.org/10.3201/eid2909.221897

Table 1. Summary of territorywide preventive measures implemented during the 5th and 6th waves of the COVID-19 outbreak in Hong Kong evaluated in study of effects of school-based preventive measures on COVID-19 incidence, 2022

Preventive measures	Focus	Period
Masks		
A person must wear a mask at all times when entering or attending school.	School staff, students	2020 Jan 23–2023 Feb 28
School closure		
Suspend face-to-face classes and on-campus activities	Kindergarten and primary school students	2022 Jan 14–2022 Apr 18
	Students in secondary schools	2022 Jan 24–2022 Apr 28
Allow some mask-wearing activities on a half-day basis	Kindergarten, primary school, and secondary school students	2022 May 19–2022 Oct 31
Resume half-day nonacademic extracurricular activities for those who received 2 vaccine doses >14 d apart	Students in primary schools	2022 Oct 25–2023 Feb 14
Resume half-day nonacademic extracurricular activities for those who received 3 vaccine doses >14 d apart	Students in secondary schools	2022 Oct 1–2023 Jan 31
Resume whole-day face-to-face classes if ≥90% of vaccination-eligible students (entire school or at individual class level) received >2 vaccine doses >14 d apart	Students in secondary schools	2022 Nov 1–2023 Jan 31
Resume whole-day face-to-face classes if ≥70% of vaccination-eligible students (entire school or at individual class level) received >2 vaccine doses >14 d apart	Students in primary schools	2022 Dec 1–2023 Feb 14
Resume whole-day face-to-face classes	Students in secondary schools	Beginning 2023 Feb 1
Resume whole-day face-to-face classes	Students in primary schools	Beginning 2023 Feb 15
COVID-19 tests		
Daily rapid antigen test result is required before returning to school for work or lessons	School staff and students	2022 Apr 19–2023 Mar 15
Vaccine pass		
A valid vaccine pass is required for school entry	School staff, students12–17 years of age	2022 Feb 23–2022 Dec 29
Vaccination		
≥1 dose	Students 5–11 years of age	2022 Sep 30–2022 Nov 29
	School staff, students 12–17 years of age	2022 Feb 24–2022 Jun 29
≥2 doses	Students 5–11 years of age	2022 Nov 30–2023 Feb 15
	School staff, students 12–17 years of age	2022 Jun 30–2022 Nov 29
≥3 doses	School staff, students 12–17 years of age	2022 Nov 30–2023 Feb 1

summer holiday on COVID-19 transmission in school-age children.

During normal school days (Table 2), the COVID-19 incidence rate for kindergarten students was 24% (95% CI 22%–25%), for primary school students was 34% (95% CI 32%–35%), and for secondary school students was 19% (95% CI 18%–20%) higher than for adults, suggesting that school-age children had a higher infection risk than adults during normal school days. During the 5th-wave school closure, the incidence rate for kindergarten students was 31% (95% CI 29%–32%), for primary students was 42% (95% CI 41%–43%), and for secondary students was 46% (95% CI 46%–47%) lower than for adults. During the summer holiday when most schools were closed during the 6th wave, the COVID-19 incidence rate for kindergarten students was 12% (95% CI 9%–15%), for primary students was 28% (95% CI 26%–30%), and for secondary students was 32% (95% CI 30%–34%) lower than for adults. Assuming that school-based interventions had no effect on adults, effectiveness of school closure on reducing COVID-19 transmission was 31%–46% during the 5th wave and 12%–32% during the 6th wave.

We collected school-related data from daily press conferences and press releases, including numbers of school-reported cases (students and staff), class suspensions, and schools reporting ≥1 case during periods of in-person learning (Appendix). Excluding summer holidays, weekly case numbers in the community were highly correlated with weekly numbers of school-reported student and staff cases (Pearson correlation coefficient r = 0.77, 95% CI 0.54–0.89), schools reporting ≥1 case (r = 0.75; 95% CI 0.51–0.88), and ≥2 cases of class suspension (r = 0.81, 95% CI 0.61–0.91) (Figure 2). Among 299 suspected school clusters, defined as schools that reported≥2 COVID-19 cases within 7 days, a total of 66 (22%) had >5 cases and 22 (7%) had >10 cases. The largest suspected cluster recorded 53 cases in a secondary school that had ≈750 students and ≈75 staff. The second-largest suspected cluster had 35 cases in an international school that had ≈960 primary and secondary students.

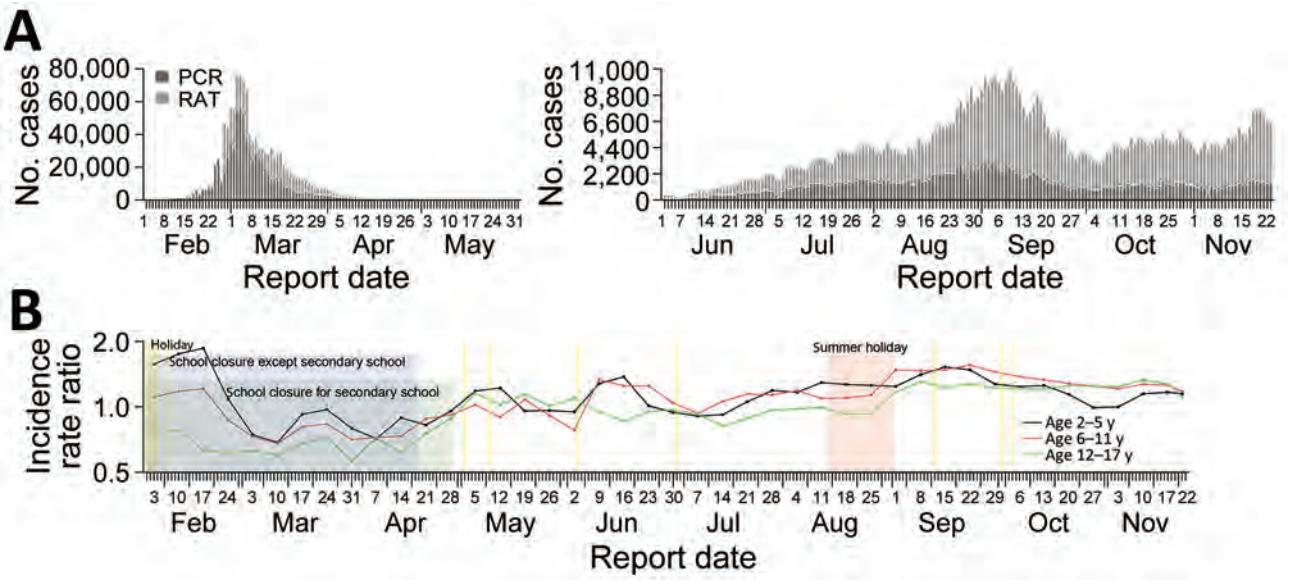

Figure 1. Epidemiology of 5th and 6th COVID-19 outbreak waves, Hong Kong, 2022, evaluated in study of effects of school-based preventive measures on COVID-19 incidence. A) Epidemic curves of 5th (February–April 2022, left) and 6th (beginning in June 2022, right) COVID-19 waves according to reporting date and test type. B) Incidence rate ratios of school-age children in kindergarten (age 2–5 y), primary schools (age 6–11 y), and secondary schools (age 12–17 y) in the 5th and 6th COVID-19 waves. Referent was adults (age ≥18 y). Yellow shading indicates a school holiday. RAT, rapid antigen test.

Conclusions

We found that school-age children had a higher SARS-CoV-2 infection risk than adults in Hong Kong, consistent with another study suggesting that children were more susceptible to Omicron variants compared with adults (*4*). School closure and summer holiday effectively reduced incidence rates in school-age children during the 5th and 6th COVID-19 waves, aligning with modeling and simulation studies demonstrating the effectiveness of school closure in reducing COVID-19 transmission (*5*–*7*). We noted that the reduction in incidence rates for school-age children during school closure in the 5th wave was greater than that during the summer holiday in the 6th wave. Potential explanations for those results are that schools might not have been completely closed during summer holiday, possibly increasing the number of contacts between children; that Omicron BA.4/BA.5 variants were more prevalent during the 6th wave (Appendix Figure 1); or that higher ascertainment rates existed among students who had RAT used to detect COVID-19.

The strong positive correlation between school-reported data and community case numbers after school reopening indicated school reopening did not cause abnormal increases in community COVID-19 incidence. The largest suspected school cluster had 53 COVID-19 cases, comparable to other superspreading events, such as the 67-case cluster caused by Omicron BA.1 and 167-case cluster caused by Omicron BA.2 in January 2022 (*8*). Those results suggest that school reopening did not pose additional superspreading risks in school settings.

The first limitation of our study is that some school-reported COVID-19 infections could have originated elsewhere in the community, such as at home, instead of in schools. Although students

Table 2. Incidence rate and incidence rate ratio estimates according to the Poisson generalized additive regression model in study of effects of school-based preventive measures on COVID-19 incidence, Hong Kong, 2022*

Period and age group	Incidence rate†	IRR (95% CI)
Normal school days		
Age, y		
≥18	169	Referent
2–5	204	1.24 (1.22–1.25)
6–11	220	1.34 (1.32–1.35)
12–17	196	1.19 (1.18–1.2)
School closure		
Age, y		
≥18	727	Referent
2–5	622	0.69 (0.68–0.71)
6–11	560	0.58 (0.57–0.59)
12–17	461	0.54 (0.53–0.54)
Summer holiday		
Age, y		
≥18	292	Referent
2–5	370	0.88 (0.85–0.91)
6–11	324	0.72 (0.7–0.74)
12–17	275	0.68 (0.66–0.7)

*Adjusted for the time trend of COVID-19 cases. IRR, incidence rate ratio.
†Per 1,000 person-years.

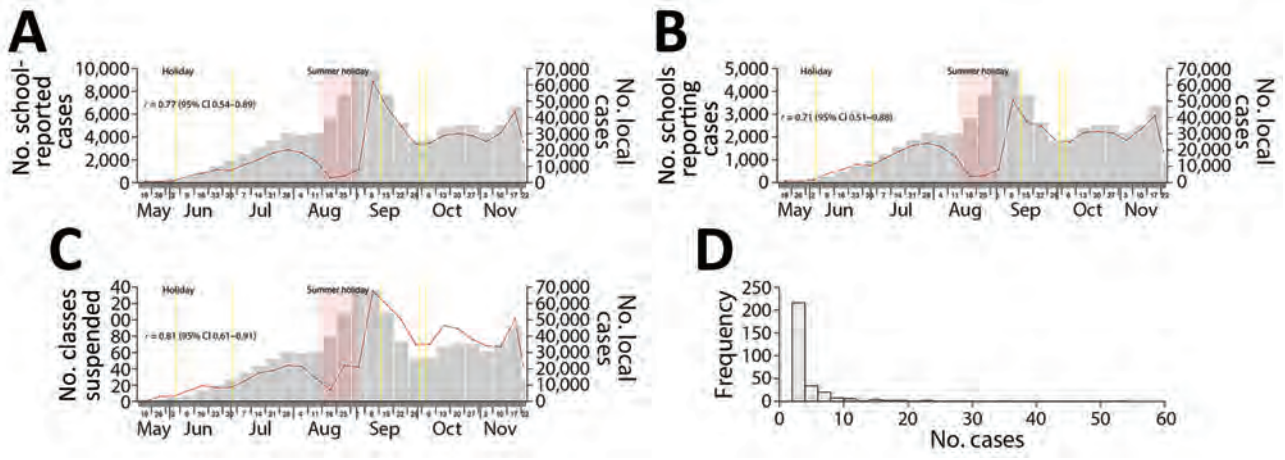

Figure 2. School-reported data during the 6th COVID-19 wave, Hong Kong, 2022, evaluated in study of effects of school-based preventive measures on COVID-19 incidence. A) Weekly numbers of school-reported cases during the 6th wave, beginning in June 2022. B) Weekly number of schools reporting ≥1 case during the 6th wave. C) Weekly number of class suspensions (classes with ≥2 COVID-19 cases) during the 6th wave. Yellow shading indicates school holiday; red shading indicates summer holiday. Pearson correlation coefficient *r* and 95% CI were calculated for data reported weekly. D) Distribution of 299 suspected school clusters of COVID-19 by size of cluster (no. cases). A school cluster was defined as a school that reported≥2 cases within 7 days. Scales for the y-axes in panels A–C differ substantially to underscore patterns but do not permit direct comparisons.

and staff were required to conduct daily rapid tests and report positive results to schools and the government, underreporting cannot be ruled out. Second, we extracted school outbreak data from press conferences; thus, some details could have been missed. Third, we cannot exclude the possibility that some schools did not fully adhere to guidelines, particularly regarding class size and lesson duration; however, we lacked school-level data to account for that possibility. Fourth, our analysis did not account for changes in dominant virus strains (Omicron BA.2 in the 5th wave, Omicron BA.5 in the 6th wave). Finally, we considered school-based measures as a collective package and were unable to determine individual effects of specific measures on COVID-19 transmission.

In summary, we evaluated school closure and school reopening accompanied by multilayer school-based preventive measures for COVID-19 in Hong Kong, which was informative as a guide for implementing and relaxing those measures. Our results might not be directly generalizable for other respiratory pathogens because of differences in transmission and intervention effectiveness. However, our results are consistent with modeling studies suggesting that safe school reopening is possible when appropriate alternative school-based preventive measures are used (*9*–*12*). If resurgence in case numbers or emergence of variants with higher transmissibility in children occurs, school closure remains an option to reduce transmission among children.

Acknowledgments

We thank Julie Au and Hang Qi for technical assistance.

This project was supported by the Health and Medical Research Fund, Health Bureau, Government of the Hong Kong Special Administrative Region (grant no. COVID190118); the Collaborative Research Fund from the University Grants Committee of Hong Kong (project no. C7123-20G); and Research Grants Council of the Hong Kong Special Administrative Region, China.

B.J.C. reports honoraria from AstraZeneca, Fosun Pharma, GSK, Haleon, Moderna, Novavax, Roche, and Sanofi Pasteur. All other authors report no other potential conflicts of interest.

About the Author

Dr Tsang is an assistant professor at the School of Public Health, University of Hong Kong. His research interests focus on infectious disease modelling and transmission and control of emerging infections.

References

1. McMenamin ME, Nealon J, Lin Y, Wong JY, Cheung JK, Lau EHY, et al. Vaccine effectiveness of one, two, and three doses of BNT162b2 and CoronaVac against COVID-19 in Hong Kong: a population-based observational study. Lancet Infect Dis. 2022;22:1435–43. https://doi.org/10.1016/S1473-3099(22)00345-0
2. Macartney K, Quinn HE, Pillsbury AJ, Koirala A, Deng L, Winkler N, et al.; NSW COVID-19 Schools Study Team. Transmission of SARS-CoV-2 in Australian educational settings: a prospective cohort study.

Lancet Child Adolesc Health. 2020;4:807–16. https://doi.org/10.1016/S2352-4642(20)30251-0
3. Viner RM, Mytton OT, Bonell C, Melendez-Torres GJ, Ward J, Hudson L, et al. Susceptibility to SARS-CoV-2 infection among children and adolescents compared with adults: a systematic review and meta-analysis. JAMA Pediatr. 2021;175:143–56. https://doi.org/10.1001/jamapediatrics.2020.4573
4. Lim DS, Choe YJ, Man Kim Y, Lee SE, Jang EJ, Kim J, et al. Household secondary attack rates of SARS-CoV-2 Omicron variant, South Korea, February 2022. Emerg Infect Dis. 2022;28:1731–4. https://doi.org/10.3201/eid2808.220384
5. Auger KA, Shah SS, Richardson T, Hartley D, Hall M, Warniment A, et al. Association between statewide school closure and COVID-19 incidence and mortality in the US. JAMA. 2020;324:859–70. https://doi.org/10.1001/jama.2020.14348
6. Bayham J, Fenichel EP. Impact of school closures for COVID-19 on the US healthcare workforce and net mortality: a modelling study. Lancet Public Health. 2020;5:e271–8. https://doi.org/10.1016/S2468-2667 (20)30082-7
7. Yang B, Huang AT, Garcia-Carreras B, Hart WE, Staid A, Hitchings MDT, et al.; UFCOVID Interventions Team. Effect of specific nonpharmaceutical intervention policies on SARS-CoV-2 transmission in the counties of the United States. Nat Commun. 2021;12:3560. https://doi.org/10.1038/s41467-021-23865-8
8. Guo Z, Zhao S, Lee SS, Mok CKP, Wong NS, Wang J, et al. Superspreading potential of COVID-19 outbreak seeded by Omicron variants of SARS-CoV-2 in Hong Kong. J Travel Med. 2022;29:taac049. https://doi.org/10.1093/jtm/taac049
9. Bilinski A, Salomon JA, Giardina J, Ciaranello A, Fitzpatrick MC. Passing the test: a model-based analysis of safe school-reopening strategies. Ann Intern Med. 2021;174:1090–100. https://doi.org/10.7326/M21-0600
10. McGee RS, Homburger JR, Williams HE, Bergstrom CT, Zhou AY. Model-driven mitigation measures for reopening schools during the COVID-19 pandemic. Proc Natl Acad Sci USA. 2021;118:e2108909118. https://doi.org/10.1073/pnas.2108909118
11. Panovska-Griffiths J, Kerr CC, Stuart RM, Mistry D, Klein DJ, Viner RM, et al. Determining the optimal strategy for reopening schools, the impact of test and trace interventions, and the risk of occurrence of a second COVID-19 epidemic wave in the UK: a modelling study. Lancet Child Adolesc Health. 2020;4:817–27. https://doi.org/10.1016/S2352-4642(20)30250-9
12. Lessler J, Grabowski MK, Grantz KH, Badillo-Goicoechea E, Metcalf CJE, Lupton-Smith C, et al. Household COVID-19 risk and in-person schooling. Science. 2021;372:1092–7. https://doi.org/10.1126/science.abh2939

Address for correspondence: Tim K. Tsang, School of Public Health, Li Ka Shing Faculty of Medicine, The University of Hong Kong, 7 Sassoon Road, Pokfulam, Hong Kong, China; email: timtsang@connect.hku.hkx

Pharyngeal Co-Infections with Monkeypox Virus and Group A *Streptococcus*, United States, 2022

Robyn M. Kaiser,[1] Shama Cash-Goldwasser,[1] Nicholas Lehnertz, Jayne Griffith, Alison Ruprecht, John Stanton, Amanda Feldpausch, Jessica Pavlick, Charles A. Bruen, David Perez-Molinar, S. Rebecca Peglow, Omobosola O. Akinsete, Sapna Bamrah Morris, Elliot Raizes, Christopher Gregory, Ruth Lynfield

We report 2 cases of pharyngeal monkeypox virus and group A *Streptococcus* co-infection in the United States. No rash was observed when pharyngitis symptoms began. One patient required intubation before mpox was diagnosed. Healthcare providers should be aware of oropharyngeal mpox manifestations and possible co-infections; early treatment might prevent serious complications.

During the ongoing mpox outbreak that began in 2022, severe oropharyngeal manifestations of mpox have been described (*1*–*3*). Co-infections have been diagnosed frequently in patients with mpox, notably sexually transmitted infections (*1*,*2*). We report on 2 cases of co-infection with pharyngeal monkeypox virus (MPXV) and group A *Streptococcus* (GAS) in patients in the United States.

The Study

In August 2022, the Centers for Disease Control and Prevention was consulted about 2 patients. Patient A had GAS pharyngitis, suspected mpox with pharyngeal manifestations, and airway compromise; patient B had confirmed mpox and pharyngitis and pharyngeal swab samples that tested positive for 3 pathogens, including MPXV.

Author affiliations: HealthPartners Regions Hospital, Saint Paul, Minnesota, USA (R.M. Kaiser, C.A. Bruen, D. Perez-Molinar, S.R. Peglow, O.O. Akinsete); Centers for Disease Control and Prevention, Atlanta, Georgia, USA (S. Cash-Goldwasser, S. Bamrah Morris, E. Raizes, C. Gregory); Minnesota Department of Health, Saint Paul (N. Lehnertz, J. Griffith, A. Ruprecht, R. Lynfield); Positive Impact Health Centers, Decatur, Georgia, USA (J. Stanton); Emory University, Atlanta (J. Stanton); Georgia Department of Public Health, Atlanta (A. Feldpausch, J. Pavlick)

DOI: https://doi.org/10.3201/eid2909.230469

In August 2022, patient A, a 39-year-old man who had a history of substance use disorder and unstable housing, was seen at an emergency department because of severe odynophagia and myalgias. Physical examination revealed posterior oropharyngeal erythema, uvula edema, and tonsillar exudates. A pharyngeal swab sample was PCR positive for GAS; he received 1 dose of oral dexamethasone and was prescribed penicillin. The patient returned 4 days later because dysphagia, dyspnea, and a new maculopapular rash on his arms and chest had developed. He was treated with epinephrine, methylprednisolone, and intravenous dexamethasone for a presumed allergic reaction to penicillin. A computed tomography scan of his neck showed substantial cervical lymphadenopathy (Figure 1, panel A) and extensive soft tissue edema and inflammation of the soft palate, uvula, tonsils, epiglottis, and retropharyngeal tissues. Flexible laryngoscopy showed ulcerative, vesicular lesions on the epiglottis. He left the emergency department against medical advice with prescriptions for clindamycin and dexamethasone.

The next day, the patient was found lying on the ground, obtunded and with labored breathing, and was brought to the emergency department. He was immediately intubated and admitted to intensive care. A repeat computed tomography scan of his neck showed that his airway was dependent on the endotracheal tube; he had extensive soft tissue edema and cervical lymphadenopathy (Figure 1, panel B). He was treated for anaphylaxis with epinephrine and methylprednisolone and also received broad-spectrum antimicrobial drugs. He had a diffuse papulopustular rash consistent with mpox (*4*). Results of HIV antigen-antibody and PCR tests were negative. Video laryngoscopy showed edema and

[1]These first authors contributed equally to this article.

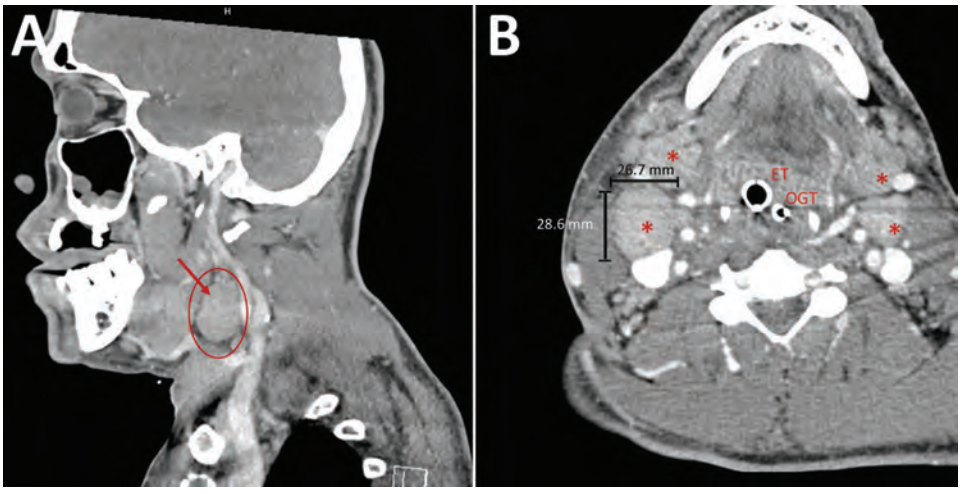

Figure 1. Computed tomography scans of patient's neck in study of pharyngeal co-infections with monkeypox virus and group A *Streptococcus*, United States, 2022. A) Sagittal view of neck of patient A (39-year-old man) showing massive cervical lymphadenopathy (red circle and arrow). B) Axial view of hypopharynx of patient A after intubation with endotracheal tube. Asterisks show enlarged cervical lymph nodes. Patient was dependent on endotracheal tube because of soft tissue edema along the airway. ET, endotracheal tube; OGT, orogastric tube.

erythema of the pharynx, uvula, and epiglottis and multiple ulcers within the pharynx (Figure 2). PCR results were negative for herpes simplex and varicella zoster virus in skin lesion samples. Swab samples were collected from skin and pharyngeal lesions to test for orthopoxvirus (OPXV) by PCR. On hospitalization day 3, histological examination of a skin lesion punch biopsy was consistent with OPXV infection, and the patient was started on intravenous tecovirimat. On hospital day 4, PCR results of all swab samples from the skin (PCR cycle threshold 16.63 for left thigh and 17.02 for right neck) and pharyngeal (cycle threshold 17.30) leisons were positive for OPXV, and he was given intravenous cidofovir. He had negative test results for Epstein-Barr virus, cytomegalovirus, syphilis, and pharyngeal gonorrhea and chlamydia. Over the next several days, the patient's skin lesions crusted, and airway edema decreased. He was extubated on hospital day 8. We obtained exposure history; the patient denied contact with persons who had mpox and said his last sexual encounter was with a female partner 4 weeks before symptom onset. He was discharged on hospitalization day 10.

In July 2022, patient B, a 36-year-old man with HIV infection (374 CD4+ cells/mm^3; viral load was suppressed on antiretroviral treatment) sought care at a clinic for a genital rash. He had engaged in anal and oral sex with multiple male partners during the previous 30 days. A swab sample from the rash tested positive for OPXV by PCR. A swab sample from his pharynx tested positive for *Neisseria gonorrhoeae* by PCR, and a rapid plasma reagin test had a positive titer of 1:16 (titer was 1:2 in March 2022). The patient received intramuscular ceftriaxone and penicillin, and his rash resolved. He returned to the clinic 8 weeks later with severe odynophagia, but no rash was observed after examination. He had a gray-white exudate and ulcers in his pharynx from which swab samples were collected. He was empirically treated with 1 dose of ceftriaxone and a course of oral doxycycline. He returned 3 days later with substantial left-sided anterior cervical lymphadenopathy (>2 cm) and was prescribed oral penicillin, after which his symptoms improved. Results from oropharyngeal swab samples were positive for GAS, *N. gonorrhoeae*, and OPXV by PCR.

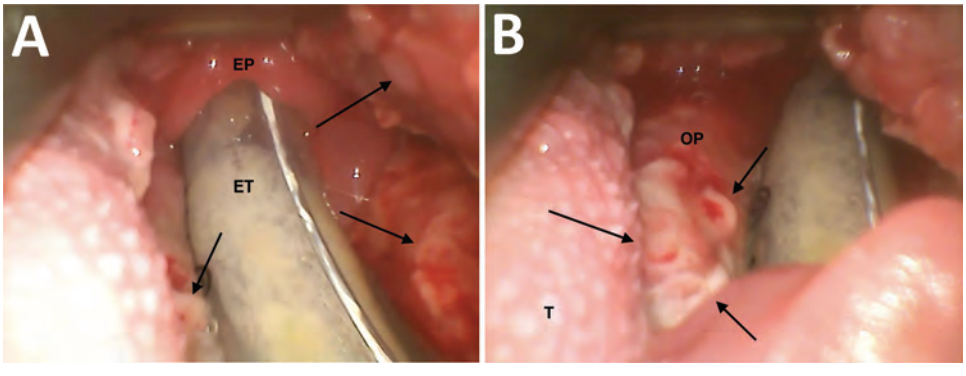

Figure 2. Video laryngoscopy images of patient larynx and pharynx in study of pharyngeal co-infections with monkeypox virus and group A *Streptococcus*, United States, 2022. A) View of oropharynx, hypopharynx, and laryngeal inlet of patient A (39-year-old man). Arrows indicate mpox lesions. B) Detailed view of mpox lesions. Arrows indicate several lesions. EP, epiglottis; ET, endotracheal tube; OP, oropharynx (lateral wall); T, tongue.

Conclusions

We show that MPXV infections of the pharynx can co-occur with other oropharyngeal infections. Similar to findings from other reported cases in the literature, patient A illustrates that mpox manifestations can be oropharyngeal and include pharyngitis, odynophagia, epiglottitis, and oral and tonsillar lesions (*1*–*3*). In both of these cases, a rash was not noted at the time of pharyngeal symptoms. If a patient is suspected of having mpox-related oropharyngeal lesions, those lesions should be tested for OPXV/MPXV; if lesions exist at multiple sites, samples from all sites should be tested. Furthermore, healthcare providers should consider testing patients with suspected or confirmed mpox and pharyngeal symptoms for GAS, sexually transmitted infections, and other infections, guided by clinical findings and epidemiologic risk.

During the 2003 mpox outbreak in the United States, oropharyngeal lesions and considerable cervical and tonsillar lymphadenopathy developed in an otherwise healthy child with mpox who was hospitalized with dyspnea and dysphagia, but intubation was not required (*5*). During the ongoing outbreak, severe or critical illness secondary to oropharyngeal mpox manifestations has been described, albeit often in persons with advanced HIV disease (*3*,*6*). In 2 reported cases, patients with mpox required intubation secondary to airway compromise. In contrast to patient A in our report, those patients had underlying immunocompromising conditions (*3*). Healthcare providers should consider early antiviral treatment for patients with suspected or laboratory-confirmed mpox disease who have severe clinical manifestations (*7*), including oropharynx involvement, or have comorbidities that increase their risk for severe disease (*8*).

We were unable to determine the relative contribution of MPXV to illness compared with other pathogens in the 2 cases. Although GAS might have been a colonizing organism, GAS carriage among adults is uncommon (*9*). Both patients had clinical features and laboratory results consistent with GAS infection (*10*,*11*), for which antimicrobial drug treatment is recommended (*11*), and were treated accordingly. OPXV detection in samples from the oropharynx of patient B might have represented ongoing infection; the effect of mpox antiviral treatment on viral clearance is unknown.

Corticosteroids were used initially in patient A until mpox was suspected. Short courses of corticosteroids are used to treat severe acute pharyngitis symptoms (*12*) and pharyngeal edema (*13*). Corticosteroids can decrease duration and severity of symptoms in patients with GAS pharyngitis; however, given the potential adverse effects of steroids and effectiveness of antimicrobial drugs, systemic steroids are generally not recommended (*11*). Further studies are needed to determine whether corticosteroids have a role in mpox treatment, including in patients with complications such as pharyngeal edema or massive cervical lymphadenopathy.

In summary, healthcare providers should be aware that MPXV infections of the pharynx can be severe, can co-occur with other pharyngeal infections, and can manifest in the absence of a rash. Early antiviral treatment of mpox in patients with oropharyngeal manifestations and early diagnosis and treatment of pharyngeal co-infections might prevent serious complications.

The Centers for Disease Control and Prevention offers an mpox clinical consultation service for the ongoing mpox outbreak. Healthcare providers seeking additional clinical guidance can contact the Centers for Disease Control and Prevention emergency operations by telephone at (770) 488-7100.

About the Author

Dr. Kaiser is an infectious disease physician at HealthPartners in Saint Paul. Her primary interests include emerging infectious diseases, bacterial resistance, and vaccine safety.

References

1. Thornhill JP, Barkati S, Walmsley S, Rockstroh J, Antinori A, Harrison LB, et al.; SHARE-net Clinical Group. Monkeypox virus infection in humans across 16 countries—April–June 2022. N Engl J Med. 2022;387:679–91. https://doi.org/10.1056/NEJMoa2207323
2. Miller MJ, Cash-Goldwasser S, Marx GE, Schrodt CA, Kimball A, Padgett K, et al.; CDC Severe Monkeypox Investigations Team. Severe monkeypox in hospitalized patients—United States, August 10–October 10, 2022. MMWR Morb Mortal Wkly Rep. 2022;71:1412–7. https://doi.org/10.15585/mmwr.mm7144e1
3. Brooks KA, Neptune NS, Mattox DE. Otolaryngologic manifestations of mpox: the Atlanta outbreak. Acta Otolaryngol. 2023;143:237–41. https://doi.org/10.1080/00016489.2023.2182911
4. Centers for Disease Control and Prevention. Mpox signs and symptoms. 2022 [cited 2022 Nov 28]. https://www.cdc.gov/poxvirus/mpox/symptoms/index.html
5. Anderson MG, Frenkel LD, Homann S, Guffey J. A case of severe monkeypox virus disease in an American child: emerging infections and changing professional values. Pediatr Infect Dis J. 2003;22:1093–8. https://doi.org/10.1097/01.inf.0000101821.61387.a5
6. Mitjà O, Alemany A, Marks M, Lezama Mora JI, Rodríguez-Aldama JC, Torres Silva MS, et al.; SHARE-NET writing group. Mpox in people with advanced HIV infection:

a global case series. Lancet. 2023;401:939–49. https://doi.org/10.1016/S0140-6736(23)00273-8
7. Centers for Disease Control and Prevention. Interim clinical guidance for the treatment of mpox [cited 2023 June 1]. https://www.cdc.gov/poxvirus/mpox/clinicians/treatment.html
8. Rao AK, Schrodt CA, Minhaj FS, Waltenburg MA, Cash-Goldwasser S, Yu Y, et al. Interim clinical treatment considerations for severe manifestations of mpox—United States, February 2023. MMWR Morb Mortal Wkly Rep. 2023;72:232–43. https://doi.org/10.15585/mmwr.mm7209a4
9. Ditchburn R, Ditchburn J. Rate of carriage of group A beta haemolytic streptococci. BMJ. 1995;311:193. https://doi.org/10.1136/bmj.311.6998.193
10. Ebell MH, Smith MA, Barry HC, Ives K, Carey M. The rational clinical examination. Does this patient have strep throat? JAMA. 2000;284:2912–8. https://doi.org/10.1001/jama.284.22.2912
11. Shulman ST, Bisno AL, Clegg HW, Gerber MA, Kaplan EL, Lee G, et al. Clinical practice guideline for the diagnosis and management of group A streptococcal pharyngitis: 2012 update by the Infectious Diseases Society of America. Clin Infect Dis. 2012;55:1279–82. https://doi.org/10.1093/cid/cis847
12. Sadeghirad B, Siemieniuk RAC, Brignardello-Petersen R, Papola D, Lytvyn L, Vandvik PO, et al. Corticosteroids for treatment of sore throat: systematic review and meta-analysis of randomised trials. BMJ. 2017;358:j3887. https://doi.org/10.1136/bmj.j3887
13. Hawkins DB, Crockett DM, Shum TK. Corticosteroids in airway management. Otolaryngol Head Neck Surg. 1983;91:593–6. https://doi.org/10.1177/019459988309100601

Address for correspondence: Robyn M. Kaiser, HealthPartners-Division of Infectious Disease, 401 Phalen Blvd, Saint Paul, MN 55130, USA; email: robyn.m.kaiser@healthpartners.com

Rapid Epidemic Expansion of Chikungunya Virus East/Central/South African Lineage, Paraguay

Marta Giovanetti,[1] Cynthia Vazquez,[1] Mauricio Lima,[1] Emerson Castro,[1] Analia Rojas, Andrea Gomez de la Fuente, Carolina Aquino, Cesar Cantero, Fatima Fleitas, Juan Torales, Julio Barrios, Maria J. Ortega, Maria L. Gamarra, Shirley Villalba, Tania Alfonzo, Joilson Xavier, Talita Adelino, Hegger Fritsch, Felipe C.M. Iani, Glauco C. Pereira, Carla de Oliveira, Gabriel Schuab, Evandra S. Rodrigues, Simone Kashima, Juliana Leite, Lionel Gresh, Leticia Franco, Houriiyah Tegally, Wesley C. Van Voorhis, Richard Lessels, Ana Maria Bispo de Filippis, Andrea Ojeda, Guillermo Sequera, Romeo Montoya, Edward C. Holmes, Tulio de Oliveira, Jairo M. Rico, José Lourenço, Vagner Fonseca, Luiz C.J. Alcantara

The spread of Chikungunya virus is a major public health concern in the Americas. There were >120,000 cases and 51 deaths in 2023, of which 46 occurred in Paraguay. Using a suite of genomic, phylodynamic, and epidemiologic techniques, we characterized the ongoing large chikungunya epidemic in Paraguay.

Chikungunya is a mosquitoborne disease caused by the chikungunya virus (CHIKV), a single-stranded positive-sense RNA virus belonging to the family *Togaviridae* (*1*), which is transmitted to humans through the bite of infected *Aedes aegypti* and *Ae. albopictus* mosquitoes. This disease is generally an acute, self-limiting illness characterized by fever and severe joint pain, although persistent or relapsing joint pain can occur (*1*). Atypical and severe manifestations (including meningoencephalitis) have been reported, and death is usually associated with older ages and other underlying diseases. Mother-to-child transmission of CHIKV occurs, and neonatal disease can be severe, with neurologic, myocardial, or hemorrhagic complications (*1*).

CHIKV can be classified into 4 distinct genotypes: West African, East/Central/South African (ECSA), Asian, and Indian Ocean lineages (*2*,*3*). An imported case of CHIKV in Paraguay was detected in June 2014 in a person from the Dominican Republic (*4*). Using on-site genomic monitoring, phylodynamic and epidemiologic approaches, we characterized the large-scale and ongoing CHIKV epidemic in Paraguay.

The Study

This study was reviewed and approved by the Pan American Health Organization (PAHO) Ethics

Author affiliations: Università Campus Bio-Medico di Roma, Italy (M. Giovanetti); Instituto Oswaldo Cruz, Belo Horizonte, Brazil (M. Giovanetti, M. Lima, E. Castro, J. Xavier, H. Fritsch, L.C.J. Alcantara); Laboratorio Central de Salud Pública, Asunción, Paraguay (C. Vazquez, A. Rojas, A. Gomez de la Fuente, C. Aquino, C. Cantero, F. Fleitas, J. Torales, J. Barrios, M.J. Ortega, M.L. Gamarra, S. Villalba, T. Alfonzo); Central de Saúde Pública do Estado de Minas Gerais, Ezequiel Dias, Brazil (M. Lima, E. Castro, T. Adelino, F.C.M. Iani, G.C. Pereira); Universidade Federal de Minas Gerais, Belo Horizonte (J. Xavier, H. Fritsch); Instituto Oswaldo Cruz, Rio de Janeiro, Brazil (C. de Oliveira, G. Schuab, A.M.B. de Filippis); University of São Paulo, São Paulo, Brazil (E.S. Rodrigues, S. Kashima); Pan American Health Organization/World Health Organization, Washington, DC, USA (J. Leite, L. Gresh, L. Franco, J.M. Rico); Stellenbosch University, Stellenbosch, South Africa (H. Tegally, T. de Oliveira); University of KwaZulu-Natal, Durban, South Africa (H. Tegally, R. Lessels, T. de Oliveira); National Institutes of Health, Bethesda, Maryland, USA (W.C. Van Voorhis); Dirección General de Vigilancia de la Salud, Asunción (A. Ojeda, G. Sequera); Organización Panamericana de la Salud/Organización Mundial de la Salud Asuncion (R. Montoya); University of Sydney, Sydney, New South Wales, Australia (E.C. Holmes); University of Lisbon, Lisbon, Portugal (J. Lourenço); Organização Pan-Americana da Saúde/Organização/Mundial da Saúde, Brasilia, Brazil. (V. Fonseca)

DOI: https://doi.org/10.3201/eid2909.230523

[1]These authors contributed equally to this article.

Review Committee (PAHO no. 2016-08-0029) and by the Paraguayan Ministry of Public Health and Social Welfare (MSPyBS/SG no. 0944/18). Samples used in this study were deidentified residual samples from routine diagnosis of arboviruses in the Paraguayan Public Health Laboratory, which is part of the public network within the Paraguayan Ministry of Health.

We partnered with PAHO to perform on-site genomic surveillance at the Laboratorio Central de Salud Pública in Asunción, Paraguay. During March 11–17, 2023, a team of molecular biologists from Brazil and Paraguay worked with selected samples (based on cycle threshold [Ct] values ≤35 and availability of epidemiologic metadata, generating 179 viral genomes deposited in GenBank under accession nos. OQ775394–567 and OQ567722–5). We performed sequencing by using Nanopore technology (*5*). We constructed phylogenetic trees to explore the evolutionary and epidemiologic relationships of CHIKV in Paraguay with those of other sequences of this viral genotype sampled globally. We retrieved from GenBank 715 CHIKV ECSA genome sequences collected through March 30, 2023, with associated lineage date and country of collection,. We compiled a description of the relevant methods used (Appendix 1, https://wwwnc.cdc.gov/EID/article/29/9/23-0523-App1.pdf) and strains analyzed (Appendix 2, https://wwwnc.cdc.gov/EID/article/29/9/23-0523-App2.xlsx).

Autochthonous infections were detected in Paraguay in 2015, and CHIKV has been detected in the country every year since that date (Appendix 1 Figure 1, panel A). On the basis of reported suspected CHIKV infections, Paraguay has had 4 epidemic waves, in 2015, 2016, 2018, and 2023, all associated with summer months (Appendix 1 Figure 1, panel A). During October 2, 2022–April 10, 2023, a total of 118,179 suspected and confirmed infections were reported, including 3,510 hospitalized case-patients and 46 deaths (*4*,*6*). Neonates have accounted for 0.3% (n = 162) of these cases and 8 deaths. In addition, 294 suspected cases

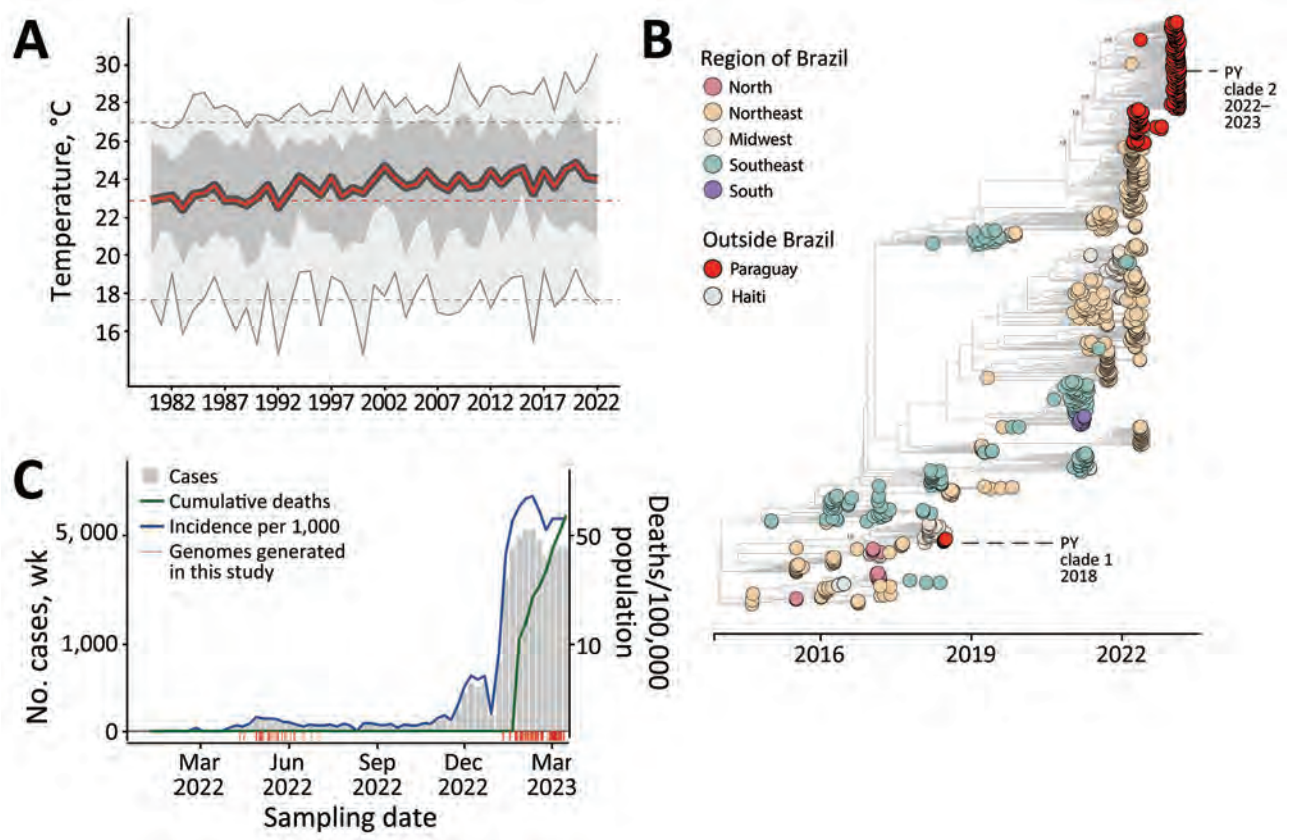

Figure 1. Spatial and temporal distribution of cases of chikungunya in Paraguay. A) Temperature trends during 1981–2022. Yearly mean (red line), yearly minimum and maximum (light gray shading), yearly 50% quantiles (dark gray shading), minimum and maximum temperatures in 1981 (dashed gray lines) and mean temperature in 1981 (dashed red line) are shown. B) Number of chikungunya virus genome sequences in Paraguay compared with Brazil (by region) and Haiti. Size of circles indicates number of new genomes generated in this study. C) Weekly reported chikungunya cases (gray area), incidence normalized per 100,000 persons (blue line), and cumulative deaths (green line) during 2022–2023 (through epidemiologic week 11). Red bars indicate dates of sample collection of genomes generated in this study. PY, patient-year.

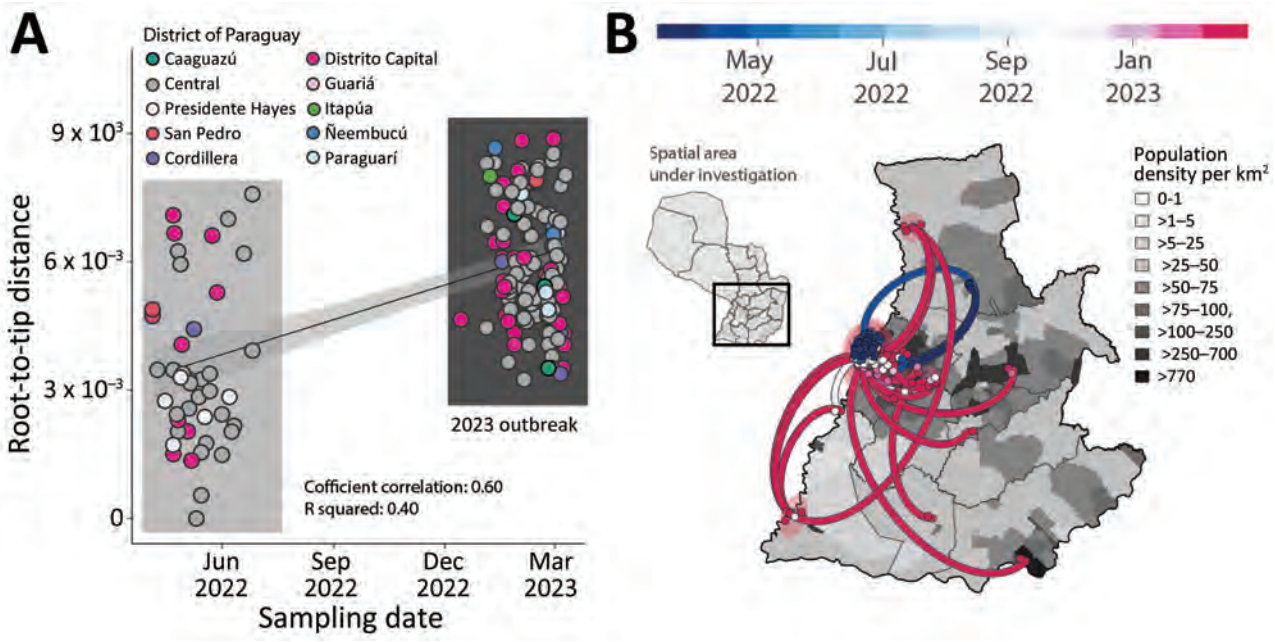

Figure 2. Expansion of the chikungunya East/Central/South/African lineage epidemic in Paraguay. A) Regression of root-to-tip genetic distances and sampling dates estimated by using TempEst version 1.5.3, (http://tree.bio.ed.ac.uk/software/tempest), buffers (shaded area) representing 90% CIs. Colors indicate geographic location of sampling. B) Spatiotemporal reconstruction of the spread of CHIKV ECSA in Paraguay. Circles represent nodes of the maximum clade credibility phylogeny, colored according to their inferred time of occurrence (scale shown). Shaded areas represent 80% highest posterior density interval and depict uncertainty of the phylogeographic estimates for each node. Solid curved lines indicate links between nodes and directionality of movement. Differences in population density are shown on a gray-white scale.

of acute meningoencephalitis have been reported, 125 (43%) of which have been attributed to CHIKV (*5*,*6*).

Although yearly minimum temperatures across Paraguay have remained stable over the past 40 years, mean and maximum yearly temperatures have been steadily increasing, and the rapid and large resurgence of CHIKV in 2022 coincided with the highest mean temperatures reported (Figure 1, panel A). Before 2022, confirmed infections were restricted to the Central, Paraguarí, and Amambay Districts; the Central District dominated the reports (Appendix 1 Figure 1, panel B). After viral resurgence in 2022, confirmed infections have been reported in all districts (Appendix 1).

We screened 179 quantitative reverse transcription PCR–positive samples for CHIKV. All contained sufficient DNA (≥2 ng/μL) to proceed with library preparation, and their PCR Ct values were a mean of 21 (range 9–34) (Appendix 2). Samples had good spatial representation of southern Paraguay (10/17 districts) (Figure 1, panel B), including several districts that had the highest historical counts of CHIKV infections (Appendix 1) and captured the out-season and in-season periods of transmission (autumn and early winter 2022 and summer 2023) (Figure 1, panel C). Analysis of sample sequence coverage versus Ct showed an average coverage of 94% among samples and a Ct of 28, below which average coverage ≥90% was achieved (Figure 2; Appendix 1). Most genomes (87%) were obtained from serum samples, the rest from cerebrospinal fluid; 54% were from female and 46% from male patients, and the mean age of the samples was 41 (range 26–95) days (Appendix 2).

Most (58%) genomes were from CHIKV infection outcomes in outpatients, followed by fatal (18%), intensive care unit (17%) and inpatient (7%) infections (Figure 1; Appendix 1). Compared with outpatient outcomes, we found a clear association of fatal outcomes in older age groups (Figure 1). The same comparison with outcomes requiring medical attention (ICU, inpatients) was not statistically significant (Figure 1). This observation contrasted the common notion that CHIKV symptomatic infections are more frequent in older age groups (*7*).

To determine the dynamics of the CHIKV ECSA in Paraguay, we performed phylodynamic analysis of a dataset comprising 715 available representative genomes combined with viruses sequenced in this study (n = 179, collected during April 6, 2022–March

10, 2023) (Figure 1). A date-stamped phylogeny indicated that all the novel isolates formed a single, large, well-supported monophyletic group, denoted Paraguay clade 2, within the CHIKV ECSA American clade. This result strongly suggests that the 2022–2023 epidemic was not related to cross-border transmission from Brazil, as reported (*8*) (Figure 1), but was more likely the result of continual transmission within Paraguay over a period of 11 months of a viral strain that was introduced in the region in early 2022 (Figures 1, 2).

To investigate evolution of the Paraguay clade 2 in more detail, we used a smaller dataset (n = 179) representing this virus clade in isolation. We found a relatively strong correlation between sampling date and root-to-tip genetic divergence in this dataset ($r^2 = 0.40$, correlation coefficient = 0.60), indicating relatively clock-like virus evolution (Figure 2). Phylogeographic analysis of Paraguay clade 2 enabled reconstruction of viral movements among different districts in Paraguay (Figure 2) and suggested a mean time of origin in late March 2022 (95% highest posterior density March 25, 2022–April 5, 2022). Viruses from this clade spread multiple times from the Midwestern District (Distrito Capital and Central Regions) toward the Southeast (Itapúa) and to the Midwest, as indicated by virus sequences from the Presidente Hayes and the Cordillera Regions (Figure 2).

Virus transmission dynamics roughly followed patterns of population density, moving most often between the most populous urban localities (Figure 1 panel B; Figure 2). Because it is recognized that both nonsynonymous and synonymous mutations can lead to changes in viral RNA (*9*,*10*), affecting splicing, stability, translation, or cotranslational protein folding, additional studies will be necessary to determine the potential effects of mutations on structure and function and, thus, on viral pathogenesis and fitness.

Conclusions

This study highlights the resurgence of CHIKV ECSA in Paraguay during 2022–2023. Our findings provide evidence of lineage persistence over a period of 11 months preceding resurgence and report the notable coincidence of virus resurgence and the highest mean temperatures recorded in Paraguay. Those 2 factors, combined with presence of the vectors and a large proportion of the population susceptible to CHIKV probably generated an ideal scenario for the observed fast and large CHIKV epidemic wave that started at the end of 2022. Given the association of ongoing resurgence with a specific lineage of CHIKV ECSA with 2 synonymous changes in nonstructural proteins 3 and 4 and uncertainty of how the ongoing epidemic will unfold, genomic surveillance should remain active to track real-time evolution and spatial spread, contributing to public health risk assessments in Paraguay and other countries in South America.

Acknowledgments

We thank the Global Consortium to Identify and Control Epidemics (https://climade.health) for providing assistance and support; PAHO/WHO for providing support; and Marcelo Korc, Alexander Rosewell, and Rodrigo Stabeli for providing major contributions and assistance. Because the paper had already reached its limit for the number of authors, we were unable to include them on the paper as coauthors.

This study was supported by the PAHO Health Emergencies Department, the National Institutes of Health USA (grant U01 AI151698) for the United World Arbovirus Research Network (UWARN), FAPESP (2021/11944-6), and the Mercosur Structural Convergence Fund (FOCEM), Mercosur, FOCEM agreement no. 03/11 Project Research, Education, and Biotechnologies Applied to Health (COF 03/11). Data analysis support was provided by the Centre for Epidemic Response and Innovation at Stellenbosch University, which was supported by the Rockefeller Foundation. M.G. was supported by PON Ricerca e Innovazione 2014-2020 and by CRP-ICGEB research grant 2020, project CRP/BRA20-03, contract CRP/20/03.

Author contributions: Study conception and design: M.G., C.V., J.L., J.M.R., L.C.J.A.; investigations: M.G., C.V., M.L., E.C., A.R., A.G.d.l.F., C.A., C.C., F.F., J.T., J.B., M.J.O., M.L.G., S.V., T.A., J.X., T.A., H.F., F.C.M.I., C.d.O., G.S., E.S.R., S.K., J.L., L.G., L.F., H.T., R.L., A.M.B.d.F., A.O., G.S., R.M., M.K., E.C.H., T.d.O., J.M.R., J.L., V.F., L.C.J.A; data analysis: M.G., H.T., J.L., V.F.; writing (original): M.G., J.L., L.C.J.A.; writing (revision): M.G., C.V., M.L., E.C., A.R., A.G.d.l.F., C.A., C.C., F.F., J.T., J.B., M.J.O., M.L.G., S.V., T.A., J.X., T.A., H.F., F.C.M.I., C.d.O., G.S., E.S.R., S.K., J.L., L.G., L.F., H.T., R.L., A.M.B.d.F., A.O., G.S., R.M., M.K., E.C.H., T.d.O., J.M.R., J.L., V.F., L.C.J.A; resources: C.V., J.M.R., L.C.J.A.

About the Author

Dr. Giovanetti is a visiting research scientist at the René Rachou Institute, Fiocruz Minas Gerais, Belo Horizonte, Brazil, and a research scientist at the University Campus Bio-Medico, Rome, Italy. Her primary research interests are patterns of gene flow in pathogen populations and

phylogenetics and phylogeography as tools to recreate and understand determinants of viral outbreaks and how that information can be translated into public policy recommendations.

References

1. Schwartz O, Albert ML. Biology and pathogenesis of chikungunya virus. Nat Rev Microbiol. 2010;8:491–500. https://doi.org/10.1038/nrmicro2368
2. de Oliveira EC, Fonseca V, Xavier J, Adelino T, Morales Claro I, Fabri A, et al. Short report: introduction of chikungunya virus ECSA genotype into the Brazilian midwest and its dispersion through the Americas. PLoS Negl Trop Dis. 2021;15:e0009290. https://doi.org/10.1371/journal.pntd.0009290
3. Rico-Hesse R. Molecular evolution and distribution of dengue viruses type 1 and 2 in nature. Virology. 1990; 174:479–93. https://doi.org/10.1016/0042-6822(90)90102-W
4. Quick J, Grubaugh ND, Pullan ST, Claro IM, Smith AD, Gangavarapu K, et al. Multiplex PCR method for MinION and Illumina sequencing of Zika and other virus genomes directly from clinical samples. Nat Protoc. 2017;12:1261–76. https://doi.org/10.1038/nprot.2017.066
5. Pan American Health Organization. CHIKV weekly report. 2023 [cited 202 Jul 14]. https://www3.paho.org/data/index.php/en/mnu-topics/chikv-en/550-chikv-weekly-en.html
6. Pan American Health Organization. Disease outbreak news. 2023 [cited 2023 Jul 14] .https://www.who.int/emergencies/disease-outbreak-news/item/2023-DON448#:~:text=Paraguay%3A%20Between%202%20October%202022,hospitalized%20cases%20and%2046%20deaths.
7. Yoon IK, Alera MT, Lago CB, Tac-An IA, Villa D, Fernandez S, et al. High rate of subclinical chikungunya virus infection and association of neutralizing antibody with protection in a prospective cohort in the Philippines. PLoS Negl Trop Dis. 2015;9:e0003764. https://doi.org/10.1371/journal.pntd.0003764
8. Gräf T, Vazquez C, Giovanetti M, de Bruycker-Nogueira F, Fonseca V, Claro IM, et al. Epidemiologic history and genetic diversity origins of chikungunya and dengue viruses, Paraguay. Emerg Infect Dis. 2021;27:1393–404. https://doi.org/10.3201/eid2705.204244
9. Faure G, Ogurtsov AY, Shabalina SA, Koonin EV. Adaptation of mRNA structure to control protein folding. RNA Biol. 2017; 14:1649–54. https://doi.org/10.1080/15476286.2017.1349047
10. Sharma Y, Miladi M, Dukare S, Boulay K, Caudron-Herger M, Groß M, et al. A pan-cancer analysis of synonymous mutations. Nat Commun. 2019;10:2569. https://doi.org/10.1038/s41467-019-10489-2

Address for correspondence: Marta Giovanetti, Instituto René Rachou, Fiocruz Minas, Avenida Augusto de Lima, 1.715, Barro Preto, Belo Horizonte, MG, CEP: 30.190-009, Brazil; email: giovanetti.marta@gmail.com

etymologia revisited

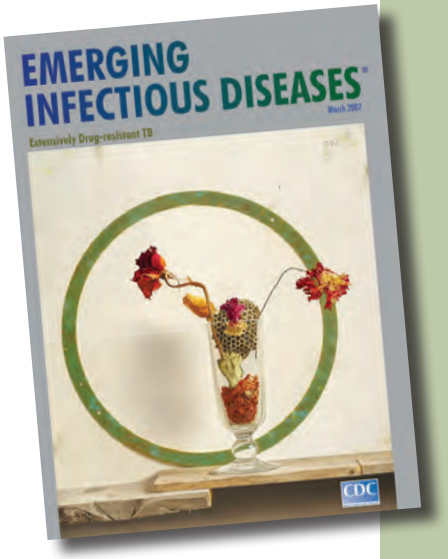

Originally published in March 2007

Norovirus

[nor′-o-vi′rəs]

Genus of viruses that cause viral gastroenteritis. Noroviruses are named after the original strain, "Norwalk virus," which caused an outbreak of acute gastroenteritis among children at an elementary school in Norwalk, Ohio, in 1968. Numerous outbreaks of disease with similar symptoms have been reported since, and the etiologic agents were called "Norwalk-like viruses" or "small round-structured viruses." Noroviruses are transmitted primarily through the fecal-oral route and are highly contagious; as few as 10 viral particles may infect a person.

Reference

Mahy BWJ. A dictionary of virology. London: Academic Press; 2001; http://www.cdc.gov/ncidod/dvrd/revb/gastro/norovirus-qa.htm; http://www.medicinenet.com/norovirus_infection/article.htm

https://wwwnc.cdc.gov/eid/article/13/3/e1-1303_article

Population-Based Serologic Survey of *Vibrio cholerae* Antibody Titers before Cholera Outbreak, Haiti, 2022

Christy H. Clutter,[1] Molly B. Klarman,[1] Youseline Cajusma, Emilee T. Cato, Md. Abu Sayeed, Lindsey Brinkley, Owen Jensen, Chantale Baril, V. Madsen Beau De Rochars, Andrew S. Azman, Maureen T. Long, Derek Cummings, Daniel T. Leung,[2] Eric J. Nelson[2]

A *Vibrio cholerae* O1 outbreak emerged in Haiti in October 2022 after years of cholera absence. In samples from a 2021 serosurvey, we found lower circulating antibodies against *V. cholerae* lipopolysaccharide in children <5 years of age and no vibriocidal antibodies, suggesting high susceptibility to cholera, especially among young children.

In October 2010, a United Nations peacekeeping mission to Haiti following a highly destructive earthquake inadvertently introduced cholera (*1*,*2*), leading to ≈820,000 cases and ≈10,000 deaths over the following 9 years (*3*). The last confirmed case from that outbreak was reported in January 2019 (*4*), commencing a 3-year period with no confirmed cases. Unfortunately, following a wave of sociopolitical instability that compromised sanitation, 2 cases of cholera were reported on October 2, 2022, and a new outbreak began thereafter; as of February 24, 2023, the outbreak had led to >33,000 suspected cases and 590 registered deaths (*5*). Phylogenetic analyses suggested the current strain descended from the *Vibrio cholerae* O1 Ogawa strain responsible for the original outbreak (*6*; C.N. Mavian et al., unpub data; http://medrxiv.org/lookup/doi/10.1101/2022.11.21.22282526). Although previous infection or vaccination can provide protective immunity, persons not exposed to cholera during the earlier outbreak would be immunologically naive and at higher risk for infection, a hypothesis supported by high reported rates of cholera in young children (*5*).

After exposure to *V. cholerae*, the predominant adaptive antibody response is to cholera toxin and lipopolysaccharide (LPS) (*7*). However, the most clearly defined nonmechanistic correlate of protection for cholera is presence of vibriocidal antibodies that target the O-specific antigen of the *V. cholerae* LPS (*8*,*9*). Circulating antibody titers peak within several weeks after infection and slowly wane to baseline over ensuing months, with high levels of variability among patients (*8*). Killed whole-cell oral cholera vaccines (OCVs), such as those distributed during vaccination campaigns in Haiti, are 58% effective for the first 2 years, but effectiveness declines to 26% by 4 years after vaccination (*10*). Children >5 years of age show ≈50% OCV protection level at 2-year follow-up compared with adults (*11*). Because no natural infections were reported and vaccinations were not administered during the 3 years preceding the 2022 outbreak, we investigated the presence of *V. cholerae*–specific antibodies in adults and children by analyzing samples collected in a cross-sectional serologic survey in 2 communes in the Ouest Department of Haiti conducted before the 2022 outbreak.

The Study

We collected dried blood spots from 861 enrolled participants, 564 adults and 297 children (<18 years

Author affiliations: University of Utah, Salt Lake City, Utah, USA (C.H. Clutter, O. Jensen, D.T. Leung); University of Florida, Gainesville, Florida, USA (M.B. Klarman, Y. Cajusma, E.T. Cato, M.A. Sayeed, L. Brinkley, V.M. Beau De Rochars, M.T. Long, D. Cummings, E.J. Nelson); Université d'État d'Haïti, Port au Prince, Haiti (C. Baril); Johns Hopkins University, Baltimore, Maryland, USA (A.S. Azman)

DOI: https://doi.org/10.3201/eid2909.230174

[1]These first authors contributed equally to this article.

[2]These senior authors contributed equally to this article.

of age) (Table 1); 62.6% were female and 37.4% male. A small percentage of participants self-reported previous cholera vaccination (1.2%; n = 10) or clinical disease (4.3%; n = 37). We performed ELISAs on all dried blood spot eluates to assess the quantity of circulating cholera toxin B (CtxB) or *V. cholerae*–specific LPS antibodies. For persons with IgG titers for either epitope ≥2 SD above the mean, we performed vibriocidal assays to assess presence of functional antibodies (Appendix, https://wwwnc.cdc.gov/EID/article/29/9/23-0174-App1.pdf).

We measured antibody titers for *V. cholerae* LPS and CtxB for both IgG and IgA isotypes in all participants (Figure 1, panel A). Children <5 years of age had significantly lower titers of both LPS IgG and IgA compared with older children and adults (p<0.0001; Figure 2, panels A, B; Appendix Table 1). CtxB IgG was elevated in children <5 years of age (p = 0.0033), especially those 1 (p = 0.0024) or 2 (p = 0.0011) years of age (Figure 2, panel C). We found significant differences in CtxB IgA among children <5 years of age, older children, and adults, but this finding was driven by results from children <1 year of age, who may lack antibodies for reasons unrelated to *V. cholerae* exposure (Figure 2, panel D; Appendix Table 1) (*12*). Using generalized additive model–based splines, we estimated a significant positive nonlinear association of IgA isotypes with age (LPS: effective degrees of freedom [EDF] 3.4, p<0.0001; CtxB: EDF 2.0, p<0.0001) (Appendix Figure 1). This association was not significant for IgG isotypes (LPS: EDF 4.9, p = 0.12; CtxB: EDF 1.0, p = 0.13). We conducted vibriocidal assays on a subset (n = 51/861, 5.9%) of samples (Appendix), but no tested samples had detectable vibriocidal responses (Figure 1, panel B).

Conclusions

In this cross-sectional serologic survey within Haiti, we detected low rates of circulating IgG and IgA for LPS and CtxB. Children 1–4 years of age had lower titers of LPS IgG and IgA compared with adults and children ≥5 years of age. Children 1–2 years of age had elevated CtxB IgG titers, which may reflect the cross-reactive nature of CtxB antibodies with the heat-labile toxin of enterotoxigenic *Escherichia coli*, which has the highest force of infection among enteric pathogens among children in Haiti (*13*). Because of that inherent cross-reactivity for CtxB, LPS IgG is a more specific measure for history of exposure to *V. cholerae,* and the IgG isotype is a more meaningful for comparisons among age groups. However, we detected no vibriocidal antibodies, the best available correlate for protection against cholera.

Table. Characteristics of 861 participants from serologic study of *Vibrio cholerae*–specific antibodies before a cholera outbreak in Haiti, 2022

Characteristic	No. (%)
Sex	
M	322 (37.4)
F	539 (62.6)
Age group, y	
Adults ≥18	564 (65.5)
Children 5–17	297 (34.5)
Children <5	112 (13)
Cholera vaccination status	
Vaccinated	10 (1.2)
Not vaccinated	847 (98.4)
Unsure	4 (0.4)
Prior infection	
Yes	37 (4.3)
No	822 (95.5)
Unsure	2 (0.2)

Association of results of serologic assays used in our study with previous *V. cholerae* O1 infection has been shown based on longitudinal studies of culture-confirmed cholera patients (*9*) and with protection against disease based on studies of household contacts of index cases and in human challenge studies (*8*,*13*,*14*). Our data were consistent with data on limited recent disease transmission and antigenic exposure in Haiti, especially among young children born during the period in which little pandemic *V. cholerae* was circulating. Those serologic data suggest that per-

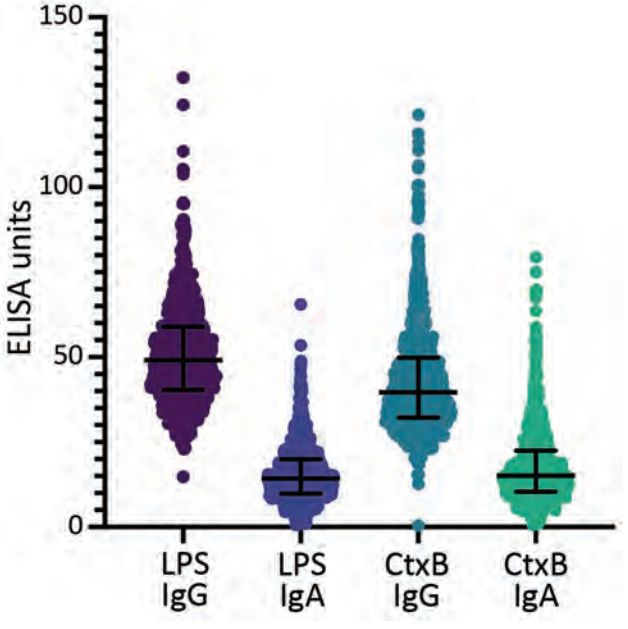

Figure 1. *Vibrio cholerae*–specific and functional antibodies among participants in a serologic study conducted before a cholera outbreak in Haiti, 2022. We performed ELISAs for both IgG and IgA serotypes on all 861 samples for LPS and CtxB. Horizontal lines indicate medians; error bars indicate interquartile ranges. CtxB, cholera toxin subunit B; LPS, lipopolysaccharide.

sons in communities in Haiti who were serosurveyed, especially children <5 years of age, may have limited preexisting immunologic protection against cholera.

The 2022 outbreak was caused by a *V. cholerae* Ogawa isolate that aligns with isolates circulating during the 2010–2019 outbreak (*6*; C.N. Mavian et al., unpub data). The degree to which *V. cholerae* circulated in human and environmental reservoirs at a level below the threshold detectable by the surveillance infrastructure during the period between outbreaks is unknown. The intersection between low levels of circulating cholera and declining population immunity, combined with the collapse of clean water and sanitation infrastructure, likely put residents of Haiti at risk for cholera and led to the 2022 outbreak.

This study was limited by risk of enrollment bias because only 28% of the households screened consented to participate. Given disproportionate sampling in low population density grid cells, true distribution of cholera incidence across the population of Haiti would need to be adjusted before using these data for future serosurveillance research. In addition, observations of relatively lower IgA titers in children 1–4 years of age might have been part of a larger trend of IgA responses increasing with age, a confounding factor that might inaccurately reflect the number of specific exposures. Third, ELISA was limited by availability of quantitative and matrix-matched controls, leading us to use convalescent plasma as positive and naive serum as negative controls. Fourth, selecting samples with high ELISA units for vibriocidal assays may have missed samples with lower antibody levels that harbored functional antibodies. Finally, our serosurvey was limited to 2 adjacent communes in the

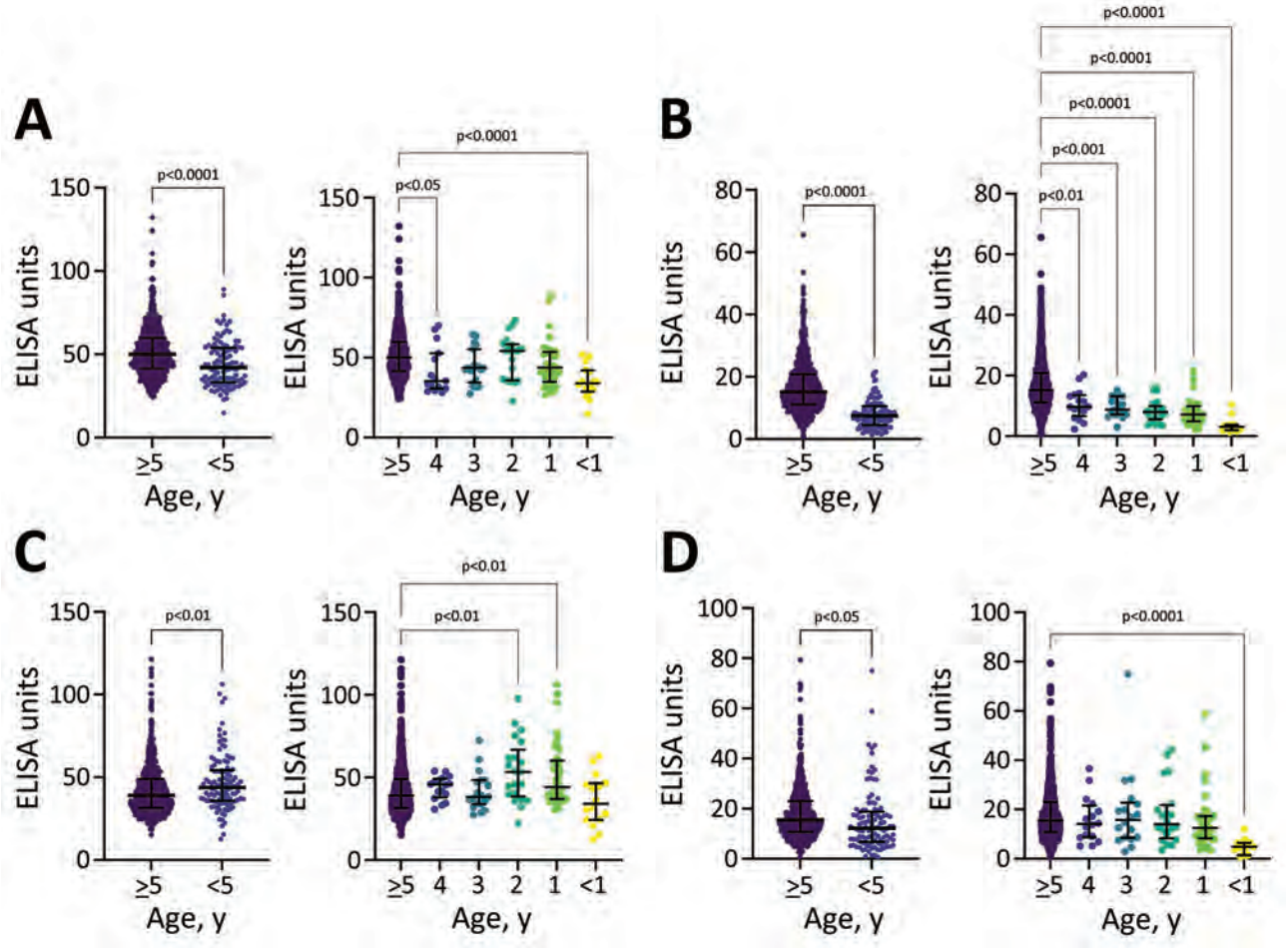

Figure 2. Antibody titers by age, vaccination status, and previous history of infection among participants in a serologic study conducted before a cholera outbreak in Haiti, 2022. We compared antibody titers for lipopolysaccharide (LPS) and cholera toxin subunit B (CtxB) between children <5 years of age (n = 112) and adults and children ≥5 years of age for LPS IgG (A), LPS IgA (B), CtxB IgG (C), and CtxB IgA (D). We made statistical comparisons between the <5- and ≥5-year age groups using an unpaired 2-tailed Student t test. Individual year-by-year comparisons were compared using 1-way analysis of variance. Horizontal lines indicate medians; error bars indicate interquartile ranges. Significant p values are indicated.

Ouest Department of Haiti; hence, findings may not be generalizable to other parts of the country.

In summary, our population-based serosurvey of 2 Haitian communities revealed a lack of functional antibodies and significantly lower *V. cholerae* LPS–specific IgG among young children than older children and adults. These findings suggest persons, especially young children, in Haiti may have high susceptibility to cholera cases and outbreaks.

Acknowledgments

We are grateful to the participants as well as the team who conducted the survey in Haiti. We would like to thank the administrators and leadership at the Emerging Pathogens Institute and the Department of Pediatrics at the University of Florida for their ongoing support. We also honor the dedication and support of the Ministry of Public Health and Population (Ministère de la Santé Publique et de la Population) for their commitment to the health of the Haitian population despite the profound period of instability.

Funding for this study was provided through grant support to D.T.L. from the National Institute of Allergy and Infectious Diseases (R01 AI135115) and to E.J.N. from the Children's Miracle Network (Florida, USA). The sponsors had no role in the design and conduct of the study; collection, management, analysis, and interpretation of the data; preparation, review, or approval of the manuscript; and decision to submit the manuscript for publication.

About the Author

Dr. Clutter is a postdoctoral fellow at the University of Utah investigating cholera seroepidemiology and adaptive immunity during metabolic disease. Ms. Klarman is director of research initiatives at the University of Florida Public Health Research Lab in Gressier, Haiti. Initiatives include surveillance of emerging diseases and efforts to improve early access to healthcare for preemergency patients in resource-limited settings.

References

1. Chin CS, Sorenson J, Harris JB, Robins WP, Charles RC, Jean-Charles RR, et al. The origin of the Haitian cholera outbreak strain. N Engl J Med. 2011;364:33–42. https://doi.org/10.1056/NEJMoa1012928
2. Frerichs RR, Keim PS, Barrais R, Piarroux R. Nepalese origin of cholera epidemic in Haiti. Clin Microbiol Infect. 2012;18:E158–63. https://doi.org/10.1111/j.1469-0691.2012.03841.x
3. World Health Organization. Cholera—Haiti [cited 2023 Feb 7]. https://www.who.int/emergencies/disease-outbreak-news/item/2022-DON427
4. World Health Organization. Cholera, 2019. Weekly Epidemiological Record. 2020;95:441–8.
5. Pan American Health Organization; World Health Organization. Epidemiological update—cholera—28 February 2023 [cited 2023 Feb 7] https://www.paho.org/en/documents/epidemiological-update-cholera-28-february-2023
6. Rubin DHF, Zingl FG, Leitner DR, Ternier R, Compere V, Marseille S, et al. Reemergence of cholera in Haiti. N Engl J Med. 2022;387:2387–9. https://doi.org/10.1056/NEJMc2213908
7. Kauffman RC, Bhuiyan TR, Nakajima R, Mayo-Smith LM, Rashu R, Hoq MR, et al. Single-cell analysis of the plasmablast response to *Vibrio cholerae* demonstrates expansion of cross-reactive memory B cells. MBio. 2016;7:e02021–16. https://doi.org/10.1128/mBio.02021-16
8. Azman AS, Lessler J, Luquero FJ, Bhuiyan TR, Khan AI, Chowdhury F, et al. Estimating cholera incidence with cross-sectional serology. Sci Transl Med. 2019;11:eaau6242. https://doi.org/10.1126/scitranslmed.aau6242
9. Iyer AS, Harris JB. Correlates of protection for cholera. J Infect Dis. 2021;224(Suppl 2):S732–7. https://doi.org/10.1093/infdis/jiab497
10. Bi Q, Ferreras E, Pezzoli L, Legros D, Ivers LC, Date K, et al.; Oral Cholera Vaccine Working Group of the Global Task Force on Cholera Control. Protection against cholera from killed whole-cell oral cholera vaccines: a systematic review and meta-analysis. Lancet Infect Dis. 2017;17:1080–8. https://doi.org/10.1016/S1473-3099(17)30359-6
11. Qadri F, Wierzba TF, Ali M, Chowdhury F, Khan AI, Saha A, et al. Efficacy of a single-dose, inactivated oral cholera vaccine in Bangladesh. N Engl J Med. 2016;374:1723–32. https://doi.org/10.1056/NEJMoa1510330
12. Arnold BF, Martin DL, Juma J, Mkocha H, Ochieng JB, Cooley GM, et al. Enteropathogen antibody dynamics and force of infection among children in low-resource settings. Elife. 2019;8:e45594. https://doi.org/10.7554/eLife.45594
13. Harris JB, LaRocque RC, Chowdhury F, Khan AI, Logvinenko T, Faruque ASG, et al. Susceptibility to *Vibrio cholerae* infection in a cohort of household contacts of patients with cholera in Bangladesh. PLoS Negl Trop Dis. 2008;2:e221. https://doi.org/10.1371/journal.pntd.0000221
14. Haney DJ, Lock MD, Simon JK, Harris J, Gurwith M. Antibody-based correlates of protection against cholera analysis of a challenge study in a cholera-naive population. Clin Vaccine Immunol. 2017;24:e00098–17. https://doi.org/10.1128/CVI.00098-17

Address for correspondence: Christy H. Clutter, Department of Internal Medicine, Division of Infectious Disease, University of Utah, Wintrobe Research Building, Rm 517, 26 North Medical Dr N, Salt Lake City, UT 84112, USA; email: christy.clutter@hsc.utah.edu

Infection-Induced SARS-CoV-2 Seroprevalence among Blood Donors, Japan, 2022

Ryo Kinoshita, Takeshi Arashiro, Noriko Kitamura, Satoru Arai, Koki Takahashi, Tadaki Suzuki, Motoi Suzuki,[1] Daisuke Yoneoka[1]

A nationwide survey of SARS-CoV-2 antinucleocapsid seroprevalence among blood donors in Japan revealed that, as of November 2022, infection-induced seroprevalence of the population was 28.6% (95% CI 27.6%–29.6%). Seroprevalence studies might complement routine surveillance and ongoing monitoring efforts to provide a more complete real-time picture of COVID-19 burden.

SARS-CoV-2 transmission has been identified in Japan since early 2020, and by the end of 2022, ≈29 million COVID-19 diagnosed cases had been reported (*1*). However, case-based surveillance of COVID-19 may underestimate the total number of infections because undiagnosed persons with mild symptoms or asymptomatic infection might not seek treatment. Seroprevalence studies targeting the SARS-CoV-2 nucleocapsid antibody can be used to estimate the proportion of persons experiencing natural infection and may provide insights to understand population immunity status independent of vaccination (*2*–*5*).

During June 2020–February 2022, four large-scale serologic surveys were conducted in 5 prefectures of Japan (Miyagi, Tokyo, Aichi, Osaka, and Fukuoka) (*6*,*7*); a comprehensive survey covering all 47 prefectures has not yet been conducted. Seroprevalence during SARS-CoV-2 Omicron variant predominance in February 2022 was 3.5% for the 5 prefectures (*6*). However, after the seventh epidemic wave started in July 2022, we analyzed residual blood donation samples to determine infection-induced seroprevalence levels in all 47 prefectures of Japan to monitor trends in community transmission across the nation (Figure 1, panel A). This study was performed as an active epidemiologic investigation in accordance with the Act on the Prevention of Infectious Diseases and Medical Care for Patients with Infectious Diseases (Infectious Disease Control Law of Japan; Act No. 114 of 1998) and did not require formal ethics review or participant consent.

The Study

Participants were blood donors to the Japanese Red Cross Society during November 6–13, 2022 (Figure 1, panel A). To be included, participants had to be 16–69 years of age at the time of donation and have provided whole blood or blood components. Persons were not permitted to donate blood if they had been diagnosed with or tested positive for COVID-19 and were <4 weeks after symptom resolution or, for asymptomatic persons, sample collection; if they had acute COVID-19–related signs or symptoms (e.g., fever, cough, breathing difficulty) or experienced altered senses of taste or smell during the period between 2 weeks after symptom onset and 3 days after resolution; or if they were close contacts of confirmed COVID-19 case-patients and <2 weeks after most recent contact.

We calculated the necessary number of samples on the basis of prefecture-level population sizes in October 2021 and expected COVID-19 prevalence from the cumulative number of cases as of September 1, 2022. We also extracted data on age and sex. We tested serum from randomly selected blood samples collected from eligible blood donors using Elecsys Anti-SARS-CoV-2 (Roche Diagnostics, https://www.roche.com), using the manufacturer-recommended seropositivity cutoff index of ≥1.0. We based

Affiliations: National Institute of Infectious Diseases, Tokyo, Japan (R. Kinoshita, T. Arashiro, N. Kitamura, S. Arai, T. Suzuki, M. Suzuki, D. Yoneoka); Japanese Red Cross Society, Tokyo, Japan (K. Takahashi)

DOI: https://doi.org/10.3201/eid2909.230365

[1]These senior authors contributed equally to this article.

seroprevalence estimates on weighted tabulation (*8*). We stratified seroepidemiologic data by prefecture, sex, and age group (16–19, 20–29, 30–39, 40–49, 50–59, or 60–69 years of age) to estimate the survey weights to adjust for the age and sex distribution of each prefecture. We used estimated population as of October 1, 2021, as baseline. We calculated 95% CIs by using the binomial exact method and set the statistical significance level at <0.05 with an acceptable 5% margin of error. For comparison, we also extracted the cumulative number of reported COVID-19 cases through October 30, 2022, from the Ministry of Health, Labour and Welfare (*1*). We extracted vaccination coverage records as of October 30, 2022, from the Digital Agency Vaccination Record System (*9*).

We tested 8,260 specimens from the November 6–13, 2022, study period. Infection-induced seroprevalence in the total population of Japan was 28.6% (95% CI 27.6%–29.6%). We stratified seroprevalence by age and sex (Figure 1, panel B). Median age of blood donors was 47 years (interquartile range 35–55 years). Among both sexes, prevalence peaked in the 20–29-year age group, in which 41.1% (95% CI 37.9%–44.4%) of men and 38.9% (95% CI 34.0%–43.9%) of women were seropositive. Prevalence decreased with age and was lowest among the 60–69-year age group: 16.1% (95% CI 13.9%–18.4%) of men and 19.0% (95% CI 15.6%–22.9%) of women were seropositive. The populations of Tokyo (34.5%, 95% CI 28.7%–40.7%), Osaka (43.0%, 95% CI 36.9%–49.3%), and Okinawa (45.1%, 95% CI 39.7%–50.6%) prefectures had higher seroprevalence than we found overall (Figure 2, panel A) (*10*).

Except in Okinawa, population density and COVID-19 prevalence appeared to have an exponential relationship (Figure 2, panel B), similar to an observed trend in the United States (*11*). Percentages of reported cases among total population were higher than percentages of seroprevalent nucleocapsid antibodies in several low–population density prefectures: 13.0% versus 9.2% in Nagano, 16.6% versus 14.9% in Gifu, 17.6% versus 17.0% in Hiroshima, and 14.3% versus 13.2% in Tokushima (Figure 2, panels C, D). In most prefectures, however, percentage prevalence of nucleocapsid antibodies was higher than percentage of reported cases among the population, although 95% CIs overlapped.

Conclusions

Using specimens from blood donations accepted in November 2022, we revealed the prevalence of nucleocapsid antibodies to SARS-CoV-2 in Japan, although we observed differences in prevalence among prefectures. For comparison over time, a previous population-based serial cross-sectional seroepidemiologic survey showed that prevalences were 3.1% in Tokyo, 4.1% in Osaka, and 1.9% in Fukuoka in December 2021 and 6.4% in Tokyo, 6.1% in Osaka, and 3.3% in Fukuoka in February 2022 (*6*).

Even after the country was largely affected by Omicron-variant disease, estimated seroprevalence was remarkably lower in Japan (28.6%) than what has been reported in the United Kingdom using blood donor samples taken during October 26–December 16, 2022; antinucleocapsid seroprevalence in the United Kingdom was 82.5% (*12*). Seroprevalence in

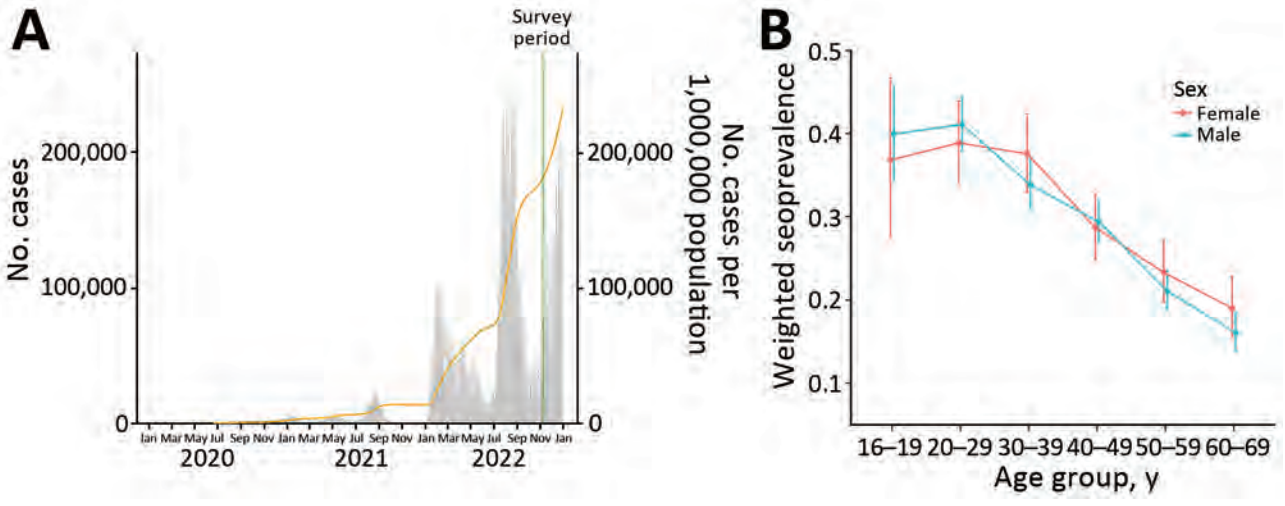

Figure 1. Reported COVID-19 cases among the general population and seroprevalence of SARS-CoV-2 among blood donors, Japan. A) Number of reported COVID-19 cases by date of report, 2020–2022. Orange line indicates cumulative number of reported cases per 1 million persons. Green shading indicates survey period. B) Weighted seroprevalence stratified of SARS-CoV-2 among blood donors from November 6–13, 2022, by age group and sex. Error bars represent 95% CIs.

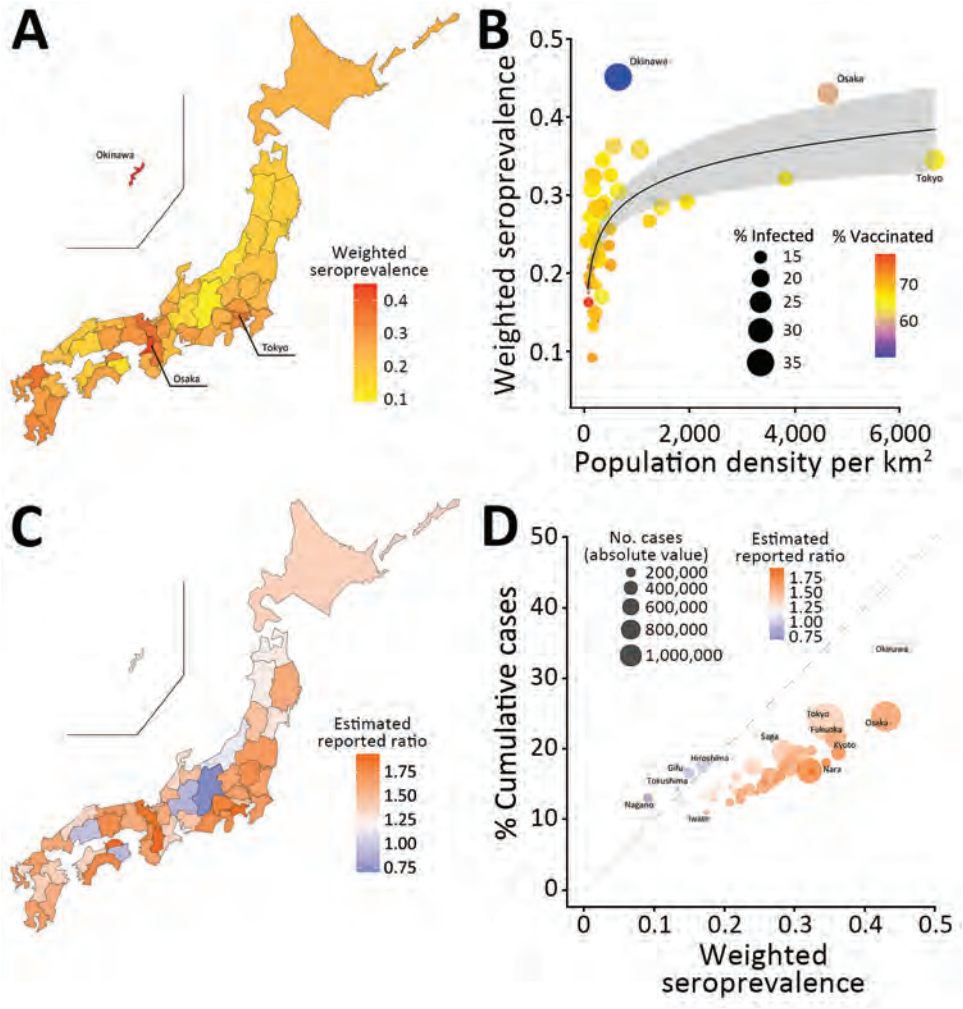

Figure 2. Analyses of weighted seroprevalence of SARS-CoV-2 among blood donors from November 6–13, 2022, compared with reported cases among the general population, Japan. A) Weighted seroprevalence by prefecture. B) Relationship between population density (persons/km^2) and weighted seroprevalence by prefecture. Circle sizes indicate percentage of infected persons based on cumulative number of reported cases; colors indicate vaccination coverage for >3 doses of COVID-19 vaccine. C) Ratio of weighted seroprevalence to the percentage of cumulative number of reported cases (estimated to reported infections) by prefecture. D) Relationship between weighted seroprevalence and percentage of cumulative number of reported cases by prefecture. Circle sizes represent absolute value of cumulative number of reported cases.

Japan in November 2022 was comparable to the estimated seroprevalence of 28.8% among blood donors in the United States as of December 2021 (*13*). Lower seroprevalence in Japan might reflect high vaccination coverage or adherence to public health and social measures. Both the United States and the United Kingdom observed similar decreasing prevalence among older age groups (*12*–*14*). Case ascertainment rate was higher in Japan than the United States, where reported infection-induced seroprevalence was 2.2–3.1 times higher than the cumulative number of reported cases (*14*).

Among limitations in this study, the first is that we adjusted demographic differences among prefectures by survey weights, but selection bias caused by the characteristics of blood donors remains. Second, eligible age in Japan for blood donation is 16–69 years of age; therefore, we could not use these data to evaluate children <16 or elderly persons >69 years of age. Third, samples were all collected within a single 1-week timeframe, which hindered exploration of temporal trends. Finally, ratio of estimated to reported infections does not consider the sensitivity or decay of nucleocapsid antibodies, which could potentially reduce detection of previously infected persons, depending on time since infection, age, sex, and vaccination status (*15*).

Despite those limitations, we comprehensively evaluated the proportion of infected persons in the overall population of Japan. Although reporting all COVID-19 cases has become increasingly challenging in most countries, seroprevalence studies could potentially complement routine surveillance and continued monitoring over time to provide a more complete real-time picture of COVID-19 burden.

Acknowledgments

We thank the prefecture governments and public health centers for surveillance, laboratory examination, and epidemiological investigation. We also thank support from staff members of the Ministry of Health, Labour and Welfare, Japan.

The survey was funded by the Ministry of Health, Labour and Welfare of Japan. R.K. reports receiving support from the Japan Society for the Promotion of Science KAKENHI program (grant no. 21K17307). D.Y. reports receiving support from the Japan Science and Technology Agency PRESTO program (grant no. JPMJPR21RC).

Author contributions: M.S. coordinated the survey. K.T. organized the acquisition of residual blood samples for serological examination. R.K. and D.Y. analyzed the dataset and drafted the article. All the authors made critical revisions to the manuscript for important intellectual content and gave final approval of the manuscript.

About the Author

Dr. Kinoshita is a researcher at the Center for Surveillance, Immunization, and Epidemiologic Research, National Institute of Infectious Diseases, Tokyo, Japan. His primary research interests include infectious diseases epidemiology and modeling with a current focus on prevention of vaccine preventable diseases.

References

1. Japan Ministry of Health Labour and Welfare. Visualizing the data: information on COVID-19 infections [cited 2023 March 15] https://covid19.mhlw.go.jp
2. Kleynhans J, Tempia S, Wolter N, von Gottberg A, Bhiman JN, Buys A, et al.; PHIRST-C Group. SARS-CoV-2 seroprevalence after third wave of infections, South Africa. Emerg Infect Dis. 2022;28:1055–8. https://doi.org/10.3201/eid2805.220278
3. Erikstrup C, Laksafoss AD, Gladov J, Kaspersen KA, Mikkelsen S, Hindhede L, et al. Seroprevalence and infection fatality rate of the SARS-CoV-2 Omicron variant in Denmark: a nationwide serosurveillance study. Lancet Reg Health Eur. 2022;21:100479.
4. Yamayoshi S, Iwatsuki-Horimoto K, Okuda M, Ujie M, Yasuhara A, Murakami J, et al. Age-stratified seroprevalence of SARS-CoV-2 antibodies before and during the vaccination era, Japan, February 2020–March 2022. Emerg Infect Dis. 2022;28:2198–205. https://doi.org/10.3201/eid2811.221127
5. Bhuiyan TR, Hulse JD, Hegde ST, Akhtar M, Islam T, Khan ZH, et al. SARS-CoV-2 seroprevalence before Delta variant surge, Chattogram, Bangladesh, March–June 2021. Emerg Infect Dis. 2022;28:429–31. https://doi.org/10.3201/eid2802.211689
6. Arashiro T, Arai S, Kinoshita R, Otani K, Miyamoto S, Yoneoka D, et al. National seroepidemiological study of COVID-19 after the initial rollout of vaccines: before and at the peak of the Omicron-dominant period in Japan. Influenza Other Respir Viruses. 2023;17:e13094. https://doi.org/10.1111/irv.13094
7. Yoshiyama T, Saito Y, Masuda K, Nakanishi Y, Kido Y, Uchimura K, et al. Prevalence of SARS-CoV-2–specific antibodies, Japan, June 2020. Emerg Infect Dis. 2021;27:628–31. https://doi.org/10.3201/eid2702.204088
8. Gideon L. Handbook of survey methodology for the social sciences. New York: Springer; 2012.
9. Japan Digital Agency. Vaccination Record System (VRS) [cited 2023 Mar 15]. https://info.vrs.digital.go.jp
10. National Institute of Infectious Diseases Japan. Analysis of the rate of existing infections using blood donated samples in November 2022 [in Japanese] [cited 2023 Feb 7]. https://www.niid.go.jp/niid/ja/2019-ncov/2484-idsc/11729-covid19-82.html
11. Sy KTL, White LF, Nichols BE. Population density and basic reproductive number of COVID-19 across United States counties. PLoS One. 2021;16:e0249271. https://doi.org/10.1371/journal.pone.0249271
12. UK Health Security Agency. COVID-19 vaccine surveillance report: week 2 (12 January 2023) [cited 2023 March 15]. https://assets.publishing.service.gov.uk/government/uploads/system/uploads/attachment_data/file/1134075/Vaccine-surveillance-report-week-2-2023.pdf
13. Jones JM, Opsomer JD, Stone M, Benoit T, Ferg RA, Stramer SL, et al. Updated US infection- and vaccine-induced SARS-CoV-2 seroprevalence estimates based on blood donations, July 2020–December 2021. JAMA. 2022;328:298–301. https://doi.org/10.1001/jama.2022.9745
14. Jones JM, Stone M, Sulaeman H, Fink RV, Dave H, Levy ME, et al. Estimated US infection- and vaccine-induced SARS-CoV-2 seroprevalence based on blood donations, July 2020–May 2021. JAMA. 2021;326:1400–9. https://doi.org/10.1001/jama.2021.15161
15. Navaratnam AMD, Shrotri M, Nguyen V, Braithwaite I, Beale S, Byrne TE, et al.; Virus Watch Collaborative. Nucleocapsid and spike antibody responses following virologically confirmed SARS-CoV-2 infection: an observational analysis in the Virus Watch community cohort. Int J Infect Dis. 2022;123:104–11. https://doi.org/10.1016/j.ijid.2022.07.053

Address for correspondence: Daisuke Yoneoka or Motoi Suzuki, Center for Surveillance, Immunization, and Epidemiologic Research, National Institute of Infectious Diseases, 1-23-1 Toyama, Shinjuku-Ku, Tokyo 162-0052, Japan; email: yoneoka@niid.go.jp or mosuzuki@niid.go.jp

Prevalence of Asymptomatic Mpox among Men Who Have Sex with Men, Japan, January–March 2023

Daisuke Mizushima,[1] Yui Shintani,[1] Misao Takano, Daisuke Shiojiri, Naokatsu Ando, Takahiro Aoki, Koji Watanabe, Takato Nakamoto, Hiroyuki Gatanaga, Shinichi Oka

We prospectively assessed asymptomatic monkeypox virus infections among men who have sex with men in Tokyo, Japan, during the initial phase of the mpox epidemic. Our findings suggest that asymptomatic infections were likely underestimated and were comparable in magnitude to symptomatic infections, highlighting the need to improve testing accessibility among high-risk populations.

During the 2022 global mpox outbreak, asymptomatic monkeypox virus (MPXV) infections or unrecognized mpox cases were reported among men who have sex with men (MSM) (*1*–*4*). Asymptomatic cases were diagnosed by using PCR on anorectal, pharyngeal, urine, and pooled samples, but the prevalence of asymptomatic infections varied by country. A recent meta-analysis reported the prevalence of asymptomatic MPXV infections worldwide (*5*), but limited cohort sizes have hindered precise estimations. Understanding the extent to which asymptomatic infections contribute to MPXV transmission is crucial for an effective public health response (*6*,*7*). In addition, further clarification on the how prevalence of asymptomatic infections affect mpox epidemics is needed.

By December 2022, only 8 mpox cases had been confirmed in Japan, and 5 of those cases were reported in Tokyo. However, since the beginning of 2023, the number of new mpox cases has steadily increased in Japan. Despite the rise in cases, vaccination for mpox remains unavailable in Japan, even for high-risk populations, such as MSM and persons with HIV. We assessed asymptomatic MPXV infections among MSM cohorts with and without HIV infection in Tokyo.

The Study

We assessed mpox prevalence among MSM across 3 sites in Tokyo during January 5–March 20, 2023. We enrolled MSM ≥18 years of age who had sexual intercourse within the previous 3 months and who provided written informed consent. We excluded persons from the study if they reported symptoms of suspected mpox at enrollment. Specifically, we excluded persons who had typical mpox symptoms, which include suspected skin lesions and any of the following: fever, lymphadenopathy, or pain in mucous membranes. We categorized atypical symptoms as having 1 typical mpox symptom, such as fever or pain, or other atypical symptoms.

Patients self-collected clinical samples for MPXV testing, including anorectal swab samples or pooled samples consisting of anorectal swabs, initial stream urine, and gargle rinse, by using a previously reported method (*8*). Persons who tested positive for MPXV were closely monitored through weekly health checks conducted via telephone and asked about their general condition, including whether they had any atypical symptoms.

We defined asymptomatic infections as mpox cases without any symptoms, including atypical symptoms, during the study period. We classified symptomatic infections as mpox cases in which any symptoms developed, including atypical symptoms, ≤3 weeks before mpox testing or during the study period. Also, to increase awareness of mpox, we provided all study participants with general information on the disease, including its mode of transmission and typical symptoms.

Author affiliations: National Center for Global Health and Medicine, Tokyo, Japan (D. Mizushima, Y. Shintani, M. Takano, D. Shiojiri, N. Ando, T. Aoki, K. Watanabe, T. Nakamoto, H. Gatanaga, S. Oka); Personal Health Clinic, Tokyo (D. Shiojiri); Kumamoto University, Kumamoto, Japan (H. Gatanaga, S. Oka)

DOI: https://doi.org/10.3201/eid2909.230541

[1]These authors contributed equally to this article.

We used the QIAamp DNA Mini Kit (QIAGEN, https://www.qiagen.com) to extract viral DNA from patient specimens and QuantStudio 12K Flex and QuantiTect Probe PCR Kit (Thermo Fisher Scientific, https://www.thermofisher.com) to subsequently detect viral DNA. To measure the copy numbers for genomic DNA of MPXV and of varicella zoster virus, which is used as a differential diagnosis, we performed a specific multiplex quantitative PCR, as previously reported (*9*). This study was approved by the Human Research Ethics Committee of National Center for Global Health and Medicine (approval no. NCGM-S-004600-00).

We recruited a total of 1,348 eligible MSM for this study (Figure 1; Appendix Table, https://wwwnc.cdc.gov/EID/article/29/9/23-0541-App1.pdf). Two persons were excluded because of suspected symptoms associated with mpox, which were subsequently confirmed outside of this study to be MPXV infection by PCR testing of skin lesions. The remaining 1,346 participants had a median age of 38 (IQR 31–47) years and underwent PCR testing for MPXV. Among participants, 5 (0.37%; 95% CI 0.12–0.86) tested positive. One positive result was obtained from an anorectal swab, and the remaining 4 were from pooled samples (Table; Appendix Figure 1). Of the 5 positive cases, cycle threshold values were 20.8–31.0. The time interval between last sexual activity and mpox diagnosis was 8–48 days. Three of the positive cases remained asymptomatic after 1 month and were classified as asymptomatic infections. However, 1 participant, upon receiving the positive result, disclosed recovering from fever and pharyngitis without experiencing typical skin manifestations of mpox 1 week before the study quantitative PCR test, and another participant reported having only skin lesions 3 days after the screening test. Consequently, we classified those 2 cases as symptomatic MPXV infections.

Of the 1,341 MSM who tested negative by PCR, 4 participants had symptoms of suspected mpox develop after the study test and were later confirmed MPXV-positive by PCR testing of skin lesions. The time from the negative PCR test to symptom onset was 13–53 days, and the time from symptom onset to

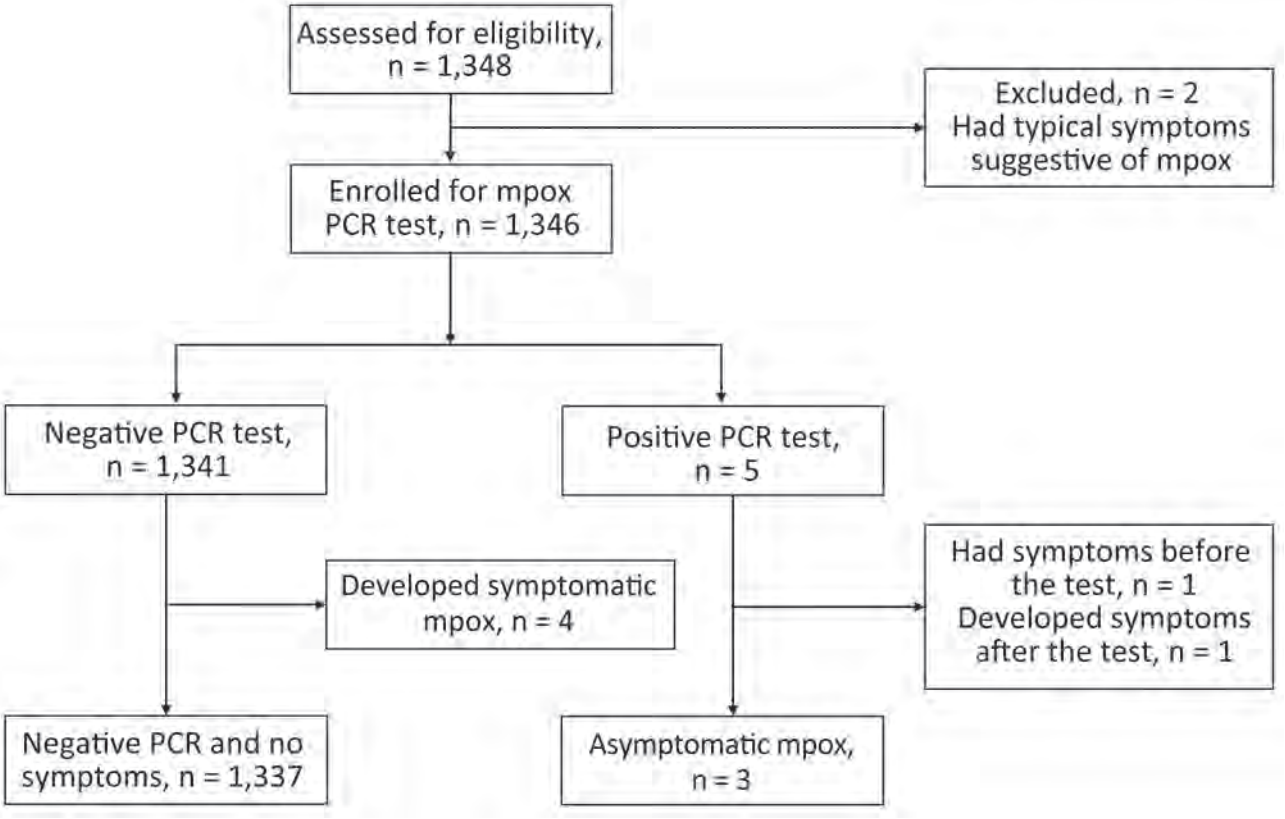

Figure 1. Flowchart of participant selection in a study of prevalence of asymptomatic mpox among men who have sex with men, Japan, January–March 2023. Of 1,348 eligible participants, 2 were excluded because of suggestive mpox symptoms. Of the remaining 1,346, a total of 5 tested positive for mpox via reverse transcription PCR; 4 of those who initially tested negative later had mpox symptoms develop. Ultimately, 6 cases were categorized as symptomatic monkeypox virus infections and 3 as asymptomatic. A total of 1,337 participants tested negative and did not exhibit any symptoms during the study period.

diagnosis was 4–9 days (Figure 2). Of all mpox cases, 4 were MSM with HIV infection; 1 was asymptomatic and 3 were symptomatic. Those 4 case-patients were receiving antiretroviral therapy, had a CD4 count >500 cells/mL, and had an undetectable HIV viral load. During the study period, a total of 44 cases were identified in Tokyo (Appendix Figure 2).

Conclusions

We conducted a large-scale study on mpox prevalence in Japan and found that prevalence of unrecognized or asymptomatic mpox might be underestimated. By applying a rigorous definition of asymptomatic MPXV infection, we identified a similar number of asymptomatic mpox cases compared with symptomatic cases among MSM cohorts in Tokyo, regardless of whether participants had typical or atypical mpox symptoms. These findings provide valuable insights into the intricacies of asymptomatic mpox cases and underscore the pressing need to enhance the availability of mpox testing for high-risk populations experiencing atypical symptoms. In addition, our prospective approach combined with the large cohort and timely surveillance conducted at the onset of the mpox epidemic in Japan (*10*) enabled us to determine a relatively precise prevalence of asymptomatic MPXV infection.

Although the specific infectivity of asymptomatic cases has not yet been determined, the potential prevalence of undetected asymptomatic mpox cases could contribute to the current global pandemic (*11*), which might be supported by our cycle threshold value data that was <30 in asymptomatic cases. To gain a comprehensive understanding of the infectivity of asymptomatic mpox cases, including the duration of viral shedding, further investigation is required. In addition, the lack of awareness of mpox could be affecting the prevalence of undetected cases; most participants in our study were not aware of mpox. Therefore, enhanced awareness, including knowledge of atypical symptoms, and research on infectivity are critically needed to mitigate the potential spread of MPXV.

This study had some limitations. First, ≈70% of the subjects were tested by using only anorectal samples and cross-sectional tests at 3-month intervals, which might have underestimated of asymptomatic mpox prevalence. Second, the infectivity and duration of viral shedding were not evaluated in asymptomatic cases, thereby limiting our understanding of the role of asymptomatic persons in MPXV transmission. Finally, the study did not use MPXV antibody testing because of the low specificity of currently available modalities (*12*,*13*); thus,

Table. Characteristics among cases in a study of prevalence of asymptomatic mpox among men who have sex with men, Japan, January–March 2023*

Case no.	Classification	HIV status	Sample type	Ct value	Timeframe, d					Symptoms
					Sexual activity to diagnosis	Sexual activity to symptom onset	Negative test to symptom onset	Symptom onset to diagnosis	Negative test to diagnosis	
1	Asymptomatic	On PrEP	Anorectal swab	21.2	10	NA	NA	NA	NA	NA
2	Asymptomatic	HIV	Pooled†	20.8	29	NA	NA	NA	NA	NA
3	Asymptomatic	On PrEP	Pooled†	28.4	ND	NA	NA	NA	NA	NA
4	Symptomatic‡	HIV	Pooled†	28.8	8	11	NA	NA	NA	Skin lesions
5	Symptomatic§	On PrEP	Pooled†	31.0	48	8	NA	NA	NA	Fever and pharyngitis
6	Symptomatic¶	HIV	Skin lesion swab	ND	22	15	32	7	39	Skin lesions
7	Symptomatic¶	On PrEP	Skin lesion swab	ND	23	18	48	5	53	Skin lesions, fever, lymphadenopathy, and pharyngitis
8	Symptomatic¶	On PrEP	Skin lesion swab	ND	18	9	13	9	22	Skin lesions, fever, lymphadenopathy, and pharyngitis
9	Symptomatic¶	HIV	Skin lesion swab	ND	8	4	53	4	57	Skin lesions and lymphadenopathy

*Ct, cycle threshold; NA, not applicable; ND, no data; PrEP, preexposure prophylaxis.
†Samples consisted of anorectal swabs, initial stream urine, and gargle rinse.
‡Initially asymptomatic but had symptoms develop during study.
§Initially asymptomatic, but patient later reported previous self-resolving symptoms.
¶Initially tested negative but had symptoms develop during study.

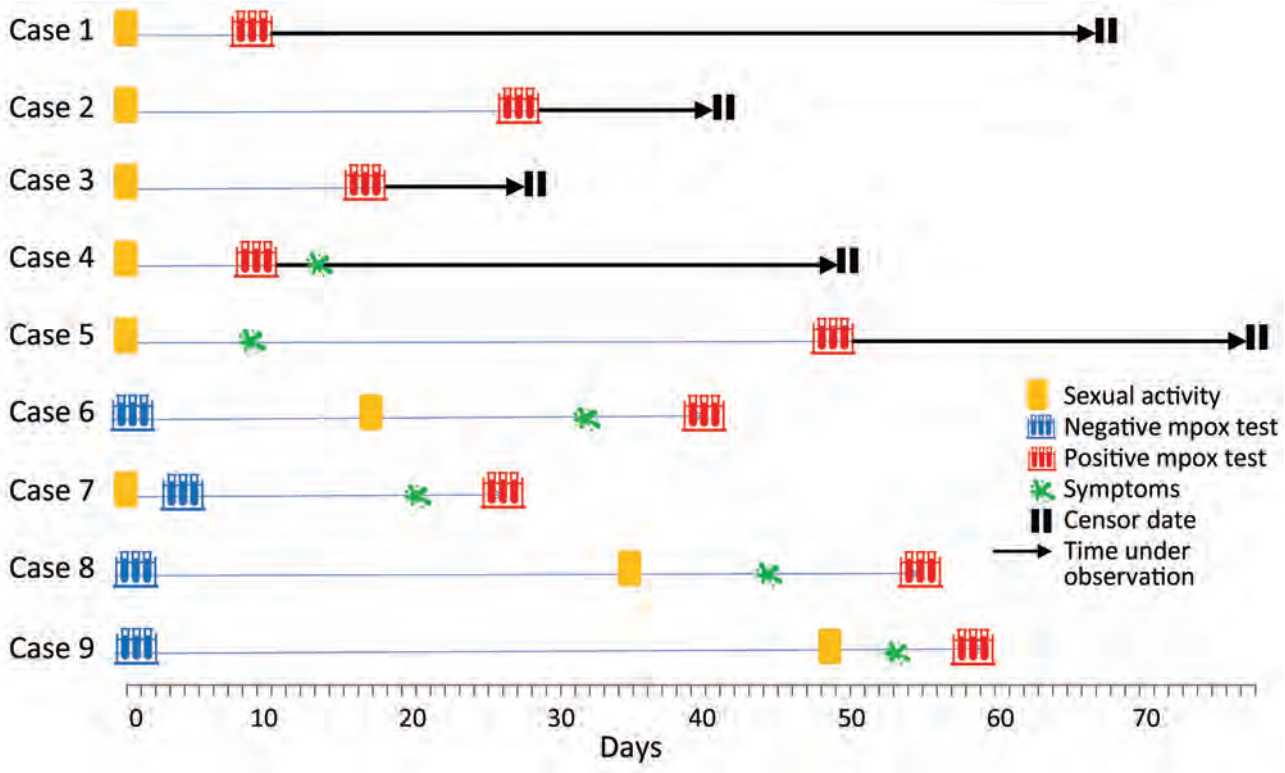

Figure 2. Timeline of sexual activity, symptoms, and testing for participants in a study of prevalence of asymptomatic mpox among men who have sex with men, Japan, January–March 2023. Data are provided for 9 participants who were positive for monkeypox virus during the study period. Cases 1–3 remained asymptomatic.

we might have missed additional asymptomatic mpox cases.

In conclusion, our study offers valuable insights into the relative magnitude between asymptomatic and symptomatic MPXV infection among MSM cohorts during the early stages of the mpox epidemic in Japan. Further research is needed to comprehend the epidemiology and clinical significance of asymptomatic mpox, including examination of the infectivity and the duration of viral shedding in asymptomatic cases. Nonetheless, our study highlights the urgent need for mpox awareness, testing, and vaccination among high-risk groups, including MSM and HIV-positive persons, in Japan.

Acknowledgments

We thank all clinical staff at AIDS Clinical Center, National Center for Global Health and Medicine, especially Kazuko Tanaka and Yoshimi Deguchi for their assistance and support in conducting this study.

S.O. has received research grants and materials from Japan Tobacco/Trii Pharmaceutical, MSD K.K., CSL Behring, Gilead Sciences, and ViiV Healthcare, Co., and has received honorariums from Torii Pharmaceutical, Co., MSD K.K., Gilead Sciences., Janssen Pharmaceutical, K.K., and ViiV Healthcare, Co. H.G. has received honorariums from MSD K.K., Abbott Japan, Co., Janssen Pharmaceutical K.K., Torii Pharmaceutical, Co., Roche Diagnostics K.K., and ViiV Healthcare, Co. Other authors declare no conflict of interest.

About the Author

Dr. Mizushima is a manager of the AIDS Clinical Center, National Center for Global Health and Medicine, Tokyo, Japan. His research interests include HIV and other sexually transmitted infections.

References

1. Moschese D, Pozza G, Mileto D, Giacomelli A, Cutrera M, Cossu MV, et al. Isolation of viable monkeypox virus from anal and urethral swabs, Italy, May to July 2022. Euro Surveill. 2022;27:2200675. https://doi.org/10.2807/1560-7917.ES.2022.27.36.2200675
2. Ferré VM, Bachelard A, Zaidi M, Armand-Lefevre L, Descamps D, Charpentier C, et al. Detection of monkeypox virus in anorectal swabs from asymptomatic men who have sex with men in a sexually transmitted infection screening program in Paris, France. Ann Intern Med. 2022;175:1491–2. https://doi.org/10.7326/M22-2183

3. De Baetselier I, Van Dijck C, Kenyon C, Coppens J, Michiels J, de Block T, et al.; ITM Monkeypox study group. Retrospective detection of asymptomatic monkeypox virus infections among male sexual health clinic attendees in Belgium. Nat Med. 2022;28:2288–92. https://doi.org/10.1038/s41591-022-02004-w
4. Ogale YP, Baird N, Townsend MB, Berry I, Griffin I, Lee M, et al. Evidence of mpox virus infection among persons without characteristic lesions or rash presenting for first dose of JYNNEOS vaccine—District of Columbia, August 2022. Clin Infect Dis. 2023 Mar 14 [Epub ahead of print]. https://doi.org/10.1093/cid/ciad145
5. Satapathy P, Mohanty P, Manna S, Shamim MA, Rao PP, Aggarwal AK, et al. Potentially asymptomatic infection of monkeypox virus: a systematic review and meta-analysis. Vaccines (Basel). 2022;10:2083. https://doi.org/10.3390/vaccines10122083
6. Reda A, El-Qushayri AE, Shah J. Asymptomatic monkeypox infection: a call for greater control of infection and transmission. Lancet Microbe. 2023;4:e15–6. https://doi.org/10.1016/S2666-5247(22)00259-2
7. Van Dijck C, De Baetselier I, Kenyon C, Liesenborghs L, Vercauteren K, Van Esbroeck M, et al.; ITM Monkeypox Study Group. Mpox screening in high-risk populations finds no asymptomatic cases. Lancet Microbe. 2023;4:e132–3. https://doi.org/10.1016/S2666-5247(22)00357-3
8. Ando N, Mizushima D, Watanabe K, Takano M, Shiojiri D, Uemura H, et al. Modified self-obtained pooled sampling to screen for *Chlamydia trachomatis* and *Neisseria gonorrhoeae* infections in men who have sex with men. Sex Transm Infect. 2021;97:324–8. https://doi.org/10.1136/sextrans-2020-054666
9. Maksyutov RA, Gavrilova EV, Shchelkunov SN. Species-specific differentiation of variola, monkeypox, and varicella-zoster viruses by multiplex real-time PCR assay. J Virol Methods. 2016;236:215–20. https://doi.org/10.1016/j.jviromet.2016.07.024
10. World Health Organization. Multi-country outbreak of mpox, external situation report #19—30 March 2023 [cited 2023 Apr 21]. https://www.who.int/publications/m/item/multi-country-outbreak-of-mpox--external-situation-report--19---30-march-2023
11. Van Dijck C, Hens N, Kenyon C, Tsoumanis A. The roles of unrecognized mpox cases, contact isolation and vaccination in determining epidemic size in Belgium: a modeling study. Clin Infect Dis. 2023;76:e1421–3. https://doi.org/10.1093/cid/ciac723
12. Karem KL, Reynolds M, Braden Z, Lou G, Bernard N, Patton J, et al. Characterization of acute-phase humoral immunity to monkeypox: use of immunoglobulin M enzyme-linked immunosorbent assay for detection of monkeypox infection during the 2003 North American outbreak. Clin Diagn Lab Immunol. 2005;12:867–72.
13. Waddell CJ, Filardo TD, Prasad N, Pellegrini GJ Jr, Persad N, Carson WC, et al. Possible undetected mpox infection among persons accessing homeless services and staying in encampments—San Francisco, California, October–November 2022. MMWR Morb Mortal Wkly Rep. 2023;72:227–31. https://doi.org/10.15585/mmwr.mm7209a3

Address for correspondence: Daisuke Mizushima, National Center for Global Health and Medicine, AIDS Clinical Center, 1-21-1 Toyama, Shinjuku, Tokyo 162-8655, Japan; email: dmizushi@acc.ncgm.go.jp

Population Analysis of *Escherichia coli* Sequence Type 361 and Reduced Cefiderocol Susceptibility, France

Agnès B. Jousset, Laura Bouabdallah, Aurélien Birer, Isabelle Rosinski-Chupin, Jean-François Mariet, Saoussen Oueslati, Cécile Emeraud, Delphine Girlich, Philippe Glaser, Thierry Naas, Rémy A. Bonnin, Laurent Dortet

Cefiderocol resistance is increasingly reported in New Delhi metallo-β-lactamase–producing Enterobacterales. Genomic and phenotypic analysis of *Escherichia coli* sequence type 361, a primary clone causing carbapenemase spread in France, revealed mutations leading to cefiderocol resistance. Continued genomic surveillance of carbapenem-resistant Enterobacterales could clarify prevalence of cefiderocol-resistant *E. coli* in Europe.

Few last-line antimicrobial agents effectively treat infections caused by New Delhi metallo-β-lactamase (NDM)–producing Enterobacterales (*1*). Cefiderocol is a novel synthetic conjugate siderophore cephalosporin that is more stable against β-lactamase hydrolysis than classical cephalosporins (*2*). However, several acquired cefiderocol-resistance mechanisms have been described in Enterobacterales, including increased bla_{NDM} copy numbers (*3*), specific bla_{KPC} variants (*4*), structural change in AmpC (*5*), and mutations or inactivation of siderophore receptors (*6*). Specific polymorphisms in penicillin-binding protein 3 (PBP3), the target of cefiderocol, also have been reported in *Acinetobacter* and *Escherichia coli* (*7*–*9*). However, prevalence of those polymorphisms and effects of cumulative resistance mechanisms have not been fully evaluated.

Since 2012, the French National Reference Center (F-NRC) for Antimicrobial Resistance has conducted active nationwide surveillance of carbapenemase-producing Enterobacterales (CPE). In 2022, the percentage of *E. coli* sequence type (ST) 361 isolates sent to F-NRC doubled to 1.2% from 0.6% of CPE in 2021. We characterized emerging *E. coli* ST361 in France and investigated cefiderocol resistance among CPE.

The Study

Since 2014, prevalence of NDM-producing Enterobacterales has been increasing in France (Figure 1, panel A). Among NDM producers, we observed a polyclonal dissemination of *E. coli* isolates, but 50% of isolates were from 4 main clones (ST410, ST167, ST361, and ST405), as reported in other countries in Europe (Appendix 1 Figure 1, https://wwwnc.cdc.gov/EID/article/29/9/23-0390-App1.pdf) (*10*). *E. coli* ST410, ST167, and ST405 have been characterized at the genomic level (*3*,*8*,*11*), but ST361 characteristics remain unclear.

During July 1, 2021–June 30, 2022, we investigated all (n = 856) nonduplicate carbapenem-nonsusceptible *E. coli* isolates sent to F-NRC. We used Sensititer broth microdilution (ThermoFisher, https://www.thermofisher.com), as previously described (*12*), to measure MICs of aztreonam, ceftazidime-avibactam, imipenem, meropenem, and cefiderocol (Figure 2). Of note, the Mueller–Hinton broths used were from batches not affected by the manufacturer's withdrawal relayed by European Committee on Antimicrobial Susceptibility Testing (https://www.eucast.org/

Author affiliations: Bicêtre Hospital Bacteriology Hygiene, Le Kremlin-Bicetre, France (A.B. Jousset, J.-F. Mariet, C. Emeraud, T. Naas, R.A. Bonnin, L. Dortet); Institut National de la Santé et de la Recherche Médicale, Paris, France (A.B. Jousset, L. Bouabdallah, S. Oueslati, C. Emeraud, D. Girlich, T. Naas, R.A. Bonnin, L. Dortet); Centre National de Référence de la Résistance aux Antibiotiques, Le Kremlin-Bicetre (A.B. Jousset, J.-F. Mariet, C. Emeraud, T. Naas, R.A. Bonnin, L. Dortet); Centre National de Référence de la Résistance aux Antibiotiques, Clermont-Ferrand, France (A. Birer); Institut Pasteur, Paris (I. Rosinski-Chupin, P. Glaser); Universite Paris-Sud, Paris (T. Naas)

DOI: https://doi.org/10.3201/eid2909.230390

ast-of-bacteria/warnings). Among tested isolates, 774 were CPE, including 243 NDM producers. The MIC_{50} (MIC to inhibit growth of 50% of isolates) of cefiderocol was higher (2 mg/L) for NDM producers among isolates tested compared with other carbapenem-resistant *E. coli* (0.12 mg/L) (Figure 1, panel B), as previously reported (*12*).

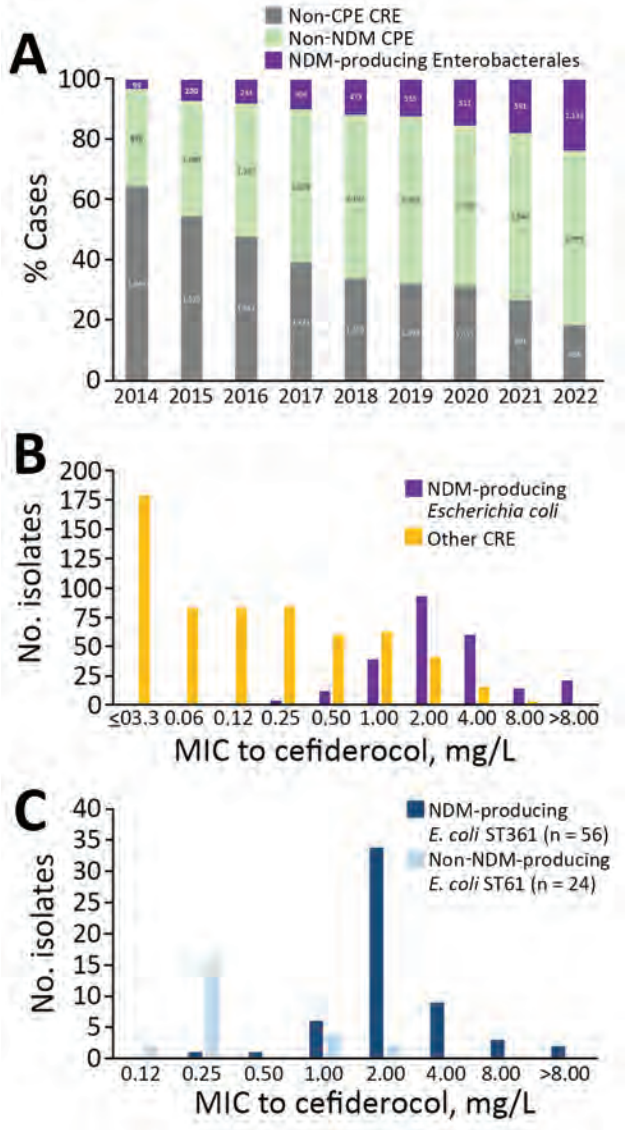

Figure 1. Evolution of NDM-producing and non–NDM-producing CPE observed in a population analysis of *Escherichia coli* ST361 and reduced cefiderocol susceptibility, France. A) Evolution of non-CPE CRE, non-NDM CRE, and non–NDM-producing Enterobacterales sent to the French National Reference Center for Antimicrobial Resistance during 2014–2022. B) Distribution of cefiderocol MICs in all (n = 856) CRE isolates collected during the study, July 1, 2021–June 30, 2022. C) Distribution of cefiderocol MICs in all (n = 80) *E. coli* ST361 isolates from the French National Reference Center for Antimicrobial Resistance collection, 2015–2022. CPE, carbapenemase-producing Enterobacterales; CRE, carbapenem-resistant Enterobacterales; NDM, New Delhi metallo-β-lactamase; non-CPE, non–carbapenemase producing; non-NDM CPE, non–NDM carbapenemase-producing Enterobacterales; ST, sequence type.

To genomically characterize *E. coli* ST361, we added all (n = 51) ST361 isolates sent to F-NRC during 2015–2021 to the 29 isolates collected during the study period. We conducted short-read sequencing on those 80 isolates by using the NextSeq500 system (Illumina, https://www.illumina.com). We assembled sequences by using Shovill 1.1.0 (https://github.com/tseemann/shovill) and SPAdes 3.14.0 (https://github.com/ablab/spades) under GenBank BioProject no. PRJNA925451 (Appendix 2 Table 1). We used Resfinder 4.1 (*13*) to analyze resistome content and PlasmidFinder 2.1 (*14*) to analyze replicon content (Appendix 2 Table 2).

Among 80 *E. coli* ST361 isolates, 50 produced NDM carbapenemase, 49 of which were NDM-5; another 20 produced oxacillinase 48–like carbapenemase; 6 coproduced NDM-5 with another carbapenemase; and 4 did not produce carbapenemase (Figure 2). Analysis of cefiderocol MIC distribution for ST361 showed that isolates with MICs >2 produced NDM, but that analysis also suggested that mechanisms besides NDM are involved in cefiderocol resistance (Figure 1, panel C). Thus, we analyzed the bla_{NDM} gene copy number on CLC Genomics Workbench 21.0 (QIAGEN, https://www.qiagen.com), where we mapped the raw data (fastq reads) on the genome (fasta) of each corresponding *E. coli* sequence. Then we normalized the average coverage of bla_{NDM} mapping reads to the average coverage of 10 different chromosomal genes used as references. However, correlation analysis did not reveal an association between bla_{NDM} gene number and the cefiderocol MIC (data not shown). Then we used *E. coli* K-12 MG1655 (GenBank accession no. NC_000913) as a reference to investigate *cirA*, *fiu*, *fepA*, *fepB*, *fecA*, *fhuA*, *tonB*, *pcnB*, *exbB*, *exbD*, *baeS/baeR*, and *ompR/envZ* gene mutations involved in siderophore-iron uptake. To eliminate polymorphisms linked to the ST itself, we only considered amino acid substitutions not shared by all ST361 isolates. A total of 14 (18%) isolates displayed a mutation in 1 of those genes (Appendix 2 Table 1, https://wwwnc.cdc.gov/EID/article/29/9/23-0390-App2.xlsx). Overall, analysis of variance multiple parameter correlation analysis in RStudio 2022.07.1 (The R Foundation for Statistical Computing, https://www.r-project.org) revealed that bla_{NDM} ($p = 0.0035$) or chromosomal mutations ($p = 0.0033$) within a siderophore receptor were associated with higher cefiderocol MICs.

We also analyzed the preferential cefiderocol target, PBP3. That analysis revealed that compared

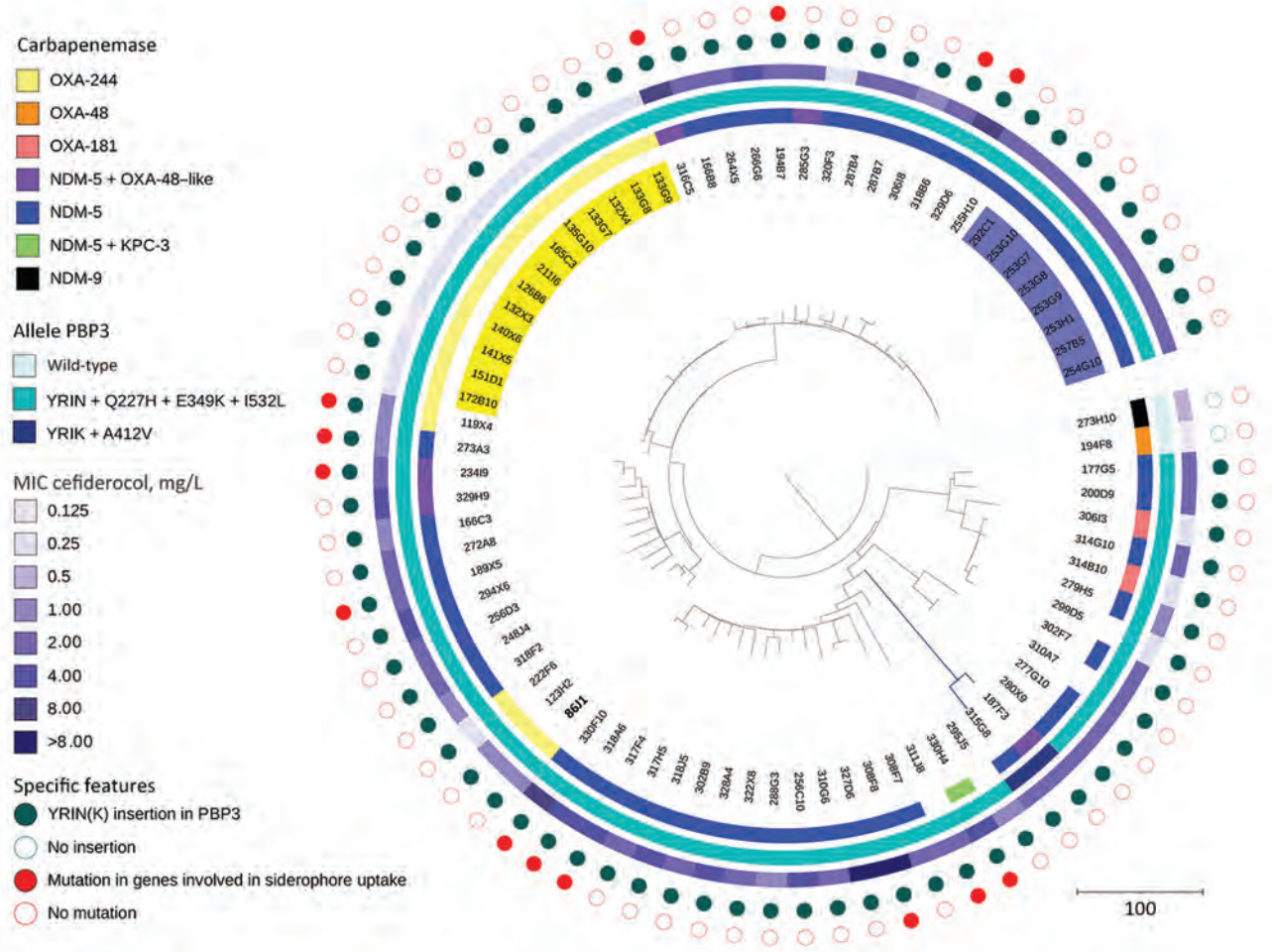

Figure 2. Phylogenetic analysis of 80 *Escherichia coli* ST361 isolates collected during 2015–2022 and used in a population analysis of *E. coli* ST361 and reduced cefiderocol susceptibility, France. Isolates were sent to the French National Reference Center for carbapenem-resistant Enterobacterales testing as part of routine surveillance. The phylogenetic tree was built by using SNIppy version 4.6.0 (https://github.com/tseemann/snippy) on whole-genome sequences. Data were visualized using iTOL 6.5.2 (https://itol.embl.de). The most ancient isolate, isolate no. 86J1 collected in 2015 (bold text, lower left of tree), was used as reference genome. A total of 4,957,882 nt positions were analyzed in the comparison. Colors indicate various outbreaks involving 13 OXA-244 producers (yellow) and 7 NDM-5 producers (blue). Two specific features are represented with filled circles: a YRIN(K) insertion in PBP3 (green) and chromosomal mutations within genes involved in siderophore-iron uptake (red). Genes investigated were *cirA, fiu, fepA, fepB, fecA, fhuA, tonB, pcnB, exbB, exbD, baeS/baeR*, and *ompR/envZ*. Scale bar indicates nucleotide substitutions per site. KPC, *Klebsiella pneumoniae* carbapenemase; NDM, New Delhi metallo-β-lactamase; OXA, oxacillinase; PBP3, penicillin-binding protein 3.

with the reference, 76 isolates shared a common allele that had a 4 amino acid insertion (YRIN motif) at position 333 and 3 substitutions (Q227H, E349K, and I532L). Two isolates had a different allele with a YRIK insertion and an A412V substitution, and 2 isolates had no insertions or mutations. Of note, the 3 different alleles were associated with 3 different nodes on the phylogenetic tree, indicating an evolution process that probably involved chromosomal recombination (Figure 2), as described for ST410 (*11*). The YRIN(K) motif insertion has been described to be involved in cephalosporin and aztreonam resistance (*8*,*9*,*11*). To study the effect of the YRIN(K) motif insertion on cefiderocol resistance, we performed susceptibility testing on the reference strain and its isogenic PBP3 encoding gene mutant with YRIN insertion (*11*). We transformed both strains by plasmid topoisomerase-based cloning $bla_{\text{NDM-1}}$ to increase the basal range of cefiderocol MIC concentrations in the microbroth dilution technique. The YRIN insertion resulted in a 4-fold increase in cefiderocol MIC, from ≤0.03 mg/L to 0.125 mg/L in the YRIN *ftsI* chromosomal mutant.

We also analyzed all (n = 321) available ST361 genomes and metadata in EnteroBase (University of Warwick, https://warwick.ac.uk/fac/sci/med/research/biomedical/mi/enterobase) on October 1,

2022 (Appendix 1 Figures 3, 4; Appendix 2 Table 3). The 401-isolate phylogenetic tree showed that isolates from F-NRC were distributed within several main branches (Appendix 1 Figure 3), confirming our collection's diversity. Of note, the YRIN(K) insertion occurred in only 36% of the EnteroBase genomes but occurred in 97% of NDM producers; however, only 7% of non–NDM producers had the modified alleles. The phylogenetic tree enabled visualization of this strong association between occurrence of NDM and PBP3 alleles possessing the YRIN(K) insertion. Furthermore, specifying isolate locations revealed international ST361 circulation.

We also examined genomes sequenced at F-NRC during 2015–2022 that are from 3 other predominant STs disseminating NDM-5 in France. Among those genomes, we noted a high prevalence of YRIN(K) insertion in PBP3, namely in 98% of ST410 (n = 273), 92% of ST167 (n = 184), and 86% of ST405 (n = 122), regardless of β-lactamase content (Appendix 1 Figure 5, panel A). YRIN(K) insertion prevalence was only 4% in *E. coli* ST131 (n = 166), another high-risk clone associated with multiple β-lactamases (*15*). Distribution analysis of cefiderocol MICs in ST410, ST167, and ST405, excluding NDM-producing isolates, revealed a MIC_{50} of 1 mg/L, confirming the role of the genetic background in reduced cefiderocol susceptibility (Appendix 1 Figure 5, panel B).

Conclusions

Our results highlight the emergence of NDM-producing *E. coli* ST361 associated with reduced cefiderocol susceptibility in France. Emergence resulted from a combination of factors: modified PBP3, a strong association with NDM-5 carbapenemase, and frequent chromosomal mutations in genes involved in siderophore-iron uptake. No feature alone is sufficient to confer cefiderocol resistance, according to published clinical breakpoints (https://www.eucast.org/clinical_breakpoints), but the combined mechanisms appear to confer resistance.

In conclusion, our study revealed that *E. coli* ST361 is becoming a key player in NDM-5 carbapenemase dissemination, and its genetic background confers reduced cefiderocol susceptibility. *E. coli* ST361 has only been sporadically reported, but its prevalence might be underestimated. To further assess prevalence and spread of cefiderocol-resistant *E. coli* in Europe, each country should continue nationwide genomic surveillance of carbapenemase-resistant bacteria.

This work was supported by grants from the French National Research Agency, project Seq2Diag PPR Antibioresistance (grant no. ANR-20-PAMR-0010).

About the Author

Dr. Jousset is an assistant professor at the Institut National de la Santé et de la Recherche Médicale (INSERM), Paris, France. Her main research interests include epidemiology, genetics, and biochemistry of β-lactamases in gram-negative bacteria.

References

1. Wright H, Bonomo RA, Paterson DL. New agents for the treatment of infections with gram-negative bacteria: restoring the miracle or false dawn? Clin Microbiol Infect. 2017;23:704–12. https://doi.org/10.1016/j.cmi.2017.09.001
2. Wang C, Yang D, Wang Y, Ni W. Cefiderocol for the treatment of multidrug-resistant gram-negative bacteria: a systematic review of currently available evidence. Front Pharmacol. 2022;13:896971. https://doi.org/10.3389/fphar.2022.896971
3. Simner PJ, Mostafa HH, Bergman Y, Ante M, Tekle T, Adebayo A, et al. Progressive development of cefiderocol resistance in *Escherichia coli* during therapy is associated with an increase in bla_{NDM-5} copy number and gene expression. Clin Infect Dis. 2022;75:47–54. https://doi.org/10.1093/cid/ciab888
4. Hobson CA, Cointe A, Jacquier H, Choudhury A, Magnan M, Courroux C, et al. Cross-resistance to cefiderocol and ceftazidime–avibactam in KPC β-lactamase mutants and the inoculum effect. Clin Microbiol Infect. 2021;27:1172.e7–10. https://doi.org/10.1016/j.cmi.2021.04.016
5. Shields RK, Iovleva A, Kline EG, Kawai A, McElheny CL, Doi Y. Clinical evolution of AmpC-mediated ceftazidime-avibactam and cefiderocol resistance in *Enterobacter cloacae* complex following exposure to cefepime. Clin Infect Dis. 2020;71:2713–6. https://doi.org/10.1093/cid/ciaa355
6. Klein S, Boutin S, Kocer K, Fiedler MO, Störzinger D, Weigand MA, et al. Rapid development of cefiderocol resistance in carbapenem-resistant *Enterobacter cloacae* during therapy is associated with heterogeneous mutations in the catecholate siderophore receptor *cirA*. Clin Infect Dis. 2022;74:905–8. https://doi.org/10.1093/cid/ciab511
7. Malik S, Kaminski M, Landman D, Quale J. Cefiderocol resistance in *Acinetobacter baumannii*: roles of β-lactamases, siderophore receptors, and penicillin binding protein 3. Antimicrob Agents Chemother. 2020;64:e01221-20. https://doi.org/10.1128/AAC.01221-20
8. Wang Q, Jin L, Sun S, Yin Y, Wang R, Chen F, et al. Occurrence of high levels of cefiderocol resistance in carbapenem-resistant *Escherichia* coli before its approval in China: a report from China CRE-Network. Microbiol Spectr. 2022;10:e0267021. https://doi.org/10.1128/spectrum.02670-21
9. Sato T, Ito A, Ishioka Y, Matsumoto S, Rokushima M, Kazmierczak KM, et al. *Escherichia coli* strains possessing a four amino acid YRIN insertion in PBP3 identified as part of the SIDERO-WT-2014 surveillance study. JAC Antimicrob Resist. 2020;2:dlaa081. https://doi.org/10.1093/jacamr/dlaa081
10. Chakraborty T, Sadek M, Yao Y, Imirzalioglu C, Stephan R, Poirel L, et al. Cross-border emergence of *Escherichia coli* producing the carbapenemase NDM-5 in Switzerland and Germany. J Clin Microbiol. 2021;59:e02238-20. https://doi.org/10.1128/JCM.02238-20

11. Patiño-Navarrete R, Rosinski-Chupin I, Cabanel N, Gauthier L, Takissian J, Madec JY, et al. Stepwise evolution and convergent recombination underlie the global dissemination of carbapenemase-producing *Escherichia coli*. Genome Med. 2020;12:10. https://doi.org/10.1186/s13073-019-0699-6
12. Bonnin RA, Emeraud C, Jousset AB, Naas T, Dortet L. Comparison of disk diffusion, MIC test strip and broth microdilution methods for cefiderocol susceptibility testing on carbapenem-resistant Enterobacterales. Clin Microbiol Infect. 2022;28:1156.e1–5. https://doi.org/10.1016/j.cmi.2022.04.013
13. Bortolaia V, Kaas RS, Ruppe E, Roberts MC, Schwarz S, Cattoir V, et al. ResFinder 4.0 for predictions of phenotypes from genotypes. J Antimicrob Chemother. 2020;75:3491–500. https://doi.org/10.1093/jac/dkaa345
14. Carattoli A, Zankari E, García-Fernández A, Voldby Larsen M, Lund O, Villa L, et al. In silico detection and typing of plasmids using PlasmidFinder and plasmid multilocus sequence typing. Antimicrob Agents Chemother. 2014;58:3895–903. https://doi.org/10.1128/AAC.02412-14
15. Dautzenberg MJD, Haverkate MR, Bonten MJM, Bootsma MCJ. Epidemic potential of *Escherichia coli* ST131 and *Klebsiella pneumoniae* ST258: a systematic review and meta-analysis. BMJ Open. 2016;6:e009971. https://doi.org/10.1136/bmjopen-2015-009971

Address for correspondence: Agnès B. Jousset, Service de Bactériologie-Hygiène, Hôpital de Bicêtre, 78 rue du Général Leclerc, 94275 Le Kremlin-Bicêtre CEDEX, France; email: agnes.jousset@aphp.fr

Acute Chagas Disease Outbreak among Military Personnel, Colombia, 2021

Hernán Darío Vergara, Carlos H. Gómez, Álvaro A. Faccini-Martínez, Ana Catalina Herrera, María José López, Camila Camacho, Lilian Muñoz, Lissa Cruz-Saavedra, Carolina Hernández, Juan David Ramírez

We report an acute Chagas disease outbreak among soldiers in Colombia. *Trypanosoma cruzi* infection was confirmed through parasitology, serology, and molecular methods. Among 9 affected soldiers, 2 died; 7 were hospitalized and received benznidazole treatment, which produced favorable outcomes. Personnel patrolling rural areas in Colombia could be at increased risk for Chagas disease.

Chagas disease, caused by *Trypanosoma cruzi* parasites, often progresses to a chronic phase that includes cardiovascular, gastrointestinal, and neurologic sequelae (*1*). However, acute forms account for ≈1% of reported cases and can have severe clinical manifestations, especially when orally acquired because of the particularly high parasitic load from this transmission route (*1*). Some populations can be at high risk for infection, including military personnel who are in endemic areas patrolling in rural or jungle environments where the parasite has been documented in multiple reservoirs (*2*,*3*). Although vectorborne transmission is most common, oral transmission has been associated with outbreaks of acute Chagas disease in Latin America and has case fatality rates of 8%–35% (*1*).

In South America, acute Chagas disease outbreaks through oral transmission have been related to food contaminated with triatomine feces or secretions from infected mammals (*1*). Colombia has reported increases in acute Chagas disease due to oral transmission since 1992 (*4*). Up to 35% of acute Chagas disease cases have complications, the most frequent of which are pericardial effusion, myocarditis, and heart failure (*1*,*5*). In rare cases, hemophagocytic lymphohistiocytosis can develop, as reported in the case of a soldier from Colombia (*6*).

We report a case series of acute Chagas disease among military personnel from a base in northeastern Colombia, where the potential risk of enzootic *T. cruzi* transmission was previously reported (*2*). We describe the clinical features observed in the hospital care of infected patients.

The Study

During the third and fourth week of November 2021, a group of 11 military personnel from a base in the municipality of La Jagua de Ibirico, Department of Cesar, Colombia, participated jungle patrols near the base. Within a few days, 9 personnel exhibited signs and symptoms compatible with acute febrile syndrome; 2 persons had severe symptoms and died, and the remaining 7 were transferred to the Hospital Militar Central, a reference military hospital in Bogota, Colombia. Hospitalization dates for the 7 admitted patients ranged from December 19, 2021, through February 4, 2022 (Figure 1).

The 7 patients had no relevant medical history; 6 (86%) required immediate transfer to the intensive care unit for monitoring. All patients had fever; other signs and symptoms included chest pain, dyspnea, abdominal pain, vomiting, and diarrhea (Table). Four (57%) patients required pericardiocentesis for moderate pericardial effusion. None required ventilatory support or vasopressors. We collected clinical and laboratory data through interviews and review of electronic medical records. None of the patients reported seeing triatomines or opossums within the military base facilities where they were located.

Author affiliations: Hospital Militar Central, Bogota, Colombia (H.D. Vergara, C.H. Gómez, Á.A. Faccini-Martínez, A.C. Herrera, M.J. López, L. Muñoz); Servicios y Asesorías en Infectología, Bogota (Á.A. Faccini-Martínez); Universidad Militar Nueva Granada, Bogota (C. Camacho); Universidad del Rosario, Bogota (L. Cruz-Saavedra, C. Hernández, J.D. Ramírez)

DOI: https://doi.org/10.3201/eid2909.230886

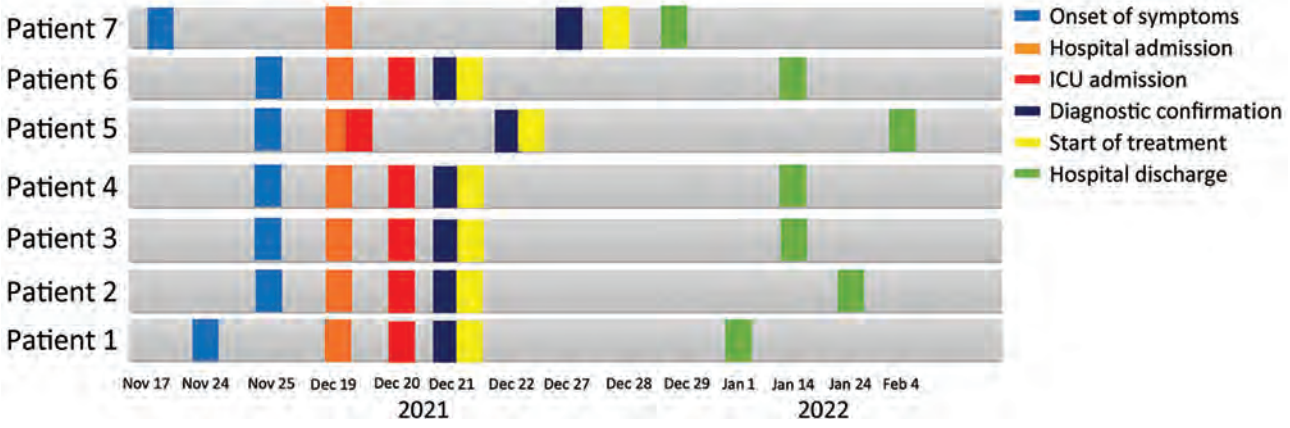

Figure 1. Timeline of acute Chagas disease illness and hospitalizations among military personnel, Colombia, 2021–2022. A group of 9 military personnel had signs and symptoms compatible with acute febrile syndrome, 2 of whom had severe symptoms and died. The remaining 7 patients were admitted to Hospital Militar Central in Bogota, and were treated with benznidazole (5–7 mg/kg/d for 60 days). All 7 had favorable outcomes.

We obtained blood and serum samples from the 7 admitted patients. Overall, diagnosis of acute Chagas disease was made by ELISA serology, Strout concentration method, and molecular tests. In blood samples, we used quantitative PCR to target *T. cruzi* satellite DNA and conventional PCR to target the mini-exon gene. Direct examination of pericardial fluid subsequently revealed parasites (Figure 2).

After Chagas disease was confirmed, we started all 7 patients on benznidazole treatment (5–7 mg/kg/d for 60 days), and all had favorable outcomes. Informed consent was obtained from the included patients. The study was approved by the ethics committee of the Hospital Militar Central.

Conclusions

We describe a group of young soldiers without underlying conditions in whom febrile illness progressed toward deterioration in an average of 24 days. Their disease courses correlate with descriptions in the medical literature of the progression of oral acute Chagas disease, which can occur in a range of 3–22 days after infection, depending on the degree of infecting inoculum (*5*,*7*,*8*).

The frequencies of clinical manifestations in the patients in this study are among the highest described in other reports of acute Chagas disease outbreaks (*5*,*7*,*8*). Our patients had fever (100%), abdominal pain (57.1%), diarrhea (71.4%), vomiting (57.1%), chest pain (71.4%), and dyspnea (71.4%) (Table). Pericardial involvement was high (57%) in our patients compared with other reports. In a report on a 2007 outbreak of acute Chagas disease in the Brazilian Amazon, up to 46.2% of the 233 cases had pericardial involvement (*8*). Another report from Colombia in 2021 analyzed 103 cases of acute Chagas disease that occurred in the department of Casanare and found that 34.9% of the patients had ≥1 complication, which consisted of pericardial effusion, myocarditis, or heart failure (*5*). The high proportion of our patients with cardiac complications might have been the result of a high parasite inoculum, which is more feasible during oral transmission.

Another finding of note is the area of origin of the cases, because a field epidemiologic study of *T. cruzi* circulation was previously conducted in that area and other military facilities in municipalities with historical reports of triatomines and Chagas disease cases (*2*). In that study, a geospatial analysis was conducted to evaluate the coexistence of triatomines and infected mammals in a training base located in La Loma, in the municipality of Jagua de Ibirico (*2*), the same municipality where the cases we report here occurred. However, that study described a low potential risk for *T. cruzi* transmission and the absence of triatomines near the dormitories or kitchens of the military facility (*2*).

The characteristics of the outbreak we describe, its temporality and the clinical severity of the cases, strongly suggest transmission via the oral route. All affected case-patients were involved in patrol activities in a rural area near the military base, which could have exposed them to a sylvatic genotype of *T. cruzi* that has been reported in Colombia in association with Chagas disease outbreaks caused by oral transmission (*4*). Although none of the patients treated at our institution died, 2 patients from the same outbreak died at the site of origin. That case-fatality rate (22.2%) is consistent with the reported case-fatality rates in acute Chagas disease, which can average

24.4% (*9*). Outbreaks of orally transmitted Chagas disease usually occur during the warmest months of the year, which coincides with the reported dates and estimated temperatures in the geographic area where our patients were during the month of November. Those conditions could favor a higher density of triatomines and a greater number of parasites in triatomine feces, which would increase the probability of food contamination and, therefore, the possibility of oral infection (*10*).

One limitation of this report is the lack of confirmation of the source of the outbreak. In previous studies in Colombia, evidence of *T. cruzi* seropositivity was demonstrated in 1% of the military population studied in 5 departments (*3*), but no similar studies have been conducted in the area where the outbreak cases in this study originated. Despite the reported low vector contact among military personnel, the geographic characteristics of the region where this outbreak originated are similar to areas with higher

Table. Clinical features and laboratory test results of acute Chagas disease among military personnel, Colombia, 2021*

Characteristics	Patient 1	Patient 2	Patient 3	Patient 4	Patient 5	Patient 6	Patient 7
No. days fever at hospital admission	26	25	25	25	25	25	33
Symptoms	Fever, asthenia, adynamia, diarrhea, vomiting, chest pain, orthopnea	Fever, asthenia, adynamia, abdominal pain, pleuritic pain, dyspnea	Fever, chills, vomiting, abdominal pain, pleuritic pain, dyspnea	Fever, headache, chills, abdominal pain, diarrhea, vomiting, pleuritic pain, dyspnea	Fever, abdominal pain, diarrhea, vomiting, dry cough, orthopnea	Fever, asthenia, malaise, diarrhea, pleuritic pain, dyspnea	Fever, asthenia, adynamia, diarrhea
ICU admission	Y	Y	Y	Y	Y	Y	N
Pericardial effusion, mL	+, 600	+, 450	+, 760	+, 600	+, 200	+, ND	No effusion
Troponin, pg/mL	1,111	225	722	671	997.3	568	4.7
Echocardiography	LVEF 29%, generalized apical hypokinesia, LVMI 131 g/m^2	LVEF 54%, hypokinesia of apical predominance, LVMI 112 g/m^2	LVEF 38%, decreased right ventricular filling pattern without contractility disorder, LVMI 120 g/m^2	LVEF 28%, generalized hypokinesia, LVMI 150 g/m^2	LVEF 35%, no contractility disorder, LVMI 120 g/m^2	LVEF 62%, no contractility disorder, LVMI 104 g/m^2	LVEF 60%, no contractility disorder, LVMI 72 g/m^2
EKG	Sinus rhythm, generalized low voltage, and anterolateral repolarization disorder	Sinus rhythm, generalized low voltage, and anterolateral repolarization disorder	Sinus tachycardia, generalized repolarization disorder, and low voltage	Sinus tachycardia, generalized repolarization disorder, and low voltage	Sinus tachycardia, generalized repolarization disorder, and low voltage	Sinus tachycardia, generalized repolarization disorder, and low voltage	Sinus rhythm
Hemoglobin, g/dL	12	10.1	10.6	13	9.5	12.2	15.6
Creatinine, mg/dL	0.94	0.75	0.82	0.92	0.88	0.76	1.04
Thick blood smear†	–	–	–	–	–	–	–
SARS-CoV-2 rapid antigen test‡	–	–	–	–	+	–	–
SARS-CoV-2 qRT-PCR‡	–	–	–	–	+	–	–
ELISA, IgG antibodies to *Trypanosoma cruzi*	+	+	+	+	+	+	–
Strout test	+	–	+	+	NP	NP	–
qPCR for *T. cruzi*, parasites/mL§	+, 0.5	+, 4.55	+, 3.25	+, 5.4	+, 5.8	+, 2.63	+, 0.5
Direct microscopic examination of pericardial fluid¶	+	+	+	+	NP	NP	NP

*EKG, electrocardiography; ICU, intensive care unit; LVEF, left ventricular ejection fraction; LVMI, left ventricular mass index; ND, no data; NP, not performed; qRT-PCR, real-time quantitative reverse transcription PCR; qPCR, quantitative PCR; +, positive; –, negative.
†Presence of trypomastigotes.
‡Nasal swab.
§Whole blood for *T. cruzi* DNA detection.
¶Detection of trypomastigotes via pericardiocentesis.

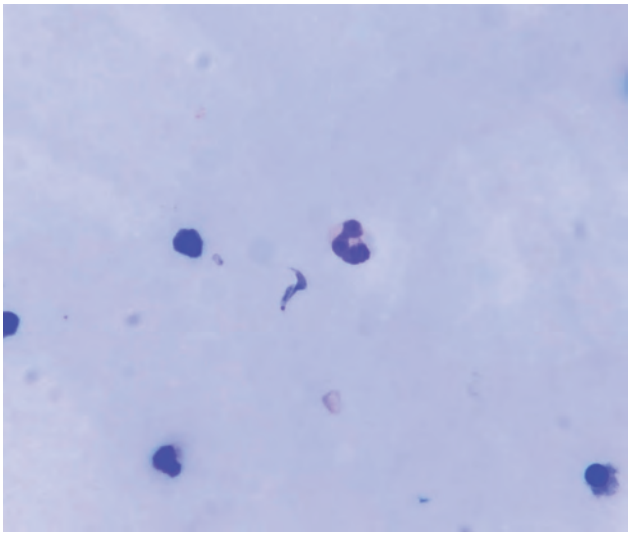

Figure 2. Pericardial fluid smear collected for diagnosis of acute Chagas disease among military personnel, Colombia, 2021. Giemsa-stained pericardial fluid smear of patient 1 shows a *Trypanosoma cruzi* parasite (center). Original magnification ×1,000.

vector populations, raising the possibility of sylvatic zoonotic oral transmission.

In summary, our study shows that military personnel could be exposed to *T. cruzi* through oral transmission while patrolling in Chagas disease–endemic areas. Thus, we advise public health and clinical practitioners who care for military personnel to be aware of acute Chagas disease as an additional parasitic zoonotic infection in cases of undifferentiated febrile syndrome associated with cardiac compromise, especially myocarditis or pericardial effusion.

About the Author

Dr. Vergara is a communicable disease epidemiologist and serves as the head of the Infectious Diseases Department at the Hospital Militar Central in Bogota, Colombia. His research interests primarily focus on tropical infectious diseases and HIV/AIDS.

References

1. Franco-Paredes C, Villamil-Gómez WE, Schultz J, Henao-Martínez AF, Parra-Henao G, Rassi A Jr, et al. A deadly feast: elucidating the burden of orally acquired acute Chagas disease in Latin America—public health and travel medicine importance. Travel Med Infect Dis. 2020;36:101565. https://doi.org/10.1016/j.tmaid.2020.101565
2. Cantillo-Barraza O, Torres J, Hernández C, Romero Y, Zuluaga S, Correa-Cárdenas CA, et al. The potential risk of enzootic *Trypanosoma cruzi* transmission inside four training and re-training military battalions (BITER) in Colombia. Parasit Vectors. 2021;14:519. https://doi.org/10.1186/s13071-021-05018-4
3. Méndez C, Duque MC, Romero Y, Pérez J, Rodríguez O, Correa-Cárdenas CA, et al. Prevalence of *Trypanosoma cruzi* infection in active military population of the Colombian National Army gathered in five departments. PLoS One. 2019;14:e0223611. https://doi.org/10.1371/journal.pone.0223611
4. Ramírez JD, Montilla M, Cucunubá ZM, Floréz AC, Zambrano P, Guhl F. Molecular epidemiology of human oral Chagas disease outbreaks in Colombia. PloS Negl Trop Dis. 2013;7:e2041. https://doi.org/10.1371/journal.pntd.0002041
5. Rincón-Acevedo CY, Parada-García AS, Olivera MJ, Torres-Torres F, Zuleta-Dueñas LP, Hernández C, et al. Clinical and epidemiological characterization of acute Chagas disease in Casanare, Eastern Colombia, 2012–2020. Front Med (Lausanne). 2021;8:681635. https://doi.org/10.3389/fmed.2021.681635
6. Gómez CH, Vargas-Hernández DA, Largo J, Hernández S, Faccini-Martínez ÁA. Hemophagocytic lymphohistiocytosis and acute Chagas disease, Colombia. Travel Med Infect Dis. 2021;44:102213. https://doi.org/10.1016/j.tmaid.2021.102213
7. Noya BA, Díaz-Bello Z, Colmenares C, Ruiz-Guevara R, Mauriello L, Muñoz-Calderón A, et al. Update on oral Chagas disease outbreaks in Venezuela: epidemiological, clinical and diagnostic approaches. Mem Inst Oswaldo Cruz. 2015;110:377–86. https://doi.org/10.1590/0074-02760140285
8. Pinto AY, Valente SA, Valente VC, Ferreira Junior AG, Coura JR. Acute phase of Chagas disease in the Brazilian Amazon region: study of 233 cases from Pará, Amapá and Maranhão observed between 1988 and 2005 [in Portuguese]. Rev Soc Bras Med Trop. 2008;41:602–14. https://doi.org/10.1590/S0037-86822008000600011
9. Álvarez-Hernández DA, García-Rodríguez-Arana R, Ortiz-Hernández A, Álvarez-Sánchez M, Wu M, Mejia R, et al. A systematic review of historical and current trends in Chagas disease. Ther Adv Infect Dis. 2021;8:20499361211033715. https://doi.org/10.1177/20499361211033715
10. Chuit R, Meiss R, Salvatella R. Epidemiology of Chagas disease. In: Altcheh J, Freilij H, editor. Chagas disease: Birkhäuser advances in infectious diseases. Geneva: Springer Nature; 2019. p. 91–109.

Address for correspondence: Hernán Darío Vergara, Servicio de Infectología, Hospital Militar Central, Tv. 3C No. 49–02, Bogotá D.C. 110231, Colombia; email: hvergara@homil.gov.co

Lymphocytic Choriomeningitis Virus in Person Living with HIV, Connecticut, USA, 2021

Jonathan Dyal, Shiv Gandhi, Caitlin M. Cossaboom, Austin Leach, Ketan Patel, Marjorie Golden, Joseph Canterino, Marie-Louise Landry, Debi Cannon, Mary Choi, Inna Krapiunaya, John D. Klena, Trevor Shoemaker

Lymphocytic choriomeningitis virus is an underreported cause of miscarriage and neurologic disease. Surveillance remains challenging because of nonspecific symptomatology, inconsistent case reporting, and difficulties with diagnostic testing. We describe a case of acute lymphocytic choriomeningitis virus disease in a person living with HIV in Connecticut, USA, identified by using quantitative reverse transcription PCR.

Lymphocytic choriomeningitis virus (LCMV) is globally occurring, Old World arenavirus. The common house mouse (*Mus musculus*) is the primary reservoir, although the virus can infect many other rodent species, including wild or domesticated rats, gerbils, and hamsters (*1*). In humans, LCMV infection is frequently asymptomatic but can present as a nonspecific viral illness, sometimes accompanied by headache or photophobia (*2*). Congenital LCMV infection carries a high risk for spontaneous abortion or serious neurologic deficits in the developing fetus. Children born after congenital LCMV infection frequently suffer from chorioretinitis, hydrocephalus, and psychomotor delay (*3*). Immunocompromised persons are also at greater risk for complications following LCMV infection because they can develop life-threatening encephalitis, seizures, and paralysis. Other groups at heightened risk for infection include transplant recipients and persons that work with rodents, such as laboratory staff and pet store workers (*4*,*5*).

Author affiliations: Centers for Disease Control and Prevention, Atlanta, Georgia, USA (J. Dyal, C.M. Cossaboom, A. Leach, K. Patel, D. Cannon, M. Choi, I. Krapiunaya, J.D. Klena, T. Shoemaker); Yale School of Medicine, New Haven, Connecticut, USA (S. Gandhi, M. Golden, J. Canterino, M. Landry)

DOI: http://doi.org/10.3201/eid2909.230087

Because of its a broad geographic distribution and potential for severe disease, clarifying the effects of LCMV on human health remains an important public health challenge.

Because of its nonspecific symptoms, lack of physician awareness, suboptimal diagnostic testing, and limited and inconsistent reporting requirements, LCMV is an underrecognized public health threat. In the United States, Wisconsin is the only state that requires hospitals and healthcare providers to report cases of LCMV (*6*). Because LCMV is not nationally notifiable, the Centers for Disease Control and Prevention (CDC) receives case reports on a voluntary basis (*7*). Although outbreaks of LCMV have been identified, sporadic cases are likely underreported, and the true burden within the United States is unknown.

Laboratory diagnosis of an acute case of LCMV is made by detection of viral nucleic acids by using real-time reverse transcription PCR (qRT-PCR) and detection of circulating LCMV IgM or a rising titer of LCMV IgG. However, few commercial laboratories offer testing services for LCMV. LCMVs causing human infection are genetically diverse, a feature that has made the design and implementation of nucleic acid–based assays challenging (*8*). Taking advantage of improved reagents for PCR and an increase in the number of complete genomes available for analysis, we developed a qRT-PCR assay for LCMV, targeting the large segment. We describe a case of LCMV infection in a patient with well-controlled HIV, diagnosed by using the qRT-PCR and IgM and IgG enzyme-linked immunosorbent assays (ELISA) at CDC. Use of the qRT-PCR can accelerate detection of acute LCMV infection and therefore has the potential to improve patient care.

The Case

A 53-year-old man residing in Connecticut, USA, with a history of well-controlled HIV and receiving antiretroviral therapy but with a chronically low CD4 count (150/μL) and percentage (14%), was admitted to the emergency department at Yale New Haven Hospital (New Haven, CT, USA) with a 2-day history of headache, nausea, and emesis. In the weeks leading up to admission, he had noted mice in his home. Approximately 2 weeks before admission, he cleaned mouse feces and urine with a vacuum while wearing gloves and a mask. At arrival to the hospital, he was febrile to 100.7°F but otherwise hemodynamically stable. Physical examination showed no neurologic deficits or nuchal rigidity. Laboratory data were notable for a hemoglobin of 11.2 g/dL (reference range 13.1–17.5), leukocyte count of 7,200/μL (reference range 4,000–10,000/μL), platelet count of 213,000/μL (reference range 150,000–400,000/μL), aspartate transaminase 59 U/L (reference range 10–35 U/L), and alanine aminotransferase 96 U/L (reference range 9–59 U/L). His HIV viral load was below the limit of detection (20 copies/mL) 1 month before admission.

The patient underwent a lumbar puncture after receiving empiric antibiotics for meningitis. Analysis of the cerebral spinal fluid (CSF) revealed a nucleated cell count of 500/μL in tube 1 and 495/μL in tube 4 (reference range 0–5/μL), which was lymphocyte predominant (≈85%). CSF protein was 116 mg/dL (reference range 15–45 mg/dL) and glucose was 66 mg/dL (reference range 40–70 mg/dL). Culture remained sterile and CSF was negative for herpes simplex virus by real-time PCR, West Nile virus IgM in CSF, and for 14 pathogens included on the BioFire FilmArray Meningitis/Encephalitis Panel (BioFire Diagnostics, LLC, https://www.biofiredx.com).

Because of concern for aseptic meningitis caused by LCMV, we sent CSF and whole blood samples to CDC for LCMV testing. LCMV IgM and IgG were determined by a CDC-developed ELISA, as previously described (*2*). For nucleic acid testing, in brief, samples were inactivated by using MagMAX Pathogen RNA/DNA Kit (ThermoFisher, https://www.thermofisher.com) and extracted on the KingFisher Duo Prime platform (ThermoFisher). Extracted samples were tested by using an qRT-PCR targeting the large segment of LCMV. RNA from samples positive by the LCMV qRT-PCR were selected for sequencing and subsequent phylogenetic analysis. RNA library sequencing, amplicon-based sequencing, and phylogenetic analysis were performed on the LCMV genome obtained from the CSF sample, as were additional

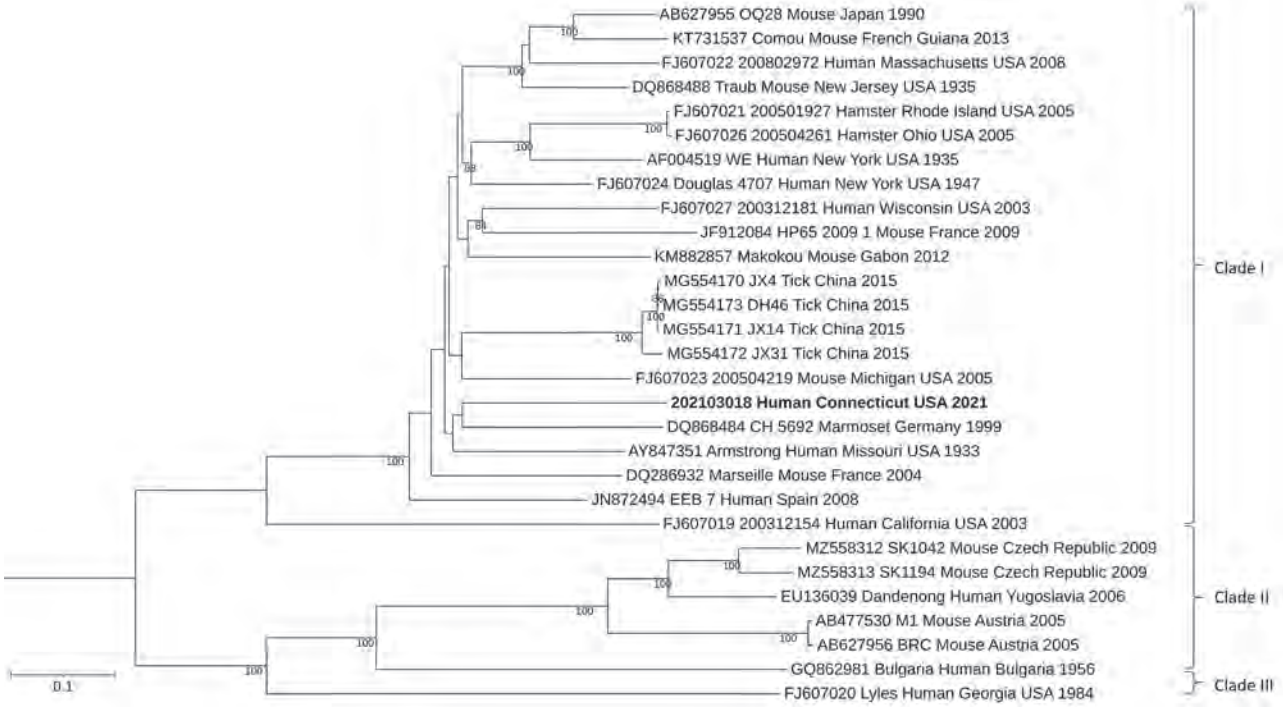

Figure 1. Maximum-likelihood analysis of the full large genome segment of lymphocytic choriomeningitis virus (LCMV) sample from a patient in Connecticut, USA (bold), compared with reference sequences. Branch nodes provide the bootstrap support values, as a percentage. Clades are indicated at right, and GenBank accession numbers are provided for reference sequences. Scale bar indicates number of substitutions per site.

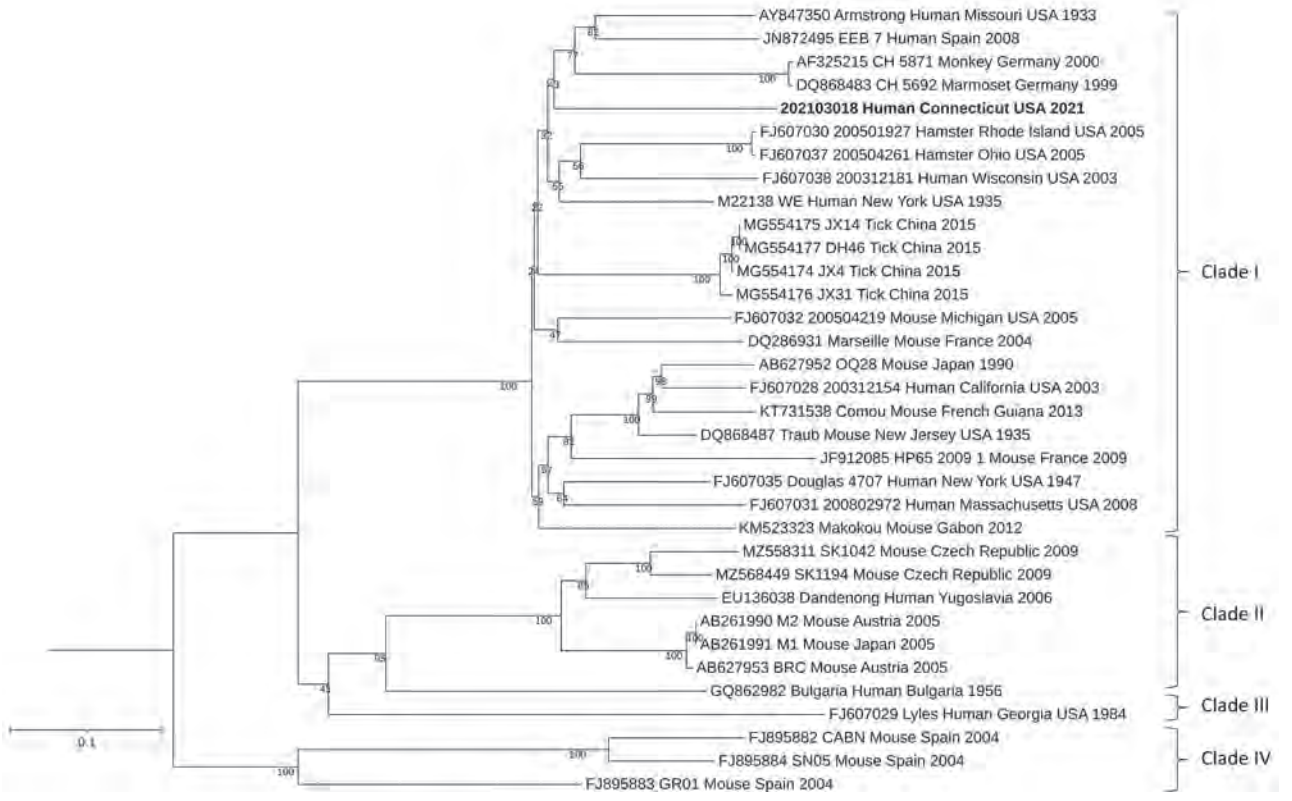

Figure 2. Maximum-likelihood analysis of the full small genome segment of lymphocytic choriomeningitis virus (LCMV) sample from a patient in Connecticut, USA (bold), compared with reference sequences. Branch nodes provide the bootstrap support values, as a percentage. Clades are indicated at right, and GenBank accession numbers are provided for reference sequences. Scale bar indicates number of substitutions per site.

laboratory methods (Appendix, https://wwwnc.cdc.gov/EID/article/29/9/23-0087-App1.pdf).

Analysis of the CSF showed that LCMV IgM and IgG ELISA results were both negative, but qRT-PCR results were positive. On blood collected 3 days after the CSF sample, LCMV IgM and IgG ELISA results were both positive (titer ≥1:400), and qRT-PCR results were negative. Sequence analysis of both the small and large segments showed the LCMV strain clustered to lineage I (Figures 1, 2). After confirming a diagnosis of LCMV meningitis in the patient, we discontinued empiric antibiotics and discharged him on hospitalization day 10. The patient's headaches resolved approximately 5 days after discharge, and he made a complete recovery.

Conclusions

Despite minimal reporting requirements, LCMV is believed to be widespread throughout the United States and the world. As in the case we report, clinicians should maintain a high index of suspicion for LCMV infection in patients with identified rodent exposures and symptoms consistent with meningitis, especially in high-risk groups such as pregnant women and the immunocompromised. LCMV viremia occurs early and is transient but may seed the central nervous system. Thus, as occurred for the patient in this report, viral RNA may no longer be detectable in blood but may be detectable in CSF in patients with clinical signs and symptoms of LCMV. Consequently, for patients with suspected LCMV infection, parallel molecular and serologic testing of both blood and CSF is likely beneficial for early diagnosis and management.

By sequencing the full genome of an LCMV strain isolated from this patient and conducting a phylogenetic analysis, we have gained valuable insights into the evolutionary relationships and genetic diversity of LCMV. The obtained phylogenetic trees provide evidence for the relatedness of the patient's strain to other known LCMV strains and contributes to our understanding of the virus's epidemiology. The LCMV strains we obtained group in clade I, which corresponds to the *M. musculus domesticus* host subspecies (*1*) and contains viruses from Asia, Europe, America, and Africa. The phylogenetic tree also shows that the

strain identified in this patient was genetically distinct from strains that have been identified from other parts of the world.

No-cost molecular and serologic testing for LCMV is available to hospitals and health departments through CDC's Viral Special Pathogens Branch (Division of High-Consequence Pathogens and Pathology, National Center for Emerging and Zoonotic Infectious Diseases). Increasing both community and healthcare provider awareness of LCMV and public health case reporting could improve surveillance efforts and clarify the true burden, risk factors, and distribution of LCMV infection in the United States.

Acknowledgments

We thank the patient for agreeing to the publication of this report. We also thank the physicians, nurses, and other members of the hospital clinical care team, the Connecticut state and local public health departments, and members of the CDC Viral Special Pathogens Branch.

About the Author

Dr. Dyal is an emergency medicine physician and epidemiologist at the University of Texas, Houston. A former Epidemic Intelligence Service Officer with CDC, he focuses on international emergency medicine, emerging infectious diseases, and public health epidemiology.

References

1. Fornůsková A, Hiadlovská Z, Macholán M, Piálek J, de Bellocq JG. New perspective on the geographic distribution and evolution of lymphocytic choriomeningitis virus, Central Europe. Emerg Infect Dis. 2021;27:2638–47. https://doi.org/10.3201/eid2710.210224
2. Park JY, Peters CJ, Rollin PE, Ksiazek TG, Katholi CR, Waites KB, et al. Age distribution of lymphocytic choriomeningitis virus serum antibody in Birmingham, Alabama: evidence of a decreased risk of infection. Am J Trop Med Hyg. 1997;57:37–41. https://doi.org/10.4269/ajtmh.1997.57.37
3. Bonthius DJ. Lymphocytic choriomeningitis virus: an underrecognized cause of neurologic disease in the fetus, child, and adult. Semin Pediatr Neurol. 2012;19:89–95. https://doi.org/10.1016/j.spen.2012.02.002
4. Knust B, Ströher U, Edison L, Albariño CG, Lovejoy J, Armeanu E, et al. Lymphocytic choriomeningitis virus in employees and mice at multipremises feeder-rodent operation, United States, 2012. Emerg Infect Dis. 2014;20:240. https://doi.org/10.3201/eid2002.130860
5. Amman BR, Pavlin BI, Albariño CG, Comer JA, Erickson BR, Oliver JB, et al. Pet rodents and fatal lymphocytic choriomeningitis in transplant patients. Emerg Infect Dis. 2007;13:719–25. https://doi.org/10.3201/eid1305.061269
6. Council of State and Territorial Epidemiologists. 2018—lymphocytic choriomeningitis virus infection [cited 2022 Aug 25]. http://srca.querytool.cste.org/Display.cshtml?year=2018&jurisdiction=0&reporters=1&reporters=2&conditions=Lymphocytic+Choriomeningitis+Virus+Infection
7. Adams DA, Thomas KR, Jajosky RA, Foster L, Baroi G, Sharp P, et al.; Nationally Notifiable Infectious Conditions Group. Summary of Notifiable Infectious Diseases and Conditions—United States, 2015. MMWR Morb Mortal Wkly Rep. 2017;64:1–143. https://doi.org/10.15585/mmwr.mm6453a1
8. Albariño CG, Palacios G, Khristova ML, Erickson BR, Carroll SA, Comer JA, et al. High diversity and ancient common ancestry of lymphocytic choriomeningitis virus. Emerg Infect Dis. 2010;16:1093–100. https://doi.org/10.3201/eid1607.091902

Address for correspondence: Trevor Shoemaker, Centers for Disease Control and Prevention, 1600 Clifton Rd NE, Mailstop HS24-12, Atlanta, GA 30329-4027, USA; email: tis8@cdc.gov

Rat Hepatitis E Virus in Norway Rats, Ontario, Canada, 2018–2021

Sarah J. Robinson, Jamie Borlang, Chelsea G. Himsworth, David L. Pearl, J. Scott Weese, Antonia Dibernardo, Carla Osiowy, Neda Nasheri, Claire M. Jardine

We tested liver samples from 372 Norway rats (*Rattus norvegicus*) from southern Ontario, Canada, during 2018–2021 to investigate presence of hepatitis E virus infection. Overall, 21 (5.6%) rats tested positive for the virus. Sequence analysis demonstrated all infections to be rat hepatitis E virus (*Rocahepevirus ratti* genotype C1).

Hepatitis E virus (HEV) is a nonenveloped, single-stranded, positive-sense RNA virus within the family Hepeviridae, subfamily Orthohepevirinae, which is divided into 4 genera: *Paslahepevirus*, *Rocahepevirus*, *Chirohepevirus*, and *Avihepevirus* (*1*). Human hepatitis E is primarily caused by *Paslahepevirus balayani* (genotypes 1–4), and infection generally causes an acute, self-limiting disease, but severe and chronic hepatitis and extrahepatic manifestations can occur in immunocompromised patients (*2*). *Paslahepevirus balayani* genotypes 1 and 2 are endemic in developing countries, circulating in humans and transmitted primarily via the fecal-oral route through contaminated drinking water. Sporadic cases of hepatitis E infection caused by zoonotic transmission of HEV (*Paslahepevirus balayani* genotypes 3 and 4) are increasingly reported in industrialized countries (*3*). Infections are acquired through direct contact with infected animals, environmental contamination with animal feces, and foodborne transmission from eating undercooked pork, venison, and wild boar meat (*3*).

Additional HEV variants have been reported in a diversity of animal species, and zoonotic transmission from animal reservoirs is a growing public health concern. Norway rats (*Rattus norvegicus*) have been shown to carry swine HEV (*Paslahepevirus balayani* genotype 3) and are natural reservoirs of HEV variants within the species *Rocahepevirus ratti* genotype C1 (rat HEV) (*4*). Since it was first detected in Germany in 2010, rat HEV has been identified in Norway rats from the United States, China, Vietnam, and 13 countries in Europe (*5*). Recently, cases of acute hepatitis caused by rat HEV have been reported in Hong Kong, Canada (infection acquired in Central Africa), and Spain (*6*–*8*). Those reports raise concerns regarding the potential risk for rat HEV transmission to humans and hepatitis E as an emerging infectious disease worldwide.

The Study

We conducted a study to investigate HEV infection in Norway rats from southern Ontario, Canada, and identify associations between host factors, season, land use, and year of collection. We obtained rat carcasses through collaboration with pest control professionals working in southern Ontario. Our rat and sample collection methods have been previously described and evaluated as a source of samples for zoonotic pathogen surveillance (*9*). We studied 372 Norway rats (species determined by external morphology) from 161 unique geographic coordinates within southern Ontario during November 2018–June 2021 (Figure 1). During necropsy, we recorded rat demographic characteristic data (Table) and collected liver samples aseptically. Most rats in our sample were sexually mature (65%), and there were more females (51.2%) than males (48.8%). We noted the body condition of rats to be poor (emaciated or underconditioned) in 69.1% and good (well conditioned or overconditioned) in 30.9%. We could not determine sex (3%), sexual maturity (3.2%), or body condition (2.4%) in a minority of rats because of poor carcass condition. We categorized rats by collection

Author affiliations: University of Guelph, Guelph, Ontario, Canada (S.J. Robinson, D.L. Pearl, J.S. Weese, C.M. Jardine); Public Health Agency of Canada, Winnipeg, Manitoba, Canada (J. Borlang, A. Dibernardo, C. Osiowy); University of British Columbia, Vancouver, British Columbia, Canada (C.G. Himsworth); Health Canada, Ottawa, Ontario, Canada (N. Nasheri); University of Ottawa, Ottawa (N. Nasheri); Canadian Wildlife Health Cooperative, Guelph (C.M. Jardine)

DOI: http://doi.org/10.3201/eid2909.230517

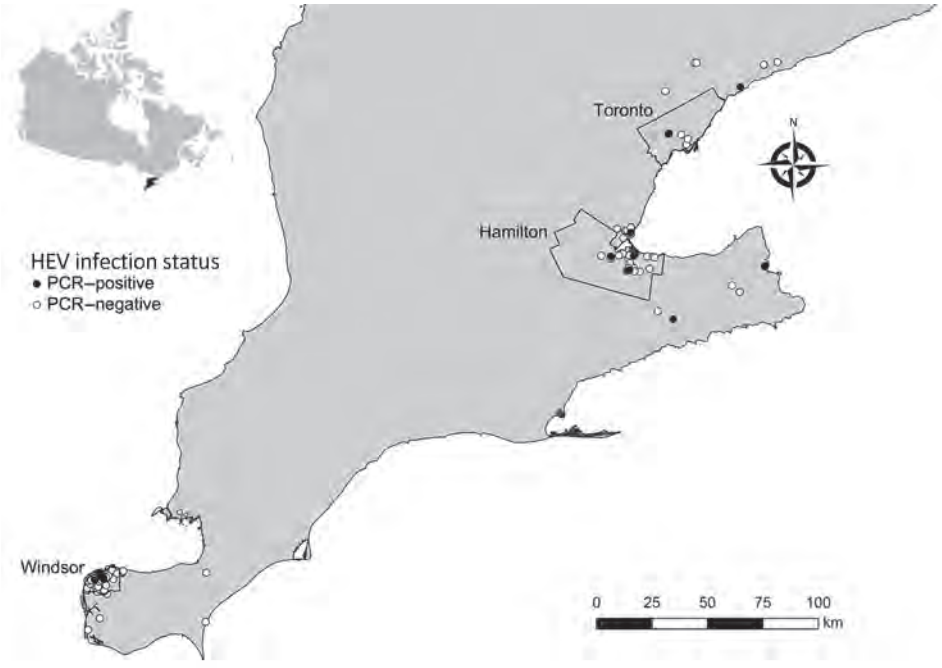

Figure 1. Sites of collection and HEV PCR status of rats submitted by pest control professionals in southern Ontario, Canada, during November 2018–June 2021. Geographic administrative boundaries of the cities of Windsor, Hamilton, and Toronto are displayed. Inset map indicates the location of southern Ontario within Canada. HEV, hepatitis E virus.

location as residential (52.4%), industrial (17.5%), institutional (15.6%), commercial (8.9%), and mixed (5.6%) land use. We collected most rats during the winter (36.8%) and fall (36.8%), followed by spring (21.8%) and summer (4.6%). To account for low sample size in the summer, we recategorized seasonal data as summer/fall (June–November) and winter/spring (December–May).

We screened liver RNA extracts for the presence of HEV by real-time PCR by using previously described primers and probes (*10*). Of 372 rats tested, 21 (5.6%, 95% CI 3.5%–8.5%) rats from 16 distinct locations in 7 cities/towns were positive for HEV (Figure 1). The odds of HEV infection were significantly higher in sexually mature rats (odds ratio 3.99, 95% CI 1.14–21.47; p = 0.025). By using exact logistic regression models, we observed no association with sex, body condition, land use, season, or year of collection (Table).

We amplified positive samples by using a previously described heminested PCR to generate an

Table. Descriptive statistics for rat demographic variables, land use, season, and year of collection and results from exact logistic regression analyses evaluating associations with hepatitis E virus PCR status among 372 Norway rats (collected in southern Ontario, Canada, during November 2018–June 2021

Category, no. with data available	No. (%)	PCR-positive (%)	PCR-negative (%)	Odds ratio (95% CI)	p value
Sex, n = 361					
F	185 (51.2)	9 (4.9)	176 (95.1)	Referent	
M	176 (48.8)	11 (6.3)	165 (93.7)	1.13 (0.43–2.95)	0.955
Sexual maturity, n = 360					
Immature	126 (35.0)	1 (0.8)	125 (99.2)	Referent	
Mature	234 (65.0)	19 (8.1)	215 (91.9)	3.99 (1.14–21.47)	0.025
Body condition, n = 363					
Poor	251 (69.1)	11 (4.4)	240 (95.6)	Referent	
Good	112 (30.9)	9 (8.0)	103 (92.0)	1.66 (0.61–4.36)	0.361
Land use, n = 372*					
Residential	195 (52.4)	11 (5.6)	184 (94.4)	Referent	
Nonresidential	177 (47.6)	10 (5.6)	167 (94.4)	0.92 (0.35–2.39)	1.000
Season, n = 372†					
Summer/fall	154 (41.4)	8 (5.2)	146 (94.8)	Referent	
Winter/spring	218 (58.6)	13 (6.0)	205 (94.0)	1.03 (0.39–2.80)	1.000
Year of collection, n = 372					
2018	43 (11.6)	4 (9.3)	39 (90.7)	Referent	
2019	193 (51.9)	11 (5.7)	182 (94.3)	0.47 (0.14–1.84)	0.307
2020	93 (25.0)	2 (2.2)	91 (97.8)	0.17 (0.02–1.12)	0.069
2021	43 (11.6)	4 (9.3)	39 (90.7)	0.80 (0.15–4.04)	1.000

*Land use was defined as residential and nonresidential (i.e., institutional, industrial, commercial, and mixed).
†Seasons were defined as winter (December–February), spring (March–May), summer (June–August), and fall (September–November).

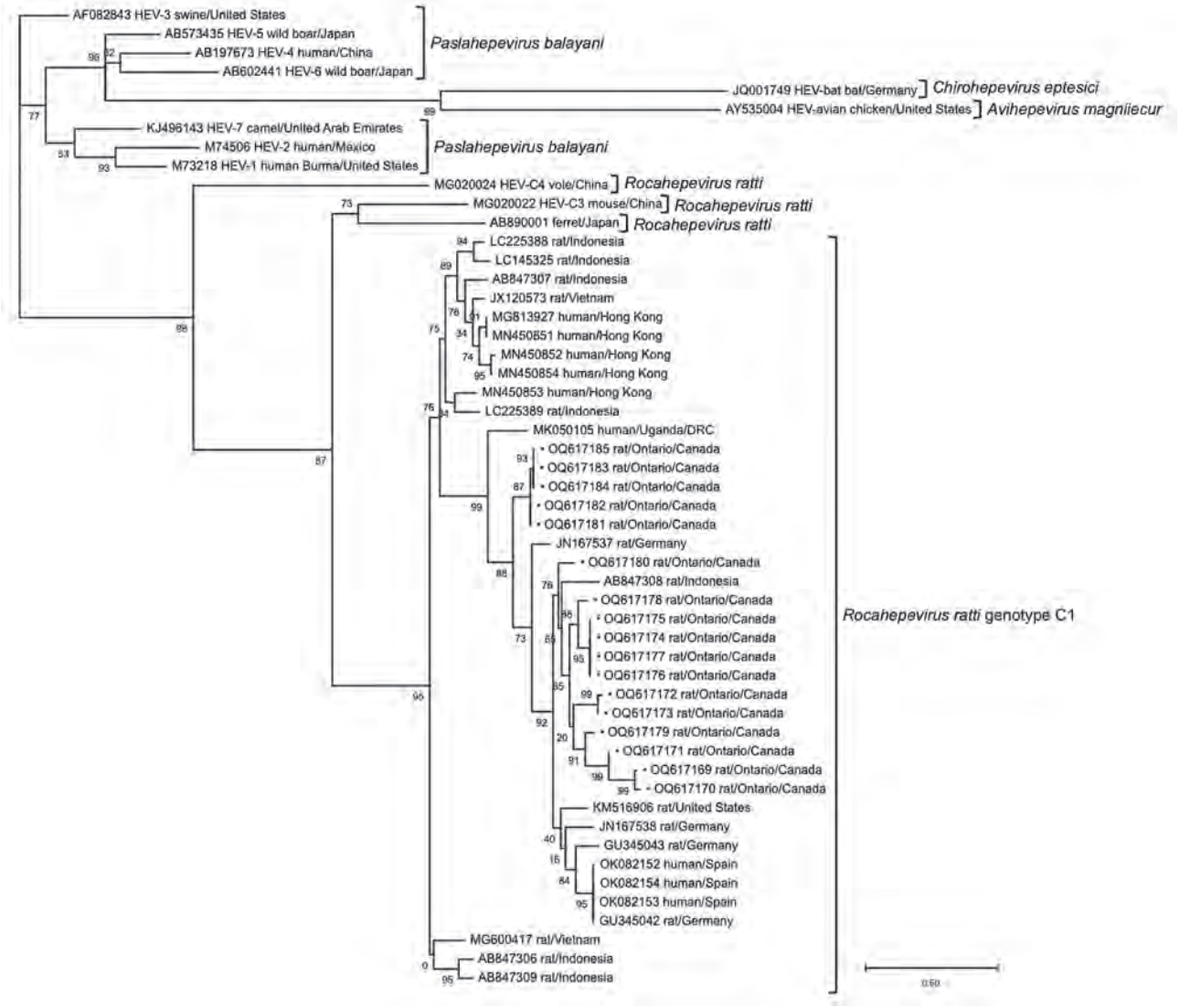

Figure 2. Phylogenetic tree based on the nucleotide alignment of hepatitis E virus (HEV) sequences from rats submitted by pest control professionals in southern Ontario, Canada, during November 2018–June 2021 (black dots), and select reference sequences from other studies in GenBank (accession numbers provided). Maximum-likelihood analysis of a 283-nt fragment of the RNA dependent RNA polymerase of open reading frame 1 was performed by the general time reversible plus gamma plus invariant sites substitution model as determined for the alignment by Smart Model Selection (*12*). Tree construction was optimized by nearest neighbor interchange and subtree pruning and regrafting with branch support computed by the approximate likelihood-ratio test based on a Shimodaira-Hasegawa-like procedure (*13*). Only bootstrap values >70% are shown. Scale bar indicates the number of nucleotide substitutions per site. DRC, Democratic Republic of the Congo.

amplicon from the open reading frame (ORF) 1 region (*11*). We retrieved a 283-nt fragment of ORF1 from 17 samples and analyzed generated sequences with Lasergene software (DNASTAR, https://www.dnastar.com). We did not obtain sequence data for 4 rats. We aligned sequences with select GenBank reference sequences representing HEV genotypes currently known to infect rats, as well as rat HEV found in humans. Phylogenetic analysis of the partial ORF1-derived sequences showed that all PCR amplicons were rat HEV. We grouped rat HEV sequences from southern Ontario (GenBank accession numbers OQ617169–85) into 4 distinct clusters (Figure 2), with relatively low genetic divergence (14%). Sequences in our study had the highest nucleotide homology with rat HEV sequences from rats in the United States (83.3%), followed by Germany (82.2%), Vietnam (71.5%), and Indonesia (71.3%). Southern Ontario shares a border with 2 US states, New York and Michigan, and the westernmost samples from

Windsor were collected directly adjacent to Detroit, Michigan. We noted Ontario rat HEV sequences to be genetically distinct (24.6% divergence) from rat HEV sequences reported in humans.

Conclusions

Laboratory analysis of samples taken from Norway rats in southern Ontario, Canada, revealed hepatitis E virus RNA in 21 (5.6%, 95% CI 3.5%–8.5%) of 372 rats, and phylogenetic analysis demonstrated that these sequences were closely related to those found in rats from other countries. Detection of rat HEV (*R. ratti* genotype C1) in Norway rats in our study shows that this virus is broadly distributed within southern Ontario, including 3 major cities (i.e., Toronto, Hamilton, and Windsor), and may be endemic in Norway rat populations. An absence of PCR-positive rats in some areas of southern Ontario may be the result of undersampling rather than an indication that HEV is absent in these populations.

We observed that sexually mature rats were at significantly greater odds of being infected with HEV than immature rats. This observation is in contrast to findings from previous studies of rats, which found no association with age and infection status (*14*,*15*). We concede that this disparity in findings might be owing to methodological differences in how age classes were defined (i.e., sexual maturity [open vaginal orifice in females, scrotal testes in males] vs. weight). The observed association in our study might be the result of cumulative exposure to HEV leading to increased risk for infection over time and behaviors in sexually mature rats that may increase transmission (e.g., exploratory and aggressive behaviors).

To date, 12 human cases of rat HEV have been reported in Hong Kong, Canada, and Spain (*6*–*8*). Although zoonotic transmission from rats to humans has been suggested, the exact source and route of transmission in these cases remains unclear. Notably, human hepatitis E caused by rat HEV may be underreported because of subclinical or mild infection, limited awareness, and diagnostic testing techniques for HEV that might not detect rat HEV. Further studies are needed to investigate potential modes and patterns of transmission and elucidate the zoonotic potential of rat HEV and associated public health risks.

This report of rat HEV (*R. ratti* genotype C1) in Canada provides further evidence that this virus has a broad geographic distribution globally and may be endemic in Norway rats. Our study highlights the importance of continued surveillance for HEV in rats and the need for additional research regarding the role of rats in human hepatitis E.

Acknowledgments

We thank Leonard Shirose, Brian Stevens, Laura Dougherty, Rachel Finer, and Simon Jeeves for their support and assistance with sample processing. We greatly appreciate Windsor Pest Control (Catherine Trudell), Abell Pest Control, and Orkin Canada for submitting carcasses.

Funding was provided by the Natural Science and Engineering Research Council. S.J.R. was supported by an Ontario Veterinary College PhD Fellowship and an Ontario Graduate Scholarship.

About the Author

Dr. Robinson is a postdoctoral researcher in the Department of Pathobiology, Ontario Veterinary College, University of Guelph, Ontario, Canada. Her research interests include the ecology and epidemiology of zoonotic pathogens associated with rats and other wildlife.

References

1. Purdy MA, Drexler JF, Meng XJ, Norder H, Okamoto H, Van der Poel WHM, et al. ICTV virus taxonomy profile: *Hepeviridae* 2022. J Gen Virol. 2022;103. https://doi.org/10.1099/jgv.0.001778
2. Pischke S, Hartl J, Pas SD, Lohse AW, Jacobs BC, Van der Eijk AA. Hepatitis E virus: infection beyond the liver? J Hepatol. 2017;66:1082–95. https://doi.org/10.1016/j.jhep.2016.11.016
3. Meng XJ. From barnyard to food table: the omnipresence of hepatitis E virus and risk for zoonotic infection and food safety. Virus Res. 2011;161:23–30. https://doi.org/10.1016/j.virusres.2011.01.016
4. Kenney SP. The current host range of hepatitis E viruses. Viruses. 2019;11:452. https://doi.org/10.3390/v11050452
5. Wang B, Harms D, Yang XL, Bock CT. *Orthohepevirus* C: an expanding species of emerging hepatitis E virus variants. Pathogens. 2020;9:154. https://doi.org/10.3390/pathogens9030154
6. Sridhar S, Yip CCY, Wu S, Chew NFS, Leung KH, Chan JFW, et al. Transmission of rat hepatitis E virus infection to humans in Hong Kong: A clinical and epidemiological analysis. Hepatology. 2021;73:10–22. https://doi.org/10.1002/hep.31138
7. Andonov A, Robbins M, Borlang J, Cao J, Hatchette T, Stueck A, et al. Rat hepatitis E virus linked to severe acute hepatitis in an immunocompetent patient. J Infect Dis. 2019;220:951–5. https://doi.org/10.1093/infdis/jiz025
8. Rivero-Juarez A, Frias M, Perez AB, Pineda JA, Reina G, Fuentes-Lopez A, et al.; HEPAVIR and GEHEP-014 Study Groups. *Orthohepevirus C* infection as an emerging cause of acute hepatitis in Spain: First report in Europe. J Hepatol. 2022;77:326–31. https://doi.org/10.1016/j.jhep.2022.01.028
9. Robinson SJ, Finer R, Himsworth CG, Pearl DL, Rousseau J, Weese JS, et al. Evaluating the utility of pest control sourced rats for zoonotic pathogen surveillance. Zoonoses Public Health. 2022;69:468–74. https://doi.org/10.1111/zph.12936
10. Mulyanto, Suparyatmo JB, Andayani IGAS, Khalid, Takahashi M, Ohnishi H, et al. Marked genomic

heterogeneity of rat hepatitis E virus strains in Indonesia demonstrated on a full-length genome analysis. Virus Research. 2014;179:102–12. https://doi.org/10.1016/j.virusres.2013.10.029
11. Drexler JF, Seelen A, Corman VM, Fumie Tateno A, Cottontail V, Melim Zerbinati R, et al. Bats worldwide carry hepatitis E virus-related viruses that form a putative novel genus within the family Hepeviridae. J Virol. 2012;86:9134–47. https://doi.org/10.1128/JVI.00800-12
12. Lefort V, Longueville JE, Gascuel O. SMS: smart model selection in PhyML. Mol Biol Evol. 2017;34:2422–4. https://doi.org/10.1093/molbev/msx149
13. Anisimova M, Gascuel O. Approximate likelihood-ratio test for branches: A fast, accurate, and powerful alternative. Syst Biol. 2006;55:539–52. https://doi.org/10.1080/10635150600755453
14. Murphy EG, Williams NJ, Jennings D, Chantrey J, Verin R, Grierson S, et al. First detection of Hepatitis E virus (*Orthohepevirus C*) in wild brown rats (*Rattus norvegicus*) from Great Britain. Zoonoses Public Health. 2019;66:686–94. https://doi.org/10.1111/zph.12581
15. Ryll R, Bernstein S, Heuser E, Schlegel M, Dremsek P, Zumpe M, et al. Detection of rat hepatitis E virus in wild Norway rats (*Rattus norvegicus*) and Black rats (*Rattus rattus*) from 11 European countries. Vet Microbiol. 2017;208:58–68. https://doi.org/10.1016/j.vetmic.2017.07.001

Address for correspondence: Sarah J. Robinson, Department of Pathobiology, Ontario Veterinary College, University of Guelph, 50 Stone Rd East, Guelph, ON N1G 2W1, Canada; email: srobin18@uoguelph.ca

Reoccurring *Escherichia coli* O157:H7 Strain Linked to Leafy Greens–Associated Outbreaks, 2016–2019

Jessica C. Chen,[1] Kane Patel,[1] Peyton A. Smith, Eshaw Vidyaprakash, Caroline Snyder, Kaitlin A. Tagg, Hattie E. Webb, Morgan N. Schroeder, Lee S. Katz, Lori A. Rowe,[2] Dakota Howard, Taylor Griswold, Rebecca L. Lindsey, Heather A. Carleton

Genomic characterization of an *Escherichia coli* O157:H7 strain linked to leafy greens–associated outbreaks dates its emergence to late 2015. One clade has notable accessory genomic content and a previously described mutation putatively associated with increased arsenic tolerance. This strain is a reoccurring, emerging, or persistent strain causing illness over an extended period.

Escherichia coli O157:H7 is estimated to cause ≈63,000 domestically acquired foodborne illnesses and 20 deaths in the United States each year (*1*). *E. coli* O157:H7 infections are typically associated with abdominal cramps, bloody diarrhea, and vomiting; however, a rare but serious condition called hemolytic uremic syndrome can develop, resulting in anemia and acute renal failure (*2*). Healthy cattle serve as the main reservoir for *E. coli* O157:H7, and contaminated food, water, and environmental sources, as well as contact with animals, have been the source of outbreaks of *E. coli* O157:H7 infections (*3*,*4*). More recently, contaminated leafy greens have been recognized as a major source of *E. coli* O157:H7 illnesses and outbreaks. In foodborne illness attribution estimates for 2020 based on outbreak data, 58.1% of *E. coli* O157:H7 illnesses were attributed to vegetable row crops, a category that includes leafy greens (https://www.cdc.gov/foodsafety/ifsac/annual-reports.html). During 2009–2018, a total of 32 confirmed or suspected outbreaks of *E. coli* O157:H7 infections linked to contaminated leafy greens occurred in the United States and Canada (*5*).

A large *E. coli* outbreak in late 2019, hereafter referred to as outbreak A, caused 167 cases, hospitalized 85 persons from 27 states, and was associated with the consumption of romaine lettuce from Salinas Valley, California, USA (https://www.cdc.gov/ecoli/2019/o157h7-11-19/index.html). We characterized isolates from outbreak A and highly related isolates by using a variety of molecular methods.

The Study

A query of the PulseNet database revealed 356 isolates related to the outbreak strain that had <15 core-genome multilocus sequence typing (MLST; cgMLST) allele differences (Table 1; Appendix 1 Table 1, https://wwwnc.cdc.gov/EID/article/29/9/23-0069-App1.xlsx) (*6*). Of those, 302 isolates corresponded to human cases associated with 6 outbreaks spanning 3 years; dates of isolation ranged from September 27, 2016, to January 3, 2020. An additional 54 isolates were either clinical isolates not associated with a recognized outbreak (n = 14) or from environmental (n = 20), food (n = 8), or animal (n = 12) samples. Seven-gene MLST and Manning clade typing revealed all isolates were sequence type (ST) 11 and belonged to Manning clade 2 (Appendix 2, https://wwwnc.cdc.gov/EID/article/29/9/23-0069-App2.pdf). In silico PCR of the Shiga toxin (stx) genes revealed that all

Author affiliations: Centers for Disease Control and Prevention, Atlanta, Georgia, USA (J.C. Chen, K. Patel, P.A. Smith, E. Vidyaprakash, C. Snyder, K.A. Tagg, H.E. Webb, M.N. Schroeder, L.S. Katz, L.A. Rowe, D. Howard, T. Griswold, R.L. Lindsey, H.A. Carleton); Oak Ridge Institute for Science and Education, Oak Ridge, Tennessee, USA (K. Patel, C. Snyder)

DOI: https://doi.org/10.3201/eid2909.230069

[1]These first authors contributed equally to this article.

[2]Current affiliation: Tulane National Primate Research Center, Covington, Louisiana, USA.

Table 1. Summary of outbreaks caused by reoccurring *Escherichia coli* O157:H7 strain REPEXH02 linked to leafy greens–associated outbreaks, 2016–2019*

Outbreak	No. sequences	Timeframe	No. sequences, subset	Median subset allele differences (min–max)	Median hqSNP subset differences (min–max)	Outbreak source	Growing region
D	20	Sep 27–Dec 5, 2016	20	2 (0–5)	3 (0–17)	Unknown	NA
C	23	Nov 10–-Dec 14, 2017	23	0 (0–3)	1 (0–5)	Leafy greens	Likely SW USA, Mexico
B3	7	Jul 31–Aug 15, 2018	7	0 (0–3)	1 (0–10)	Unknown	NA
B2	71	Oct 8–Dec 7, 2018	69	1 (0–4)	2 (0–10)	Romaine lettuce	Santa Maria, CA
B1	19	Nov 1–Dec 18, 2018	18	2 (0–5)	4 (0–10)	Leafy greens	NA
A	179	Sep 27, 2019–Jan 3, 2020	84	1 (0–5)	2 (0–12)	Romaine lettuce	Salinas Valley, CA
Nonhuman samples collected in Santa Maria	23	Nov 14, 2019	12	0 (0–1)	1 (0–5)	NA	Santa Maria, CA
Not associated with known outbreak	14	Oct 18, 2016–Aug 4, 2019	12	1 (0–3)	8 (0–18)	NA	NA
All	356	Sep 27, 2016–Jan 3, 2020	245	2 (0–8)	10 (0–39)	NA	NA

*hqSNP, high-quality single nucleotide polymorphism; NA, not applicable.

but 2 isolates contained *stx2a*, whereas 2 remaining isolates had no detectable stx genes. We generated a closed-reference genome, 2019C-3201 (Strain: PNUSAE020169; BioSample: SAMN10432148), using PacBio Sequel technology (https://www.pacb.com) and assembled with Flye version 2.6 (*7*). The sequence data assembled into a single complete chromosomal contig and 3 plasmids (Table 2).

We selected a subset of 245 isolates for further genomic analysis to more evenly sample across outbreaks and to reduce computational demands. Isolates were characterized by core genome MLST implemented in BioNumerics 7.6 (*6*) and high-quality single-nucleotide polymorphism (SNP; hqSNP) methods using Lyve-SET version 1.1.4f (*9*), using the chromosomal sequence of 2019C-3201 as a reference and the Lyve-SET presets for *E. coli*. Overall, hqSNP was more discriminatory, differentiating isolates by a median of 10 pairwise hqSNPs (0–39 SNPs), whereas cgMLST differentiated isolates by a median of 2 allele differences (0–8 alleles) (Table 1). This finding was foreseeable because hqSNP does not depend on a predefined scheme; therefore, intergenic SNPs between loci, multiple SNP differences within a given locus, or SNPs in loci not included in the cgMLST schema can result (*9*).

Time-tree analysis using BEAST version 2.6.3 (*10*) revealed the divergence of this strain into 2 clades that last shared a common ancestor around late 2015 (median December 19, 2015; 95% highest posterior density interval December 7, 2014–July 10, 2016) (Figure 1). After outbreak D in 2016, sequences corresponding to a given outbreak belonged to 1 of 2 clades; outbreaks B2 and C were associated with clade 1, and outbreaks A, B1, and B3 were associated with clade 2. Of note, outbreak A was traced to romaine lettuce from Salinas Valley, whereas traceback and sampling in outbreak B2 linked some illnesses to romaine lettuce from Santa Maria, California (https://www.fda.gov/food/outbreaks-foodborne-illness/investigation-summary-factors-potentially-contributing-contamination-romaine-lettuce-implicated-fall; https://www.fda.gov/food/outbreaks-foodborne-illness/outbreak-investigation-e-coli-romaine-salinas-california-november-2019). Lettuce from Salinas was not considered a source of any illnesses in outbreak B2.

Table 2. Genomic attributes of the 2019C-3201 reference genome of reoccurring *Escherichia coli* O157:H7 strain REPEXH02 linked to leafy greens–associated outbreaks, 2016–2019*

Contig name	GenBank accession no.	Length, bp	Sequence coverage	Replicon	PTU (*8*)
2019C-3201 chromosome	CP090856	5,488,442	866	None	NA
p2019C-3201_1	CP090857	87,920	732	IncI1-I(gamma)	PTU-I1
p2019C-3201_2	CP090858	61,933	560	IncFII(pHN7A8), IncFII(pSFO)	PTU-F_E
p2019C-3201_3	CP090859	92,724	623	IncFIB, IncFII	PTU-E5

*PTU, plasmid taxonomic unit.

Environmental sampling in Santa Maria in 2019 yielded isolates clustering closely with outbreak B2 in the time tree.

We analyzed the closed reference sequence of 2019C-3201 using Prokka version 1.8 to enable SNP annotation (*11*). We examined output from Lyve-SET to determine the SNPs differentiating the 2 clades in our phylogenetic analysis (Appendix 1 Table 2). This work confirms a previous study reporting a nonsense mutation in the *arsR* gene, an arsenical resistance operon repressor (*12*). All clade 1 isolates in this study possess a G→A mutation resulting in a premature stop codon. This mutation could decrease the activity of this repressor and lead to constitutive expression of this operon. Agricultural soils and water sources can contain increased arsenic levels because of natural processes, industrial sources, or agricultural uses of arsenic, such as application of arsenic-containing herbicides,

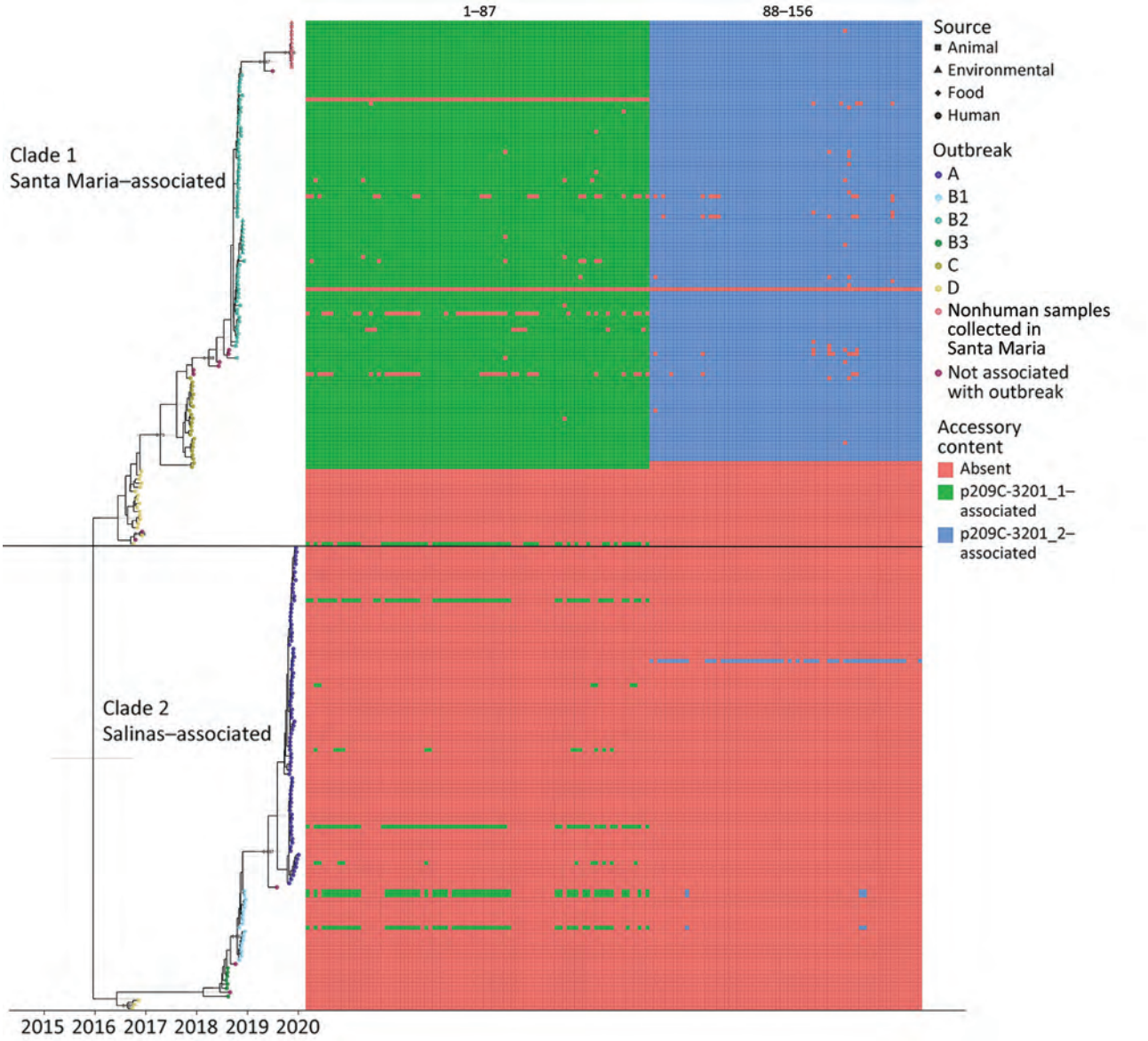

Figure 1. Tip-dated maximum clade credibility tree of 245 isolates of reoccurring *Escherichia coli* O157:H7 strain REPEXH02 linked to leafy greens–associated outbreaks, 2016–2019, generated in BEAST2 (https://www.beast2.org). Tips are aligned with the date of collection; calendar year is shown on the x-axis. Tips are colored according to the outbreak to which each isolate belonged; the shape corresponds to sample type (e.g., human, animal, environmental, or food). A horizontal black line segregates the two identified clades. Clade 1 contains outbreak B2 where some illness was traced back to Santa Maria, California, USA, as well as environmental samples collected in that region. Clade 2 contains outbreak A, which was traced back to the Salinas Valley, California. The presence/absence matrix to the right of the tree displays accessory genome content identified using Roary/scoary with 90% sensitivity and specificity to a subset of clade 1 isolates. A legend for accessory genome feature labels is included in Appendix 1 Table 5 (https://wwwnc.cdc.gov/EID/article/29/9/23-0069-App1.pdf).

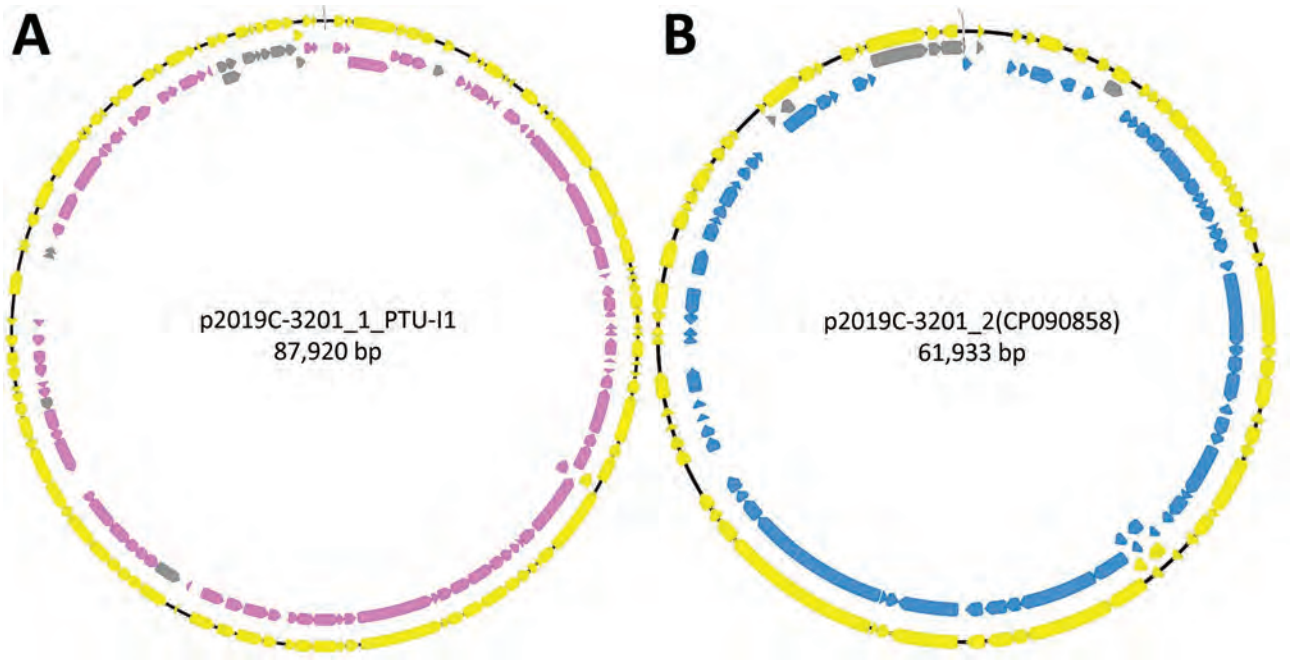

Figure 2. Annotated plasmids of reference genome 2019C-3201 of *Escherichia coli* O157:H7 containing clade-specific genomic features. A) p2019C-3201_1 annotated with prokka version 1.14.5 (yellow annotations) (*11*). Mapped list of Roary features (pan_genome_references.fa) onto plasmid (95% nucleotide identity; gray annotations) (*14*). Features highlighted had ≥90 sensitivity and ≥90 specificity to a subset of clade 1 isolates (pink annotations). The region with specific/sensitive features covers a large portion of the plasmid and predominately contains genes encoding hypothetical proteins with unknown functions and common plasmid-associated genes. Three features did not map in Geneious because they were either below 95% identity (2 features) or were identified as partial copy (1 feature). B) p2019C-3201_2 annotated with prokka v1.14.5 (yellow annotations). Mapped list of Roary features (pan_genome_references.fa) onto plasmid (100% nucleotide identity; gray annotations). Features highlighted had ≥90 sensitivity and ≥97 specificity (blue annotations) to a subset of clade 1 isolates. The region with specific/sensitive features covers a large portion of the plasmid and is associated with conjugation. Image was generated using Geneious version 2021.2 (https://www.geneious.com).

pesticides, or animal drugs (*13*). This mutation could provide an ecologic advantage in environments containing high levels of arsenic. This finding underscores the potential need to routinely screen enteric bacterial strains for heavy metal resistance determinants, as well as to consider heavy metal levels in soil as part of traceback investigations.

We further characterized isolates through assembly and annotation using Shovill-SPAdes version 1.0.9 and Prokka version 1.14.5 (*11*) and subsequent analysis in Roary version 3.11.2 (*14*) and scoary version 1.6.16 (*15*) to identify differences in the pangenome among isolates. We compared differentially distributed genes with the reference genome using BLASTn (https://blast.ncbi.nlm.nih.gov/Blast.cgi) to identify feature location (chromosome/plasmid). Roary/scoary analysis revealed a subset of clade 1 isolates with additional genomic content. A total of 156 genomic features had ≥90 sensitivity and ≥90 specificity to this subset of clade 1. Of those, 87 (56%) are on plasmid p2019C-3201_1, and 69 (44%) are on p2019C-3201_2 (Figure 2; Appendix 1 Tables 3, 4). Prokka-annotated features associated with p2019C-3201_1 (Figure 2; Appendix 1 Table 3) were predominantly genes encoding hypothetical proteins with unknown functions and common plasmid-associated genes. Annotated features associated with p2019C-3201_2 (Figure 2; Appendix 1 Table 4) were predominantly associated with conjugation and span a large portion of that plasmid. Additional work is necessary to characterize the role of these plasmids in clade 1. When visualizing the distribution of these clade 1–specific features alongside the maximum-clade credibility tree (Figure 1; Appendix 1 Table 5), it appears those features were acquired after clade 1 and clade 2 diverged. Given the geographic distribution of isolates, these features might be a result of adaptation to a particular niche or environment.

Conclusions

In summary, a specific strain of *E. coli* O157:H7 associated with leafy greens has been the source of ongoing enteric illness since late 2016. This strain is estimated to have emerged in late 2015 and consists of 2 clades with different geographic distributions, 1 of which has notable genomic features. After this analysis, an additional outbreak associated with this strain was

detected in late 2020 in which a reported 40 infections occurred in 19 states; 20 persons were hospitalized, and 4 developed hemolytic uremic syndrome (https://www.cdc.gov/ecoli/2020/o157h7-10-20b/index.html). After that outbreak, no further outbreaks have been detected, and only a single clinical isolate associated with this strain has been identified by PulseNet. The Centers for Disease Control and Prevention has classified this strain as a reoccurring, emerging, or persistent (REP) strain (https://www.cdc.gov/ncezid/dfwed/outbreak-response/rep-strains.html) with the designation REPEXH02. REP strains represent a new paradigm in enteric molecular surveillance, distinct from discrete outbreaks where numerous cases occur in a relatively short time frame. Detailed genomic characterization of additional REP strains, using the types of approaches outlined in this study, is necessary to elucidate factors contributing to their emergence and persistence in specific environments.

Acknowledgments

We thank state and local health departments for sequencing of *E. coli* O157:H7 associated with these outbreaks. The authors also thank Matthew Wise for helpful discussions and feedback.

This work was made possible by support from the Advanced Molecular Detection initiative at the Centers for Disease Control and Prevention and is covered by activities approved by the Centers for Disease Control and Prevention Internal Review Board (approval no. 7172).

About the Author

Dr. Chen is a bioinformatician in the Division of Foodborne, Waterborne, and Environmental Diseases, National Center for Emerging and Zoonotic Infectious Diseases, CDC. Her research interests are focused on understanding the evolution of bacterial foodborne pathogens of public health concern. Mr. Patel was an epidemiologist in Division of Foodborne, Waterborne, and Environmental Diseases, CDC, leading the response to multistate foodborne and zoonotic *E. coli* and *Salmonella* outbreaks within the Outbreak Response and Prevention Branch, as well as focusing on the response to REP strains of various pathogens. He now leads a team focused on building disease surveillance and outbreak response technology platforms in the private sector.

References

1. Scallan E, Hoekstra RM, Angulo FJ, Tauxe RV, Widdowson MA, Roy SL, et al. Foodborne illness acquired in the United States—major pathogens. Emerg Infect Dis. 2011;17:7–15. https://doi.org/10.3201/eid1701.P11101
2. Mead PS, Griffin PM. *Escherichia coli* O157:H7. Lancet. 1998; 352:1207–12. https://doi.org/10.1016/S0140-6736(98)01267-7
3. Bielaszewska M, Schmidt H, Liesegang A, Prager R, Rabsch W, Tschäpe H, et al. Cattle can be a reservoir of sorbitol-fermenting Shiga toxin–producing *Escherichia coli* O157:H(-) strains and a source of human diseases. J Clin Microbiol. 2000;38:3470–3. https://doi.org/10.1128/JCM.38.9.3470-3473.2000
4. Heiman KE, Mody RK, Johnson SD, Griffin PM, Gould LH. *Escherichia coli* O157 outbreaks in the United States, 2003–2012. Emerg Infect Dis. 2015;21:1293–301. https://doi.org/10.3201/eid2108.141364
5. Marshall KE, Hexemer A, Seelman SL, Fatica MK, Blessington T, Hajmeer M, et al. Lessons learned from a decade of investigations of Shiga toxin–producing *Escherichia coli* outbreaks linked to leafy greens, United States and Canada. Emerg Infect Dis. 2020;26:2319–28. https://doi.org/10.3201/eid2610.191418
6. Tolar B, Joseph LA, Schroeder MN, Stroika S, Ribot EM, Hise KB, et al. An overview of PulseNet USA databases. Foodborne Pathog Dis. 2019;16:457–62. https://doi.org/10.1089/fpd.2019.2637
7. Lin Y, Yuan J, Kolmogorov M, Shen MW, Chaisson M, Pevzner PA. Assembly of long error-prone reads using de Bruijn graphs. Proc Natl Acad Sci U S A. 2016;113:E8396–405. https://doi.org/10.1073/pnas.1604560113
8. Redondo-Salvo S, Bartomeus-Peñalver R, Vielva L, Tagg KA, Webb HE, Fernández-López, et al. COPLA, a taxonomic classifier of plasmids. BMC Bioinfo. 2021;22:390. https://doi.org/10.1186/s12859-021-04299-x
9. Katz LS, Griswold T, Williams-Newkirk AJ, Wagner D, Petkau A, Sieffert C, et al. A comparative analysis of the Lyve-SET phylogenomics pipeline for genomic epidemiology of foodborne pathogens. Front Microbiol. 2017;8:375. https://doi.org/10.3389/fmicb.2017.00375
10. Bouckaert R, Vaughan TG, Barido-Sottani J, Duchêne S, Fourment M, Gavryushkina A, et al. BEAST 2.5: an advanced software platform for Bayesian evolutionary analysis. PLOS Comput Biol. 2019;15:e1006650. https://doi.org/10.1371/journal.pcbi.1006650
11. Seemann T. Prokka: rapid prokaryotic genome annotation. Bioinformatics. 2014;30:2068–9. https://doi.org/10.1093/bioinformatics/btu153
12. Cherry JL. Recent genetic changes affecting enterohemorrhagic *Escherichia coli* causing recurrent outbreaks. Microbiol Spectr. 2022;10:e0050122. https://doi.org/10.1128/spectrum.00501-22
13. Punshon T, Jackson BP, Meharg AA, Warczack T, Scheckel K, Guerinot ML. Understanding arsenic dynamics in agronomic systems to predict and prevent uptake by crop plants. Sci Total Environ. 2017;581-582:209–20. https://doi.org/10.1016/j.scitotenv.2016.12.111
14. Page AJ, Cummins CA, Hunt M, Wong VK, Reuter S, Holden MTG, et al. Roary: rapid large-scale prokaryote pan genome analysis. Bioinformatics. 2015;31:3691–3. https://doi.org/10.1093/bioinformatics/btv421
15. Brynildsrud O, Bohlin J, Scheffer L, Eldholm V. Rapid scoring of genes in microbial pan-genome-wide association studies with Scoary. Genome Biol. 2016;17:238. https://doi.org/10.1186/s13059-016-1108-8

Address for correspondence: Jessica C. Chen, Centers for Disease Control and Prevention, 1600 Clifton Rd NE, Mailstop H23-7, Atlanta, GA 30329-4027, USA; email: lly3@cdc.gov

Human Neural Larva Migrans Caused by *Ophidascaris robertsi* Ascarid

Mehrab E Hossain, Karina J. Kennedy, Heather L. Wilson, David Spratt, Anson Koehler, Robin B. Gasser, Jan Šlapeta, Carolyn A. Hawkins, Hari Priya Bandi, Sanjaya N. Senanayake

We describe a case in Australia of human neural larva migrans caused by the ascarid *Ophidascaris robertsi*, for which Australian carpet pythons are definitive hosts. We made the diagnosis after a live nematode was removed from the brain of a 64-year-old woman who was immunosuppressed for a hypereosinophilic syndrome diagnosed 12 months earlier.

Ophidascaris species are nematodes exhibiting an indirect lifecycle; various genera of snakes across the Old and New Worlds are definitive hosts. *O. robertsi* nematodes are native to Australia, where the definitive hosts are carpet pythons (*Morelia spilota*). The adult nematodes inhabit the python's esophagus and stomach and shed their eggs in its feces. Eggs are ingested by various small mammals, in which larvae establish, serving as intermediate hosts (*1*). Larvae migrate to thoracic and abdominal organs (*1*–*3*) where, particularly in marsupials, the third-stage larvae may reach a considerable length (7–8 cm), even in small hosts (*3*,*4*). The lifecycle concludes when pythons consume the infected intermediate hosts (*3*). Humans infected with *O. robertsi* larvae would be considered accidental hosts, although human infection with any *Ophidascaris* species has not previously been reported. We report a case of human neural larva migrans caused by *O. robertsi* infection.

Author affiliations: Canberra Health Services, Canberra, Australian Capital Territory, Australia (M. Hossain, K.J. Kennedy, H.L. Wilson, C.A. Hawkins, H. Bandi, S.N. Senanayake); Australian National University, Canberra (K.J. Kennedy, C.A. Hawkins, H. Bandi, S.N. Senanayake); Commonwealth Scientific and Industrial Research Organization Australian Capital Territory, Canberra (D. Spratt); University of Melbourne, Melbourne, Victoria, Australia (A. Koehler, R.B. Gasser); University of Sydney, Sydney, New South Wales, Australia (J. Šlapeta); The University of Sydney Institute for Infectious Diseases, Sydney (J. Šlapeta)

DOI: http://doi.org/10.3201/eid2909.230351

The Study

A 64-year-old woman from southeastern New South Wales, Australia, was admitted to a local hospital in late January 2021 after 3 weeks of abdominal pain and diarrhea, followed by dry cough and night sweats. She had a peripheral blood eosinophil count (PBEC) of 9.8×10^9 cells/L (reference range $<0.5 \times 10^9$ cells/L), hemoglobin 99 g/L (reference range 115–165 g/L), platelets 617×10^9 cells/L (reference range 150–400 $\times$ 10^9 cells/L), and C-reactive protein (CRP) 102 mg/L (reference range <5 mg/L). Her medical history included diabetes mellitus, hypothyroidism, and depression. She was born in England and had traveled to South Africa, Asia, and Europe 20–30 years earlier. She was treated for community-acquired pneumonia with doxycycline and had not recovered fully.

A computed tomography (CT) scan revealed multifocal pulmonary opacities with surrounding ground-glass changes, as well as hepatic and splenic lesions. Bronchoalveolar lavage revealed 30% eosinophils without evidence of malignancy or pathogenic microorganisms, including helminths. Serologic testing was negative for *Strongyloides*. Autoimmune disease screening results were negative. The patient's diagnosis was eosinophilic pneumonia of unclear etiology; she began taking prednisolone (25 mg/d) with partial symptomatic improvement.

Three weeks later, she was admitted to a tertiary hospital with recurrent fever and a persistent cough while on prednisolone. PBEC was 3.4×10^9 cells/L and CRP was 68.2 mg/L. CT scans revealed persistent hepatic and splenic lesions and migratory pulmonary opacities (Figure 1, panels A, B). The pulmonary and hepatic lesions were 18F-fluorodeoxyglucose–avid on positive emission tomography scan. Lung biopsy specimen was consistent with eosinophilic pneumonia but not with eosinophilic granulomatosis with polyangiitis (EGPA) (Figure 1, panel C). Bacterial, fungal, and mycobacterial cultures were negative.

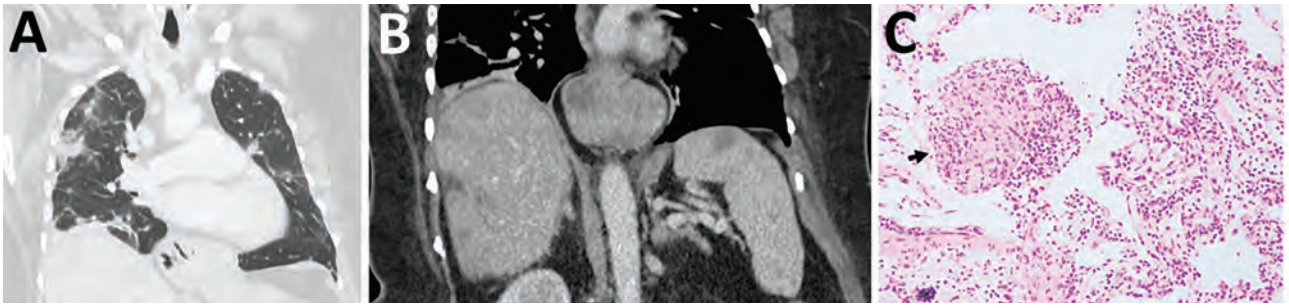

Figure 1. Early testing conducted during investigation of illness in a 64-year-old woman from southeastern New South Wales, Australia, who was later determined to have *Ophidascaris robertsi* nematode infection. A) Computed tomography scan of chest with venous contrast demonstrating multiple bilateral airspace opacities and nodules with a peripheral bronchovascular distribution. The opacities have surrounding ground-glass changes. Many were present in the patient's study from a previous hospitalization; however, some had resolved while others were new, indicating a migratory pattern. B) Computed tomography scan of abdomen with venous contrast demonstrating multiple ill-defined hypoattenuated lesions within the liver and spleen. C) Hematoxylin and eosin stain (original magnification ×200) of a pulmonary lesion revealing prominent eosinophil infiltration of stroma and vessel walls. Arrow indicates a granuloma composed of histiocytes and eosinophils. The prominent eosinophilia was inconsistent with hypersensitivity pneumonitis, and the absence of vessel wall damage did not support a diagnosis of eosinophilic granulomatosis with polyangiitis.

Echinococcus, *Fasciola*, and *Schistosoma* antibodies were not detected; concentrated and fixed-stain techniques did not reveal parasites on fecal specimens.

We detected a monoclonal T-cell receptor gene rearrangement, suggesting T-cell driven hypereosinophilic syndrome (HES). Other hematologic and vasculitis investigations were unremarkable. HES treatment began with prednisolone (50 mg/d) and mycophenolate (1 g 2×/d). Because of her travel history, possibility of false-negative *Strongyloides* serology, and increased immunosuppression, she received ivermectin (200 μg/kg orally) for 2 consecutive days and a repeat dose after 14 days.

A CT scan in mid-2021 showed improvement in the pulmonary and hepatic lesions but unchanged splenic lesions. PBEC was 0.76×10^9 in September 2021. We added mepolizumab (interleukin-5 monoclonal antibody, 300 mg every 4 wk) in January 2022 because we were unable to reduce the prednisolone below 20 mg daily without a flare of respiratory symptoms. When PBEC returned within normal range, we tapered the prednisolone dose.

During a 3-month period in 2022, the patient experienced forgetfulness and worsening depression while continuing prednisolone (7.5 mg/d) and mycophenolate and mepolizumab at the same doses. PBEC was within reference range; CRP was 6.4 mg/L. Brain magnetic resonance imaging showed a 13 × 10 mm peripherally enhancing right frontal lobe lesion (Figure 2, panel A). In June 2022, she underwent an open biopsy. We noted a stringlike structure within the lesion, which we removed; it was a live and motile helminth (80 mm long, 1 mm diameter) (Figure 2, panels B, C). We performed a circumferential durotomy and

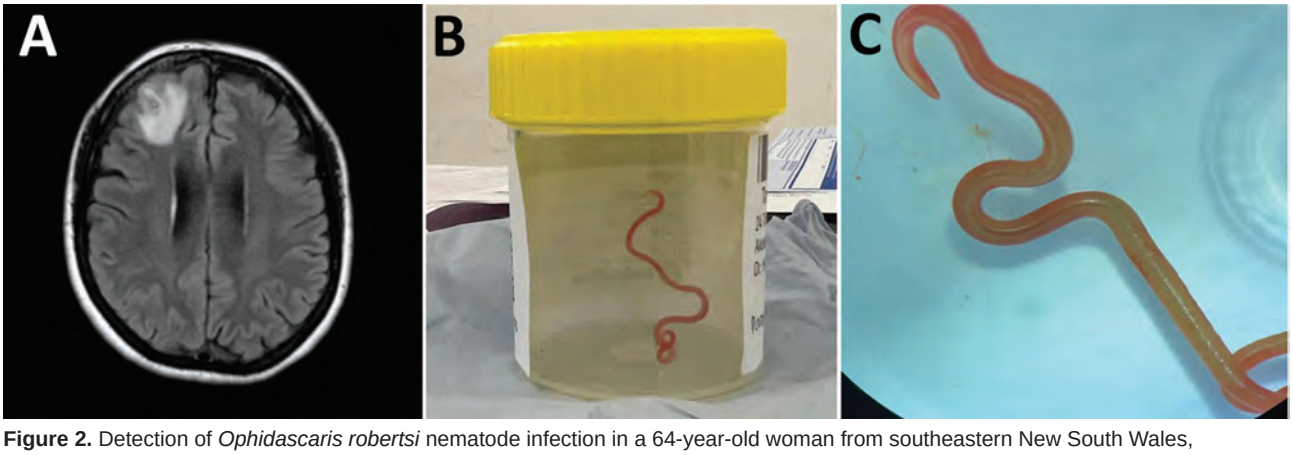

Figure 2. Detection of *Ophidascaris robertsi* nematode infection in a 64-year-old woman from southeastern New South Wales, Australia. A) Magnetic resonance image of patient's brain by fluid-attenuated inversion recovery demonstrating an enhancing right frontal lobe lesion, 13 × 10 mm. B) Live third-stage larval form of *Ophidascaris robertsi* (80 mm long, 1 mm diameter) removed from the patient's right frontal lobe. C) Live third-stage larval form of *O. robertsi* (80 mm long, 1 mm diameter) under stereomicroscope (original magnification ×10).

corticotomy and found no other helminths. Histopathology of the dural tissue revealed a benign, organizing inflammatory cavity with prominent eosinophilia.

We provisionally identified the helminth as a third-stage larva of *Ophidascaris robertsi* on the basis of its distinctive red color, 3 active ascaridoid-like lips, presence of a cecum, and absence of a fully developed reproductive system, in the context of the known epidemiologic distribution of this species. The head and tail were preserved at the Australian National Wildlife Collection (W/LHC no. N5758). Small segments underwent independent PCR-based sequencing targeting the cytochrome oxidase c subunit 1 (*cox*1) (*5*,*6*) at the University of Sydney and the second internal transcribed spacer (ITS) 2 of nuclear ribosomal DNA (*7*) at the University of Melbourne. Both sequencing results provided >99.7% sequence match to *Ophidascaris* (formerly *Amplicecum*) *robertsi* isolates in the National Center for Biotechnology Information and in-house databases (Appendix, https://wwwnc.cdc.gov/EID/article/29/9/23-0351-App1.pdf).

A progress CT scan revealed resolution of pulmonary and hepatic lesions but unchanged splenic lesions. The patient received 2 days of ivermectin (200 μg/kg/d) and 4 weeks of albendazole (400 mg 2×/d). She was given a weaning course of dexamethasone (starting 4 mg 2×/d) over 10 weeks, while all other immunosuppression was discontinued. Six months after surgery (3 months after ceasing dexamethasone), the patient's PBEC remained normal. Neuropsychiatric symptoms had improved but persisted.

Conclusions

The patient in this case resided near a lake area inhabited by carpet pythons. Despite no direct snake contact, she often collected native vegetation, warrigal greens (*Tetragonia tetragonioides*), from around the lake to use in cooking. We hypothesized that she inadvertently consumed *O. robertsi* eggs either directly from the vegetation or indirectly by contamination of her hands or kitchen equipment.

The patient's clinical and radiologic progression suggests a dynamic process of larval migration to multiple organs, accompanied by eosinophilia in blood and tissues, indicative of visceral larva migrans syndrome. We suspect that the splenic lesions are a separate pathology because they remained stable and were not PET avid, unlike the pulmonary and hepatic lesions.

This case highlights the difficulty in obtaining a suitable specimen for parasitic diagnosis and the challenging management decisions regarding immunosuppression in the presence of potentially life-threatening HES. Although visceral involvement is common in animal hosts, the invasion of the brain by *Ophidascaris* larvae had not been reported previously. The patient's immunosuppression may have enabled the larvae to migrate into the central nervous system (CNS). The growth of the third-stage larva in the human host is notable, given that previous experimental studies have not demonstrated larval development in domesticated animals, such as sheep, dogs, and cats, and have shown more restricted larval growth in birds and nonnative mammals than in native mammals (*4*).

After we removed the larva from her brain, the patient received anthelmintics and dexamethasone to address potential larvae in other organs. *Ophidascaris* larvae are known to survive for long periods in animal hosts; for example, laboratory rats have remained infected with third-stage larvae for ≥4 years (*4*). The rationale for ivermectin and albendazole was based on data from the treatment of nematode infections in snakes and humans (*8*,*9*). Albendazole has better penetration into the CNS than ivermectin (*10*). Dexamethasone has been used in other human nematode and tapeworm infections to avoid deleterious inflammatory CNS responses following treatment (*11*).

In summary, this case emphasizes the ongoing risk for zoonotic diseases as humans and animals interact closely. Although *O. robertsi* nematodes are endemic to Australia, other *Ophidascaris* species infect snakes elsewhere, indicating that additional human cases may emerge globally.

Acknowledgments

We thank Mitali Fadia and Sophie Hale for their assistance.

About the Author

Dr. Hossain is an infectious diseases physician in Australia. Her primary research interest is in parasitology.

References

1. Sprent JFA. The life history and development of *Amplicaecum robertsi*, an ascaridoid nematode of the carpet python (*Morelia spilotes variegatus*). I. Morphology and functional significance of larval stages. Parasitology. 1963;53:7–38. https://doi.org/10.1017/S0031182000072498
2. Gallego-Agúndez M, Villaluenga Rodríguez JE, Juan-Sallés C, Spratt DM. First report of parasitism by *Ophidascaris robertsi* (Nematoda) in a sugar glider (*Petaurus breviceps*, Marsupialia). J Zoo Wildl Med. 2014;45:984–6. https://doi.org/10.1638/2014-0107.1
3. Gonzalez-Astudillo V, Knott L, Valenza L, Henning J, Allavena R. Parasitism by *Ophidascaris robertsi* with associated pathology findings in a wild koala

(*Phascolarctos cinereus*). Vet Rec Case Rep. 2019;7:e000821. https://doi.org/10.1136/vetreccr-2019-000821
4. Sprent J. The life history and development of *Amplicaecum robertsi*, an ascaridoid nematode of the carpet python (*Morelia spilotes variegatus*). II. Growth and host specificity of larval stages in relation to the food chain. Parasitology. 1963;53:321–37. https://doi.org/10.1017/S0031182000072796
5. Baron HR, Šlapeta J, Donahoe SL, Doneley R, Phalen DN. Compensatory gastric stretching following subtotal gastric resection due to gastric adenocarcinoma in a diamond python (*Morelia spilota spilota*). Aust Vet J. 2018;96:481–6. https://doi.org/10.1111/avj.12764
6. Folmer O, Black M, Hoeh W, Lutz R, Vrijenhoek R. DNA primers for amplification of mitochondrial cytochrome c oxidase subunit I from diverse metazoan invertebrates. Mol Mar Biol Biotechnol. 1994;3:294–9.
7. Mullis K, Faloona F, Scharf S, Saiki R, Horn G, Erlich H. Specific enzymatic amplification of DNA in vitro: the polymerase chain reaction. Cold Spring Harb Symp Quant Biol. 1986;51:263–73. https://doi.org/10.1101/SQB.1986.051.01.032
8. Wilson S, Carpenter JW. Endoparasitic diseases of reptiles. J Exot Pet Med. 1996;5:64–74. https://doi.org/10.1016/S1055-937X(96)80019-3
9. Herman JS, Chiodini PL. Gnathostomiasis, another emerging imported disease. Clin Microbiol Rev. 2009;22:484–92. https://doi.org/10.1128/CMR.00003-09
10. Nau R, Sörgel F, Eiffert H. Penetration of drugs through the blood-cerebrospinal fluid/blood-brain barrier for treatment of central nervous system infections. Clin Microbiol Rev. 2010;23:858–83. https://doi.org/10.1128/CMR.00007-10
11. Katchanov J, Sawanyawisuth K, Chotmongkol V, Nawa Y. Neurognathostomiasis, a neglected parasitosis of the central nervous system. Emerg Infect Dis. 2011;17:1174–80. https://doi.org/10.3201/eid1707.101433

Address for correspondence: Sanjaya N. Senanayake, Infectious Diseases Unit, Canberra Health Services, The Canberra Hospital, Yamba Dr, Garran, Australian Capital Territory, Postcode 2605, Australia; email: sanjaya.senanayake@anu.edu.au

Anaplasma bovis–Like Infections in Humans, United States, 2015–2017

Sandor E. Karpathy, Luke Kingry, Bobbi S. Pritt, Jonathan C. Berry, Neil B. Chilton, Shaun J. Dergousoff,[1] Roberto Cortinas, Sarah W. Sheldon, Stephanie Oatman,[2] Melissa Anacker, Jeannine Petersen, Christopher D. Paddock

We detected the DNA of an *Anaplasma bovis*–like bacterium in blood specimens from 4 patients from the United States with suspected tickborne illnesses. Initial molecular characterization of this novel agent reveals identity to *A. bovis*–like bacteria detected in *Dermacentor variabilis* ticks collected from multiple US states.

The genus *Anaplasma* includes several species of tickborne, zoonotic pathogens of global importance. Three recognized species (*Anaplasma phagocytophilum*, *Anaplasma ovis*, and *Anaplasma bovis*) and one provisionally named species (*Anaplasma capra*) are associated with moderately severe to severe disease in humans (*1*). Human infections with *A. bovis*, a pathogen first identified in monocytes of cattle in Algeria in 1936 and subsequently detected in other countries in Africa, Asia, and the Americas, were reported from China in 2017 (*1*–*3*). In 2015, a targeted metagenomic approach designed to amplify the V1–V2 region of the bacterial 16S rRNA (*rrs*) gene identified DNA of an *A. bovis*–like agent in blood specimens from 2 US patients with suspected tickborne illnesses (*4*). The agent demonstrated 100% identity across a 357-bp region of *rrs* to *A. bovis*–like sequences amplified from several human-biting *Dermacentor* tick species in North America (*4*). An additional 2 US patients positive for this same *Anaplasma* species were identified in 2017 (L. Kingry et al., unpub. data), although the genetic identity of this pathogen remained limited to the same 357-bp sequence of *rrs* (*5*–*7*). To further characterize the phylogenetic position of this novel agent, we evaluated additional sequences to determine the uniqueness of this strain among the expanding global complex of *A. bovis*–like bacteria.

The Study

We extracted DNA from 100 μL of EDTA-treated whole blood obtained from 4 patients from whom partial *rrs* sequences of an *A. bovis*–like agent were identified from a targeted metagenomics assessment of whole blood specimens collected from US patients with suspected tickborne disease (*4*; L. Kingry et al., unpub. data). DNA extracts containing *A. bovis* DNA were also available from an adult *Dermacentor andersoni* tick collected in Saskatchewan Landing Provincial Park in Saskatchewan, Canada, and from 5 adult *Dermacentor variabilis* ticks collected in Washita County, Oklahoma; Floyd County, Iowa; and Sarpy and Cass Counties, Nebraska, from which partial *rrs* sequences most similar with *A. bovis* were amplified previously (*5*,*6*).

We amplified segments of the *rrs*, citrate synthase (*glt*A), and heat shock chaperon (*gro*EL) genes using Taq PCR Master Mix Kit (QIAGEN, https://www.qiagen.com) (Table 1). Each 20-μL primary reaction consisted of 1 μM of each primer, 10 μL Taq Master Mix, 2 μL DNA, and 6 μL molecular-grade water. Secondary reactions (*gro*EL only) consisted of 1 μM of each primer, 10 μL Taq Master Mix, 1 μL primary PCR product, and 7 μL molecular-grade water. We resolved PCR amplicons on a 1% agarose gel in Tris-acetate-EDTA buffer and cut amplicons from the gel and purified using a Wizard SV Gel and PCR Clean-up kit (Promega, https://www.promega.com). We sequenced each purified amplicon (1 μL) bidirectionally

Author affiliations: Centers for Disease Control and Prevention, Atlanta, Georgia, USA (S.E. Karpathy, C.D. Paddock); Centers for Disease Control and Prevention, Fort Collins, Colorado, USA (L. Kingry, S.W. Sheldon, S. Oatman, J. Petersen); Mayo Clinic, Rochester, Minnesota, USA (B.S. Pritt, J.C. Berry); University of Saskatchewan, Saskatoon, Saskatchewan, Canada (N.B. Chilton, S.J. Dergousoff); University of Nebraska, Lincoln, Nebraska, USA (R. Cortinas); Minnesota Department of Health, St. Paul, Minnesota, USA (M. Anacker)

DOI: https://doi.org/10.3201/eid2909.230559

[1]Current affiliation: Agriculture and Agri-food Canada, Lethbridge, Alberta, Canada.

[2]Current affiliation: Mayo Clinic, Jacksonville, Florida, USA.

Table 1. PCR primers used in study of *Anaplasma bovis*–like infections in humans, United States, 2015–2017

Gene	Primer name	Sequence, 5′ → 3′	Annealing temperature*	Reference
rrs	Out2F	GAT AGC GGA ATT CCT AGT GTA GAG GTG	56°C	(*8*)
	317Pan	AAA GGA GGT AAT CCA GC		
*glt*A	Abov_gltA2F	CGG AAA TTA CTT TTA TAG ATG G	49°C	This study
	Abov_gltA2R	CAT ACC AYT GAG AAA CCC AAC		
gro*EL*	HS1-f	CGT CAG TGG GCT GGT AAT GAA	54°C	(*9*,*10*)
	HS6-r	CCW CCW GGT CWA CAC CTT C	50°C	(*11*)
	HS3-f	ATA GTY ATG AAG GAG AGT GAT		
	HSVR	TCA ACA GCA GCT CTA GTW G		

*Cycling conditions: 95°C for 3 min followed by 35 cycles of 95°C for 30 s, 1 min at the annealing temperature listed above, and an extension at 72°C for 1 min 30 s. This was followed by a final extension at 72°C for 10 min.

using a Big Dye Terminator v3.1 Cycle Sequencing Kit, purified using a BigDye XTerminator Purification Kit, and sequenced using an ABI 3500 Genetic Analyzer (all from ThermoFisher Scientific, https://www.thermofisher.com).

We used Geneious Prime version 2021.0.3 (https://www.geneious.com) to assemble and align consensus sequences and infer the phylogenetic relationships between DNA sequences (*12*). Only 3 sources of genetic information for *A. bovis* were available in GenBank that provided complete or partial sequence data at all 3 loci, including those amplified from the blood of a raccoon (*Procyon lotor*) captured in Hokkaido, Japan (*13*); a goat (*Capra* sp.) from Shaanxi Province, China; and a cow (*Bos taurus*) from Shaanxi Province, China. The *rrs, glt*A, and *gro*EL nucleotide sequences amplified from the human samples were submitted to GenBank and assigned the accession numbers OQ693620 (*rrs*), OQ694770 (*glt*A), and OQ693619 (*gro*EL).

The *rrs* sequences (599-bp) of the 4 human samples were 100% identical to each other and to those amplified from a *D. andersoni* tick and 5 *D. variabilis* ticks; the sequences also showed 98.3% identity to the *rrs* sequences amplified from blood specimens obtained from the cow from China, 98% to those from the goat from China, and 97.8% identity to those from the raccoon from Japan. The 826-bp *glt*A sequences from the 4 human samples were 100% identical to each other and to all sequences from *D. variabilis* ticks; they also were 99.4% identical to the 827-bp sequence from the *D. andersoni* tick. When trimmed to 356 bp to match the sequence lengths available in GenBank of those from the cow and goat from China, the North America sequences amplified from humans and ticks shared only 78.6%–79.4% identity with the sequences from China. The *gro*EL sequences (1,079-bp) of the human samples were 100% identical to each other and to the corresponding sequences amplified from all 5 *D. variabilis* ticks and showed 99.4% identity to the *gro*EL sequence amplified from the *D. andersoni* tick. Those samples showed only 85.4% identity to the *A. bovis* sequences from the raccoon from Japan and 84.6% identity to the sequences from the cow and goat from China. Phylogenetic analyses using concatenated sequences from the 3 loci produced an inferred consensus tree that grouped human and North America *Dermacentor* spp. tick samples with the other *A. bovis* sequences but with strong statistical support (100%) for the separation of *A. bovis*–like sequences from North America and those from China and Japan (Figure).

Conclusions

A novel and presumably tickborne pathogen of humans was identified in blood of patients from the central and upper midwestern United States during 2015–2017 (Table 2). The amplification of a thus far genetically identical agent from *D. variabilis* ticks suggests that this tick species could represent a vector of this *A. bovis*–like agent in the United States. This bacterium is also related to a worldwide complex of bacteria, detected in multiple species of ticks and domesticated and wild animals, designated collectively as *A. bovis*. Because *A. bovis* has never been cultured in vitro, neither a type strain nor a complete genome exist for this pathogen. Only 3 genetic loci from *A. bovis* exist in GenBank, and few sources provide complete sequences for all loci from the same sample. As seen in this evaluation, the level of nucleotide identity among samples can vary considerably at an individual locus and hamper efforts to establish genetic relatedness of *A. bovis*–like bacteria.

The spectrum of disease and epidemiology associated with human infections caused by this novel *A. bovis*–like agent remains unknown. Presumably, human infections with this agent in the United States are uncommon, because this bacterium was detected only 4 times from 29,928 residual clinical samples obtained during 2014–2019. By comparison, 1,236 infections with *A. phagocytophilum* and 345 infections with *Ehrlichia* spp. were identified from this investigation during the same period (*5*; L. Kingry et al., unpub. data). The study design that enabled the discovery of

this novel agent also precluded the collection of clinical details of infected patients; nonetheless, an *A. bovis*–like pathogen was detected recently in blood of patients from Anhui and Jiangxi Provinces in China who had illnesses characterized predominantly by fever, myalgia, fatigue, anorexia, and thrombocytopenia (*3*). In the United States, *A. bovis*–like bacteria have been detected in blood samples from cottontail

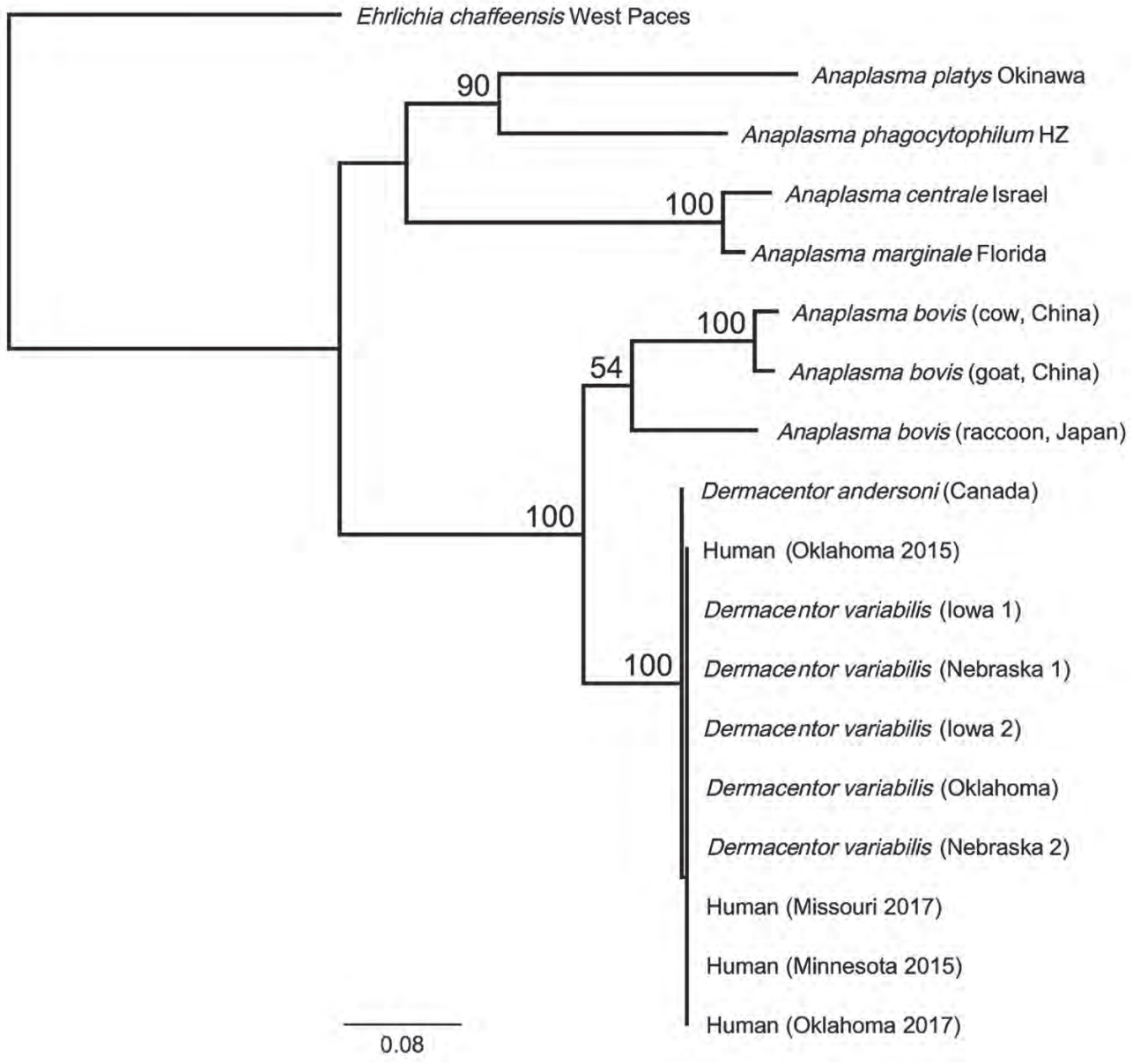

Figure. Phylogenetic relationship of novel human *Anaplasma bovis*–like pathogen associated with human cases in the United States, 2015–2017, to other *A. bovis*–like and related *Anaplasma* species based on 2,039 bp of concatenated *rrs*, *glt*A, *gro*EL nucleotide sequences. Phylogenetic relationships were inferred using the RAxML method using the general time reversible plus gamma model (*13*). One thousand bootstrap replicates were used to estimate the likelihood of the tree; bootstrap values are displayed next to the nodes. Only bootstrap values of >50 are shown. GenBank accession numbers for the samples in this study: OQ772254;, *glt*A; OQ772255, *gro*EL; and OQ724830, *rrs*; those for the *D. andersoni* sample were assigned the following numbers: OQ772256, *glt*A; OQ772257, *gro*EL; and OQ724821, *rrs.* Reference sequences from GenBank: *Anaplasma bovis* (cow, China): MH255937, 16S; MH594290, *glt*A; MH255906.1, *gro*EL; *A. bovis* (goat, China): MH255939, 16S; MH255915.1, *glt*A; MH255907, *gro*EL; *A. bovis* (raccoon, Japan): GU937020, 16S; JN588561, *glt*A; JN588562, *gro*EL; *Anaplasma platys* strain Okinawa: AY077619, 16S; AY077620, *glt*A; AY077621, *gro*EL; *A. phagocytophilum* strain HZ NC_007797; *A. centrale* strain Israel NC_013532; *A. marginale* strain Florida NC_012026. *Ehrlichia chaffeensis* strain West Paces (NZ_CP007480) was used as the outgroup. Scale bar represents mean number of nucleotide substitutions per site.

Table 2. Demographic and geographic characteristics associated with human cases of *Anaplasma bovis*–like infection identified in the United States, 2015–2017

Specimen	Patient age, y/sex	State of origin	Date of collection
Oklahoma 2015	71/F	Oklahoma	2015 Jun 9
Minnesota 2015	34/M	Minnesota	2015 Aug 12
Oklahoma 2017	67/F	Oklahoma	2017 May 21
Missouri 2017	54/M	Missouri	2017 Jun 14

rabbits (*Sylvilagus* spp.) from Massachusetts, Georgia, and Texas and from black-tailed jackrabbits (*Lepus californicus*) from Texas (*14*,*15*). Developing a specific molecular assay could help identify additional patients infected with this novel agent and clarify the tick and wildlife species involved in its natural history and transmission to humans.

Acknowledgments

We thank Paula Lado, Michelle Allerdice, Joy Hecht, and Maria F.B.M. Galletti for providing DNA from the *D. variabilis* tick samples used in the molecular evaluations. We also thank the TickNet AMD Emerging Infections Program Team at the Minnesota Department of Health, the Mayo Clinic, and Bacterial Diseases Branch in the Division of Vector-Borne Diseases at the Centers for Disease Control and Prevention for assistance with the identification of the human cases.

S.J.D. is an employee of the Government of Canada (His Majesty the King in Right of Canada, 2023).

About the Author

Dr. Karpathy is a microbiologist for the Division of Vector-Borne Diseases, National Center for Emerging and Zoonotic Infectious Diseases, Centers for Disease Control and Prevention. His research interests include the genetic characterization and genomics of rickettsial pathogens.

References

1. Li H, Zheng Y-C, Ma L, Jia N, Jiang B-G, Jiang R-R, et al. Human infection with a novel tick-borne *Anaplasma* species in China: a surveillance study. Lancet Infect Dis. 2015;15:663–70. https://doi.org/10.1016/S1473-3099(15)70051-4
2. Donatien A, Lestoquard F. Rickettsiose bovine Algerienne a *R. bovis*. Bull Soc Pathol Exot. 1940;33:245–8.
3. Lu M, Chen Q, Qin X, Lyu Y, Teng Z, Li K, et al. *Anaplasma bovis* infection in fever and thrombocytopenia patients—Anhui Province, China 2021. China CDC Wkly. 2022;4:249–53. https://doi.org/10.46234/ccdcw2022.053
4. Kingry L, Sheldon S, Oatman S, Pritt B, Anacker M, Bjork J, et al. Targeted metagenomics for clinical detection and discovery of bacterial tick-borne pathogens. J Clin Microbiol. 2020;58:e00147–20. https://doi.org/10.1128/JCM.00147-20
5. Chilton NB, Dergousoff SJ, Lysyk TJ. Prevalence of *Anaplasma bovis* in Canadian populations of the Rocky Mountain wood tick, *Dermacentor andersoni*. Ticks Tick Borne Dis. 2018;9:1528–31. https://doi.org/10.1016/j.ttbdis.2018.07.003
6. Lado P, Luan B, Allerdice MEJ, Paddock CD, Karpathy SE, Klompen H. Integrating population genetic structure, microbiome, and pathogens presence data in *Dermacentor variabilis*. PeerJ. 2020;8:e9367. https://doi.org/10.7717/peerj.9367
7. Lane RS, Mun J, Peribáñez MA, Fedorova N. Differences in prevalence of *Borrelia burgdorferi* and *Anaplasma spp.* infection among host-seeking *Dermacentor occidentalis, Ixodes pacificus*, and *Ornithodoros coriaceus* ticks in northwestern California. Ticks Tick Borne Dis. 2010;1:159–67. https://doi.org/10.1016/j.ttbdis.2010.09.004
8. Zhuang L, Du J, Cui XM, Li H, Tang F, Zhang PH, et al. Identification of tick-borne pathogen diversity by metagenomic analysis in *Haemaphysalis longicornis* from Xinyang, China. Infect Dis Poverty. 2018;7:45. https://doi.org/10.1186/s40249-018-0417-4
9. Sumner JW, Nicholson WL, Massung RF. PCR amplification and comparison of nucleotide sequences from the groESL heat shock operon of *Ehrlichia* species. J Clin Microbiol. 1997;35:2087–92. https://doi.org/10.1128/jcm.35.8.2087-2092.1997
10. Rar VA, Livanova NN, Panov VV, Doroschenko EK, Pukhovskaya NM, Vysochina NP, et al. Genetic diversity of *Anaplasma* and *Ehrlichia* in the Asian part of Russia. Ticks Tick Borne Dis. 2010;1:57–65. https://doi.org/10.1016/j.ttbdis.2010.01.002
11. Rar V, Livanova N, Tkachev S, Kaverina G, Tikunov A, Sabitova Y, et al. Detection and genetic characterization of a wide range of infectious agents in *Ixodes pavlovskyi* ticks in Western Siberia, Russia. Parasit Vectors. 2017;10:258. https://doi.org/10.1186/s13071-017-2186-5
12. Stamatakis A. RAxML version 8: a tool for phylogenetic analysis and post-analysis of large phylogenies. Bioinformatics. 2014;30:1312–3. https://doi.org/10.1093/bioinformatics/btu033
13. Sashika M, Abe G, Matsumoto K, Inokuma H. Molecular survey of *Anaplasma* and *Ehrlichia* infections of feral raccoons (*Procyon lotor*) in Hokkaido, Japan. Vector Borne Zoonotic Dis. 2011;11:349–54. https://doi.org/10.1089/vbz.2010.0052
14. Goethert HK, Telford SR III. Enzootic transmission of *Anaplasma bovis* in Nantucket cottontail rabbits. J Clin Microbiol. 2003;41:3744–7. https://doi.org/10.1128/JCM.41.8.3744-3747.2003
15. Yabsley MJ, Romines J, Nettles VF. Detection of *Babesia* and *Anaplasma* species in rabbits from Texas and Georgia, USA. Vector Borne Zoonotic Dis. 2006;6:7–13. https://doi.org/10.1089/vbz.2006.6.7

Address for correspondence: Sandor E. Karpathy, Centers for Disease Control and Prevention, 1600 Clifton Rd NE, Mailstop H17-3, Atlanta, GA 30329-4027, USA; email: skarpathy@cdc.gov

Novel Echarate Virus Variant Isolated from Patient with Febrile Illness, Chanchamayo, Peru

Gilda Troncos, Dina Popuche, Bishwo N. Adhikari, Kyle A. Long, Jane Ríos, Michel Valerio, Carolina Guevara, Regina Z. Cer, Kimberly A. Bishop-Lilly, Julia S. Ampuero, Maria Silva, Cristhopher D. Cruz

A new phlebovirus variant was isolated from an acute febrile patient in Chanchamayo, Peru. Genome characterization and p-distance analyses based on complete open reading frames revealed that the virus is probably a natural reassortant of the Echarate virus (large and small segments) with a yet-unidentified phlebovirus (M segment).

The genus *Phlebovirus* (order Bunyavirales, family Phenuiviridae) consists of 66 species according to the International Committee on Taxonomy of Viruses (*1*). Phleboviruses are globally distributed and can be transmitted by phlebotomine sandflies, mosquitoes, or ticks (*2*,*3*). Sandfly phlebovirus can cause unspecific symptoms in humans and often is misdiagnosed as dengue fever, malaria, or influenza (*4*,*5*); however, its clinical symptoms can range from high fever, severe headache, muscle pain, and aseptic meningitis to mild or severe meningoencephalitis (*6*). In Peru, 3 of 9 phleboviruses that cause febrile illness in Central and South America (*3*–*5*,*7*) have been identified: Echarate virus (ECHV), Maldonado virus (*7*), and Candiru virus (*7*).

During the last decade, isolates characterized by whole-genome sequencing have contributed to increased detection of novel and recombinant pathogenic and nonpathogenic phleboviruses worldwide (*2*,*5*,*7*), demonstrating a high viral diversity within this genus. Therefore, continuous public health surveillance, including genome characterization as a complementary tool, is critical to identifying novel and emerging viruses of clinical relevance in the Americas. We report the identification and characterization of a novel ECHV virus variant isolated from a patient with acute febrile illness (AFI) in Peru.

The Study

As part of passive clinic-based surveillance for AFI in Peru approved by Peru's Ministry of Health and the US Naval Medical Research Unit South Institutional Review Board (protocol no. NMRCD.2010.0010) (*8*), a 20-year-old man who worked in civil construction was admitted to Hospital Regional Docente de Medicina Tropical Julio César Demarini Caro, located in the city of Chanchamayo in the northern region of Junín Department in central Peru, on June 25, 2019 (Figure 1). He had a 2-day history of fever, malaise, chills, systemic muscle pain, arthralgias, generalized head pain, drowsiness, photophobia, retroocular pain, and anorexia. He had conjunctival injection and an axillary temperature of 39.0°C, and the tourniquet test was negative.

We inoculated the acute serum sample into African green monkey kidney cells (Vero ATCC CCL-81) and *Aedes albopictus* mosquito cells (C6/36) and maintained them at 37°C (Vero cells) and 33°C (mosquito cells). The sample showed ≈50% cytopathic effect at day 7 in Vero cells, but no cytopathic effect occurred in C6/36 cells after 10 days. We prepared spot slides of both cell lines and tested them by indirect immunofluorescence assay (IFA) using pooled polyclonal antisera against flaviviruses (yellow fever virus and dengue virus serotype 3),

Author affiliations: US Naval Medical Research Unit SOUTH, Lima, Peru (G. Troncos, D. Popuche, J. Ríos, C. Guevara, J.S. Ampuero, M. Silva, C.D. Cruz); Defense Threat Reduction Agency, Fort Belvoir, Virginia, USA (B.N. Adhikari); Biological Defense Research Directorate, Naval Medical Research Command, Fort Detrick, Maryland, USA (B.N. Adhikari, K.A. Long, R.Z. Cer, K.A. Bishop-Lilly); Leidos, Reston, Virginia (K.A. Long); Hospital Regional Docente de Medicina Tropical Julio César Demarini Caro, Chanchamayo, Peru (M. Valerio); Universidad Peruana Cayetano Heredia, Lima (M. Valerio)

DOI: https://doi.org/10.3201/eid2909.230374

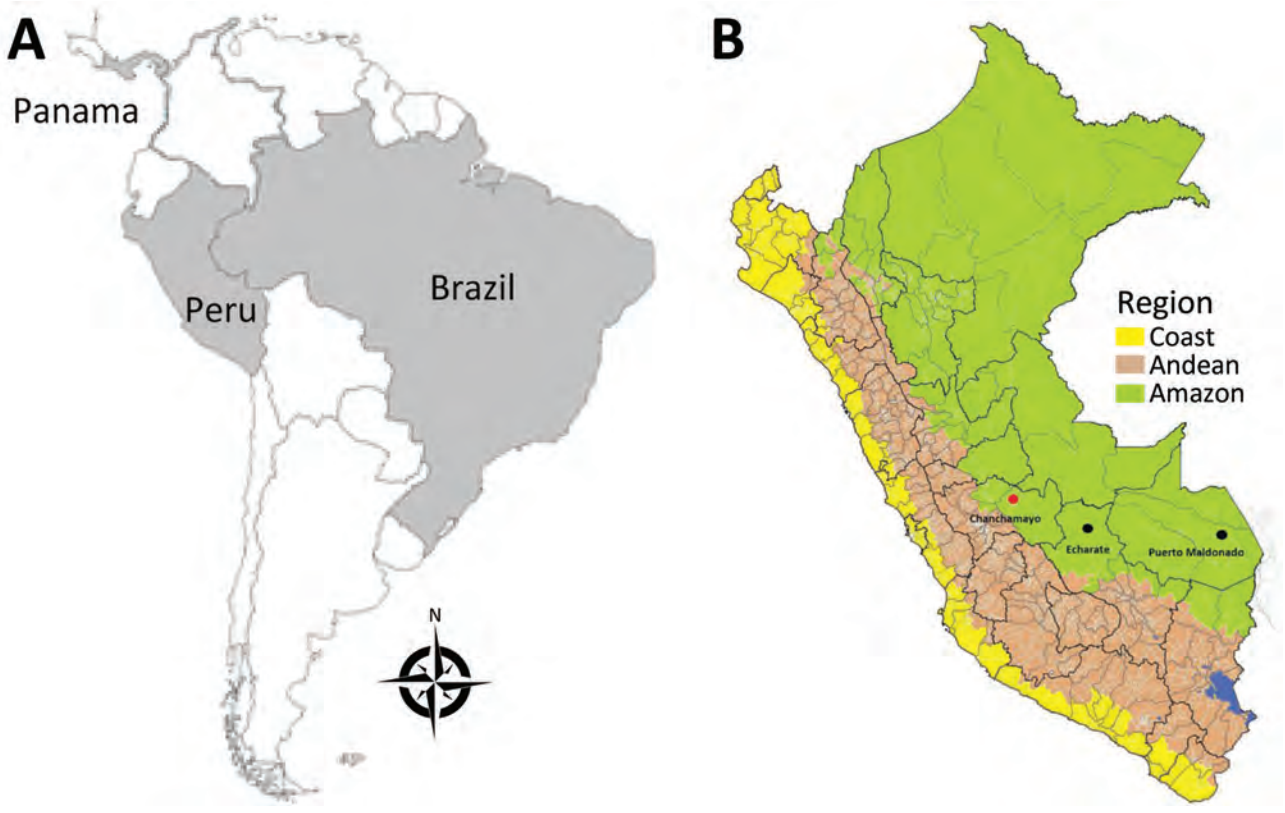

Figure 1. Geographic distribution of Candiru complex virus in Central and South America in study of novel ECHV variant isolated from patient with febrile illness, Chanchamayo, Peru. A) Countries where viruses were identified (shaded in gray). B) Geographic distribution of the Candiru complex viruses in Peru identified from patients with acute febrile illness. Red dot indicates location of the novel ECHV variant: ECHV variant (Chanchamayo–Junín), ECHV (Echarate-Cuzco, 1998); Maldonado virus (Puerto Maldonado–Madre de Dios, 2004); Candiru virus (Puerto Maldonado–Madre de Dios, 2010). ECHV, Echarate virus.

alphaviruses (Mayaro virus and Venezuelan equine encephalitis virus), orthobunyaviruses (Oropouche virus, Guaroa virus, Caraparu virus, and Maguari virus), arenaviruses (Allpahuayo virus and Tacaribe virus), and cardiovirus. Only the Vero cells spot slide was reactive by IFA (≈25% of cells fluoresced) with pooled bunyaviruses polyclonal antibody. The second IFA with individual polyclonal antibody components also detected a weak reaction (≈25% of cells fluoresced) with Oropouche and Maguari polyclonal antibodies. Because of a weak positive signal at this level, we submitted the isolate for molecular characterization.

We extracted RNA from infected Vero cell supernatant by using the QIAamp Viral RNA Mini Kit (QIAGEN, https://www.qiagen.com), according to the manufacturer's instructions. We amplified the viral genome by using 2 unbiased approaches, a modified sequence-independent, single-primer amplification (SISPA) protocol (*9*), and whole-transcriptome amplification (WTA) (*10*) using REPLI-g WTA Single Cell Kit (QIAGEN) according to manufacturer's guidelines. We prepared libraries by using Nextera XT DNA Library Preparation Kit (Illumina, https://www.illumina.com) and sequenced them on the Illumina MiSeq platform by using MiSeq Reagent Kit version 3 (600-cycle) according to the manufacturer's instruction.

We processed raw reads from both sequencing approaches (SISPA and WTA) for quality control, de novo assembly, host read subtraction, taxonomic classification, and gene family analysis by using 3 different bioinformatics pipelines: EDGE Bioinformatics tools (*11*), VirusSeeker (*12*), and MetaDetector (K.A. Bishop-Lilly et al., unpub. data). Both unbiased methods showed similar read quality. Results of taxonomic analysis of the reads and contigs obtained from SISPA and WTA showed Candiru phlebovirus as the unique human viral pathogen in the isolate, indicating that both techniques successfully amplified the isolated virus. We searched consensus sequences (GenBank accession nos. OQ623470–2) against a nucleotide database by using BLASTn and protein database

Table 1. Summary of nucleotide and amino acid similarity for a novel Echarate virus variant isolated from patient with febrile illness, Chanchamayo, Peru*

Segment	% Nucleotide identity; % coverage (accession no.)	% Amino acid identity (accession no.)
Large	83.2; 99 (HM119410.1)	97.01 (AEA30058.1)
Medium	76.5; 97† (HM119411.1)	86.36 (AEA30046.1)
Small	91.32; 100 (HM119412.1)	96.37‡ (AEA30072.1); 100§ (AEA30073.1)

*Accession nos. represent best hits on GenBank.
†Result after a BLASTn (https://blast.ncbi.nlm.nih.gov) search was optimized for more dissimilar sequences (discontiguous megablast).
‡Nonstructural.
§Nucleoprotein.

by using BLASTx (both at https://blast.ncbi.nlm.nih.gov). Candiru phlebovirus large and small segments had >95% amino acid identity compared with those of ECHV. Of note, the medium (M) segment had 76.5% identity with that of ECHV at nucleotide level and 86.36% identity at amino acid level (Table 1). The M segment typically encodes for 3 polypeptides (NSm, Gn, and Gc), which are co-translationally cleaved. The NSm polypeptide is a virulence factor associated with the inhibition of apoptosis in infected cells and plays a role in viral mosquito infection (*13*). The amino acid identity value of the predicted NSm sequence of our isolated virus ranged from <30% with the other members of Candiru complex to 78.6% with ECHV. For average coverage calculation, we mapped the trimmed reads back to contigs obtained from de novo assembly and to the corresponding Echarate reference sequences as an orthogonal verification at 0.8 length fraction and 0.8 similarity fraction. The minimum coverage was 1,583× in the M segment with ECHV and the maximum was 10,224× in the M segment with the obtained contig (Table 2).

We performed pairwise sequence comparison between our isolate and Candiru complex viruses for the RNA-dependent RNA polymerase, glycoprotein precursor, nucleoprotein, and nonstructural genes. The p-distance value of the glycoprotein precursor gene 0.237 (nucleotide) between our isolate and ECHV was similar to those observed among other members of the Candiru complex (Appendix 1 Table, https://wwwnc.cdc.gov/EID/article/29/9/23-0374-App1.xlsx) and consistent with values previously reported in the literature among members of the Candiru complex (0.2–0.46) and among members of the same complex but not among strains of the same virus (0.01–0.12) (*7*,*14*,*15*). Furthermore, considering the new variant was isolated and characterized 21 years later, we also calculated the overall mean distance values (0.079 for nucleotide, 0.039 for amino acid) for 74 complete M segment sequences of Oropouche virus published over time (1955–2021 [67 years]). Those values suggest that the difference could not be explained by virus mutation because the new isolate has a nucleotide difference value of 0.24 with ECHV. The low M segment identity value together with distance values probably indicate the uniqueness of this segment and support the concept that this is a novel ECHV variant that could be generated by a recombinant event between ECHV and an unknown phlebovirus.

To determine the evolutionary relationship of our isolate to other known members of the genus, we conducted maximum-likelihood phylogenetic analyses on the aligned amino acid sequence of the RNA-dependent RNA polymerase, glycoprotein precursor, nucleoprotein, and nonstructural genes (Appendix 2, https://wwwnc.cdc.gov/EID/article/29/9/23-0374-App2.pdf). All the phylogenetic trees placed our isolate among the Candiru virus complex within a well-supported clade with ECHV. However, the NSm or glycoprotein tree clustered the new variant together with ECHV within a well-supported clade separate from other Candiru complex viruses (Figure 2).

Conclusions

Our findings indicate that a novel ECHV variant is circulating in the jungle of central Peru. Because the clinical symptoms of infection with this variant

Table 2. Depth and breadth of coverage based on reads mapped to references for a novel Echarate virus variant isolated from patient with febrile illness, Chanchamayo, Peru*

Segment	Reference	No. mapped reads	Depth coverage	Breadth coverage, %
Large	Contig	111,471	8,163.64×	100
	ECHV (HM119410, 6,411 bp)	201,837	4,777.26×	100
Medium	Contig	164,685	10,224.69×	100
	ECHV (HM119411, 4,287 bp)	24,756	1,583.69×	48
Small	Contig	20,585	6,358×	100
	ECHV (HM119412,1,818 bp)	24,690	3,561.94×	100

*GenBank accession numbers and sequence length for each ECHV segment are in parentheses. ECHV, Echarate virus.

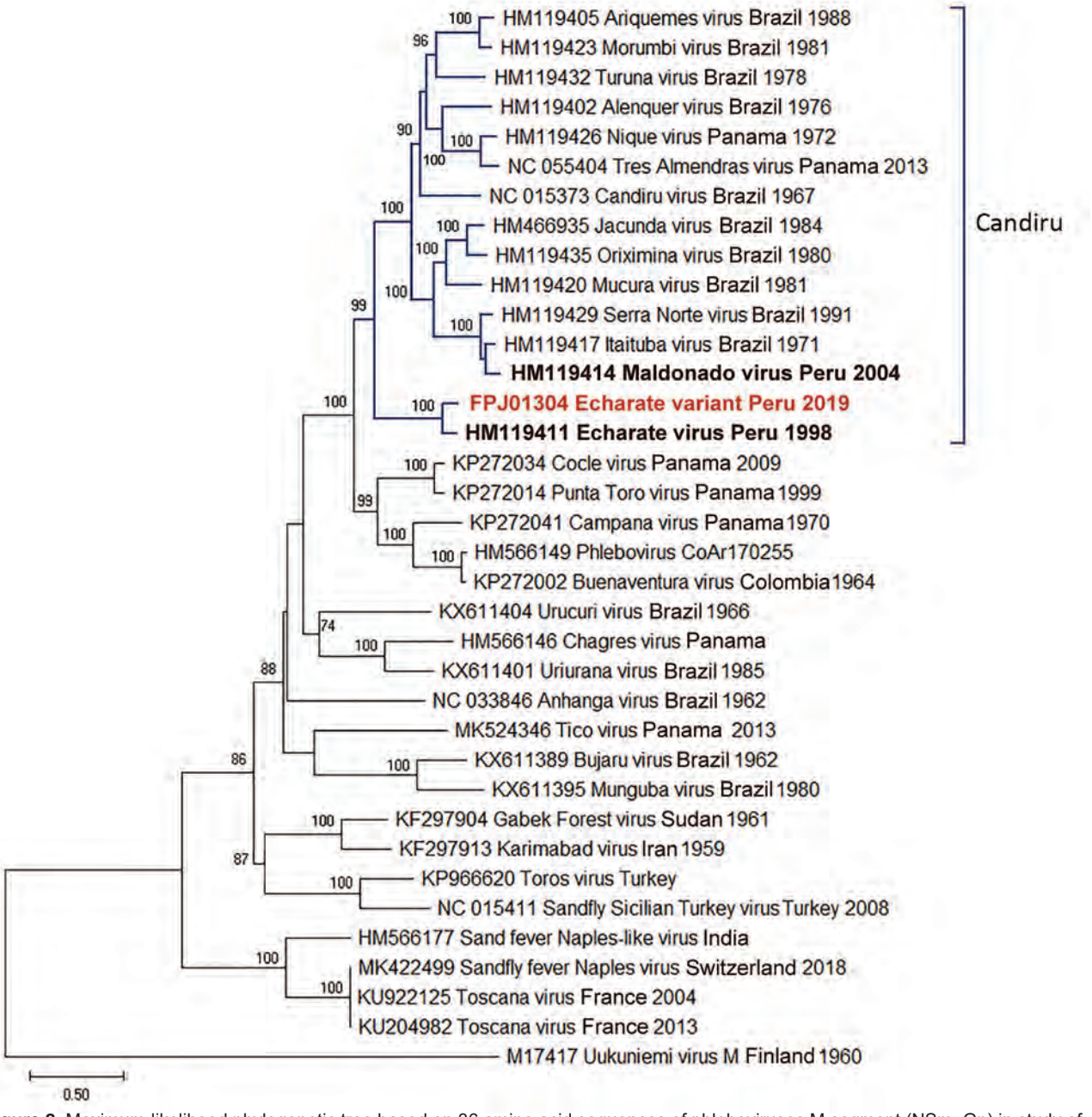

Figure 2. Maximum-likelihood phylogenetic tree based on 36 amino acid sequences of phleboviruses M segment (NSm–Gn) in study of novel Echarate virus variant isolated from patient with febrile illness, Chanchamayo, Peru. Strains from Peru are in bold, and the novel variant is in red. Only bootstrap values >70% are shown at key nodes. Uukuniemi virus was considered as the outgroup. Scale bar indicates nucleotide substitutions per site.

are also characteristic of dengue, malaria, and other tropical infectious diseases common in this region (*4*,*5*) continued AFI biosurveillance is needed to detect novel and emerging pathogens to protect the health of the population and US service members deployed in affected areas in Peru. Ecologic studies are necessary to determine how widespread the new variant is within this region, to identify potential vectors and reservoirs involved in its transmission, and to support decision-making for keeping service members medically prepared and protected from health and safety threats both on and off duty.

Acknowledgments

We thank the local Ministry of Health authorities in Peru, Red de Salud Chanchamayo, and Hospital Docente de

Medicina Tropical Julio César Demarini Caro for their support to allow us to execute this study. We thank Patricia Aguilar for reviewing the manuscript.

This study was funded by the Armed Forces Health Surveillance Division, Global Emerging Infections Surveillance Branch, Proposal Management Information System identification nos. P0143_19_N6_01.01, P_0149_19_AH_02_NMRC and P0013_20_AH_01.01 and Navy work unit no. A1417.

About the Author

Ms. Troncos is a research technician in the Virology and Emerging Infections Department of US Naval Medical Research Unit SOUTH, Lima, Peru. Her primary research interests include identification and characterization of viruses that cause illnesses in humans.

References

1. Abudurexiti A, Adkins S, Alioto D, Alkhovsky SV, Avšič-Županc T, Ballinger MJ, et al. Taxonomy of the order *Bunyavirales*: update 2019. Arch Virol. 2019;164:1949–65. https://doi.org/10.1007/s00705-019-04253-6
2. de Carvalho MS, de Lara Pinto AZ, Pinheiro A, Rodrigues JSV, Melo FL, da Silva LA, et al. Viola phlebovirus is a novel Phlebotomus fever serogroup member identified in *Lutzomyia (Lutzomyia) longipalpis* from Brazilian Pantanal. Parasit Vectors. 2018;11:405. https://doi.org/10.1186/s13071-018-2985-3
3. Elliott RM, Brennan B. Emerging phleboviruses. Curr Opin Virol. 2014;5:50–7. https://doi.org/10.1016/j.coviro.2014.01.011
4. Gundacker ND, Carrera JP, Castillo M, Díaz Y, Valenzuela J, Tamhane A, et al. Clinical manifestations of Punta Toro virus species complex infections, Panama, 2009. Emerg Infect Dis. 2017;23:872–4. https://doi.org/10.3201/eid2305.161925
5. Palacios G, Wiley MR, Travassos da Rosa APA, Guzman H, Quiroz E, Savji N, et al. Characterization of the Punta Toro species complex (genus *Phlebovirus*, family *Bunyaviridae*). J Gen Virol. 2015;96:2079–85. https://doi.org/10.1099/vir.0.000170
6. Baldelli F, Ciufolini MG, Francisci D, Marchi A, Venturi G, Fiorentini C, et al. Unusual presentation of life-threatening Toscana virus meningoencephalitis. Clin Infect Dis. 2004;38:515–20. https://doi.org/10.1086/381201
7. Palacios G, Tesh R, Travassos da Rosa A, Savji N, Sze W, Jain K, et al. Characterization of the Candiru antigenic complex (*Bunyaviridae*: *Phlebovirus*), a highly diverse and reassorting group of viruses affecting humans in tropical America. J Virol. 2011;85:3811–20. https://doi.org/10.1128/JVI.02275-10
8. Forshey BM, Guevara C, Laguna-Torres VA, Cespedes M, Vargas J, Gianella A, et al.; NMRCD Febrile Surveillance Working Group. Arboviral etiologies of acute febrile illnesses in western South America, 2000–2007. PLoS Negl Trop Dis. 2010;4:e787. https://doi.org/10.1371/journal.pntd.0000787
9. Djikeng A, Halpin R, Kuzmickas R, Depasse J, Feldblyum J, Sengamalay N, et al. Viral genome sequencing by random priming methods. BMC Genomics. 2008;9:5. https://doi.org/10.1186/1471-2164-9-5
10. Jiang H, Xing Z, Liu X, Chai Q, Xin Z, Zhu C, et al. Comparison and development of a metagenomic next-generation sequencing protocol for combined detection of DNA and RNA pathogens in cerebrospinal fluid. BMC Infect Dis. 2022;22:326. https://doi.org/10.1186/s12879-022-07272-y
11. Li PE, Lo CC, Anderson JJ, Davenport KW, Bishop-Lilly KA, Xu Y, et al. Enabling the democratization of the genomics revolution with a fully integrated web-based bioinformatics platform. Nucleic Acids Res. 2017;45:67–80. https://doi.org/10.1093/nar/gkw1027
12. Zhao G, Wu G, Lim ES, Droit L, Krishnamurthy S, Barouch DH, et al. VirusSeeker, a computational pipeline for virus discovery and virome composition analysis. Virology. 2017;503:21–30. https://doi.org/10.1016/j.virol.2017.01.005
13. Eifan S, Schnettler E, Dietrich I, Kohl A, Blomström AL. Non-structural proteins of arthropod-borne bunyaviruses: roles and functions. Viruses. 2013;5:2447–68. https://doi.org/10.3390/v5102447
14. Collao X, Palacios G, de Ory F, Sanbonmatsu S, Pérez-Ruiz M, Navarro JM, et al. Granada virus: a natural phlebovirus reassortant of the sandfly fever Naples serocomplex with low seroprevalence in humans. Am J Trop Med Hyg. 2010;83:760–5. https://doi.org/10.4269/ajtmh.2010.09-0697
15. Amaro F, Hanke D, Zé-Zé L, Alves MJ, Becker SC, Höper D. Genetic characterization of Arrabida virus, a novel phlebovirus isolated in South Portugal. Virus Res. 2016;214:19–25. https://doi.org/10.1016/j.virusres.2016.01.004

Address for correspondence: Gilda Troncos, US Naval Medical Research Unit SOUTH, 3230 Lima Pl, Washington, DC 20521-3230, USA; email: gilda.troncos.ln@health.mil

High Prevalence of *Candida auris* Colonization during Protracted Neonatal Unit Outbreak, South Africa

Liliwe Shuping, Tsidiso G. Maphanga, Serisha D. Naicker, Ruth Mpembe, Nqobile Ngoma, Sithembiso Velaphi, Firdose Nakwa, Jeannette Wadula, Prenika Jaglal, Nelesh P. Govender

One third of patients were colonized by *Candida auris* during a point-prevalence survey in a neonatal unit during an outbreak in South Africa. The sensitivity of a direct PCR for rapid colonization detection was 44% compared with culture. The infection incidence rate decreased by 85% after the survey and implementation of isolation/cohorting.

Candida auris has been recognized as a critical priority pathogen globally, causing invasive infections and persistent outbreaks in healthcare facilities (*1*). In June 2019, an outbreak dominated by *C. auris* clade III occurred in a 185-bed neonatal unit of a national central hospital located in Gauteng Province, South Africa. To contain the outbreak, multiple infection prevention and control (IPC) measures were implemented (Appendix, https://wwwnc.cdc.gov/EID/article/29/9/23-0393-App1.pdf), including colonization screening for contact patients housed in the same cubicle as babies who had positive cultures. Despite those measures, sustained control was not achieved, similar to the case for other prolonged outbreaks (*2*,*3*). Although small section-wide colonization point-prevalence surveys (PPS) were conducted earlier for control (Figure 1), a comprehensive unit-wide PPS was never undertaken. We describe a unit-wide PPS conducted before the neonatal unit was relocated to a new facility as part of a longstanding renovation plan.

Author affiliations: National Institute for Communicable Diseases, Johannesburg, South Africa (L. Shuping, T.G. Maphanga, S.D. Naicker, R. Mpembe, N. Ngoma, N.P. Govender); Chris Hani Baragwanath Academic Hospital, Johannesburg (S. Velaphi, F. Nakwa); University of the Witwatersrand, Johannesburg (S. Velaphi, F. Nakwa, J. Wadula, P. Jaglal, N.P. Govender); National Health Laboratory Service, Johannesburg (J. Wadula, P. Jaglal); University of Cape Town, Cape Town, South Africa (N.P. Govender); St. George's University of London, London, UK (N.P. Govender); University of Exeter, Devon, UK (N.P. Govender)

DOI: https://doi.org/10.3201/eid2909.230393

The Study

Institutional ethics approval for public health surveillance and outbreak investigations was granted by the University of the Witwatersrand HREC (Medical) (M210752). Permission to conduct the survey was granted by the hospital's Medical Advisory Committee, Chief Executive Officer, and the Paediatric Department management.

The aim of the PPS was to reduce *C. auris* transmission in the new facility. The PPS was conducted on November 2, 2021 (3 days before the relocation), to establish colonization status and implement cohorting/isolation for affected infants. We used a direct reverse transcription PCR (RT-PCR)–based method for rapid detection and compared this to culture as the reference standard. We collected composite skin swab specimens from the axilla and groin (*4*) and used selective and enrichment methods to isolate *C. auris* in culture (Appendix). We used the one-step SYBR PrimeScript RT-PCR Kit II (TaKaRa Bio, Inc., https://www.takarabio.com), according to Sexton et al. (*5*).

We swabbed 195 infants; RT-PCR results for 55 (93%) of 59 infants admitted to the neonatal intensive care unit and transitional care unit were available within 24 hours of specimen collection. Samples from those sections were prioritized because of high previous number of infections (Appendix Figure 1). Processing of the remaining swab samples was completed within 48 hours. The prevalence of *C. auris* colonization by RT-PCR was 15% (29/195) (Table 1). All culture results were available within 17 days after

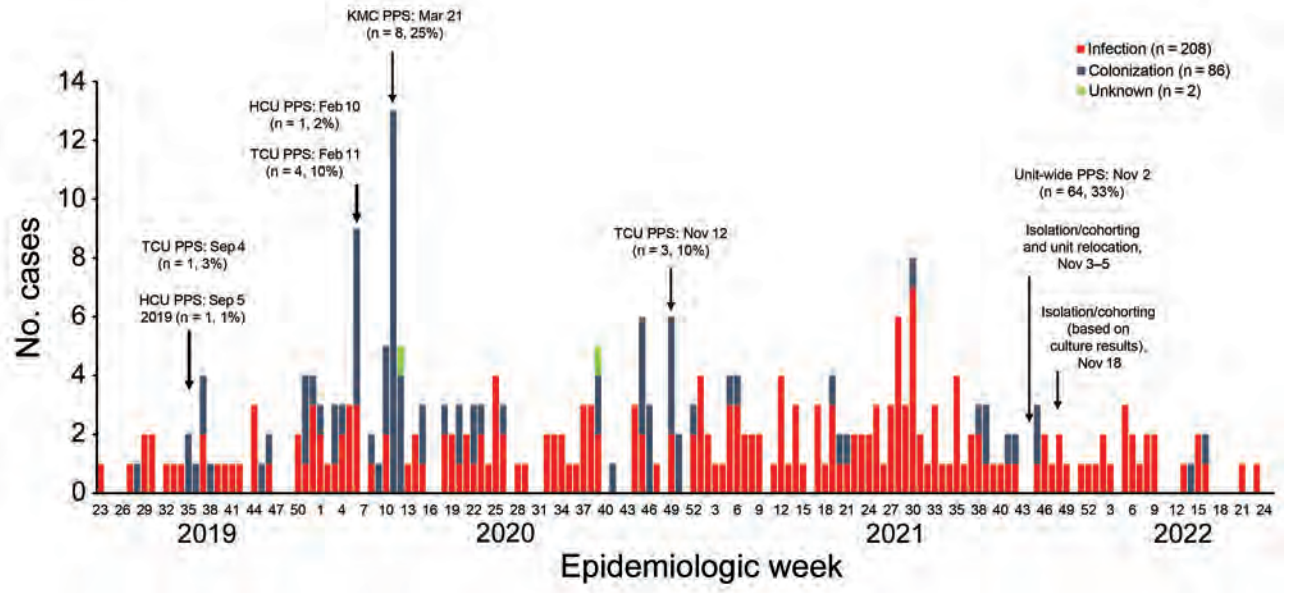

Figure 1. Timeline of culture-confirmed *Candida auris* infection and colonization in neonatal unit, Chris Hani Baragwanath Academic Hospital, Johannesburg, South Africa, June 1, 2019–June 24, 2022. HCU, high care unit; KMC, kangaroo mother and child care; PPS, point-prevalence survey; TCU, transitional care unit.

specimen collection because of multiple processing steps (Appendix Figure 2). With culture, the prevalence of *C. auris* was 32% (63/195). The overall prevalence was 33% (64/195). The sensitivity of the RT-PCR compared with culture was 44% (95% CI, 32%–58%). The sensitivity was highest in the high-care surgical unit and the neonatal intensive care unit, where the prevalence of colonization was highest on the day of the unit-wide PPS (Table 2).

All infants who were colonized with *C. auris* were immediately placed in isolation/cohorted in a separate section with contact precautions after either a positive PCR result or culture result. Infants who were positive for *C. auris* based on PPS results or who had a previous culture-positive diagnostic specimen for *C. auris* were not transferred to the new facility. Instead, they remained in the isolation/cohorting section of the old neonatal unit until discharge. Because swab specimen culture results were still unknown on the relocation day, admitted PCR-negative and subsequently admitted infants were housed in separate wings in the new unit. Apart from that measure and the allocation of dirty and clean equipment areas, IPC practices in the new unit remained largely unchanged.

Using archived laboratory data, we analyzed incidence rates of *C. auris* infection (isolation from normally sterile specimens) or colonization (isolation from nonsterile specimens) in the unit before the PPS (January 1, 2019–November 2, 2021) and after the PPS and relocation (November 3, 2021–June 24, 2022) (Figure 2). Before the PPS, 167 new cases of *C. auris* infection were diagnosed, an incidence rate of 1.3 cases/1,000 patient-days. After the survey, 27 new cases of infection were diagnosed, an 85% decrease in the infection incidence rate to 0.2 cases/1,000 patient-days after PPS. The incidence rate of *C. auris* colonization was 0.6 cases/1,000 patient-days (n = 82) before the PPS and 0.1 cases/1,000 patient-days after (n = 4).

Table 1. Prevalence of *Candida auris* colonization by direct SYBR PrimeScript RT-PCR and selective/enrichment culture with MALDI-TOF mass spectrometry identification in neonatal unit of Chris Hani Baragwanath Academic Hospital, Johannesburg, South Africa, November 2, 2021*

Neonatal unit	No. swabbed	Prevalence by RT-PCR	Prevalence by culture	Overall prevalence
Intensive care	12	6 (50)	10 (83)	10 (83)
Transitional care	46	8 (17)	14 (30)	14 (30)
High care surgical	10	5 (50)	6 (60)	7 (70)
High care	97	7 (7)	27 (28)	27 (28)
Kangaroo mother and child care	30	3 (10)	6 (20)	6 (20)
Total	195	29 (15)†	63 (32)	64 (33)

*Values are no. (%) except as indicated. MALDI-TOF, matrix-assisted laser desorption/ionization time-of-flight; RT-PCR, reverse transcription PCR.
†One infant had insufficient sample for PCR; however, this infant was included in the denominator when calculating prevalence.

Table 2. Diagnostic accuracy measures for a direct SYBR PrimeScript RT-PCR compared with culture (standard) during a *Candida auris* colonization survey in neonatal unit of Chris Hani Baragwanath Academic Hospital, Johannesburg, South Africa, November 2, 2021*

Neonatal unit	Sensitivity	Specificity	Positive predictive value	Negative predictive value	Diagnostic accuracy
Intensive care	60 (26–88)	100 (16–100)	100 (54–100)	33 (4.0–78)	67 (35–90)
Transitional care	57 (29–82)	100 (89–100)	100 (63–100)	84 (69–94)	87 (74–95)
High care surgical	67 (22–96)	75 (19–99)	80 (28–9)	60 (15–95)	70 (35–93)
High care	26 (11–46)	100 (95–100)	100 (59–93)	78 (67–86)	79 (70–87)
Kangaroo mother and child care	50 (12–88)	100 (86–100)	100 (29–100)	89 (71–98)	90 (73–98)
Overall	44 (32–58)	99 (96–100)	97 (82–100)	79 (72–85)	81 (74–85)

*Values in parentheses are 95% CIs. One patient had a positive RT-PCR result but a negative culture. A heavy growth of *Staphylococcus aureus* from this patient's sample could have overgrown *C. auris*. RT-PCR, reverse transcription PCR.

Conclusions

Compared with previous limited surveys in the unit, we determined a high prevalence of *C. auris* colonization during the unit-wide PPS, probably a major factor in ongoing transmission within the neonatal unit (*6*,*7*). Screening of direct contacts and surveys limited to specific sections of the unit probably missed colonized patients in other areas, and our results emphasize the need for routine unit-wide surveys, which are more effective in detecting the true extent of colonization during protracted *C. auris* outbreaks.

In the months after the unitwide PPS, infection and colonization incidence decreased. However, infections and colonization (albeit to a lesser extent) continued to occur. Assuming that skin colonization always precedes invasive infection, the continued occurrence of *C. auris* infections suggests the PPS was only partially successful at control. Culture-based methods used for identification delayed implementation of contact precautions because of a long turnaround time. The RT-PCR intended for rapid identification of colonization had a lower sensitivity than the >90% reported previously (*5*). The low observed sensitivity was possibly caused by low fungal load in the swab specimens, supported by a longer time-to-culture-positivity for PCR-negative/culture-positive swab specimens than for PCR-positive/culture-positive swab specimens (Appendix Table 1). In addition, a higher fungal burden on patient skin in high-prevalence neonatal unit sections might have improved detection (*7*). Nonetheless, we could not exclude PCR inhibitors as a reason for low sensitivity because our assay lacked an internal control.

Despite the limitations of our case detection methods during the PPS, the substantial decrease in infection incidence strongly suggests that the PPS and related IPC measures played a crucial role in control. Although colonization incidence also decreased after the PPS, we are uncertain whether that was a real decrease. The incidence in the period before the PPS included colonized patients identified during limited surveys, resulting in more colonization cases potentially being detected in that period compared with the post-PPS period.

Undetected colonization and persisting IPC challenges, such as staff shortages and bed occupancy

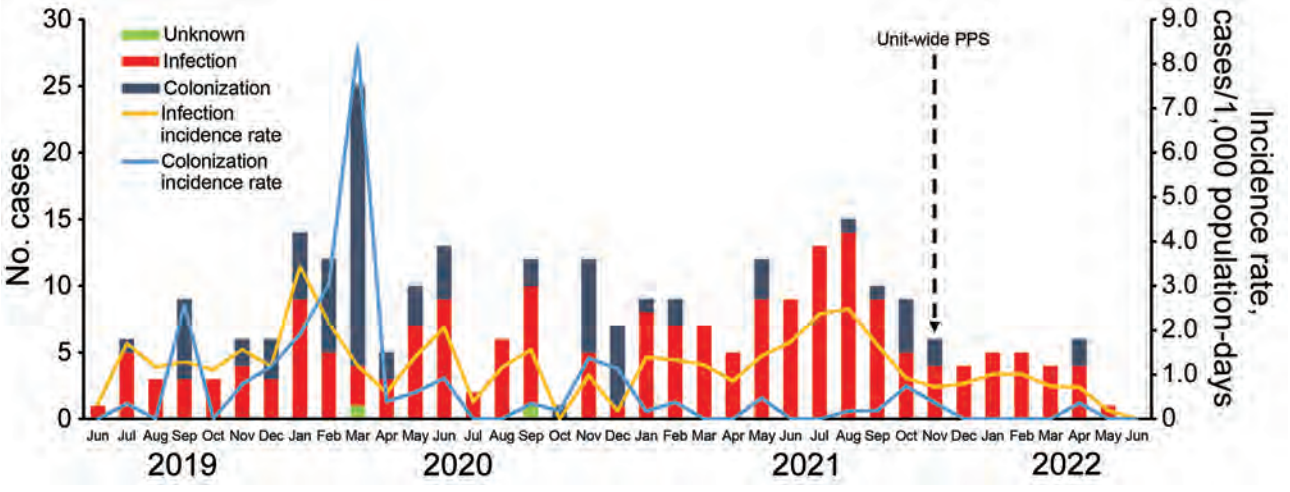

Figure 2. Timeline of new cases and incidence rate of culture-confirmed *Candida auris* infection (n = 194) and colonization (n = 86) in neonatal unit, Chris Hani Baragwanath Academic Hospital, Johannesburg, South Africa, June 1, 2019–June 24, 2022. PPS, point-prevalence survey.

in excess of capacity, all probably contributed to the continued transmission within the unit. Topical chlorhexidine gluconate or terbinafine could lead to skin decolonization (*8*,*9*). However, determining the optimal skin concentration, required contact time, and number of applications for sustained *C. auris* clearance and ensuring safety in neonatal populations remain unresolved (*10*). A comprehensive bundle of IPC measures, which includes routine PPS to assess skin colonization, preferably using a more sensitive PCR method (such as TaqMan chemistry) (*7*,*11*), along regular audits of adherence to contact precautions, surgical aseptic technique, device care protocols, and periodic environmental sampling to guide cleaning and decontamination efforts, should be implemented. This system could be challenging and costly to maintain in a large unit; however, these measures are crucial for control. In conclusion, regular PPS should be conducted in neonatal units experiencing ongoing *C. auris* outbreaks to identify colonized persons and implement IPC precautions to prevent spread.

Acknowledgments

We thank Inge Kleinhans, Husna Ismail, Amanda Shilubane, Silondiwe Nzimande, Dikeledi Kekana, and Siphiwe Kutta for providing support during the PPS; the neonatal unit nursing staff for helping to plan the survey; and the National Institute for Communicable Diseases Surveillance Information Management Unit for providing surveillance data throughout the outbreak investigation.

This work was supported by the National Institute for Communicable Diseases. a division of the National Health Laboratory Service.

About the Author

Ms. Shuping is an epidemiologist at the Centre for Healthcare-Associated Infections, Antimicrobial Resistance and Mycoses at the National Institute for Communicable Diseases, Johannesburg, South Africa. Her primary research interests are neonatal infection epidemiology, antimicrobial resistance, and infection prevention and control.

References

1. World Health Organization. WHO fungal priority pathogens list to guide research, development and public health action. Oct 25, 2022 [cited 2023 Jul 10]. https://www.who.int/publications/i/item/9789240060241
2. Ruiz-Gaitán A, Moret AM, Tasias-Pitarch M, Aleixandre-López AI, Martínez-Morel H, Calabuig E, et al. An outbreak due to *Candida auris* with prolonged colonisation and candidaemia in a tertiary care European hospital. Mycoses. 2018;61:498–505. https://doi.org/10.1111/myc.12781
3. Eyre DW, Sheppard AE, Madder H, Moir I, Moroney R, Quan TP, et al. A *Candida auris* outbreak and its control in an intensive care setting. N Engl J Med. 2018;379:1322–31. https://doi.org/10.1056/NEJMoa1714373
4. Center for Disease Control and Prevention. Screening for *Candida auris* colonization [cited 2022 Jun 8]. https://www.cdc.gov/fungal/candida-auris/c-auris-screening.html
5. Sexton DJ, Kordalewska M, Bentz ML, Welsh RM, Perlin DS, Litvintseva AP. Direct detection of emergent fungal pathogen *Candida auris* in clinical skin swabs by SYBR green-based quantitative PCR assay. J Clin Microbiol. 2018;56:1–6. https://doi.org/10.1128/JCM.01337-18
6. Moema I, Ismail H, van Schalkwyk E, Shuping L, Govender N. Outbreak of culture-confirmed *Candida auris* bloodstream infection in the neonatal unit of a public-sector hospital, South Africa, July through September 2017. FEAD: the Field Epidemiology Abstract Database. 2017 [cited 2022 Jun 25]. https://www.tephinet.org/learning/fead/outbreak-of-culture-confirmed-candida-auris-bloodstream-infection-in-the-neonatal-unit
7. Sexton DJ, Bentz ML, Welsh RM, Derado G, Furin W, Rose LJ, et al. Positive correlation between *Candida auris* skin-colonization burden and environmental contamination at a ventilator-capable skilled nursing facility in Chicago. Clin Infect Dis. 2021;73:1142–8. https://doi.org/10.1093/cid/ciab327
8. Huang X, Hurabielle C, Drummond RA, Bouladoux N, Desai JV, Sim CK, et al. Murine model of colonization with fungal pathogen *Candida auris* to explore skin tropism, host risk factors and therapeutic strategies. Cell Host Microbe. 2021;29:210–221.e6. https://doi.org/10.1016/j.chom.2020.12.002
9. Ghannoum M, Herrada J, McCormick TS, Long L. A novel transdermal application for clearing skin colonization by *Candida auris*. Antimicrob Agents Chemother. 2023;95:1–6. https://doi.org/10.1128/AAC.02303-20
10. Proctor DM, Dangana T, Sexton DJ, Fukuda C, Yelin RD, Stanley M, et al.; NISC Comparative Sequencing Program. Integrated genomic, epidemiologic investigation of *Candida auris* skin colonization in a skilled nursing facility. Nat Med. 2021;27:1401–9. https://doi.org/10.1038/s41591-021-01383-w
11. Ahmad A, Spencer JE, Lockhart SR, Singleton S, Petway DJ, Bagarozzi DA Jr, et al. A high-throughput and rapid method for accurate identification of emerging multidrug-resistant *Candida auris*. Mycoses. 2019;62:513–8. https://doi.org/10.1111/myc.12907

Address for correspondence: Liliwe Shuping, Centre for Healthcare-Associated Infections, Antimicrobial Resistance and Mycoses, National Institute for Communicable Diseases, National Health Laboratory Service, 1 Modderfontein Rd, Sandringham, Johannesburg, 2131, South Africa; email: liliwes@nicd.ac.za

Fatal Necrotizing Enterocolitis in Neonate Caused by *Cronobacter sakazakii* Sequence Type 64 Strain of CRISPR Sublineage b

Haiyan Zeng,[1] Chengsi Li,[1] Jumei Zhang, Bingshao Liang, Hanjie Mei, Qingping Wu

We report fatal neonatal necrotizing enterocolitis in China caused by *Cronobacter sakazakii* capsular profile K1:CA1, sequence type 64, and CRISPR type 197. Phylodynamic analyses indicated that the strain originated from the ancient, widespread, and antimicrobial drug–sensitive CRISPR sublineage b. Enhanced surveillance and pathogenesis research on this organism are required.

Cronobacter sakazakii is a major foodborne pathogen that is associated with outbreaks of life-threatening necrotizing enterocolitis, meningitis, and sepsis in neonates and infants. Although the incidence of this pathogen is low, the case-fatality rate is high in premature and immunocompromised infants (*1*,*2*). Multilocus sequence typing (MLST) is a powerful tool for effectively identifying and discriminating different *Cronobacter* strains. Specific sequence types (STs) and clonal complexes are closely related to infections (*3*).

Compared with MLST, CRISPR (clustered regularly interspaced short palindromic repeats) typing is superior for distinguishing similar strains (*4*). *C. sakazakii* ST64, the major ST in food samples, was further divided into 2 sublineages based on CRISPR diversity (*5*). We report a *C. sakazakii* ST64 strain that caused necrotizing enterocolitis in a neonate in China and further examine its origin and phylogenetic relationship with ST64 strains based on CRISPR diversity and whole-genome single-nucleotide polymorphism (wgSNP).

Author affiliations: Guangdong University of Technology, Guangzhou, China (H. Zeng); Institute of Microbiology, Guangzhou (H. Zeng, C. Li, J. Zhang, Q. Wu); Guangzhou Women and Children's Medical Center, Guangzhou (B. Liang)

DOI: https://doi.org/10.3201/eid2909.230537

The Study

This study was approved by the Ethics Committee of Guangzhou Women and Children's Medical Center (Guangzhou, China; no. 2016081029). Experiments were performed at the Institute of Microbiology, Guangdong Academy of Sciences, and analyses and manuscript preparation were completed at Guangdong University of Technology.

On April 28, 2019, a 17-day-old male neonate born with severe congenital heart disease and perioral cyanosis for 2 hours was hospitalized in a children's hospital in Guangzhou, China. The patient had necrotizing enterocolitis symptoms develop on May 6 and was given meropenem and metronidazole as antiinfection therapy. However, his symptoms did not improve, and intestinal perforation and peripheral hydrocephalus developed a few days later. Despite the efforts of the doctor, the patient died.

We identified a *Cronobacter* species isolated from ascites by using an automated VITEK 2 Compact system (bioMérieux, https://www.biomerieux.com). An isolate, GZfs, was identified as *C. sakazakii* ST64 of serotype O2. This ST has not previously been reported to cause neonatal necrotizing enterocolitis (*6*). *C. sakazakii* GZfs were susceptible to almost all antimicrobial drugs tested, except cephalothin (Appendix Table, https://wwwnc.cdc.gov/EID/article/29/9/23-0537-App1.pdf). We sequenced genomic and plasmid DNA by using the PacBio RS II (Pacific Biosciences, https://www.pacb.com) and HiSeq (Illumina, https://www.illumina.com) platforms, assembled, and annotated as described (*1*,*7*). *C. sakazakii* GZfs had a single circular chromosome, 4.2 Mb, 57.11% GC content, and 2 plasmids (denoted as pFS1, 115,925

[1]These authors contributed equally to this article.

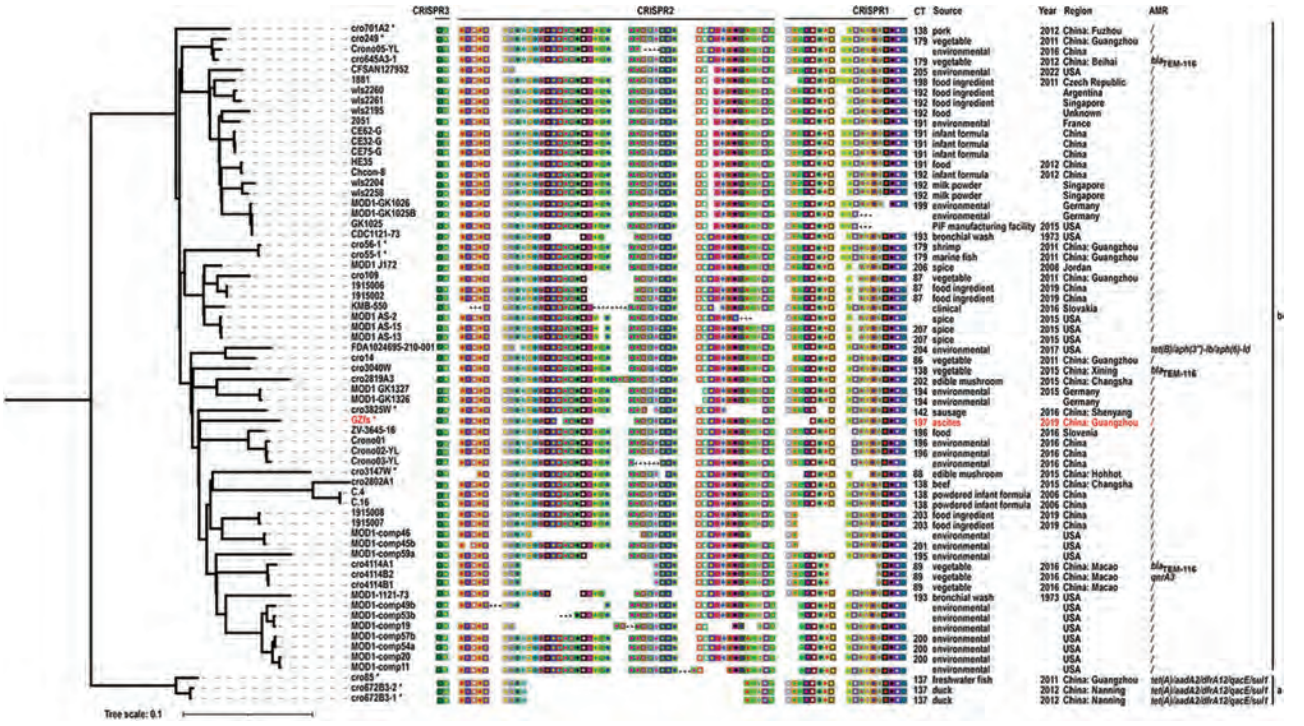

Figure 1. Multilocus sequence typing phylogenetic tree based on whole-genome sequencing single-nucleotide polymorphisms of a Cronobacter sakazakii ST64 strain from a fatal case of necrotizing enterocolitis in a 17-day-old male neonate, China, compared with reference strains. Asterisks indicate newly sequenced strains in this study; red text indicates isolate from the neonate. CRISPR spacers arrangement, CT, source, year, region and genes are listed next to corresponding strains. Color schemes in CRISPR arrays are provided at the spacer level to illustrate differences among strains by using CRISPRStudio software (https://www.semanticscholar.org). Ellipsis in spacers indicate partial CRISPR arrays without determined end (incomplete CRISPR arrays). Scale bar indicates nucleotide substitutions per site. AMR, antimicrobial resistance; CR, CRISPR type; CRISPR, clustered regularly interspaced short palindromic repeats; ST, sequence type.

bp, 57.09% GC; and pFS2, 110,391 bp, 50.10% GC) (GenBank accession nos. CP123201–3).

In our previous study, we divided *C. sakazakii* ST64 strains into 2 CRISPR sublineages, a and b, and compared antimicrobial drug resistance profile strains in sublineage a with strains in sublineage b (*5*). To explore the origin of this pathogenic strain and its phylogenetic relationship with other *C. sakazakii* ST64 strains, we performed whole-genome sequencing of 9 ST64 strains (GenBank accession nos. JARUQD000000000–L000000000) and downloaded all ST64 strains with whole-genome sequences from the *Cronobacter* PubMLST database (https://pubmlst.org/organisms/cronobacter-spp) and GenBank genome databases. We provide antimicrobial drug resistance results of 14 food-source ST64 strains (Appendix Table).

After deleting all poor-quality sequences and duplicate strains, we used 66 whole-genome sequences for further analyses. We extracted CRISPR arrays and spacers from those sequences and assigned CRISPR type (CT) numbers to 55 strains with intact CRISPR arrays, according to methods from our previous study (*4*). All ST64 strains had the same 2 spacers: CRISPR3, which was not detected in our previous study because of the lack of *cas* genes (*7*), and CRISPR3, which was not useful for CT in this ST. There were 25 CTs, including 17 new, and we identified *C. sakazakii* GZfs as a new type of CT197 (Appendix). Based on spacer composition, GZfs belonged to CRISPR sublineage b. However, no other strain was found to have an identical spacer profile.

We calculated the wgSNP of ST64 strains by using Harvest software (*8*) and extracted those strains by using SNP-sites software (*9*). We constructed a maximum-likelihood phylogenetic tree by using FastTree software (*10*) and edited in iTOL (*11*). We used a Bayesian phylogenetic approach to estimate the nucleotide substitution rates and divergence times of *C. sakazakii* ST64 according to a previous study (*7*). The maximum-likelihood tree based on the wgSNPs of ST64 strains also showed 2 distinct phylogenetic clusters in accordance with the CRISPR sublineages (Figure 1). The strains in sublineage a were all from food sources.

Sublineage b contained more strains and diverse sources. Moreover, *C. sakazakii* GZfs and all clinical source strains (*C. sakazakii* KMB-550, MOD1-1121-73, and CDC1121-73) in public databases belonged to this cluster. *C. sakazakii* MOD1-1121-73 and CDC1121-73 were isolated from bronchial washes; there was no other patient or disease information regarding those clinical strains.

The genome-wide substitution rate of *C. sakazakii* ST64 was estimated to be 2.3×10^{6} substitutions/site/year (95% CI 1.0×10^{7}–5.3×10^{6} substitutions/site/year). According to the maximum clade credibility (MCC) tree (Figure 2), the likely most recent common ancestor of CRISPR sublineage b was 47,500 (95% CI 11,600–300,700) years ago, earlier than for sublineage a, which was 10,900 (95% CI 1,300–11,600) years ago. *C. sakazakii* GZfs had a relatively close phylogenetic relationship with the food-source *C. sakazakii* strain ZV-3645-16 in Slovenia; environmental strains *C. sakazakii* Crono01, Crono02-YL, and Crono03-YL; and the food-source strain *C. sakazakii* cro3825W in China (Figures 1, 2). This finding indicates a close environment food-clinic relationship in dissemination.

We identified acquired drug resistance genes by using ResFinder 2.1. (https://cge.cbs.dtu.dk/services/ResFinder-2.1). All 3 strains in sublineage a acquired the antimicrobial resistance (AMR) genes *tet(A)/aadA2/dfrA12/qacE/sul1*, in accordance with their resistance to tetracycline and trimethoprim/sulfamethoxazole (Figure 1; Appendix Table). Five strains in sublineage b had AMR genes; 3 strains (*C. sakazakii* cro645A3-1, cro3040W, cro4114A1) and 1 strain (*C. sakazakii* cro4114B2) isolated from vegetables harbored the AMR genes $bla_{\text{TEM-116}}$ and *qnrA3*. Four strains were susceptible to all tested antimicrobial drugs (Appendix Table). One environmental strain, *C. sakazakii* FDA1024695-210-001, had *tet(B)/aph(3'')-Ib/aph(6)-Id* genes. A total of 92.1% (58/63) strains in sublineage b lacked AMR genes. All 4 clinical strains, including *C. sakazakii* GZfs, did not have AMR genes. In a previous study, *C. sakazakii* ST494 strain was sensitive to all antimicrobial drugs used for treatment; however, the patient died (*12*). Those results suggested that AMR might not be the major reason for the high case-fatality rate associated with this pathogenic infection. Both *C. sakazakii* ST494 and ST64 did not belong to the common pathogenic clonal complex. Enhanced surveillance and pathogenesis research of this organism are warranted.

The virulence genes in *C. sakazakii* remain unclear (*13*), and 2 T6SS and 1 prophage on the chromosome of GZfs might contribute to pathogenicity. The capsular profile of the GZfs was determined to be K1:CA1, as in our previous study (*1*), and plasmid pFS1 was closely related to the IncFIB-type virulence plasmid pESA3 identified in pathogenic *C. sakazakii* strains and pGW2 in *C. sakazakii* GZcsf-1, which causes

Figure 2. Timed phylogeny in maximum clade credibility tree of *Cronobacter sakazakii* ST64 strain from a fatal case of necrotizing enterocolitis in a 17-day-old male neonate, China, compared with reference strains. Red text indicates isolate from the neonate. Numbers along branches are bootstrap values. Posterior probabilities are shown in the nodes. ST, sequence type.

meningitis in neonates (*1*,*14*). More attention should be given to the study of virulence and pathogenesis.

Conclusions

We report 1 *C. sakazakii* ST64 strain, GZfs, causing fatal neonatal necrotizing enterocolitis in China that did not belong to the previously identified common pathogenic clonal complexes or STs (*3*). It belongs to the ancient, widespread, and antimicrobial drug–sensitive CRISPR cluster b of ST64. AMR might not be the major reason for the high case-fatality rate for this pathogen. Public health would benefit from identification of virulence genes and pathogenic mechanisms of *C. sakazakii*.

Acknowledgment

We thank Editage (https://www.editage.cn) for English language editing.

This study was supported by grants from the National Natural Science Foundation of China (32072327) and Guangdong Basic and Applied Basic Research Foundation (2021A1515010865).

About the Author

Dr. Zeng is an associate professor at Guangdong University of Technology, Guangzhou, China. Her primary research interests are adaptive evolution, drug resistance, and phage treatment of major pathogenic bacteria.

References

1. Zeng H, Lei T, He W, Zhang J, Liang B, Li C, et al. Novel multidrug-resistant *Cronobacter sakazakii* causing meningitis in neonate, China, 2015. Emerg Infect Dis. 2018;24:2121–4. https://doi.org/10.3201/eid2411.180718
2. Taylor MG, Amerson-Brown MH, Hulten K, Cameron LH, Holzmann-Pazgal G, Edwards MS, et al. Two cases of *Cronobacter sakazakii* meningitis in infants: the importance of early advanced brain imaging and public health reporting. Pediatr Infect Dis J. 2021;40:e346–8. https://doi.org/10.1097/INF.0000000000003184
3. Ogrodzki P, Forsythe SJ. DNA-sequence based typing of the *Cronobacter* genus Using MLST, CRISPR-*cas* array and capsular profiling. Front Microbiol. 2017;8:1875. https://doi.org/10.3389/fmicb.2017.01875
4. Zeng H, Li C, He W, Zhang J, Chen M, Lei T, et al. *Cronobacter sakazakii*, *Cronobacter malonaticus*, and *Cronobacter dublinensis* genotyping based on CRISPR locus diversity. Front Microbiol. 2019;10:1989. https://doi.org/10.3389/fmicb.2019.01989
5. Zeng H, Li C, Ling N, Zhang J, Chen M, Lei T, et al. Prevalence, genetic analysis and CRISPR typing of *Cronobacter* spp. isolated from meat and meat products in China. Int J Food Microbiol. 2020;321:108549. https://doi.org/10.1016/j.ijfoodmicro.2020.108549
6. Gopinath GR, Chase HR, Gangiredla J, Eshwar A, Jang H, Patel I, et al. Genomic characterization of malonate positive *Cronobacter sakazakii* serotype O:2, sequence type 64 strains, isolated from clinical, food, and environment samples. Gut Pathog. 2018;10:11. https://doi.org/10.1186/s13099-018-0238-9
7. Zeng H, Zhang J, Wu Q, He W, Wu H, Ye Y, et al. Reconstituting the history of *Cronobacter* evolution driven by differentiated CRISPR activity. Appl Environ Microbiol. 2018;84:e00267–18. https://doi.org/10.1128/AEM.00267-18
8. Treangen TJ, Ondov BD, Koren S, Phillippy AM. The Harvest suite for rapid core-genome alignment and visualization of thousands of intraspecific microbial genomes. Genome Biol. 2014;15:524. https://doi.org/10.1186/s13059-014-0524-x
9. Page AJ, Taylor B, Delaney AJ, Soares J, Seemann T, Keane JA, et al. *SNP-sites*: rapid efficient extraction of SNPs from multi-FASTA alignments. Microb Genom. 2016;2:e000056. https://doi.org/10.1099/mgen.0.000056
10. Price MN, Dehal PS, Arkin AP. FastTree 2—approximately maximum-likelihood trees for large alignments. PLoS One. 2010;5:e9490. https://doi.org/10.1371/journal.pone.0009490
11. Letunic I, Bork P. Interactive Tree Of Life (iTOL) v5: an online tool for phylogenetic tree display and annotation. Nucleic Acids Res. 2021;49(W1):W293–6. https://doi.org/10.1093/nar/gkab301
12. Chaves CE, Brandão ML, Lacerda ML, Rocha CA, Leone de Oliveira SM, Parpinelli TC, et al. Fatal *Cronobacter sakazakii* sequence type 494 meningitis in a newborn, Brazil. Emerg Infect Dis. 2018;24:1948–50. https://doi.org/10.3201/eid2410.180373
13. Phair K, Pereira SG, Kealey C, Fanning S, Brady DB. Insights into the mechanisms of *Cronobacter sakazakii* virulence. Microb Pathog. 2022;169:105643. https://doi.org/10.1016/j.micpath.2022.105643
14. Joseph S, Desai P, Ji Y, Cummings CA, Shih R, Degoricija L, et al. Comparative analysis of genome sequences covering the seven *Cronobacter* species. PLoS One. 2012;7:e49455. https://doi.org/10.1371/journal.pone.0049455

Address for correspondence: Qingping Wu, Guangdong Provincial Key Laboratory of Microbial Safety and Health, State Key Laboratory of Applied Microbiology, Southern China, Institute of Microbiology, Guangdong Academy of Sciences, Xianlie Zhong Rd 100, Guangzhou City 510070, China; email: wuqp203@163.com; or Haiyan Zeng, School of Biomedicine and Pharmaceutical Science, Guangdong University of Technology, Waihuan West Rd 100, Guangzhou City 510006, China; email: zenghy@aliyun.com or zenghy@gdut.edu.cn

Home-Based Testing and COVID-19 Isolation Recommendations, United States

Patrick K. Moonan, Jonathan P. Smith, Brian F. Borah, Divya Vohra, Holly H. Matulewicz, Nickolas DeLuca, Elise Caruso, Penny S. Loosier, Phoebe Thorpe, Melanie M. Taylor, John E. Oeltmann

Using a nationally representative panel survey, we examined isolation behaviors among persons in the United States who had positive SARS-CoV-2 test results during January 2021–March 2022. Compared with persons who received provider-administered results, persons with home-based results had 29% (95% CI 5%–47%) lower odds of following isolation recommendations.

Self-administered home-based tests are increasingly used as the primary method to detect SARS-CoV-2, the virus that causes COVID-19 (*1*). In contrast to tests performed at a public health department, laboratory, or other healthcare setting and administered by a provider, home-based tests require little or no interaction with the healthcare system (*2*,*3*). The Centers for Disease Control and Prevention (CDC) recommends isolation for persons who test positive for SARS-CoV-2 (*4*); however, it is unclear if test administration type is associated with following isolation recommendations. We used data from a nationally representative survey of persons in the United States with COVID-19 (*5*) to explore differences in proportions among those who isolated, followed contemporary isolation recommendations, and self-notified contacts by test administration type.

The Study

We conducted a probability-based, web-based panel survey that provided a representative sampling frame, weighted to demographically represent all noninstitutionalized adults >18 years of age residing in the United States during January 2020–March 2022 (Appendix, https://wwwnc.cdc.gov/EID/article/29/9/23-0494-App1.pdf). For persons with multiple SARS-CoV-2 test results, isolation behaviors and self-notification of contacts corresponded to the first episode only. Because home tests were approved in late 2020 (*6*) and the recommended length of isolation duration evolved over time, we restricted survey respondents to persons with COVID-19 diagnoses that occurred during January 1, 2021–March 31, 2022, and categorized participants by whether they achieved the minimum number of days recommended for isolation on the basis of CDC-recommended contemporary isolation policies. During January 1–December 31, 2021, the minimum recommended isolation period was 10 days; during January 1–March 31, 2022 (the end date of the survey), the minimum recommended isolation period was 5 days (*7*).

We developed survey-weighted multivariable logistic models to examine the association between test administration type and 1) any isolation, 2) adherence to contemporary guidelines among those who isolated, and 3) self-reporting to contacts. We also developed a survey-weighted multivariable linear regression model to examine the association between test administration type and days of isolation. In multivariable models we controlled for age, sex, race/ethnicity, US state of residence, household size, household income, and urbanicity (i.e., urban, suburban, and rural). We transformed logistic models to compute adjusted odds ratios (aORs) and accompanying 95% CI, considering CIs that did not contain the null to be statistically significant.

Using population-weighted survey responses, we estimated 48,518,190 adults in the United States had ≥1 positive SARS-CoV-2 test result during the 15-month analytic period. Among those, 11,468,111

Author affiliations: Centers for Disease Control and Prevention, Atlanta, Georgia, USA (P.K. Moonan, B.F. Borah, N. DeLuca, E. Caruso, P.S. Loosier, P. Thorpe, M.M. Taylor, J.E. Oeltmann); Yale University, New Haven, Connecticut, USA (J.P. Smith); Vermont Department of Health, Burlington, Vermont, USA (B.F. Borah); Mathematica, Princeton, New Jersey, USA (D. Vohra, H.H. Matulewicz)

DOI: http://doi.org/10.3201/eid2909.230494

(24%) adults had results exclusively from home-based tests and 37,050,079 (76%) had results exclusively from provider-administered tests.

After we adjusted for potential confounders, persons who received results from home-based tests were significantly less likely to isolate for any duration compared with those who received provider-administered tests (78% vs. 84%; aOR 0.72 [95% CI 0.57–0.89]) (Figure). Similarly, among those who did isolate, the odds that their isolation met contemporary guidelines were significantly lower among persons who received results from home-based tests than among those with provider-administered tests (64% vs, 73%; aOR 0.71 [95% CI 0.53–0.95]). The adjusted mean duration of isolation was 2 (95% CI 1.59–2.45) days shorter among persons with results from home-based tests than those with provider-administered tests ($p<0.001$). Participants who home tested also had decreased odds of self-notifying their contacts; however, that association was not statistically significant (78% vs. 84%; aOR 0.79 [95% CI 0.53–1.18]) (Figure).

Conclusions

Using a nationally representative survey of persons with COVID-19, we found that persons in the United States who exclusively used SARS-CoV-2 home-based tests were significantly less likely to isolate or follow contemporary isolation recommendations and, on average, isolated for fewer days than those who exclusively used provider-administered tests. This analysis adds to a limited number of reports that investigated the actual behaviors of persons after they received a positive SARS-CoV-2 result. A randomized trial by Woloshin et al. (*8*) demonstrated that persons who used home-based tests might not follow CDC guidelines. Those findings suggest that persons who test at home may be unaware of or misinformed about the need for, or duration of, recommended isolation and indicates that health providers may potentially influence isolation behaviors and reinforce contemporary recommendations. Ritchey et al. (*9*) found that, despite the increased availability of home-based tests, only a small fraction of persons in the United States self-reported home-based test results to a public health surveillance system. Those findings have potential implications for initiating important public health activities, such as formal case investigation for surveillance and contract tracing to interrupt ongoing transmission. Oeltmann et al. (*5*) reported that most persons with any positive test results self-notified contacts irrespective of whether they participated in formal case investigation and contact tracing. In

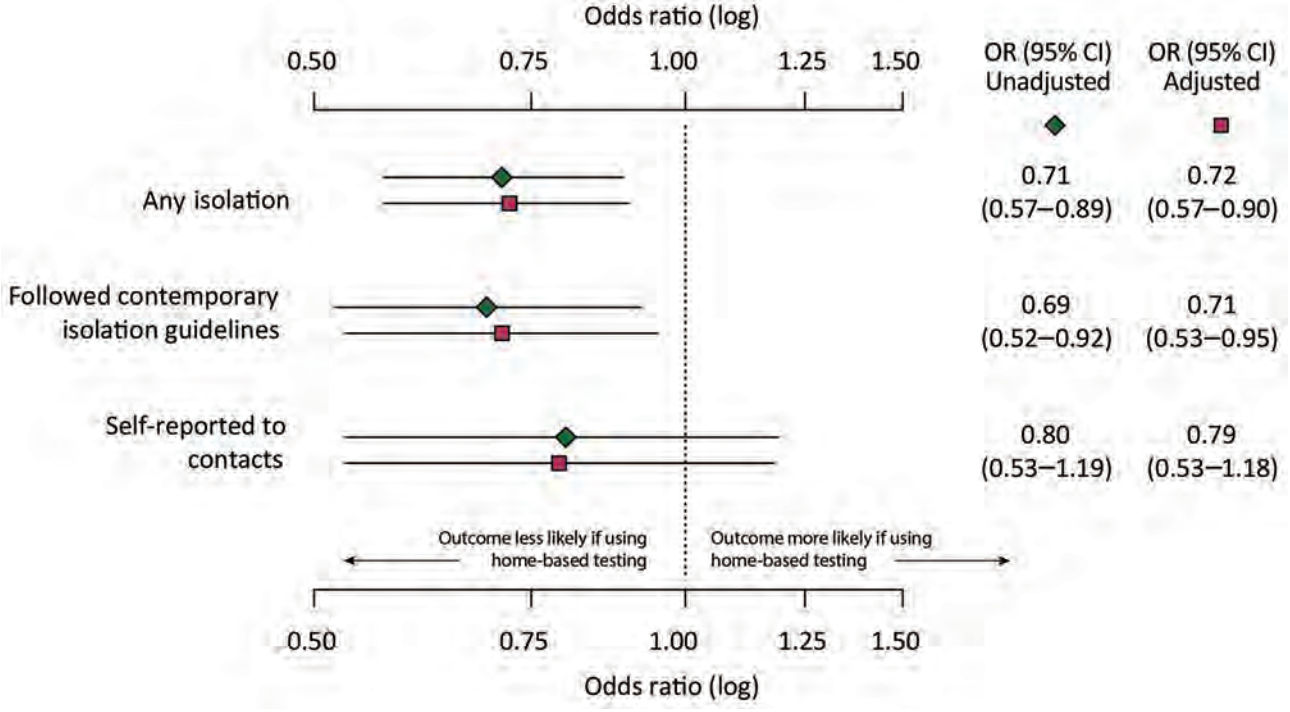

Figure. Crude and adjusted odds ratios and 95% CIs comparing COVID-19 isolation, isolation duration, and self-notification of contacts by SARS-CoV-2 test administration type, United States, January 2021–March 2022. Multivariable models included population-weighted individual survey responses controlled for age, sex, race/ethnicity, US state of residence, household size, household income, and urbanicity (i.e., urban, suburban, or rural). Isolation and notification likelihood of home-based testing is in comparison to provider-administered tests. Vertical dashed line indicates the null or no statistical association. OR, odds ratio.

addition, Bien-Gund et al. found that persons who tested positive were motivated to distribute test kits to potential contacts (*10*), suggesting that persons with positive results might engage in constructive health behaviors without formal public health interactions.

The first limitation of our study is that responses were self-reported, meaning those who agreed to participate in the survey might be more health conscious and, thus, have a higher propensity to follow public health guidelines. We did not include those too ill to respond (e.g., hospitalized persons) or persons experiencing homelessness, and we only administered the survey to participants proficient in English or Spanish. Conversely, persons with mild or asymptomatic disease were plausibly less motivated to test and, thus, may have been unaware of a potential COVID-19 diagnosis, resulting in a potential misclassification in the survey. The pace of home-based testing availability and use in the study population might not reflect the true practice in the United States over time. Finally, the survey was limited to questions describing the first episode of COVID-19. For persons with multiple episodes or test results, isolation behaviors and self-notification of contacts might have changed over time.

Rapid, home-based tests for SARS-CoV-2 have both individual and public health benefits (*9*). Home-based tests greatly expanded access to COVID-19 diagnosis, especially among those without primary healthcare providers and those without stable medical benefits. However, although home-based tests increase convenience and may hasten the time to diagnosis (*2*–*4*), home-based tests eliminate the opportunity for providers to offer health education, reinforce complex and often rapidly evolving COVID-19 recommendations, and emphasize the importance of behavior change to mitigate ongoing transmission. Clear public health messaging about when and how to test, and the efficacy of each type of test, may help to ensure that persons are testing at the appropriate time, even if they do not experience any symptoms (*11*).

In our study, a notable proportion of persons with home-based test results (64%) and provider-administered test results (73%) followed contemporary isolation recommendations. Because the proportion of individuals using home-based tests has increased over time, there is a need to better integrate these results into tangible public health actions. Developing mechanisms that encourage self-report of positive home-based tests results to health departments will likely improve COVID-19 surveillance, formal case investigation, and contact tracing efforts, but also offer opportunities for additional clinical, educational, and emotional support that may further reinforce contemporary COVID-19 recommendations. Examining specific individual-level or community-level behavioral factors associated with self-reporting and other public health actions may extend these findings and deepen our understanding of optimal strategies to mitigate future pandemics with rapid widespread transmission.

Study participation was voluntary; all participants had privacy and confidentiality protections. US Centers for Disease Control and Prevention reviewed this study and deemed it not to be research as defined in 45 CFR 46.102(l) (U.S. Department of Health and Human Services, Title 45 Code of Federal Regulations 46, Protection of Human Subjects).

This work was supported by funding from the Centers for Disease Control and Prevention (no. RFA-DR-21-087.2).

Author contributions: P.K.M. had full access to all of the data in the study and takes responsibility for the integrity of the data and the accuracy of the data analysis. Concept and design: P.K.M., J.P.S., B.F.B., J.E.O. Acquisition, analysis, or interpretation of data: P.K.M., D.V., H.H.M., M.M.T., J.E.O. Drafting of the manuscript: P.K.M., J.P.S., B.F.B., J.E.O. Critical revision of the manuscript for important intellectual content: P.K.M., J.P.S., B.F.B., D.V., H.H.M., N.D., P.S.L., E.C., P.H., M.M.T., J.E.O. Statistical analysis: J.P.S., P.K.M. Administrative, technical, or material support: P.K.M., H.H.M., M.M.T., J.E.O. Supervision: P.K.M., H.H.M., J.E.O.

About the Author

Dr. Moonan is an epidemiologist in the Global TB Branch, Division of Global HIV and TB, Global Health Center, US Centers for Disease Control and Prevention. He was a member of CDC's COVID-19 Response Team during the study period. During his deployment, he focused on evaluating the effectiveness of case investigation and contact tracing and the impact of COVID-19 isolation and quarantine in the United States.

References

1. Rader B, Gertz A, Iuliano AD, Gilmer M, Wronski L, Astley CM, et al. Use of at-home COVID-19 tests—United States, August 23, 2021–March 12, 2022. MMWR Morb Mortal Wkly Rep. 2022;71:489–94. https://doi.org/10.15585/mmwr.mm7113e1
2. Siegler AJ, Hall E, Luisi N, Zlotorzynska M, Wilde G, Sanchez T, et al. Willingness to seek diagnostic testing for SARS-CoV-2 with home, drive-through, and clinic-based specimen collection locations. Open Forum Infect Dis. 2020;7:ofaa269. https://doi.org/10.1093/ofid/ofaa269

3. Embrett M, Sim SM, Caldwell HAT, Boulos L, Yu Z, Agarwal G, et al. Barriers to and strategies to address COVID-19 testing hesitancy: a rapid scoping review. BMC Public Health. 2022;22:750. https://doi.org/10.1186/s12889-022-13127-7
4. Massetti GM, Jackson BR, Brooks JT, Perrine CG, Reott E, Hall AJ, et al. Summary of guidance for minimizing the impact of COVID-19 on individual persons, communities, and health care systems—United States, August 2022. MMWR Morb Mortal Wkly Rep. 2022;71:1057–64. https://doi.org/10.15585/mmwr.mm7133e1
5. Oeltmann JE, Vohra D, Matulewicz HH, DeLuca N, Smith JP, Couzens C, et al. Isolation and quarantine for COVID-19 in the United States, 2020–2022. Clin Infect Dis. 2023 [Epub ahead of print]. https://doi.org/10.1093/cid/ciad163
6. Harmon A, Chang C, Salcedo N, Sena B, Herrera BB, Bosch I, et al. Validation of an at-home direct antigen rapid test for COVID-19. JAMA Netw Open. 2021;4:e2126931-e.
7. Centers for Disease Control and Prevention. CDC updates and shortens recommended isolation and quarantine period for general population. 2021 Dec 27 [cited 2023 Feb 2]. https://www.cdc.gov/media/releases/2021/s1227-isolation-quarantine-guidance.html
8. Woloshin S, Dewitt B, Krishnamurti T, Fischhoff B. Assessing how consumers interpret and act on results from at-home COVID-19 self-test kits: a randomized clinical trial. JAMA Intern Med. 2022;182:332–41. https://doi.org/10.1001/jamainternmed.2021.8075
9. Ritchey MD, Rosenblum HG, Del Guercio K, Humbard M, Santos S, Hall J, et al. COVID-19 self-test data: challenges and opportunities—United States, October 31, 2021–June 11, 2022. MMWR Morb Mortal Wkly Rep. 2022;71:1005–10. https://doi.org/10.15585/mmwr.mm7132a1
10. Bien-Gund C, Dugosh K, Acri T, Brady K, Thirumurthy H, Fishman, J, et al. Factors associated with US public motivation to use and distribute COVID-19 self-tests. JAMA Netw Open. 2021;4:e2034001-e.
11. DeLuca N, Caruso E, Gupta R, Kemmerer C, Coughlin R, Chan O, et al.; CDC COVID-19 Case Investigation and Contact Tracing Task Force. Experiences with COVID-19 case investigation and contact tracing: a qualitative analysis. SSM Qual Res Health. 2023;3:100244. https://doi.org/10.1016/j.ssmqr.2023.100244

Address for correspondence: Patrick K. Moonan, Centers for Disease Control and Prevention, 1600 Clifton Rd NE, Mailstop US1-2, Atlanta, GA 30329-4027, USA; email: pmoonan@cdc.gov

etymologia revisited

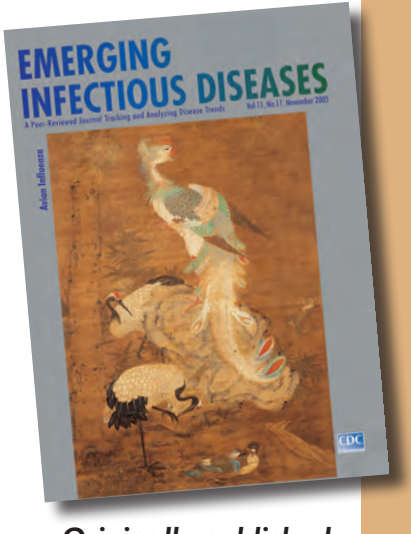

Originally published in November 2007

Tularemia

[t-lə-rē-mē-ə]

An infectious, plaguelike, zoonotic disease caused by the bacillus *Francisella tularensis*. The agent was named after Tulare County, California, where the agent was first isolated in 1910, and Edward Francis, an Officer of the US Public Health Service, who investigatedthe disease. Dr. Francis first contracted deer fly fever from a patient he visited in Utah in the early 1900s. He kept a careful record of his 3-month illness and later discovered that a single attack confers permanent immunity. He was exposed to the bacterium for 16 years and even deliberately reinfected himself 4 times.

Tularemia occurs throughout North America, many parts of Europe, the former Soviet Union, the Peoples Republic of China, and Japan, primarily in rabbits, rodents, and humans. The disease is transmitted by the bites of deerflies, fleas, and ticks; by contact with contaminated animals; and by ingestion of contaminated food or water.

Clinical manifestations vary depending on the route of introduction and the virulence of the agent. Most often, an ulcer is exhibited at the site of introduction, together with swelling of the regional lymph nodes and abrupt onset of fever, chills, weakness, headache, backache, and malaise.

Reference

Dorland's illustrated medical dictionary, 31st edition. Philadelphia: Saunders; 2007; Benenson AS, editor. Control of communicable diseases manual. Washington: American Public Health Association; 1995; https://www.whonamedit.com

https://wwwnc.cdc.gov/eid/article/13/11/e1-1311_article

Evaluating SARS-CoV-2 Saliva and Dried Blood Spot Surveillance Strategies in a Congregate Population

Liana R. Andronescu, Stephanie A. Richard, Eric D. Laing, Nora Pisanic, Si'Ana A. Coggins, Magdielis Gregory Rivera, Kate Kruczynski, Adam K. Saperstein, Jitendrakumar Modi, Jamie A. Fraser, Saira Shaikh, Christopher C. Broder, Timothy H. Burgess, Christopher D. Heaney, Simon D. Pollett, Eugene Millar, Christian L. Coles, Mark P. Simons

The optimal approach to COVID-19 surveillance in congregate populations remains unclear. Our study at the US Naval Academy in Annapolis, Maryland, USA, assessed the concordance of antibody prevalence in longitudinally collected dried blood spots and saliva in a setting of frequent PCR-based testing. Our findings highlight the utility of salivary-based surveillance.

Congregate populations, including those in university and military settings, are at high risk for SARS-CoV-2 transmission because of crowding, frequent physical contact, and environmental contamination (*1*). Using self-collected saliva for surveillance may be a noninvasive alternative to serum and warrants further evaluation to guide population surveillance strategies.

Assessment of SARS-CoV-2 infection prevalence often is underestimated because of asymptomatic and paucisymptomatic infections that are not often captured by screening test strategies (*2*–*4*), but those infections contribute to high attack rates in congregate populations (*5*–*9*). This study evaluated the use of saliva to estimate the prevalence of SARS-CoV-2 infection among a congregate population of young and initially immunologically naive adults at the US Naval Academy (USNA) in Annapolis, Maryland, USA.

Author affiliations: Uniformed Services University of the Health Sciences, Bethesda, Maryland, USA (L.R. Andronescu, S.A. Richard, E.D. Laing, S.A. Coggins, A.K. Saperstein, J.A. Fraser, S. Shaikh, C.C. Broder, T.H. Burgess, S.D. Pollett, E. Millar, C.L. Coles, M.P. Simons); The Henry M. Jackson Foundation for the Advancement of Military Medicine, Inc., Bethesda (L.R. Andronescu, S.A. Richard, S.A. Coggins, J.A. Fraser, S. Shaikh, S.D. Pollett, E. Millar, C.L. Coles); Johns Hopkins University, Baltimore, Maryland, USA (N. Pisanic, M. Gregory Rivera, K. Kruczynski, C.D. Heaney); Naval Health Clinic, Annapolis, Maryland, USA (A.K. Saperstein, J. Modi)

DOI: https://doi.org/10.3201/eid2909.230417

The Study

The Observational Seroepidemiologic Study of COVID-19 at the USNA (TOSCANA) study enrolled male and female midshipmen to estimate the SARS-CoV-2 attack rate and assess the concordance of seroprevalence between blood and saliva. All midshipmen at USNA (≈4,500) reside in a single dormitory. During the time of the study, nonpharmaceutical interventions included mask wearing, weekly PCR-based surveillance, and isolation of cases (Appendix, https://wwwnc.cdc.gov/EID/article/29/9/23-0417-App1.pdf). Pharmaceutical interventions included receipt of the Moderna (https://www.modernatx.com) SARS-CoV-2 mRNA vaccine in March 2021 (first dose) and April 2021 (second dose); >96% of all midshipmen had documented receipt of 2 doses.

We initiated the process of recruiting, enrolling, and acquiring consent of participants at the start of the academic year. After providing consent, participants completed the baseline questionnaire regarding demographic information, risk factors for acute respiratory infection, and previous infections or exposures to SARS-CoV-2. Paired self-collected saliva and dried blood spots were collected at enrollment (August 2020, visit 1 [V1]) and follow-up visits in December 2020 (V2), February 2021 (V3, saliva only), and April–May 2021 (V4) (Appendix Table).

Methods for dried blood spot (DBS) collection and testing has been described previously (*10*). We collected blood samples by using the Mitra Blood

Table 1. New SARS-CoV-2 infections detected among 79 study participants, by PCR and serologic test, at each specimen collection timepoint, US Naval Academy, Annapolis, Maryland, USA, August 2020–May 2021*

Test	2020 Aug (V1)	2020 Dec (V2)	2021 Feb (V3)	2021 May (V4)†	Total
Saliva seroconversion‡	0	2	3	13	18
Dried blood spot seroconversion	0	3	NA	16	19
PCR-positive	1	3	5	10	19

*Sample restricted to participants who had a PCR test on record (from screening or medically attended SARS-CoV-2) and were not seropositive at the first visit in August 2020. V1, V2, V3, and V4 note the visit timepoint that matches to the corresponding month.
†Collection time is postvaccination; nucleocapsid IgG and not spike IgG seroconversion alone was used to measure infection.
‡Salivary nucleocapsid IgG positivity defined as receptor-binding domain IgG and nucleocapsid IgG positive; salivary spike IgG positivity used a receptor-binding domain target.

Collection Kit (Neoteryx, https://www.neoteryx.com) and tested them for SARS-CoV-2 reactive IgG by using an in-house multiplex microsphere-based immunoassay. The antigenic targets were a prefusion-stabilized SARS-CoV-2 spike glycoprotein ectodomain trimer and a nucleocapsid protein; we detected antigen-specific IgG levels by using a Bio-Plex 200 HTF multiplexing systems (Bio-Rad, https://www.bio-rad.com) and reported results as median fluorescence intensity (MFI).

We collected saliva samples by using an Oracol S14 collection device (Malvern Medical Developments, https://www.malmed.co.uk) and tested them as previously described (*11*). We tested samples for IgG binding to any of 7 SARS-CoV-2 antigen components (2 SARS-CoV-2 nucleocapsid proteins, 3 receptor-binding domain [RBD] proteins, and 2 spike proteins) by using a multiplex immunoassay. After background subtraction, we classified samples positive for RBD and nucleocapsid IgG as indicative of prior infection, whereas we classified samples positive for only RBD IgG as indicative of SARS-CoV-2 vaccination.

As part of routine clinical care, USNA's Brigade Medical Clinic collected nasopharyngeal swab specimens from all returning midshipmen in August and throughout the school year when they visited the clinic with symptoms of respiratory illness. In addition, each week we randomly selected 15% of the asymptomatic midshipmen population for reverse transcription PCR (RT-PCR) screening; we also tested 100% of in-season varsity athletes each week. We excluded from weekly testing all participants who had confirmed positive SARS-CoV-2 infection during the preceding 90 days. We tested nasopharyngeal swab samples by using SARS-CoV-2 RT-PCR and made results accessible through electronic medical records.

We compared seroconversion rates with cumulative frequencies of molecularly confirmed infections. We calculated correlation coefficients for spike IgG and nucleocapsid IgG MFI in saliva and DBS. We used the Cohen kappa coefficient (κ) to measure concordance of saliva with DBS nucleocapsid IgG and spike IgG positivity and to measure concordance of PCR tests with seroconversions.

This study was approved by the Uniformed Services University Institutional Review Board under protocol IDCRP-129. All participants provided written informed consent.

In August 2020, a total of 104 midshipmen enrolled in the study; 64.4% were men, 92.3% were white, 8 (7.7%) reported COVID-19 exposure, and 11 (10.6%) reporting a COVID-19 diagnosis before arrival at USNA. At baseline, 17 (16%) participants

Table 2. Saliva and DBS serologic test concordance for detection of SARS-CoV-2 infection among study participants, by specimen collection timepoint, US Naval Academy, Annapolis, Maryland, USA, August 2020–May 2021*

	Aug 2020, n = 41		Dec 2020, n = 47		May 2021, n = 55	
Serologic test	DBS-negative	DBS-positive	DBS-negative	DBS-positive	DBS-negative	DBS-positive
Spike IgG†						
Saliva-negative	31 (75.6)	5 (12.2)	37 (78.7)	5 (10.6)	0	2 (3.6)
Saliva-positive	1 (2.4)	4 (9.8)	0	5 (10.6)	0	53 (96.4)
Kappa coefficient (95% CI)	0.49 (0.15–0.83)		0.61 (0.32–0.91)		N/A	
Observed agreement	0.85		0.89		0.96	
Nucleocapsid IgG‡						
Saliva-negative	37 (90.24)	1 (2.4)	40 (85.1)	2 (4.3)	23 (41.8)	5 (9.1)
Saliva-positive	1 (2.4)	2 (4.9)	1 (2.1)	4 (8.5)	5 (9.1)	22 (40.0)
Kappa coefficient (95% CI)	0.64 (0.18–1.00)		0.69 (0.36–1.00)		0.64 (0.43–0.84)	
Observed agreement	0.95		0.94		0.82	

*Sample restricted to participants with both DBS and saliva specimens available. Values are no. (%) except as indicated. DBS, dried blood spot.
†Receptor-binding domain target for salivary assay.
‡Salivary nucleocapsid IgG positivity defined as receptor-binding domain IgG and nucleocapsid IgG positivity.

showed evidence of SARS-CoV-2 infection based on spike IgG values in DBS.

Among the participants who were serologically negative for SARS-CoV-2 at enrollment, 18 seroconversions were detected in saliva, 19 were detected in DBS, and 19 were detected by PCR by the end of follow-up (Table 1); however, at V4 (postvaccination), additional cases were detected by DBS and saliva that were missed by PCR testing. One participant had a positive PCR result before a serologic result; the PCR test was conducted in August 2020, and the participant had no record of seroconversion through the end of the study.

By V4, 100% of remaining participants were spike IgG seropositive, and 49.1% of remaining participants with both DBS and saliva seroconverted to nucleocapsid IgG as evaluated by DBS (Table 2). Among participants with both DBS and saliva samples (n = 55), spike IgG results had an observed agreement of 0.85 and a κof 0.49 (95% CI 0.15–0.83) at V1. By V2 the observed agreement rose to 0.89 and κ to 0.61 (95% CI 0.32–0.91); by V4 the observed agreement reached 0.96. Nucleocapsid IgG results had an observed agreement of 0.95 and a κof 0.64 (95% CI 0.18–1.00) at V1 (Table 2). At V2 the observed agreement was 0.94 and κ was 0.69 (95% CI 0.36–1.00), and by V4 the observed agreement was 0.82 and κ was 0.64 (95% CI 0.43–0.84).

Spike IgG MFI in saliva and DBS were significantly correlated at all 3 timepoints (Figure 1); high spike IgG values at V4 were consistent with the participants receiving vaccinations in March–April 2021. Nucleocapsid IgG MFI in saliva and DBS also were significantly correlated at all 3 timepoints (Figure 2).

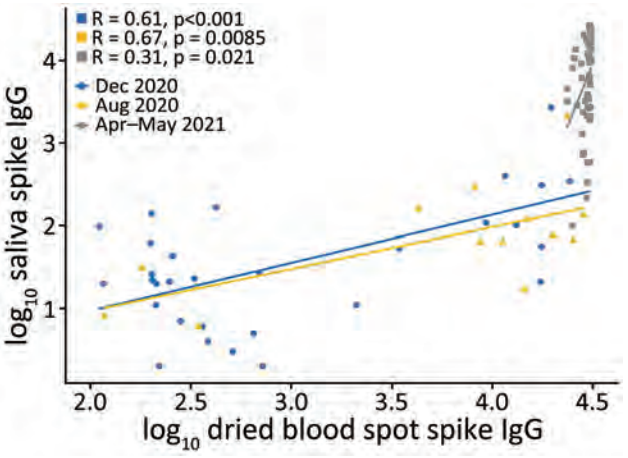

Figure 1. Quantitative comparison of spike IgG in saliva and dried blood spots among 79 study participants, US Naval Academy, Annapolis, Maryland, USA, December 2020–May 2021.

Conclusions

This study, conducted among a population of midshipmen at USNA in the first year of the COVID-19 pandemic, employed blood and saliva collection at multiple visits to evaluate the validity of salivary antibody surveillance. We observed concordance between DBS and saliva for the detection of spike and nucleocapsid IgG, and both biospecimen types were similar to RT-PCR for detection of cases. We noted that all vaccinees mounted a spike IgG response in DBS by V4, consistent with the known immunogenicity of these vaccines, but only 49.1% vaccinees had detectable nucleocapsid IgG at V4, indicating a substantive SARS-CoV-2 infection attack rate in the first half of 2021.

This assessment of SARS-CoV-2 detection in a congregate setting can help inform approaches for detection of SARS-CoV-2 in populations before and after vaccination. Prior evidence shows that PCR testing is an efficient method of infection control in congregate communities if administered regularly but that asymptomatic cases may still be undetected (*12*). These findings may apply to surveillance for other respiratory infections, such as influenza. A limitation to this study was the inability to directly match RT-PCR testing with blood and saliva collection, small sample size with paired samples, and loss to follow-up after the end of the academic year.

In summary, this assessment supports using saliva testing as a less invasive, more feasible surveillance method for monitoring changes in disease prevalence and susceptibility in large populations. Future directions include validation of alternative antibody targets, in both serum and saliva, which can discriminate antibody prevalence in the context of preexisting vaccination and postinfection hybrid immunity.

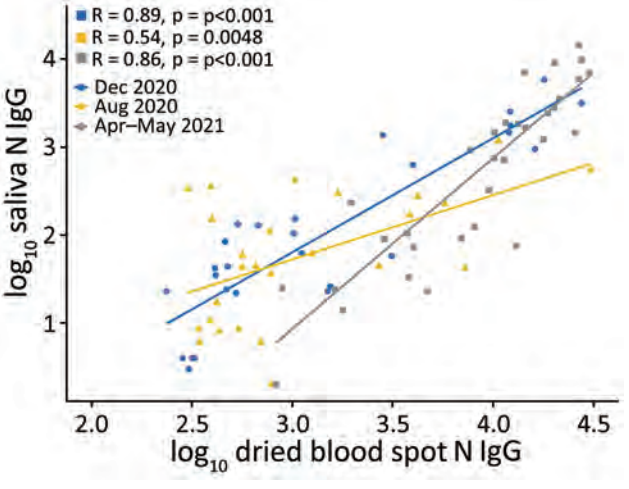

Figure 2. Quantitative comparison of nucleocapsid IgG in saliva and dried blood spots among 79 study participants, US Naval Academy, Annapolis, Maryland, USA, December 2020–May 2021. N, nucleocapsid.

This study (IDCRP-129) was conducted by the Infectious Disease Clinical Research Program, a Department of Defense program executed by the Uniformed Services University of the Health Sciences through a cooperative agreement with the Henry M. Jackson Foundation for the Advancement of Military Medicine, Inc. This work was supported by awards from the Defense Health Program (HU00012020067) and the National Institute of Allergy and Infectious Disease (HU00011920111). This project has been funded in part by the National Institute of Allergy and Infectious Diseases at the National Institutes of Health, under an interagency agreement (Y1-AI-5072).

The contents of this publication are the sole responsibility of the authors and do not necessarily reflect the views, opinions or policies of Uniformed Services University of the Health Sciences; the Henry M. Jackson Foundation for the Advancement of Military Medicine, Inc.; the Defense Health Agency; US Naval Academy; Departments of the Army, Navy, or Air Force; Department of Defense; or the US Government. Mention of trade names, commercial products, or organizations does not imply endorsement by the US Government.

About the Author

Dr. Andronescu is a postdoctoral fellow supporting research on SARS-CoV-2 with the Infectious Disease Clinical Research Program in the Department of Preventive Medicine and Biostatistics at the Uniformed Services University. Her other research interests include global health, control of infectious diseases, and surveillance in resource-limited settings.

References

1. Diepstra K, Bullington BW, Premkumar L, Shook-Sa BE, Jones C, Pettifor A. SARS-CoV-2 seroprevalence: demographic and behavioral factors associated with seropositivity among college students in a university setting. J Adolesc Health. 2022;71:559–69. https://doi.org/10.1016/j.jadohealth.2022.06.015
2. Gao Z, Xu Y, Sun C, Wang X, Guo Y, Qiu S, et al. A systematic review of asymptomatic infections with COVID-19. J Microbiol Immunol Infect. 2021;54:12–6. https://doi.org/10.1016/j.jmii.2020.05.001
3. Ralli M, Morrone A, Arcangeli A, Ercoli L. Asymptomatic patients as a source of transmission of COVID-19 in homeless shelters. Int J Infect Dis. 2021;103:243–5. https://doi.org/10.1016/j.ijid.2020.12.031
4. Sah P, Fitzpatrick MC, Zimmer CF, Abdollahi E, Juden-Kelly L, Moghadas SM, et al. Asymptomatic SARS-CoV-2 infection: A systematic review and meta-analysis. Proc Natl Acad Sci U S A. 2021;118:e2109229118. https://doi.org/10.1073/pnas.2109229118
5. Kimball A, Hatfield KM, Arons M, James A, Taylor J, Spicer K, et al.; Public Health–Seattle & King County; CDC COVID-19 Investigation Team. Asymptomatic and presymptomatic SARS-CoV-2 infections in residents of a long-term care skilled nursing facility—King County, Washington, March 2020. MMWR Morb Mortal Wkly Rep. 2020;69:377–81. https://doi.org/10.15585/mmwr.mm6913e1
6. Wei WE, Li Z, Chiew CJ, Yong SE, Toh MP, Lee VJ. Presymptomatic transmission of SARS-CoV-2—Singapore, January 23–March 16, 2020. MMWR Morb Mortal Wkly Rep. 2020;69:411–5. https://doi.org/10.15585/mmwr.mm6914e1
7. Goldberg SA, Lennerz J, Klompas M, Mark E, Pierce VM, Thompson RW, et al. Presymptomatic transmission of severe acute respiratory syndrome coronavirus 2 among residents and staff at a skilled nursing facility: results of real-time polymerase chain reaction and serologic testing. Clin Infect Dis. 2021;72:686–9. https://doi.org/10.1093/cid/ciaa991
8. Rivett L, Sridhar S, Sparkes D, Routledge M, Jones NK, Forrest S, et al. CITIID-NIHR COVID-19 BioResource Collaboration. Screening of healthcare workers for SARS-CoV-2 highlights the role of asymptomatic carriage in COVID-19 transmission. eLife. 2020;9:9. https://doi.org/10.7554/eLife.58728
9. Han D, Li R, Han Y, Zhang R, Li J. COVID-19: Insight into the asymptomatic SARS-COV-2 infection and transmission. Int J Biol Sci. 2020;16:2803–11. https://doi.org/10.7150/ijbs.48991
10. Epsi NJ, Richard SA, Laing ED, Fries AC, Millar E, Simons MP, et al.; EPICC COVID-19 Cohort Study Group. Clinical, immunological, and virological SARS-CoV-2 phenotypes in obese and nonobese military health system beneficiaries. J Infect Dis. 2021;224:1462–72. https://doi.org/10.1093/infdis/jiab396
11. Katz MJ, Heaney CD, Pisanic N, Smith L, Bigelow BF, Sheikh F, et al. Evaluating immunity to SARS-CoV-2 in nursing home residents using saliva IgG. J Am Geriatr Soc. 2022;70:659–68. https://doi.org/10.1111/jgs.17660
12. Hakre S, Lakhal-Naouar I, King DB, Burns JL, Jackson KN, Krauss SW, et al. Virological and serological assessment of US Army trainees isolated for coronavirus disease 2019. J Infect Dis. 2022;226:1743–52. https://doi.org/10.1093/infdis/jiac198

Address for correspondence: Mark P. Simons, Infectious Disease Clinical Research Program, Department of Preventive Medicine and Biostatistics, Uniformed Services University of the Health Sciences, 6720A Rockledge Dr, Bethesda, MD 20817, USA; email: mark.simons@usuhs.edu

Seroprevalence of *Vibrio cholerae* in Adults, Haiti, 2017

Wilfredo R. Matias, Yodeline Guillaume, Gertrude Cene Augustin, Kenia Vissieres, Ralph Ternier, Richelle C. Charles, Jason B. Harris, Molly F. Franke, Louise C. Ivers

In Haiti in 2017, the prevalence of serum vibriocidal antibody titers against *Vibrio cholerae* serogroup O1 among adults was 12.4% in Cerca-la-Source and 9.54% in Mirebalais, suggesting a high recent prevalence of infection. Improved surveillance programs to monitor cholera and guide public health interventions in Haiti are necessary.

In 2010, cholera, caused by the bacterium *Vibrio cholerae*, was introduced into Haiti, resulting in >800,000 cases and >10,000 deaths (*1*,*2*). Case incidence peaked in 2012, then decreased, and the last case of confirmed cholera was reported in February 2019 (*3*). More than 3 years later, in October 2022, cholera was again detected in Haiti, and that outbreak is ongoing (*4*,*5*).

The response to cholera in Haiti and globally has been hampered by inaccuracies in estimating the actual prevalence of disease (*6*). In resource-limited settings where infectious diseases surveillance systems and laboratory capacity are limited, clinical case count–guided public health interventions can be suboptimal because of limitations in the accuracy of clinical case definitions (*7*). More accurate estimates of cholera disease prevalence and transmission dynamics are key for guiding and monitoring control efforts. Serosurveillance represents a promising tool to address the limitations of clinical surveillance (*8*,*9*). However, seroepidemiologic data are lacking from settings like Haiti where cholera has resurged. In 2017, we conducted a seroepidemiologic survey to measure the prevalence of cholera in Haiti during the waning phase of the first cholera epidemic in that country.

Author affiliations: Brigham and Women's Hospital Division of Infectious Diseases, Boston, Massachusetts, USA (W.R. Matias); Massachusetts General Hospital Center for Global Health, Boston (W.R. Matias, Y. Guillaume); Massachusetts General Hospital Division of Infectious Diseases, Boston (W.R. Matias, R.C. Charles, J.B. Harris, L.C. Ivers); Zanmi Lasante, Croix-des-Bouquets, Haiti (G. Cene Augustin, K. Vissieres, R. Ternier); Harvard Medical School, Boston (R.C. Charles, J.B. Harris, M.F. Franke, L.C. Ivers); Harvard School of Public Health, Boston (R.C. Charles); Harvard Global Health Institute, Cambridge, Massachusetts, USA (L.C. Ivers)

DOI: https://doi.org/10.3201/eid2909.230401

The Study

This study was conducted as part of a campaign to control and eliminate cholera transmission in 2 communities in Haiti. The first, Cerca-la-Source, is a rural, mountainous community of ≈50,000 persons. The second, Mirebalais, is an urban commune of ≈100,000 persons. Both communities are located in the Centre Department of Haiti, a historically underserved and particularly impoverished region of the country.

We conducted a census of both communities. During the census, a subset of households was invited to participate in a household survey and a serologic survey at fixed sampling intervals during March–August 2017 (Appendix Table 1, https://wwwnc.cdc.gov/EID/article/29/9/23-0401-App1.pdf). Trained study enumerators implemented study procedures in their native language of Haitian Creole; the procedures included surveys to measure self-reported sociodemographic and cholera risk factors.

We obtained dried blood spots from consenting adults ≥18 years of age and shipped them to a laboratory in Boston, Massachusetts, USA, where we performed vibriocidal assays by using a drop-plate method from dried blood spots specimens, as described previously (*10*), except we used Advance Dx100 Serum Separator cards (Advance Dx, Inc., https://adx100.com) instead of the cards used in that study. We used target *V. cholerae* strains 19479 El Tor Inaba and X25049 El Tor Ogawa.

To ensure estimates were representative of the populations of Mirebalais and Cerca-la-Source, we used a raking procedure to apply survey weights on the basis of the population distribution of age, sex, and communal sections from the census in those regions. We used a random intercept to account for clustering by household. The primary outcome was

Table 1. Unweighted demographic characteristics of *Vibrio cholerae* serosurvey participants compared with census participants in 2 communities, Centre Department, Haiti, March–August 2017*

	Cerca-la-Source		Mirebalais	
Characteristic	Census†	Serosurvey	Census†	Serosurvey
Total no.	24,500	156	45,365	121
Sex				
M	12,157 (49.6)	74 (47.4)	21,397 (47.2)	56 (46.3)
F	12,343 (50.4)	82 (52.6)	23,968 (52.8)	65 (53.7)
Mean age (SD)	37.1 (16.4)	42.3 (16.1)	37.1 (16.3)	44.6 (16.8)
Age group, y				
18–30	11,162 (45.6)	47 (30.1)	20,700 (45.6)	31 (25.6)
31–40	4,899 (20.0)	29 (18.6)	9,214 (20.3)	25 (20.7)
41–50	3,728 (15.2)	32 (20.5)	6,519 (14.4)	25 (20.7)
>50	4,711 (19.2)	48 (30.8)	8,932 (19.7)	40 (33.1)
Communal section				
1st Acajou Bruler	9,298 (38.0)	51 (32.7)	NA	NA
2nd Acajou Bruler	7,952 (32.5)	59 (37.8)	NA	NA
3rd Lamielle (Cerca-la-Source)	7,250 (29.6)	46 (29.5)	NA	NA
3rd Grand Boucan	NA	NA	26,202 (57.8)	67 (55.4)
6th Sarazin	NA	NA	19,163 (42.2)	54 (44.6)

*Values are no. (%) except as indicated. NA, data not applicable for this category.
†Census only includes persons ≥18 years of age because that was the population included in the serosurvey.

the overall seroprevalence (either Ogawa or Inaba) of vibriocidal antibody responses against *V. cholerae* for each community. We defined seropositivity as a vibriocidal antibody response titer threshold of ≥320 on the basis of the best available evidence, a recent study in Bangladesh that estimated that a vibriocidal modal titer of 320 had a sensitivity of 80.6% and specificity of 83.0% for infections within the preceding year (*9*). We also calculated serotype-specific seroprevalence estimates for each region. For potential risk factors for seropositivity, we provided descriptive statistics, weighted seroprevalence estimates, and 95% CIs (for categorical variables) and odds ratios (ORs) with 95% CIs. We calculated ORs by using univariable logistic regression followed by multivariable logistic regression analysis, including only those risk factors associated with cholera at a significance level of p<0.20 in univariable analysis. We conducted analyses using the survey package in R 4.2.2 (The R Project for Statistical Computing, https://cran.r-project.org) (*11*).

The study was approved by the Partners Healthcare Institutional Review Board (protocol 2016P002781) and the Zanmi Lasante Institutional Review Board (protocol ZL IRB ID AK). All study participants provided written informed consent.

Overall, we enrolled 265 (27.6%) of 960 invited households in the study. Samples from 48 households were lost during tumultuous sociopolitical events, resulting in samples from 217 households available for analysis: 99 households with 156 persons in Cerca-la-Source and 118 households with 121 persons in Mirebalais.

We analyzed unweighted demographic characteristics for the census population and for serosurvey participants (Table 1). Serosurvey participants were representative of the census population. The weighted seroprevalence of *V. cholerae* was 12.4% (95% CI 6.76%–20.0%) in Cerca-la-Source and 9.54% (95% CI 4.91%–16.0%) in Mirebalais (Table 2). We analyzed the frequency distribution of vibriocidal antibody titers for both serotypes (Figure). Only 4 of 277 persons reported having received oral cholera vaccine, consistent with the fact that no major public health oral cholera vaccine campaign had been undertaken in those regions before sample collection.

We calculated seroprevalence estimates for potential risk factors for cholera (Appendix Table 2). Seropositivity varied across multiple subgroups; however, 95% CIs were wide. Only the poverty likelihood index (OR 2.33, 95% CI 0.93–5.84) and reporting having an unimproved toilet compared with

Table 2. Weighted seroprevalence based on vibriocidal antibody titers in *Vibrio cholerae* serosurvey participants in 2 communities, Centre Department, Haiti, March–August 2017*

	Cerca-la-Source			Mirebalais		
Strain	No. tested	No. positive	% Seroprevalence (95% CI)	No. tested	No. positive	% Seroprevalence (95% CI)
Either Ogawa or Inaba	156	16	12.4 (6.76–20.0)	121	12	9.54 (4.91–16.0)
Ogawa only	156	14	9.73 (5.38–16.0)	121	11	8.75 (4.28–15.0)
Inaba only	156	2	2.69 (0.49–8.00)	121	3	2.73 (0.57–7.00)

*Based on a vibriocidal antibody assay positivity threshold titer of 320. Weights were computed as the inverse probability of selection and adjusted so that the marginal distribution of age group, sex, and communal section agreed with those from census estimates.

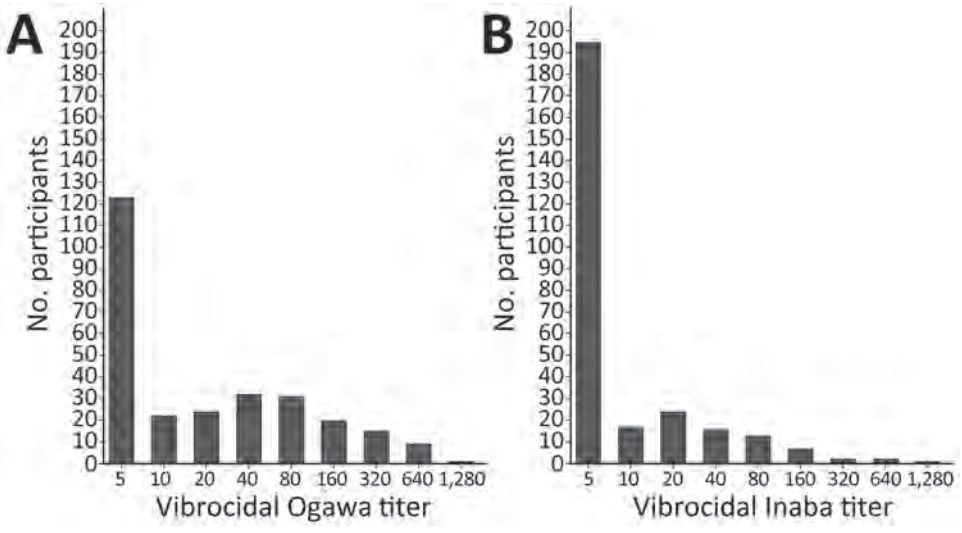

Figure. Serosurvey participants with vibriocidal antibody titers for Ogawa (A) and Inaba (B) *Vibrio cholerae* serotypes in 2 communities, Centre Department, Haiti, March–August 2017. Samples came from 217 total households, 99 (156 persons) in Cerca-la-Source and 118 (121 persons) in Mirebalais. All participants were adults ≥18 years of age.

open defecation (OR 0.26, 95% CI 0.04–1.53) met our predetermined p value threshold for inclusion into a multivariable model, so we did not perform multivariable analysis.

Conclusions

The vibriocidal antibody is a complement-dependent, bactericidal antibody directed against the lipopolysaccharide O-antigen of *V. cholerae* and is the best characterized immunologic marker of recent exposure to cholera. However, there is no widely agreed-upon threshold to quantify exposure over a given period, and our understanding of the relationship between symptom severity and antibody kinetics is limited. In the study from Bangladesh, a vibriocidal titer of ≥320 was the best marker of infection in the preceding year (*9*).

Limited serologic data on *V. cholerae* are available from Haiti. One prior serosurvey, conducted during March–April 2011, within the first 6 months of the onset of the epidemic in the Artibonite Department of Haiti, estimated that 39% of persons had a vibriocidal titer ≥320, whereas 64% had titers ≥80, which suggested extensive infection and was consistent with high early case counts (*12*).

The findings from this study should be interpreted considering several limitations. Only adults ≥18 years of age in 1 department of Haiti participated, so the data cannot be directly extrapolated to younger age groups and other regions; however; during 2017–2018, that department was the most affected according to case counts (*13*). We were unable to account for uncertainty in vibriocidal assay performance characteristics. Ideally, seroprevalence estimates should integrate data on the local sensitivity and specificity of a serologic assay, which are not available for Haiti (*14*). Last, the survey was cross-sectional and did not account for temporal waning of serologic markers.

In summary, in 2017, the seroprevalence of *V. cholerae* vibriocidal antibodies was 12.4% in Cerca-la-Source and 9.54% in Mirebalais in Haiti, suggesting a high rate of recent infection even at a time when case incidence was declining. Although commune-level incidence data were not available for direct comparison, in 2017, the reported annual incidence for the Centre Department, where Cerca-la-Source and Mirebalais are located, was 4.3 cases/1,000 inhabitants, which offers a general frame of reference (*13*,*15*). Those findings inform our understanding of cholera epidemic dynamics in Haiti, which is now experiencing a resurgence of cholera after nearly 3 years without a confirmed case. Our results demonstrate a higher-than-expected disease prevalence and suggest the need for improved surveillance to monitor cholera and guide public health interventions, especially during the waning phase of outbreaks.

Acknowledgments

We thank all the study participants and Zanmi Lasante staff for supporting this work.

This work was supported by the US National Institutes of Allergy and Infectious Diseases (grant no. T32 AI007433, awarded to W.R.M., and grant no. AI099243, awarded to L.C.I. and J.B.H.) and the Bill and Melinda Gates Foundation (grant no. OPP1148213, awarded to L.C.I. and R.T.). Funding sources played no role in study design; in the collection, analysis, and interpretation of data; in the writing of the report; and in the decision to submit the paper for publication.

About the Author

Dr. Matias is an infectious diseases fellow at Massachusetts General Hospital and Brigham and Women's Hospital and a global health fellow at the Massachusetts General Hospital's Center for Global Health. His research focuses on epidemic disease response and global health equity.

References

1. Chin CS, Sorenson J, Harris JB, Robins WP, Charles RC, Jean-Charles RR, et al. The origin of the Haitian cholera outbreak strain. N Engl J Med. 2011;364:33–42. https://doi.org/10.1056/NEJMoa1012928
2. World Health Organization. Cholera—Haiti. 2022 Dec 22 [cited 2023 Jan 4]. https://www.who.int/emergencies/disease-outbreak-news/item/2022-DON415
3. Rebaudet S, Dély P, Boncy J, Henrys JH, Piarroux R. Toward cholera elimination, Haiti. Emerg Infect Dis. 2021;27:2932–6. https://doi.org/10.3201/eid2711.203372
4. Rubin DHF, Zingl FG, Leitner DR, et al. Reemergence of cholera in Haiti. N Engl J Med. 2022;387:2387–9. https://doi.org/10.1056/NEJMc2213908
5. Vega Ocasio D, Juin S, Berendes D, Heitzinger K, Prentice-Mott G, Desormeaux AM, et al.; CDC Haiti Cholera Response Group. Cholera outbreak—Haiti, September 2022–January 2023. MMWR Morb Mortal Wkly Rep. 2023;72:21–5. https://doi.org/10.15585/mmwr.mm7202a1
6. Luquero FJ, Rondy M, Boncy J, Munger A, Mekaoui H, Rymshaw E, et al. Mortality rates during cholera epidemic, Haiti, 2010–2011. Emerg Infect Dis. 2016;22:410–6. https://doi.org/10.3201/eid2203.141970
7. Nadri J, Sauvageot D, Njanpop-Lafourcade BM, Baltazar CS, Banla Kere A, Bwire G, et al. Sensitivity, specificity, and public-health utility of clinical case definitions based on the signs and symptoms of cholera in Africa. Am J Trop Med Hyg. 2018;98:1021–30. https://doi.org/10.4269/ajtmh.16-0523
8. Azman AS, Moore SM, Lessler J. Surveillance and the global fight against cholera: setting priorities and tracking progress. Vaccine. 2020;38(Suppl 1):A28–30. https://doi.org/10.1016/j.vaccine.2019.06.037
9. Azman AS, Lessler J, Luquero FJ, Bhuiyan TR, Khan AI, Chowdhury F, et al. Estimating cholera incidence with cross-sectional serology. Sci Transl Med. 2019;11:eaau6242. https://doi.org/10.1126/scitranslmed.aau6242
10. Iyer AS, Azman AS, Bouhenia M, Deng LO, Anderson CP, Graves M, et al. Dried blood spots for measuring *Vibrio cholerae*–specific immune responses. PLoS Negl Trop Dis. 2018;12:e0006196. https://doi.org/10.1371/journal.pntd.0006196
11. Lumley T. survey: analysis of complex survey samples. 2020 Apr 3 [cited 2021 May 6]. https://CRAN.R-project.org/package=survey
12. Jackson BR, Talkington DF, Pruckler JM, Fouché MDB, Lafosse E, Nygren B, et al.; The Cholera Serosurvey Working Group. Seroepidemiologic survey of epidemic cholera in Haiti to assess spectrum of illness and risk factors for severe disease. Am J Trop Med Hyg. 2013;89:654–64. https://doi.org/10.4269/ajtmh.13-0208
13. Lee EC, Chao DL, Lemaitre JC, Matrajt L, Pasetto D, Perez-Saez J, et al. Achieving coordinated national immunity and cholera elimination in Haiti through vaccination: a modelling study. Lancet Glob Health. 2020;8:e1081–9. https://doi.org/10.1016/S2214-109X(20)30310-7
14. Azman AS, Lauer SA, Bhuiyan TR, Luquero FJ, Leung DT, Hegde ST, et al. *Vibrio cholerae* O1 transmission in Bangladesh: insights from a nationally representative serosurvey. Lancet Microbe. 2020;1:e336–43. https://doi.org/10.1016/S2666-5247(20)30141-5
15. Haiti Ministry of Health and Population. Report of the National Surveillance Network: cholera. 52nd epidemiologic week, 2017 [in French]. 2017 [cited 2023 Jan 25]. https://mspp.gouv.ht/site/downloads/Profil%20statistique%20Cholera%2052eme%20SE2017version%20finale.pdf

Address for correspondence: Wilfredo R. Matias, Massachusetts General Hospital, Division of Infectious Diseases, 55 Fruit St, BUL-130, Boston, MA 02114, USA; email: wmatias@bwh.harvard.edu

Who is this person?

Here is a clue: He played a key role in containing the spread of severe acute respiratory syndrome.

A) Ronald Ross

B) David Bruckner

C) Carlo Urbani

D) Li Wenliang

E) Norman Edward Shumway

Decide first.
Then see next page for the answer.

Carlo Urbani

Mariano Martini

This is a photograph of Carlo Urbani (1956–2003), who was a communicable disease expert for the World Health Organization (WHO) in Hanoi, Vietnam. In 2003, he identified what later became known as SARS and alerted WHO and colleagues elsewhere about his concerns. The disease was originally characterized as pneumonia of unknown origin.

Dr. Urbani was born in Castelplanio, Ancona, Italy, on October 19, 1956. In 1981, he graduated from the University of Ancona with a degree in medicine and surgery and, subsequently, specialized in infectious and tropical diseases at the University of Messina. He worked as a general practitioner and began organizing trips abroad to help poor populations, especially in Africa. In 1993, he became a WHO consultant for control of parasitic diseases and conducted numerous missions in Africa. In 1996, he was appointed as a coordinator of a Médecins Sans Frontières (MSF, of which he was a member) project designed to control parasitic diseases in Cambodia and lived with his entire family in Phnom Penh until 1997. After returning to Italy, he resumed his work as assistant director of the Department of Infectious Diseases at Macerata Hospital, was increasingly involved in MSF missions, and became a WHO consultant for the Western Pacific area. In 1999, he was appointed president of MSF Italia and was a member of the delegation that received the Nobel Peace Prize in Oslo, Norway, that same year.

In 2000, Dr. Urbani made a decision that changed his life; he declined the directorship at Macerata Hospital and accepted an appointment as a WHO expert for the Western Pacific region. He left Italy and moved to Hanoi, Vietnam. Highly aware of the importance of this appointment, which enabled him to assist countries in the region with their efforts to control parasitic diseases, he traveled frequently on missions to critical areas in China, Laos, Cambodia, and the Philippines.

Author affiliation: University of Genoa, Genoa, Italy

DOI: https://doi.org/10.3201/eid2909.212412

Dr. Urbani was the first WHO doctor to identify SARS in Vietnam, which occurred in a businessman from America who was hospitalized in Hanoi in 2003. SARS cases had been identified earlier in Guangdong Province, China, and exported cases led to hospitalizations in Hong Kong before the first case in Vietnam. One of those patients was hospitalized in Hong Kong on February 17, 2003, after returning from Guangdong Province and had infected close contacts, including healthcare workers and a doctor from that province; the doctor was admitted to an intensive care unit with severe pneumonia on February 22. On February 28, 2003, Dr. Urbani was notified by the Hanoi French Hospital about a patient who was hospitalized with atypical pneumonia. He visited the hospital on Monday, March 3, and realized that he was facing a new, severe, and highly contagious disease. He learned that the patient from the United States had recently stayed at a Hong Kong hotel, where other guests had also been infected; this connection represented the beginning of the international spread of the virus.

Several sources in the scientific literature have indicated that Dr. Urbani understood the situation

was critical not only for the hospital staff but also for the entire community because of further contagion risk. However, no one (including Dr. Urbani) would have likely concluded that the situation was critical for the entire community merely from examining the index patient in Vietnam. Indeed, a sporadic case of severe pneumonia in a healthy adult would not raise the alarm of an impending global pandemic, which was what SARS actually became, although it was fortunately contained by rapid and vigorous intervention from WHO. What would have alerted Dr. Urbani to the unusual nature of this disease was the anomalous cluster of severe pneumonia cases that occurred after the index case, especially in young healthcare workers.

Dr. Urbani alerted the government and WHO about the gravity of the situation and possible risks, urging prompt implementation of measures necessary to prevent disease transmission. All infected patients with pneumonia in the Hanoi hospital were isolated, infection control measures were implemented, and the hospital was cordoned off by security guards. On Sunday, March 9, 2003, Dr. Urbani and a WHO representative, Pascale Brudon, called for urgent action against the dangerous new illness, and the Vice Minister of Health in Vietnam immediately assigned a local team to review the situation at the Hanoi French Hospital. A crucial decision was the appointment of 2 experts to help investigate and control the outbreak: Hitoshi Oshitani, WHO's regional adviser for Communicable Disease Surveillance and Response, arrived on March 10 to head the WHO team, and Tim Uyeki, an influenza expert from the US Centers for Disease Control and Prevention (CDC), arrived on March 11.

On March 11, while flying from Hanoi to Bangkok, Thailand, Dr. Urbani noticed that he had what he believed to be the first symptoms of SARS. Upon his arrival at the Bangkok airport, he warned colleagues who had come to pick him up to keep their distance and asked to be immediately placed in hospital isolation. He asked Scott Dowell from the CDC's Emerging Infections Program to take 2 swab samples to ensure a good sample was obtained, which became a source of some of the first CDC isolates of SARS-CoV, the cause of SARS.

In Hanoi, Ms. Brudon, Dr. Oshitani, and Dr. Uyeki held an emergency meeting on March 12 with the Vietnam Vice Minister of Health and the director of the National Institute of Hygiene and Epidemiology to discuss recommendations for controlling the outbreak. On March 15, WHO declared that the disease identified by Dr. Urbani was a world health threat, and Ms. Brudon persuaded local authorities to adopt adequate quarantine measures and close the country's ports and borders to curb virus spread. Over the next days, specialists in epidemiology from around the world, including CDC, traveled to Hanoi to join the WHO Vietnam SARS team to help contain and study the outbreak.

On March 29, 2003, after 19 days in isolation, Dr. Urbani died. His dedication to science prompted him to authorize samples of his lung tissues to be collected postmortem and used for research purposes. Dr. Urbani was 1 of ≈80 persons in Vietnam, including many healthcare workers, whose SARS-CoV infections were linked back to the businessman from the United States. At the end of the outbreak, 774 deaths were attributed to SARS worldwide.

The fact that Dr. Urbani immediately reported the first outbreak of SARS in Vietnam was of fundamental importance not only to the local community but also worldwide. His timely action enabled prompt global surveillance of SARS cases, which meant that many patients were identified and isolated before hospital staff could be infected and, above all, before the outbreak of SARS could snowball into a pandemic, which occurred in 2020 for SARS-CoV-2. On April 8, 2003, UN Secretary General Kofi Annan said, "Dr. Carlo Urbani dedicated his life to helping protect and save the lives of others. It was characteristic of his vigilance, professionalism, and expertise that he was instrumental in ensuring an early response by the international community to SARS. Had it not been for his recognition that the outbreak of the virus was something out of the ordinary, many more would have fallen victim to SARS. It was the cruelest of ironies that he lost his own life to SARS while seeking to safeguard others from the disease. Dr. Urbani leaves an inspiring legacy in the United Nations family and the global public health community. For his contribution on the front lines of the fight against disease, he will be remembered as a hero in the best and truest sense of the word."

About the Author

Dr. Martini is professor of history of medicine, medical humanities, public health ethics, and hygiene and a scientific advisor for the Unesco Chair of anthropology of health, biosphere, and healing system at the University of Genoa. His research interests focus on medical humanities, history of epidemiology, infectious diseases, hygiene, public health, ethics, and history of vaccines.

Suggested Reading

1. Centers for Disease Control and Prevention. Update: outbreak of severe acute respiratory syndrome—worldwide, 2003. MMWR Morb Mortal Wkly Rep. 2003;52:241–8.
2. Desenclos JC, van der Werf S, Bonmarin I, Levy-Bruhl D, Yazdanpanah Y, Hoen B, et al. Introduction of SARS in France, March–April, 2003. Emerg Infect Dis. 2004;10:195–200. https://doi.org/10.3201/eid1002.030351
3. Fleck F. Carlo Urbani (obituary). BMJ. 2003;326:825. https://doi.org/10.1136/bmj.326.7393.825
4. World Health Organization. Summary of probable SARS cases with onset of illness from 1 November 2002 to 31 July 2003 [cited 2022 Dec 15]. https://www.who.int/csr/sars/country/table2004_04_21/
5. Centers for Disease Control and Prevention. Emerging infections program [cited 2023 Jan 15]. https://www.cdc.gov/ncezid/dpei/eip/index.html
6. Mahase E. Covid-19: quarantine works when introduced early alongside other measures, finds review. BMJ. 2020;369:m1450. https://doi.org/10.1136/bmj.m1450
7. Meletti J. Il medico del mondo. Vita e morte di Carlo Urbani. Milan: IL Saggiatore; 2004.
8. Oransky I. Carlo Urbani (obituary). Lancet. 2003;361:1481. https://doi.org/10.1016/S0140-6736(03)13107-8
9. Ksiazek TG, Erdman D, Goldsmith CS, Zaki SR, Peret T, Emery S, et al; SARS Working Group. A novel coronavirus associated with severe acute respiratory syndrome. New Engl J Med. 2003;348:1953–66. https://doi.org/10.1056/NEJMoa030781
10. World Health Organization. SARS: how a global epidemic was stopped. June 15, 2006 [cited 2023 Jan 15] https://www.who.int/publications/i/item/sars-how-a-global-epidemic-was-stopped

Address for correspondence: Mariano Martini, Department of Health Sciences, University of Genoa, Via Pastore, n.1, Genoa 16132, Italy; email: mariano.martini@unige.it

Group A *Streptococcus* Meningitis in Adults, Denmark

Henrik Nielsen, Merete Storgaard, Jannik Helweg-Larsen, Lykke Larsen, Micha P.G. Jepsen, Birgitte R. Hansen, Lothar Wiese, Jacob Bodilsen

Aalborg University Hospital, Aalborg, Denmark (H. Nielsen, J. Bodilsen); Aalborg University, Aalborg (H. Nielsen, J. Bodilsen); Aarhus University Hospital, Aarhus, Denmark (M. Storgaard); Rigshospitalet, Copenhagen, Denmark (J. Helweg-Larsen); Odense University Hospital, Odense, Denmark (L. Larsen); Nordsjællands Hospital, Hillerød, Denmark (M.P.G. Jepsen); Hvidovre University Hospital, Hvidovre, Denmark (B.R. Hansen); Zealand University Hospital, Roskilde, Denmark (L. Wiese)

DOI: http://doi.org/10.3201/eid2909.230627

We report a 21-fold increase in group A *Streptococcus* meningitis in adults in Denmark during October 13, 2022–April 12, 2023, concurrent with an outbreak of invasive streptococcal disease. We describe clinical characteristics of the outbreak cases and prognosis for patients in comparison to those for previous sporadic cases.

Emergence of increased group A *Streptococcus* (GAS) disease, initially expressed as activity of scarlet fever in childhood, has been observed in multiple countries; some countries reported the toxigenic $M1_{UK}$ clone (*1*–*3*). A report from the Netherlands suggested an increase in GAS meningitis cases, mainly from the toxicogenic $M1_{UK}$ lineage (*4*). This increase is likely result of the rise in invasive GAS infections (*5*), because ≈1% of invasive GAS manifests as meningitis (*6*). However, it is unclear if this outbreak differs clinically from previous sporadic cases, as acknowledged by van der Putten et al. (*4*). To address this limitation, we compared all cases of GAS meningitis in adults in Denmark during 2015–2022 with cases during the outbreak, October 2022–April 2023.

The Danish Study Group for Infections of the Brain (DASGIB) has performed active, real-time nationwide surveillance of community-acquired bacterial meningitis in adults (≥18 years of age) since January 1, 2015, as described previously (*7*). In brief, data on demographics, comorbidities, clinical signs and symptoms, microbiology and biochemical examinations, radiology, treatment, and outcome are aggregated in an online platform. The legal department of the North Denmark Region (record no. 2023-012693) and the Danish Board of Health (record nos. 3-3013-2579/1 and 3-3013-3168/1) approved the DASGIB database. Patient consent or permission from an ethical committee is not required.

For this study, a definition of GAS meningitis required (*7*) clinical symptoms suggestive of bacterial meningitis (e.g., headache, neck stiffness, fever,

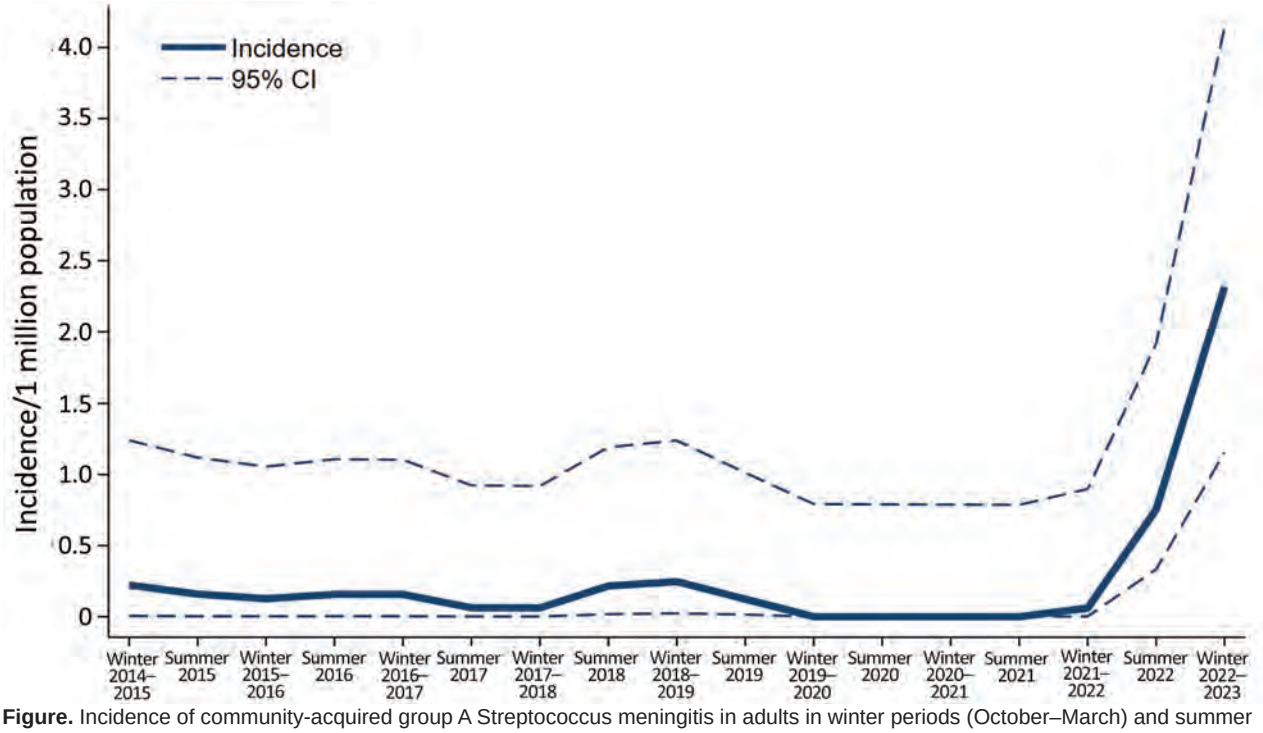

Figure. Incidence of community-acquired group A Streptococcus meningitis in adults in winter periods (October–March) and summer periods (April–September), Denmark, January 1, 2015–2023, illustrating outbreak during October 13, 2022–April 12, 2023.

Table. Characteristics of adults with community-acquired group A streptococcal meningitis, Denmark, 2015–2023

Characteristic	Jan 1, 2015–Oct 12, 2022	Oct 13, 2022–Apr 13, 2023	p value†
Total no. cases	8	11	
Age	57 (35–66)	58 (40–69)	0.53
Sex, no. (%)			
M	5 (62)	7 (64)	
F	3 (38)	4 (36)	1.0
Comorbidity, no. (%)	0	4 (36)	0.09
Duration of symptoms, d	5.5 (1–7)	2 (1–4)	0.35
Glasgow Coma Score‡	15 (15–15)	13 (11–15)	0.01
Temperature	37.7 (37.0–39.0)	39.1 (37.7–39.4)	0.23
Systolic blood pressure	131 (113–136)	125 (119–125)	0.25
Ear-nose-throat focus, no. (%)	7 (88)	9 (82)	1.0
C-reactive protein, mg/L	305 (228–367)	216 (105–313)	0.46
Time until lumbar puncture, h	3.0 (1.8–3.6)	2.2 (1.6–7.8)	0.85
CSF leukocytes, 10^6 cells/L	111 (40–385)	1,726 (534–3,990)	0.03
CSF protein, g/L	1.7 (0.7–3.2)	1.6 (0.9–2.6)	0.79
CSF culture positive, no. (%)	3 (38)	3 (27)	1.0
Bacteremia, no. (%)	5 (63)	7 (64)	1.0
Time until antimicrobial drugs, h	3.7 (1.7–7.0)	4.4 (0.3–12.3)	0.95
Dexamethasone, no. (%)	8 (100)	8 (73)	0.23
Intensive care unit stay, no. (%)	4 (50)	7 (64)	0.66
Progressive or new neurologic deficits, no. (%)	3 (38)	1 (9)	0.26
Seizures, no. (%)	2 (25)	1 (9)	0.55
Septic shock, no. (%)	3 (38)	1 (9)	0.26
Death, no. (%)	1 (13)	1 (9)	1.0

*Values are median (IQR) except as indicated. CSF, cerebrospinal fluid; IQR, interquartile range.
†p value determined by Fisher exact test for categorial variables and Mann-Whitney rank sum test for continuous variables.
‡Glasgow Coma Score based on eye opening (*1–4*), verbal response (*1–5*) and motor response (*1–6*), maximum 15 points.

altered mental status) and either of the following criteria: positive culture or bacterial DNA/antigen analysis of cerebrospinal fluid (CSF); positive blood culture and CSF leukocytes >10 × 10^6 cells/L; or culture-confirmed otitis or mastoiditis and CSF leukocytes >10 × 10^6 cells/L. Incidence was computed as no. cases/no. adults in Denmark during each study period.

During January 1, 2015–October 12, 2022, we observed a total of 8 cases of GAS meningitis, corresponding to a mean of 0.11/1 million adults/6 months (Figure). Because of the increase in invasive GAS in Denmark beginning in October 2022 (*8*), we then assessed the incidence of GAS meningitis during October 13, 2022–April 12, 2023. We observed 11 cases of GAS meningitis in adults, corresponding to 2.32/1 million/6 months, an increase in incidence by a factor of 21. The diagnosis was confirmed by culture in 9 patients, whereas it was established by PCR in 2 patients for whom antimicrobial treatment began before lumbar puncture. We examined isolates of *emm*-1.0 type in 4 cases, *emm*-12.0 in 2 cases, and *emm*-87.0 in 1 case; isolate type was not available in 2 cases.

Patients with GAS meningitis had lower Glasgow Coma Scale scores at admission and higher CSF leukocyte counts in the last 6 months of the study than overall (Table); otherwise, clinical characteristics and prognosis did not differ between the 2 study periods. We observed a high percentage of patients with streptococcal infection in the upper respiratory tract (Table). We observed 2 serious complications, endophthalmitis (1 case) and subdural empyema (1 case), but no increase in deaths in the second study period.

We conclude that in October 2022–April 2023, an outbreak of GAS meningitis occurred in Denmark, showing a 21-fold increase in incidence compared with the baseline in previous years. The baseline incidence agrees with earlier findings in Denmark (*9*). Our case definition included cases confirmed by positive PCR of CSF, positive blood cultures or other cultures combined with CSF pleocytosis, and clinical manifestations of bacterial meningitis, in addition to positive CSF culture, which may explain why our incidence is higher than that recently reported for adults from the Netherlands (*4*).

The rise in invasive GAS infections was initially seen in children (*5*), but our study indicates an increase of severe infections in adults as well. The toxicogenic *emm*-1.0 type is currently the predominant strain in Denmark (*8*) and other countries (*4*,*5*). However, we found no differences in clinical characteristics or prognosis for GAS meningitis during this surge compared with those of previous years.

About the Author

Dr. Nielsen is a clinical professor of infectious diseases at Aalborg University Hospital, Aalborg, Denmark. His research interest is infections in the brain, including bacterial meningitis.

References

1. Lynskey NN, Jauneikaite E, Li HK, Zhi X, Turner CE, Mosavie M, et al. Emergence of dominant toxigenic M1T1 *Streptococcus pyogenes* clone during increased scarlet fever activity in England: a population-based molecular epidemiological study. Lancet Infect Dis. 2019;19:1209–18. https://doi.org/10.1016/S1473-3099(19)30446-3
2. Demczuk W, Martin I, Domingo FR, MacDonald D, Mulvey MR. Identification of *Streptococcus pyogenes* $M1_{UK}$ clone in Canada. Lancet Infect Dis. 2019;19:1284–5. https://doi.org/10.1016/S1473-3099(19)30622-X
3. Li Y, Nanduri SA, Van Beneden CA, Beall BW. $M1_{UK}$ lineage in invasive group A streptococcus isolates from the USA. Lancet Infect Dis. 2020;20:538–9. https://doi.org/10.1016/S1473-3099(20)30279-6
4. van der Putten BCL, Vlaminckx BJM, de Gier B, Freudenburg-de Graaf W, van Sorge NM. Group A streptococcal meningitis with the $M1_{UK}$ variant in the Netherlands. JAMA. 2023;329:1791–2. 10.1001/jama.2023.5927 https://doi.org/10.1001/jama.2023.5927
5. Guy R, Henderson KL, Coelho J, Hughes H, Mason EL, Gerver SM, et al. Increase in invasive group A streptococcal infection notifications, England, 2022. Euro Surveill. 2023;28:2200942. https://doi.org/10.2807/1560-7917.ES.2023.28.1.2200942
6. Davies HD, McGeer A, Schwartz B, Green K, Cann D, Simor AE, et al.; Ontario Group A Streptococcal Study Group. Invasive group A streptococcal infections in Ontario, Canada. N Engl J Med. 1996;335:547–54. https://doi.org/10.1056/NEJM199608223350803
7. Bodilsen J, Larsen L, Brandt CT, Wiese L, Hansen BR, Andersen CØ, et al. Existing data sources for clinical epidemiology: the Danish Study Group of Infections of the Brain Database (DASGIB). Clin Epidemiol. 2021;13:921–33. https://doi.org/10.2147/CLEP.S326461
8. Statens Serum Institut. Increase in the number of group A streptococcal infections. 2023 [cited 2023 Jun 29]. https://www.ssi.dk/sygdomme-beredskab-og-forskning/sygdomsudbrud/streptokker
9. Kjærgaard N, Bodilsen J, Justesen US, Schønheyder HC, Andersen CØ, Ellermann-Eriksen S, et al.; DASGIB Study Group. Community-acquired meningitis caused by beta-haemolytic streptococci in adults: a nationwide population-based cohort study. Eur J Clin Microbiol Infect Dis. 2019;38:2305–10. https://doi.org/10.1007/s10096-019-03678-w

Address for correspondence: Henrik Nielsen, Department of Infectious Diseases, Aalborg University Hospital, 18 Hobrovej, DK9000 Aalborg, Denmark; email: henrik.nielsen@rn.dk

Patient Characteristics During Early Transmission of SARS-CoV-2, Palau, January 13–February 24, 2022

Braiden Eilers, Myra D. Adelbai-Fraser, Johnrey R. Collado, Miriam Van Dyke, Melanie Firestone, Angie S. Guinn, Michael T. Dillon, Richard Brostrom, Michael H. Kinzer, Nick Muñoz, Kazuhiro Okumura, Vance Brown, Oluwatomiloba Ademokun, Ritter Udui, Gaafar J. Uherbelau, W. Thane Hancock

Author affiliations: Centers for Disease Control and Prevention, Atlanta, Georgia USA (B. Eilers, M. Van Dyke, M. Firestone, A.S. Guinn, M.T. Dillon, R. Brostrom, M.H. Kinzer, V. Brown, O. Ademokun, W.T. Hancock); Palau Ministry of Health and Human Services, Koror, Palau (M.D. Adelbai-Fraser, J.R. Collado, R. Udui, G.J. Uherbealu); US Department of Health and Human Services, Washington, DC, USA (N. Muñoz, K. Okumura)

DOI: https://doi.org/10.3201/eid2909.230182

Palau had no reported evidence of COVID-19 community spread until January 2022. We chart reviewed hospitalized patients who had a positive SARS-CoV-2 test result during early community transmission. Booster vaccinations and early outpatient treatment decreased hospitalizations. Inadequate hospital infection control practices contributed to iatrogenic COVID-19 and preventable deaths.

Palau is a Pacific Island country that has a population of ≈17,500 persons (*1*). This country has a small health system, remote location, and high prevalence of chronic disease (*2*), which made it exceptionally vulnerable to the effects of COVID-19. Palau took extraordinary steps to prevent the introduction of SARS-CoV-2 by initially closing borders in March 2020 and later transitioning to strict testing and quarantine procedures. The country also expanded testing capacity, maximized vaccinations, and acquired novel COVID-19 therapeutics.

In July 2021, Palau discontinued its mandatory travel quarantine after 95% of the population ≥18 years of age were fully vaccinated against COVID-19. Limited SARS-CoV-2 infections were soon identified in travelers, but no cases of community transmission were documented until January 13, 2022, when community transmission of SARS-CoV-2 (Omicron BA.1.1) was confirmed. At that time, 98% of the eligible population was fully vaccinated and 31% had received a booster vaccination within the previous 2 months.

Cases increased rapidly (859 in the first 2 weeks), and the first known COVID-19 related hospitalization occurred on January 20, 2022. Rapid antigen testing was offered at a central location and rurally by mobile teams. The Community COVID-19 Care Center (C4) was established to immediately evaluate patients who tested positive for SARS-CoV-2 and, if indicated, provided a novel COVID-19 therapeutic (monoclonal antibody sotrovimab or antiviral drugs molnupiravir or nirmatrelvir/ritonavir) as outpatient treatment. Persons who had abnormal vital signs or severe symptoms were referred to the emergency department.

At Belau National Hospital, the only hospital in Palau, all patients were tested for COVID-19 at admission, and periodic surveillance testing was conducted on patients admitted for non–COVID-19 health conditions. We examined characteristics of all hospitalized patients who had a positive SARS-CoV-2 test result during the early surge of COVID-19 community transmission, January 13–February 24, 2022. During that period, Palau identified 3,656 patients who had SARS-CoV-2 infection; 57 (1.6%) were hospitalized. We abstracted patient information on demographics, concurrent conditions, vaccination status, oxygen requirement, treatment, and disposition.

Of the 57 hospitalized patients, more were female (32 [56%]) than male (25 [44%]) ; 28 (49%) were ≥65 years of age. Four (7%) patients were children <5 years of age, including 1 infant born to a mother who had COVID-19 and who tested positive on the first day of life. Fifty-two (91%) patients had ≥1 known medical condition, putting them at risk for severe COVID-19 (*3*); 29 (51%) patients had ≥4 risk factors (≥65 years of age or medical conditions), putting them at higher risk for severe COVID-19. The 5 (9%) patients who did not have concurrent conditions were the 4 hospitalized children and 1 adult (30–40 years of age).

Twenty-seven (47%) hospitalized patients were unvaccinated or incompletely vaccinated (5 patients had partial primary vaccination; 4 patients were ineligible for vaccination because they were <5 years old). Twenty (35%) patients had completed their primary vaccination but had not received an appropriate booster (15 patients were eligible for a booster at the time of COVID-19 diagnosis). Ten (18%) had completed their primary vaccination with an appropriate booster (≥14 days before COVID-19 diagnosis).

Eighteen (32%) patients required oxygen supplementation during hospitalization. Of those, 4 required high-flow nasal cannula; all were unvaccinated. Although some patients met criteria for intubation, none were mechanically ventilated because of their goals of care.

Seven patients died during hospitalization; 1 death was deemed not related to COVID-19 disease and excluded from the death analysis. Of the 6 (11%) COVID-19 related deaths, 4 (67%) patients were unvaccinated and 2 (33%) had completed primary vaccination but had not received an appropriate booster. All patients who had COVID-19–related deaths had ≥2 risk factors for developing severe disease. All required oxygen supplementation.

A total of 29 (50%) patients were hospitalized primarily because of COVID-19 pneumonia; 3 of those patients died. Ten patients received remdesivir during their admission. Only 1 patient who received treatment from the C4 returned for admission because of worsening symptoms; that patient survived.

A total of 20 (35%) patients were determined to have hospital-acquired SARS-CoV-2 infection because they tested negative on admission but later tested positive during their hospitalization. Three of those patients died. Eight of the hospital-acquired infections were long-term hospital admissions (Palau has no skilled nursing facilities); 5 patients were unvaccinated, and 1 died.

This analysis characterized hospitalized patients who had SARS-CoV-2 infections in a recently exposed Pacific Islander population that had high rates of chronic illness but excellent COVID-19 immunization coverage and good access to testing and COVID-19 therapeutics. Booster vaccinations appear protective because the risk for hospitalization with COVID-19 was crudely estimated to be 18.6 times higher for unvaccinated persons than for persons who had completed primary vaccination and an appropriate booster. There were no deaths for any of the COVID-19 patients who received novel COVID-19 therapeutics at the C4, suggesting that therapy at time of diagnosis provided additional protection against severe disease. The large proportion of hospital-acquired infections and subsequent preventable deaths highlighted inadequate infection control practices and motivated revision of hospital protocols.

Acknowledgments

We thank the patients for participating in this study; Catherine Decherong, Edolem Ikerdeu, Antonnette Merur, Mere Cama, Clarette Matlab, and Ngirachisau Mekoll for providing assistance; and staff of Belau National Hospital, the outpatient clinics, and the Palau Ministry of Health and Human Services for working diligently to protect the health of all Palauans.

About the Author

Dr. Eilers is an epidemic intelligence service officer, emergency medicine physician, and epidemiologist in the Global Health Center, Centers for Disease Control and Prevention, Atlanta, GA. Her primary research interests are global health and outbreak prevention and management.

References

1. Office of Planning and Statistics. 2020 Census of population and housing of the Republic of Palau, volume: basic tables. 2022 [cited 2022 Nov 4]. https://www.palaugov.pw/wp-content/uploads/2022/09/2020-Census-of-Population-and-Housing.pdf
2. Watson BM, Chiang C, Ikerdeu E, Yatsuya H, Honjo K, Mita T, et al. Profile of non-communicable disease risk factors among adults in the Republic of Palau: findings of a national STEPS survey. Nagoya J Med Sci. 2015; 77:609–19.
3. Centers for Disease Control and Prevention. COVID-19: people with certain medical conditions. October 19, 2022 [cited 2023 Jun 25]. https://www.cdc.gov/coronavirus/2019-ncov/need-extra-precautions/people-with-medical-conditions.html

Address for correspondence: Braiden Eilers, Centers for Disease Control and Prevention, 1600 Clifton Rd NE, Mailstop H21-1, Atlanta, GA, 30329-4027, USA; email: riq4@cdc.gov

Partial Genome Characterization of Novel Parapoxvirus in Horse, Finland

Jenni Virtanen, Maria Hautaniemi, Lara Dutra, Ilya Plyusnin, Katja Hautala, Teemu Smura, Olli Vapalahti, Tarja Sironen, Ravi Kant, Paula M. Kinnunen

Author affiliations: University of Helsinki, Helsinki, Finland (J. Virtanen, L. Dutra, I. Plyusnin, K. Hautala, T. Smura, O. Vapalahti, T. Sironen, R. Kant, P.M. Kinnunen), Finnish Food Authority, Helsinki (M. Hautaniemi), Medical University of Gdansk, Gdynia, Poland (R. Kant)

DOI: https://doi.org/10.3201/eid2909.230049

We report a sequencing protocol and 121-kb poxvirus sequence from a clinical sample from a horse in Finland with dermatitis. Based on phylogenetic analyses, the virus is a novel parapoxvirus associated with a recent epidemic; previous data suggest zoonotic potential. Increased awareness of this virus and specific diagnostic protocols are needed.

Parapoxviruses (PPVs) usually cause contagious skin infections in ruminants and occasionally infect other species such as humans (*1*). The genus *Parapoxvirus* encompasses the following recognized species: Orf virus, bovine papular stomatitis virus, pseudocowpoxvirus, red deerpox virus, and grey sealpox virus (GSEPV) (*2*). All of those, except GSEPV and deerpox virus, are zoonotic. PPV genomes are usually 130–140 kb (*2*). Recently, poxviruses have emerged in humans and horses (*3*,*4*).

A severe infection caused by a parapox-like virus (F14.1158H) was first verified from a horse euthanized in Finland in 2013 (*5*). According to the short sequences (1.1 kb in total) obtained from envelope phospholipase (open reading frame [ORF] 011) and RNA polymerase subunit RPO147 (ORF056) genes, F14.1158H is most closely related to PPVs and is similar to the 585-bp sequences detected in lesions from humans after contact with horses and donkeys in the United States (*5*,*6*). However, the actual classification remained unclear because of limited sequence data and lack of amplification in numerous PPV PCR assays (*5*). No other clinical cases were confirmed until 2022, when an epidemic of dermatitis emerged in horses across Finland. PPV infection was subsequently identified in several cases using pan-PPV PCR (*7*) and Sanger sequencing (Appendix, https://wwwnc.cdc.gov/EID/article/29/9/23-0049-App1.pdf). Partial ORF011 sequences were 97% identical to the sequences from the 2013 case, with identity of 79%–87% to other PPVs (Appendix Table). This finding highlighted the need to properly characterize F14.1158H.

To better characterize the virus, we analyzed DNA extracted directly from a skin lesion of the 2013 equine case (*5*) and subjected it to next-generation sequencing with 2 different protocols (Appendix). The first protocol, relying on a pool of poxvirus primers, was insufficient to acquire enough sequence data. With a PCR-free approach, using enrichment of the viral DNA, we acquired as much as 121 kb of nucleotide sequence, almost the full genome, with coverage values of ≈100 in 5 contigs (BioProject no. PRJNA922554; GenBank accession nos. OQ248663–7). We noted the overall guanine-cytosine content to be 68.4%, which is similar to that

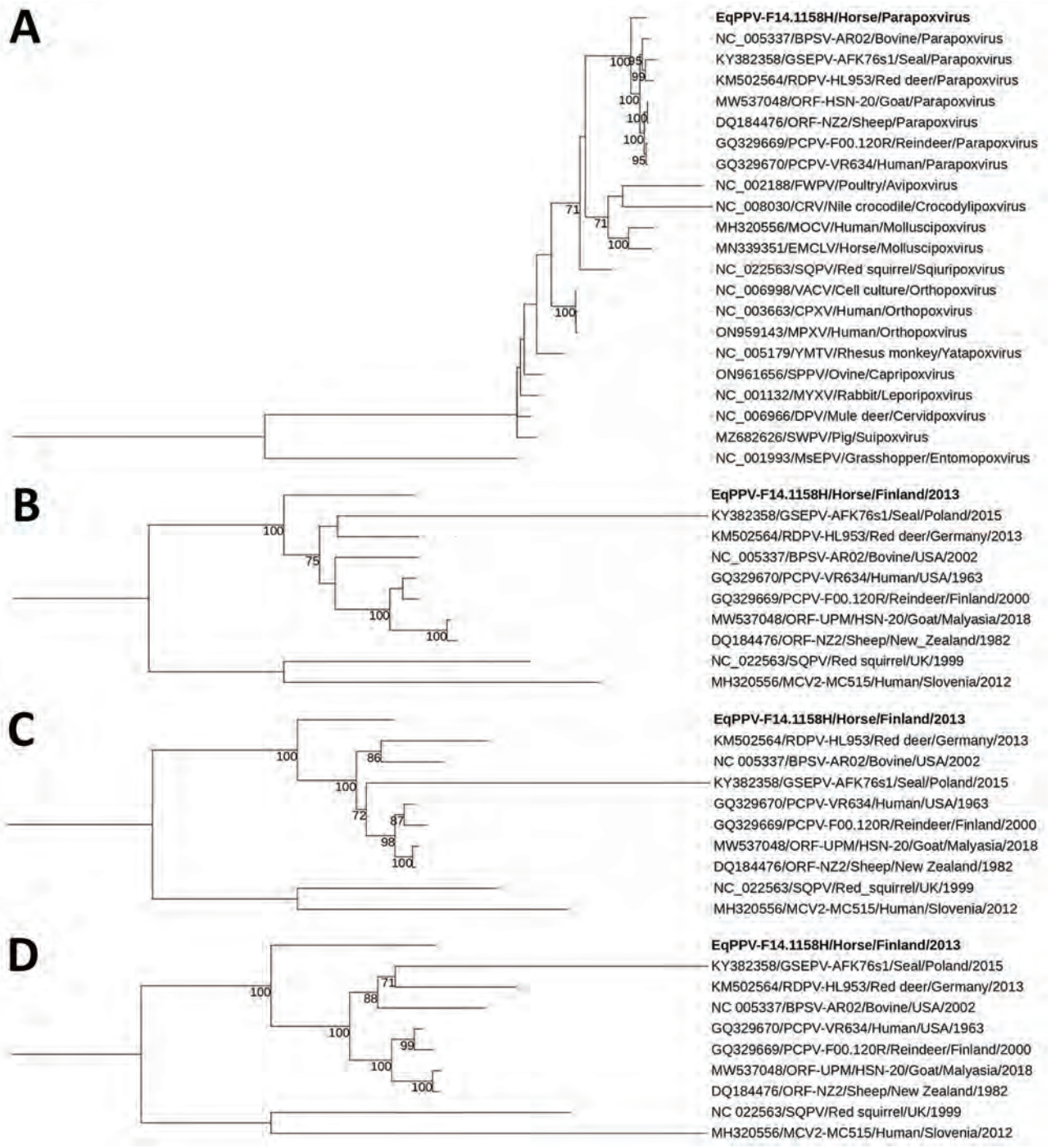

Figure. Phylogenies of PPV isolate F14.1158H from a skin lesion of an infected horse in Finland, 2013. A) Grouping of F14.1158H among all the genera of the subfamily Chordopoxvirinae in a phylogenetic tree based on amino acid sequences of the DNA polymerase (ORF025) gene. B–D) Grouping of F141158H among the genus *Parapoxvirus* in phylogenetic trees based on the nucleotide sequences of the early transcription factor (ORF083) (B), RNA polymerase (ORF101) (C), and topoisomerase 1 (ORF062) (D) genes. Bootstrap values >70% are shown next to the nodes. GenBank accession numbers are provided for reference sequences. MsEPV is used as an outgroup in panel A and SQPV and MOCV in panels B–D. Findings indicate that F14.1158H represents a novel PPV, designated EqPPV. CPXV, cowpox virus; CRV, crocodilepox virus; DPV, deerpox virus; EMCLV, equine molluscum contagiosum-like virus; EqPPV, equine PPV; FWPV, fowlpox virus; MOCV, molluscum contagiosum virus; MPXV, monkeypox virus; MsEPV, melanoplus sanguinipes entomopoxvirus; MYXV, myxoma virus; ORF, open reading frame; PPV, parapoxvirus; SPPV, sheeppox virus; SQPV, squirrelpox virus; SWPV, swinepox virus; VACV, vaccinia virus; YMTV, yaba monkey tumor virus.

of PPVs (*2*). We were unable to fully assemble and orient the data because we had no reference genome, a critical component in future investigations like ours. The lack of high-quality DNA and unsuccessful virus isolation attempts (Appendix) further complicated the sequencing process. In another study, researchers used a combination of short- and long-read sequencing to recover the full genome of the GSEPV (*8*). However, with our clinical sample, the small amount of DNA available for sequencing led to an alternative approach.

We conducted phylogenetic analysis for the following poxvirus core genes (*9*) (ORF numbers designated according to PPV ORFs) (*10*): DNA polymerase (ORF025), early transcription factor (ORF083), DNA-directed RNA polymerase subunit RPO132 (ORF101), and DNA topoisomerase type 1 (ORF062) (Figure). Consistent with earlier observations based on partial sequences of ORF11 and ORF056, F14.1158H grouped clearly closer to PPVs than other poxviruses (Figure, panel A), although distinctly separate from the 5 recognized species (Figure, panels B–D). We found the amino acid sequences to be more similar to PPV species than to other chordopoxviruses. For example, amino acid identity of DNA polymerase was 46%–60% between F14.1158H and viruses from other genera, 76%–80% between F14.1158H and PPVs, and 84%–95% among the previously recognized PPV species (Appendix Table 3). Within the PPVs, F14.1158H generally showed the second lowest pairwise nucleotide identity of the group (after the most divergent GSEPV) (Table); identities to other PPVs were 74%–83% (ORF025), 73%–83% (ORF083), 78%–87% (ORF101), and 84%–91% (ORF062). GSEPV was consistently furthest from F14.1158H, whereas F14.1158H identities to other

Table. Nucleotide identity comparison between the PPV isolate F14.1158H and other PPVs and *Molluscum contagiosum* virus in 4 selected core genes based on DNA extracted directly from a skin lesion of an infected horse in Finland, 2013*

	% Identity							
Core gene and virus	*Molluscum contagiosum* (MC515)	Grey sealpox	Red deerpox	Bovine papular stomatitis (AR02)	Orf (UPM/HSN-20)	Orf (NZ2)	Pseudocowpox (F00.120R)	Pseudocowpox (VR634)
DNA polymerase (ORF025)								
Grey sealpox	62	NA	NA	NA	NA	NA	NA	NA
Red deerpox	68	79	NA	NA	NA	NA	NA	NA
Bovine papular stomatitis (AR02)	68	79	86	NA	NA	NA	NA	NA
Orf (UPM/HSN-20)	69	79	87	87	NA	NA	NA	NA
Orf (NZ2)	69	79	87	87	99	NA	NA	NA
Pseudocowpox (F00.120R)	69	79	87	87	94	94	NA	NA
Pseudocowpox (VR634)	70	80	88	88	95	95	98	NA
F14.1558H	69	74	81	81	82	82	82	83
Early transcription factor (ORF083)								
Grey sealpox	65	NA	NA	NA	NA	NA	NA	NA
Red deerpox	73	80	NA	NA	NA	NA	NA	NA
Bovine papular stomatitis (AR02)	74	80	90	NA	NA	NA	NA	NA
Orf (UPM/HSN-20)	73	79	88	89	NA	NA	NA	NA
Orf (NZ2)	73	79	88	89	99	NA	NA	NA
Pseudocowpox (F00.120R)	74	80	90	91	95	95	NA	NA
Pseudocowpox (VR634)	74	80	90	91	95	95	98	NA
F14.1558H	74	78	87	87	86	86	87	87
RNA polymerase (ORF101)								
Grey sealpox	73	NA	NA	NA	NA	NA	NA	NA
Red deerpox	79	84	NA	NA	NA	NA	NA	NA
Bovine papular stomatitis (AR02)	80	85	93	NA	NA	NA	NA	NA
Orf (UPM/HSN-20)	80	86	93	93	NA	NA	NA	NA
Orf (NZ2)	80	86	93	93	100	NA	NA	NA
Pseudocowpox (F00.120R)	80	86	92	94	97	97	NA	NA
Pseudocowpox (VR634)	80	86	93	94	98	98	98	NA
F14.1558H	80	84	89	91	91	91	91	91
Topoisomerase 1 (ORF062)								
Grey sealpox	62	NA	NA	NA	NA	NA	NA	NA
Red deerpox	68	79	NA	NA	NA	NA	NA	NA
Bovine papular stomatitis (AR02)	68	79	86	NA	NA	NA	NA	NA
Orf (UPM/HSN-20)	69	79	87	87	NA	NA	NA	NA
Orf (NZ2)	69	79	87	87	99	NA	NA	NA
Pseudocowpox (F00.120R)	69	79	87	87	94	94	NA	NA
Pseudocowpox (VR634)	70	80	88	88	95	95	98	NA
F14.1558H	69	74	81	81	82	82	82	83

*Findings indicate that F14.1158H represents a novel PPV, designated equine PPV. NA, not applicable; ORF, open reading frame; PPV, parapoxvirus.

PPVs were similar. A relatively high difference explains why F14.1158H was not detected by several PCRs designed for detecting PPV, which should be considered when designing diagnostic protocols. These phylogenetic results and sequence identities, together with the high guanine and cytosine content and disease characteristics, indicate that F14.1158H represents a novel PPV, designated equine parapoxvirus (EqPPV). The final taxonomic position and the possible differences of human and equine-derived variants (*6*) will require more data.

Most known PPVs are zoonotic, and any novel virus detected in animals should be treated with concern (*6*). Thus, considering the tendency of PPVs to cause diseases in humans, EqPPV has a zoonotic potential. It is therefore important to sample humans and other animals in contact with infected horses. It is also critical to establish diagnostic protocols due to low specificity and sensitivity of pan-PPV PCR for EqPPV (Appendix). In terms of veterinary importance, this virus poses a threat for horses that could translate to financial losses for owners. The information provided here will inform development of proper diagnostic tools and also enable establishment of prevention measures.

Acknowledgments

We thank Niina Airas for her expert support regarding equine medicine. We also thank Mira Utriainen for technical assistance.

This study was financially supported by the Niemi Foundation, Finnish Foundation of Veterinary Research, and the Erkki Rajakoski Fund of Hippos Finland.

About the Author

Ms. Virtanen is a postdoctoral researcher at the University of Helsinki in the field of clinical microbiology. Her research interests include zoonotic viruses and pathogens in human–animal interface.

References

1. Essbauer S, Pfeffer M, Meyer H. Zoonotic poxviruses. Vet Microbiol. 2010;140:229–36. https://doi.org/10.1016/j.vetmic.2009.08.026
2. McInnes CJ, Damon IK, Smith GL, McFadden G, Isaacs SN, Roper RL, et al. ICTV virus taxonomy profile: *Poxviridae* 2023. J Gen Virol. 2023;104:00184. https://doi.org/10.1099/jgv.0.001849
3. Capobianchi MR, Di Caro A, Piubelli C, Mori A, Bisoffi Z, Castilletti C. Monkeypox 2022 outbreak in non-endemic countries: Open questions relevant for public health, nonpharmacological intervention and literature review. Front Cell Infect Microbiol. 2022;12:1005955. https://doi.org/10.3389/fcimb.2022.1005955
4. Ehmann R, Brandes K, Antwerpen M, Walter M, V Schlippenbach K, Stegmaier E, et al. Molecular and genomic characterization of a novel equine molluscum contagiosum-like virus. J Gen Virol. 2021;102:001357. https://doi.org/10.1099/jgv.0.001357
5. Airas N, Hautaniemi M, Syrjä P, Knuuttila A, Putkuri N, Coulter L, et al. Infection with possible novel parapoxvirus in horse, Finland, 2013. Emerg Infect Dis. 2016;22:1242–5. https://doi.org/10.3201/eid2207.151636
6. Osadebe LU, Manthiram K, McCollum AM, Li Y, Emerson GL, Gallardo-Romero NF, et al. Novel poxvirus infection in 2 patients from the United States. Clin Infect Dis. 2015;60:195–202. https://doi.org/10.1093/cid/ciu790
7. Inoshima Y, Morooka A, Sentsui H. Detection and diagnosis of parapoxvirus by the polymerase chain reaction. J Virol Methods. 2000;84:201–8. https://doi.org/10.1016/S0166-0934(99)00144-5
8. Günther T, Haas L, Alawi M, Wohlsein P, Marks J, Grundhoff A, et al. Recovery of the first full-length genome sequence of a parapoxvirus directly from a clinical sample. Sci Rep. 2017;7:3734. https://doi.org/10.1038/s41598-017-03997-y
9. Yu Z, Zhang W, Fu H, Zou X, Zhao M, Liang S, et al. Genomic analysis of Poxviridae and exploring qualified gene sequences for phylogenetics. Comput Struct Biotechnol J. 2021;19:5479–86. https://doi.org/10.1016/j.csbj.2021.09.031
10. Hautaniemi M, Ueda N, Tuimala J, Mercer AA, Lahdenperä J, McInnes CJ. The genome of pseudocowpoxvirus: comparison of a reindeer isolate and a reference strain. J Gen Virol. 2010;91:1560–76. https://doi.org/10.1099/vir.0.018374-0

Address for correspondence: Jenni Virtanen, Department of Veterinary Biosciences, Faculty of Veterinary Medicine, PO Box 66 00014 University of Helsinki, Helsinki, Finland; email: jenni.me.virtanen@helsinki.fi

Rickettsial Disease Outbreak, Mexico, 2022

Ricardo J. Estrada-Mendizabal, Oscar Tamez-Rivera, Emelina Hinojosa Vela, Paulina Blanco-Murillo, Cordelia Alanis-Garza, Jaime Flores-Gouyonnet, Jessica Suhail Sauceda Garza, Gloria Yolanda Carranza Medina, Lilia Elida García Rodriguez, Alma Rosa Marroquin Escamilla

Author affiliations: Tecnologico de Monterrey, Escuela de Medicina y Ciencias de la Salud, Monterrey, Mexico (R.J. Estrada-Mendizabal, O. Tamez-Rivera, P. Blanco-Murillo, C. Alanis-Garza); Secretary of Health of Nuevo Leon, Monterrey (E. Hinojosa Vela, J.S. Sauceda Garza, G.Y. Carranza Medina, L.E. Garcia Rodriguez, A.R. Marroquin Escamilla); Autonomous University of San Luis Potosi, San Luis Potosi, Mexico (J. Flores-Gouyonnet)

DOI: http://doi.org/10.3201/eid2909.230344

Beginning in 2022, Nuevo Leon, Mexico, experienced an outbreak of rickettsioses that is still ongoing despite multidisciplinary control efforts. A total of 57 cases have been confirmed, particularly affecting children. We report a high mortality rate among hospitalized persons in Nuevo Leon. Continuing efforts are required to control the outbreak.

Rickettsioses are life-threatening vectorborne infections transmitted by several arthropods, such as ticks, lice, fleas, and mites (*1*,*2*). Rickettsial diseases are an emerging threat in Mexico, particularly in the northern regions, where previous outbreaks have been reported (*3*). In 2022, the local epidemiologic surveillance department reported 57 confirmed and >500 probable rickettsial disease cases in Nuevo Leon, a semiarid state in northeast Mexico. This unprecedented and alarming increase represents the highest number of rickettsial disease cases in a single year in this region, showing significant contrast with 2021, when only 13 confirmed cases were reported. Although surveillance and preventive measures are continuously in place, additional multidisciplinary strategies were established after the outbreak was declared in May 2022.

The Mexican Institute of Epidemiology defines a probable case of rickettsiosis as a patient with fever and ≥2 compatible clinical and laboratory signs. Technicians at the State Laboratory of Public Health of Nuevo Leon perform real-time PCR targeting the *gltA* gene on all probable cases identified <7 days after symptom onset. A positive PCR result requires the presence of a well-defined sigmoid curve, where the 3 PCR-reaction phases are distinguished, plus a quantification cycle value ≤38. State laboratory staff use an indirect immunofluorescence antibody assay to analyze all samples collected 7–14 days after symptom onset and confirm cases through real-time PCR or, retrospectively, with seroconversion by immunofluorescence

Table. Clinical and paraclinical characteristics of patients with rickettsioses during outbreak in Neuvo Leon, Mexico, 2022

Characteristic	Total, n = 57	No. (%) patients		p value†
		Cured, n = 21	Died, n = 36	
Patient age, y				0.106
<4	8	1 (1.7)	7 (12.2)	
4–12	28	12 (21)	16 (28)	
13–18	8	1 (1.7)	7 (12.2)	
>18	13	7 (12.2)	6 (10.5)	
Patient sex				0.768
F	34	12 (21)	22 (38.5)	
M	23	9 (15.7)	14 (24.5)	
Clinical signs‡	n = 48	n = 14	n = 34	
Anemia				**0.012**
Yes	32	11 (22.9)	21 (43.7)	
No	16	3 (6.2)	13 (27)	
Thrombocytopenia				**0.007**
Yes	47	13 (27)	34 (70.8)	
No	1	1 (2)	0	
Leukocytosis				**0.01**
Yes	17	3 (6.2)	14 (29.1)	
No	31	11 (22.9)	20 (41.6)	
Leukopenia				**0.014**
Yes	4	2 (4.1)	2 (4.1)	
No	44	12 (25)	32 (66.6)	
Treatment with doxycycline				0.074
Yes	52	21 (36.8)	31 (54.3)	
No§	5	0	5 (8.7)	
Time to treatment initiation, h	n = 52	n = 21	n = 31	**0.007**
≤24	4	4 (7.6)	0	
>24	48	17 (32.6)	31 (59.6)	

*n values within columns indicate number of patients in category.
†By χ^2 test. Bold indicates statistical significance.
‡Anemia: female, hemoglobin <11.6 g/dL; male, hemoglobin <13.2 g/dL). Thrombocytopenia: female, platelets <157 × 10^9/L; male, platelets <135 × 10^9/L. Leukocytosis: leukocytes >9.6 × 10^9 cells/L. Leukopenia: leukocytes <3.4 × 10^9 cells/L.
§Five patients died before treatment and had their diagnosis confirmed by autopsy.

antibody analysis (*4*). The data discussed in this report comprise all 57 confirmed cases in 2022.

Compared with results from 2021, the incidence rate of rickettsioses in Nuevo Leon in 2022 rose from 0.2 to 0.9 cases/100,000 inhabitants. Most cases occurred in October (n = 14) and December (n = 9). The median patient age was 10 years (range 1–61 years); 59.6% of case-patients were female and 40.4% male. The pediatric population (≤18 years of age) represented 77% of all cases (Appendix Table, https://wwwnc.cdc.gov/EID/article/29/9/23-0344-App1.pdf). Most patients required hospitalization (n = 50), and all had a positive history of tick exposure within 2 weeks before symptom onset. More than half of cases (54%) originated in 2 remote municipalities of Nuevo Leon, where most patients had a positive contact history with stray dogs or cats. The most frequent clinical signs were fever (100%), petechial rash (56%), and tachycardia (40%) (Table). Predominant symptoms were headache (75%), abdominal pain (75%), myalgia (74%), and arthralgia (58%). Laboratory findings at hospital admission included anemia in 66% of case-patients, thrombocytopenia in 98% (median platelet count 25 × 10^3/μL), leukocytosis in 35%, and leukopenia in 8%.

Of the 57 case-patients, 52 were treated with doxycycline; the remaining 5 died before treatment and had their infections diagnosed through autopsy. The median time-to-treatment initiation from symptom onset was 4 days, and only 8% of the patients received prompt antibiotic therapy within the first 24 hours of symptom onset. More than half (63%) of the total case-patient population died, and median time from symptom onset to death was 5 days (range 2–17); median length of hospital stay was 1 day (range 0–41). The annual rickettsiosis mortality rate for the region was 0.6 deaths/100,000 inhabitants.

Figure. Brown dog ticks collected by the vector control department of Nuevo Leon, Mexico, in a hard-to-reach municipality.

To determine clinical, laboratory, and demographic associations with mortality, we performed χ^2 testing by using SPSS Statistics software (IBM, https://www.ibm.com). We found statistically significant associations with mortality in patients with anemia (p = 0.012), thrombocytopenia (p = 0.007), leukocytosis (p = 0.01), and leukopenia (p = 0.014) at hospital admission. Likewise, a time-to-treatment initiation of 24 hours was associated with survival (p = 0.007). Among the 57 cases, 4 were confirmed as spotted fever group rickettsiosis because of seroconversion to *Rickettsia rickettsii* antigens, 5 seroconverted to *R. typhi* and were confirmed as typhus group rickettsiosis, and the remaining 48 cases were tested by molecular analysis and were confirmed as simply rickettsiosis (*Rickettsia* sp.)—that is, PCR did not discriminate between spotted fever group and typhus group rickettsiae.

An alarming feature of this ongoing outbreak is its high fatality rate (63%). The most recent outbreaks of rickettsiosis in Mexico reported fatality rates of 40% in Sonora and 29% Baja California (*5*,*6*). In northeastern Mexico, the brown dog tick (*Rhipicephalus sanguineus*) is highly prevalent (Figure), posing a high risk for rickettsioses (*7*). Social determinants of health in hard-to-reach municipalities are thought to contribute to the rise in rickettsial disease cases. The abundance of stray animals, lack of healthcare accessibility, and poor disease knowledge may play a significant role in this outbreak.

To date, the local epidemiologic surveillance department has led various interventions in an attempt to control the outbreak by implementing vector control strategies, educating healthcare personnel of high-risk municipalities, designating community champions against rickettsioses, and raising public awareness through media. Clinicians on the Mexico–United States border should have a high index of suspicion of rickettsiosis among febrile patients and consider early empiric antibiotic treatment to reduce mortality risk.

The work on which this report is based was carried out at the Secretary of Health of Nuevo Leon.

About the Author

Mr. Estrada-Mendizabal is a senior medical student at Tecnologico de Monterrey, Escuela de Medicina y Ciencias de la Salud Nuevo Leon, Mexico. His research interests are in public health and infectious diseases, and he is currently undergoing a social service year at the healthcare jurisdictions management department of Nuevo Leon.

References

1. Zhang YY, Sun YQ, Chen JJ, Teng AY, Wang T, Li H, et al. Mapping the global distribution of spotted fever group rickettsiae: a systematic review with modelling analysis. Lancet Digit Health. 2023;5:e5–15. https://doi.org/10.1016/S2589-7500(22)00212-6
2. Fang R, Houhamdi L, Raoult D. Detection of *Rickettsia prowazekii* in body lice and their feces by using monoclonal antibodies. J Clin Microbiol. 2002;40:3358–63. https://doi.org/10.1128/JCM.40.9.3358-3363.2002
3. Álvarez-Hernández G, Roldán JFG, Milan NSH, Lash RR, Behravesh CB, Paddock CD. Rocky Mountain spotted fever in Mexico: past, present, and future. Lancet Infect Dis. 2017;17:e189–96. https://doi.org/10.1016/S1473-3099(17)30173-1
4. General de Epidemiologia D. Lineamientos para la Vigilancia por Laboratorio de las Rickettsiosis (2022). [cited 2023 April 08] https://www.gob.mx/cms/uploads/attachment/file/694561/LVL_Rickettsiosis_200122.pdf
5. Drexler NA, Yaglom H, Casal M, Fierro M, Kriner P, Murphy B, et al. Fatal Rocky Mountain spotted fever along the United States–Mexico border, 2013–2016. Emerg Infect Dis. 2017;23:1621–6. https://doi.org/10.3201/eid2310.170309
6. Straily A, Drexler N, Cruz-Loustaunau D, Paddock CD, Alvarez-Hernandez G. Notes from the field: community-based prevention of Rocky Mountain spotted fever—Sonora, Mexico, 2016. MMWR Morb Mortal Wkly Rep. 2016;65:1302–3. https://doi.org/10.15585/mmwr.mm6546a6
7. Salomon J, Fernandez Santos NA, Zecca IB, Estrada-Franco JG, Davila E, Hamer GL, et al. Brown dog tick (*Rhipicephalus sanguineus* Sensu Lato) infection with endosymbiont and human pathogenic *Rickettsia* spp., in northeastern México. Int J Environ Res Public Health. 2022;19:6249. https://doi.org/10.3390/ijerph19106249

Address for correspondence: Oscar Tamez-Rivera, Av. Batallon de San Patricio 112, Real San Agustin, 66278 San Pedro Garza Garcia, Neuvo Leon, Mexico; email: oscar.tamez@tec.mx

etymologia revisited

Zika [zēkə] Virus

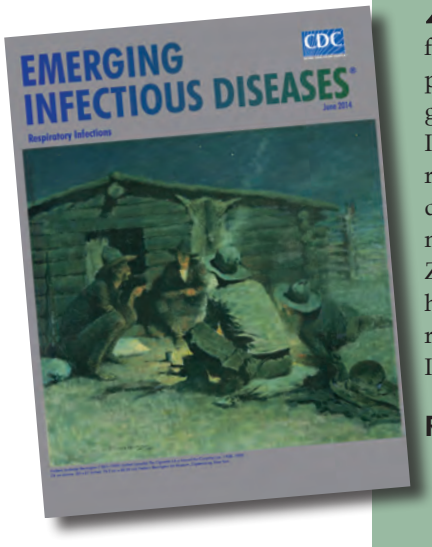

Originally published in June 2014

Zika virus is a mosquito-borne positive-sense, single-stranded RNA virus in the family *Flaviviridae*, genus *Flavivirus* that causes a mild, acute febrile illness similar to dengue. In 1947, scientists researching yellow fever placed a rhesus macaque in a cage in the Zika Forest (*zika* meaning "overgrown" in the Luganda language), near the East African Virus Research Institute in Entebbe, Uganda. A fever developed in the monkey, and researchers isolated from its serum a transmissible agent that was first described as Zika virus in 1952. It was subsequently isolated from a human in Nigeria in 1954. From its discovery until 2007, confirmed cases of Zika virus infection from Africa and Southeast Asia were rare. In 2007, however, a major epidemic occurred in Yap Island, Micronesia. More recently, epidemics have occurred in Polynesia, Easter Island, the Cook Islands, and New Caledonia.

References

1. Dick GW, Kitchen SF, Haddow AJ. Zika virus. I. Isolations and serological specificity. Trans R Soc Trop Med Hyg. 1952;46:509–20. http://dx.doi.org/10.1016/ 0035-9203 (52)90042-4
2. Hayes EB. Zika virus outside Africa. Emerg Infect Dis. 2009; 15:1347–50. http://dx.doi.org/10.3201/eid1509.090442
3. MacNamara FN. Zika virus: a report on three cases of human infection during an epidemic of jaundice in Nigeria. Trans R Soc Trop Med Hyg. 1954;48:139–45. http://dx.doi.org/10.1016/0035-9203(54)90006-1
4. Murphy JD. Luganda–English dictionary. Washington (DC): The Catholic University of America Press; 1972.

https://wwwnc.cdc.gov/eid/article/20/6/et-2014_article

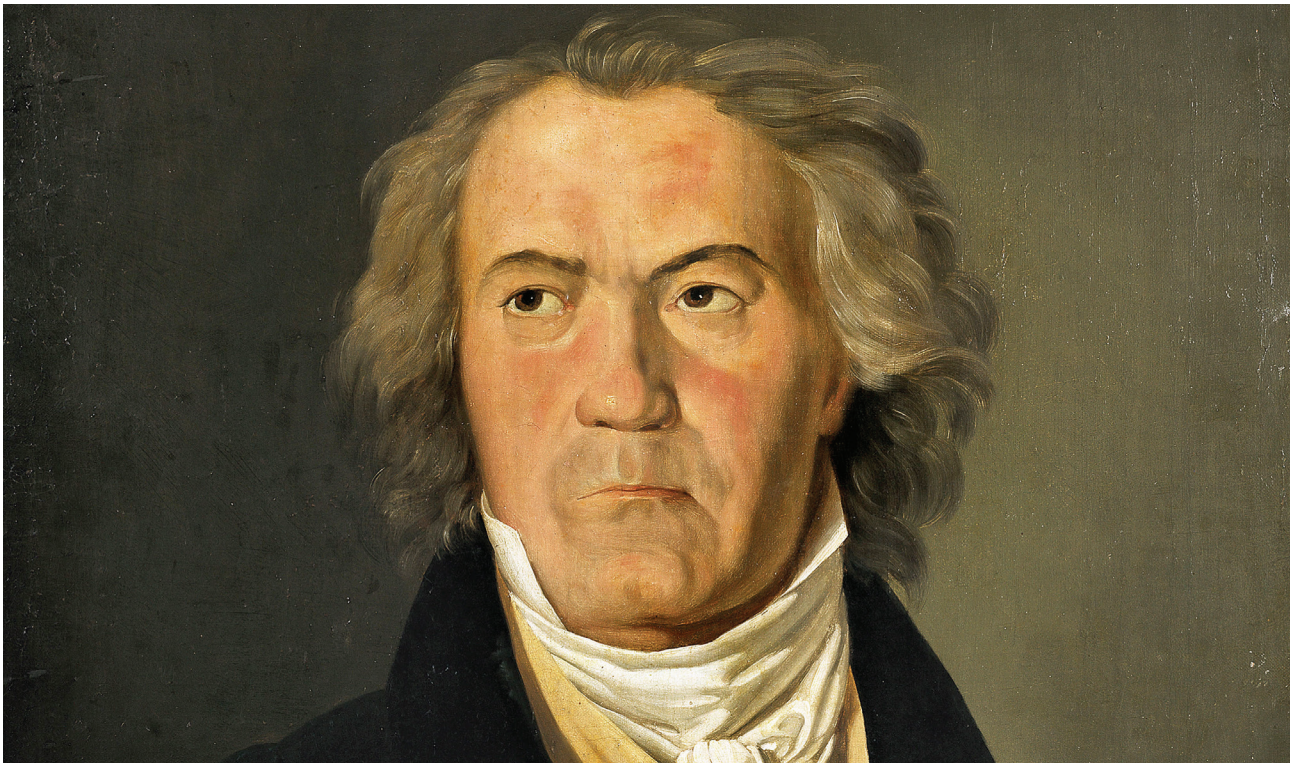

Attributed to Ferdinand Georg Waldmüller (1793–1869), *Portrait of Beethoven*, 1823 (detail). Oil on canvas, 28.1 in x 30.5 in/71.5 cm x 77.5 cm. Kunsthistorisches Museum, Vienna, Austria. Digital image from Art Resource, New York, New York, USA.

B for Beethoven

Terence Chorba

Ludwig van Beethoven (1770–1827) is one of the most renowned and admired composers in the development of Western Classical music. He was perhaps the greatest contributor to the musical style transition from Classical (roughly 1750–1820), with linear compositional styles, to Romantic (roughly 1798–1837), with dramatic expansion of orchestra size and development of lyrical, less formulaic melodic styles. The German composer's contributions vastly widened the scope and development of the concerto, quartet, sonata, and symphony. In March 1827, after a prolonged illness, Beethoven died at age 56 in his apartment in Vienna. Discussions of Beethoven's health have been voluminous, fraught with controversy, and limited by an absence of evidence, characteristic of the first half of the 19th century before the availability of radiologic and microbiologic diagnostics. Starting at age 28, the composer suffered hearing deficits that were initially characterized as tinnitus and high-frequency hearing loss. Letters, journals, and other documents of that era indicate that, in his final decade of his life, Beethoven's health and hearing progressively declined, yet he produced many works that were expansive and departing from the more conservative structure of his earlier works.

In 1823, Ferdinand Georg Waldmüller (1793–1865), a Vienna-born painter, was commissioned by Christoph Härtel, one of Beethoven's Leipzig publishers, to paint a portrait of the composer. Waldmüller is credited with being one of the most influential painters of the Biedermeier period, the era between the Congress of Vienna in 1815 and the onset of the revolutions throughout Europe in 1848. Beginning at age 14, Waldmüller studied portrait, still life, and nature painting at the Academy of Fine Arts in Vienna. In a painting attributed to Waldmüller that is featured on this month's cover, he captured an older Beethoven whose hair, though still wild, was a bit more tame than in images from his younger years. Beethoven was already suffering from hearing loss, but that was the same year in

Author affiliation: Centers for Disease Control and Prevention, Atlanta, Georgia, USA

DOI: https://doi.org/10.3201/eid2909.AC2909

which he completed one of his supreme achievements, his Missa Solemnis (https://archive.org/details/lp_missa-solemnis_ludwig-van-beethoven-leonard-bernstein-the). The composer sat for Waldmüller only once and that sitting was brief, so it is assumed that only the composer's face was captured; later on, the painter would have added the clothes and portions of the hair. A second, more finished, oil-on-canvas version of the portrait was made from that study but was destroyed in a fire during the 1943 Allied bombing of Leipzig. Later in his career, Waldmüller focused on painting landscapes; his most notable works, principally in Italy, emphasized nature and color. He died in 1865 in Hinterbrühl, Austria, near his native Vienna.

The day after Beethoven's death, an autopsy performed by one of the leading pathologists of the era, Karl Rokitansky, found Beethoven to have a uniformly dense skull vault; together with Beethoven's prominent forehead and enlarged jaw with protruding chin, that finding is thought to have been consistent with Paget's disease of bone (osteitis neoformans), not described until 1877. Paget's is a disease of unknown etiology in which there is cellular remodeling and bone deformity from breakdown and disorganized new bone formation. Progressive hearing loss is a common symptom of Paget's disease, the result of the eighth cranial nerve being compressed by bony overgrowth or the small bones of the middle ear being disrupted. Another autopsy finding, an atrophic nodular and cirrhotic liver, together with the account of a friend that Beethoven consumed wine in excess near the end of his life, has long led historians to believe that Beethoven also suffered from and died of alcoholism-associated liver disease. There is no identified record of his having palmar erythema, spider angiomata, asterixis (liver flap), or gynecomastia, all commonly associated with chronic liver disease; however, Beethoven endured 2 attacks of jaundice (the first at age 51), swelling of his limbs, and ascites requiring repeated paracentesis. In most cases worldwide, cirrhosis of the liver is attributable to the interplay of individual genetic predisposition and the effects of alcohol or infection with hepatitis B virus (HBV) or hepatitis C virus (HCV).

In a fortuitous recent development in the study of the human genome, hair has been identified as a potential resource for evidence of HBV DNA in persons with acute or chronic HBV infection. Recently, 8 independently sourced locks of hair attributed to Beethoven from public and private collections underwent genomic sequencing, 5 of which we now know originated from the same man with predominantly central European ancestry and are deemed to be authentic. DNA extracted from those 5 locks yielded 2 copies of a particular variant of the *PNPLA3* gene that has been associated with developing liver cirrhosis. The 5 locks also had single copies of 2 variants of the *HFE* gene that most often cause hereditary hemochromatosis, which can also contribute to liver damage. Based on metagenomic analyses, it seems that Beethoven also had HBV infection, at least in the months immediately before his death, although it is unknown whether the infection was recent, chronic, or reactivated. Thus, a potential explanation for Beethoven's recurrent bouts of jaundice and the severe liver disease observed at autopsy, often credited as his principal cause of death, may be the contribution of any or all of the triad of excess alcohol consumption, genetic predisposition for liver disease, and HBV infection.

Bibliography

1. Anonymous. Ludwig van Beethoven: lithograph by I.G. Fritzsche after a painting by Ferdinand Georg Waldmüller [in German]. Beethoven-Haus, Bonn [cited 2023 Jul 18]. https://www.beethoven.de/en/media/view/6234496605093888
2. Begg TJ, Schmidt A, Kocher A, Larmuseau MH, Runfeldt G, Maier PA, et al. Genomic analyses of hair from Ludwig van Beethoven. Curr Biol. 2023;33:1431–47.e22. https://doi.org/10.1016/j.cub.2023.02.041
3. Brotto D, Fellin R, Sorrentino F, Gheller F, Trevisi P, Bovo R. A modern case sheds light on a classical enigma: Beethoven's deafness. Laryngoscope. 2021;131:179–85. https://doi.org/10.1002/lary.28464
4. Davies PJ. Beethoven in person: his deafness, illnesses, and death. Praeger (Westport, CT); 2001.
5. De Sapio M. The mystique of late Beethoven [cited 2023 Jul 18]. https://theimaginativeconservative.org/2020/10/mystique-late-beethoven-michael-de-sapio.html
6. Erfurth A. Ludwig van Beethoven: a psychiatric perspective. Wien Med Wochenschr. 2021;171:381–90. https://doi.org/10.1007/s10354-021-00864-4
7. Harada T, Komatsu H, Inui A, Tsunoda T, Hashimoto T, Fujisawa T. Hepatitis B virus DNA in the fingernails and hair of children with acute hepatitis B. J Infect Chemother. 2022;28:82–6. https://doi.org/10.1016/j.jiac.2021.08.014
8. Hopfner R. Portrait Ludwig van Beethoven [cited 2023 Jul 18]. https://www.khm.at/en/objectdb/detail/85675
9. Perz JF, Armstrong GL, Farrington LA, Hutin YJ, Bell BP. The contributions of hepatitis B virus and hepatitis C virus infections to cirrhosis and primary liver cancer worldwide. J Hepatol. 2006;45:529–38. https://doi.org/10.1016/j.jhep.2006.05.013
10. Shield K, Manthey J, Rylett M, Probst C, Wettlaufer A, Parry CD, et al. National, regional, and global burdens of disease from 2000 to 2016 attributable to alcohol use: a comparative risk assessment study. Lancet Public Health. 2020;5:e51–61. https://doi.org/10.1016/S2468-2667(19)30231-2
11. Wolf P. Creativity and chronic disease. Ludwig van Beethoven (1770–1827). West J Med. 2001;175:298. https://doi.org/10.1136/ewjm.175.5.298

Address for correspondence: Terence Chorba, Centers for Disease Control and Prevention, 1600 Clifton Rd NE, Mailstop US12-4, Atlanta, GA 30329-4027, USA; email: tlc2@cdc.gov

EMERGING INFECTIOUS DISEASES®

Upcoming Issue • Bacterial Infections, Including Syphilis

- Spike in Congenital Syphilis, Mississippi, USA, 2016–2022
- Serotype Distribution and Disease Severity in Adults Hospitalized with *Streptococcus pneumoniae* Infection, Bristol and Bath, UK, 2006–2022
- Comprehensive Case-Control Study of Protective and Risk Factors for Buruli Ulcer, Southeastern Australia
- Posttransfusion Sepsis Attributable to Bacterial Contamination in Platelet Collection Set Manufacturing Facility, United States\
- Ancestral Origin and Dissemination Dynamic of Reemerging Toxigenic *Vibrio cholerae,* Haiti
- Emergence of SARS-CoV-2 Delta Variant and Effect of Nonpharmaceutical Interventions, British Columbia, Canada
- Characteristics and Mortality of 333 Persons with Tuberculosis and COVID-19 in a Cross-sectional Sample from 25 Jurisdictions, United States
- Managing Risk for Congenital Syphilis, Perth, Western Australia, Australia
- *Listeria monocytogenes* Transmission from Donated Blood to Platelet Transfusion Recipient, Italy
- Human Tularemia Epididymo-Orchitis Caused by *Francisella tularensis* Subspecies *holartica*
- Imported Toxigenic *Corynebacterium Diphtheriae* in Refugees with Polymicrobial Skin Infections, Germany, 2022
- Estimated Costs of 4-Month Pulmonary Tuberculosis Treatment Regimen, United States
- Limited Outbreak of Highly Pathogenic Influenza A(H5N1) Virus in Herring Gull Colony, Canada, 2022
- SARS-CoV-2 Mortality, China, December 2022–February 2023
- Pseudomonas aeruginosa High-Risk Sequence Type 463 Co-Producing KPC-2 and AFM-1 Carbapenemases, China, 2020–2022
- Reemergence of Cosmopolitan Genotype of Dengue Virus Serotype 2, Southern Vietnam
- *Bacillus subtilis* Bacteremia from Gastrointestinal Perforation after Natto Ingestion, Japan
- Parasites: The Inside Story
- One Health Approach to Globalizing, Accelerating, and Focusing Amphibian and Reptile Disease Research
- Stability of Monkeypox Virus in Body Fluids and Wastewater

Complete list of articles in the October issue at https://wwwnc.cdc.gov/eid/#issue-303

Earning CME Credit

To obtain credit, you should first read the journal article. After reading the article, you should be able to answer the following, related, multiple-choice questions. To complete the questions (with a minimum 75% passing score) and earn continuing medical education (CME) credit, please go to http://www.medscape.org/journal/eid. Credit cannot be obtained for tests completed on paper, although you may use the worksheet below to keep a record of your answers.

You must be a registered user on http://www.medscape.org. If you are not registered on http://www.medscape.org, please click on the "Register" link on the right hand side of the website.

Only one answer is correct for each question. Once you successfully answer all post-test questions, you will be able to view and/or print your certificate. For questions regarding this activity, contact the accredited provider, CME@medscape.net. For technical assistance, contact CME@medscape.net. American Medical Association's Physician's Recognition Award (AMA PRA) credits are accepted in the US as evidence of participation in CME activities. For further information on this award, please go to https://www.ama-assn.org. The AMA has determined that physicians not licensed in the US who participate in this CME activity are eligible for *AMA PRA Category 1 Credits*™. Through agreements that the AMA has made with agencies in some countries, AMA PRA credit may be acceptable as evidence of participation in CME activities. If you are not licensed in the US, please complete the questions online, print the AMA PRA CME credit certificate, and present it to your national medical association for review.

Article Title

Characteristics of Hard Tick Relapsing Fever Caused by *Borrelia miyamotoi*, United States, 2013–2019

CME Questions

1. Which one of the following statements regarding *Borrelia miyamotoi* is most accurate?

A. It is a gram-negative spirochete
B. It is an agent of soft tick relapsing fever
C. It is transmitted by ticks of the *Argasidae* genus
D. The prevalence of *B. miyamotoi* in its vector tick is about 30% in the US

2. Which one of the following statements regarding cases of *B. miyamotoi* infections in the current study is most accurate?

A. There were a total of 4,000 cases
B. The prevalence of infections increased over time
C. The median age of individuals with infection was 20 years
D. More than 80% of individuals with infection were male

3. Which month was associated with the peak of *B. miyamotoi* infections in the current study?

A. April
B. June
C. August
D. October

4. Which one of the following clinical characteristics of *B. miyamotoi* infection in the current study is most accurate?

A. The median time from symptom onset to seeking medical attention was 5 days
B. The most common symptom was rash
C. Laboratory abnormalities occurred in less than 25% of patients
D. The mortality rate of infection was 4%

Earning CME Credit

To obtain credit, you should first read the journal article. After reading the article, you should be able to answer the following, related, multiple-choice questions. To complete the questions (with a minimum 75% passing score) and earn continuing medical education (CME) credit, please go to http://www.medscape.org/journal/eid. Credit cannot be obtained for tests completed on paper, although you may use the worksheet below to keep a record of your answers.

You must be a registered user on http://www.medscape.org. If you are not registered on http://www.medscape.org, please click on the "Register" link on the right hand side of the website.

Only one answer is correct for each question. Once you successfully answer all post-test questions, you will be able to view and/or print your certificate. For questions regarding this activity, contact the accredited provider, CME@medscape.net. For technical assistance, contact CME@medscape.net. American Medical Association's Physician's Recognition Award (AMA PRA) credits are accepted in the US as evidence of participation in CME activities. For further information on this award, please go to https://www.ama-assn.org. The AMA has determined that physicians not licensed in the US who participate in this CME activity are eligible for AMA PRA Category 1 Credits™. Through agreements that the AMA has made with agencies in some countries, AMA PRA credit may be acceptable as evidence of participation in CME activities. If you are not licensed in the US, please complete the questions online, print the AMA PRA CME credit certificate, and present it to your national medical association for review.

Article Title

Foodborne Botulism, Canada, 2006–2021

CME Questions

1. What was the average annual incidence of foodborne botulism between 2006 and 2021 in the current study?

A. 0.01 per 100,000 population
B. 1 per 100,000 population
C. 10 per 100,000 population
D. 22 per 100,000 population

2. Which one of the following serotypes of botulinum neurotoxins was most common in the current study?

A. Type A
B. Type B
C. Type E
D. Type F

3. Which one of the following types of foods accounted for most of the cases of foodborne botulism in the current study?

A. Uncooked marine mammal products
B. Juices
C. Food from restaurants
D. Commercially prepared fish

4. Which one of the following statements regarding clinical outcomes of foodborne botulism in the current study is most accurate?

A. 70% of patients with botulism required mechanical ventilation
B. The mortality rate was less than 2%
C. Serotype E was associated with a longer hospital stay
D. Serotype B was associated with a longer hospital stay